UNIVERSITAT DE BARCELONA

Novel approaches toward anti-Alzheimer and antiprotozoal drug candidates

Irene Sola Lao

FACULTAT DE FARMÀCIA I CIÈNCIES DE L'ALIMENTACIÓ

LABORATORI DE QUÍMICA FARMACÈUTICA
DEPARTAMENT DE FARMACOLOGIA, TOXICOLOGIA I QUÍMICA TERAPÈUTICA

NOVEL APPROACHES TOWARD ANTI-ALZHEIMER AND ANTIPROTOZOAL DRUG CANDIDATES

Irene Sola Lao

Barcelona, 2016

UNIVERSITAT DE BARCELONA

FACULTAT DE FARMÀCIA I CIÈNCIES DE L'ALIMENTACIÓ

Programa de doctorat:
Química Orgànica Experimental i Industrial

NOVEL APPROACHES TOWARD ANTI-ALZHEIMER AND ANTIPROTOZOAL DRUG CANDIDATES

Memòria presentada per Irene Sola
per optar al títol de Doctora per la Universitat de Barcelona

Director i tutor: Dr. Diego Muñoz-Torrero López-Ibarra

Doctoranda: Irene Sola Lao

Irene Sola Lao
Barcelona, 2016

Resum

La present Tesis Doctoral pretèn el desenvolupament de nous candidats de fàrmacs anti-Alzheimer i antiprotozoaris, gràcies a l'ús de tres diferents i innovadores aproximacions: "**Teràpies Multidiana**", "**Reposicionament de fàrmacs**" i "**Validació d'una nova diana terapèutica pel tractament de Malària**".

En referència a la malaltia d'Alzheimer, l'estratègia terapèutica basada en fàrmacs multidiana ha representat la base del disseny molecular i posterior síntesis de dos noves famílies estructurals proveïdes d'interaccions addicionals a aquelles establertes amb els enzims de tipus colinesteràsics, les quals s'ha demostrat que tan sols confereixen un alleujament simptomàtic de l'Alzheimer. En primer lloc, la família de compostos rhein-huprina conté una estructura híbrida constituïda per un potent inhibidor d'AChE, com és l'huprina Y, a més de per un fragment de tipus antraquinona derivat del compost rhein, que resulta en un efecte antiagregant del pèptid β-amiloide (Aβ) a part dels efectes convencionals derivats de l'inhibició dual de l'enzim AChE. D'altra banda, la família d'híbrids basats en levetiracetam es composen a més d'un inhibidor d'AChE, d'una unitat relacionada amb el fàrmac antiepilèptic levetiracetam (registrat com a Keppra®), el qual reverteix l'activitat epileptiforme causada per l'agregació d'Aβ.

Respecte les malalties de la Tripanosomiasis Africana i de la Malària, els fàrmacs que actualment existeixen al mercat són problemàtics, requereixen d'administració parenteral i la majoria donen lloc a molts efectes adversos, a més de produir resistències que comprometen la seva efectivitat clínica. Per aquesta raó, en el context de la present Tesis Doctoral, l'estratègia terapèutica de reposicionament de fàrmacs amb estructura d'aminoquinolina i la seva posterior optimització farmacològica ha estat usada per la ràpida recerca de noves teràpies eficaces contra la Tripanosomiasis Africana. Pel que fa a la Malària, l'enzim bifuncional de *Plasmodium falciparum* glucosa-6-fosfat deshidrogenasa-6-fosfogluconolactonasa (*Pf*GluPho) ha estat validat com a diana terapèutica, gràcies a la síntesis i evaluació farmacològica d'una sèrie de compostos glucosídics amb una estructura anàloga al substrat de l'enzim, la glucosa-6-fosfat.

Summary

This PhD Thesis pursues the development of novel anti-Alzheimer and antiprotozoal drug candidates upon exploitation of three different novel approaches: **Multitarget therapies**, **Drug repurposing**, and **Validation of a novel anti-malarial target**.

The work carried out in the frame of this PhD Thesis has followed three research lines, thus dividing the next report on three main objectives, namely the development of novel disease-modifying anti-Alzheimer agents, novel potential 4-aminoquinoline-based anti-tripanosomatid compounds, and so far unexplored substrate analog *Pf*G6PD inhibitors for the treatment of malaria.

In the context of the anti-Alzheimer therapeutic strategies, the innovative so-called Multi-Target Directed Ligands (MTDLs) approach has inspired the structure-based design and synthesis of two novel classes of hybrid compounds endowed with additional key target interactions beyond cholinesterases, whose modulation has shown to only confer a relief of the very late symptoms of the disease. On the one hand, rhein-huprine hybrids combine the activity of the potent catalytic anionic site (CAS) AChE inhibitor, huprine Y, with that of an anthraquinone fragment derived from rhein to afford a tau antiaggregating effect, apart from the conventional effects derived from dual site AChE interaction. Levetiracetam-based hybrids, on the other hand, comprise, apart from a CAS AChE inhibitor unit, a moiety related to the antiepileptic drug levetiracetam which tackles the Aβ-induced aberrant epileptiform activity across the neuronal network.

Regarding HAT and malaria treatment, current registered drugs are problematic, most of them display a range of toxic side effects, require strict and complicated parenteral administration regimens and produce resistances that undermine clinical effectiveness. For this reason, there is an acute need to find novel drugs that can circumvent the limitations of existing therapies. In the context of this PhD Thesis, drug repurposing and further optimization of 4-aminoquinoline-based compounds has been considered as a useful approach to potentially speed up the drug development in the HAT field. We have demonstrated that homodimerization, heterodimerization, and side chain modification of the anti-Alzheimer investigational 4-aminoquinoline derivative huprine Y can result in potent brain permeable antitrypanosomal agents, with decreased but still significant anticholinesterasic activity. On the other hand, the

bifunctional *Plasmodium falciparum* glucose-6-phosphate dehydrogenase-6-phosphogluconolactonase enzyme (*Pf*GluPho) has recently emerged as attractive druggable alternative for the development of innovative antimalarial therapeutic strategies. Starting from a homology model of *Pf*G6PD (G6PD domain of *Pf*GluPho), a new family of selective substrate analog-based inhibitors against the parasite *Pf*G6PD active site has been designed and synthesized, on the basis of the structural differences found at the catalytic site of the parasite and human enzymes.

Abbreviations

ACh	Acetylcholine
AChE	Acetylcholinesterase
AChEI	Acetylcholinesterase inhibitor
AcOH	Acetic acid
AD	Alzheimer's disease
ADI	Alzheimer's Disease International
aMCI	amnestic mild cognitive impairment
AMPK	Adenosine monophosphate-activated protein kinase
apoE	Apolipoprotein E
APP	β-Amyloid precursor protein
aq.	Aqueous
Aβ	β-Amyloid peptide
$A\beta_{40}$	40 amino acid β-amyloid peptide
$A\beta_{42}$	42 amino acid β-amyloid peptide
BACE-1	β-Secretase
bAChE	Bovine acetylcholinesterase
BBB	Blood-brain barrier
BChE	Butyrylcholinesterase
BChEI	Butyrylcholinesterase inhibitor
BMGF	Bill and Melinda Gates Foundation
CAS	Catalytic Anionic Site
CH_2Cl_2	Dichloromethane; methylene chloride
CH_3CN	Acetonitrile
$ClCO_2Et$	Ethyl chloroformate
CNS	Central Nervous System
CQ	Chloroquine
CSP	Circumsporozoite protein
C83 or CTFα	a carboxy-terminal α fragment composed of 83 amino acids
DALYs	Disability adjusted life-years
DBS	Dual Binding Site

DCC	Dicyclohexylcarbodiimide
DFMO	α-Difluoromethylornithine or eflornithine
DHFR	Dihydrofolate reductase
DHODase	Dihydroorotate dehydrogenase
DHPS	Dihydropteroate synthase
DMAP	Dimethylaminopyridine
DMF	N,N-dimethylformamide
DMPK	Drug Metabolism and Pharmacokinetic
DMSO	Dimethyl sulfoxide
DNDi	Neglected Diseases initiative
eeAChE	Electrophorus electricus acetylcholinesterase
EMP	Embden-Meyerhof-Parnas
Et_3N	Triethylamine
ER	Endoplasmic reticulum
FAD	Familial Alzheimer's Disease
FDA	Food and Drug Administration
FP	toxic free heme; ferri/ferroprotoporphyrin IX
FV	food vacuole
GBD	Global Burden Disease
GluPho	Glucose-6-phosphate dehydrogenase–6-phosphogluconolactonase
GSH	Glutathione
GSSG	Glutathione disulfide
GSK-3β	Glycogen Synthase Kinase 3β
G6PD	Glucose-6-phosphate dehydrogenase
G6PDd	Glucose-6-phosphate dehydrogenase deficiency
*h*AChE	Human Acetylcholinesterase
hAPP	Human amyloid precursor protein
HAT	Human African Trypanosomiasis
Hb	Hemoglobin
hBChE	Human Butyrylcholinesterase
HEP	Human hepatoma cells
hG6PD	Human glucose-6-phosphate dehydrogenase
HMS	Hexose monophosphate shunt

H_2O_2	Hydrogen peroxide
HPIA	Haem polymerization inhibitory activity
HPLC	High-performance liquid chormatography
HT	Hexose transporter
HTS	High-throughput screening
IC_{50}	Concentration that inhibits 50% of the enzymatic activity
IL-1β	Interleukin-1 β
i-PrOH	Isopropyl alcohol; isopropanol
K*i*	Inhibition constant
KOH	Potassium hydroxide
$LiAlH_4$	Lithium aluminium hydride
LiOH	Lithium hydroxide
LTP	Long term potentiation
*m*AChE	Mouse acetylcholinesterase
MAO	Monoamine Oxidase
MCPBA	*meta*-Chloroperoxybenzoic acid
MCR	Multicomponent Reaction
MeOH	Methanol
Ms	Mesylate
MsCl	Methanesulfonyl chloride; mesyl chloride
MTDLs	Multi-Target Directed Ligands
MVI	Malaria Vaccine Initiative
$NaBH_3CN$	Sodium cyanoborohydride
NADP or $NADP^+$	Nicotinamide adenine dinucleotide phosphate
NADPH	reduced form of nicotinamide adenine dinucleotide phosphate
NaCN	Sodium cyanide
NaH	Sodium Hydride
$NaHCO_3$	Sodium bicarbonate
NaOH	Sodium Hydroxide
NaOMe	Sodium methoxide
NECT	Nifurtimox/Eflornitine Combination Therapy
NMDA	N-Methyl-di-Aspartate
NMEs	New Molecule Entities

NMT	*N*-Myristoyl transferase
NO	Nitric oxide
NTDs	Neglected Tropical Diseases
NFTs	Neurofibrillary Tangles
OxPPP	Oxidative pentose phosphate pathway
PAMPA-BBB	Parallel Artificial Membrane Permeability Assay to evaluate passive BBB permeability
PAS	Peripheral Anionic Site
PDB	Protein Data Bank
PDEB	Phosphodiesterase
PDPs	Product Development Partnerships
P_e	Effective permeability
Pf	*Plasmodium falciparum*
PHF	Paired Helical Filaments
PPP	Pentose phosphate pathway
PSEN	Presenilin
PTR	Pteridine reductase
RBC	Red blood cell
RNAi	RNA interference
r. t.	Room temperature
ROS	Reactive Oxygen Species
sAPPα	Secreted Amyloid Precursor Protein-α
SAR	Structure-Activity Relationships
SI	Selectivity Index
SOD	Superoxide dismutase
SV2A	Synaptic vesicle protein 2A
T.b.	*Trypanosoma brucei*
T. b. g.	*T. b. gambiense*
T. b. r.	*T. b. rhodiense*
*Tc*AChE	*Torpedo californica* Acetylcholinesterase
THF	Tetrahydrofuran
TNF-α	Tumor necrosis factor α
TryR	Trypanothione reductase
TryS	Trypanothione synthase

WHO	World Health Organization
6PGD	6-Phosphogluconate dehydrogenase
6PGL	6-phosphogluconolactonase

Table of contents

1. Introduction to Alzheimer's disease 1

1.1. Present scenario 3

1.2. The AD puzzle 4

1.2.1. Amyloid cascade hypothesis 5

1.2.2. Cholinergic hypothesis 8

1.2.3. Mutations and risk factors associated with AD 11

1.3. Current treatments and trends against AD 12

1.3.1. Acetylcholinesterase inhibitors (AChEIs) 13

1.3.1.1. Revisiting AChEIs as disease-modifying therapies 14

1.3.1.2. A cross-talk between AChE and Aβ 15

1.3.1.3. Dual binding site AChEIs 17

1.3.2. BACE-directed chemotherapy 19

1.3.3. Multitarget chemotherapy 21

2. Introduction to Human African Trypanosomiasis (HAT) 25

2.1. Present scenario 27

2.2. HAT epidemiology 28

2.3. Current treatment and trends against HAT 31

2.3.1. Phenotypic whole-cell high-throughput screening (HTS) 34

2.3.2. Other drug discovery strategies for HAT 36

2.4. The concept of privileged structures in rational drug design 37

2.4.1. Quinolines as privileged motifs 38

2.4.2. Quinoline and protozoan diseases 40

2.4.3. Antiprotozoal quinoline compounds developed in our research group 41

3. Introduction to Malaria 43

3.1. Present scenario 45

3.2. Cause and spread of malaria 47

3.3. Current treatment and trends against malaria 50

3.3.1. Oxidative stress and antioxidant defense in malaria parasites 54

3.3.2. Pentose Phosphate Pathway (PPP) and Glucose-6-Phosphate Dehydrogenase (G6PD) 56

3.3.3. G6PD deficiency and malaria 59

3.3.4. Glucose-6-Phosphate Dehydrogenase-6-Phosphogluconolactonase from *P. falciparum* (*Pf*GluPho) 62

4. Objectives 65

4.1. Synthesis and *in vitro* and *in vivo* pharmacological evaluation of two novel classes of multitarget anti-Alzheimer drug candidates *(J. Med. Chem.* **2014***, 57,* 2549; *Curr. Alzheimer Res.* **2016**, *13*, 1017; and *J. Med. Chem.* **2015***, 58,* 6018) 67

4.2. Repurposing and further optimization of 4-aminoquinoline-based anti-Alzheimer AChE inhibitors toward new HAT therapies (*Bioorg. Med. Chem. Lett.* **2014**, *24*, 5435; *Bioorg. Med. Chem*. **2015**, *23*, 5156; and *Bioorg. Med. Chem.* **2016**, in press) 68

4.3. Searching for new safe and cost-effective antimalarial treatments: novel substrate analog PfG6PD inhibitors (Draft of the manuscript) 69

5. Multitarget therapies for AD 71

5.1. Multitarget therapy for AD treatment 73

5.2. Rhein−huprine hybrids

(*J. Med. Chem*. **2014**, *57*, 2549; and *Curr. Alzheimer Res.* **2016**, *13*, 1017) 76

5.2.1. Synthesis of rhein−huprine hybrids 79

5.2.2. *In vitro*, *ex vivo*, and *in vivo* evaluation of rhein−huprine hybrids 81

5.3. Levetiracetam−huprine and levetiracetam−(6-chloro)tacrine hybrids

(*J. Med. Chem.* **2015**, *58*, 6018) 85

5.3.1. Synthesis of levetiracetam-based hybrids 90

5.3.2. Pharmacological evaluation of levetiracetam-based hybrids 96

5A. *J. Med. Chem*. **2014**, *57*, 2549 97

5B. *Curr. Alzheimer Res*. **2016**, *13*, 1017 209

5C. *J. Med. Chem.* **2015**, *58*, 6018 251

6. Exploitation of the huprine scaffold for HAT drug development 313

6.1. Drug repurposing strategy from anti-Alzheimer compounds to antiprotozoal agents 315

6.2. Hit-to-lead optimization by huprine dimerization 317

6.2.1. *Bis*(+)-Huprines (*Bioorg. Med. Chem. Lett*. **2014**, *24*, 5435) 318

6.2.1.1. Preparation of *bis*(+)-huprines (+)-**101a**–**e** 319

6.2.1.2. Pharmacological evaluation of *bis(+)*-huprines (+)-**101a–e** 320

6.2.2. Huprine-based heterodimers (*Bioorg. Med. Chem*. **2015**, *23*, 5156) 321

6.2.2.1. Preparation of huprine-based heterodimers 322

6.2.2.2. Phenotypic screening of huprine-based heterodimers and mechanistic studies 326

6.3. Hit-to-lead optimization by side chain modification (*Bioorg. Med. Chem*. **2016**, in press) 329

6.3.1. Synthesis of ω-cyanoalkyl-, ω-aminoalkyl-, and ω-guanidinoalkylhuprine (tacrine) derivatives 330

6.3.2. Pharmacological evaluation 332

6A. *Bioorg. Med. Chem. Lett*. **2014**, *24*, 5435 335

6B. *Bioorg. Med. Chem*. **2015**, *23*, 5156 355

6C. *Bioorg. Med. Chem*. **2016**, in press 371

7. Ongoing battle against drug resistant malaria 431

7.1. *Pf*G6PD, a new target to combat drug resistant malaria 433

7.2. Substrate analog inhibitors of *Pf*G6PD designed from an enzyme homology model (Draft of the manuscript) 436

7.2.1. Synthesis of substrate analog *Pf*G6PD inhibitors 438

7.2.2. *In vitro* biological profiling of substrate analog *Pf*G6PD inhibitors 441

7.A. Draft of the manuscript 445

CONCLUSIONS **489**

REFERENCES **495**

COMMUNICATION OF RESULTS **521**

CHAPTER 1

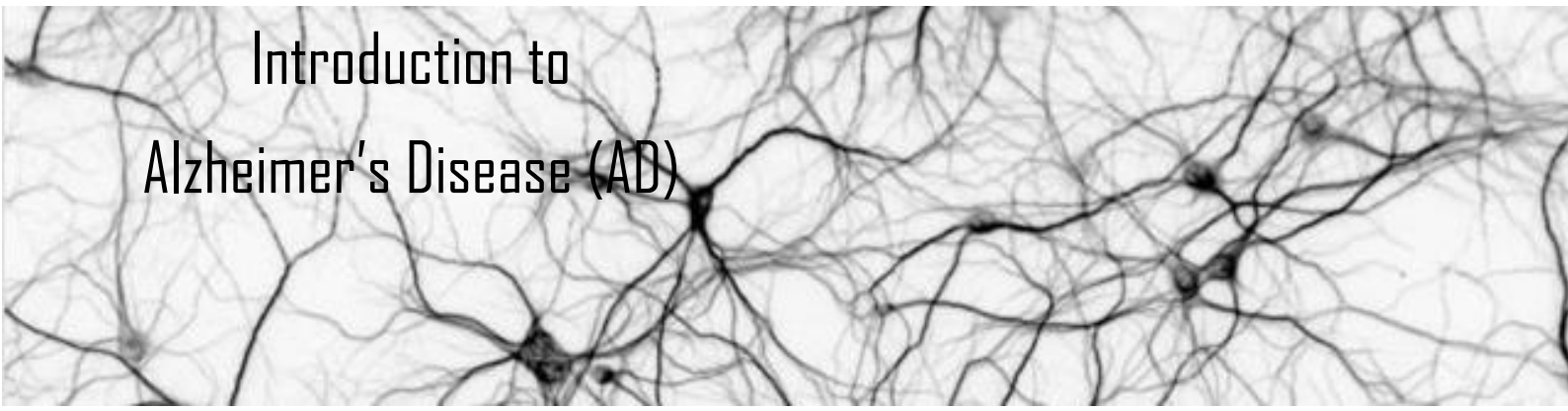

Introduction to Alzheimer's Disease (AD)

1.1. Present scenario

The constant improvement of living conditions in most western countries is leading to an increasing human life span and to the corresponding spread of age-related neurodegenerative disorders, among which Alzheimer's disease (AD) is one of the commonest and the most challenging.

AD is a chronic neurodegenerative disorder marked by a severe and progressive worsening of cognitive functions, especially memory processes, but thinking, language, behavior, orientation, and the ability to perform everyday activities are also affected.[1] The earliest symptoms are usually subtle, intermittent deficits in the remembrance of minor events of everyday life, referred to as loss of episodic memory. After many months of gradual memory loss, other cognitive symptoms appear and slowly advance. Over a further period of years, profound dementia develops and affects multiple cognitive and behavioral spheres. In the final stages of the disease people are bed-bound and require around-the-clock care, and ultimately death usually comes by way of minor respiratory complications, such as aspiration or pneumonia.[1,2,3]

The prevalence of AD ranges from 1 to 2% in the 65 years age group to 35% or higher in the 85 years age.[4] As of 2015, according to Alzheimer's Disease International (ADI) 46.8 million people worldwide are living with dementia, and this number is projected to triple by 2050, over 131.5 million people, the majority of whom are thought to suffer AD. Today, the vast majority of people with dementia (94%) live in low and middle income countries where access to social protection, services, support, and care are very limited. The current prevalence estimates are 12−13% higher when compared to 2009 estimates, with these estimates being particularly higher in East Asia and Africa (**Figure 1.1**).[5]

[1] 2015 Facts and Figures. Alzheimer's Association Home Page. https://www.alz.org (accessed February 2, 2016)

[2] Cummings, J. L.; Askin-Edgar, S. *CNS Drugs* **2000**, *13*, 385−395.

[3] Leonard, B. E. *Hum. Psycopharmacol*. **1998**, *13*, 83−90.

[4] Tayeb, H. O.; Yang, H. K.; Price, B. H. *et al. Pharmacol. Ther.* **2012**, *134*, 8–25.

[5] World Alzheimer Report 2015: The Global Impact of Dementia - An analysis of prevalence, incidence, cost and trends. Alzheimer's Disease International Home Page. http://www.alz.co.uk (accessed January 12, 2016).

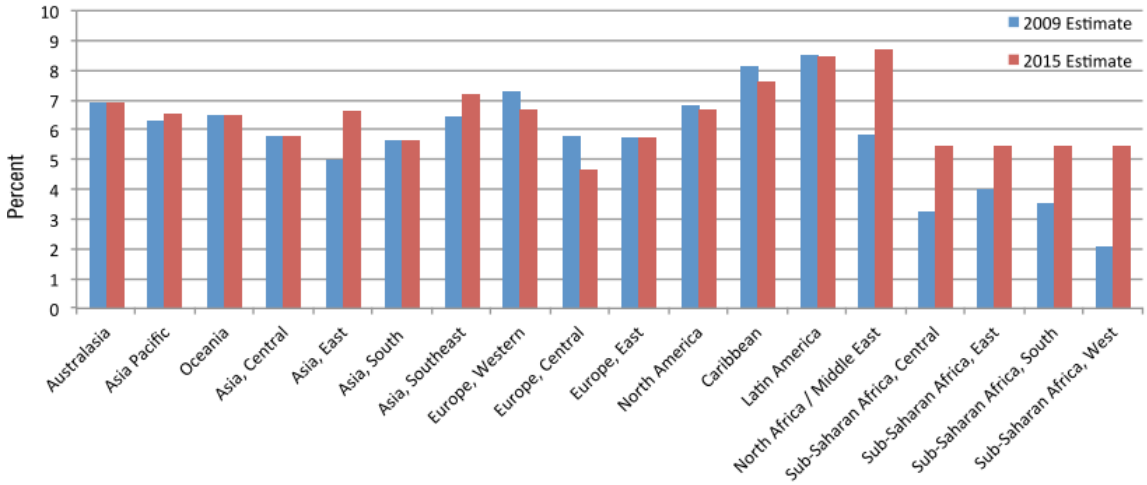

Figure 1.1. Estimated prevalence of dementia for patients aged ≥ 60, standardized to Western Europe population, by Global Burden Disease (GBD) region (Image source: World Alzheimer Report 2015: The Global Impact of Dementia - An analysis of prevalence, incidence, cost and trends. Alzheimer's Disease International Home Page. http://www.alz.co.uk)

Not only are there numerous health-related reasons for concern, but AD and dementia also suppose a huge economic impact. In 2015, the total estimated worldwide cost of dementia was US$ 818 billion, and it will become a trillion dollar disease by 2018, rising to US$ 2 trillion by 2030. Altogether, these figures stress the importance of AD as the biggest global public health and social care challenges today and in the future, and the urgent need for new treatments that allow an early effective intervention before irreversible pathological changes occur.[1,5]

1.2. The AD puzzle

AD was first diagnosed more than 100 years ago by Dr. Alois Alzheimer. He described numerous globs of sticky proteins in the interneuronal space and a tangle of fibrils throughout the cortex in the place where neurons were previously located, after the postmortem brain assessment of a 51-years-old female patient diagnosed with a new disease called "presenile dementia".[6] But it was not until 70 years thereafter that AD was recognized as the most common cause of

[1] 2015 Facts and Figures. Alzheimer's Association Home Page. https://www.alz.org (accessed February 2, 2016)
[5] World Alzheimer Report 2015: The Global Impact of Dementia - An analysis of prevalence, incidence, cost and trends. Alzheimer's Disease International Home Page. http://www.alz.co.uk (accessed January 12, 2016).
[6] Stelzmann, R. *Clinical Anat.* **1995**, *1*, 429–431.

dementia and a "major killer" in elderly people.[7] Although intensive research efforts have been directed toward deciphering the mechanisms of AD, much is yet to be discovered about the precise biological changes that cause it, why it progresses more quickly in some than in others, and how the disease can be prevented, slowed, or stopped.[1]

There has been a number of single factor theories that have been proposed to explain the etiology of AD, but to date, no one theory can adequately explain all aspects of this disorder and, hence, the disease origin remains still enigmatic. However, there is a quite general consensus that several pathological hallmarks can explain the underlying AD pathogenesis, such as formation of amyloid β-protein (Aβ) plaques, abnormal posttranslational modifications of tau protein to yield neurofibrillary tangles (NFTs), and deterioration of neurotransmitter systems.[8,9]

1.2.1. Amyloid cascade hypothesis

The so-called "amyloid cascade" hypothesis is one of the most widely accepted as a centerpiece of AD pathogenesis.[10] β-Amyloid plaques are extracellular deposits of which the major component is Aβ, a small polypeptide released by cleavage of a much larger transmembrane β-amyloid precursor protein (APP)[11,12] through the successive action of two proteases: β-secretase 1 (BACE-1) and γ-secretase; which is known as amyloidogenic processing. The initial cleavage of APP by BACE-1 takes place within the endosome at low pH, to produce a 99 amino acid length soluble peptide fragment (C99 or CNTβ), and is the rate-limiting step in Aβ formation. This peptide is further processed by γ-secretase to 36−43 amino acid length Aβ species, of which the longer isoforms, especially Aβ42, are the most fibrillogenic and neurotoxic (**Figure 1.2**). Alternatively, a non-amyloidogenic cleavage of APP by α-secretase allows for the release of a large soluble fragment of APP (sAPPα), which may actually have neurotrophic and neuroprotective properties, and a carboxy-terminal α fragment composed of 83 amino acids (C83 or CTFα). This is, in fact, the predominant pathway for amyloid metabolism.[4]

---

[1] 2015 Facts and Figures. Alzheimer's Association Home Page. https://www.alz.org (accessed February 2, 2016)
[7] Katzman R. *Arch. Neurol.* **1976**, *33*, 217–218.
[4] Tayeb, H. O.; Yang, H. K.; Price, B. H. *et al. Pharmacol. Ther.* **2012**, *134*, 8–25.
[8] a) Tomiyama, T.; Shoji, A.; Kataoka, K. *et al. J. Biol. Chem*. **1996**, *271*, 6839–6844. b) Lahiri, D. K.; Farlow, M. R.; Sambamurti, K. *et al. Curr. Drug Targets* **2003**, *4*, 97–112. c) Cummings, J. *Rev. Neurol. Dis.* **2004**, *1*, 60–69. d) Bartolini, M.; Bertucci, C.; Bolognesi, M. L. *et al. ChemBioChem* **2007**, *8*, 2152–2161. e) Gauthier, S.; Poirier, J. *Alzheimers Dement.* **2008**, *4* (Suppl. 1), S48–50.
[9] Krall, W. J; Sramek, J. J.; Cutler, N. *Ann. Pharmacother.* **1999**, *33*, 441–450.
[10] Hardy, J.; Allson, D. *Trends Pharmacol. Sci.* **1991**, *12*, 383−388.
[11] Masters, C. L.; Simms, G.; Weinman, N. A. *et al. Proc. Natl. Acad. Sci. USA* **1985**, *82*, 4245–4249.
[12] Kang, J.; Lemaire, H. G.; Unterbeck, A. *et al. Nature* **1987**, *325*, 733–736.

The amyloid hypothesis suggests that the soluble Aβ oligomers can impair synaptic function between neurons. Simultaneously, the oligomers may cluster into insoluble β-sheet amyloid fibrils (senile plaques) in the extracellular compartment through a process that depends on proteoglycans and apolipoproteins. Over time, the subsequent oxidative stress and biochemical changes ultimately lead to the death of neurons and the development of the "senile plaques" typical of AD.

In parallel, amyloid hypothesis also proposes that changes in tau and subsequent neurofibrillary tangle formation are triggered by toxic concentrations of Aβ.[13] Tau is a soluble protein that is physiologically present in the neuronal axons where it promotes microtubule assembly and stability. The binding of tau to microtubules is regulated by phosphorylation. In AD, tau becomes hyperphosphorylated due to an imbalance of different kinases activities of the glycogen synthase kinase-3 (GSK-3) family, losing the capacity to bind microtubules and therefore giving rise to its aggregation first into oligomers and then into β-sheet structures before forming macroscopic NFTs, evident in post mortem Alzheimer's disease tissues.[14] The latter will disrupt the structure and function of the neuron.[15]

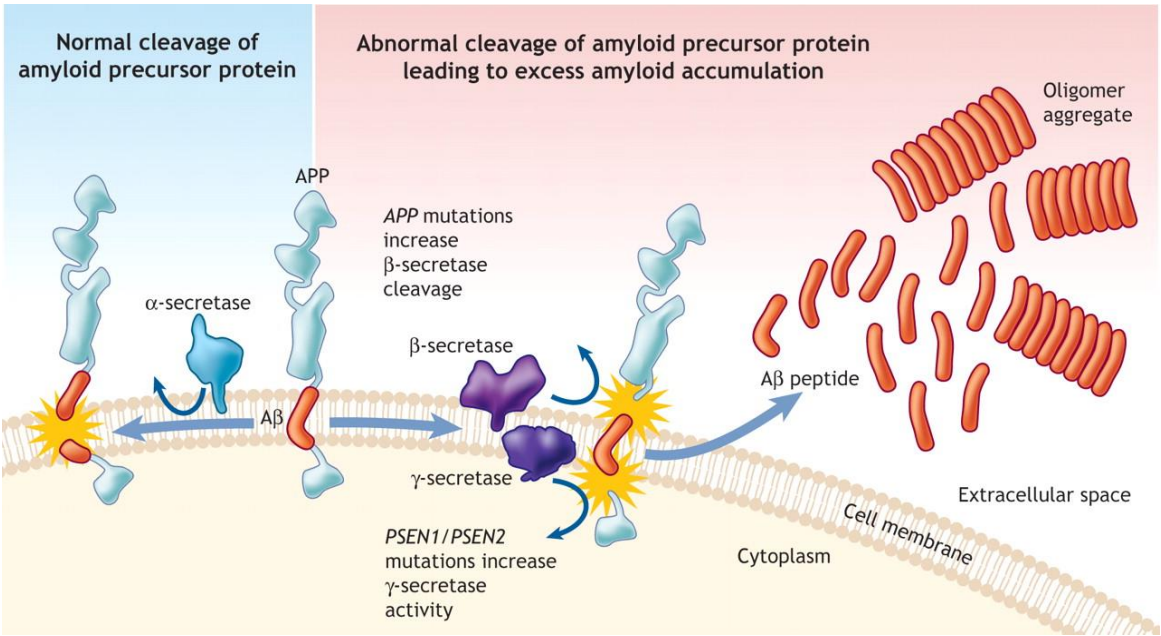

Figure 1.2. APP can undergo a series of proteolytic cleavages by secretase enzymes (Image source: Patterson, C.; Feightner, J. W.; Hsiung, G. Y.; MacKnight, C.; Sadvnick, A. D. *CMAJ* **2008**, *178*, 548–556).

[13] Churcher, I. *Curr. Top. Med. Chem.* **2006**, *6*, 579–595.
[14] Ferrer, I.; Gomez-Isla, T.; Puig, B. *et al. Curr. Alzheimer Res.* **2005**, *2*, 3–18.
[15] Ballard, C.; Gauthier, S.; Corbett, A. *et al. Lancet* **2011**, *377*, 1019–1031.

Though the amyloid hypothesis offers a broad framework to explain AD development, some researchers argue that it does not capture all crucial components of the pathophysiologic processes.[16] Several discrepancies in human and mouse studies point out that abundant amyloid deposition does not necessarily correlate with memory deficits or neuronal toxicity.[17] Cerebral amyloid plaques can exist in normal individuals, without associated cognitive impairment. Up to 30% of population in their 70s can have amyloid plaques without cognitive dysfunction.[18] Furthermore, whilst a significant body of genetic evidence suggests that increased synthesis or decreased clearance of Aβ is the primary pathogenic event in AD, post-mortem analyses show that the degree of tau-related pathology correlates much better with the severity of the dementia than does Aβ burden suggesting a key role for tau in the neurodegenerative cascade of the disease. This, coupled to the observations that extensive neurodegeneration is observed in both clinical tauopathies and transgenic animal models of disease in the absence of any Aβ pathology, demonstrates that tau is able to mediate neuronal loss in its own right rather than simply being an accessory to Aβ-induced injury.[13] In fact, more recent theories tie together Aβ pathology with NFT, but the relationship between them has been difficult to discover. Increasing evidence suggests that apoptotic mechanisms involving activation of cysteine aspartyl proteases (caspases) may be the missing link between Aβ and NFT.[19] Extracellular Aβ oligomers may activate caspases through activation of cell surface death receptors. Alternatively, intracellular Aβ may activate caspases through a process that involves endoplasmic reticulum (ER) stress or mitochondrial stress. One of the consequences of caspase activation is cleavage of tau, which favors conformational changes characteristic of paired helical filaments (PHF-tau). Progressive accumulation of tau leads to cytoskeletal disruption, failure of axoplasmic and dendritic transport, and subsequent loss of trophic support that culminates in neuronal death. The extracellular amyloid deposits in senile plaques also trigger reactive glial changes and neuroinflammation that can also contribute to neuronal loss through production of reactive oxygen species (ROS), nitric oxide (NO), and proinflammatory cytokines such as tumor necrosis factor α (TNF-α) and interleukin-1 β (IL-1β) (**Figure 1.3**).[20]

[13] Churcher, I. *Curr. Top. Med. Chem.* **2006**, *6*, 579−595.
[16] Hardy, J.; Selkoe, D. J. *Science* **2002**, *297*, 353−356.
[17] Knopman, D. S.; Parisi, J. E.; Salviati, A. *et al. J. Neuropathol. Exp. Neurol*. **2003**, *62*, 1087–1095.
[18] a) Fagan, A. M.; Mintun, M. A.; Shah, A. R. *et al. EMBO Mol. Med*. **2009**, *1*, 371–380. b) Morris, J.; Roe, C. M.; Grant, E. A. *et al*. *Arch. Neurol*. **2009**, *66*, 1469–1475. c) Rentz, D.; Locascio, J. J.; Becker, J. A. *et al.* M. *Ann. Neurol.* **2010**, *67*, 353–364.
[19] Rissman, R. A.; Poon, W. W.; Blurton-Jones, M. *et al. J. Clin. Invest.* **2004**, *114*, 121–130.
[20] Dickson, D. W. *J. Clin. Invest.* **2004**, *114*, 23−27.

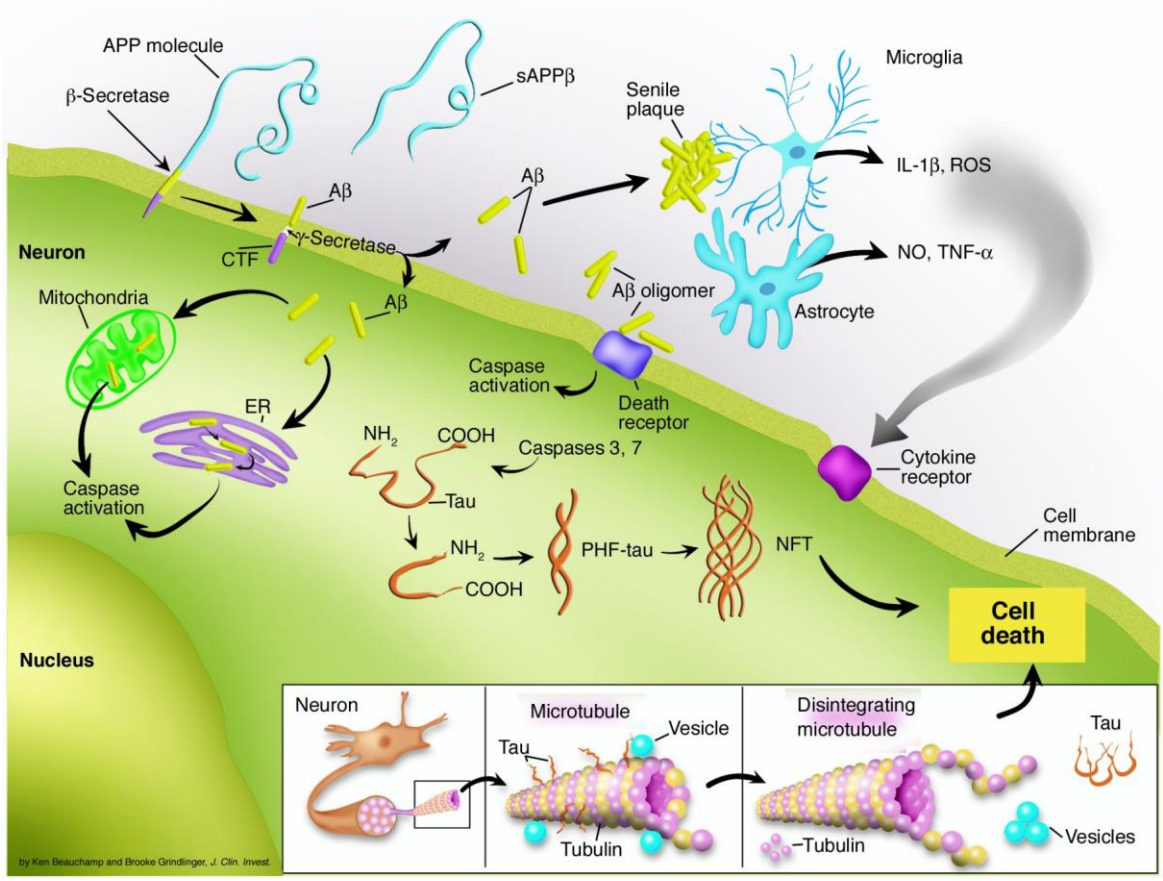

Figure 1.3. Factors involved in AD pathogenesis (Image source: Dickson, D. W. *J. Clin. Invest.* 2**004**, *114*, 23–27).

1.2.2. Cholinergic hypothesis

Another common feature in AD patients is a cholinergic deficiency. As of "cholinergic hypothesis" claimed over 20 years ago, a deficit of neurotransmitter acetylcholine (ACh) in the central nervous system (CNS), which is especially present in brain areas dealing with learning, memory, behavior, and emotional responses that include the neocortex and the hippocampus, contributes substantially to the cognitive decline observed in those with advanced age and AD. Considerable evidences support this theory;[21] antimuscarinic agents such as scopolamine and atropine have been shown to impair memory performance in a variety of behavioral paradigms in rodents.[22,23]

[21] Camps, P.; Muñoz-Torrero, D. *Mini-Rev. Med. Chem*. **2002**, *2*, 11–25.
[22] Decker, M. W.; McGaugh, J. L. *Synapse* **1991**, *7*, 151–168.
[23] Terry, A. V.; Buccafusco, J. J. *J. Pharmacol. Exp. Ther.* **2003**, *306*, 821–827.

There are two major classes of enzymes responsible for ACh degradation, acetylcholinesterase (AChE) and butyrylcholinesterase (BChE), both of which are present in the central and peripheral compartments. Functionally, both enzymes hydrolyze ACh efficiently but at different rates; BChE hydrolyzes butyrylcholine (BCh) at rates faster than ACh, while AChE degrades BCh much more slowly than ACh.[9,24]

Human AChE (hAChE) is a 583 amino acid residues protein, additionally provided with a 31 residues signal peptide (**Figure 1.4**). The hydrolysis of ACh takes place inside the catalytic site of the enzyme (catalytic anionic site, CAS), localized at the bottom of a 20 Å long gorge. The CAS is constituted by a catalytic triad consisting of residues Ser203-His447-Glu334 that are involved in neurotransmitter hydrolysis, and a neighbouring anionic hydrophobic site (Trp86, Glu202, Tyr337, Tyr341, and Phe338) responsible for cation−π interactions stabilizing the positive charge of the quaternary ammonium group of ACh and allowing to position its ester group in an orientation that enables it to face the CAS. Moreover, a second AChE binding site is the peripheral anionic site (PAS), a larger region rich in aromatic residues, which is located at the mouth of this narrow gorge and is responsible of the early binding of the substrate and directs it towards the CAS (**Figure 1.5**).[25]

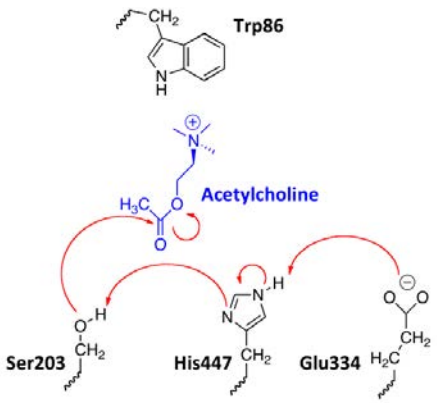

Figure 1.4. Schematic representation of the hydrolytic degradation of ACh in the CAS of AChE.

[9] Krall, W. J; Sramek, J. J.; Cutler, N. *Ann. Pharmacother.* **1999**, *33*, 441–450.
[24] Savini, L.; Gaeta, A.; Fattorusso, C. *et al. J. Med. Chem*. **2003**, *46*, 1−14.
[25] Sussman, J. L.; Harel, M.; Frolow, F. *et al. Science*, **1991**, *253*, 872−879.

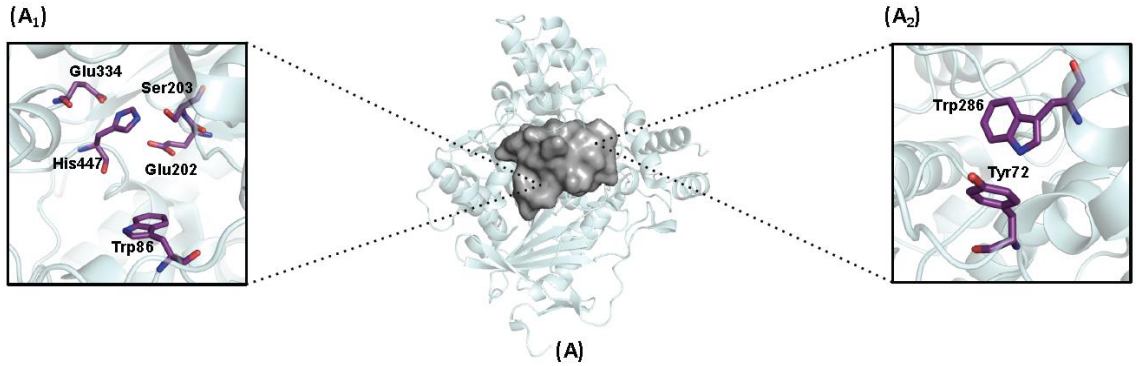

Figure 1.5. X-ray structure of human recombinant AChE (**A**, PDB ID: 3LII) with the details of the CAS (**A1**) and the PAS (**A2**).

In healthy brains, AChE hydrolyses the majority of ACh while BChE, mainly present in human blood, plays a secondary role. Nevertheless, based on research studies that highlight the relevance of BChE in advanced stages of AD, dual inhibition of AChE and BChE is increasingly pursued in the search for novel AD treatments.[26] Recent studies have noted that as AD progresses the activity of AChE decreases but increased levels of BChE (40-90%) are observed in the most affected areas of the brain, such as hyppocampus and temporal cortex, likely working as a co-regulator and helping in the maintenance and progression of the disease.[27,28,29] Different experimental evidences have placed BChE alongside AChE as an important contributor to the occurrence, symptoms, and progression of AD.[30] Thus, postmortem studies have shown that both AChE and BChE colocalise with Aβ deposits, although BChE at late stages of plaques formation, whereas AChE only at early stages.[31] Moreover, *in vivo* studies in rodents have demonstrated that selective BChE inhibition elevates ACh in brain and enables learning recovery and Aβ reduction.[32]

[26] Macdonald, I. R.; Rockwood, K.; Martin, E. *et al. Alzheimers Dis*. **2014**, *42*, 379−384.
[27] Perry, E. K.; Perry, R. H. *Neuropathol. Appl. Neurobiol.* **1978**, *4*, 273−277.
[28] Lane, R. M.; Potkin, S. G.; Enz, A. *Int. J. Neuropsychopharmacol.* **2006**, *9*, 101−124.
[29] Fernández-Bachiller, M. I.; Pérez, C.; Monjas, L. *et al. J. Med. Chem*. **2012**, *55*, 1303−1317.
[30] Mesulam, M. M.; Geula, C. *Ann. Neurol.* **1994**, *36*, 722−727.
[31] a) Guillozet, A. L.; Smiley, J. F.; Mash, D. C. *et al. Ann. Neurol.* **1997**, *42*, 909−918. b) Geula, C.; Darvesh, S. *Drugs Today* **2004**, *40*, 711−721. c) Ballard C. G.; Greig, N. H.; Guillozet-Bongaarts, A. L. *et al. Curr. Alzheimer Res.* **2005**, *2*, 307−318. d) Anand, P.; Singh, B. *Arch. Pharm. Res.* **2013**, *36*, 375–399.
[32] Greig, N. H.; Utsuki, T.; Ingram, D. K. *et al. Proc. Natl. Acad. Sci. U. S. A.* **2005**, *102*, 17213−17218.

1.2.3. Mutations and risk factors associated with AD

The amount of risk of Alzheimer's disease that is attributable to genetics is estimated to be around 70%. Among them only a small percentage of Alzheimer's cases (around 1%) can develop AD in midlife as a result of any of single-gene mutations on chromosome 21, 14, and 1, which encode APP, presenilin 1 (PSEN1), and presenilin 2 (PSEN2), respectively (**Figure 1.6**), producing familial AD (FAD).[15]

Mutations in the APP gene (the Swedish and A673V mutations, **Figure 1.6**)[33,34] tend to inhibit cleavage by α-secretase and consequently enable preferential cleavage by BACE-1. Mutations in PSEN1 and PSEN2, which are components of the γ-secretase complex, increase cleavage by γ-secretase at this site. In both situations, the result is an increased Aβ peptide production or a shift toward the most aggregation prone Aβ peptide. Those inheriting a mutation to the APP or PSEN1 genes are guaranteed to develop AD, whilst those inheriting a mutation in the PSEN2 gene have a 95% chance of developing the disease. Individuals with mutations in any of these three genes usually have onset of clinical symptoms between 30 and 60 years old, while the vast majority of individuals with AD have late-onset disease, occurring at age 65 or later.[35]

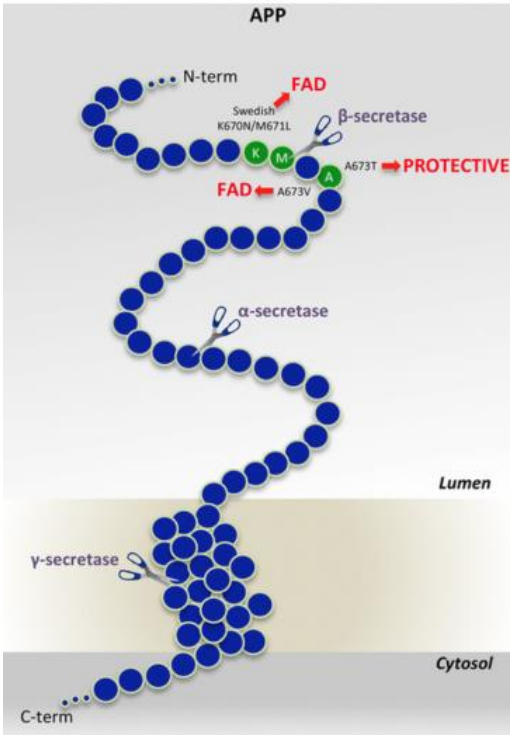

Figure 1.6. APP gene mutations related to AD (Image source: Vassar, R. *Alzheimers Res. Ther.* **2014**, *6*, 89).

The major genetic risk factor for late-onset AD is apolipoprotein E ε4 (ApoE ε4), which promotes Aβ aggregation and colocalizes with Aβ in senile plaques.[20] This is one of the three forms of the ApoE gene, which encodes a major cholesterol carrier in the blood and CNS. Those who inherit

[15] Ballard, C.; Gauthier, S.; Corbett, A. *et al. Lancet* **2011**, *377*, 1019–1031
[20] Dickson, D. W. *J. Clin. Invest.* **2004**, *114*, 23−27.
[33] Haass, C.; Lemere, C. A.; Capell, A. *et al. Nat. Med.* **1995**, *1*, 1291−1296.
[34] Jahn, H. *Dialogues Clin. Neurosci*. **2013**, *15*, 445−454.
[35] Citron, M.; Eckman, C. B.; Diehl, T. S. *et al*. *Neurobiol. Dis.* **1998**, *5*, 107−116.

one ApoE ε4 gene have about a threefold increased risk of developing AD, while those with two ApoE ε4 genes have a 12- to 15-fold increased risk.[36]

On the other hand, a coding mutation (A673T, **Figure 1.6**) in the APP gene has been found to exert a strong protective effect against AD. This substitution is adjacent to the aspartyl protease β-site in APP, and results in an approximately 40% reduction in the formation of amyloidogenic peptides.[37]

Other factors seem to be involved in late-onset AD development apart from genetic mutations. Although AD is not necessarily the outcome of aging,[38] it becomes the greatest contributing risk factor since the short course of human evolution has not shaped our biology to cope with the consequences of greatly extended longevity.[39] Furthermore, traumatic brain injury, cardiovascular disease, metabolic disorders, education or life style, to name a few, are other known risk factors for AD, which, in fact, are modifiable factors.[40]

1.3. Current treatments and trends against AD

AD, as we have already seen, appears to have a heterogeneous etiology. This, along with a late diagnosis of the disease, because pathological events seem to begin decades before measurable symptoms are obvious, is hindering the search for an efficient therapy that halts AD progression.

Despite tremendous investments made to increase the number of drugs approved and the targets engaged, in an effort to alter the disease course, symptomatic medications prevail as the mainstay of treatment options to date. Disappointingly, most clinical trials of potential drug candidates failed and no new drug (beyond medical foods) has been approved for the treatment of AD in the last decade.[41] As a result of this disheartening situation, valuable disease-modifying therapies are still needed.

Hereafter, it is summarized the current treatments against AD and some attempts to target the underlying pathogenesis through novel drug strategies, mainly AChEI inhibitors and Aβ-directed strategies, which are indeed of our particular field of interest.

[36] Raber, J.; Huang, Y.; Ashford, J. W. *Neurobiol. Aging* **2004**, *25*, 641–650.
[37] Jonsson, T.; Atwal, J. K.; Steinberg, S. *et al. Nature* **2012**, *488*, 96−99
[38] Den Dunnen, W. F.; Brouwer, W. H.; Bijlard, E. *et al. Neurobiol. Aging* **2008**, *29*, 1127−32.
[39] Narayan, P.; Ehsani, S.; Lindguist, S. *Nat. Chem. Biol.* **2014**, *10*, 911−920.
[40] Schmitt, B.; Bernhardt, T.; Moeller, H. J. *et al. CNS Drugs* **2004**, *18*, 827−844.
[41] Berk, C.; Sabbagh, M. N. *Drugs Aging* **2013**, *30*, 783–792.

1.3.1. Acetylcholinesterase inhibitors (AChEIs)

Since cholinergic deficiency in CNS has been widely associated with AD, ChEIs have become viable options to tackle the disease pathogenesis and are, indeed, the first-line treatment for dementia associated with AD. With the only exception of the non-competitive *N*-methyl-D-aspartate (NMDA) receptor antagonist memantine, **1** (marketed by Merz Pharmaceuticals as Axura™ in 2002, **Figure 1.7**)[42] which is believed to work by reducing excitotoxicity mediated by the neurotransmitter glutamate,[43] the other four commercialized anti-Alzheimer drugs, namely tacrine, **2** (Cognex™, Parke-Davis, 1993),[44,45] donepezil, **3** (Aricept™, Pfizer, 1996),[46,47] rivastigmine, **4** (Exelon™, Novartis, 2000),[48] and galantamine, **5** (Reminyl™, Janssen, 2001),[49] are cholinomimetic agents with the pharmacological profile of AChEIs. All of them increase the levels of ACh at the synapse and provide, however, only modest symptomatic relief to certain extent, achieving a stabilization of the cognitive function at a steady level during at least 1-year period in approximately 50% patients.[50] Moreover, not all AD patients are responsive to the effects of AChEIs and to date the differences between 'responders' and 'non-responders' remain unclear.[51,48] Connelly *et al.*[52] have reported that AD patients with high levels of medial temporal lobe atrophy are less likely to respond to donepezil and other studies have suggested that patients carrying the apolipoprotein ε4 (APOE ε4) allele are more likely to benefit from donepezil than non-APOE ε4 carriers.[53,54] It is important to note that tacrine was withdrawn from the market, although in some countries it is still available,[55] due to its dose-dependent hepatotoxicity, among other side effects.[56,57]

Tacrine, donepezil, and galantamine are reversible AChEIs, and rivastigmine is considered a pseudoirreversible AChEI as it contains a carbamate group that reacts with the residue Ser 203,

[42] Lipton, S. A. *Nature* **2004**, *428*, 473.
[43] Waxman, E. A.; Lynch, D. R. *Neuroscientist* **2005**, *11*, 37−49.
[44] Gualtieri, F.; Dei, S.; Manetti, D. *et al. Farmaco* **1995**, *50*, 489−503.
[45] Davis, K. L.; Thal, L. J.; Gamzu, E. R. *et al. N. Engl. J. Med.* **1992**, *327*, 1253−1259.
[46] Marx, J. *Science* **1996**, *273*, 50−53.
[47] Sugimoto, H.; Iimura, Y.; Yamanishi, Y. *et al. Med. Chem.* **1995**, *38*, 4821−4829.
[48] Polinsky, R. J. *Clin. Therap.* **1998**, *20*, 634−647.
[49] Sramek, J. J.; Frackiewicz, E. J.; Cutler, N. R. *Expert Opin. Investig. Drugs* **2000**, *9*, 2393−2402.
[50] Giacobini, E. *Pharmacol. Res.* **2004**, *50*, 433−440.
[51] Lemstra, A. W.; Richard, E.; van Gool, W. A. *Age Aging* **2007**, *36*, 625–627.
[52] Connelly, P. J.; Prentice, N. P.; Fowler, K. G. *J. Neurol. Neurosur. Ps.* **2005**, *76*, 320–324
[53] Bizzarro, A.; Marra, C.; Acciarri, A. *et al. Dement. Geriatr. Cogn.* **2005**, *20*, 254–261.
[54] Choi, S. H.; Kim, S. Y.; Na, H. R.; Kim, B. K. *et al. Dement. Geriatr. Cogn*. **2008**, *25*, 445–450.
[55] Zemek, F.; Drtinova, L.; Nepovimova, E. *et al. Expert Opin. Drug Saf.* **2014**, *13*, 759−774.
[56] Watkins, P. B.; Zimmerman, H. J.; Knapp, M. J. *et al. JAMA* **1994**, *271*, 992–998.
[57] Winker, M. A. *JAMA* **1994**, *271*, 1023–1024.

carbamoylating the enzyme, whose activity is slowly recovered after hydrolysis of the serine carbamate group. In principle, the four commercialized AChEIs were developed to inhibit the hydrolysis of ACh, and, therefore they were expected to interact with the active site of the enzyme. Nevertheless, the analysis of the X-ray structures of the four commercialized AChEIs in complex with AChE pointed out that while tacrine, **2**, rivastigmine, **4**, and galantamine, **5**, do clearly interact within the active site of the enzyme, conversely donepezil, **3**, is the sole marketed AChEI exhibiting a dual-site binding mode of interaction.[58] In fact, it spans the whole length of the gorge, simultaneously interacting with both Trp86, a characteristic residue of the CAS, and Trp286 in the PAS (**Figure 1.7**).

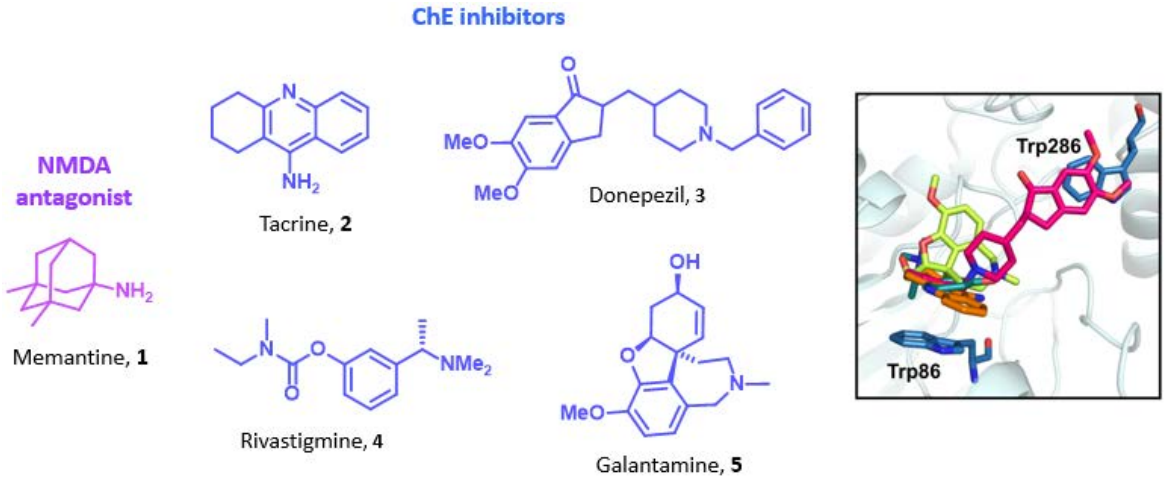

Figura 1.7. Left: Structure of the five marketed anti-Alzheimer drugs. Right: Binding mode of the four AChEIs in the gorge of AChE: tacrine, **2** (orange structure, PDB ID: 1ACJ); donepezil, **3** (magenta structure, PDB ID: 1EVE); rivastigmine, **4** (green structure, PDB ID: 1GQR); galantamine, **5** (yellow structure, PDB ID: 4EY6).

1.3.1.1. Revisiting AChEIs as disease-modifying therapies

Until now, the use of ChEIs has been only indicated for symptomatic treatment of AD, since they have not been able to prevent the progress of the disease in clinical trials.[59,60] However, in the last years, the use of AChEIs have again come into the focus of drug development efforts, in hopes of designing a viable therapeutic approach that amplifies the action of ACh in the brain of AD patients.

[58] Giacobini, E. *Neurochem. Res.* **2000**, *25*, 1185−1190.
[59] Mohs, R. C.; Doody, R. S.; Morris, J. C. *et al. Neurology* **2001**, *57*, 481–488.
[60] Winblad, B.; Engedal, K.; Soininen, H. *et al*. *Neurology* **2001**, *57*, 489–495.

Selective cholinergic depletions have shown to have multiple effects, one directly on specific cognitive processes like attention and flexibility,[61] and another by making the hippocampus less plastic and more susceptible to secondary insults.[62] In particular, the blockade of the glutamate-induced excitotoxicity through antagonism of NMDA receptors,[63] the overexpression of the antiapoptotic protein bcl-2 following stimulation of α4β2 nicotinic receptors,[64,65] and the mobilization of calcium pools from the intracellular reticulum following activation of σ1 receptors[66] have been proposed among the putative mechanisms proposed to explain the neuroprotective effects of AChEIs. These latter functions seem to be related to secondary non-cholinergic effects of ACh. In this regard, some studies have revealed two major forms of AChE in the mammal brain, tetrameric and monomeric species.[67] The major forms in the non-AD adult brain are tetramers (G4) that are anchored in the cell membrane of neurons, while in the AD brain there is a selective loss in the G4 form and the lighter species, monomers or dimers, are preserved or even increased in severely affected cases of AD. The tetramers probably constitute the true cholinergic species, but the significance of the particular increase in monomeric AChE is unclear to date.[68]

Moreover, recent clinical trials have shown that patients treated with both AChE and BChE inhibitors show minor cortical atrophic changes and attenuated loss of brain volumes.[69] These findings are consistent with the hypothesis that inhibitors of both enzymes may have neuroprotective and disease-modifying effects.[70]

1.3.1.2. A cross-talk between AChE and Aβ

Most of the above mentioned neuroprotection mechanisms may depend on protein–protein interactions rather than the AChE catalytic activity, thus making it difficult any structural rationalization to assist the design of novel drugs hitting these specific targets.[71] A distinct scenario is found when considering an additional neuroprotection mechanism connected with

[61] McGaughy, J.; Everitt, B. J.; Robbins, T. W. *et al. Behav. Brain Res.* **2000**, *115*, 251–263.
[62] Cutuli, D.; Foti, F.; Mandolesi, L. *et al. J. Alzheimers Dis.* **2009**, *17*, 161–176.
[63] Wang, X. D.; Chen, X. Q.; Yang, H. H. *et al. Neurosci. Lett.* **1999**, *272*, 21−24.
[64] Takada-Takatori, Y.; Kume, T.; Sugimoto, M. *et al. Neuropharmacology* **2006**, *51*, 474−486.
[65] Kihara, T.; Sawada, H.; Nakamizo, T. *et al*. *Biochem. Biophys. Res. Commun.* **2004**, *325*, 976−982.
[66] Meunier, J.; Ieni, J.; Maurice, T. *Br. J. Pharmacol.* **2006**, *149*, 998−1012.
[67] Massoulié, J.; Pezzementi, L.; Bon, S. *et al. Prog. Neurobiol*. **1993**, *41*, 31–91.
[68] García-Ayllón, M. S.; Small, D. H.; Avila, J. *et al. Front. Mol. Neurosci*. **2011**, *4*, 22.
[69] a) Greig, N.; Utsuki, T.; Ingram, D. *et al. Proc. Natl. Acad. Sci. U.S.A*. **2005**, *102*, 17213−17218. b) Lane, R. M.; Potkin, S. G.; Enz, A. *Int. J. Neuropsychoph.* **2006**, *9*, 101−124. c) Venneri, A.; Lane, R. *Neuroreport* **2009**, *20*, 285−288.
[70] Shanks, M.; Kivipelto, M.; Bullok, R. *et al. Curr. Med. Res. Opin.* **2009**, *25*, 2439−2446.
[71] Muñoz-Torrero, D. *Curr. Med. Chem.* **2008**, *15*, 2433−2455

the effect of AChEIs on Aβ aggregation. As reported by Prof. N. Inestrosa (*Pontificia Universidad Católica de Chile*), AChE, which colocalizes with Aβ in the senile plaques, participates in a non-cholinergic mechanism by means of a binding to Aβ, accelerating Aβ assembly *in vitro* and increasing its neurotoxicity potency,[72,73,74,75,76] which contributes to an unfavorable feedback loop leading to the cognitive impairment seen in AD.[77,78,79] Thus, these previous reports indicate that AChE act as a "pathological chaperone" promoting the assembly of Aβ1-40 peptides towards a β-sheet rich conformer endowed with an increased tendency to form more neurotoxic aggregates (**Figure 1.8**), by a mechanism that involves the PAS of AChE, located at the rim of the active site gorge of the enzyme. [73,74,78,80]

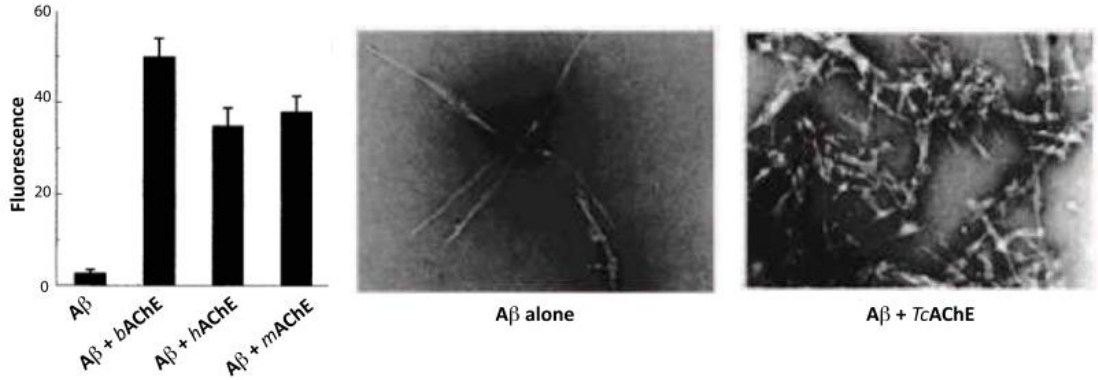

Figure 1.8. Left: Aβ aggregation in the presence of bovine AChE (*b*AChE), human AChE (*h*AChE), or mouse AChE (*m*AChE), quantified according to the increase of fluorescence due to thioflavin T, a compound that binds the β-sheets of Aβ when it is forming aggregates (Aβ 240 μM, AChE 2.4−9.6 μM, r. t., 48 h). Right: Electronic micrographies of Aβ fibrils alone or in the presence of *Torpedo californica* AChE (*Tc*AChE).

[72] Inestrosa, N. C.; Alvarez, A.; Pérez, C. A. *et al*. *Neuron* **1996**, *16*, 881−891.
[73] Alvarez, A.; Opazo, C.; Alarcon, R. *et al. J. Mol. Biol.* **1997**, *272*, 348−361.
[74] Alvarez, A.; Alarcón, R.; Opazo, C. *et al*. *J. Neurosci.* **1998**, *18*, 3213−3223.
[75] Inestrosa, N. C.; Sagal, J. P.; Colombres, M. *Subcell Biochem.* **2005**, *38*, 299−317.
[76] Inestrosa, N. C.; Dinamarca, M. C.; Alvarez, A. *FEBS J.* **2008**, *275*, 625−632.
[77] Chacón, M. A.; Reyes, A. E.; Inestrosa, N. C. *J. Neurochem.* **2003**, *87*, 195−204.
[78] Reyes, A. E.; Chacón, M. A.; Dinamarca, M. C. *et al. Am. J. Pathol.* **2004**, *164*, 2163−2174.
[79] Dinamarca, M. C.; Arrázola, M.; Toledo, E. *et al. Chem. Biol. Interact*. **2008**, *175*, 142−149.
[73] Alvarez, A.; Opazo, C.; Alarcon, R. *et al. J. Mol. Biol.* **1997**, *272*, 348−361.
[74] Alvarez, A.; Alarcón, R.; Opazo, C. *et al*. *J. Neurosci.* **1998**, *18*, 3213−3223.
[78] Reyes, A. E.; Chacón, M. A.; Dinamarca, M. C. *et al. Am. J. Pathol.* **2004**, *164*, 2163−2174.
[80] Muñoz, F. J.; Inestrosa, N. C. *FEBS Lett*. **1999**, *450*, 205−209.

Indeed, propidium, **6**, a specific PAS-binding inhibitor, is known to inhibit (at 50 μM) by 75% the AChE-induced Aβ aggregation, while the CAS-binding inhibitor edrophonium, **7**, has no effect on Aβ aggregation at 100 μM (**Figure 1.9**).[81]

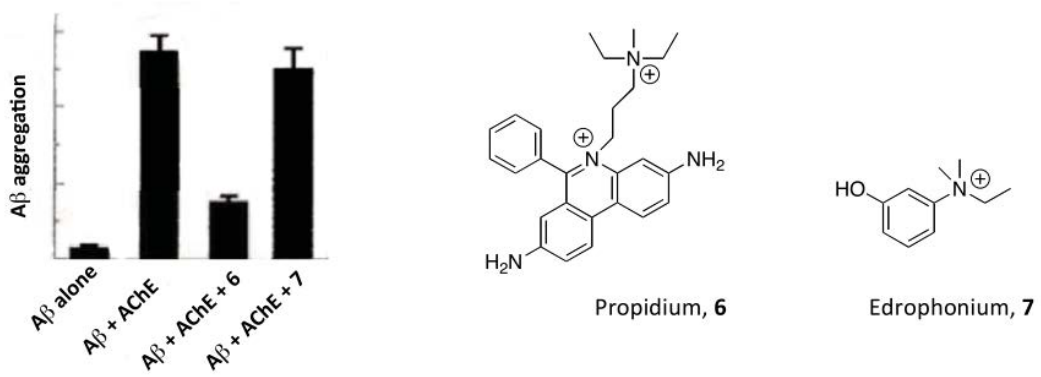

Figure 1.9. Aβ aggregation alone and in the presence of AChE, propidium (**6**), and edrophonium (**7**) quantified according to the increase of fluorescence due to thioflavin T.

Overall, these findings paved the way to the exploitation of AChE-induced Aβ aggregation inhibitors as a promising disease-modifying strategy for the treatment of AD. Taking into account the structure of AChE, where active and peripheral sites are close enough as to be simultaneously spanned by donepezil, **3**, the development of dual binding site AChEIs has strongly emerged in the last decades as a much more promising alternative to the design of selective CAS- or PAS-binding AChEIs. Accordingly, this strategy offers the advantantage of providing compounds with enhanced AChE affinity and AChE-induced Aβ antiaggregating properties, thereby being effective at the early stages of the neurodegenerative cascade.[82]

1.3.1.3. Dual binding site AChEIs

A large number of dual binding site AChEIs (DBS) with a well-documented Aβ antiaggregating activity has been reported in literature so far.[83] It is worth mentioning *bis*(7)-tacrine, **8**,[84] which

[81] De Ferrari, G. V.; Canales, M. A.; Shin, I. *et al. Biochemistry* **2001**, *40*, 10447−10457.
[82] Castro, A.; Martínez, A. *Curr. Pharm. Design* **2006**, *12*, 4377−4387.
[83] Brogi, S.; Butini, S.; Maramai, S.; Colombo, R. *et al*. *CNS Neurosci. Ther.* **2014**, *20*, 624−632.
[84] a) Pang, Y. P.; Quiram, P.; Jelacic, T. *et al. Biol. Chem*. **1996**, *271*, 23646−23649. b) Carlier, P. R.; Han, Y. F.; Chow, E. S. *et al. Bioorg. Med. Chem.* **1999**, *7*, 351−357. c) Bolognesi, M. L.; Cavalli, A.; Valgimigli, L. *et al. J. Med. Chem*. **2007**, *50*, 6446−6449.

was the pioneering work in DBS, the donepezil-coumarine derivative AP2238, **9**,[85] and the tacrine-indole hybrid **10**, among a host of described DBS (**Figure 1.10**).[86]

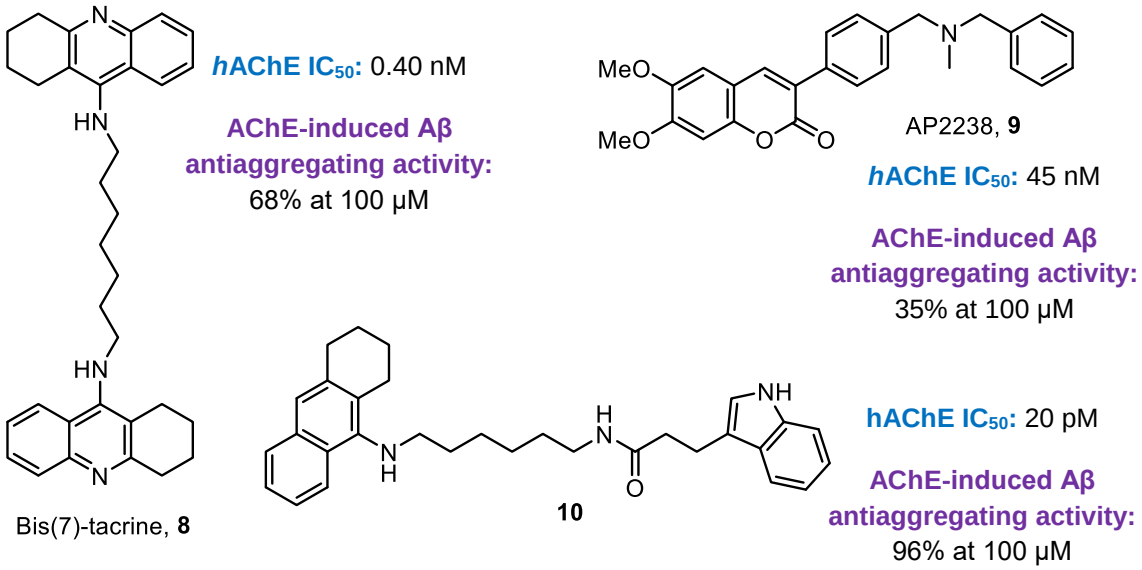

Figure 1.10. Structure of some dual binding site AChEIs.

Our research group has also made a contribution in this field. It all began about 15 years ago when Profs. P. Camps and D. Muñoz-Torrero (Universitat de Barcelona, Spain) reported a novel class of potent CAS-binding AChEIs referred to as huprines (**Figure 1.11**), which turned out to be among the most potent reversible AChEIs described so far.[87] Huprines were designed by combination of the 4-aminoquinoline moiety of tacrine, **2**, with the carbobicyclic substructure of (−)-huperzine A, a potent AChEI isolated from *Huperzia serrata* that is commercialized as a nutraceutical in the USA (Cerebra®) and approved in China as a palliative treatment for AD. Several families of huprine- and tacrine-based DBS displaying Aβ antiaggregating effect have been developed in our research group.[88] Among them, it is worth noting the series of donepezil−huprine hybrids (**Figure 1.11**), which was designed with the support of molecular modelling studies by linkage of a unit of huprine, **11−12**, and the 5,6-dimethoxy-2-[4-piperidinyl)methyl]-1-indanone moiety of donepezil (or the indane derivative thereof). The donepezil−huprine family resulted in a highly potent inhibition of the catalytic activity of *h*AChE (IC_{50} = 2.61−49.9 nM) and moderate *h*BChE inhibition (IC_{50} = 61−419 nM). More importantly,

[85] Piazzi, L.; Rampa, A.; Bisi, A. *et al. J. Med. Chem*. **2003**, *46*, 2279−2282.
[86] Muñoz-Ruiz, P.; Rubio, L.; García-Palomero, E. *et al. J. Med. Chem*. **2005**, *48*, 7223−7233.
[87] a) Camps, P.; El Achab, R.; Görbig, D. M. *et al. J. Med. Chem.* **1999**, *42*, 3227−3242. b) Muñoz-Torrero, D.; Camps, P. *Expert Opin. Drug Dis.* **2008**, *3*, 65−81
[88] a) Camps, P.; Formosa, X.; Galdeano, C. *et al. J. Med. Chem.* **2009**, *52*, 5365−5379. b) Galdeano, C.; Viayna, E.; Sola I. et al. *J. Med. Chem*. **2012**, *55*, 661−669. c) Viayna, E.; Sabate, R.; Muñoz-Torrero, D. *Curr. Top. Med. Chem*. **2013**, *13*, 1820−1842.

these hybrids exhibited a significant *in vitro* neutralization of the pathological chaperoning effect of AChE toward the aggregation of Aβ (25−50% of inhibition at 100 μM concentration of inhibitor) and the self-induced Aβ-aggregation (16−30% of inhibition at 10 μM concentration of inhibitor), apart from an outstanding *in vitro* inhibitory activity towards BACE-1 (12−31% inhibition at 5 μM concentration of inhibitor), thus making them suitable leads amenable to further optimization.[89]

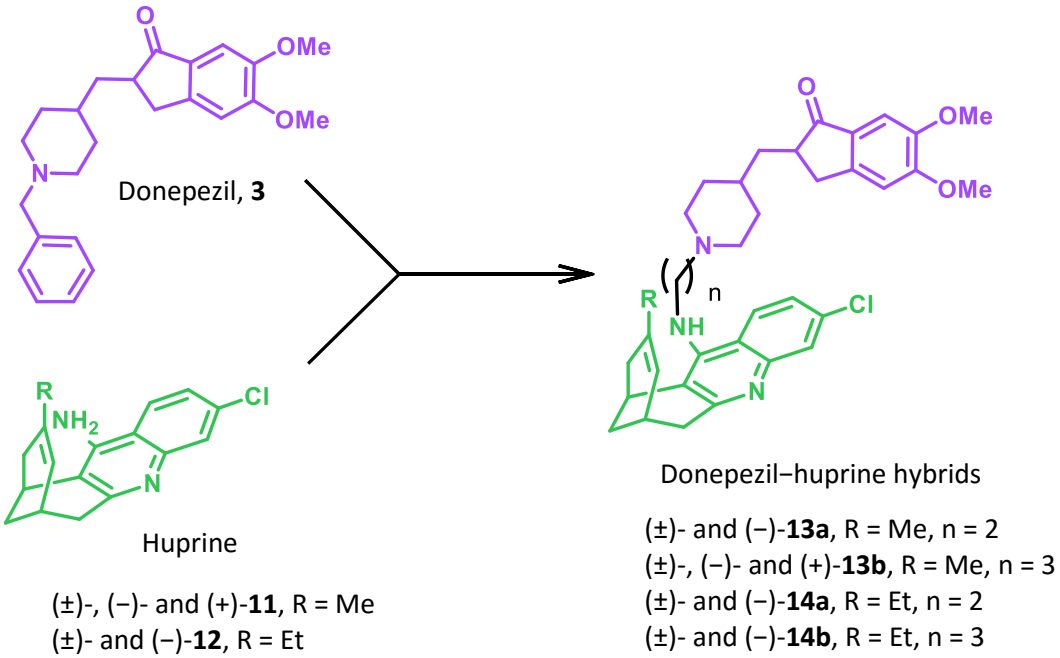

Figure 1.11. Design of donepezil−huprine hybrids **13**−**14**.

1.3.2. BACE-directed chemotherapy

Aβ seems to be the main target in order to prevent the neurodegenerative process of AD. Thus, in the last years important efforts to develop anti-Alzheimer drugs capable of positively modify the progression of the disease by inhibiting the formation and aggregation of Aβ have been made.[90,91] In this light, both secretases responsible for Aβ formation (γ- and β-secretase, BACE-1) have been actively pursued as drug targets by the pharmaceutical industry. Nevertheless, BACE-1 has gained more traction as it is involved in the initial and rate-limiting step of the proteolytic

[89] a) Camps, P.; Muñoz-Torrero, D.; Formosa, X. *et al.* WO 2007/122274A1. b) Camps, P.; Formosa, X.; Galdeano, C. *et al. J. Med. Chem*. **2008**, *51*, 3558−3598. c) Muñoz-Torrero, D.; Camps, P.; Gómez, T. *et al.* WO 2011/076969A1. d) Viayna, E.; Gómez, T.; Galdeano, C. *et al*. *ChemMedChem* **2010**, *5*, 1855−1870. e) Sola, I.; Viayna, E.; Gómez, T. *et al. Molecules* **2015**, *20*, 4492−4515.

[90] Melnikova, I. *Nat. Rev. Drug Discov.* **2007**, *6*, 341−342.

[91] Skovronsky, D. M.; Lee, V. M.; Trojanowski, J. Q. *Annu. Rev. Pathol.* **2006**, *1*, 151−170

cleavage of APP to Aβ,[92] and due also in part to recent genetic evidence[93] as well as human clinical trial results showing a correlation of BACE-1 inhibition with Aβ reduction.[94] BACE-1 is a 501 amino acid membrane-associated, pepsin-like aspartic protease whose active site is a hydrophilic 20 Å long cavity of nearly 1000 $Å^3$. Two characteristic aspartic acid residues, namely Asp32 and Asp228, are responsible for the hydrolytic cleavage of the substrate inside the binding cleft, which results partially covered by a highly flexible antiparallel hairpin-loop, referred to as the "flap" (**Figure 1.12**).[95]

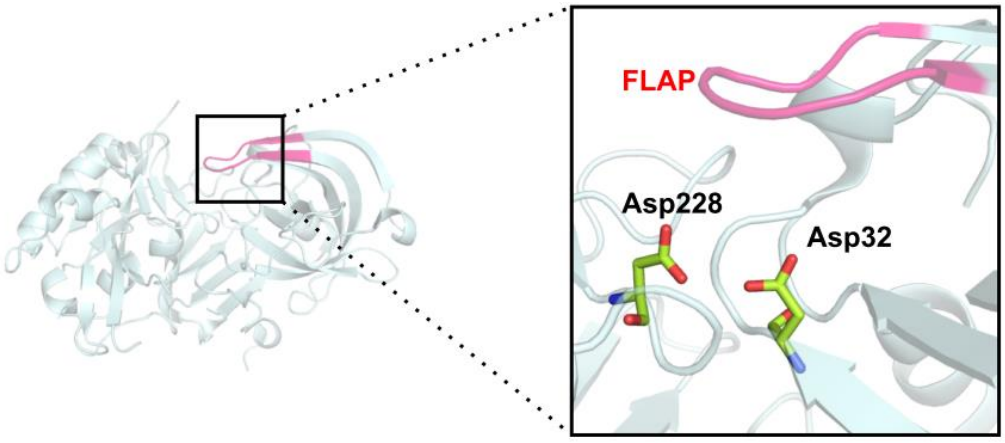

Figure 1.12. X-ray structure of BACE-1 (PDB ID: 1SGZ) with the details of the catalytic anionic dyad.

In addition to processing APP, BACE-1 is also responsible for cleaving other peptides, which may reduce its usefulness as a drug target.[96] Particularly, some subtle effects on both peripheral and central myelin formation have been associated to administration of BACE-1 inhibitors,[97] which continues to produce considerable attrition in this target space. For instance, BACE-1 inhibitors from Eli Lilly (LY2811376) and Amgen (AMG-8718) led to accumulation of autofluorescent material and degeneration of the retinal pigment epithelium (RPE) layer of the eye in rat safety

[92] De Strooper, B.; Vassar, R.; Golde, T. *Nat. Rev. Neurol*. **2010**, *6*, 99−107.
[93] Jonsson, T.; Atwal, J. K.; Steinberg, S. *et al*. *Nature* **2012**, *488*, 96–99.
[94] a) May, P. C.; Dean, R. A.; Lowe, S. L. *et al. J. Neurosci.* **2011**, *31*, 16507−16516. b) Stone, J.; Kleijn, H. J.; Dockendorf, M. *et al*. *Alzheimer's Dementia* **2013**, 9(4) Supplement, P690–P691.
[95] Kacker, P.; Bottegoni, G.; Cavalli, A. *Curr. Med. Chem*. **2012**, *19*, 6095−6111.
[96] a) Cheret, C.; Willem, M.; Fricker, F. R. *et al*. *EMBO J*. **2013**, *32*, 2015–2028. b) Kandalepas, P. C.; Vassar, R. *J. Neurochem*. **2012**, *120* (Suppl 1), 55–61. c) Kuhn, P. H.; Koroniak, K.; Hogl, S. *al*. *EMBO J*. **2012**, *31*, 3157–3168. d) Zhou, L.; Barao, S.; Laga, M. *et al*. *J. Biol. Chem*. **2012**, *287*, 25927–25940. e) Cai, J.; Qi, X.; Kociok, N. *et al*. *EMBO Mol. Med*. **2012**, 4, 980–991. f) Alzforum. "Cloistered Retreat Takes the Pulse of BACE Research." http://www.alzforum.org/news/conference-coverage/cloistered-retreat-takes-pulse-bace-research. February 18, 2016.
[97] Willem, M.; Garratt, A. N.; Novak, B. *et al. Science* **2006**, *314*, 664–666.

studies.[94a,98] Moreover, Lilly terminated a phase II study with LY2886721 as a result of abnormal liver biochemical tests. Thus, among the few BACE-1 inhibitors currently in clinical trials, only AZD3293 and MK-8931 have reached the phase II/III.[99] Therefore, novel small molecule BACE-1 inhibitors able to cross the blood-brain barrier (BBB) are urgently needed.[100]

1.3.3. Multitarget chemotherapy

As we have reported above, in the last decade, new significant insights concerning the cellular and molecular basis of AD pathogenesis have highlighted that the different strategies are not antithetical; rather, they tend to overlap in different areas. In light of these considerations, an alternative multiple combinations of co-factors model of AD was proposed by McDonald in 2002, where different factors set in motion a self-sustaining, amplifying cycle which culminates in cell death processes.[101] As a consequence, drug discovery in AD is gradually moving from the development of molecules able to modulate the biological function of a single target ("one drug−one target" paradigm) to polypharmacologic approaches aimed at hitting several of the key biological targets or events of the AD pathological network.[102] The most traditional polypharmacologic strategies consist of combination of drugs in a cocktail (multiple-medication therapy) or in a single formulation (multiple-compounded medication), but unfortunately these appear to be disadvantageous for patients in terms of compliance issues, drug−drug interactions, problems of bioavailability, and metabolism. Thus, the multifactorial nature of AD calls for the development of Multitarget-Directed Ligands (MTDLs) which comprise a single chemical entity capable of modulating simultaneously multiple targets ("one drug−more targets" approach). Besides reducing the pharmacokinetic and interaction problems linked to multiple-medication therapy, MTDLs generally show a synergistic pharmacologic effect.[103] However, the main challenge associated with this strategy is to optimize a compound series for multiple targets. We should achieve a proper activity at different targets and stages of the disease, but it

[98] Fielden, M. R.; Werner, J.; Coppi, A. *et al*. *Toxicol. Pathol.* **2015**, *43*, 581−592.
[99] LY2886721. https://investor.lilly.com/releaseDetail.cfm?ReleaseID=771353.
[100] Vassar, R. *Alzheimers Res. Ther*. **2014**, *6*, 89
[101] McDonald, R. J. *Can. J. Exp. Psychol*. **2002**, *56*, 221–339.
[102] a) Hopkins, A. L. *Nat. Biotechnol.* **2007**, *25*, 1110−1111. b) Hopkins, A. L. *Nat. Chem. Biol.* **2008**, *4*, 682−690. c) Janga, S. C.; Tzakos, A. *Mol. BioSyst.* **2009**, *5*, 1536−1548.
[103] a) Buccafusco, J. J.; Terry, A. V., Jr. *J. Pharmacol. Exp. Ther.* **2000**, *295*, 438−444. b) Youdim, M. B.; Buccafusco, J. J. *J. Neural Transm.* **2005**, *112*, 519−537. c) Nicolotti, O.; Giangreco, I.; Introcaso, A. *et al. Expert Opin. Drug Dis.* **2011**, *6*, 871−884.

becomes even harder since we do not even know how much potency at each single target is required and what the desired balance is between the potencies.[104]

With each passing year, an ever-increasing number of MTDL drug candidates towards AD treatment have entered the fray; just some of which are depicted below (**Figure 1.13**).[105,106] One of the most widely adopted strategy in this field has been to modify the molecular structure of AChEIs often by the use of hybrid agents in order to complement it with additional biological activities that are useful for treating AD, like M2 receptor antagonism,[107] inhibition of spontaneous Aβ aggregation,[108]AChE-dependent amyloid aggregation inhibition (dual-binding site inhibitors), or providing it with antioxidant properties[109] linked to MAO-B inhibition,[110] calcium channel blockage,[111] or control oxidative damage properties.[112]

[104] a) Morphy, R.; Rankovic, Z. *J. Med. Chem.* **2005**, *48*, 6523−6543 b) Morphy, R.; Rankovic, Z. *Drug Discov. Today* **2007**, *12*, 156–160. c) Bottegoni, G.; Favia, A. D.; Recanatini, M. *et al. Drug Discov. Today* **2012**, *17*, 23–34. d) Viayna, E.; Sola, I.; Di Pietro, O. *et al. Curr. Med. Chem.* **2013**, *20*, 1623−1634.

[105] Recent reviews: a) Cavalli, A.; Bolognesi, M. L.; Minarini, A. *et al. J. Med. Chem.* **2008**, *51*, 347−372. b) Carmo Carreiras, M.; Mendes, E.; Jesus Perry, M. *et al. Curr. Top. Med. Chem*. **2013**, *13*, 1745−1770. c) Rampa, A.; Gobbi, S.; Belluti, F. *et al. Curr. Top. Med. Chem*. **2013**, *13*, 1879−1904. d) Geldenhuys, W. J.; Van der Schyf, C. J. *Curr. Med. Chem*. **2013**, *20*, 1662−1672. e) Chen, X.; Decker, M. *Curr. Med. Chem.* **2013**, *20*, 1673−1685. f) Guzior, N.; Wieckowska, A.; Panek, D. *et al. Curr. Med. Chem.* **2015**, *22*, 373−404.

[106] Recent examples: a) Farina, R.; Pisani, L.; Catto, M. *et al*. *J. Med. Chem*. **2015**, *58*, 5561−5578. b) Prati, F.; De Simone, A.; Bisignano, P. *et al. Angew. Chem. Int. Ed.* **2015**, *54*, 1578−1582. c) Rochais, C.; Lecoutey, C.; Gaven,F. *et al. J. Med. Chem.* **2015**, *58*, 3172−3187. d) Guzior, N.; Bajda, M.; Skrok, M. *et al. Eur. J. Med. Chem*. **2015**, *92*, 738−749.
e) Xie, S.S.; Lan, J.S.; Wang, X.B. *et al. Eur. J. Med. Chem*. **2015**, 93, 42−50. f) Sang, Z.; Qiang, X.; Li, Y. *et al. Eur. J. Med. Chem*. **2015**, *94*, 348−366. g) Benchekroun, M.; Bartolini, M.; Egea, J. *et al. ChemMedChem* **2015**, *10*, 523−539. h) Liu, Q.; Qiang, X.; Li, Y. *et al. Bioorg. Med. Chem*. **2015**, *23*, 911−923.

[107] Melchiorre, C.; Andrisano, V.; Bolognesi, M. L. *et al*. *J. Med. Chem.* **1998**, *41*, 4186−4189.

[108] a) Bolognesi, M.; Andrisano, V.; Bartolini, M. *et al. Med. Chem*. **2005**, *48*, 24−27. b) Huang, W.; Tang, L.; Shi, Y. *et al*. *Bioorg. Med. Chem*. **2011**, *19*, 7158−7167. c) Li, Y.; Peng, P.; Tang, L. *et al. Bioorg. Med. Chem*. **2014**, *22*, 4717−4725. d) Rosini, M.; Simoni, E.; Bartolini, M. *et al*. *J. Med. Chem*. **2008**, *51*, 4381−4384.

[109] a) Holmquist, L.; Stuchbury, G.; Berbaum, K. *et al*. *Pharmacol. Ther.* **2007**, *113*, 54−164. b) Bolognesi, M. L.; Rosini, M.; Andrisano, V. *et al*. *Curr. Pharm. Des*. **2009**, *15*, 601−613.

[110] a) Sterling, J.; Herzig, Y.; Goren, T. *et al. J. Med. Chem*. **2002**, *45*, 5260−5279. b) Youdim, M. B.; Amit, T.; Bar-Am, O. *et al. Neurotoxic. Res.* **2006**, *10*, 181−192. c) Bolea, I.; Gella, A.; Unzeta, M. *J. Neural Transm*. **2013**, *120*, 893−902. d) Pisani, L.; Catto, M.; Leonetti, F. *et al. Curr. Med. Chem*. **2011**, *18*, 4568−4587.

[111] Marco-Contelles, J.; León, R.; de Los Ríos, C. *et al. J. Med. Chem.* **2006**, *49*, 7607−7610.

[112] Cavalli, A.; Bolognesi, M. L.; Capsoni, S. *et al. Angew. Chem. Int. Ed. Engl.* **2007**, *46*, 3689−3692.

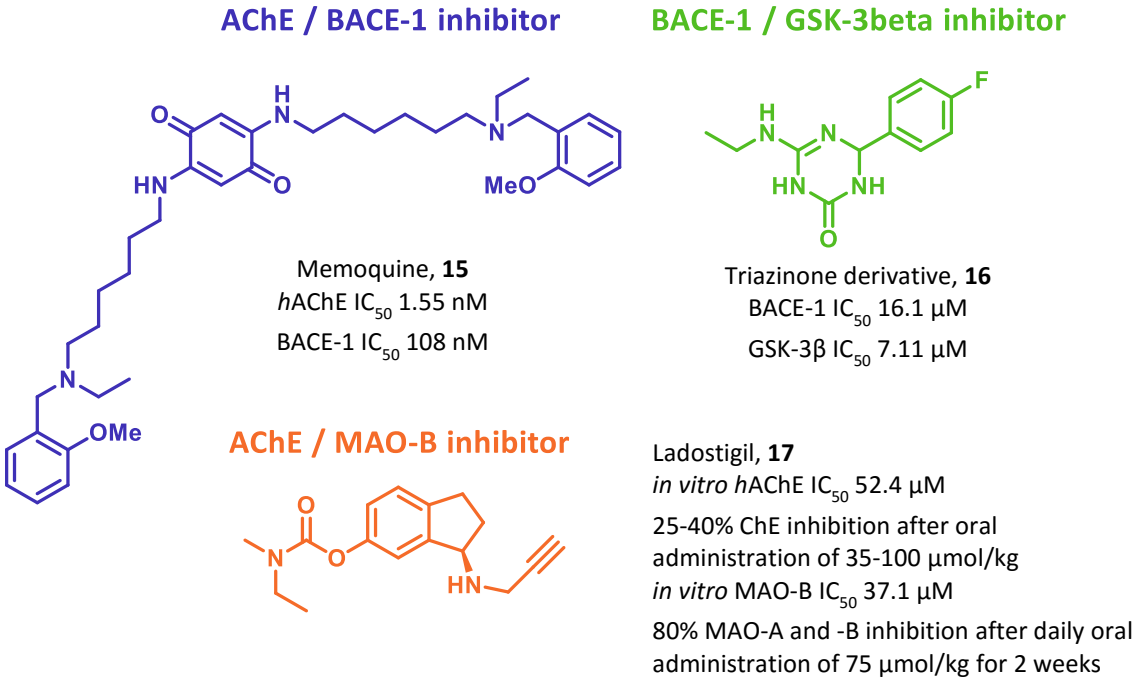

Figure 1.13. Structure and activities of some multitarget anti-Alzheimer agents.

CHAPTER 2

Introduction to Human African Trypanosomiasis (HAT)

2.1. Present scenario

Human African Trypanosomiasis (HAT), also known as "sleeping sickness", is a vector-borne protozoan disease included by the World Health Organization (WHO) among the so-called 17 Neglected Tropical Diseases (NTDs). Particularly, HAT poses a notable health burden in 36 countries throughout sub-Saharan Africa where nowadays nearly 30 million people are estimated to be at risk of acquiring it, entailing more than 1.2 million disability-adjusted life years (DALYs) per year.[113,114,115]

Although HAT figures appear to be quite alarming, these were even worse over the last century as a result of devastating epidemics (300,000 to 500,000 deaths between 1896 and 1906), after which sleeping sickness was almost eradicated.[116] In response to a dramatic resurgence of HAT because of the last epidemic in 1998 that caused nearly 38,000 new cases, strengthened control and surveillance programmes by the WHO and partners in endemic areas have led to a steady decline in its burden, dropping below 10,000 the number of new cases in 2009 and more recently, in 2014, there were 3,796 cases recorded, the lowest level ever reported.[114,115] In this light, the global eradication of the disease as a public health problem has been targeted by WHO as a feasible goal by 2020. [117,118]

If we take in account that HAT affects mostly remote impoverished rural zones, where it coexist with animal trypanosomiasis ("nagana"), its control and its proper diagnosis turn out to be especially hard. Mainly due to these reasons, the true impact of the disease is unknown, largely because of under-reporting.[119] Therefore, despite impressive achievements in the control and treatment of HAT over the past decade, much more endeavours are, certainly, still necessary to achieve HAT elimination, such as stronger control on vector transmission, new methods to early diagnose and treat patients, as well as the development of safer and more effective and affordable drugs.[120,121,122]

---

[113] Simarro, P. P.; Diarra, A.; Ruiz-Postigo, J. A. *et al. PLoS Negl. Trop. Dis*. **2011**, *5*, e1007.
[114] WHO. http://www.who.int/mediacentre/ factsheets/fs259/en/ (accessed November 27, 2015)
[115] DNDi. http://www.dndi.org/diseases-projects/hat/ (accessed December 15, 2015)
[116] Maurice, J. *Lancet* **2013**, *381*, 13−14.
[117] WHO. *Working to Overcome the Global Impact of Neglected Tropical Diseases,* **2010**.
[118] WHO. *Investing to Overcome the Global Impact of Neglected Tropical Diseases,* **2015**.
[119] Fèvre, E. M.; Wissmann, B. V.; Weburn, S. C. *et al*. *PLoS Negl. Trop. Dis*. **2008**, *2*, e333.
[120] Welburn, S. C.; Maudlin, I.; Simarro, P. P. *Parasitology* **2009**, *136*, 1943–1949.
[121] Barrett, M. P. *Lancet* **2006**, *367*, 1377–1378.
[122] Simarro, P. P.; Jannin, J. G.; Cattand, P. *PLoS Med.* **2008**, *5*, e55.

2.2. HAT epidemiology

The causative agent of HAT is the unicellular protozoa *Trypanosoma brucei,* namely *T. b. gambiense* (*T. b. g.*) and *T. b. rhodiense* (*T. b. r.*) subspecies, which are transmitted by the tsetse fly (31 species and subspecies of the genus *Glossina*),[123] its unique vector.[124] The distribution in Africa of both infecting subspecies is different, since it is closely correlated to that of their insect vector.[125] Gambian sleeping sickness (caused by *T. b. g.* infection) is spread over 24 countries in West and Central Africa and currently accounts for over 98% of reported cases, while Rhodesian sleeping sickness (caused by *T. b. r*.) is found in 13 countries in Eastern and Southern Africa and is responsible for only about 2% of cases (**Figure 2.1**).[126,127] It is worth mentioning that both HAT variants exist in Uganda, what raises the possibility that some patients become co-infected with both *T. brucei* subspecies.[128,129] Moreover, imported HAT caused by *T. b. gambiense* has occasionally been reported in short-term travellers[130] but is more often encountered in migrants and expatriates residing in rural or coastal foci.[131]

[123] Franco, J. R.; Simarro, P. P.; Diarra, A. *et al*. *Clin. Epidemiol*. **2014**, *6*, 257−275.
[124] Brun, R.; Blum, J.; Chappuis, F. *et al*. *Lancet* **2010**, *375*, 148–59.
[125] Hoare, C. A. The mammalian trypanosomes of Africa. *The African trypanosomiasis*. George Allen and Unwin LTD, London, **1970**, 3−23.
[126] Malvy, D.; Chappuis, F. *CMI* **2011**, *17*, 986–995.
[127] Barrett, M. P.; Burchmore R. J. S.; Stich, A. *et al. Lancet* **2003**, *362*, 1469–1480.
[128] Kennedy, P. G. E. The fatal sleep. Edinburgh: Luath Press, **2010**.
[129] Picozzi, K.; Fèvre, E. M.; Odiit, M.; Carrington, M. *et al. BMJ* **2005**, *331*, 1238–1241.
[130] Malvy, D.; Djossou, F.; Longy-Boursier, M. *et al. Eur. J. Dermatol*. **2000**, *10*, 561–562.
[131] Gautret, P.; Clerinx, J.; Caumes, E. *et al. Euro Surveill*. **2009**, *14*, 19327.

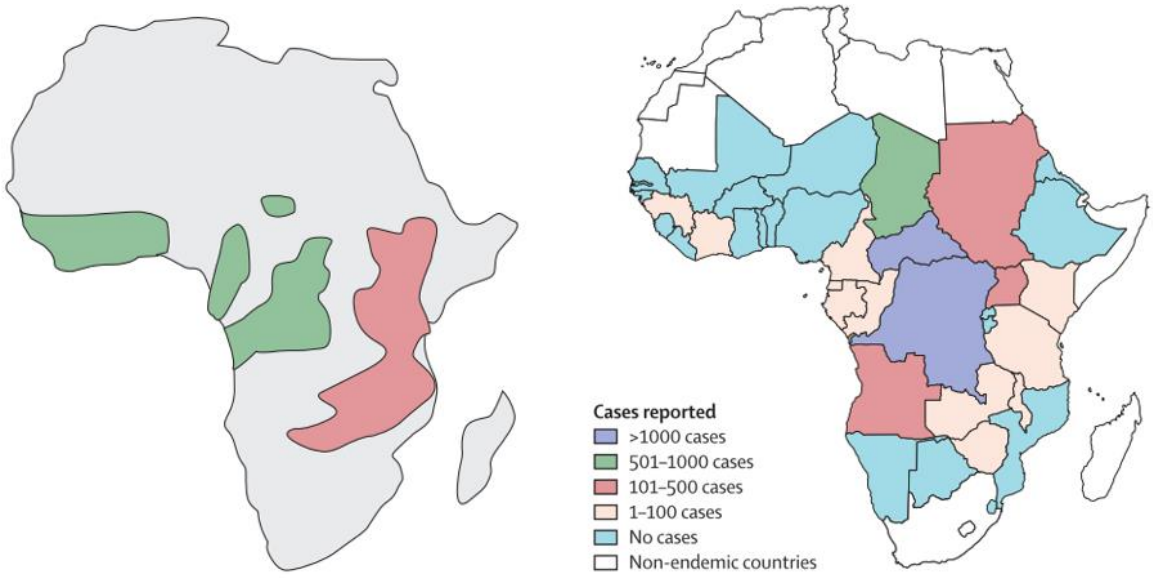

Figure 2.1. Left: Diagrammatic representation of HAT distribution, in green Gambian sleeping sickness and in red the Rhodesian form of the disease. Right: number of reported cases in 2009 in endemic African countries (Image source: Kennedy, P. G. E. *Lancet Neurol*. **2013**, *12*, 186−194).

During the lifecycle of *T. brucei*, the blood-sucking tsetse fly bites an infected host such as wild or domestic cattle which are reservoirs in *T. b. rhodesiense* form or human beings, mainly, in the case of *T. b. gambiense* HAT and it ingests trypanosomes during the blood meal.[132] Of note, the fact that *T. b. r*. is a zoonosis makes it difficult the control of the disease since it involves interrupting the fly−animal−human cycle.[133]

Once parasites enter to fly's midgut, they undergo dramatic morphological and biochemical changes, which results in highly infective trypanosome forms reaching the salivary glands of the vector (**Figure 2.2**). Later, when an infected tsetse fly bites human, trypanosomes are inoculated into the host bloodstream. A primary lesion in the skin is a painful trypanosomal chancre that appears 5–15 days after the bite. Over the following few weeks, during the so-called first or hemolymphatic stage, the parasites multiply within the lymphatic and vascular system producing nonspecific clinical symptoms, such as malaise, arthralgia, headache, and intermittent fever, which often lead to misdiagnosis as malaria. Acute manifestations can be diverse and include gastrointestinal complaints, cardiac features, ophthalmological complications, and endocrine dysfunction, to name a few.[134] If not treated adequately, after a variable period, depending on the HAT variant, the parasites cross the blood-brain barrier (BBB) and invade the CNS. Once this

[132] Kennedy, P. G. E. *Lancet Neurol*. **2013**, *12*, 186−194.
[133] Welburn, S. C.; Maudlin, I. *Adv. Parasitol.* **2012**, *79*, 299–337.
[134] Nagle, A. S.; Khare, S.; Kumar, A. B. *et al. Chem. Rev.* **2014**, *114*, 11305−11347.

has happened the disease has entered the encephalopatic or CNS stage (also known as second or late stage), pathologically marked by a host of symptoms including psychiatric, motor, and sensorial disorders along with abnormal reflexes.[135] Approximately three-quarters of patients experience the most indicative feature of CNS HAT, daytime somnolence alternated with nocturnal insomnia, from which HAT derives its description as sleeping sickness.[136] It is important to note, *T. b. g.* produces a chronic disease with average infection lasting around 3 years, and when symptoms emerge the patient is often already in an advanced CNS stage. By contrast, Rhodesian disease presents an acute infection which rapidly progresses and invades CNS, and unless patients are treated, it leads to patient death within months.[137,138]

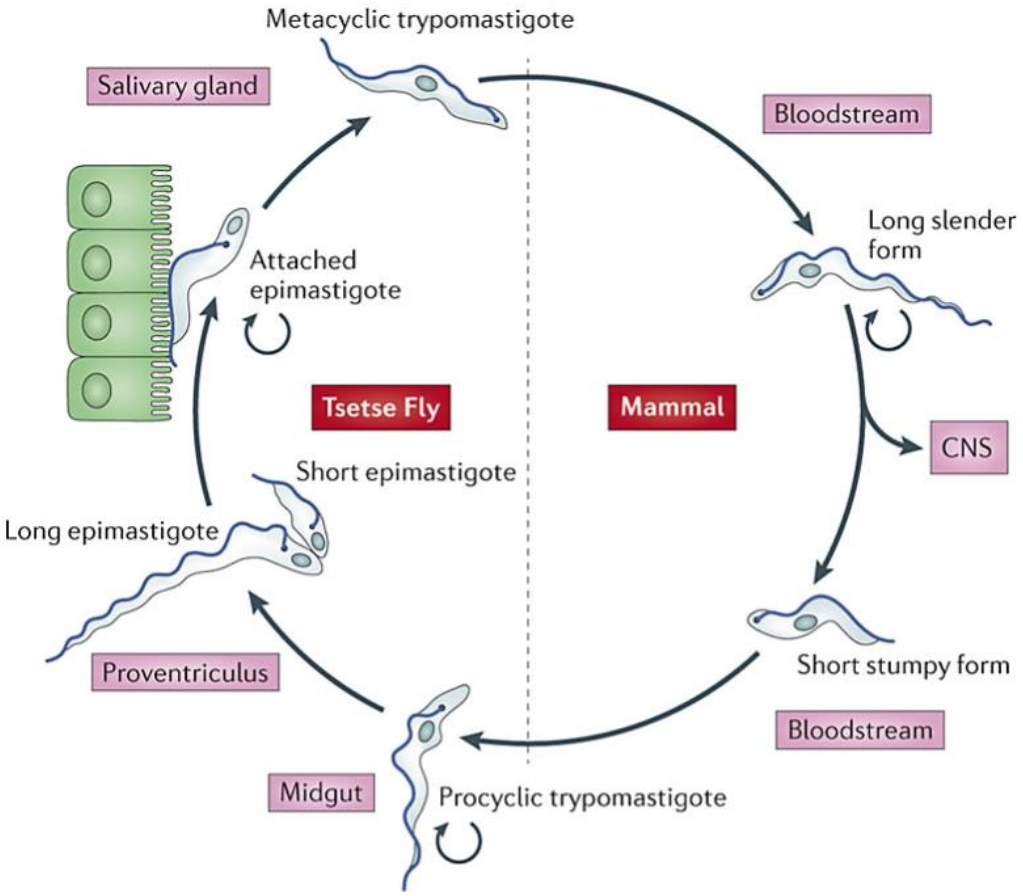

Figure 2.2. *Trypanosoma brucei* life cycle: Infection of a mammalian host initiates through the release of growth-arrested metacyclic trypomastigotes to the mammalian bloodstream by the tsetse bite. Metacyclic trypomastigotes then differentiate into proliferating long slender forms that establish and maintain a bloodstream infection, and eventually penetrate the blood vessel

[135] Atouguia, J. L. M.; Kennedy, P. G. E.; Davis, L. E. Neurological aspects of human African trypanosomiasis. Butterworth-Heinemann, Oxford, **2000**, 321−372.
[136] Blum, J.; Schmid, C.; Burri, C. *Acta Tropica* **2006**, *97*, 55−64.
[137] Bentivoglio, M.; Grassi-Zucconi, G.; Olsson, T. *et al*. *Trends Neurosci*. **1994**, *17*, 325−329.
[138] Lundkvist, G.B.; Kristensson, K.; Bentivoglio, M. *Physiology* **2004**, *19*, 198−206.

endothelium and invade extravascular tissues, including CNS. Then, the latter forms are differentiated into short stumpy forms that are transmitted to the vector through its bite.[139] In the fly's midgut the latter change into procyclic trypomastigotes, which multiply by binary fission (indicated with a circular arrow), producing long epimastigote forms that embark on a migration that ends in the salivary glands, where they attach to the salivary gland epithelium. Attached epimastigotes replicate and ultimately complete the life cycle via an asymmetric division to generate again metacyclic trypomastigotes,[140] which are the infective forms and can be inoculated into the human bloodstream when the fly bites human beings (Image source: Langousis, G.; Hill, K. L. *Nat. Rev. Microbiol*. **2014**, *12*, 505−518).

2.3. Current treatment and trends against HAT

As we have just mentioned above, HAT represents a huge threat in large parts of the world, resulting almost always in death if untreated or inadequately treated. Vaccine research has long been a global priority, however, it has been impeded for HAT treatment by some key technical hurdles.[141] As a consequence, chemotherapy seems to be the only therapeutic option for controlling infection, even though current HAT drugs by no means reflect the clinical need.

At the present time, the therapeutic arsenal of HAT relies on a handful of outdated, toxic, difficult to administer, and increasingly ineffective drugs due to the growing emergence of resistance (**Figure 2.3**).[142,143] Novel strategies are hence desperately needed to defeat this disease.

Pentamidine (**18**) and suramin (**19**) are used to treat the hemolymphatic stage of *T. b. gambiense* and *rhodesiense*, respectively, since they are incapable of crossing BBB and are thus ineffective against CNS-stage. These drugs are moderately well tolerated, with rare severe adverse reactions occurring and among minor adverse reactions may cause mild proteinuria, nausea, vomiting, fever, and exfoliative dermatitis after suramin treatment. In the encephalopathic stage, melarsoprol (**20**), an arsenic-based derivative, remains the most widely used in *T. b. r.* infections and the only drug for the treatment of *T. b. g.* infection, despite the fact it is poorly tolerated and frequently provokes adverse reactions that can be life threatening; for instance, around 5−10% patients suffer encephalopathic syndrome, half of which are fatal. A newer drug,

[139] MacGregor, P.; Savill, N. J.; Hall, D. *et al*. *Cell Host Microbe* **2011**, *9*, 310–318.
[140] Rotureau, B.; Subota, I.; Buisson, J. *et al*. *Development* **2012**, *139*, 1842–1850.
[141] Bethony, J. M.; Cole, R. N.; Guo, X. T. *et al. Immunol. Rev*. **2011**, *239*, 237–270.
[142] Delespaux, V.; de Koning, H. P. *Drug Resist. Updates* **2007**, *10*, 30−50.
[143] Rodgers, J. *J. Neuroimmunol*. **2009**, *211*, 16−22.

eflornithine (**21**, DFMO) represented a decisive breakthrough as it let a safer alternative for late-stage *gambiense* HAT and indeed, it gradually replaced melarsoprol as the first-line treatment. As a result, the use of melarsoprol decreased from 88% of the total late-stage cases reported in 2006 to 51% in 2008.[113] Eflornithine, nevertheless, shows a key drawback due to a long-term administration treatment, involving four infusions each day during 2 weeks, which is obviously not feasible within the context of undeveloped public health systems. However, the recent introduction of nifurtimox−eflornithine combination treatments (NECT) has allowed to reduce the treatment time to 7 days of intravenous eflornithine plus 10 days of oral nifurtimox (**22**, traditionally used to treat Chagas disease).[144] NECT currently represents the first-line treatment for late-stage *T. b. gambiense*.[145,146]

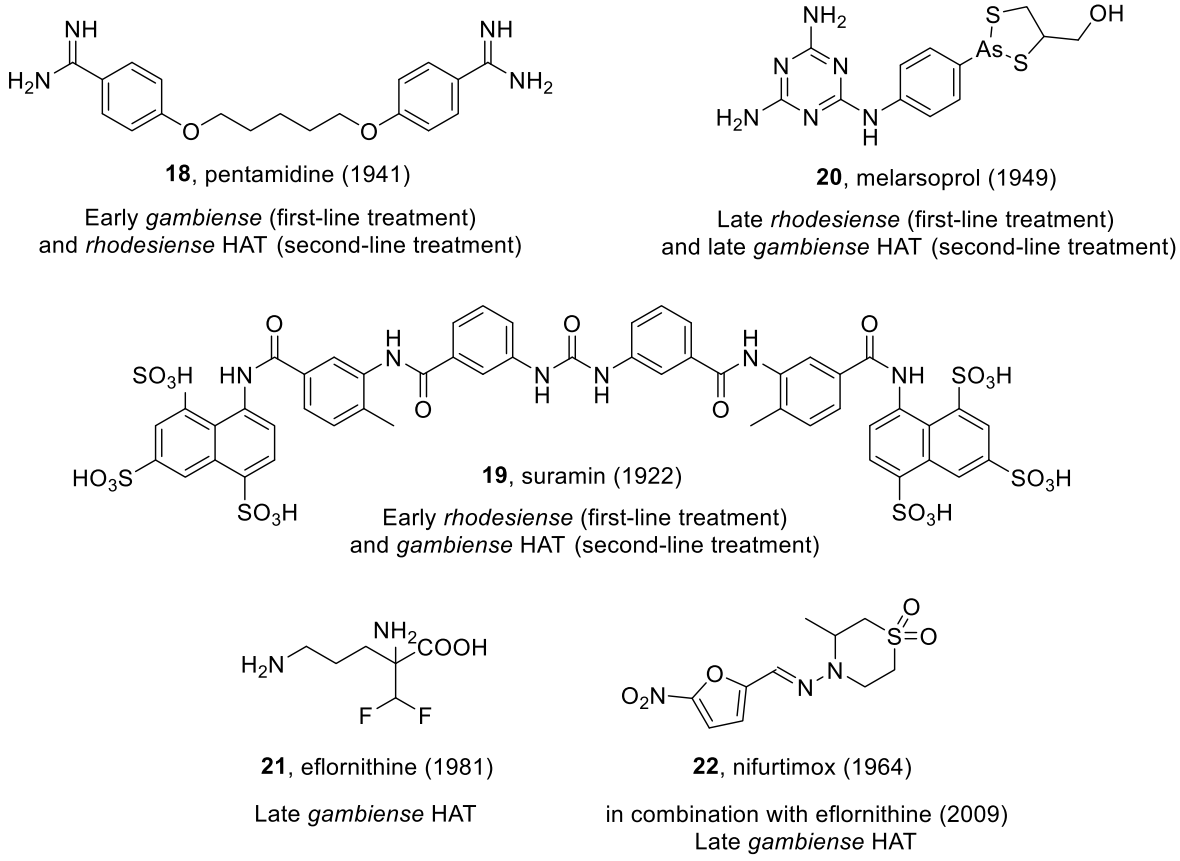

Figure 2.3. Current drugs to treat HAT[132] and their introduction date.[147]

[113] Simarro, P. P.; Diarra, A.; Ruiz-Postigo, J. A. *et al*. *PLoS Negl. Trop. Dis*. **2011**, *5*, e1007.
[132] Kennedy, P. G. E. *Lancet Neurol*. **2013**, *12*, 186−194.
[144] Priotto, G.; Kasparian, S.; Mutombo, W. *et al. Lancet* **2009**, *374*, 56–64.
[145] Burri, C. *Parasitology* **2010**, *137*, 1987–1994.
[146] Fairlamb, A. H. *Trends Parasitol*. **2003**, *19*, 488−494.
[147] DNDi: Home Page. http://www.dndi.org (accessed December 15, 2015).

Set against the spectacular advances in other chemotherapy areas over the past half-century, there has been a deficit in registered new drugs against parasitic diseases in general, and trypanosomiasis in particular; for instance, only 4% of new registered drugs (with none of them being a new chemical entity) were launched for the treatment of NTD between 2000 and 2011.[147]

The deficit in this drug discovery field could be explained by the difficulties linked to NTDs, as they mainly affect poor disadvantaged people who have limited access to health care systems. Moreover, a lack of knowledge regarding validated drug targets and the complex nature of the pathogens themselves pose serious challenges in drug efficacy, including drug-resistance mechanisms, latent and persistent forms, intracellular location, and multiple life forms for those transmitted by vectors. Nevertheless, the most constraining factor in this context is the historical underinvestment by governments and pharmaceutical companies in this not-for-profit area, as they are very unlikely to see a financial return.[148]

Against this outrageous outlook, intense research efforts have been made and strong drug development pipelines for NTDs have been applied during the last decade thanks to the substantial engagement and support of both private and nongovernmental, nonprofit organizations such as the Drugs for Neglected Diseases initiative (DNDi) and the Bill and Melinda Gates Foundation (BMGF).[149] In this light, a number of novel drug discovery strategies such as target-based screening, virtual docking studies, and genomic-based approaches have been used to identify new drug candidates for NTDs. Particularly, phenotypic whole-cell high-throughput screening of large compound libraries has recently emerged as a very useful tool especially for parasitic diseases, for which the mode of action is poorly understood, and for many, it is likely to involve interaction with a number of different targets. Furthermore, simultaneous inhibition of two or more key biological targets with combination therapies or multitarget-directed ligands, along with repurposing, repositioning and rescue of known molecules have also arisen as feasible therapeutic strategies from an economic point of view.[150]

[147] DNDi: Home Page. http://www.dndi.org (accessed December 15, 2015).
[148] Goupil, L. S.; McKerrow, J. H. *Chem. Rev.* **2014**, *114*, 11131–11137.
[149] Njoroge, M.; Njuguna, N. M.; Mutai, P. *et al. Chem. Rev.* **2014**, *114*, 11138–11163.
[150] Renslo, A. R.; McKerrow, J. H. *Nat. Chem. Biol.* **2006**, *2,* 701–710.

2.3.1. Phenotypic whole-cell high-throughput screening (HTS)

The advances in genomics and combinatorial chemistry have allowed the use of whole cell parasite approaches in HTS mode. In fact, HTS has developed over the years from simple 96-well assays to fully automated 384-well assays, enabling nowadays the screening of more than 100,000 compounds per day. Phenotypic whole-cell screening has proven as a successful strategy in drug discovery, as is detailed in a recent interesting review by Swinney and Anthony[151] who disclosed that despite the fact that the majority of new molecular entities (NME) registered between 1999 and 2008 were discovered through target-based approaches, a bigger proportion were found through phenotypic approaches when considering *First in Class* NME (**Figure 2.4**).

Figure 2.4. Origins of NMEs in the period of 1999−2008. (Image source: Gilbert, I. H. *J. Med. Chem.* **2013**, *56*, 7719−7726).

The main advantage of phenotypic approaches with respect to target-based ones is the identification of compounds active against the whole parasite, interacting with different components and not individual components of it, and also meaning issues such as cell uptake and cell efflux are also taken into account, thus yielding hits capable of penetrating cell membranes and reaching the intracellular target/s.[152] Phenotypic approaches also allow counter-screens against mammalian cells to obtain a preliminary idea of cytotoxicity and selectivity.[153] Moreover, as we have just highlighted above, this strategy is very advantageous when the disease biology is poorly understood, as is the case of HAT, inasmuch as it often leads to the identification of molecules acting on a completely novel and unknown target or acting simultaneously on more than one target, thereby hampering selection of resistance.[153] However, the major drawback of phenotypic approaches is the subsequent extensive target-based study in

[151] Swinney, D. C.; Anthony, J. *Nat. Rev. Drug Discov*. **2011**, *10*, 507−519.
[152] Gilbert, I. H. *J. Med. Chem.* **2013**, *56*, 7719−7726.
[153] Kotz, J. *SciBX* **2012**, *5*, 1−3.

order to identify the intracellular target/s upon which the compounds act, which includes chemical proteomics and metabolomics screening against a panel of purified, recombinant *T.b. brucei* proteins, receptors, and enzymes.[154,155,156]

In recent years, a broad spectrum of chemical scaffolds displaying promising activity against *T. brucei* strains has been reported from phenotypic whole-cell HTS studies.[134,149,157] In fact, to date, the two only compounds that have successfully progressed into clinical trials were discovered through phenotypic studies: the nitroimidazole fexinidazole, **23**, and the oxaborole SCYX-7158, **24** (**Figure 2.5**). However, both compounds were identified by screening small, focused libraries in standard 96-well assay plates and not by large HTS of very diverse compound libraries.[158]

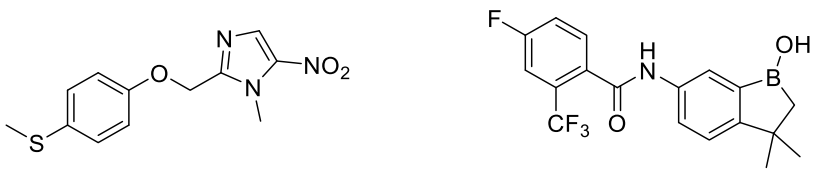

fexinidazole, **23** SCYX-7158, **24**

Figure 2.5. Chemical structure of the sole compounds that are currently undergoing clinical trials for treatment of HAT.

Fexinidazole, **23**, was originally synthesized and shown to have trypanocidal activity in the 1970s. In 2006, it was rediscovered by the DNDi through an extensive screening of >700 novel and described nitroheterocyclic molecules as potential drug candidates for treatment of late-stage HAT.[159] SCYX-7158, **24**, a second potential CNS-stage HAT drug, resulted from screening a library of boron-based compounds from Anacor Pharmaceuticals and a lead-optimisation programme conducted by Scynexis.[160,161] Both compounds were evaluated by preclinical pharmacological and safety studies with no untoward effects that have precluded them from further evaluation in human patients.

[134] Nagle, A. S.; Khare, S.; Kumar, A. B. *et al. Chem. Rev.* **2014**, *114*, 11305−11347.
[149] Njoroge, M.; Njuguna, N. M.; Mutai, P. *et al. Chem. Rev.* **2014**, *114*, 11138–11163.
[154] Kuettel, S.; Mosimann, M.; Mäser, P. *et al. PLoS Negl. Trop. Dis*. **2009**, *3*, e506.
[155] Mercer, L.; Bowling, T.; Perales, J. *et al. PLoS Negl. Trop. Dis.* **2011**, *5*, e956.
[156] König, J.; Wyllie, S.; Wells, G. *et al*. *J. Biol. Chem.* **2011**, *286*, 8523-8533.
[157] Brun, R.; Don, R.; Jacobs, R. T. *et al*. *Future Microbiol*, **2011**, *6*, 677−691.
[158] Jones, A. J.; Avery, V. M. *Expert Opin. Drug Discov.* **2013**, *8*, 495−507.
[159] Torreele, E.; Bourdin, T. B.; Tweats, D.; Kaiser, M. *et al. PLoS Negl. Trop. Dis.* **2010**, *4*, e923.
[160] Jacobs, R. T.; Nare, B.; Wring, S. A. *et al*. *PLoS Negl. Trop. Dis*. **2011**, *5*, e1151.
[161] DNDi. http://www.dndi.org/diseases-projects/portfolio/oxaborole-scyx-7158.html.

2.3.2. Other drug discovery strategies for HAT

Target-based strategies become also a feasible option in drug discovery of HAT. This approach involves screening a library of compounds against a given protein that is known to take part in the development of a disease and then optimizing the compounds for potency against the enzyme, selectivity, cellular activity, and pharmacokinetic properties. The selection of a target for drug discovery is of key importance, and it should be truly validated, that happens when it is already in the clinic for treating the disease. Although ornithine decarboxylase (ODC), which is the target of the drug eflornithine, is the only one fully validated target for the treatment of HAT the publication of the *T. brucei* genome in 2005 accelerated the understanding of its complex biology and revealed several potential interesting targets to be considered in drug discovery.[162] *N*-Myristoyl transferase (NMT), pteridine reductase 1 (PTR1), trypanothione synthase (TryS), phosphodiesterases (PDEB1 and PDEB2), trypanosomal Aurora kinase 1, and the cysteine protease rhodesain are some examples of trypanosome enzymes that have been suggested as promising targets and for whom potent inhibitors have been developed (**25**–**28**, **Figure 2.6**).[149,163]

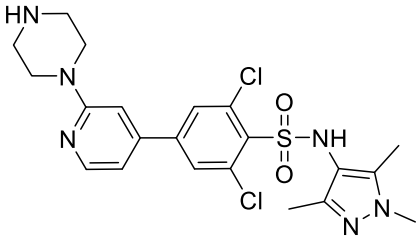

25, *Tb*NMT IC_{50} = 0.002 μM

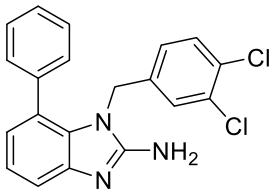

26, *Tb*PTR1 Ki^{app}= 0.007 μM

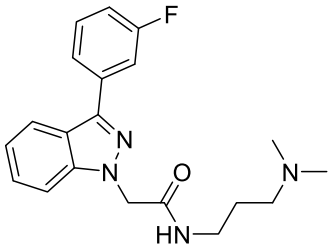

27, *Tb*TryS IC_{50} = 0.045 μM

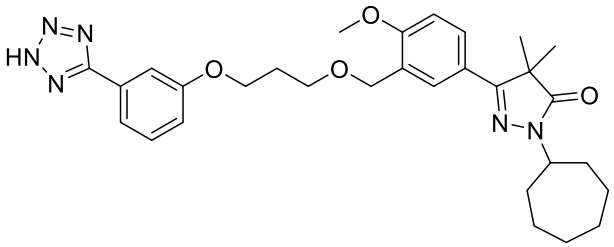

28, *Tb*PDEB1 IC_{50} = 0.062 μM

Figure 2.6. Inhibitors of potential targets for the treatment of HAT.[149,164]

[149] Njoroge, M.; Njuguna, N. M.; Mutai, P. *et al. Chem. Rev.* **2014**, *114*, 11138–11163.
[162] Berriman, M.; Ghedin, E.; Hertz-Fowler, C. *et al*. *Science* **2005**, *309*, 416–422.
[163] Gilbert, I. H. *Parasitology* **2014**, *141*, 28–36.
[164] Hannaert, V. *Planta Med.* **2011**, *77*, 586–597.

Other strategies that have been used in drug discovery for HAT are, for instance, the development of amidine and diamidine compounds structurally related to pentamidine, **1**, structural modification of known trypanocidal natural products,[164,165] and, more importantly, repositioning of known molecules that have been used for the treatment of other protozoan diseases.[166,167,168,169,170] Nevertheless, so far whole-cell HTS has proved to be the most valuable tool providing a reliable starting point for the discovery of hits that already possess drug-like properties as well as for the identification and validation of new targets. When used in isolation, no one drug discovery approach is ideal, but by utilizing two or three complementary methods together, the shortcomings of each individual approach can be overcome and the success rate increased. Furthermore, funding and resources need to be in place to progress the molecules identified into preclinical development; otherwise, molecules will continue to remain at the initial identification stage.[149]

2.4. The concept of privileged structures in rational drug design

It is well known the fact that the pharmaceutical sector is dealing in the last decades with a 'productivity crisis', what has been mainly caused for the excessively long, complex, and costly drug discovery and development processes.[171] To put into context, only 19 NMEs (including biologics) were registered by the FDA in 2007, it being the least productive year of the past two decades, and this number slightly increased to 21 in 2008. Conversely, the costs associated with the development of a novel drug have increased from $500 million to $1.8 billion. The introduction of HTS methodologies in the early 1990 was expected to boost the number of robust drugs released to the market, nevertheless, despite some successful cases, a third of drug candidates either failed before arriving at the market or were later withdrawn generally due to lack of efficacy, toxicity and unfavorable drug metabolism and pharmacokinetic (DMPK) properties.[172]

[149] Njoroge, M.; Njuguna, N. M.; Mutai, P. *et al. Chem. Rev.* **2014**, *114*, 11138–11163.
[164] Hannaert, V. *Planta Med.* **2011**, *77*, 586–597.
[165] Jones, A. J.; Grkovic, T.; Sykes, M. L. *et al*. *Mar. Drugs* **2013**, *11*, 4058–4082.
[166] Croft, S. L.; Barrett, M. P.; Urbina, J. A. *Trends Parasitol.* **2005**, *21,* 508–512.
[167] Steverding, D.; Tyler, K. M. *Expert Opin. Investig. Drugs* **2005**, *14*, 939–955.
[168] Barrett, M. P.; Croft, S. L. *Br. Med. Bull.* **2012**, *104*, 175–196.
[169] Tang, S. C.; Shapiro, T. A. *Antimicrob. Agents Chemother.* **2010**, *54*, 620–62629.
[170] Patel, G.; Karver, C. E.; Behera, R. *et al. J. Med. Chem.* **2013**, *56*, 3820−3832.
[171] Munos, B. *Nat. Rev. Drug Discov.* **2009**, *8*, 959−968.
[172] Paul, S. M.; Mytelka, D. S.; Dunwiddie, C. T. *et al*. *Nat. Rev. Drug Discov*. **2010**, *9*, 203−214.

To overcome this problem of attrition in the post-HTS era, significant efforts have been addressed on designing more chemically diverse and drug-like compound libraries.[173] Well-designed libraries should produce higher quality compounds that will lead to an increase in overall efficiency and productivity further downstream. In this light, the use of 'privileged structures' has emerged over the past two decades as a fruitful approach to overcome these deficiencies in the discovery and optimization of novel biologically active molecules.[174]

From the original definition of privileged structures provided by Evans in 1988, the concept has greatly evolved in most cases to describe not only basic molecular structures (*core scaffolds*) found to exert promiscuous binding properties towards a range of different biological targets, but also structures that modulate proteins lacking a strict target class relation. In addition, privileged structures typically exhibit good drug-like properties, thus leading to more drug-like compound libraries.[175] Benzodiazepines, dihydropyridines, quinazolines, acridines, and quinolines are some examples of privileged scaffolds. Of particular interest are quinolines, which are recurrent structural motifs in compounds active against two quite different pathologies, such as neurodegenerative and protozoan diseases.[176]

2.4.1. Quinolines as privileged motifs

Quinoline is a "promiscuous" heterocyclic ring moiety prevalent in a variety of pharmacologically active synthetic and natural compounds[177] displaying a broad range of biological activities, covering antimalarial, **29**,[178,179] antifungal, **30**,[180] and antiviral, **31**,[181] effects, amongst others. Moreover, they have also been investigated as potential anti-obesity, **32**,[182] anti-cancer, **33**,[183]

[173] Bleicher, K. H.; Böhm, H. J.; Müller, K. *et al*. *Nat. Rev. Drug Discov.* **2003**, *2*, 369−378.
[174] Fattori, D. *Drug Discov. Today* **2004**, *9*, 229−238.
[175] De Simone, R. W.; Currie, K. S.; Mitchell, S. A. *et al*. *Comb. Chem. High Throughput Screen*. **2004**, *7*, 473−494.
[176] Bongarzone, S.; Bolognesi, M. L. *Expert Opin. Drug Discov.* **2011**, *6*, 251−268.
[177] Welsch, M. E.; Snyder, S. A.; Stockwell, B. R. *Curr. Opin. Chem. Biol.* **2010**, *14*, 347−361.
[178] O'Neil, P. M.; Ward, S. A.; Berry, N. G. *et al. Curr. Top. Med. Chem*. **2006**, *6*, 479−507.
[179] Kaur, K.; Jain, M.; Reddy, R. P. *et al*. *Eur. J. Med. Chem.* **2010**, *45*, 3245–3264.
[180] Musiol, R.; Serda, M.; Hensel-Bielowka, S. *et al*. *Curr. Med. Chem*. **2010**, *17*, 1960−1973.
[181] López, A. E. Privileged scaffolds in medicinal chemistry: Design, synthesis, evaluation. Chapter 6 − Quinolines: Privileged scaffolds in medicinal chemistry. Bräse, S. (Ed.) Royal Society of Chemistry Publishing, **2015**, 132−146.
[182] Högberg, T.; Frimurer, T. M.; Sasmai, P. K. *Bioorg. Med. Chem. Lett*. **2012**, *22*, 6039−6047.
[183] Afzal, O.; Kumar, S.; Haider, M. R. *et al*. *Eur. J. Med. Chem*. **2015**, *97*, 871−910.

immunosupressive agents, **34**,[184] and included for treatment of neurodegenerative disorders, **2** and **35** (**Figure 2.7**).[185,186,187,188]

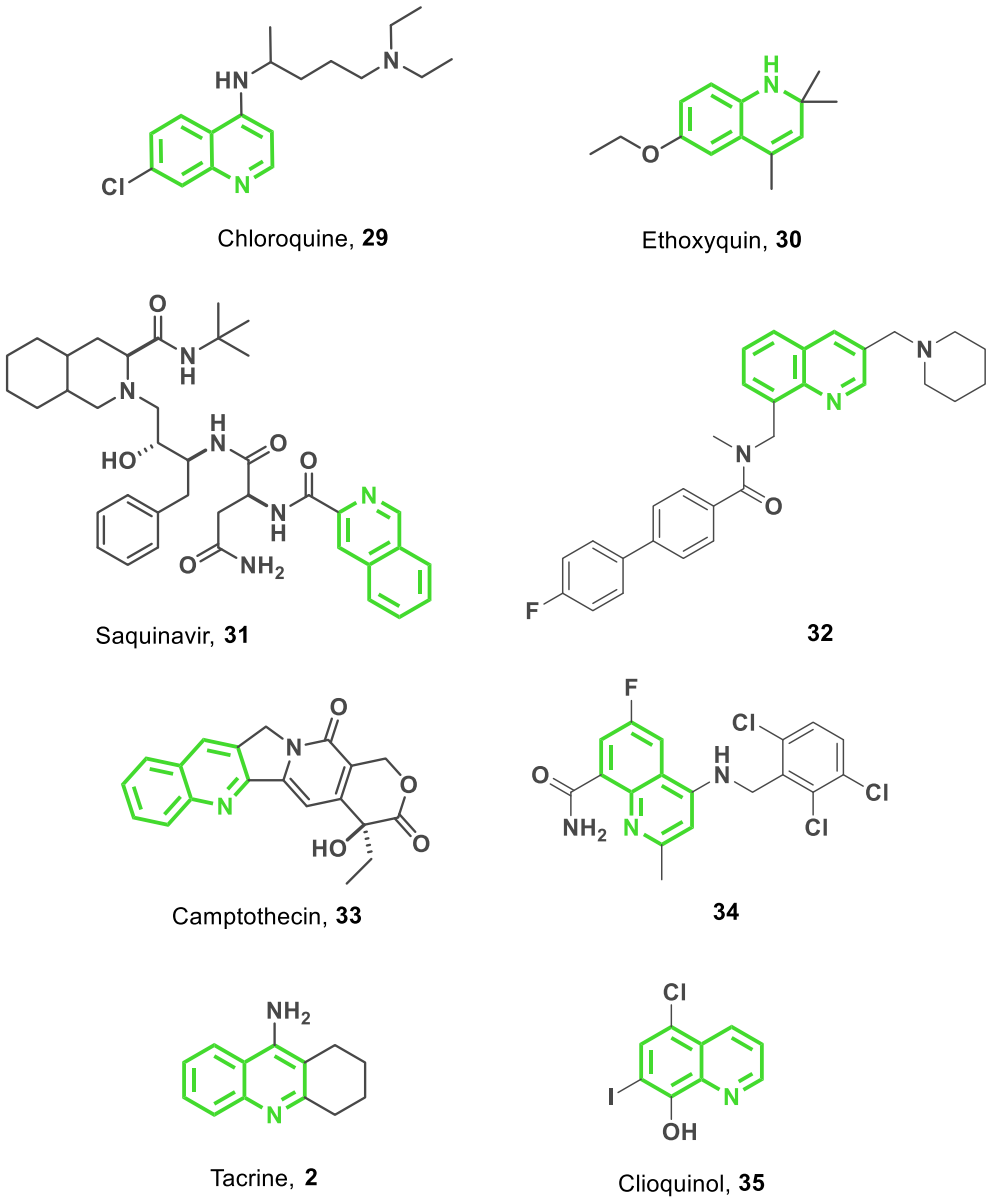

Figura 2.7. Drug examples bearing a common quinoline scaffold.

[184] Becherer, J. D.; Boros, E. E.; Carpenter, T. Y. *et al. J. Med. Chem*. **2015**, *58*, 7021−7056.
[185] Okamura, N.; Suemoto, T.; Furumoto, S. *et al. J. Neurosci.* **2005**, *25*, 10857−10862.
[186] Adlard, P. A.; Cherny, R. A.; Finkelstein, D. I. *et al. Neuron.* **2008**, *59*, 43−55.
[187] Navarrete, L. P.; Guzmán, L.; San Martín, A. *et al. J. Alzheimers Dis.* **2012**, *29*, 79−88.
[188] Alzforum: http://www.alzforum.org/therapeutics/clioquinol (Accessed 14 February 2016).

2.4.2. Quinoline and protozoan diseases

The extreme versatility displayed by quinolines makes them a very appealing scaffold in the search for new and effective antiprotozoan drug candidates, since the possibility to act on multiple metabolic pathways in parasitic cells constitutes a preferentially pursued requisite in NTDs drug discovery from an economic point of view. The administration of a sole drug for more than a single parasitic infection implies cost-effective treatments that are of special relevance for both pharmaceutical companies and public health systems in developing countries.

In this light, some quinoline derivatives have shown multi-trypanosomatid profile, displaying trypanocidal, leishmanicidal, and/or antimalarial properties simultaneously. In particular, the design of homo- and heterodimers (or hybrids) that combine two equal or distinct drug entities, respectively, in one molecule through tethers of different length and chemical nature has emerged as a fast growing approach in NTD drug discovery. This approach allows a synergistic biological improvement by the combination of the properties of each component of the dimer,[189,190,191,192,193,194] besides it may also avoid the emergence of drug resistance by means of the inhibition of multiple targets within the same parasite, as it is widely used in the case of antimalarials such as chloroquine (**29**, **Figure 2.7**).[195,196,197,198,199] For instance, piperaquine, **36**, a bis-chloroquine derivative, is a "double drug" extensively used in China and Indochina for prophylaxis and treatment of malaria,[200] while **37**–**39** [193,194,195] are examples of "hybrid" molecules that exhibit two or more antiparasitic activities (**Figure 2.8**).

[189] Musonda, C. C.; Gut, J.; Rosenthal, P. J. *et al*. *Bioorg. Med. Chem.* **2006**, *14*, 5605–5615.
[190] Musonda, C. C.; Yardley, V.; de Souza, R. C. C. *et al*. *Org. Biomol. Chem.* **2008**, *6*, 4446–4451.
[191] Glans, L.; Hu, W.; Jöst, C. *et al*. *Dalton Trans.* **2012**, *41*, 6443–6450.
[192] Gehrke, S. S.; Pinto, E. G; Steverding, D. *et al*. *Bioorg. Med. Chem.* **2013**, *21*, 805–813.
[193] Leverrier, A.; Bero, J.; Frédérich, M. *et al*. *Eur. J. Med. Chem*. **2013**, *66*, 355−363.
[194] Coa, J. C.; Castrillón, W.; Cardona, W. *et al. Eur. J. Med. Chem.* **2015**, *101*, 746–753.
[195] Kouznetsov, V. V.; Gomez-Barrio, A. *Eur. J. Med. Chem.* **2009**, *44*, 3091−3113.
[196] Muregi, F. W.; Ishih, A. *Drug Dev. Res.* **2010**, 71, 20−32.
[197] Gemma, S.; Camodeca, C.; Sanna Coccone, S. *et al. J. Med. Chem.* **2012**, *55*, 6948−6967.
[198] Fisher, G. M.; Tanpure, R. P.; Douchez, A. *et al*. *Chem. Biol. Drug Des.* **2014**, *84*, 462−472.
[199] Kannan, M.; Raichurkar, A. V.; Khan, F. R. *et al*. *Bioorg. Med. Chem. Lett.* **2015**, *25*, 1100−1103.
[200] Davis, T. M.; Hung, T. Y.; Sim, I. K. *et al*. *Drugs* **2005**, *65*, 75−87.

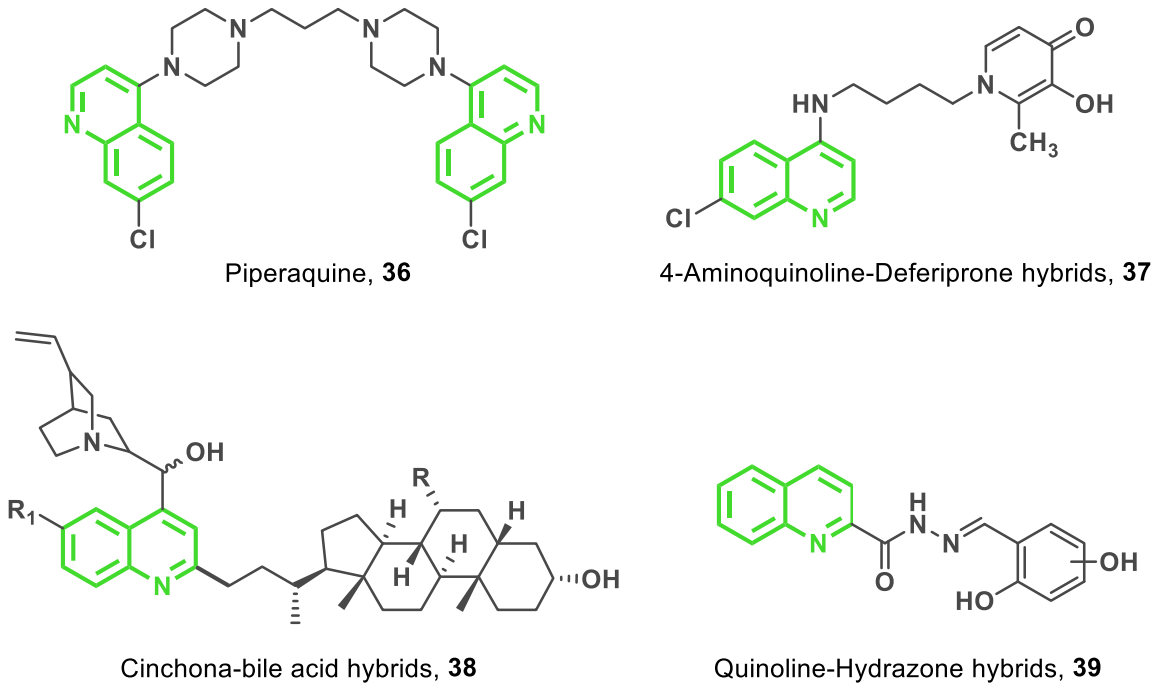

Figure 2.8. Examples of dimerization strategies for NTD therapy.

2.4.3. Antiprotozoal quinoline compounds developed in our research group

Huprines, a class of 4-aminoquinoline derivatives developed about fifteen years ago in our research group as brain permeable inhibitors of acetylcholinesterase (AChE), endowed with potential anti-Alzheimer activity,[201] were further evaluated as antiprotozoal agents, given their highly structural similarity with some recently described 4-aminoquinoline-based antiprotozoal compounds.[190,191,202,203,204,205] Moreover, the proven ability of huprines to penetrate into the CNS was considered as an additional interesting feature for the treatment of HAT given the lack of a satisfying treatment for the late-stage of this disease.

Within this context, an evaluation of 19 different huprines against *T. brucei* showed them to be moderately potent and selective trypanocidal agents, with the so-called huprine Y, **11** (**Figure 2.9**), displaying the most potent activity against *T. brucei* (IC_{50} = 0.61 µM; IC_{90} = 2.94 µM) and one of the best selectivity indices over rat myoblast L6 cells (SI = 13). Some of these huprines were

[190] Musonda, C. C.; Gut, J.; Rosenthal, P. J. *et al*. *Bioorg. Med. Chem.* **2006**, *14*, 5605–5615.
[191] Musonda, C. C.; Yardley, V.; de Souza, R. C. C. *et al*. *Org. Biomol. Chem.* **2008**, *6*, 4446–4451.
[201] Camps, P.; El Achab, R.; Morral, J. *et al*. *J. Med. Chem.* **2000**, *43*, 4657–4666.
[202] Oluwafemi, A. J.; Okanla, E. O.; Camps, P. *et al*. *Nat. Prod. Commun.* **2009**, *4*, 193–198.
[203] Upadhayaya, R. S.; Dixit, S. S.; Földesi, A. *et al. Bioorg. Med. Chem. Lett.* **2013**, *23*, 2750–2758.
[204] Rashad, A. A.; Jones, A. J.; Avery, V. M. *et al*. ACS Med. Chem. Lett. 2014, 5, 496−500.
[205] Mushtaque, S. *Eur. J. Med. Chem*. **2015**, *90*, 280−295.

also found to be moderately potent against chloroquine-resistant *Plasmodium falciparum* strains,[206] the infectious agent responsible for malaria, which made them interesting hits with dual trypanocidal-antimalarial activity.

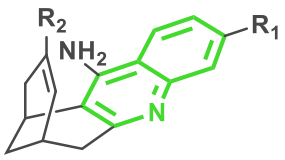

R_1= Cl, R_2= Me, **11**, *T. brucei* IC_{50}= 0.61 µM

R_1= Cl, R_2= Et, **40**, *T. brucei* IC_{50}= 0.84 µM

R_1= Cl, R_2= Allyl, **41**, *T. brucei* IC_{50}= 0.76 µM

R_1= H, R_2= Allyl, **42**, *T. brucei* IC_{50}= 4.08 µM

R_1= H, R_2= *n*-Bu, **43**, *T. brucei* IC_{50}= 0.70 µM

R_1= H, R_2= *t*-Bu, **44**, *T. brucei* IC_{50}= 0.88 µM

Figure 2.9. Structure and activity of some huprines (**11** and **40**–**44**) evaluated against *T. brucei*.

Following the last strategy, in the context of the PhD Thesis of Ornella di Pietro, a series of tricyclic heterofused quinolines with potential anti-Alzheimer activity synthesized by Povarov Multicomponent Reactions (MCR)[207] were later evaluated as antiprotozoal agents too. Surprisingly, compound **45**, one of these anticholinesterasic compounds (**Figure 2.10**), was found to show moderate activity against *T. brucei* (IC_{50} = 3.33 µM), what fostered a further exploitation of the resource of Povarov reaction in the search of novel quinoline-based antiprotozoal hits. In this light, two new benzonaphthyridines (**46** and **47** in **Figure 2.10**) were synthesized in order to explore the best substitution pattern at positions 5 and 9. The pharmacological results pointed out that the presence of 4-(aminomethyl)phenyl group and a chloro substituent at position 5 and 9, respectively, led to slightly increased potency against *T. brucei* (IC_{50} = 1.00 µM).[208]

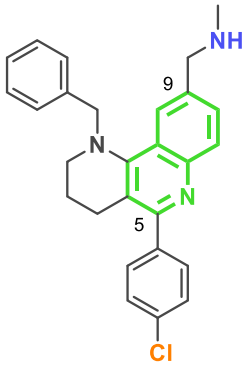

45, *T. brucei* IC_{50} = 3.33 µM

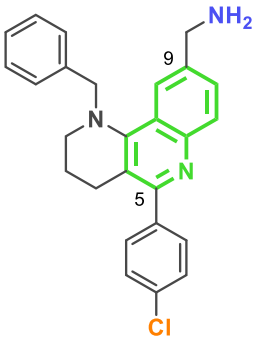

46, *T. brucei* IC_{50} = 2.10 µM

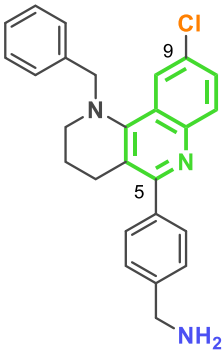

47, *T. brucei* IC_{50} = 1.00 µM

Figure 2.10. Benzonaphthyridines evaluated against *T. brucei*.

[206] Defaux, J.; Sala, M.; Formosa, X. *et al. Bioorg. Med. Chem.* **2011**, *19*, 1702–1707.
[207] Di Pietro, O.; Viayna, E.; Vicente-García, E. *et al. Eur. J. Med. Chem.* **2014**, *73*, 141–152.
[208] Di Pietro, O.; Vicente-García, E.; Taylor, M. C. *et al. Eur. J. Med. Chem.* **2015**, *105*, 120–137.

CHAPTER 3

Introduction to Malaria

3.1. Present scenario

Malaria is an ongoing devastating health problem in tropical and subtropical countries and, to a lesser extent, a life-threatening disease for non-immune travelers from malaria-free areas. In 2015 alone, WHO estimated 214 million new malaria cases with 438,000 associated deaths, being malaria still a major killer of children younger than 5 years accounting for about 70% of deaths across the globe.[209] What is worse, the mortality rate is supposed to be twice as high when including cases of malaria that are undiagnosed or untreated.[210,211]

In addition to the characteristic fever and anemia, malaria gives rise to respiratory distress due to systemic acidemia, renal failure, neurological impairments in the case of cerebral malaria that may lead to an unarousable coma and ultimately death unless it is treated.[212] In young children and non-immune adults in particular, the clinical picture can change within 24 hours, from an apparently mild condition to a life-threatening illness. If a child survives severe malaria, his or her ability to learn may be injured,[213] reducing his or her lifelong potential. An additional major consequence of the disease has been the decreased productivity and economic growth in endemic areas driving them to poverty over the years.[214]

Today the spread of malaria is more limited, having reached, indeed, total eradication in four countries, United Arab Emirates, Morocco, Turkmenistan, and Armenia,[215,216] thanks to the reinforcement of malaria control campaigns after the unexpected resurgence of the disease in 1960.[217,218] Progress was made possible through the massive rollout of effective prevention and treatment tools. For instance, today more than half of the population is now sleeping under insecticide-treated mosquito bed nets in sub-Saharan Africa, compared to just 2% in 2000. Furthermore, a rapid expansion in diagnostic testing, and in the availability of antimalarial

[209] World Malaria Report 2015, World Health Organization Home Page, **2015**. http://apps.who.int/iris/bitstream/10665/200018/1/9789241565158_eng.pdf
[210] Murray, C. J.; Rosenfeld, L. C.; Lim, S. S. *et al*. *Lancet* **2012**, *379*, 413−431.
[211] Fernando, S. D.; Rodrigo, C.; Rajapakse, S. *Malar. J.* **2010**, *9*, 366.
[212] Marsh, K.; Forster, D.; Waruiru, C. *et al*. *N. Engl. J. Med*. **1995**, *332*, 1399–1404.
[213] Boivin, M. J.; Bangirana, P.; Byarugaba, J. *et al. Pediatrics* **2007**, *119*, e360–e366.
[214] Sacks, J.; Malaney, P. *Nature* **2002**, *415*, 680–685.
[215] Overview of malaria elimination. World Health Organization Home Page. http://www.who.int/malaria/areas/elimination/overview/en/
[216] Snow, R. W.; Guerra, C. A.; Noor, A. M. *et al*. *Nature* **2005**, *434*, 214–217.
[217] Flannery, E. L.; Chatterjee, A. K.; Winzeler, E. A. *Nat. Rev. Microbiol.* **2013**, *11*, 849−862.
[218] Kumar, S.; Kumari, R.; Pandey, R. *Protoplasma* **2015**, *252*, 717−753.

medicines, has allowed many more people to access timely and appropriate treatment. As a result, since 2000 malaria mortality rates have fallen once more by 60% among all age groups, and by 71% among children under five.[219,220]

Prevention and treatment efforts are saving millions of dollars in healthcare costs as well. Notable reductions in malaria cases in sub-Saharan Africa saved an estimated US $900 million over 14 years. Mosquito nets contributed the largest savings, followed by artemisinin-based combination therapies and indoor residual spraying.[209] However, malaria threat is far from over.

Malaria has a broad distribution in both the subtropics and tropics, with many areas of the tropics where the temperature and rainfall are most suitable for the development of malaria parasites inside the vectors.[221] Thus, the vast majority of malaria deaths are concentrated in just 15 countries, mainly in Africa (**Figure 3.1**), also due to weak health systems that continue to impede progress, what evoke millions of people without access to proper services necessary to prevent and treat malaria. Consequently, 3.2 billion people – nearly half of the world's population – were at risk of malaria in 2015.[209]

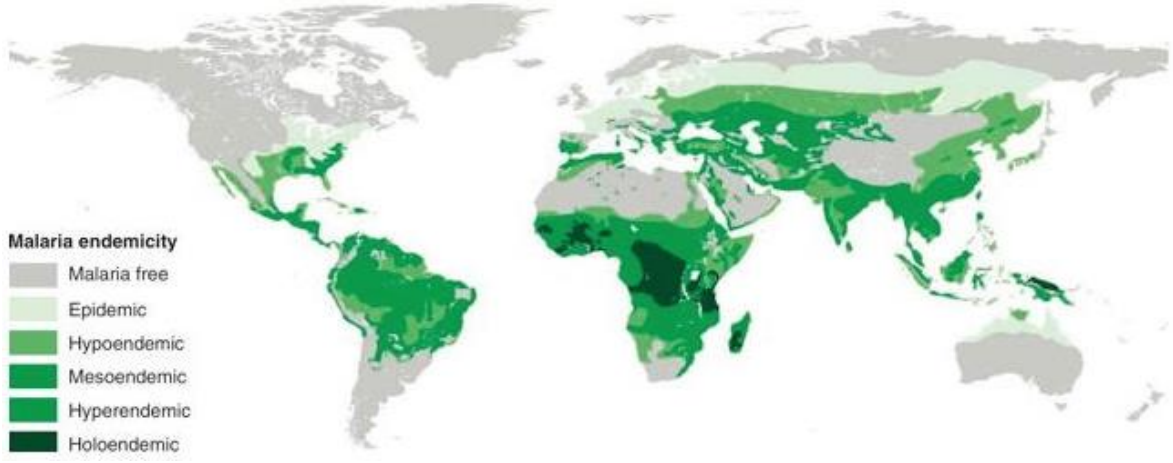

Figure 3.1. *P. falciparum* endemicity distribution within the global limits of risk (Image source: Piel, F. B.; Patil, A. P.; Howes, R. E.; Nyangiri, O. A.; Gething, P. W. *et al. Nature Comm.* **2010**, *1*, 104).

[209] World Malaria Report 2015, WHO Home Page, **2015**.
http://apps.who.int/iris/bitstream/10665/200018/1/9789241565158_eng.pdf
[219] Hay, S. I; Guerra, C. A.; Tatem, A. J. *et al*. *Lancet Infect. Dis*. **2004**, *4*, 327–336.
[220] WHO releases new guidance on insecticide-treated mosquito nets. WHO Home Page.
http://www.who.int/mediacentre/news/releases/2007/pr43/en/index.html
[221] Zucker, J. R. *Emerg. Infect. Dis.* **1996**, *2*, 37–43.

3.2. Cause and spread of malaria

Different species of *Plasmodium* protozoa can cause malaria in humans: *Plasmodium falciparum*, *P. vivax*, *P. ovale*, *P. malariae*, and *P. knowlesi*. Among them, *P. falciparum* and *P. vivax* pose the greatest threat. *P. falciparum* is the most prevalent and virulent species causing the vast majority of deaths in Africa, even though South and East Asia, South America, the Caribbean, and the Middle East also suffer this type of malaria infection.[222] It increases the risk of death in individuals without immunity due to its ability to bind the endothelium during the blood stage of the infection and to sequester in vital organs, including the brain, and also due to the rapid spread of resistance towards most antimalarial drugs available in malaria-endemic countries. Conversely, *P. vivax* has a wider distribution than *P. falciparum*, predominantly in tropical areas outside Africa; it is endemic in India, Latin America, and parts of the Eastern Mediterranean, because most Africans lack the Duffy blood group antigen that is expressed on the surface of erythrocytes and is a necessary receptor for *P. vivax* red blood cell (RBC) invasion.[223] *P. vivax* together with *P. ovale* are typically non-lethal though highly disabling, since they remain dormant for months as hypnozoites in the liver producing no outward manifestations of disease but resulting in relapses months or years after the first infection, what makes their infection difficult to eradicate. Furthermore, there is growing evidence that the lethality of *P. vivax* has been underestimated.[224,225,226,227]On the other hand, *P. malariae* does not form hypnozoites, but it can persist for decades as an asymptomatic blood stage infection. The fifth species, *P. knowlesi*, was originally described as a malaria parasite of the long-tailed and pig-tailed macaques, but more recently it is also known to produce rare human infections in some areas, such as Malaysia.[228,229]

Infection of the human host with a *Plasmodium* parasite begins with the bite of an infected *Anopheles* mosquito (malaria vector). About 40 different *Anopheles* species are important worldwide, with different species predominating in different regions. Most of the main vector species are especially active during the night and breed preferably in fresh and clean water.[230] Moreover, the malaria transmission depends on factors related to parasite, vector, human host,

[222] Gething, P. W.; Patil, A. P.; Smith, D. L. *et al. Malar. J.* **2011**, *10*, 378.
[223]Zimmerman, P. A.; Ferreira, M. U.; Howes, R. E. *et al*. *Adv. Parasitol*. **2013**, *81*, 27−76.
[224] Baird, J. K. *Trends Parasitol.* **2007**, *23*, 533–539.
[225] Guerra, C. A.; Howes, R. E.; Patil, A. P. *et al. PLoS Negl. Trop. Dis.* **2010**, *4*, e774.
[226] Battle, K. E.; Gething, P. W.; Elyazar, I. R. *et al. Adv. Parasitol.* **2012**, 80, 1−111.
[227] Rahimi, B. A.; Thakkinstian, A.; White, N. J. *et al. Malar. J.* **2014**, *13*, 481.
[228] Singh, B.; Sung, K. L.; Matusop, A. *et al*. *Lancet* **2004**, *363*, 1017–1024.
[229] Singh, B.; Daneshvar, C. *Clin. Microbiol*. *Rev*. **2013**, *26*, 165–184.
[230] Stresman, G. H. *Acta Trop.* **2010**, *116*, 167–172.

and environment and it is more intense in places where mosquito lifespan is long enough to allow the parasites to complete their growth cycle in the mosquito host and where mosquito prefers to bite humans rather than animals. For these latter reasons, over 90% of malaria deaths are occurring in sub-Saharan Africa.

Through the vector bite hundreds of **sporozoite** forms of the parasite are released into the vertebrate host's bloodstream (**Figure 3.2**), from where they migrate to the liver −passing through some cell types such as Kupfer cells− and form parasitophorous vacuoles in **hepatocytes**. At this stage they can either remain dormant as a **hypnozoite** form (*P. vivax* or *P. ovale*), or initiate development, which results in the production of tens of thousands haploid forms, called **merozoites**. The parasites then induce detachment of the infected hepatocyte, allowing it to move to the liver sinusoid where budding of parasite-filled vesicles called **merosomes** occurs.[231] New merozoites quickly invade and develop within erythrocytes where they replicate from small ring forms to the **trophozoites** after about 24 hours of invasion. Approximately 36 hours after merozoites invasion repeated nuclear division takes place to form **schizonts** or the segmenter form. This then ruptures and releases merozoites (at least 8−20 per schizont every 48 hours or 72 hours for *P. malariae*) from erythrocytes which can invade other red blood cells and continue its replication resulting in thousands of parasite-infected cells in the host bloodstream, in a cycle, sometimes synchronous, that may correspond to the cycle of fever and chills in malaria. In some cases, the merozoites enter red blood cells but do not divide. Instead they differentiate into sexual forms of the parasite, male and female **gametocytes** that circulate in the bloodstream. When the female mosquito bites an infected human, it ingests the **gametocytes** which once in the mosquito gut, the infected red blood cells burst, release the gametocytes and they in turn rapidly undergo transition into activated **gametes**. Then, male and female gametes fuse to form the motile and short-lived diploid parasite form, **ookinete** that migrates out of the blood meal, across the peritrophic matrix to the mid-gut wall where an **oocyst** is formed. Growth and division of each oocyst produces thousands of **sporozoites**. Eventually the oocyst ruptures and the sporozoites quickly find their way to the salivary glands where they await transfer to the vertebrate host. When the female mosquito feeds again, the transmission cycle is complete. The mosquito becomes infectious to its next blood meal donor approximately two weeks after ingesting gametocytes, a time frame that is influenced by the external temperature. Development of *P. vivax* within the mosquito can occur at a lower

[231] Sturm, A.; Amino, R.; Van de Sand, C. *et al*. *Science* **2006**, *313*, 1287–1290.

environmental temperature than that required for the development of *P. falciparum*, explaining the preponderance of *P. vivax* infections outside tropical and subtropical regions.[232]

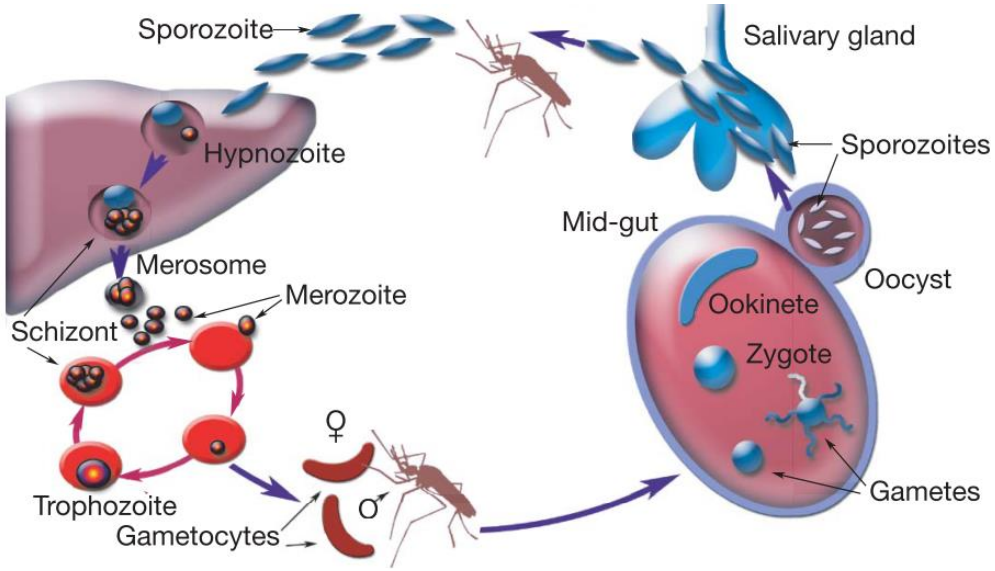

Figure 3.2. Diagram of the malaria parasite's life cycle. Liver, blood (= erythrocytic), transmission, and mosquito stages. See text above for details (Image source: Winzeler, E. A. *Nature* **2008**, *455*, 751−756).

During its itinerant existence, the unicellular malaria parasite uses a toolkit of more than 5,000 genes[233] to undergo radical metamorphoses that are suited to the numerous environments and barriers it encounters. These changes include the development, at different points in its life cycle, of motile, invasive, encysted, intracellular, sexual, and dormant forms, as we have just detailed, that enable it to complete its full life cycle (**Figure 3.2**). Each of these stages represents a potential target at which the life cycle can be interrupted. Vaccines, drugs, and anti-vector measures are being developed to prevent infection, disease, and transmission. Despite numerous potential targets, the most widely used treatments are the old compound, quinine, and the best new compound, artemisinin. These limitations stem, in part, from the fact that since its discovery in 1880 the parasite has been slow to reveal its secrets, including its metabolic pathways and its antigens that are targeted by protective immunity.[234] However, recent advances in determining the genome sequences for humans, *Anopheles* mosquitoes, and *Plasmodium* parasites have raised hopes that developing new interventions might be feasible.[235]

[232] Biamonte, M. A.; Wanner, J.; Le Roch, K. G. *Bioorg. Med. Chem. Lett.* **2013**, *23*, 2829−2843.
[233] Gardner, M. J.; Hall, N.; Fung, E.; White, O. *et al*. *Nature* **2002**, *419*, 498–511.
[234] Greenwood, B. M.; Fidock, D. A.; Kyle, D. E. *et al*. *J. Clin. Invest.* **2008**, *118*, 1266−1276.

3.3. Current treatments and trends against malaria

The treatment of malaria symptoms has a long history (**Figure 3.3**), beginning with qinghaosu (artemisinin) in ancient China[235] and **quinine** (**48**, **Figure 3.4**) isolated from Cinchona bark in the 17th century,[236] which was the mainstay of severe malaria treatment until the end of the Second World War when the first synthetic antimalarial drug, **chloroquine**, **29**, was widely deployed. During the following years, it was used to treat hundreds of millions of malaria patients and help to achieve sustainable malaria control until parasite resistance to this drug emerged. Trying to solve the health problem, the combination **sulfadoxine**/**pyrimethamine**, **49**/**50**, replaced chloroquine as a first-line drug, but again the emergence of resistance appeared soon and spread widely. At present WHO is recommending the use of drugs containing **artemisinin**, **51**, an antiprotozoal endoperoxide from sweet wormwood purified from *Artemisia annua* in 1972, as first-line treatment for uncomplicated and severe malaria and as a significant tool in the fight to eradicate the disease. [237]

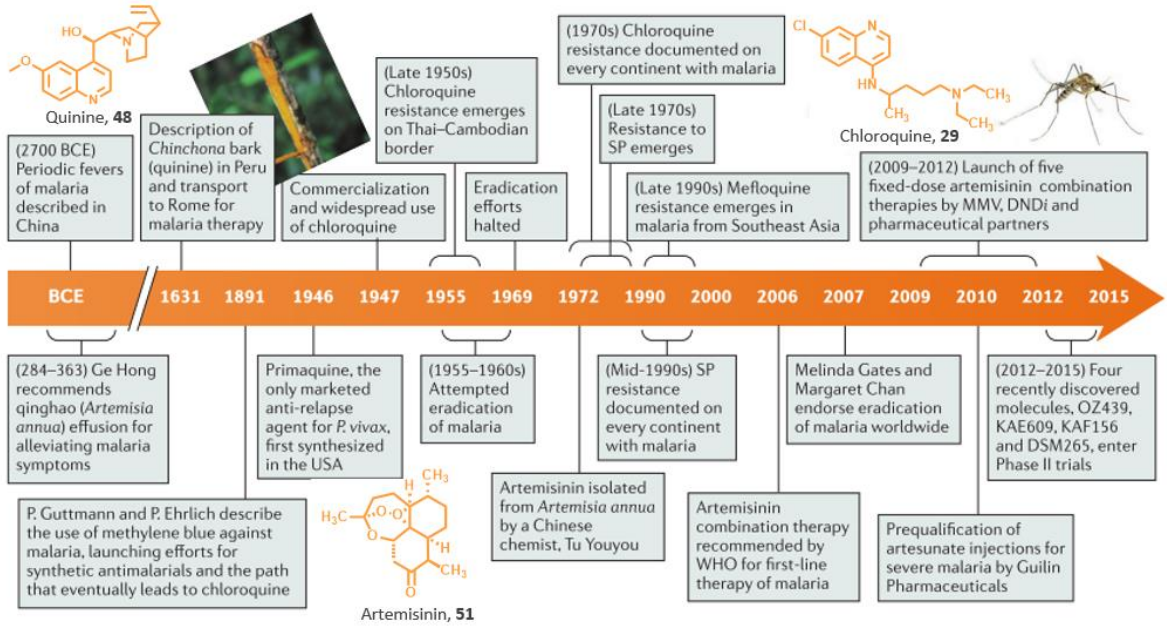

Figure 3.3. Historical timeline of the antimalarial drugs discovery (Image source: Wells, T. N.; Hooft van Huijsduijnen, R.; Van Voorhis, W. C. *Nat. Rev. Drug Discov.* **2015**, *14*, 424–442).

Although artemisinin, **51**, and its derivatives (artesunate, artemether, arteether, dihydroartemisinin) have many attractive features including potency and fast onset of action,

[235] Faurant, C. *Parasite* **2011**, *18*, 215–218.
[236] Achan, J.; Talisuna, A. O.; Erhart, A. *et al*. *Malar. J.* **2011**, *10*, 144.
[237] White, N. J. *Science* **2008**, *230*, 330–334.

they are rapidly cleared[238] and have a complex chemical structure, which has thwarted researchers' attempts to synthesize them inexpensively in the laboratory.[239] Thus, artemisinin-based compounds are often combined with slow-clearing drugs. The most popular combination consists of tablets containing artemether (**52**, 20 mg) and **lumefantrin** (**53**, 120 mg) sold as Coartem™ (Novartis).[240] For the liver stages, **primaquine**, **54**, is the only drug approved to eliminate hypnozoites and remains the only licensed drug that can provide a radical cure of *P. vivax*, but this drug, in addition to its other liabilities, produces hemolytic anemia in individuals with glucose-6-phosphate dehydrogenase (G6PD) deficiency.[241] On the other hand, **atovaquone–proguanil** (**55/56**, Malarone™, GlaxoSmithKline) is usually preferred for prophylactic treatment because it is well tolerated, but is expensive.[232]

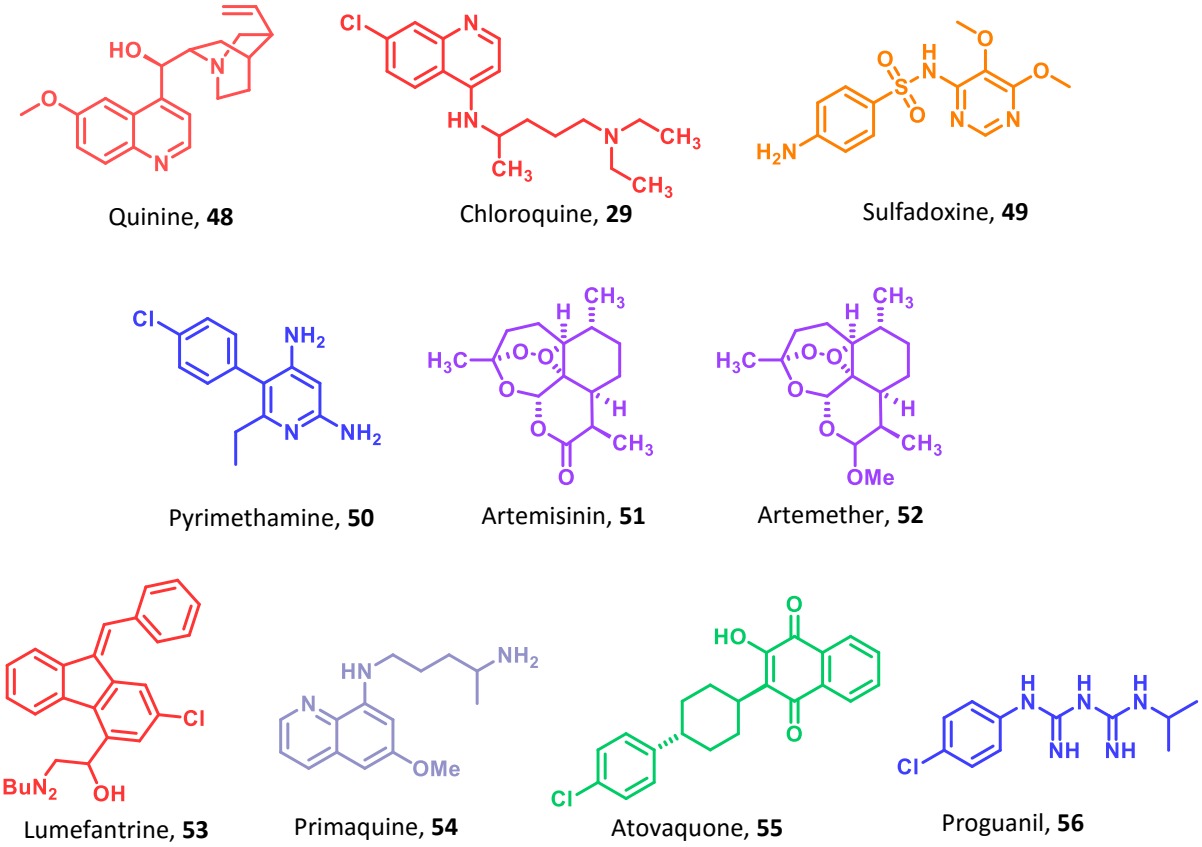

Figure 3.4. Current malaria chemotherapy. Drug mechanisms: heme polymerization depicted in red, dihydropteroate synthase (DHPS) in orange, dihydrofolate reductase (DHFR) in blue, SERCA-type Ca^{2+}-ATPase (ref) in purple, Cytochrome bc1 in green and mechanisms unknown in grey.

[232] Biamonte, M. A.; Wanner, J.; Le Roch, K. G. *Bioorg. Med. Chem. Lett.* **2013**, *23*, 2829–2843.
[238] Morris, C. A.; Duparc, S.; Borghini-Fuhrer, I. *et al. Malar. J.* **2011**, *10*, 263.
[239] Ro, D. K.; Paradise, E. M.; Ouellet, M. *et al*. *Nature* **2006**, *440*, 940–943.
[240] Djimdé, A.; Lefèvre, G. *Malar. J.* **2009**, *8* (Suppl. 1), S4.
[241] Beutler, E. *Blood* **1959**, *14*, 103–139.

Although drugs currently work well against malaria, a vaccine that targets *P. vivax* or *P. falciparum* would probably reduce much of the poverty associated with malaria and greatly assist in complete malaria eradication.[242] More than 30 *P. falciparum* malaria vaccine candidates are at either advanced preclinical or clinical stages of evaluation,[243] but only the RTS,S/AS01 (RTS,S) vaccine has completed Phase 3 evaluation and received a positive regulatory assessment. RTS,S was developed through a partnership between GlaxoSmithKline Biologicals (GSK) and the PATH Malaria Vaccine Initiative (MVI) with the support of Bill & Mellinda Gates Foundation and from a network of African research centers that performed the clinical studies. This vaccine contains a recombinant malaria protein fused to the surface of a hepatitis B protein and is based on the *P. falciparum* circumsporozoite protein (CSP), an abundant surface protein associated with the pre-erythrocytic phases of parasite development. It has been shown to reduce the number of severe cases of malaria[244] produced by *P. falciparum* infection in clinical trials, whereas it does not offer protection against *P. vivax* malaria. Unfortunately, the same studies also noted that several age groups in children still developed malaria after vaccine shot.[38,245,246]

Therefore, science has still no magic bullet for malaria and in the meantime *Plasmodium* parasites are developing unacceptable levels of resistance to one drug after another and many insecticides are no longer useful against *Anopheles* mosquitoes transmitting the disease.[247,248] Chloroquine resistance is caused by mutations of the *Pf*mdr1,[249] *Pf*cg2,[250] and *Pf*crt[251] genes. Atovaquone resistance is associated with mutations at positions 133, 144, and 248 of cytochrome b.[252] Resistance to antifolates (pyrimethamine and proguanil) is caused by point mutations at positions 51, 59, 108, and 164 of dihydrofolate reductase (DHFR). Sulfonamides and sulfones become ineffective owing to mutations at 436, 437, 540, 581, and 613 of dihydropteroate synthase (DHPS).[253] Artemisinin and their derivatives, the safest treatment against multidrug-resistant *P. falciparum* malaria, are not an exception to drug resistance,

[242] Verma, R.; Khanna, P.; Chawla, S. *Hum. Vaccin. Immunother*. **2013**, *9*, 1268−1271.
[243] WHO Home Page. Tables of malaria vaccine projects globally «The Rainbow Tables» 2015. http://www.who.int/immunization/research/development/Rainbow_tables/en/
[244] Aponte, J. J.; Aide, P.; Renom, M. *et al. Lancet* **2007**, *370*, 1543–1551.
[245] WHO Home Page. *Weekly epidemiological record*, 29th January **2016**, *91*, 33–52.
[246] Todryk, S. M.; Hill, A. V. S. *Nat. Rev. Microbiol*. **2007**, *5*, 487–489.
[247] Baird, J. K. *N. Engl. J. Med.* **2005**, *352*, 1565–1577.
[248] Alam, A.; Goyal, M.; Igbal, M. S. *et al*. *Expert Rev. Clin. Pharmacol*. **2009**, *2*, 469–489.
[249] Price, R. N.; Cassar, C.; Brockman, A. *et al. Antimicrob. Agents Chemother*. **1999**, *43*, 2943–2949.
[250] Olliaro, P. *Pharmacol. Ther*. **2001**, *89*, 207–219.
[251] Fidock, D. A.; Nomura, T.; Talley, A. K. *et al. Mol. Cell.* **2000**, *6*, 861–871.
[252] Syafruddin, D.; Siregar, J. E.; Marzuki, S. *Mol. Biochem. Parasitol.* **1999**, *104*, 185–194.
[253] Plowe, C. V.; Kublin, J. G.; Doumbo, O. K. *Drug Resist. Updat*. **1998**, *1*, 389–396.

although combining drugs can limit the emergence of resistance.[254] Malaria parasites become resistant to artemisinins due to the mutation of *Pf*ATPase6 at S769N, A623E, and E431K.[255] For that reason, antimalarial therapy urgently needs an effective treatment that not only is simple to administer and active against all the stages of the parasites life cycle, but is also endowed with mechanisms of action different from those of conventional antimalarial drugs in order to overcome the previously described resistances.

The advent of genomics and proteomics approaches including functional genomics,[256] evolutionary patterning,[257] system biology,[258] interactome studies,[259] gene network,[260] and structure-based drug design[261] have made it possible a whole synergistic outlook to identify novel drug targets. The advantages of the major metabolic differences of *Plasmodium* with its host have been considered in the design of antimalarial drugs. Several enzymes, channels, transporters, interacting molecules on the parasites (**Figure 3.5**) for RBC invasion, and molecules responsible for oxidative stress in the human malaria parasite *P. falciparum* have been identified and suggested as potential drug targets.[262,263,264] Although a few have been validated,[265] several still need to be validated to establish a specific antimalarial target.[266]

[254] Daily, J. P. *J. Clinical Pharmacol.* **2006**, *46*, 1487−1497.
[255] Mugittu, K.; Genton, B.; Mshinda, H. *et al*. *Malar. J.* **2006**, *5*, 126.
[256] Birkholtz, L.; van Brummelen, A. C.; Clark, K. *et al. Acta Trop.* **2008**, *105*, 113–123.
[257] Durand, P. M.; Naidoo, K.; Coetzer, T. L. *PLoS ONE* **2008**, *3*, e3685.
[258] Johnson, P. C.; Higgins, A. J. *Drug Discovery World Summer* **2004**, 55–62.
[259] Wuchty, S. *PLoS ONE* **2007**, *2*, e335.
[260] Jiang, Z.; Zhou, Y. *J. Integr. Bioinform.* **2005**, *2*, 14.
[261] Jana, S.; Paliwal, J. *Int. J. Antimicrob. Agents* **2007**, *30*, 4–10.
[262] Allen, R. J.; Kirk, K. *Trends Parasitol.* **2004**, *20*, 7–10.
[263] Becker, K.; Tilley, L.; Vennerstrom, J. L. *et al*. *Int. J. Parasitol.* **2004**, *34*, 163–189.
[264] Cowman, A. F.; Crabb, B. S. *Cell* **2006**, *124*, 755–766.
[265] Choi, S. R.; Mukherjee, P.; Avery, M. A. *Curr. Med. Chem.* **2008**, *15*, 161–171.
[266] Biagini, G. A.; O'Neill, P. M.; Nzila, A. *et al*. *Trends Parasitol.* **2003**, *19*, 479−487.

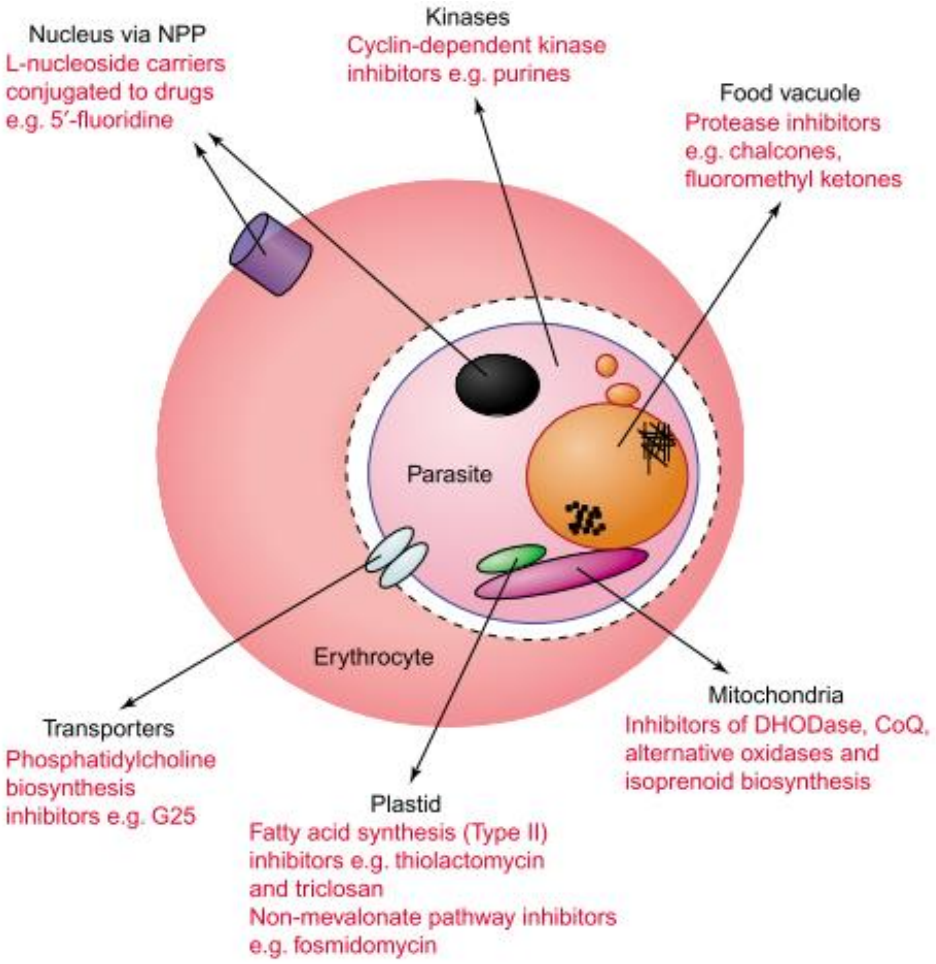

Figure 3.5. Novel drug targets as candidates for chemotherapeutic attack. Abbreviations: Coq, ubiquinone; DHODase, dihydroorotate dehydrogenase; NPP, new permeability pathway (Image source: Biagini, G. A. *et al. Trends Parasitol.* **2003**, *19*, 479−487).

A detailed description of all current potential drug malaria targets goes beyond the scope of this report. Herein, we touch upon the role of oxidative stress in malaria infection and, in particular, the pentose phosphate pathway and the recent validated target, the bifunctional enzyme glucose-6-phosphate dehydrogenase−6-phosphogluconolactonase of *P. falciparum* (*Pf*GluPho).

3.3.1. Oxidative stress and antioxidant defense in malaria parasites

Malaria parasites are continuously exposed to oxidative and nitrosative stress. Such stress might be classified as exogenous or endogenous. Exogenous stress is produced by the immune response of the host, whereas endogenous stress could either be a result of the high metabolic rate of the rapidly growing and multiplying parasite which generates large quantities of toxic redox active by-products or the degradation of host hemoglobin by the parasite.[267] Hemoglobin

[267] Becker, K. et al. Ed. Sherman, I. W. ASM Press, Washington, D.C, **2005**, 365−383.

represents the major source of amino acids for *Plasmodium*, but its degradation in an acidic food vacuole (FV) results in the production of toxic free heme (ferri/ferroprotoporphyrin IX; FP) and reactive oxygen species (ROS), conferring oxidative stress on the host cell (**Figure 3.6**). Most of the FP is sequestered into a crystalline form, known as hemozoin or malaria pigment.[268,269] To avoid this disaster, most of the free heme is detoxified by alternative pathways, including FP degradation,[270,271] reaction with glutathione,[272] and the binding to FP binding proteins. However, even if a small amount (e.g. 0.5 %) of the free heme escapes the neutralization processes, it may cause oxidative damage to host proteins and membranes, inhibit parasite enzymes, and lyse erythrocytes. Apart from this metabolically derived oxidative stress, the production of ROS by the host immune system adds to the overall oxidative burden of the parasitized cell.[248]

In this regard, it is worth noting that the potential susceptibility of the parasite–host cell unit to pro-oxidants agents is highlighted by the effectiveness of antimalarial drugs currently in clinical use that enhance oxidative stress directly or block the detoxification of hemoglobin breakdown products.[273] For instance, chloroquine acts by preventing the parasite from polymerizing toxic heme into hemozoin and/or by inhibiting glutathione-mediated degradation of heme.[274] The redox cycling of the metabolites of primaquine exerts a substantial oxidative stress, and the current front-line drug, artemisinin, seems to damage lipids and proteins by generation of ROS.[275]

Malaria parasites are equipped with a range of antioxidant defense mechanisms in order to sustain a redox equilibrium to survive, comprising low-molecular antioxidants molecules such as tripeptide glutathione (GSH), the most prominent, and varied antioxidant enzymes. The key enzymes of *P. falciparum* directly or indirectly involved in redox metabolism include glutathione- and thioredoxin-dependent proteins as well as superoxide dismutase (SOD).[276,277] In addition, pentose phosphate pathway (PPP) in *Plasmodium* species has been recently reinforced as

[248] Alam, A.; Goyal, M.; Igbal, M. S. *et al*. *Expert Rev. Clin. Pharmacol*. **2009**, *2*, 469–489.
[268] Egan, T. J.; Combrinck, J. M.; Egan, J. *et al. Biochem J*. **2002**, *365*, 343–347.
[269] Slater, A. F.; Cerami, A. *Nature* **1992**, *355*, 167–169.
[270] Zhang, F.; Schmidt, W. G.; Hou, Y. *et al. Proc. Natl. Acad. Sci. USA* **1992**, *89*, 5231–5235.
[271] Loria, P.; Miller, S.; Foley, M. *et al*. *Biochem J*. **1999**, *339*, 363–370.
[272] Ginsburg, H.; Famin, O.; Zhang, J. *et al*. *Biochem. Pharmacol.* **1998**, *56*, 1305–1313.
[273] Goldberg, D. E. *Curr. Top. Microbiol. Immunol*. **2005**, *295*, 275–291.
[274] Ginsburg, H.; Ward, S. A.; Bray, P. G. *Parasitol. Today* **1999**, *15*, 357–360.
[275] O'Neill, P. M.; Posner, G. H. *J. Med. Chem*. **2004**, *47*, 2945–2964.
[276] Rahlfs, S.; Becker, K. *Eur. J. Biochem*. **2001**, *268*, 1404–1409.
[277] Müller, S. *Mol. Microbiol.* **2004**, 53, 1291−1305.

oxidative arm.[278] Some of the enzymes responsible for the maintenance of redox equilibrium have been studied in functional and structural detail over the last few years and based on the mounting evidence they have been proved as an effective therapeutic principle in malaria (**Figure 3.6**).[263]

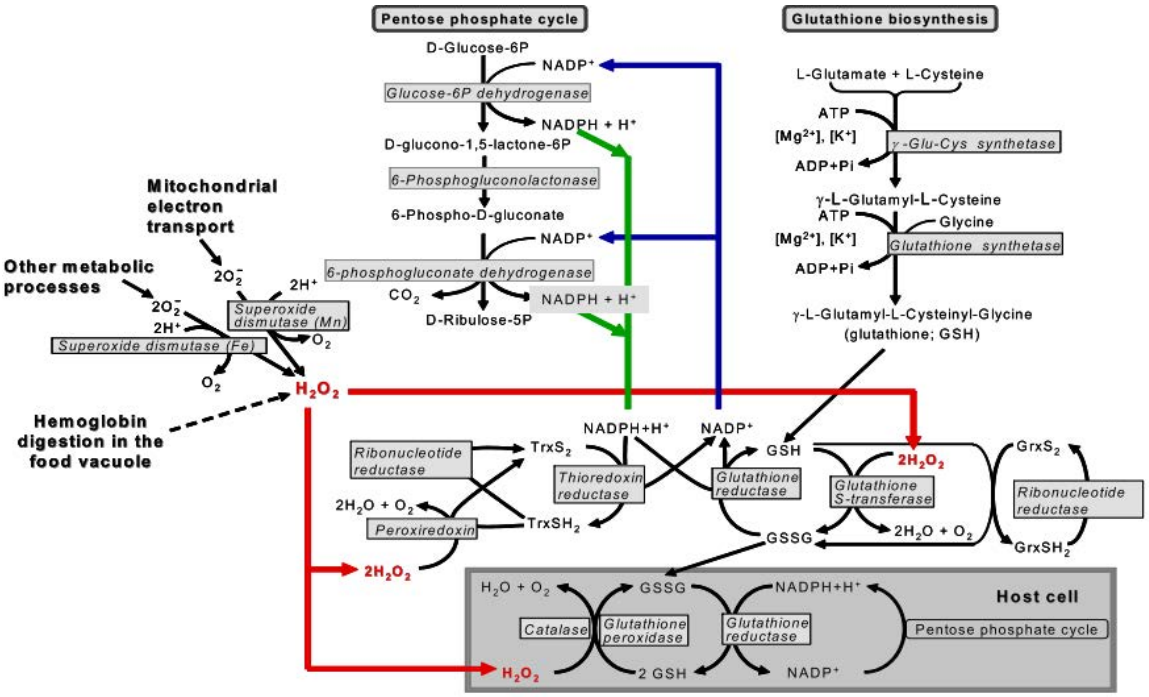

Figure 3.6. A schematic representation of the antioxidant defense in the *Plasmodium*-infected erythrocyte (Image source: Becker, K. *et al*. *Int. J. Parasitol.* **2004**, *34*, 163–189).

3.3.2. Pentose Phosphate Pathway (PPP) and Glucose-6-Phosphate Dehydrogenase (G6PD)

In human beings, glucose is metabolized apart from by the Embden-Meyerhof-Parnas (EMP) or glycolytic pathway that oxidize glucose to pyruvate with concomitant production of ATP, also by a second route, the PPP also known as the hexose monophosphate shunt (HMS). This latter pathway takes place in the cytosol and is divided into two phases: the oxidative generation of NADPH and the non-oxidative interconversion of sugars.[279] The oxidative pentose phosphate pathway (OxPPP) represents a major source of reducing power to all cells through the recycling of $NADP^+$ to NADPH (reduced form of nicotinamide adenine dinucleotide phosphate), which is formed when glucose-6-phosphate is oxidized to ribose 5-phosphate by the action of glucose-6-

[263] Becker, K.; Tilley, L.; Vennerstrom, J. L. *et al*. *Int. J. Parasitol.* **2004**, *34*, 163–189.
[278] Kruger, N. J.; von Shaewen, A. *Curr. Opin. Plant. Biol.* **2003**, *6*, 236−246.
[279] Berg, J. M.; Tymoczko, J. L.; Stryer, L. Biochemistry, 5th edn. New York, Freeman, W. H., **2002**.

phosphate dehydrogenase (G6PD) and 6-phosphogluconate dehydrogenase (6PGD) (**Figure 3.7**).[278] Ribose-5-phosphate is involved in the synthesis of RNA and DNA, as well as ATP, NADH, FAD, and CoA. NADPH, in turn, is able to act as an electron donor for several enzymatic reactions that are essential in reductive biosynthesis, and also as a proton donor for the regeneration of the reduced form of glutathione which is crucial for the reduction of hydrogen peroxide, oxygen radicals as well as the maintenance of hemoglobin and other RBC proteins in the reduced state.[280] Since RBC do not contain mitochondria, the pentose phosphate pathway is their only source of NADPH; therefore, defense against oxidative damage is dependent on G6PD.[281]

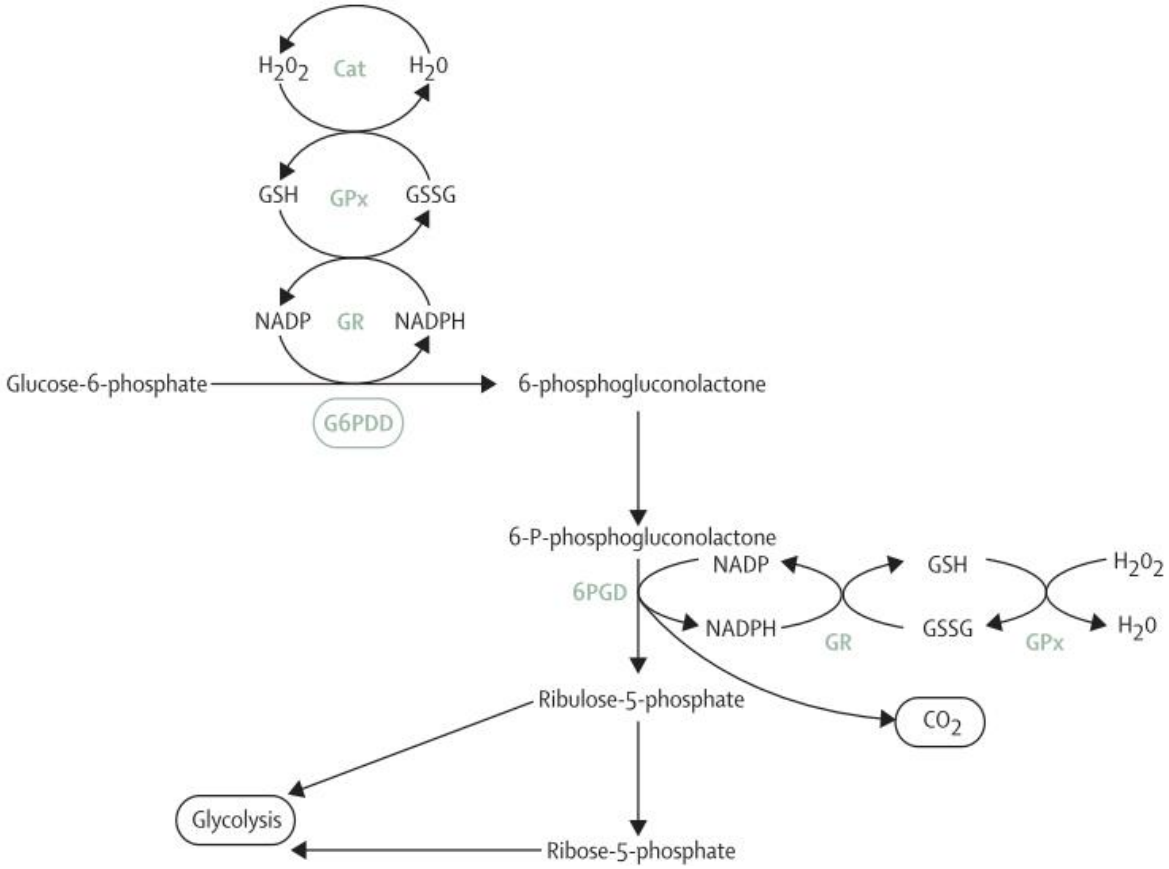

Figure 3.7. Diagram of the pentose phosphate pathway (PPP) (Image source: Naylor, C. E. *et al*. *Blood* **1996**, 87, 2974–2982).

The monomer of human G6PD (hG6PD) consists of 515 amino acids, with a molecular weight of about 59 kDa. A model of the three-dimensional structure of G6PD was published in 1996 (**Figure 3.8**),[282] and subsequently the crystal structure of hG6PD was elucidated.[283] The enzyme is

[280] Cappellini, M. D.; Fiorelli, G. *Lancet* **2008**, *371*, 64–74.
[281] Luzzatto, L.; Metha, A.; Vulliamy, T. 8th ed. Columbus: McGraw-Hill, **2001**: 4517–4553.
[282] Naylor, C. E.; Rowland, P.; Basak, K. *et al*. *Blood* **1996**, 87, 2974–2982.
[283] Au, S. W. N.; Gover, S.; Lam, V. M. S. *et al*. *Structure* **2000**, *8*, 293–303.

active as a tetramer or dimer, in a pH-dependent equilibrium. Every monomer consists of two domains: the N-terminal domain (amino acids 27–200), with a β–α–β dinucleotide binding site (amino acids 38–44); and a second, larger, β+α domain, consisting of an antiparallel nine-stranded sheet. The dimer interface lies in a barrel arrangement, in this second part of the G6PD molecule. The two domains are linked by an α-helix, containing the totally conserved eight-residue peptide that acts as the substrate binding site (amino acids 198–206).[283] Viewing the structure, at 3 Å (0.3 nm) resolution, reveals an $NADP^+$ (a coenzyme) molecule in every subunit of the tetramer, distant from the active site but close to the dimer interface. Stability of the active quaternary structures is crucial for normal G6PD activity. G6PD is present in all cells; however, its concentration varies in different tissues. In healthy red blood cells, the enzyme operates at only 1–2% of its maximum potential (even under oxidative stress generated by methylene blue): a large reserve of reductive potential exists, which is substantially decreased in G6PD-deficient red-blood cells, leading to pathophysiological features.[284,285]

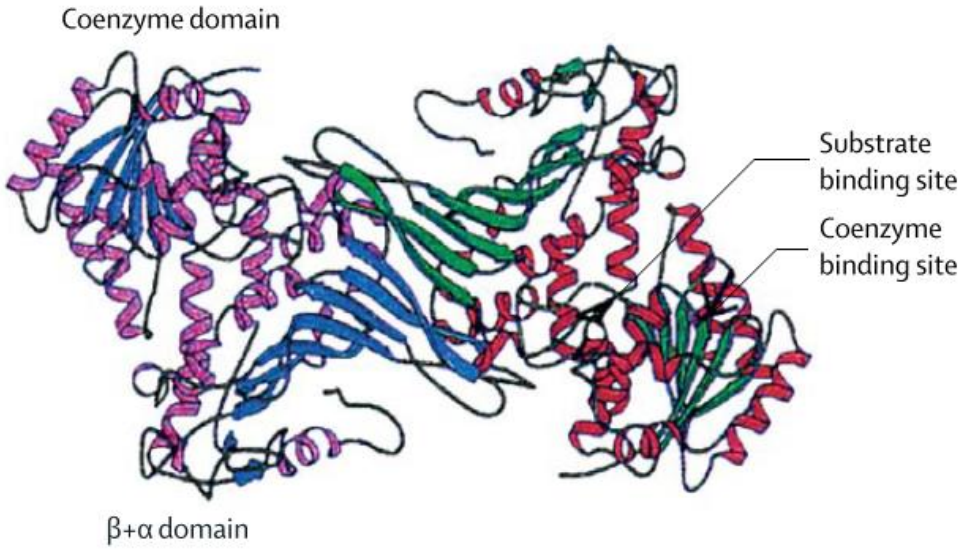

Figure 3.8. Three-dimensional model of active G6PD dimer. The two identical subunits are located across a symmetrical axis (Image source: Naylor, C. E. *et al*. *Blood* **1996**, 87, 2974–2982).

[284] Battistuzzi, G.; d'Urso, M.; Toniolo, D. *et al. Proc. Natl. Acad. Sci. USA* **1985**, *82*, 1465–1469.
[285] Gaetani, G. D.; Parker, G. C.; Kirkman, H. N. *Proc. Natl. Acad. Sci. USA* **1974**, *71*, 3584–3587.

3.3.3. G6PD deficiency and malaria

G6PD deficiency (G6PDd) is an X-linked recessive hereditary genetic disorder of red blood cells (RBC) caused by missense mutations at the so-called "housekeeping" G6PD gene, thus, showing a higher incidence in males than in females. Males are hemizygous for the G6PD gene and can, therefore, have normal gene expression or be G6PD-deficient, showing the severe phenotype, whereas females, who have two copies of the G6PD gene on each X chromosome, can be homozygote but are less common or heterozygote. Heterozygote females with only one affected X-chromosome vary in severity depending on the balance between the expression of the normal and the abnormal X chromosomes.[286,287,288]

This deficit was discovered as an outgrowth of a series of investigations performed to understand why some persons were uniquely sensitive to the development of hemolytic anemia when they ingested the 8-amino-6-metoxyquinoline antimalarial drug primaquine.[289,290] Later it was known that not only exogenous agents such as numerous drugs or fava beans, for instance, triggered acute hemolytic crisis, but both viral and bacterial infections and diabetes mellitus, amongst others causes, might also shorten RBC life span in G6PD-deficient persons and precipitate fall on hemoglobin (Hb). Other clinical manifestations are neonatal jaundice and chronic hemolysis, leading to congenital non-spherocytic hemolytic anemia, this taking place to a limited extent in some G6PD variants.[291]

Since 1967 when the WHO made an initial recommendation for the characterization of the G6PD deficiency, more than 400 biochemical variants corresponding to 140 mutations of the G6PD gene[292] have been characterised according to their physicochemical properties (such as thermostability and chromatographic behaviour), kinetic properties (involving substrates G6P, NADP and substrate analogues) and pH dependence.[293] These variants can be grouped into five classes in accordance of their enzyme activity and clinical manifestations or classified as sporadic or polymorphic.[294,295]

---

[286] Beutler, E.; Yeh, M.; Fairbanks, V. F. *Proc. Natl. Acad. Sci. USA* **1962**, *48*, 9–16.
[287] Luzzatto, L. *Haematologica* **2006**, *91*, 1303−1306.
[288] Mason, P. J.; Bautista, J. M.; Gilsanz, F. *Blood Rev.* **2007**, *21*, 267–283.
[289] Beutler, E. ed. Blood Pure and Eloquent, McGraw-Hill, New York, **1980**, 141−168.
[290] Dern, R. J.; Beutler, E.; Alving, A. S. *J. Lab. Clin. Med.* **1955**, *45*, 30-39.
[291] Beutler, E. *Blood Rev.* **1996**, *10*, 45−52.
[292] Beutler, E. *Semin. Hematol*. **1990**, *27*, 137–164.
[293] Beutler, E. 3rd edn. Grune and Stratton New York, **1984**.
[294] Betke, K.; Brewer, G. J.; Kirkman, H. N. *et al*. *World Health Organ. Tech. Rep. Ser.* **1967**, *366*, 1–53.
[295] WHO working group. *Bull. World Health Organ.* **1989**, *67*, 601–611.

Although many other RBC enzymopathies are now known, such as thalassemia, sickle cell trait and hemoglobin C,[296,297,298,299] G6PD deficiency still reigns as the most common of all clinically significant enzyme defect, not only in hematology, but in human biology as a whole, being present in more than 400 million people worldwide.

The highest prevalence of G6PD deficiency is reported in Africa, southern Europe, the Middle East, Southeast Asia, and the central and southern Pacific islands; however, because of fairly recent migration, G6PD deficiency is nowadays quite prevalent in North and South America and in parts of northern Europe.[300,301] Strikingly, the geographical distribution of this disorder is remarkably similar to that of malaria, which has lent support to the so-called "malaria protection hypothesis" that likely arose as a direct result of evolutionary natural selection in human population. This selective advantage was originally suggested over 60 years ago by Motulsky,[302] Siniscalco *et al*.,[303] and Allison and Clyde[304,305] and was later supported by Luzzatto *et al*.,[306,307,308] and Ruwende *et al*.[309,310]

A clinical protective effect in G6PDd carriers against fulminating malaria infection (*P. falciparum*) has been widely verified through various studies mainly performed in many locations of Africa, [306,311,311] however, there is no a clear association with *Vivax* malaria; it has not been accurately tested and remains anecdotal with few exceptions in some reports.[312]

---

[296] Zanella, A.; Colombo, M. B.; Rossi, F. *et al*. *Haematologica* **1989**, *74*, 387−396.
[297] Beutler, E. Williams Hematology. New York, NY, McGraw- Hill. **1995**, 564.
[298] Valentine, W. N.; Paglia, D. E. *J. Lab. Clin. Med*. **1990**, *115*, 12−20.
[299] Valentine, W. N.; Tanaka, K. R.; Paglia, D. E. *Ann. Intern. Med.* **1985**, *103*, 245−257.
[300] Frank, J. E. *Am. Fam. Physician.* **2005**, *72*, 1277–1282.
[301] Greene, L. S. *Yearbook Phys. Anthropol*. **1993**, 17 (suppl 3), 153−178.
[302] Motulsky, A. G. *Lancet* **1961**, *277*, 1168−1169.
[303] Allison, A. C. *Nature* **1960**, *186*, 531−532.
[304] Allison, A C.; Clyde, D. F. *Br. Med. J.* **1961**, *1*, 1346−1349.
[305] Siniscalco, M.; Bemini, L.; Filippi, G.*et al. Bull World Health Organ*. **1966**, *34*, 379−393.
[306] Luzzatto, L.; Usanga, E. A.; Reddy, S. *Science* **1969**, *164*, 839−842.
[307] Luzzatto, L.; Bienzle, U. *Lancet* **1979**, *1*, 1183–1184.
[308] Luzzatto, L. *et al.* Glucose-6-Phosphate Dehydrogenase, Orlando, FL, Academic, **1986**, 181.
[309] Ruwende, C.; Khoo, S. C.; Snow, R. W. *et al*. *Nature* **1995**, *376*, 246–249.
[310] Ruwende, C.; Hill, A. *J. Mol. Med.* **1998**, *76*, 581–588.
[311] a) Kruatrachue, M.; Charoenlarp, P.; Chongsuphajaisiddhi, T. *et al. Lancet* **1962**, *2*, 1183−1186. b) Bienzle, U.; Ayeni, O.; Lucas, A. O. *et al*. *Lancet* **1972**, *1*, 107−110. c) Kar, S.; Seth, S.; Seth, P. K. *Hum. Biol.* **1992**, *64*, 187−197. d) Mombo, L.; Ntoumi, F.; Bisseye, C. *et al*. *Am. J. Trop. Med. Hyg.* **2003**, *68*, 186−190. e) Guindo, A.; Fairhurst, R. M.; Doumbo, O. K. *et al*. *Plos Med.* **2007**, *4*, e66. f) Ouattara, A. K.; Bisseye, C.; Bazie, B. V. *et al*. *Pac. J. Trop. Biomed.* **2014**, *4*, 655−658.
[312] a) Louicharoen, C.; Patin, E.; Paul, R. *et al*. *Science* **2009**, *326*, 1546−1549. b) Khim, N.; Benedet, C.; Kim, S. *et al. Malaria J.* **2013**, *12*, 171−180. c) Peixoto, H. M.; Brito, M. A. M.; Romero, G. A. S. *et al*. *Malaria J.* **2015**, *14*, 126−134.

The precise mechanism of this selective advantage remains uncertain, although it overall seems to be related to the effects on RBC by increasing oxidative stress. At the molecular level the most likely explanation attributes the protection hypothesis to decreased parasite growth rate in deficient RBC, probably as a result of the intracellular accumulation of toxic oxidised substances such as oxidised glutathione and hemozoin.[313,314,315] However, there is some evidence that infected RBCs are more susceptible to hemolysis as a result of increased methaemoglobin and release of ferriheme, a known cytolytic agent,[316] and that in addition they are more readily phagocytosed by cells of the reticuloendothelial system as a result of the RBC changes (i.e. methaemoglobin and Heinz body formation, membrane damage) that are finally associated with oxidative stress imposed by the parasite infection (**Figure 3.9**).[317]

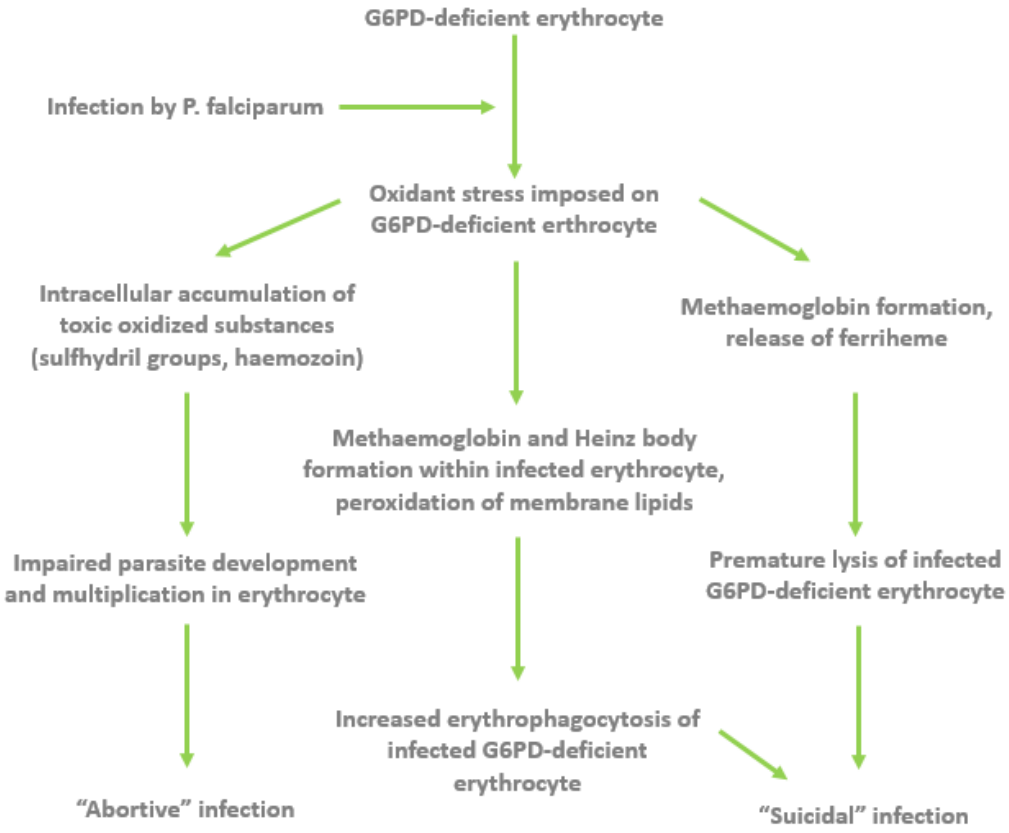

Figure 3.9. Putative protective mechanisms of the G6PD deficiency against severe malaria (Image source: Ruwende, C.; Hill, A. *J. Mol. Med.* **1998**, *76*, 581–588).

[313] Turrini, F.; Schwarzer, E.; Arese, P. *Parasitol. Today* **1993**, *9*, 297-300.
[314] Miller, J.; Golenser, J.; Kullgren, B. *et al*. *Exp. Parasitol.* **1984**, *57*, 239−247.
[315] Golenser, J.; Miller, J.; Spira, D. T. *et al*. *Trop. Med. Parasitol.* **1988**, *39*, 273−276.
[316] Janney, S. K.; Joist, J. H.; Fitch, C. D. *Blood* **1986**, *67*, 331−333.
[317] a) Cappadoro, M.; Giribaldi, G.; O'Brien, E. *et al*. *Blood* **1998**, *92*, 2527−2534. b) Arese, P.; Turrini, F.; Schwarzer, E. *Cell. Physiol. Biochem*. **2005**, *16*, 133−146. c) López, C.; Saravia, C.; Gomez, A. *et al*. *Gene* **2010**, *467*, 1–12. d) Méndez, D.; Linares, M.; Diez, A. *et al*. *Free Radic. Biol. Med*. **2011**, *50*, 1305−1313.

3.3.4. Glucose-6-Phosphate Dehydrogenase–6-Phosphogluconolactonase from P. falciparum (PfGluPho)

The pleiotropic consequences of G6PD deficiency reflect the fact that the oxidative arm of PPP is the only source of NADPH in red blood cells. In contrast, *Plasmodium* has several potential pathways in addition to PPP, as we have mentioned above, to generate NADPH. [318] These include the cytosolic enzyme glutamate dehydrogenase and the mitochondrial isocitrate dehydrogenase. However, it has been demonstrated that glutamate dehydrogenase is non-essential for asexual stage growth, and the contribution of isocitrate dehydrogenase is still unclear.[319,320]

G6PD activity in *Plasmodium* was firstly discovered more than 45 years ago in *P. berghei* by Langer et al.,[321] but the inability to confirm these findings through several subsequent investigations[322] coupled with the clear documentation and reproducible findings on the existence of the second enzyme (6-phosphogluconolactonase) of the PPP[323] raised questions about the existence of a complete PPP in the *Plasmodium* parasite and suggested that the parasite made use of the host G6PD enzyme to carry out the initial step of the PPP.[324] Nevertheless, Hempelmann and Wilson reported the presence of *P. falciparum* G6PD (*Pf*G6PD) activity 14 years later,[325] and further studies on the enzyme led not only to its identification and partial purification but also showed that the enzyme was present at similar levels in both G6PD deficient and normal host cells, what suggested that G6PD activity in malaria parasites was expressed independently from induction and adaptation to deficient cells.[326,327]

The nucleotide sequence encoding the *Pf*G6PD enzyme has been cloned and sequenced.[328,329] The primary structure as predicted from the gene sequence was found to be remarkably different from any of the 50 or so other G6PDs whose structure is known or inferred. The deduced protein has a subunit molecular weight of 107 kDa. The C-terminal part (residues 311-

[318] Preuss, J.; Jortzik, E.; Becker, K. *IUBMB Life* **2012**, *64*, 603–611.
[319] Wrenger, C.; Müller, S. *Eur. J. Biochem.* **2003**, *270*, 1775–1783.
[320] Storm, J.; Perner, J.; Aparicio, I. *et al*. *Malaria J.* **2011**, *10*, 193−204.
[321] Langer, B. W.; Phisphumvidhi, P.; Friedlander, Y. *Exp. Parasitol.* **1967**, *20*, 68−76.
[322] Sherman, I. W. *Microbiol. Rev.* **1979**, *43*, 453−495.
[323] Fletcher, K. A.; Canning, M. V.; Theakston, R. D. G. *Ann. Trop. Med. Parasitol.* **1977**, *71*, 125−130.
[324] Eckman, J.; Eaton, J. W. *Nature* **1979**, *278*, 754−756.
[325] Hempelmann, E.; Wilson, R. J. M. *Mol. Biochem. Parasitol*. **1981**, *2*, 197−204.
[326] Ling, I. T., Wilson, R. J. M. *Mol. Biochem. Parasitol*. **1988**, *31*, 47−56.
[327] Kurdi-Haidar, B.; Luzzatto, L. *Mol. Biochem. Parasitol*. **1990**, *41*, 83−91.
[328] Shahabuddin, M.; Rawlings, D. J.; Kaslow, D. C. *Biochim. Biophys. Acta.* **1994**, *1219*, 191−194.
[329] O'Brien, E.; Kurdihaidar, B.; Wanachiwanawin, W. *et al. Mol. Biochem. Parasitol.* **1994**, *64*, 313−326.

911) is clearly homologous to other described G6PDs.[330] The 310 amino acid protein sequence of the *N*-terminal region clearly differs from most eukaryotic and prokaryotic G6PDs and shows 6-phosphogluconolactonase (6PGL) activity.[331] Genes encoding very similar enzymes have also been found in four other *Plasmodium* parasites namely, *P. berghei*, *P. yoelii*, *P. chabaudi*, and *P. knowlesi*.[332]

Furthermore, it has been recently unveiled that the first two steps of the PPP in *Plasmodium* are catalyzed by a unique bifunctional protein harbouring both enzyme activities which is encoded by only one gene, named glucose-6-phosphate dehydrogenase−6-phosphogluconolactonase (GluPho)[333,334] which is found in *Plasmodium* species and in many other *Apicomplexa*.[335] A unique feature in *P. falciparum* GluPho (*Pf*GluPho) is the 62 amino acid insert (within the G6PD part) found between the structurally predicted $NADP^+$ and G6P binding site that has no similarity found to date. Similar inserts which differ in size and sequence are present in other *Plasmodium* GluPho and have however been demonstrated to be essential for GluPho activity (**Figure 3.10**).[332] *Pf*GluPho is constitutively expressed through the asexual blood stages of *Plasmodium*,[336] where its activity was originally verified.[325]

Figure 3.10. Sequence comparison of inserts within five *Plasmodium* GluPho proteins and human G6PD. Completely conserved amino acids are shaded black, highly conserved amino acids are shaded grey, and insertion sequences are italicised. Potential N-glycosylation sites are underlined. (Image source: Clarke, J. L. *et al. Mol. Biochem. Parasitol.* **2003**, *127*, 1–8).

[325] Hempelmann, E.; Wilson, R. J. M. *Mol. Biochem. Parasitol*. **1981**, *2*, 197−204.
[330] Jeffery, J.; Persson, B.; Wood, I. *et al*. *Eur. J. Biochem*. **1993**, *212*, 41−49.
[331] Scopes, D. A.; Bautista, J. M.; Vulliamy, T. J. *et al*. *Mol. Microbiol.* **1997**, *23*, 847−848.
[332] Clarke, J. L.; Sodeinde, O.; Mason, P. J. *Mol. Biochem. Parasitol.* **2003**, *127*, 1–8.
[333] Clarke, J. L.; Scopes, D. A.; Sodeinde, O. *et al*. *Eur. J. Biochem*. **2001**, *268*, 2013–2019.
[334] Jortzik, E.; Mailu, B. M., Preuss, J. *et al. Biochem. J*. **2011**, *436*, 641–650.
[335] Stover, N. A.; Dixon, T. A.; Cavalcanti, A. R. *PLoS ONE* **2011**, *6*, e22269.
[336] Bozdech, Z.; Ginsburg, H. *Malar. J*. **2005**, *4*, 17.

CHAPTER 4

Objectives

4.1. Synthesis and in vitro and in vivo pharmacological evaluation of two novel classes of multitarget anti-Alzheimer drug candidates (*J. Med. Chem.* **2014**, *57,* 2549; *Curr. Alzheimer Res.* **2016**, *13*, 1017; and *J. Med. Chem.* **2015**, *58,* 6018)

The aim of these published works herein presented involved the synthesis of multitarget compounds that displayed various interesting biological properties for the treatment of AD, by hitting several key targets for such disease. Taking into account the interesting multitarget biological profile of the donepezil–huprine hybrids,[89c,d] we devised the synthesis of novel classes of huprine-based multitarget compounds that might display additional biological properties beyond cholinesterase and Aβ aggregation inhibition. Within this context, a family of rhein–huprine hybrids (**Figure 4.1**) was firstly designed, synthesized, and evaluated *in vitro*, in *Escherichia coli* cells, and *ex vivo* (*J. Med. Chem.* ***2014***, *57*, 2549–2567) in close collaboration with the group of Prof. Nibaldo Inestrosa (Pontificia *Universidad Católica de Chile*). The excellent results obtained prompted us to further perform deeper *in vivo* studies (*Curr. Alzheimer Res*. **2016**, *13*, 1017–1029). Secondly, a series of heptamethylene-linked levetiracetam–huprine and levetiracetam–(6-chloro)tacrine hybrids was synthesized and their biological profile was assessed *in vitro* and *in vivo* (*J. Med. Chem.* **2015**, *58*, 6018–6032) thanks to the collaboration of Prof. Isidre Ferrer and Dr. Ester Aso (*IDIBELL - Hospital Universitari de Bellvitge*).

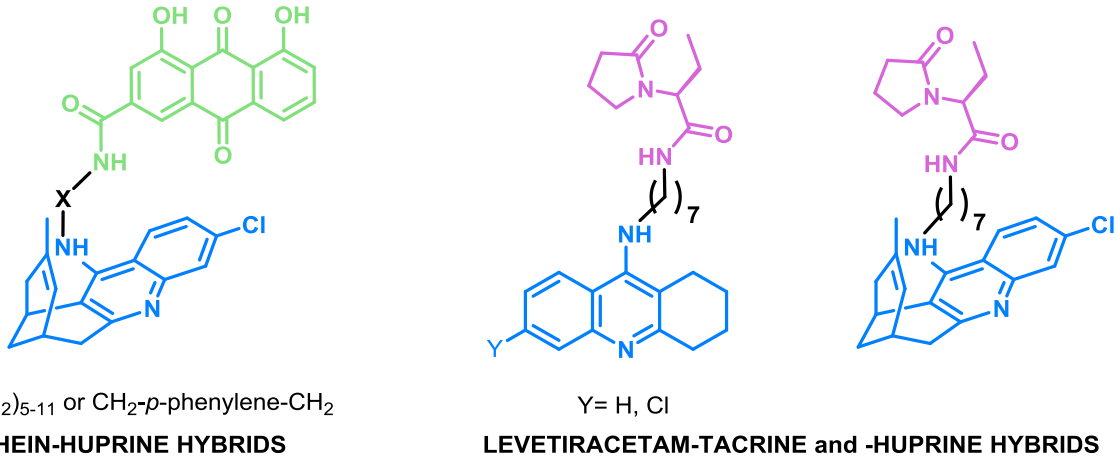

Figure 4.1. Multitarget hybrids synthesized in the frame of these published works.

[89c] Muñoz-Torrero, D.; Camps, P.; Gómez, T. *et al*. WO 2011/076969A1.
[89d] Viayna, E.; Gómez, T.; Galdeano, C. *et al. ChemMedChem* **2010**, *5*, 1855–1870.

4.2. Repurposing and further optimization of 4-aminoquinoline-based anti-Alzheimer AChE inhibitors toward new HAT therapies (*Bioorg. Med. Chem. Lett*. **2014**, *24*, 5435; *Bioorg. Med. Chem*. **2015**, *23*, 5156; and *Bioorg. Med. Chem*. **2016**, in press)

Given the astonishing trypanocidal activity of huprine Y (**11**, *T. brucei* IC_{50} = 0.61 µM and IC_{90}= 2.94 µM, **Figure 4.2**),[206] an originally anticholinesterasic compound with potential anti-Alzheimer activity,[201] but the unexpected lack of antiplasmodial activity despite its structural similarity with chloroquine, the next projects to be developed in this PhD thesis envisaged the hit-to-lead optimization of huprine derivatives regarding trypanocidal activity. For that purpose, we firstly wanted to carefully explore the trypanocidal activity of huprine homo- and heterodimers (**series I-IV, Figure 4.2**), as molecular dimerization constitute nowadays a widely used strategy in NTD drug discovery, and in particular in trypanosomiasis, aimed at improving biological properties as well as overcoming drug resistances[179] (*Bioorg. Med. Chem. Lett.* **2014**, *24*, 5435; and *Bioorg. Med. Chem.* **2015**, *23*, 5156). Furthermore, because side chain modification of 4-aminoquinoline derivatives has been also used to improve antiprotozoal potency and to overcome resistance, the synthesis and antitrypanosomal evaluation of a novel series of *N*-cyanoalkyl-, *N*-aminoalkyl- and *N*-guanidinoalkyl-huprine or (6-chloro)tacrine derivatives (**series V, Figure 4.2**) was also envisioned (*Bioorg. Med. Chem.* **2016**, submitted).

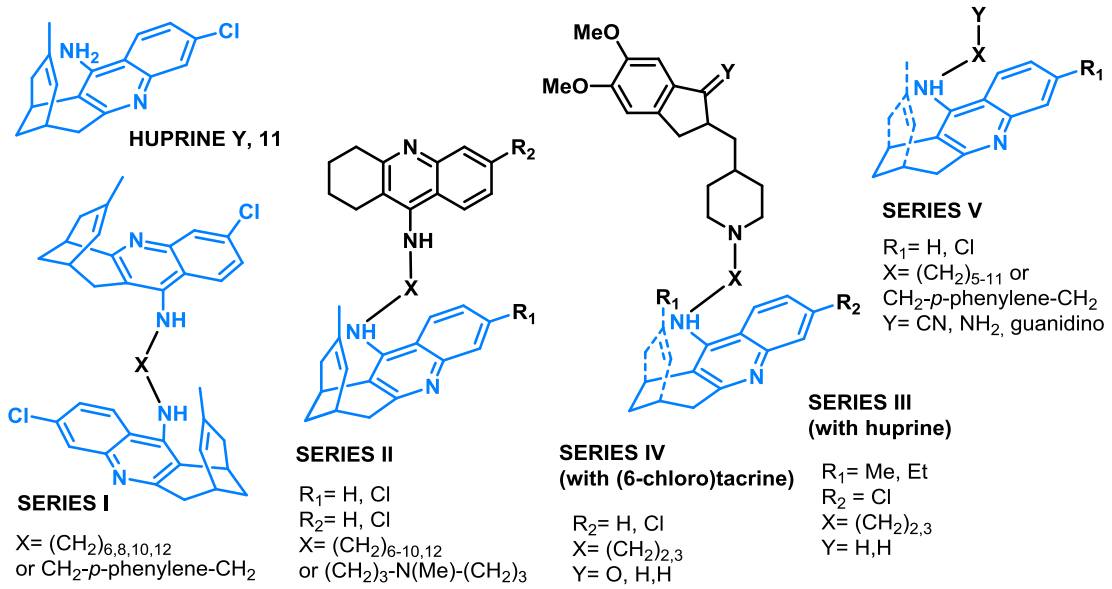

Figure 4.2. Series of huprine-based homodimers, heterodimers, and modified side chain derivatives for HAT treatment.

[179] Kaur, K.; Jain, M.; Reddy, R. P. *et al*. *Eur. J. Med. Chem.* **2010**, *45*, 3245–3264.
[201] Camps, P.; El Achab, R.; Morral, J. *et al. J. Med. Chem.* **2000**, *43*, 4657–4666.
[206] Defaux, J.; Sala, M.; Formosa, X. *et al*. *Bioorg. Med. Chem.* **2011**, *19*, 1702–1707.

4.3. Searching for new safe and cost-effective antimalarial treatments: novel substrate analog PfG6PD inhibitors (*Draft of the manuscript*)

A collaboration with Prof. Javier Luque (*Universitat de Barcelona*) embarked us in a new project towards the development of a novel antimalarial treatment. Starting from a homology model of *Pf*G6PD, a molecular modelling-guided design and synthesis of a novel family of substrate analog selective inhibitors of *Pf*G6PD (**Figure 4.3**) was envisioned, by exploiting the structural differences found at the catalytic site between the parasite and human enzymes.

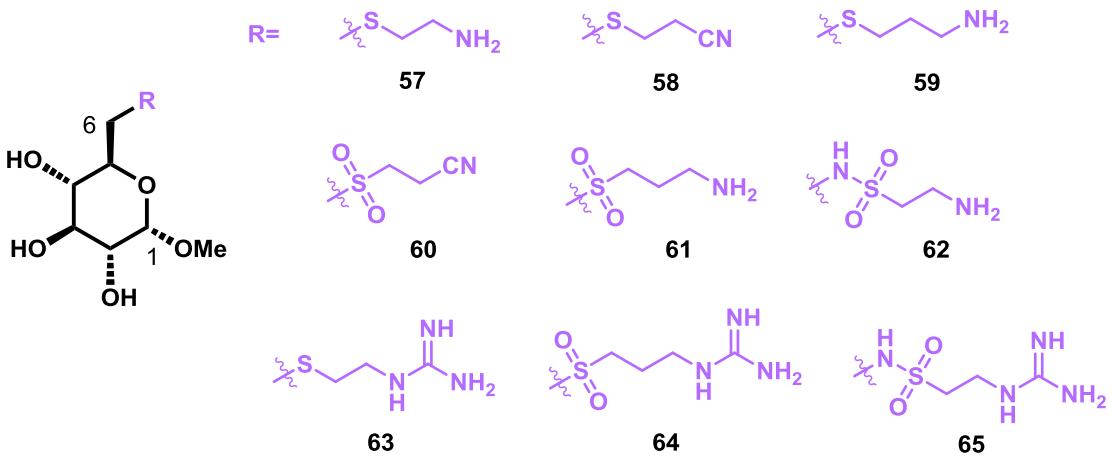

Figure 4.3. General structure of these glucose-based compounds (at the left hand) and the different chemical modifications at position 6 (at the right hand).

For the preparation of this short series of compounds, straightforward synthetic routes were envisaged, involving the common starting material methyl 6-chloro-6-deoxy-α-D-glucopyranoside, **67**, easily accessible from the commercially available methyl α-D-glucopyranoside, **66** (**Scheme 4.1**).

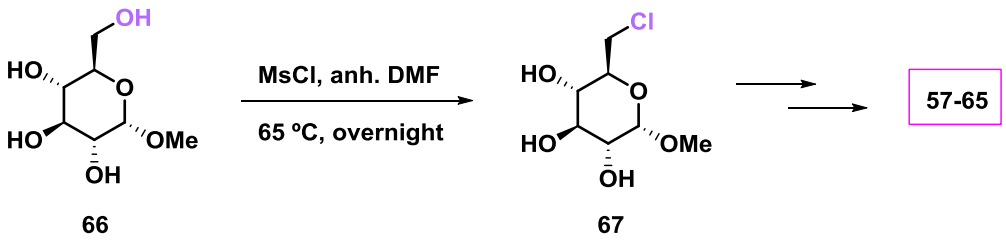

Scheme 4.1. Preparation of the starting material for the synthesis of the target substrate analog inhibitors **57–65**.

CHAPTER 5

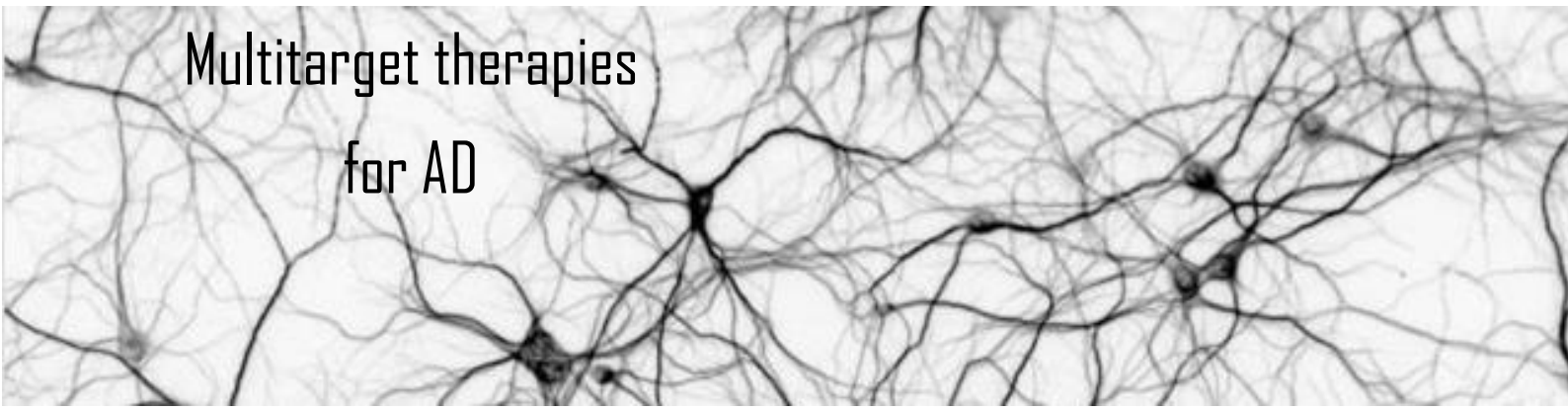

Multitarget therapies for AD

5.1. Multitarget therapy for AD treatment

The elusive finding of an effective disease-modifying anti-Alzheimer drug has been ascribed in a great part to the use of a single target-based reductionist approach rather than a multitarget therapeutic strategy.[337,338,339] This derives from the growing conception that AD pathology might not result from a straightforward process that begins with Aβ formation and aggregation[16,340] but from a robust network of interconnected events, whereby Aβ is just one and not the root cause of AD, together with tau hyperphosphorylation and aggregation, synaptic dysfunction, or neuroinflammation.[341] Therefore, a complex therapeutic approach that does not modulate single proteins but imbalances of multiple proteins within an interaction network is required to efficiently tackle such complex neurodegenerative disorder.[104d]

With this aim in mind, the MTDL strategy has emerged to provide new opportunities to help in the reduction of the neurodegenerative changes observed in AD.[342] In most cases, MTDL have been purposely designed to simultaneously hit at least Aβ formation and aggregation, and AChE activity,[343,344,345,346,347,348,349] especially prompted by the breakthrough that the PAS of AChE can bind Aβ, thereby promoting its aggregation in an early stage of the neurodegenerative cascade and increasing its neurotoxicity (see section **1.3.1.2.** and **1.3.1.3.**).[76] Moreover, another extensively pursued MTDL approach also involves the combination of two distinct pharmacophoric moieties in a single molecule, usually through a hybrid molecule formation,

[16] Hardy, J.; Selkoe, D. J. *Science* **2002**, *297*, 353−356.
[76] Inestrosa, N. C.; Dinamarca, M. C.; Alvarez, A. *FEBS J.* **2008**, *275*, 625−632.
[104d] Viayna, E.; Sola, I.; Di Pietro, O. *et al*. *Curr. Med. Chem.* **2013**, *20*, 1623−1634.
[337] Bajda, M.; Guzior, N.; Ignasik, M. *et al*. *Curr. Med. Chem*. **2011**, *18*, 4949−4975.
[338] Russo, P.; Frustaci, A.; Del Bufalo, A. *et al*. *Curr. Med. Chem*. **2013**, *20*, 1686−1693.
[339] Muñoz-Torrero, D. *Curr. Med. Chem.* **2013**, *20*, 1621−1622.
[340] Kung, H. F. *ACS Med. Chem. Lett*. **2012**, *3*, 265−267.
[341] Pimplikar, S. W. *Int. J. Biochem. Cell Biol*. **2009**, *41*, 1261−1268.
[342] Citron, M. *Nature Rev. Drug Discovery* **2010**, *9*, 387−398.
[343] Du, D. M.; Carlier, P. R. *Curr. Pharm. Des.* **2004**, *10*, 3141−3156.
[344] Recanatini, M.; Valenti, P. *Curr. Pharm. Des.* **2004**, *10*, 3157−3166.
[345] Li, W. M.; Kan, K. K. W.; Carlier, P. R. *et al*. *Curr. Alzheimer Res.* **2007**, *4*, 386−396.
[346] Holzgrabe, U.; Kapková, P.; Alptüzün, V. *et al. Expert Opin. Ther. Targets* **2007**, *11*, 161−179.
[347] Musial, A.; Bajda, M.; Malawska, B. *Curr. Med. Chem.* **2007**, *14*, 2654−2679.
[348] Haviv, H.; Wong, D. M.; Silman, I. *et al*. *Curr. Top. Med. Chem.* **2007**, *7*, 375−387.
[349] Rampa, A.; Belluti, F.; Gobbi, S. *et al*. *Curr. Top. Med. Chem.* **2011**, *11*, 2716−2730.

endowing it with additional key target interactions related to the underlying mechanism of AD pathogenesis.[350,351]

It is important to note that a suitable MTDL therapy should not only have the ability of blocking several key targets simultaneously, but also balancing the most appropriate ratio of potencies of the drug at its different targets, which becomes, even though not impossible, a tricky task. Despite that, it has proved to be feasible as evidenced by the clinical efficacy of many known drugs retrospectively found to be inherently multitarget, and also of some rationally designed MTDLs (see section **1.3.3**). [104d,352]

On the basis of these premises, some MTDL families have been also prepared in our research group. The huprines' finding, among them the eutomer of the so-called huprine Y, (−)-**11** (**Figure 5.1.**), which turned out to be one of the highest affinity AChE CAS inhibitor (hAChE IC_{50} = 0.74 nM),[87] spurred the development of several huprine-based dual binding site AChEIs families (DBS, see section **1.3.1.3.**). These DBS inhibitors comprise a huprine or related aminoquinoline moiety, as the active site interacting unit, attached through a linker to another pharmacophoric moiety, usually containing an aromatic ring capable of establishing π−π stacking interactions with the characteristic aromatic residue at the PAS of AChE, namely Trp286, as huprine-tacrine heterodimers do,[88b] besides cation−π interactions, as pyrido[3,2-c]quinoline-chlorotacrine hybrids are able to perform,[88a,353] thereby reinforcing its enzyme affinity (**Figure 5.2**).

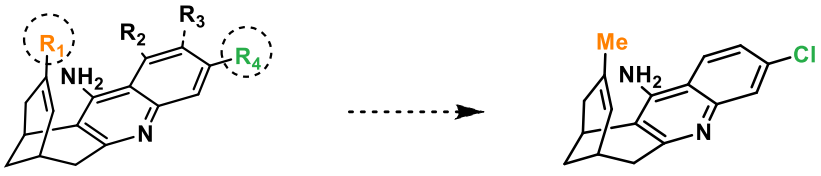

General structure of huprines

R_1 = Me, Et; **R_2** = H, CH_3, F, Cl;
R_3 = H, Cl; **R_4** = H, CH_3, F, Cl

Huprine Y, **11**

(±)-**11**, hAChE IC_{50}= 1.07 nM
(+)-**11**, hAChE IC_{50}= 321 nM
(−)-**11**, hAChE IC_{50}= 0.74 nM

Figure 5.1. Left: General structure of the most potent huprines. Right: Huprine Y structure and its inhibitory activities against AChE.

[87] a) Camps, P.; El Achab, R.; Görbig, D. M. *et al. J. Med. Chem.* **1999**, *42*, 3227−3242. b) Muñoz-Torrero, D.; Camps, P. *Expert Opin. Drug Dis.* **2008**, *3*, 65−81.
[88] a) Camps, P.; Formosa, X.; Galdeano, C. *et al. J. Med. Chem.* **2009**, *52*, 5365−5379. b) Galdeano, C.; Viayna, E.; Sola I. et al. *J. Med. Chem*. **2012**, *55*, 661−669.
[104d] Viayna, E.; Sola, I.; Di Pietro, O. *et al*. *Curr. Med. Chem.* **2013**, *20*, 1623−1634.
[350] Bolognesi, M. L. *Curr. Med. Chem*. **2013**, *20*, 1639−1645.
[351] Morphy, R.; Rankovic, Z. *J. Med. Chem*. **2006**, *49*, 4961−4970.
[352] Weinreb, O.; Amit, T.; Bar-Am, O. *et al*. *Curr. Drug Targets* **2012**, *13*, 483−494.
[353] Di Pietro, O.; Viayna, E.; Vicente-García, E. *et al. Eur. J. Med. Chem.* **2014**, *73*, 141−152.

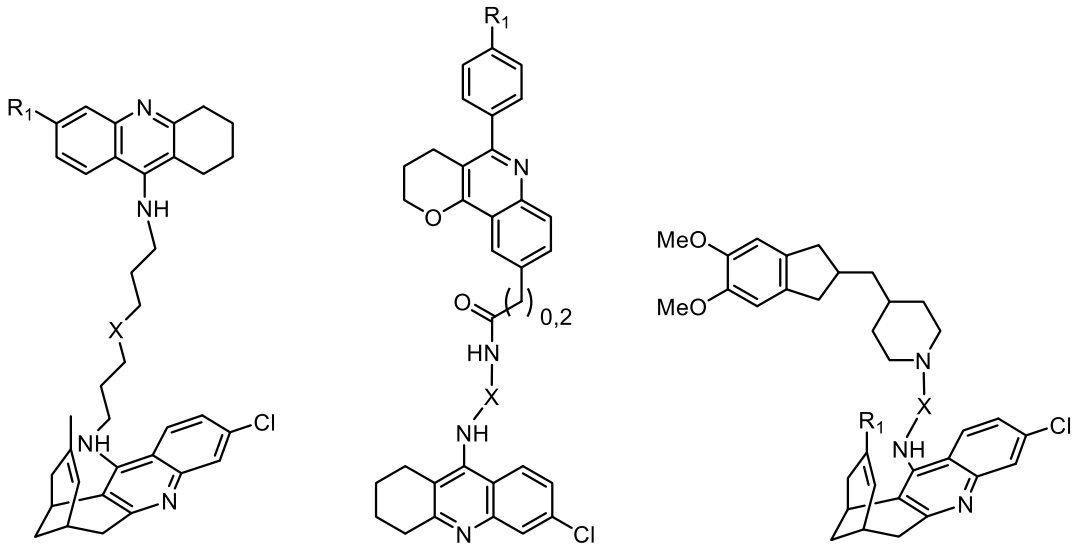

Huprine-tacrine heterodimers | **Pyrido[3,2-*c*]quinoline-chlorotacrine hybrids** | **Donepezil-huprine hybrids**

Figure 5.2. DBS AChEIs developed in our research group.

Among some DBS developed, the series of donepezil−huprine hybrids (**Figure 5.2**) has recently been shown to exhibit apart from a highly potent hAChE inhibition (IC_{50} = 2.61−49.9 nM), a moderate hBChE inhibition (IC_{50} = 61−419 nM), and reduction of the hAChE-induced Aβ40 aggregation (25−50% of inhibition at 100 μM concentration of inhibitor) and the self-induced Aβ-aggregation (16−30% of inhibition at 10 μM concentration of inhibitor), an astonishing *in vitro* inhibitory activity towards BACE-1 (12−31% inhibition at 5 μM concentration of inhibitor),[89d] as it has been found in several DBS AChEIs[112,354] even though they were not purported to display this activity.[355] Indeed, this excellent multitarget profile led to an *in vivo* study in APPSL mice for 3 months, partially supported by "Fundación para el Desarrollo de la Investigación en Genómica y Proteómica (Fundación Genoma España)", with the hit compound AVCRI104P4 (**68**, **Figure 5.3**) of the donepezil-huprine series. The *in vivo* study resulted in an improved short-term memory in the Morris Water Maze test, but AVCRI104P4 did not alter brain levels of Aβ peptides nor cortical and hippocampal amyloid plaque load. Therefore, despite the clear protective and cognitive effects that **68** showed *in vitro* (**Figure 5.3**), this lack of Aβ lowering effect *in vivo* might be a consequence of an imbalance of potencies at the different targets.[89e]

[89d] Viayna, E.; Gómez, T.; Galdeano, C. *et al*. *ChemMedChem* **2010**, *5*, 1855−1870.
[89e] Sola, I.; Viayna, E.; Gómez, T. *et al. Molecules* **2015**, *20*, 4492−4515.
[112] Cavalli, A.; Bolognesi, M. L.; Capsoni, S. *et al. Angew. Chem. Int. Ed. Engl.* **2007**, *46*, 3689−3692.
[354] Fu, H.; Li, W.; Luo, J. *et al*. *Biophys. Res. Commun.* **2008**, *366*, 631−636.
[355] Galdeano, C.; Viayna, E.; Arroyo, P. *et al. Curr. Pharm. Des*. **2010**, *16*, 2818−2836.

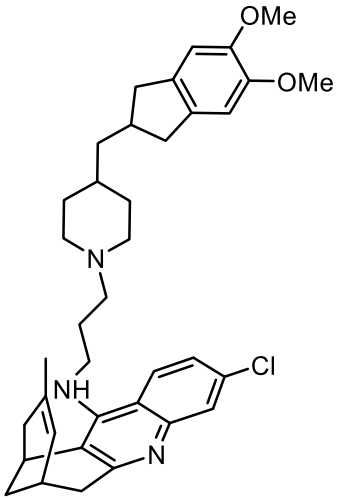

(−)-(7*S*,11*S*)-**68,** AVCRI104P4

IC_{50} hAChE (nM) = **2.61 ± 0.2**

IC_{50} hBChE (nM) = **349 ± 20**

Inhibition of hAChE-induced Aβ40 aggregation at 100 μM concentration (**%**): **41.5 ± 2.4**

Inhibition of self-induced Aβ-aggregation at 10 μM concentration (**%**): **29.0 ± 2.0**

BACE-1 inhibition at 5 μM concentration (**%**): **30.8 ± 4.1**

Figure 5.3. Hit compound of donepezil-huprine series and its *in vitro* results.

These new evidences and knowledge on the design of MTDLs prompted us to further synthesize novel hybrid molecules potentially endowed with additional interesting pharmacological properties.

5.2. Rhein−huprine hybrids (*J. Med. Chem*. **2014**, *57*, 2549; and *Curr. Alzheimer Res.* **2016**, *13*, 1017)

The group of Dr. Eckhard Mandelkow from the Max-Plank Unit for Structural Molecular Biology in Hamburg found out five hit compounds, from a HTS test of 200,000 compounds, with the special feature of possessing a polycyclic aromatic ring system derived from hydroxyanthraquinone, hydroxybenzophenone, or hydroxynaphthacendione, **69**−**73**, (Figure **5.4**) and the shared ability of inhibiting tau protein assembles into abnormal fibers (PHF) (**Figure 5.5.**).[356] Specifically, they all showed to be able to inhibit the transition from soluble to aggregated PHFs,[357,358] using fixed protein concentrations, and measuring the extent of aggregation via the fluorescence of thioflavine S, with IC_{50} values in the low micromolar range (IC_{50}= 1−5 μM).[359,360] More interestingly, the ability of compounds **69**−**73** to dissolve preformed PHFs was also tested using the thioflavine S assay to find that they exhibited again IC_{50} values in the low micromolar range (IC_{50}= 2−4 μM).

[356] Pickhardt, M.; Gazova, M.; von Bergen, M. *et al. Biol. Chem*. **2005**, *5*, 3628−3635.
[357] Von Bergen, M.; Friedhoff, P.; Biernat, J. *et al. Proc. Natl. Acad. Sci. U. S. A.* **2000**, *97*, 5129−5134.
[358] Von Bergen, M.; Barghorn, S.; Li, L. *et al*. *J. Biol. Chem*. **2001**, *276*, 48165−48174.
[359] Friedhoff, P.; Schneider, A.; Mandelkow, E. M. *et al*. *Biochemistry* **1998**, *37*, 10223−10230.
[360] Bulic, B.; Pickhardt, M.; Schmidt, B. *et al. Angew. Chem. Int. Ed*. **2009**, *48*, 1740−1752.

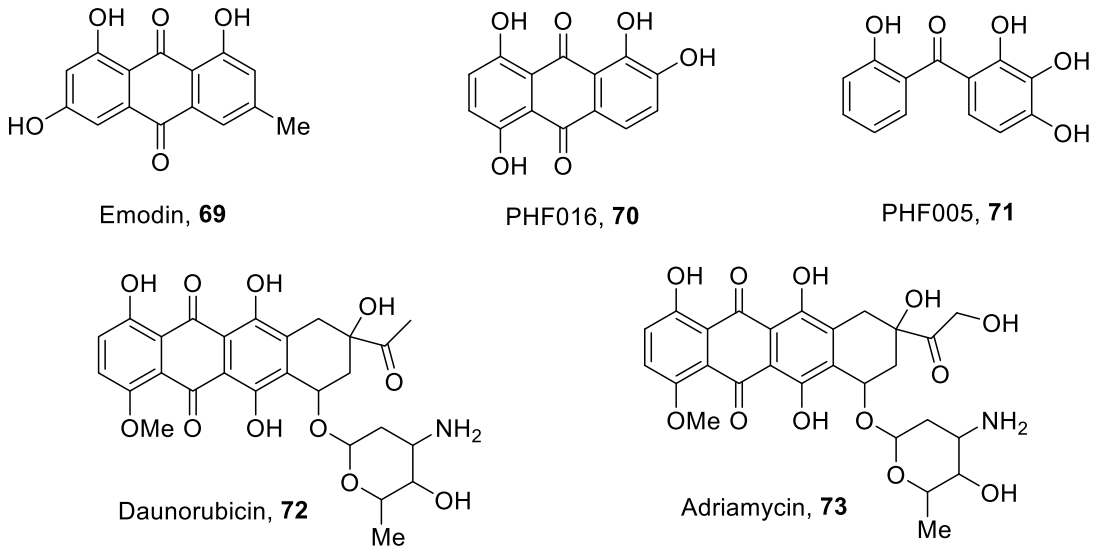

Figure 5.4. Structure of tau protein aggregation inhibitor hits **69–73**.

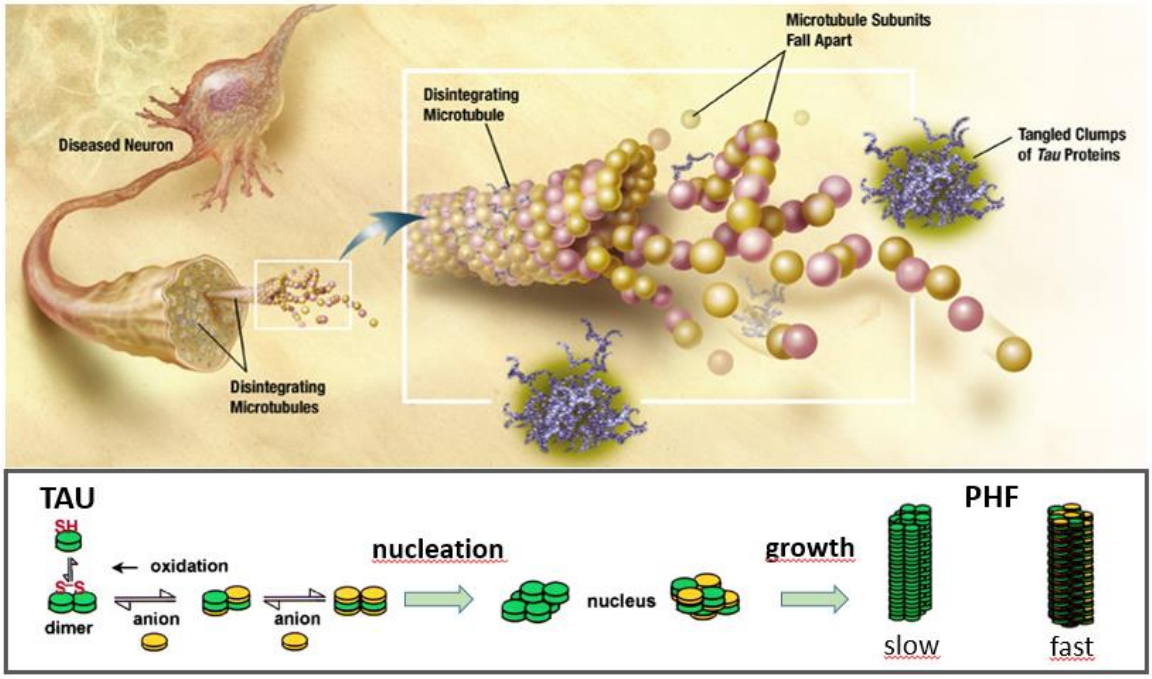

Figure 5.5. Above: Diagram showing disintegration of brain cells, as a result of tau hyperphosphorylation that leads to microtubule disintegration and tau aggregation into PHF assembles. Below: Nucleated assembly mechanism of Alzheimer's PHF. Tau monomers form homodimers by oxidation of SH groups; these dimers represent the effective assembling species of PHFs. About 4–7 dimers can form nuclei, which then elongate into PHFs. This process is normally very slow (days to weeks), but both nucleation and elongation of PHFs might greatly

accelerate by anionic cofactors (Image source: Freiedhoff, P. *et al. Proc. Natl. Acad. Sci. U. S. A*. **1998**, *95*, 15712−15717).

With these results in mind and taking into account that the intraneuronal accumulation of hyperphosphorylated tau protein and aggregation into PHFs and, later on, into NFT, is one of the hallmarks of AD[361,362] and that inhibition or reversal of tau aggregation seems likely to protect the affected neurons,[356] in the present PhD Thesis work and that of Dr. Elisabeth Viayna, a novel MTDL family named "rhein-huprine hybrids", **74a–g,** was prepared according to the retrosynthetic route depicted below (**Scheme 5.1**). This novel family combines the potent catalytic anionic site (CAS) AChE inhibitor, huprine Y (in a racemic form), (±)-**11**, and an anthraquinone fragment derived from rhein, **75**, a natural product found in the traditional Chinese herbal medicine rhubarb with anticarcinogenic properties,[363] connected through an amide-containing oligomethylene or aromatic linker. Thus, the rationale behind this design strategy was to enable a putative tau antiaggregating effect from the rhein unit, apart from the conventional effects derived from dual site AChE interaction.

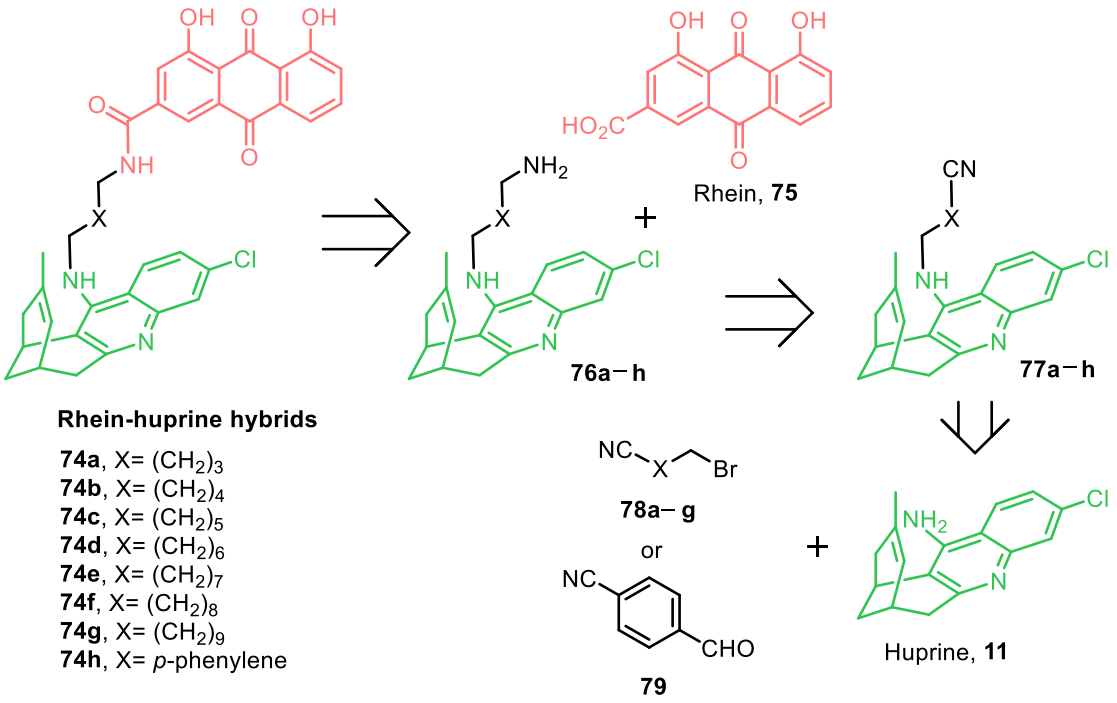

Scheme 5.1. General structure and retrosynthetic analysis of the rhein−huprine hybrids, (±)-**74a−h**.

[356] Pickhardt, M.; Gazova, M.; von Bergen, M. *et al. Biol. Chem*. **2005**, *5*, 3628−3635.
[361] Freiedhoff, P.; von Bergen, M. *et al. Proc. Natl. Acad. Sci. U. S. A*. **1998**, *95*, 15712−15717.
[362] NIH website. The hallmarks of AD. (https://www.nia.nih.gov/alzheimers/publication/part-2-what-happens-brain-ad/hallmarks-ad).
[363] Yang, X.; Sun, G.; Yang, C. *et al*. *ChemMedChem* **2011**, *6*, 2294−2301.

As the racemic nonamethylene rhein−huprine hybrid, (±)-**74e**, showed the best *in vitro* pharmacological profile, the corresponding enantiomers, (+)- and (−)-**74e** were also prepared, and later evaluated *in vitro*, *ex vivo*, and *in vivo* in transgenic AβPPswe/PS1 mice model.

5.2.1. Synthesis of rhein−huprine hybrids

For the synthesis of the desired rhein−huprine hybrids, a first alkylation of racemic or enantiopure huprine Y, (±)-, (+)-, and (−)-**11**, with the corresponding ω-bromoalkanenitrile **78a–g** in the presence of NaOH in DMSO at r. t. overnight was performed. This reaction gave crude mixtures of the desired cyanoalkylhuprines, unreacted huprine Y, and dialkylation byproducts which were purified through silica gel column chromatography to provide separately pure racemic cyanoalkylhuprines (±)-**77a–g**, and enantiopure (+)- and (−)-**77e** (**Scheme 5.2**) in moderate to good yields (25−87%). It is important to note that ω-bromoalkanenitriles **78a–c** were commercially available, however, **78d–g** had to be prepared by reaction of the appropriate dibromoalkanes with NaCN, followed by microdistillation of the reaction crudes in order to isolate the desired ω-bromoalkanenitrile from the unreacted dibromoalkane and direaction byproducts. Of note, some cyanoalkylhuprines and dialkylation byproducts were further assessed as antiprotozoal agents, as we will see in the next chapter (see **section 6.3**).

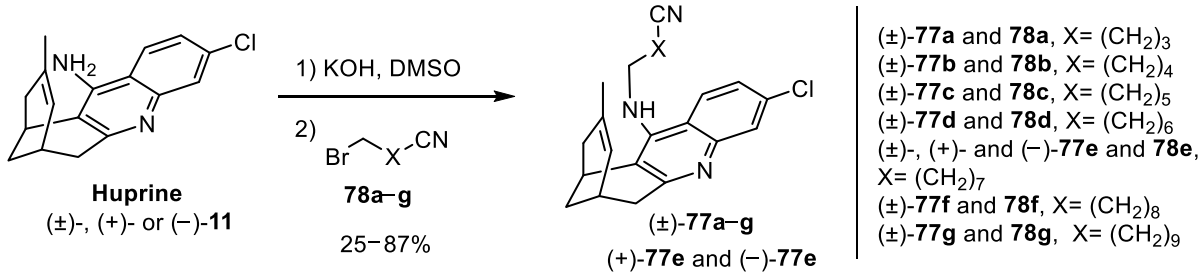

Scheme 5.2. Synthesis of racemic and enantiopure cyanoalkylhuprine products, (±)-**77a–g**, (+)- and (−)-**77e.**

The rhein−huprine hybrid (±)-**77h**, containing a *p*-phenylene moiety in the linker (**Scheme 5.3**), which was designed in order to gain additional π−π stacking interactions with AChE mid-gorge residues, was synthesized by reductive alkylation, because usual nucleophilic substitution with the corresponding 4-(bromomethyl)benzonitrile, **80**, did not work. Thus, reaction of (±)-huprine Y, (±)-**11**, with *p*-cyanobenzaldehyde, **79**, in the presence of freshly distilled morpholine, in toluene, heating under reflux for 48 h, provided after purification through silica gel column chromatography (±)-**81** in 79% yield. Imine (±)-**81** was then reduced with $NaBH_3CN$ in glacial AcOH at r. t. for 3 h to give (±)-**77h** in 91% yield.

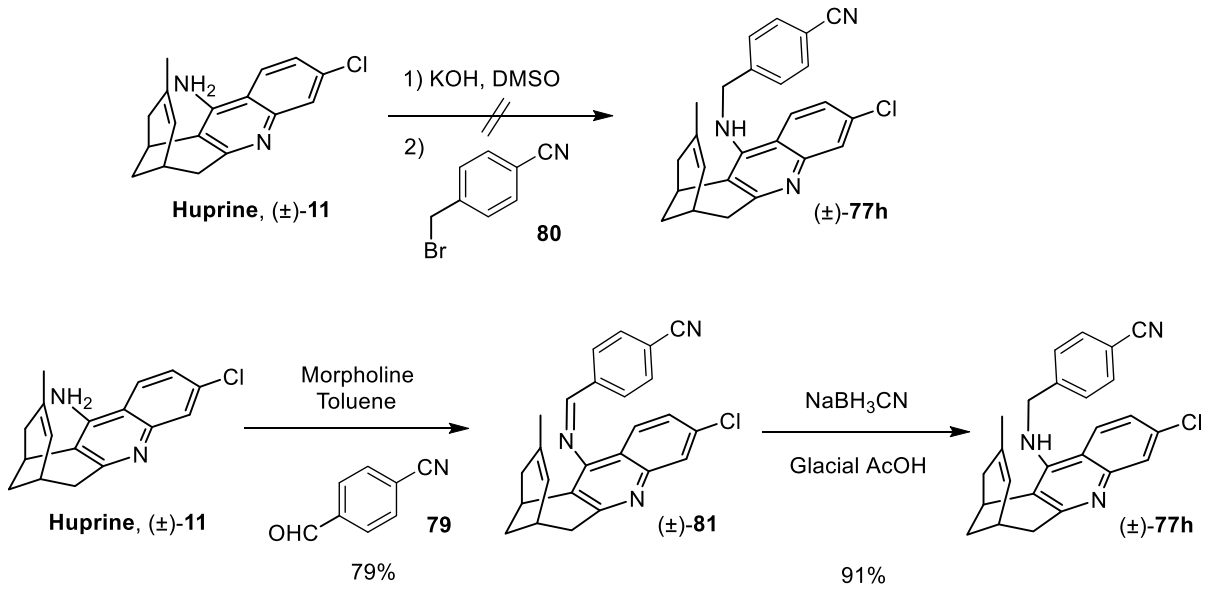

Scheme 5.3. Preparation of cyanoarylalkylhuprine (±)-**77h.**

Afterwards, cyanoalkyl- and cyanoarylalkylhuprines (±)-**77a–h,** (+)- and (−)-**77e**, were reduced with $LiAlH_4$ in Et_2O at r. t. overnight to afford the corresponding aminoalkylhuprines (±)-**76a–h,** (+)- and (−)-**76e** in excellent yields and with no need of purification (**Scheme 5.4**).

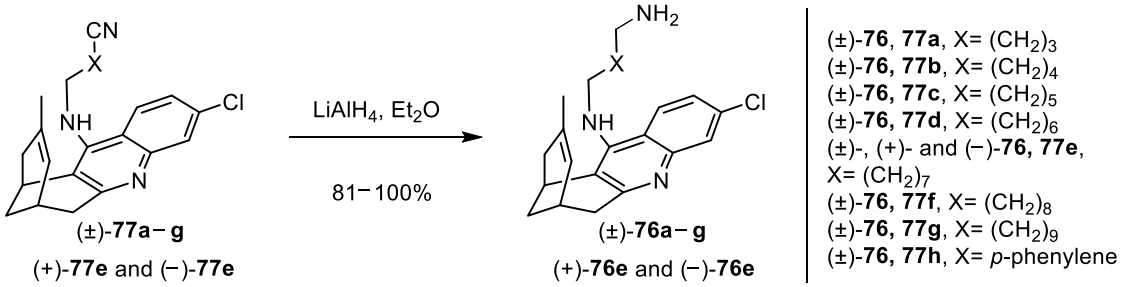

Scheme 5.4. Reduction of cyano intermediates to obtain aminoalkylhuprines (±)-**76a–h,** (+)- and (−)-**76e**.

Finally, rhein, **75**, was treated with freshly distilled Et_3N and $ClCO_2Et$ in CH_2Cl_2 at 0 °C for 30 min and the resulting mixed anhydrides were reacted with aminoalkylhuprines (±)-**76a–h,** (+)- and (−)-**76e** at r. t. for three days, to afford the desired racemic hybrids, (±)-**74a–h**, and enantiopure hybrids, (+)- and (−)-**74e**, in low to moderate yields (9–27%) after a tedious silica gel column chromatography purification (**Scheme 5.5**).

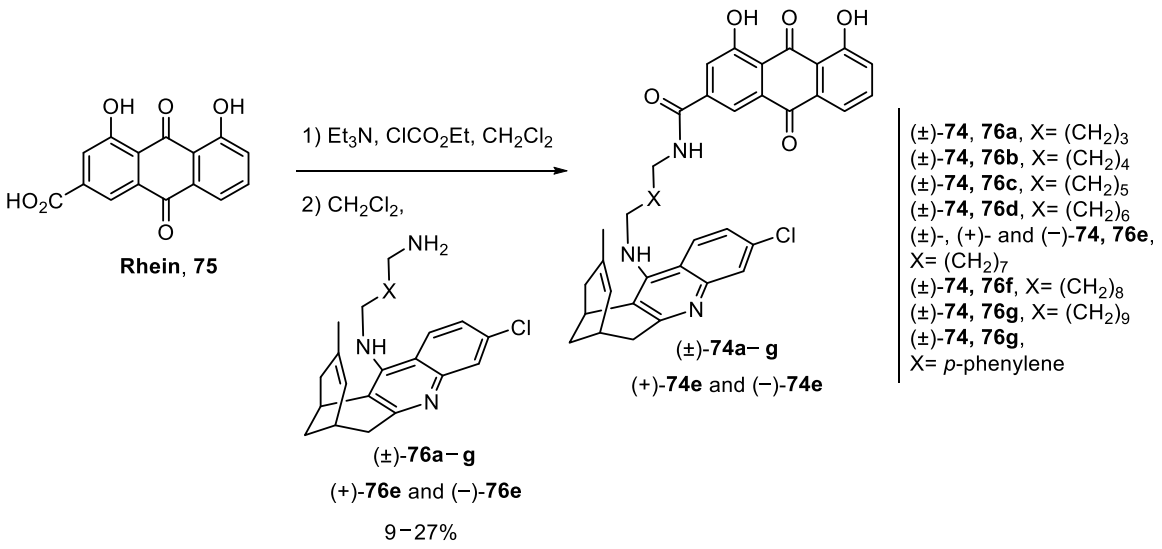

Scheme 5.5. Final step for the obtention of the target rhein–huprine hybrids (±)-**74a–h,** (+)- and (–)-**74e**.

5.2.2. In vitro, ex vivo, and in vivo evaluation of rhein–huprine hybrids

The *in vitro* biological profiling of the rhein–huprine hybrids was carried out by the groups of Drs. M. Victòria Clos and Belén Pérez (Universitat Autònoma de Barcelona), Raimon Sabaté (Universitat de Barcelona), and Vincenza Andrisano, Manuela Bartolini, and Angela De Simone (Università di Bologna), whereas the *ex vivo* and *in vivo* assays were carried out by the group of Nibaldo Inestrosa (Pontificia Universidad Católica de Chile). The molecular modeling studies of the interaction of these compounds with two of their main biological targets, AChE and BACE-1, were carried out by the group of Dr. F. Javier Luque (Universitat de Barcelona).

In vitro biological assays as well as molecular modeling studies have demonstrated, in agreement with the design rationale, that rhein–huprine hybrids, (±)-**74a–h**, act as multitarget agents. Hybrids (±)-**74a–h** were able to induce AChE inhibition (hAChE IC_{50} = 1.07–18.2 nM) and reduction of Aβ aggregation (29–52% inhibition of hAChE-induced Aβ40 aggregation with inhibitor at 100 μM concentration and 32–41% inhibition of self-induced Aβ42 aggregation at 10 μM concentration), mainly as a result of simultaneous blockade of CAS and PAS of AChE. All this series was also shown to be moderately potent BChEIs (hBChE IC_{50} = 620–1460 nM); inhibitory potency recently pursued due to the observed co-regulator BChE role in advanced stages of AD.[32] Moreover, in a simplified *in vivo* assay with intact *Escherichia coli* cells, developed by

[32] Greig, N. H.; Utsuki, T.; Ingram, D. K. *et al. Proc. Natl. Acad. Sci. U. S. A.* **2005**, *102*, 17213–17218.

Dr. Raimon Sabaté from *Universitat de Barcelona*,[364,365] the ability of our compounds to inhibit tau aggregation was also tested, ranging from 23 to 57% at 10 μM concentration of inhibitor, whereas the inhibition of Aβ aggregation by this method, was 40 to 68% inhibition of Aβ aggregation at 10 μM concentration of inhibitor, slightly higher than those found *in vitro*. Interestingly, separately rhein showed moderate inhibition of Aβ (50%) and tau aggregation (41%) whereas huprine did not show any activity. Additionaly, using the widely known parallel artificial membrane permeability assay (PAMPA-BBB)[366] with a lipid extract of porcine brain as artificial membrane, these compounds were predicted to be able to cross the blood–brain barrier, and, therefore, to reach their multiple targets in central nervous system.

More strikingly, longer hybrids (±)-**74d**, (±)-**74f**, and (±)-**74g**, as well as (±)-**74h** showed to be moderately potent BACE-1 inhibitors with IC_{50} values around 1−2 μM, whereas the nonamethylene-linked hybrid (±)-**74e** displayed the most potent BACE-1 inhibitory activity (IC_{50} = 120 nM). In contrast, the shorter homologues, from pentamethylene- to heptamethylene-linked hybrids (±)-**74a–c**, were totally inactive.

Of note, molecular modeling studies suggested that the rhein−huprine hybrids can establish a dual site binding not only within AChE, but also within BACE-1, in the latter case involving a so far unexplored secondary binding site, which is adjacent to the catalytic site. The dual site binding to both AChE and BACE-1 would account for their high potency against these enzymes.

In the light of the outstanding BACE-1 inhibitory effect of (±)-**74e**, which additionally displayed one of the best profile against other crucial targets of the AD pathogenesis, hAChE, hBChE and dual Aβ and tau aggregation, we were prompted to also synthesize separately both enantiomers of **74e** following the same methodology as that used for the rest of the series but in this case using enantiopure huprines Y, (+)-**11** and (−)-**11**, as starting material. Then, pharmacological evaluation of enantiopure nonamethylene rhein−huprine hybrids, (+)- and (−)-**74e**, revealed them as the most potent BACE-1 inhibitors ever synthesized in our research group, with an IC_{50} value of 80 nM, a 3-fold higher inhibitory potency than that exerted by Lilly's candidate LY2811376 (IC_{50} = 239 nM), whose phase I clinical trials were recently discontinued due to toxicity issues unrelated to BACE-1 inhibition.[367] It is important to note, no enantioselectivity for the different target interactions were unveiled between both enantiomers, with the exception of hAChE inhibition which was sharply different, with (−)-**74e** being >1000-fold more potent

[364] Martson, F. A. *Biochem. J.* **1986**, *240*, 1−12.
[365] Waldo, G. S.; Standish, B. M.; Berendzen, J. *et al*. *Nat. Biotechnol*. **1999**, *17*, 691−695.
[366] Di, L.; Kerns, E. H.; Fan, K. *et al*. *Eur. J. Med. Chem*. **2003**, *38*, 223−232.
[367] May, P. C.; Dean, R. A.; Lowe, S. L. *et al. J. Neurosci.* **2011**, *31*, 16507−16516.

anticholinesterasic than its counterpart (+)-**74e** (**Figure 5.6**), as it analogously happens for huprine Y enantiomers [(7*S*,11*S*)- or (−)-**11,** hAChE IC_{50} = 0.74 nM and (7*R*,11*R*)- or (+)-**11**, hAChE IC_{50} = 321 nM][87a] and other huprine-based hybrids previously developed in our research group.[88b]

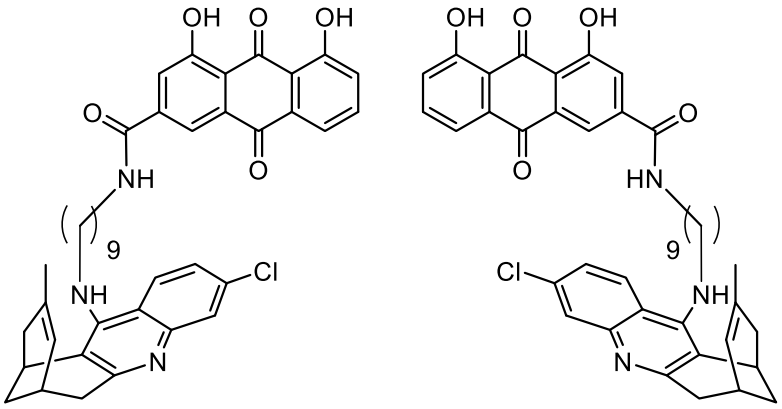

IN VITRO

hAChE IC_{50}	2.39 nM	2930 nM
hBChE IC_{50}	513 nM	265 nM
BACE-1 IC_{50}	80 nM	80 nM
Inhibition of Aβ42 aggregation (10 μM)	43%	38%

IN VIVO (intact *E. coli* cells)

Inhibition of Aβ42 aggregation (10 μM)	47%	59%
Inhibition of tau aggregation (10 μM)	34%	25%

Figure 5.6. Lead compounds of the rhein−huprine series, (−)- and (+)-**74e**, and their biological profile (*in vitro* and in *E. coli* cells).

To gain further insight into the disease-modifying effects of these novel hybrids, the two selected leads, enantiomers (+)-**74e** and (−)-**74e**, were assessed *ex vivo* using hippocampal slices from 2-month-old C57bl6 mice and further tested *in vivo* in an appropriate animal model of AD, bearing the AβPP and PS-1 mutant transgenes (AβPPswe/PS1) mice model, thanks to the

[87a] Camps, P.; El Achab, R.; Görbig, D. M. *et al. J. Med. Chem.* **1999**, *42*, 3227−3242.
[88b] Galdeano, C.; Viayna, E.; Sola I. *J. Med. Chem*. **2012**, *55*, 661−669.

collaboration with the renowned group of Prof. Nibaldo Inestrosa at the *Pontificia Universidad Católica de Chile*. This animal model presents a progressive neurodegeneration with the pass of time, featuring an increase in the amount of Aβ oligomers in the hippocampus and cortex,[368,369] which is associated with a reduction of synaptic functions and neurotransmission, producing a disruption of synaptic plastic events such as long term potentiation (LTP),[370,371,372,373] which in turn, is a widely accepted model of learning and memory especially in the CA1 region of the hippocampus[374,375] and is the parameter used to assess the state of synaptic strength.[376,377] In this context, an inhibition of the induction of LTP is related with a loss of cognitive process such as the spatial learning and memory.[378,379]

Ex vivo experiments revealed a protective effect of the lead compounds against the synaptic dysfunction induced by Aβ oligomers, in terms of induction of LTP, in the case of (+)-**74e**, and preservation of the levels of synaptic proteins, more evident for (–)-**74e** during the *ex vivo* assay. *In vivo* assays also showed protective effects, which were more evident for (+)-**74e**, including reduction of amyoid burden and neuroinflammation events, mainly astrogliosis, as well as a reduction of tau hyperphosphorylation and rescue of the cognitive deficits.

Of note, a relevant decrease in the levels of toxic Aβ42 peptide and amyloid 42/40 ratio in the hippocampus of transgenic mice was also observed only after treatment with hybrid (+)-**74e**, in accordance with the remarkable *in vitro* BACE-1 inhibition (IC_{50} = 80 nM).

Overall, the rhein−huprine hybrid (+)-**74e** emerges as a very promising multitarget anti-Alzheimer drug candidate with potential to prevent and slow disease progression. The rhein−huprine hybrid are currently protected under a US patent (Muñoz-Torrero, D.; Inestrosa, N. M.; Viayna, E.; Sola, I.; Vázquez, S. US 9,238,626 B2).

[368] Serrano-Pozo, A.; Frosch, M, P.; Masliah, E. *et al. Cold Spring Harb. Perspect. Med.* **2011**, *1*, a006189.
[369] Garcia-Alloza, M.; Robbins, E. M.; Zhang-Nunes, S. X. *et al*. *Neurobiol. Dis.* **2006***, 24*, 516−524.
[370] Walsh, D. M.; Klyubin, I.; Fadeeva, J. V. *et al. Nature* **2002**, *416*, 535−539.
[87a] Camps, P.; El Achab, R.; Görbig, D. M. *et al. J. Med. Chem.* **1999**, *42*, 3227−3242.
[88b] Galdeano, C.; Viayna, E.; Sola I. *et al. J. Med. Chem*. **2012**, *55*, 661−669.
[371] Selkoe, D. J. *Science* **2002**, *298*, 789−791.
[372] Shankar, G. M.; Li, S.; Mehta, T. H.; Garcia-Muñoz, A. *et al*. *Nat. Med*. **2008**, *14*, 837−842.
[373] Selkoe, D. J. *Behav. Brain Res*. **2008**, *192*, 106−113.
[374] Ashe, K. H. *Learn Mem.* **2001**, *8*, 301−308.
[375] Martin, S. J.; Grimwood, P. D.; Morris, R. G. *Annu. Rev. Neurosci.* **2000**, *23*, 649-711.
[376] Whitlock, J. R.; Heynen, A. J.; Shuler, M. G. *et al*. *Science* **2006**, *313*, 1093−1097.
[377] Morris, R. G.; Anderson, E.; Lynch, G. S. *et al*. *Nature* **1986**, *319*, 774−776.
[378] Caroni, P.; Donato, F.; Muller, D. *Nat. Rev. Neurosci.* **2012**, *13*, 478−490.
[379] Morris, R. G.; Garrud, P.; Rawlins, J. N. *et al*. *Nature* **1982**, *297*, 681−683.

5.3. Levetiracetam–huprine and levetiracetam–(6-chloro)tacrine hybrids (*J. Med. Chem*. **2015**, *58*, 6018)

Since age is the major risk factor for epilepsy and dementia, both are frequently seen together in the elderly. The incidence of epileptic seizures in patients with dementia is 5–10 times greater than that expected in the general older population. Indeed, between 10−22% of patients with AD experienced at least one spontaneous seizure.[380,381]

It has been recently suggested that aberrant neuronal network activity may be another major and early contributor of AD pathogenesis,[382] which in turn has been associated with high levels of Aβ and causally linked to Aβ-induced synaptic and cognitive deficits.[383] Indeed, AD patients have an increased incidence of epileptic seizures, as we have just mentioned, especially those patients with early onset AD who overexpress human amyloid precursor protein (hAPP) and Aβ as a result of mutations in some deterministic genes such as presenilin 1 and presenilin 2.[384] Increased epileptiform activity also occurs in other conditions which are associated with elevated levels of Aβ such as patients with Down syndrome, which feature three copies of chromosome 21, where the APP gene is located, and the incidence is still higher in individuals with Down syndrome who develop AD.[385]

On the other hand, during an *in vivo* study conducted in transgenic mice that express human mutated APP and thus overproduce Aβ, a relevant emergence of epileptiform activity and seizures was detected.[386] Very interestingly, among multiple antiepileptic drugs tested, only levetiracetam (**82**, Keppra™, **Figure 5.8**) effectively suppressed epileptiform activity in hAPPJ20 and APP/PS1 mouse models of AD;[387,388] for instance, phenytoin and pregabaline conversely increased the abnormal spike activity. In fact, prolonged reduction of abnormal spike activity due to chronic treatment with **82** ameliorated impairments in learning and memory and fully reversed deficits in synaptic transmission and plasticity in the hippocampus of hAPP mice.[380] Moreover, levetiracetam treatment in APP/PS1 mice also alleviated behavioral deficits as well as diminished amyloid plaque burden and tau phosphorylation. The mechanism underlying these

[380] Hommet, C.; Mondon, K.; Camus, V. *et al*. *Dement. Geriatr. Cogn. Disord.* **2008**, *25*, 293−300.
[381] Mendez, M.; Lim, G. *Drugs Aging* **2003***, 20,* 791−803*.*
[382] Palop, J. J.; Mucke, L. *Arch. Neurol.* **2009**, *66*, 435−440.
[383] Palop, J. J.; Mucke, L. *Nat. Neurosci.* **2010**, *13*, 812−818.
[384] Vossel, K. A.; Beagle, A. J.; Rabinovici, G. D. *et al*. *JAMA Neurol.* **2013**, *70*, 1158−1166.
[385] McCarron, M.; Gill, M.; McCallion, P. *et al*. *J. Intellect. Disabil. Res.* **2005**, *49*, 560−566.
[386] Palop, J. J.; Chin, J.; Roberson, E. D. *et al. Neuron* **2007**, *55*, 697−711.
[387] Sanchez, P. E.; Zhu, L.; Verret, L. *et al. Proc. Natl. Acad. Sci. U. S. A.* **2012***, 109,* E2895−E2903.
[388] Shi, J. Q.; Wang, B. R.; Tian, Y. Y. *et al*. *CNS Neurosci. Ther*. **2013**, *19*, 871−881.

observed effects involved increased Aβ clearance and up-regulated Aβ autophagic degradation through GSK-3β deactivation and AMPK activation.[388] Furthermore, chronic treatment with levetiracetam in patients with amnestic mild cognitive impairment (aMCI)[389] also reversed their behavioral abnormalities, cognitive impairments, remodeling of hippocampal circuits, and synaptic deficits, suggesting that these alterations are casually linked to aberrant network activity, thereby highlighting the critical therapeutic potential of targeting excess neuronal network activity, especially in combination with other copathogenic factors that fuel the progression of AD such as Aβ and tau aggregation and accumulation.[383]

The exact mechanism by which levetiracetam counteracts epileptic activity is still under investigation. The antiepileptic efficacy of this drug is not the consequence of inhibiting voltage-gated Na^+ channels, neither the modulation of GABA receptors, as commonly antiepileptic drugs do, but it is established that levetiracetam binds a presynaptic protein, namely the so-called synaptic vesicle protein 2A (SV2A), located in the membrane of synaptic vesicles (**Figure 5.7**).[390]

The binding to SV2A allows levetiracetam to inhibit calcium release from intraneuronal stores and to counteract the activity of negative modulators of GABA- and glycin-gated currents, therefore inhibiting excessive synchronized activity between neurons.[391] Because SV2A plays a modulatory but not an essential role in neurotransmission, it is unclear how a ligand binding to SV2A might alter neurotransmitter release.[392] The most parsimonious interpretation to the beneficial effects exerted by **82** could be the following causal chain: suppression of aberrant network activity, reversal of hippocampal remodeling, and recovery of synaptic and cognitive functions. Interestingly, **82** has been found to reduce neurotransmitter release in a synaptic activity-dependent manner and particularly in excitatory neurons with a sustained and high frequency of firing.[392] In addition, **82** may promote glutamate uptake by increasing glutamate transporter expression.[393] By modulating presynaptic release or glutamate uptake, levetiracetam might prevent excessive glutamate accumulation at the synaptic cleft, preventing overstimulation of postsynaptic glutamate receptors. This mechanism could counteract the pathogenic effects of Aβ, which may cause an increase in glutamate release.[387] Additionally, the

[383] Palop, J. J.; Mucke, L. *Nat. Neurosci.* **2010**, *13*, 812−818.
[388] Shi, J. Q.; Wang, B. R.; Tian, Y. Y. *et al*. *CNS Neurosci. Ther*. **2013**, *19*, 871−881.
[389] Bakker, A.; Krauss, G. L.; Albert, M. S. *et al*. *Neuron* **2012**, *74*, 467−474.
[390] Lynch, B. A.; Lambeng, N.; Nocka, K. *et al. Proc. Natl. Acad. Sci. U. S. A.* **2004**, *101*, 9861−9866.
[387] Sanchez, P. E.; Zhu, L.; Verret, L. *et al. Proc. Natl. Acad. Sci. U. S. A.* **2012***, 109,* E2895−E2903.
[391] Vogl, C.; Mochida, S.; Wolff, C. *et al*. *Mol. Pharmacol.* **2012**, *82*, 199−208.
[392] Meehan, A. L.; Yang, X.; McAdams, B. D. *et al*. *J. Neurophysiol.* **2011***, 106,* 1227−1239.
[393] Ueda, Y.; Doi, T.; Nagatomo, K. *et al*. *Brain Res.* **2007***, 1151,* 55−61.

reduction of calcium release from intraneuronal stores by levetiracetam might help to prevent Aβ-induced calcium dysregulation, and eventually avoid the neuronal apoptosis, as Dr. Inestrosa claimed about calcium blockade effect.[394]

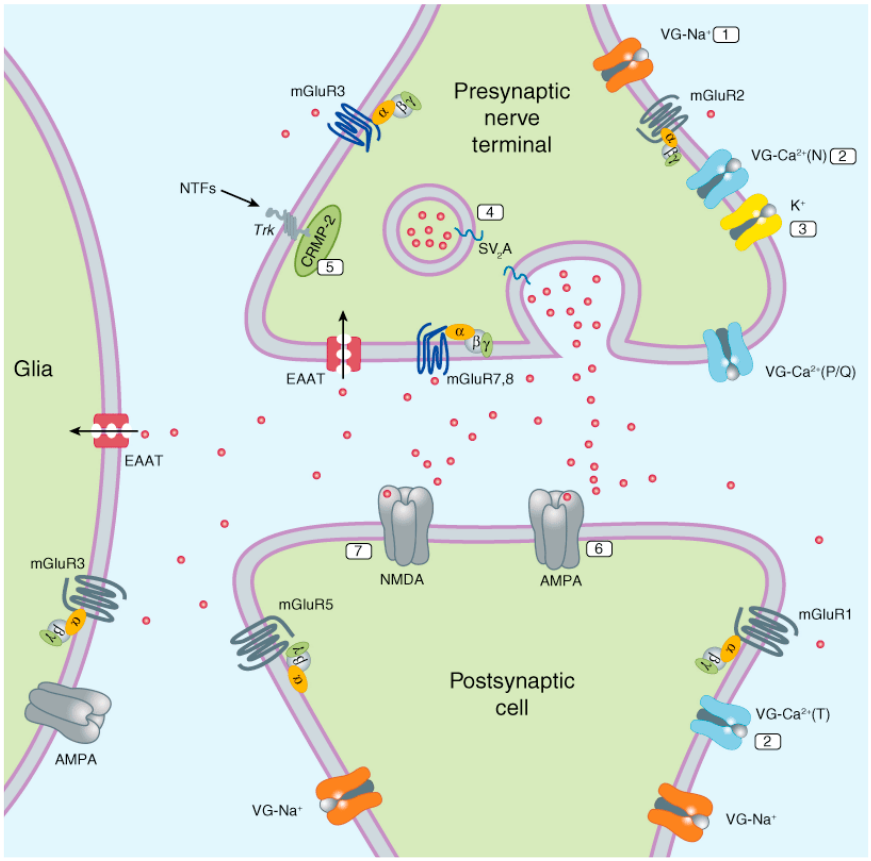

Figure 5.7. SV2A in the presynaptic terminal (Image source: Katzung, B. G.; Masters, S.B.; Trevor, A. J. Basic & Clinical Pharmacology. 11th Edition McGraw-Hill Companies. http://www.accesmedicine.com).

It is worth noting that the antiepileptic levetiracetam, (*S*)- or (−)-**82**, is the eutomer of etiracetam (**82, Figure 5.8**), a cyclic derivative of the amino acid neurotransmitter γ-aminobutyric acid, GABA. It is also structurally similar to piracetam, **83**, the prototype of the so-called "nootropic" or "smart" drugs, also known as cognitive enhancers, which are thought to modulate neurotransmission, at the level of cholinergic and glutamatergic systems, and to improve neuroplasticity.[395] Piracetam is used in many countries to treat cognitive impairment in aging, brain injuries, as well as dementia.[396,397] Clinical studies provided compelling evidence for the

[394] Godoy, J. A.; Rios, J. A.; Zolezzi, J. M. *et al*. *Cell Commun. Signal.* **2014**, *12*, 1–12.
[395] Lanni, C.; Lenzken, S. C.; Pascale, A. *et al*. *Pharmacol. Res.* **2008**, *57*, 196–213.
[396] Croisile, B.; Trillet, M.; Fondarai, J. *et al. Neurology* **1993**, *43*, 301–305.
[397] Waegemans, T.; Wilsher, C. R.; Danniau, A. *et al. Dement. Geriatr. Cogn. Disord*. **2002**, *13*, 217–224.

global efficacy of piracetam in a diverse group of older subjects with cognitive impairment.[394] In a similar way, it has also been shown to improve cognitive function in a number of animal models,[398,399] however, little or no benefit in young healthy animals has been seen after its treatment,[400,401] which has led to the speculation that piracetam's mechanism of action is associated with biochemical deficits of the aged brain. Finally, a recent *in vivo* study in rodents has brought to light protection against mitochondrial dysfunction, improved ATP production, and prevention of apoptotic signals as putative explanations of piracetam's beneficial effects in aging and neurodegeneration.

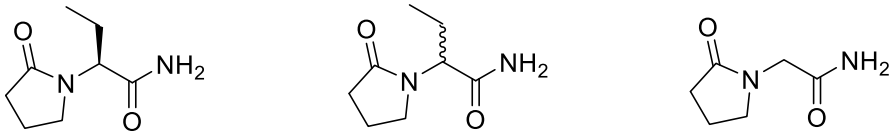

Levetiracetam, (*S*)-**82** Etiracetam, (±)-**82** Piracetam, **83**

Figure 5.8. Structures of levetiracetam, (S)-**82**, etiracetam, (±)-**82**, and piracetam, **83**.

The outstanding effects found for levetiracetam prompted us to develop a small series of levetiracetam-based hybrids with potential multipotent anti-Alzheimer profile. First, we synthesized four hybrids containing a moiety of tacrine or 6-chlorotacrine linked to 2-(2-oxopyrrolidin-1-yl)butanoic acid, either in the racemic, (±)-**86**, the distomer, (+)-**86**, or the eutomer form, (−)-**86**, related to levetiracetam [(±)-, (*R*)-, and (*S*)-**84**, and (±)-**85 Scheme 5.6**]. Secondly, two diastereomeric hybrids formed by linkage of enantiomerically pure huprine Y, (+)- or (−)-**11** with (*S*)-(−)-**86** were also synthesized [(2*S*,7'''*S*,11'''*S*)-**92** and (2*S*,7'''*R*,11'''*R*)-**93**, **Scheme 5.7**]. All hybrids were connected through an heptamethylene chain, as it is known to enable hybrids to span the whole length of the active site gorge of AChE, one of their putative targets, as supported by the evidence that recently developed heptamethylene-linked huprine-based hybrids were found to be among the most potent AChE inhibitors of the corresponding structural families, as huprine−tacrine heterodimers[88b] and rhein−huprine hybrids (**see section 5.2**). Thus, this design rationale was purported to derive a multitarget drug able to perform a dual site binding in AChE, and to tackle the aberrant epileptiform activity, as one of the mechanisms by which Aβ exerts its neurotoxic effects.

[398] Giurgea, C. E. *Drug Dev. Res.* **1982***, 2*, 441–446.
[399] Müller, W. E.; Eckert, G. P.; Eckert, A. *Pharmacopsychiatry* **1999**, *32*, Suppl 1: 2–9.
[400] Valzelli, L.; Bernasconi, S.; Sala, A. *Int. Pharmacopsychiatry* **1980**, *15*, 150–156.
[401] Müller, W. E.; Koch, S.; Scheuer, K. *et al*. *Biochem. Pharmacol.* **1997**, *53*, 135–140.

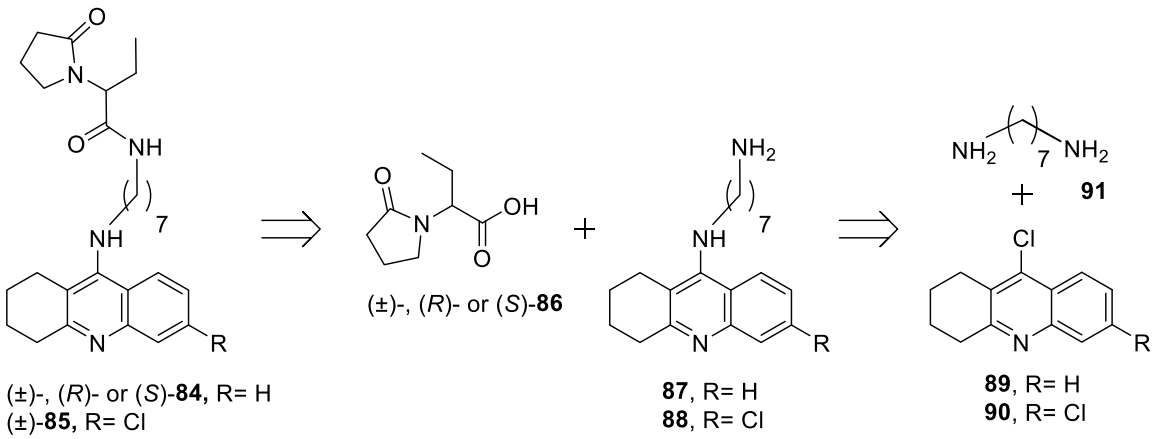

Scheme 5.6. Retrosynthesis of racemic 6-chlorotacrine-based hybrid (±)-**85,** and racemic and enantiopure levetiracetam−tacrine hybrids (±)-, (*R*)-, and (*S*)-**84.**

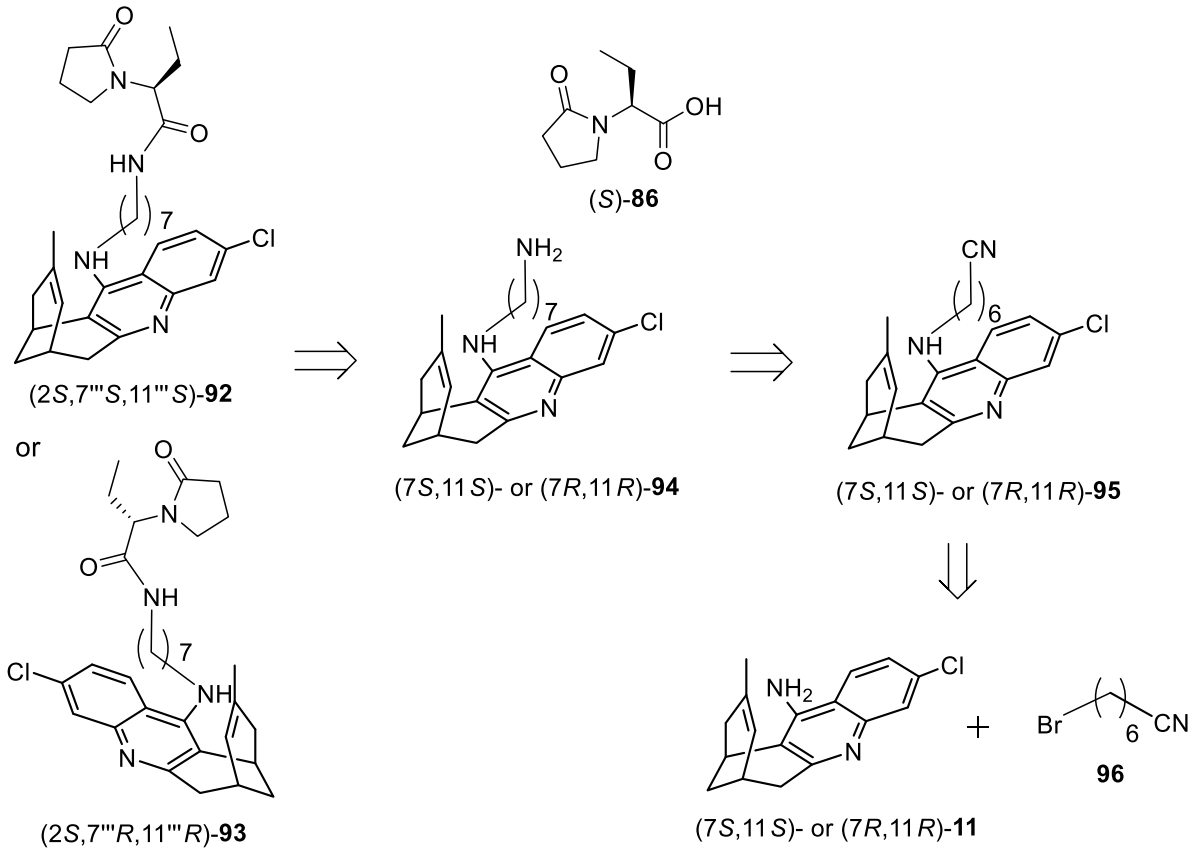

Scheme 5.7. Retrosynthesis of levetiracetam−huprine diastereomers (2*S*,7'''*S*,11'''*S*)-**92** and (2*S*,7'''*R*,11'''*R*)-**93.**

[88b] Galdeano, C.; Viayna, E.; Sola I. *et al. J. Med. Chem*. **2012**, *55*, 661−669.

5.3.1. Synthesis of levetiracetam-based hybrids

The synthesis of 2-(2-oxopyrrolidin-1-yl)butanoic acid, (±)-**86**, was carried out via nucleophilic substitution between 2-pyrrolidinone, **97**, and (±)-2-bromobutanoic acid, (±)-**98**, in the presence of NaH in anhydrous THF. Enantiopure carboxylic acids, (*S*)-**86** or (*R*)-**86**, were then obtained through a methodology previously developed in our group,[402] based on the resolution of the racemic mixture of **86** by treatment with the chiral auxiliary (*S*)-phenylpantolactam, (*S*)-**99**, in order to provide a diastereomeric mixture of esters, (α*S*,3'*S*)-**100** and (α*R*,3'*S*)-**100**, through a Steglich esterification in the presence of dicyclohexylcarbodiimide (DCC) and dimethylaminopyridine (DMAP). The diastereomeric mixture of esters **100** was then purified by silica gel column chromatography to provide pure (α*S*,3'*S*)-**100** and (α*R*,3'*S*)-**100**. Afterwards, hydrolysis of ester (α*S*,3'*S*)-**100** with LiOH/H_2O_2 at 0 °C in THF gave the desired enantiopure carboxylic acid, (*S*)-**86**, in mild conditions that preclude the racemization of **86** (**Scheme 5.8**).

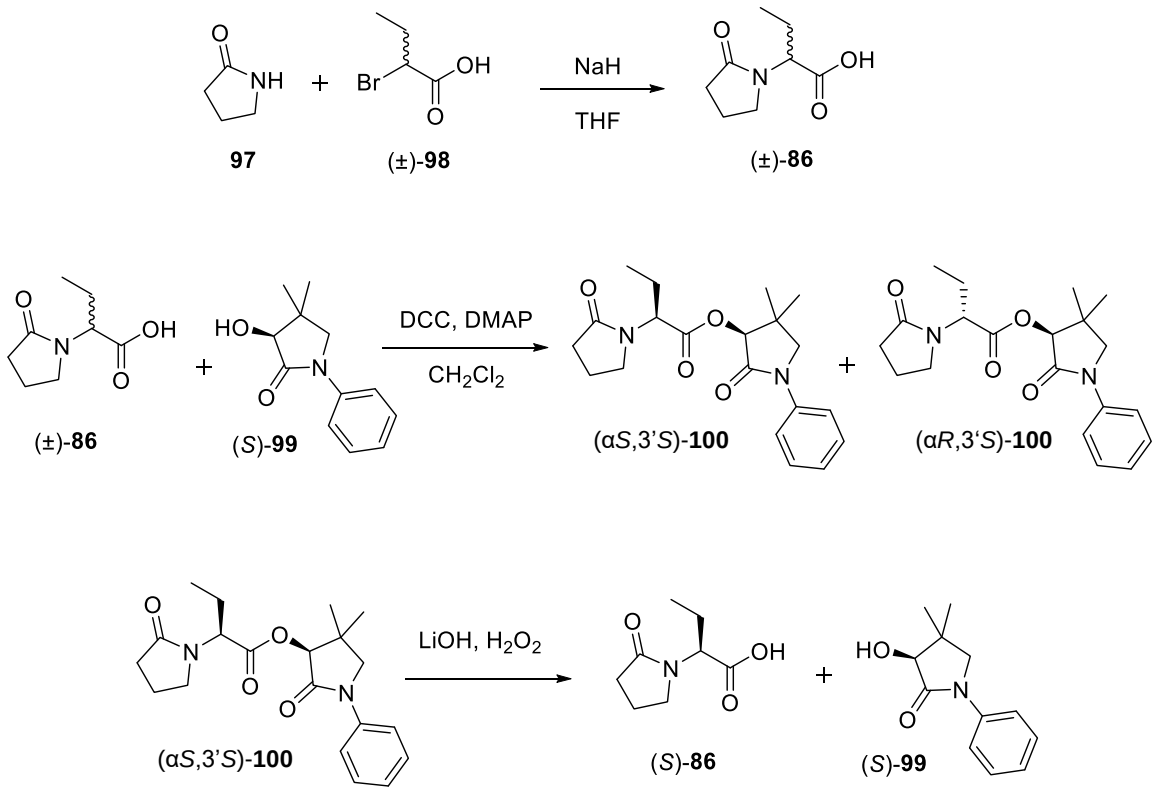

Scheme 5.8. Synthesis of enantiopure 2-(2-oxopyrrolidin-1-yl)butanoic acid, (*S*)-**86**.

[402] Boschi, F.; Camps, P.; Comes-Franchini, M. *et al. Tetrahedron: Asymmetry* **2005**, *16*, 3739–3745.

On the other hand, the second moiety of the hybrid was prepared through an easy synthetic route. For the preparation of racemic hybrids (±)-**84** and (±)-**85** we firstly performed a known nucleophilic substitution of the corresponding 4-chloroquinoline, **89** and **90**, derived from tacrine and 6-chlorotacrine, respectively, with the commercially available 1,7-diaminoheptane, **91**, to afford 9-(7-aminoheptyl)tacrine and 9-(7-aminoheptyl)-6-chlorotacrine, **87**[403] and **88**[86] (**Scheme 5.9**). Afterwards, racemic acid (±)-**86** was treated with 1 equiv of ethyl chloroformate and 2 equiv of Et_3N in CH_2Cl_2, followed by reaction of the resulting mixed anhydride with 1 equiv of the previously prepared **87** and **88** at room temperature for 3 days, and final purification by silica gel column chromatography of the crude products to afford racemic (±)-**84** and (±)-**85** in 93% and 78% yield, respectively. Regarding the preparation of enantiopure levetiracetam−tacrine hybrids, coupling of aminoheptyltacrine **87** with carboxylic acids (*S*)-**86** or (*R*)-**86** under the same reaction conditions used before afforded enantiopure hybrids, (*S*)- or (*R*)-**84**, in 60% and 27% yield, respectively (**Scheme 5.10**).

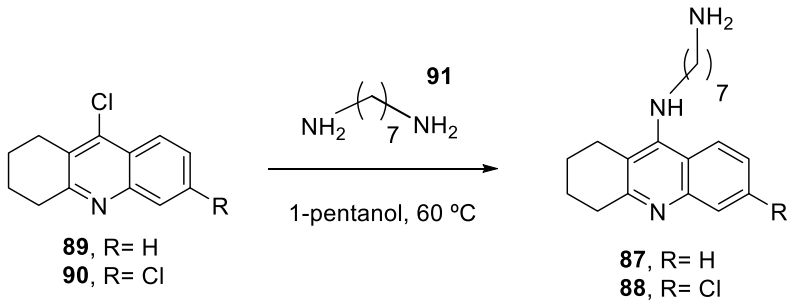

Scheme 5.9. Obtention of 9-(7-aminoheptyl)tacrine and 9-(7-aminoheptyl)-6-chlorotacrine intermediates, **87** and **88**, by aromatic nucleophilic substitution with 4-chloroquinolines **89** and **90**, respectively.

[86] Muñoz-Ruiz, P.; Rubio, L.; García-Palomero, E. *et al*. *J. Med. Chem*. **2005**, *48*, 7223−7233.
[403] Carlier, P. R.; Chow, E. S. H.; Han, Y. *et al*. *Med. Chem.* **1999**, *42*, 4225−4231.

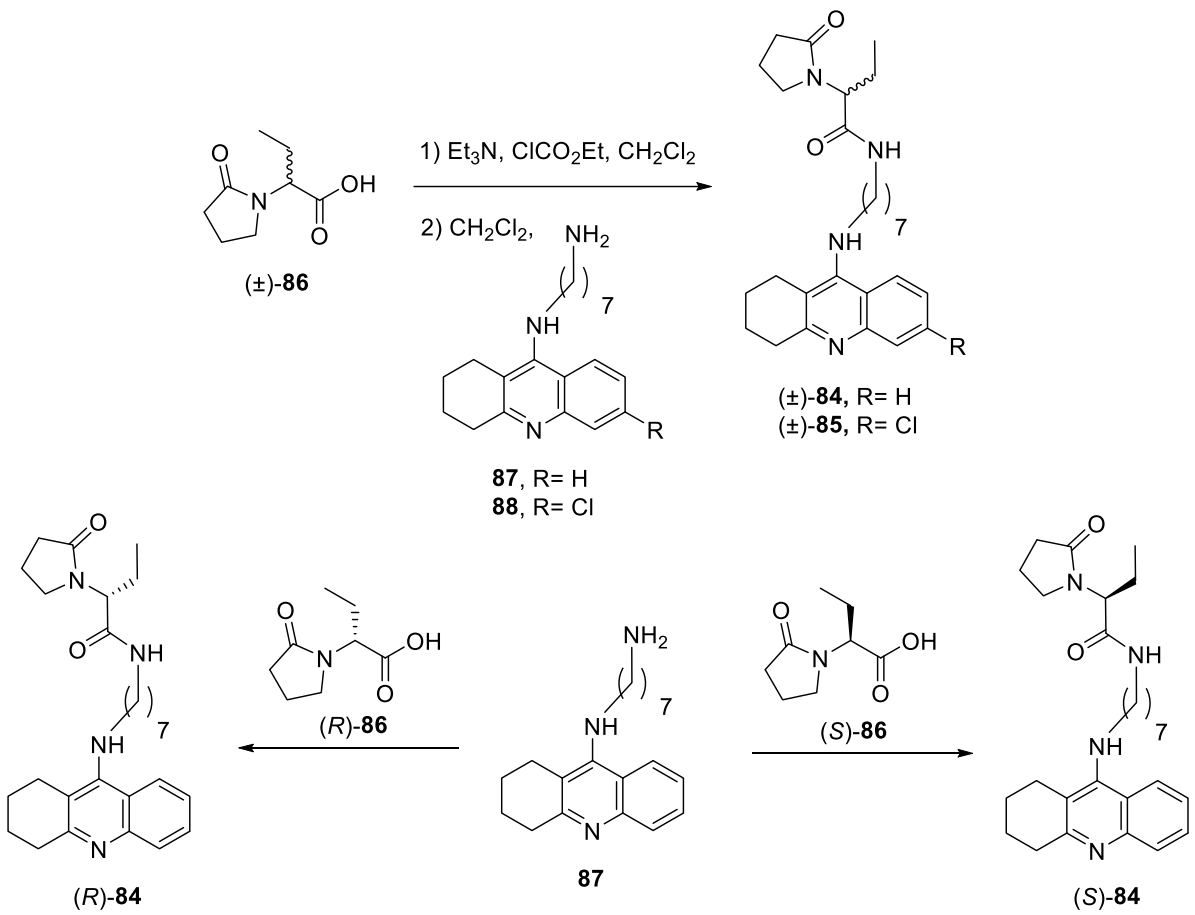

Scheme 5.10. Preparation of racemic levetiracetam−tacrine hybrid (±)-**84** and levetiracetam−6-chlorotacrine hybrid (±)-**85** (up), and enantiopure levetiracetam−tacrine hybrids (*S*)- and (*R*)-**84** (down).

For the synthesis of levetiracetam−huprine hybrids, first of all, the preparation of both enantiomeric cyanoalkyhuprines (7*S*,11*S*)- and (7*R*,11*R*)-**95**, was undertaken starting from enantiopure huprines (7*S*,11*S*)- and (7*R*,11*R*)-**11**, which are readily available even at multigram amounts by chromatographic resolution.[89e,404,] Thus, alkylation of (7*S*,11*S*)- and (7*R*,11*R*)-**11** with 7-bromoheptanenitrile, **96**, in the presence of NaOH in DMSO afforded the novel enantiopure nitriles (7*S*,11*S*)- and (7*R*,11*R*)-**95** in moderate yields (52% and 55%, respectively), which were subsequently treated with $LiAlH_4$ in anhydrous Et_2O at 0 °C to obtain amine (7*S*,11*S*)-**94** in excellent yield (91%) with no need of further purification and (7*R*,11*R*)-**94** in 45% yield, after silica gel column chromatography purification (**Scheme 5.11**).

[89e] Sola, I.; Viayna, E.; Gómez, T. *et al. Molecules* **2015**, *20*, 4492−4515.
[404] Camps, P.; Contreras, J.; Font-Bardia, M. *et al. Tetrahedron: Asymmetry* **1998**, *9*, 835−849.

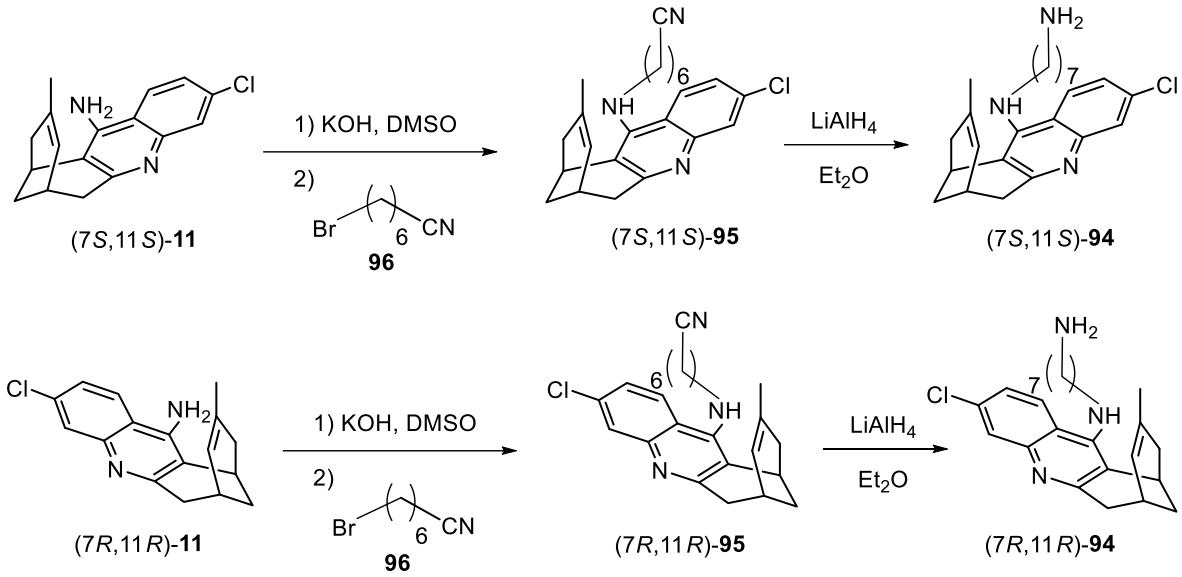

Scheme 5.11. Preparation of aminoalkylhuprine intermediates (7*S*,11*S*)- and (7*R*,11*R*)-**94**.

The final step of this work consisted of the treatment of the mixed anhydride derived from carboxylic acid (*S*)-**86** and ethylchloroformate with amines (7*S*,11*S*)- and (7*R*,11*R*)-**94** to afford the desired enantiopure levetiracetam−huprine hybrids (2*S*,7‴*S*,11‴*S*)-**92** and (2*S*,7‴*R*,11‴*R*)-**93** in 30% and 56% yield respectively, after silica gel column chromatography purification (**Scheme 5.12**).

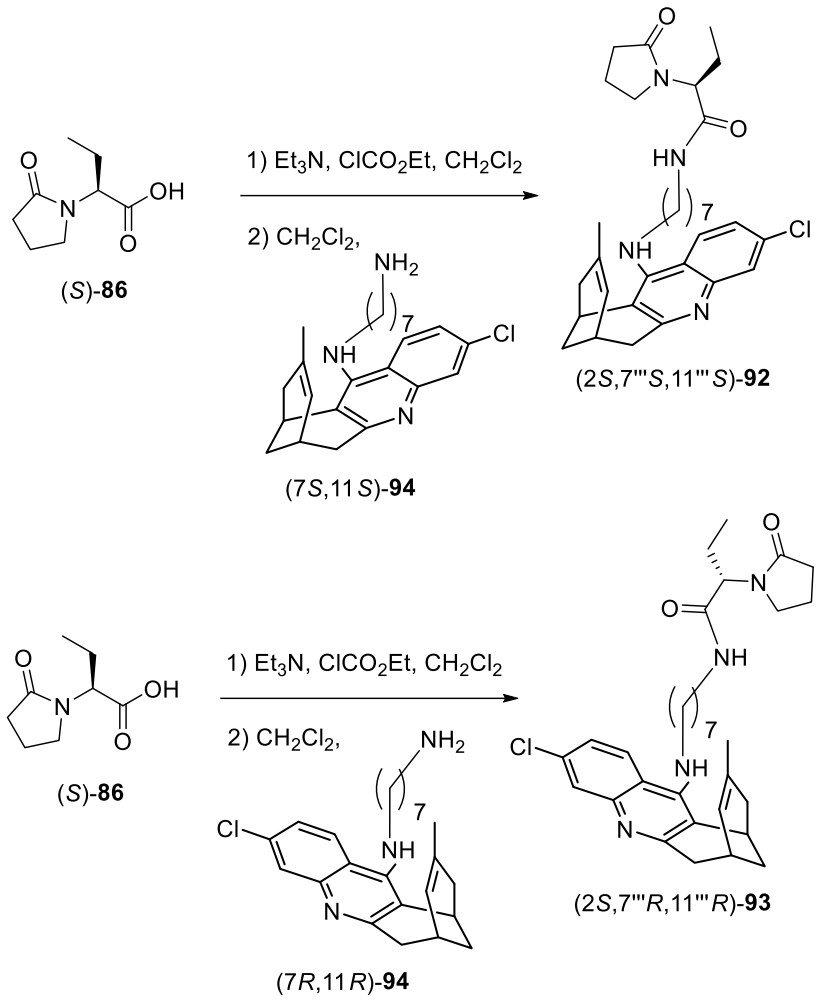

Scheme 5.12. Final step for the obtention of the enantiopure levetiracetam−huprine hybrids (2*S*,7‴*S*,11‴*S*)-**92** and (2*S*,7‴*R*,11‴*R*)-**93.**

The enantiopurity of the levetiracetam−tacrine hybrids (*S*)- and (*R*)-**84** was confirmed by chiral HPLC, carried out with a PerkinElmer model 200 chromatograph equipped with a variable λ UV detector, using a CHIRALPAK IC column, a mixture of heptane/*i*-PrOH/diethylamine 55:45:0.1 as the eluent, flow 1 mL/min, λ = 235 nm; (*R*)-**84**, retention time = 38.05 min; (*S*)-**84**, retention time = 60.49 min. The enantio- and diastereopurity of the levetiracetam−huprine hybrids (2*S*,7‴*S*,11‴*S*)-**92** and (2*S*,7‴*R*,11‴*R*)-**93** was also confirmed by chiral HPLC, using the above described equipment and conditions but with a mixture of heptane/*i*-PrOH/diethylamine 63:37:0.1 as the eluent; (2*S*,7‴*R*,11‴*R*)-**93**, retention time = 34.65 min; (2*S*,7‴*S*,11‴*S*)-**92**, retention time = 44.85 min (**Figure 5.13**).

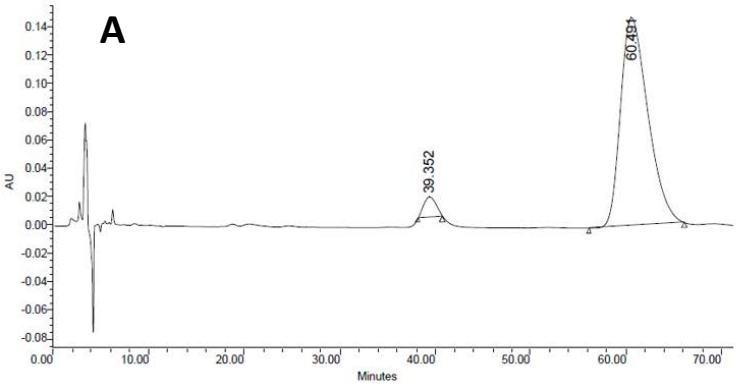

	RT (min)	Area (µV*sec)	% Area	Height (µV)	% Height
1	39.352	1333143	4.34	14537	8.99
2	60.491	29398007	95.66	147104	91.01

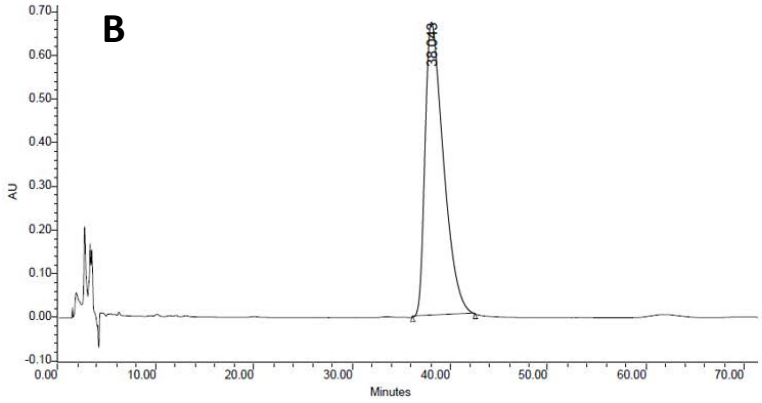

	RT (min)	Area (µV*sec)	% Area	Height (µV)	% Height
1	38.043	88308336	100.00	671972	100.00

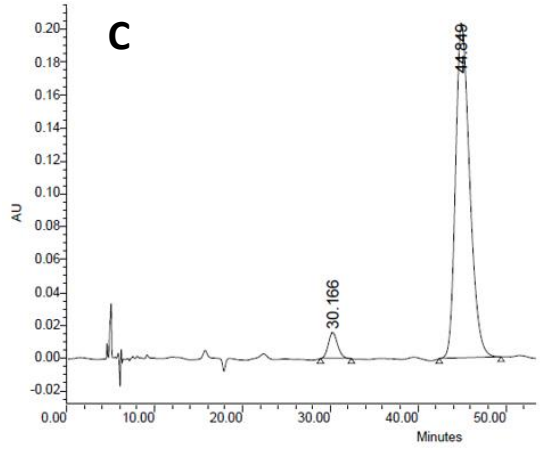

	RT (min)	Area (µV*sec)	% Area	Height (µV)	% Height
1	30.166	1189986	4.96	15918	7.26
2	44.849	22800976	95.04	203191	92.74

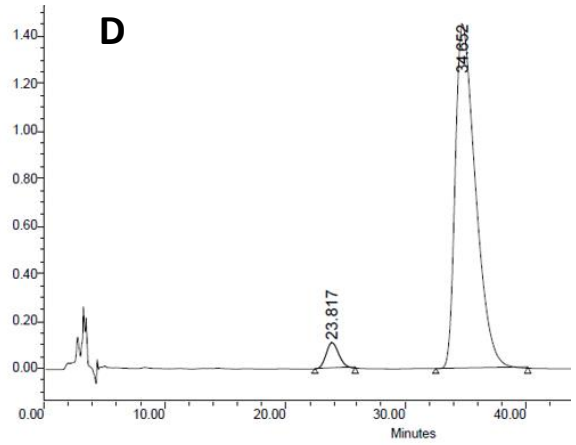

	RT (min)	Area (µV*sec)	% Area	Height (µV)	% Height
1	23.817	8112096	4.57	108798	6.99
2	34.652	169504997	95.43	1448324	93.01

Figure 5.13. Chromatograms of levetiracetam–tacrine enantiomers (*S*)- and (*R*)-**84** (**A** and **B**, respectively), and levetiracetam–huprine diastereomers (2*S*,7'''*S*,11'''*S*)-**92** and (2*S*,7'''*R*,11'''*R*)-**93** (**C** and **D**).

5.3.2. Pharmacological evaluation of levetiracetam-based hybrids

The *in vitro* biological profiling of the levetiracetam-based hybrids was carried out by the groups of Dr. M. Victòria Clos (Universitat Autònoma de Barcelona) and Dr. Raimon Sabaté (Universitat de Barcelona), whereas the *in vivo* assays were carried out by the group of Drs. Isidre Ferrer and Ester Aso (IDIBELL). The molecular modeling studies of the interaction of these compounds with AChE, which confirmed their dual site binding to the enzyme, were carried out by the group of Dr. F. Javier Luque (Universitat de Barcelona).

In agreement with the design rationale, the novel levetiracetam-based hybrids have exhibited a dual nanomolar hAChE and hBChE *in vitro* inhibition (AChE IC_{50}= 3−89 nM and BChE IC_{50}= 12−232 nM). The enantiopure levetiracetam−huprine hybrid (2*S*,7'''*S*,11'''*S*)-**92** has shown the best pharmacological profile with moderately potent dual Aβ42 and tau antiaggregation effect in a simple *in vivo* model of amyloid aggregation in intact *E. coli* cells (36% and 54% of inhibition, respectively), besides being one of the most potent and selective AChE inhibitors (AChE IC_{50} = 4.2 nM, and BChE IC_{50} = 232 nM).

Very interestingly, after a 4-week treatment with a 5 mg/kg dose in transgenic APP/PS1 mice, the number of epileptic seizures registered was lower in all of the animal groups treated with the novel hybrids relative to the control transgenic group treated with vehicle, even though only for the group treated with the levetiracetam−huprine hybrid (2*S*,7'''*S*,11'''*S*)-**92** the reduction of the incidence of epileptic seizures was statistically significant. Moreover, hybrid (±)-**84** bearing a tacrine moiety and (2*S*,7'''*S*,11'''*S*)-**92** led to a clear cognitive improvement in APP/PS1 mice after 4 days without receiving the compounds. Cortical amyloid burden and neuroinflammation around Aβ plaques were significantly reduced in transgenic animals treated with (2*S*,7'''*S*,11'''*S*)-**92**, without altering the levels of soluble Aβ40 and Aβ42, but not in animals treated with (±)-**84**, which discouraged us from testing *in vivo* any of its enantiomers.

In the case of the levetiracetam−huprine hybrid (2*S*,7'''*S*,11'''*S*)-**92**, its putative effect on epileptiform activity was complemented with a direct effect on amyloid and tau pathologies, neuroinflammation, and cholinesterases, thereby emerging as a very promising disease-modifying anti-Alzheimer drug candidate.

The levetiracetam-based hybrids are currently protected under a WO patent (Muñoz-Torrero D.; López-González, I; Sola, I.; Aso, E. WO 2014/206877 A1).

5. A.

J. Med. Chem. **2014**, *57*, 2549

Synthesis and multi-target biological profiling of a novel family of rhein derivatives as disease-modifying anti-Alzheimer agents

Elisabet Viayna,[†,‡,Δ] *Irene Sola,*[†,‡] *Manuela Bartolini,*[§] *Angela De Simone,*[¶] *Cheril Tapia-Rojas,*[#] *Felipe G. Serrano,*[#] *Raimon Sabaté,*[⊥,//] *Jordi Juárez-Jiménez,*[‡,⊥] *Belén Pérez,*[◊] *F. Javier Luque,*[‡,⊥] *Vincenza Andrisano,*[¶] *M. Victòria Clos,*[◊] *Nibaldo C. Inestrosa,*[#] *and Diego Muñoz-Torrero*[*,†,‡]

[†] Laboratori de Química Farmacèutica (Unitat Associada al CSIC), Facultat de Farmàcia, Universitat de Barcelona, Av. Joan XXIII 27-31, E-08028, Barcelona, Spain

[‡] Institut de Biomedicina (IBUB), Universitat de Barcelona, Barcelona, Spain

[§] Department of Pharmacy and Biotechnology, Alma Mater Studiorum University of Bologna, Via Belmeloro 6, I-40126, Bologna, Italy

[¶] Department for Life Quality Studies, University of Bologna, Corso d'Augusto 237, I-47921-Rimini, Italy

[#] Centro de Envejecimiento y Regeneración (CARE), Departamento de Biología Celular y Molecular, Facultad de Ciencias Biológicas, Pontificia Universidad Católica de Chile, Alameda 340, 8331150-Santiago, Chile

[⊥] Departament de Fisicoquímica, Facultat de Farmàcia, Universitat de Barcelona, Barcelona, Spain

[||] Institut de Nanociència i Nanotecnologia (IN^{2}UB), Universitat de Barcelona, Barcelona, Spain

[◊] Departament de Farmacologia, de Terapèutica i de Toxicologia, Institut de Neurociències, Universitat Autònoma de Barcelona, E-08193, Bellaterra, Barcelona, Spain

ABSTRACT: We have synthesized a family of rhein–huprine hybrids to hit several key targets for Alzheimer's disease. Biological screening performed *in vitro* and in *Escherichia coli* cells has shown that these hybrids exhibit potent inhibitory activities against human acetylcholinesterase butyrylcholinesterase, and BACE-1, dual Aβ42 and tau anti-aggregating activity, and brain permeability. *Ex vivo* studies with the leads (+)- and (–)-**7e** in brain slices of C57bl6 mice have revealed that they efficiently protect against the Aβ-induced synaptic dysfunction , preventing the loss of synaptic proteins and/or have a positive effect on the induction of long term potentiation. *In vivo* studies in APP-PS1 transgenic mice treated i.p. for 4 weeks with (+)- and (–)-**7e** have shown a central soluble Aβ lowering effect, accompanied by an increase in the levels of mature amyloid precursor protein (APP). Thus, (+)- and (–)-**7e** emerge as very promising disease-modifying anti-Alzheimer drug candidates.

INTRODUCTION

Alzheimer's disease (AD), the most common type of dementia, is associated with ever increasing unacceptable personal and economic costs, owing to its high prevalence, mortality and, worryingly, to the elusiveness of efficacious drugs.[1]

There has been a general consensus that β-amyloid peptide (Aβ) is the main culprit of a straightforward cascade process that begins with its increased formation by processing of the amyloid precursor protein (APP) by β-secretase (BACE-1) and γ-secretase, and aggregation into oligomers and fibrils. This follows with a series of downstream events including synaptic dysfunction, tau protein hyperphosphorylation and aggregation, neuroinflammation and oxidative stress, and eventually leads to neuronal death and neurotransmitter deficits.[2,3] Because these deficits account for the cognitive and functional decline, which are the main diagnostic criteria for AD, the first and so far the sole marketed anti-Alzheimer drugs, namely the acetylcholinesterase (AChE) inhibitors tacrine, donepezil, rivastigmine and galantamine and the NMDA receptor antagonist memantine, were developed to hit those neurotransmitter deficits, particularly cholinergic and glutamatergic, but are regarded as merely symptomatic.

In the past years, there has been an intense research activity for developing drugs able to tackle the underlying mechanism of AD, by hitting Aβ formation or aggregation or, to a minor extent, other downstream targets.[4] However, despite the acute need and the hopes raised for the discovery of effective disease-modifying anti-Alzheimer drugs, a number of clinically advanced Aβ-directed drug candidates have recently failed to show efficacy over placebo or they have been discontinued because of their toxicity. The efficacy issues of these drug candidates have been ascribed, at least partly, to the fact that AD pathology might not result from a straightforward process, but from a robust network of interconnected events, whereby Aβ

aggregation is not *the* cause but just *one* of the causes, together with tau hyperphosphorylation and aggregation, synaptic dysfunction or neuroinflammation.[5] This novel conception of AD would allow explaining why modulation of a single target might be ineffective, whereas simultaneous modulation of several targets of the network, including Aβ, holds promise for deriving the eagerly awaited effective disease-modifying anti-Alzheimer drugs.[6–10]

In the past years, many research groups have pursued the development of multi-target anti-Alzheimer drugs as an advantageous approach over multi-target multi-drug strategies (drug cocktails and fixed-dose combinations).[11–15] Multi-target compounds have been usually designed to hit at least Aβ formation and aggregation and AChE activity,[16] especially prompted by the finding that AChE can bind Aβ, thereby promoting its aggregation and increasing its neurotoxicity.[17–19] The recognition site of Aβ within AChE is the so-called peripheral anionic site (PAS) and it is located at the entrance of a 20 Å deep narrow gorge that leads to the catalytic anionic site (CAS).[20] The design of inhibitors able to simultaneously reach both sites of AChE, i.e. dual binding site AChE inhibitors (AChEIs), emerged some years ago as a promising source of multi-target anti-Alzheimer compounds, inasmuch as they should be endowed at least with potent anticholinesterase and Aβ anti-aggregating effects.[21–29] Moreover, the multi-target profile of these compounds can be enlarged by introducing pharmacophoric moieties that are also suitable for separate interactions with additional targets of interest other than AChE and Aβ. Two major challenges in the design and therapeutic potential of multi-target anti-Alzheimer agents are the choice of the targets to be hit and the potency of the compounds at the different targets. Indeed, it must be recognized that the timing of the different events in the progression of AD can be overlooked when selecting the biological targets to be hit. However, this issue will remain very difficult to be addressed until a precise description of the sequence of events that give rise

to the neuropathogenesis of AD becomes available. On the other hand, a multi-target action will be only effective when balanced activities are achieved at the different targets, which is also not an easy task.

Recently, the hydroxyanthraquinone derivatives emodin, **1**, and PHF016, **2** (Chart 1), have been shown to inhibit tau aggregation *in vitro* with IC_{50} values in the low micromolar range.[30,31] The structurally related compound rhein, **3** (Chart 1) is a natural product found in the traditional Chinese herbal medicine rhubarb, which is well tolerated in humans.[32] In the form of a doubly acetylated prodrug, diacerein, it is used for the treatment of arthritis. Even though rhein has been reported to be essentially inactive as inhibitor of AChE[33,34] and of Aβ aggregation,[35] its aromatic rings seem appropriate for establishing π-stacking interactions with the characteristic aromatic residue at the PAS of AChE, namely Trp286 (human AChE (hAChE) numbering). Moreover, its hydroxyanthraquinone scaffold might confer tau anti-aggregating properties to its derivatives. Thus, we inferred that combination in a hybrid of the hydroxyanthraquinone system of rhein with a moiety with high affinity for the CAS of AChE might result in a multi-target compound of interest for the treatment of AD, which should be endowed at least with AChE, Aβ aggregation and tau aggregation inhibitory activities.

Chart 1. Structures of tau aggregation inhibitors 1 and 2, rhein and huprine Y

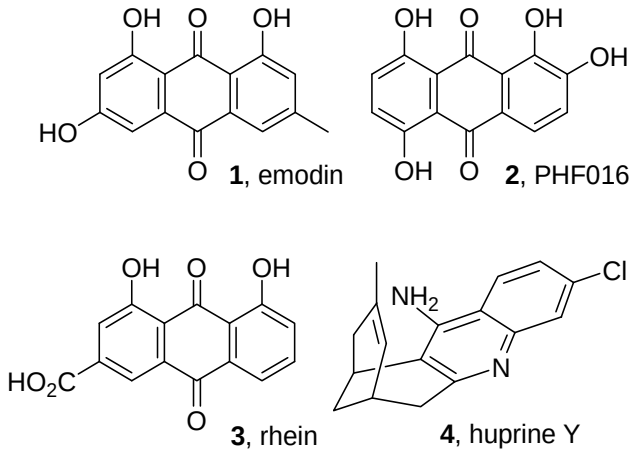

Herein, we describe the synthesis, biological profiling, and investigation of the mechanism of action of a novel family of multi-target hybrid compounds, which are composed of a unit of rhein attached, through different linkers, to a unit of huprine Y, **4** (Chart 1), a high affinity AChE's CAS inhibitor, developed in our group some years ago.[36–39] The biological profiling includes i) the *in vitro* evaluation of the inhibitory activities against hAChE, human butyrylcholinesterase (hBChE), hAChE-induced and self-induced Aβ aggregation, and human BACE-1 (hBACE-1), ii) the evaluation of the Aβ and tau anti-aggregating activities in intact *Escherichia coli* cells overexpressing these peptides, iii) the evaluation of the protective effects on synaptic integrity from Aβ-induced alterations by measuring the induction of long term potentiation and levels of synaptic proteins in hippocampal slices of 2-month-old C57bl6 mice, and iv) the assessment of their brain permeability using an artificial membrane model. Furthermore, kinetic and molecular modeling studies have been performed to shed light on the binding mode of these compounds with two of their main targets, namely AChE and BACE-1.

RESULTS AND DISCUSSION

Chemistry. The linkage between the huprine and rhein moieties was envisioned at one end through an N–C bond from the exocyclic amino group of huprine Y, as in a recently reported family of huprine-based dual binding site AChEI hybrids,[40] and at the other end through an amide bond from the carboxylic acid of rhein. Such linkages have proven to be chemically stable at physiological pH up to 4 days at 37 ºC in a structurally related family of hybrid compounds.[41] Chains from 5 to 11 methylene groups were considered for the linkers (in hybrids **7a**–**g**, Scheme 1), to afford suitable distances between huprine and rhein moieties to achieve a dual site binding to AChE and to explore the effect of the length of the linker in a target with a large binding site such as BACE-1. The incorporation of an aromatic ring within the linker, i.e. a 1,4-phenylene-bis(methylene) linker (in hybrid **7h**, Scheme 1), was also envisaged to explore potential additional interactions with the targets, i.e. interactions with midgorge residues of AChE or disruption of protein–protein interactions in the case of Aβ and tau aggregation.

Rhein–huprine hybrids **7a**–**h** were synthesized through a three- or four-step sequence from readily available racemic or enantiopure huprine Y, (±)-, (–)- or (+)-**4**,[36–38] and commercial rhein, **3** (Scheme 1). Alkylation of racemic huprine Y with commercial or described ω-bromoalkanenitriles[42–44] in the presence of KOH in DMSO afforded nitriles (±)-**5a**–**g** in moderate yields (25–87%). Nitrile (±)-**5h** was prepared in 72% overall yield by condensation of racemic huprine with 4-cyanobenzaldehyde followed by $NaBH_3CN$ reduction of the resulting imine. $LiAlH_4$ reduction of nitriles (±)-**5a**–**h** gave in excellent yields amines (±)-**6a**–**h**, which were reacted with the mixed anhydride formed from rhein and ethyl chloroformate to afford in 9–27% yield the rhein–huprine hybrids (±)-**7a**–**h**.

Scheme 1. Synthesis of the rhein–huprine hybrids 7a–h

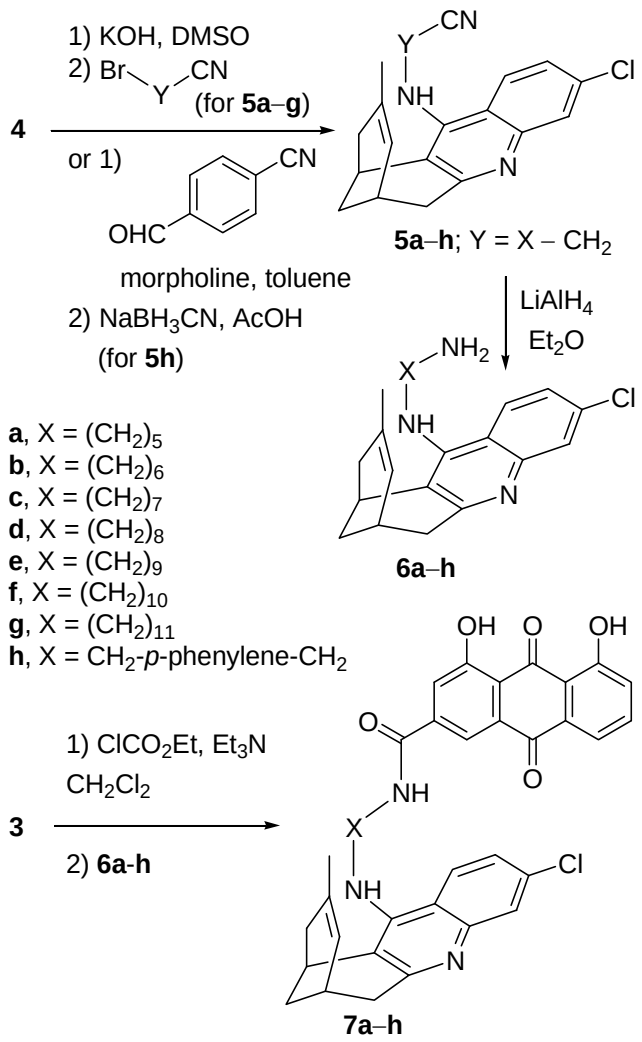

In the light of the biological results obtained for the racemic hybrids **7a**–**h**, we decided to synthesize the two enantiomers of the most interesting racemic hybrid, namely **7e**. Thus, enantiopure (–)- and (+)-**7e** were prepared from (–)- and (+)-**4** (>99% ee) using the same methodology.

The novel rhein–huprine hybrids were fully characterized in the form of hydrochloride salts through their spectroscopic data (IR, ^{1}H and ^{13}C NMR), HRMS and elemental analysis. Hydrochloride salts were also used for the activity profile assessment.

***In Vitro* Biological Profiling of Racemic Rhein–Huprine Hybrids.** *Inhibition of human cholinesterases and molecular modeling study of hAChE inhibition.* Apart from AChE, BChE is another target of interest in the search for anti-Alzheimer drugs, inasmuch as this enzyme exerts a compensatory effect in response to a greatly decreased AChE activity in central nervous system (CNS) when AD progresses.[45] Accordingly, the inhibitory activity of the novel rhein–huprine hybrids and of the reference compounds rhein and huprine Y against human recombinant AChE (hAChE) and human serum BChE (hBChE) was evaluated by the method of Ellman *et al.*[46]

All the racemic hybrids, (±)-**7a**–**h**, turned out to be potent inhibitors of hAChE, with IC_{50} values in the low nanomolar range (Table 1), even though both the length of the linker and the presence of an aromatic ring in the linker seemed to have only a moderate effect on the hAChE inhibitory activity. Indeed, the inhibitory potency gradually decreased from the shortest pentamethylene-linked hybrid (±)-**7a** to the longest undecamethylene homologue, (±)-**7g** (16-fold less potent), whereas introduction of an aromatic ring within the linker seemed to be detrimental for hAChE inhibitory activity, hybrid (±)-**7h** being 12-fold less potent than hybrid (±)-**7b** with a similar tether length. Hybrid (±)-**7a,** the most potent hAChEI of the series (IC_{50} 1.07 nM), was equipotent to the parent racemic huprine Y [(±)-**4**]. In agreement with the reported data,[33,34] the parent rhein, **3**, was found essentially inactive against hAChE.

Table 1. Inhibitory Activities of the Hydrochlorides of Rhein–Huprine Hybrids and Reference Compounds toward AChE, BChE, BACE-1, and AChE-Induced and Self-Induced Aβ Aggregation and BBB Predicted Permeabilities[a]

compd	hAChE IC_{50} (nM)[b]	hBChE IC_{50} (nM)[b]	hBACE-1 IC_{50} (nM)[b]	hAChE-induced Aβ40 aggregation (% inhib.)[c]	self-induced Aβ42 aggregation (% inhib.)[d]	P_e (10^{-6} cm s^{-1})[e] (Prediction)
(±)-**7a**	1.07 ± 0.05	950 ± 30	na[f]	45.0 ± 7.5	38.7 ± 5.0	20.0 ± 1.0 (CNS+)
(±)-**7b**	1.52 ± 0.08	1070 ± 40	na[f]	50.5 ± 8.7	40.8 ± 5.7	nd[g]
(±)-**7c**	3.18 ± 0.16	1460 ± 160	na[f]	52.5 ± 2.9	40.6 ± 1.9	27.5 ± 0.7 (CNS+)
(±)-**7d**	4.36 ± 0.22	350 ± 20	980 ± 170	44.7 ± 8.4	33.1 ± 5.4	22.4 ± 1.3 (CNS+)
(±)-**7e**	3.60 ± 0.21	620 ± 20	120 ± 90	48.7 ± 8.4	38.0 ± 4.6	21.5 ± 0.7 (CNS+)
(+)-**7e**	2930 ± 285	265 ± 21	80 ± 10	36.9 ± 3.4	38.4 ± 5.5	nd[g]
(–)-**7e**	2.39 ± 0.17	513 ± 58	80 ± 10	38.1 ± 0.7	43.2 ± 4.7	nd[g]
(±)-**7f**	7.61 ± 0.45	1100 ± 40	1190 ± 180	29.2 ± 2.4	40.9 ± 4.4	18.1 ± 0.7 (CNS+)
(±)-**7g**	17.4 ± 2.2	645 ± 67	1200 ± 150	38.2 ± 2.6	35.3 ± 4.0	16.4 ± 1.0 (CNS+)
(±)-**7h**	18.2 ± 2.2	510 ± 20	2020 ± 440	35.2 ± 1.8	32.4 ± 3.6	16.3 ± 2.5 (CNS+)
3	>10000	17000 ± 4220	na[h]	nd[g]	nd[g]	2.7 ± 0.1 (CNS+/–)
(±)-**4**	1.07 ± 0.05	181 ± 15	nd[g]	17.1 ± 4.5	nd[g]	23.8 ± 2.7 (CNS+)
(+)-**4**	321 ± 16	170 ± 17	>5000[i]	9.1 ± 3.6	13.2 ± 1.9	25.4 ± 2.9 (CNS+)
(–)-**4**	0.74 ± 0.06	222 ± 17	>5000[j]	24.7 ± 1.3	11.5 ± 5.2	23.6 ± 1.1 (CNS+)

[a] Values are expressed as mean ± standard error of the mean (SEM) of at least three experiments (n=3), each performed in duplicate. [b] IC_{50} inhibitory concentration (nM) of human recombinant AChE, human serum BChE, or human recombinant BACE-1. [c] % inhibition with inhibitor at 100 μM, Aβ40 at 230 μM and hAChE at 2.3 μM. [d] % inhibition with inhibitor at 10 μM and Aβ42 at 50 μM ([Aβ]/[I]=5/1). [e] Permeability values from the PAMPA-BBB assay. [f] Not active at 1 μM. [g] Not determined. [h] Not active. [i] 13.6 ± 2.3% inhibition at 5 μM. [j] 14.0 ± 0.1% inhibition at 5 μM.

The binding mode of the rhein–huprine hybrids to AChE was explored for compound **7h**, taking advantage of the reduced flexibility imposed by the aromatic ring. Docking studies showed that (–)-**7h** binds much more favorably than (+)-**7h**, as expected from the fact that the eutomer of huprines for AChE inhibition is the levorotatory (7*S*,11*S*)-enantiomer, (–)-**4**. The results show that (–)-**7h** may fit the hAChE gorge (Figure 1) placing i) the huprine moiety in an orientation that perfectly matches the arrangement of (–)-huprine X, the 9-ethyl-analog of (–)-huprine Y, in the CAS (PDB entry 1E66, Figure S1), and ii) the hydroxyanthraquinone system of rhein stacked between the aromatic rings of Trp286 and Tyr72 in the PAS, mimicking the arrangement of the tacrine unit of *bis*(7)-tacrine (PDB entry 2CKM, Figure S2).[47] Even though these findings support the ability of the hybrids to interact simultaneously at both CAS and PAS, the inhibitory potencies in Table 1 suggest that the rhein unit has a weak contribution to the binding, presumably due to the lack of a positive charge that would reinforce the stacking interaction, as compared with the inhibitory potency of *bis*(7)-tacrine (IC_{50} hAChE 0.81 nM)[48] and huprine–tacrine hybrids (IC_{50} hAChE up to 0.31 nM),[40] and to the lack of specific interactions formed by the polar groups of the hydroxyanthraquinone moiety at the PAS, thereby preventing a net gain in potency compared to huprine Y, (±)-**4**.

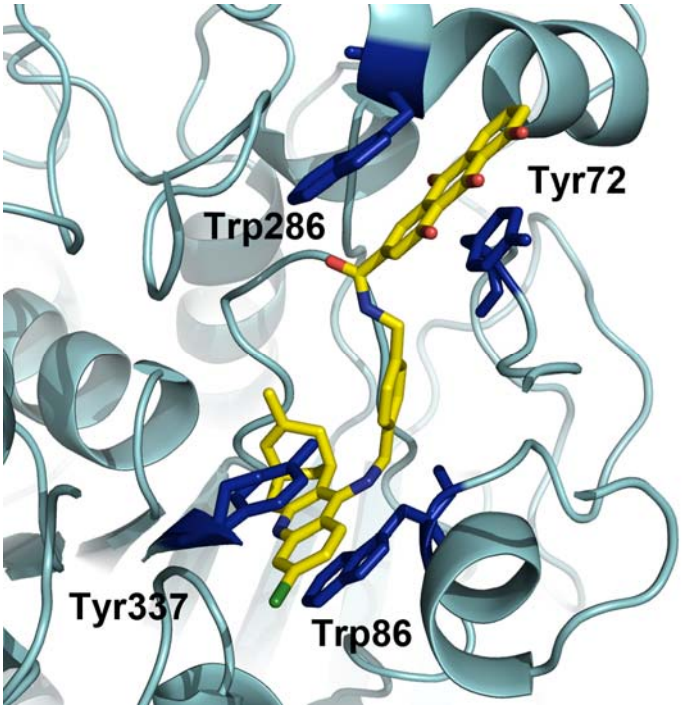

Figure 1. Binding mode of compound (–)-**7h** (shown as yellow sticks) in the AChE gorge.

All the rhein–huprine hybrids turned out to be selective for hAChE over hBChE inhibition, with selectivities in the range 28–888. However, these hybrids still exhibited a moderately potent hBChE inhibitory activity, with IC_{50} values in the submicromolar to low micromolar range (Table 1). The most potent hBChE inhibitor of the series, (±)-**7d** (IC_{50} = 350 nM), was slightly less potent than the parent huprine (2-fold) but 50-fold more potent than the parent rhein, **3**.

Inhibition of AChE-induced Aβ aggregation. The occupancy of the AChE's PAS by the rhein–huprine hybrids, predicted by docking simulations (see above), should result in a hindrance of the interaction of Aβ with AChE, and, hence, in a blockade of the Aβ proaggregating action of the enzyme. The inhibitory activity of these hybrids and the parent rhein and huprine Y against the AChE-induced aggregation of Aβ40 was assessed using a thioflavin T-based fluorescent method.[49] Rhein–huprine hybrids exhibited a significant inhibitory activity against the AChE-

induced Aβ40 aggregation, exhibiting percentages of inhibition ranging from 29 to 52% at a 100 μM concentration, which are clearly superior to that found for the AChE's CAS inhibitor huprine Y, **4** (Table 1). These activities are similar to those reported for other families of dual binding site AChEIs,[40,50–55] even though more potent inhibitors of the AChE-induced Aβ40 aggregation have been described.[56,57] In agreement with the hypothesis that both inhibitory activities are related to some extent to the ability of interacting with the AChE's PAS, the inhibitory activities of the rhein–huprine hybrids against the AChE-induced Aβ40 aggregation roughly matches the SAR trends for hAChE inhibition, i.e. the shorter homologues are the most potent and the presence of a benzene ring in the linker is slightly detrimental for the activity.

Inhibition of self-induced Aβ aggregation. The inhibitory activity of the rhein–huprine hybrids against the spontaneous aggregation of Aβ42 was determined *in vitro* using a thioflavin T-based fluorometric assay.[58] These compounds exhibit a significant Aβ42 anti-aggregating activity, displaying percentages of inhibition in the narrow range 32-41% when tested at a concentration equal to 1/5 of that of Aβ42 ([I] = 10 μM, [Aβ42] = 50 μM), they being clearly more potent than the parent huprine Y (Table 1). Of note, rhein could not be evaluated because of solubility problems under the assay conditions.

Inhibition of human BACE-1 and molecular modeling study. BACE-1 catalyzes the first and rate-limiting step of the biosynthesis of Aβ from APP, thereby constituting a prime target in the search for disease-modifying anti-Alzheimer drugs.[59,60] Strikingly, a number of dual binding site AChEIs have been found to be potent or moderately potent inhibitors of BACE-1, even if they were not purported to display this activity.[61] In most cases, these compounds inhibit BACE-1 with low micromolar IC_{50} values, as it happens with the prototypic dual binding site AChEI *bis*(7)-tacrine (IC_{50} 7.5 μM)[62] or with huprine–tacrine heterodimers (IC_{50} 4.9–7.3 μM).[40]

However, another dual binding site AChEI with more potent BACE-1 inhibitory activity, i.e. memoquin (IC_{50} 108 nM),[56] has also been reported.

In the light of these results, the novel racemic rhein–huprine hybrids were tested *in vitro* against human recombinant BACE-1 using a FRET assay.[63] Results clearly showed the importance of the linker chain length. The pentamethylene- to heptamethylene-linked hybrids (±)-**7a**–**c** were inactive for BACE-1 inhibition at a concentration of 1 μM, whereas the longer homologues (±)-**7d**, (±)-**7f**, and (±)-**7g**, as well as (±)-**7h**, containing an aromatic ring in the linker, exhibited a moderately potent BACE-1 inhibitory activity, with IC_{50} values around 1–2 μM (Table 1). Far beyond our expectations, the BACE-1 inhibitory activity in this series peaked for the nonamethylene-linked hybrid (±)-**7e**, with a remarkable IC_{50} value of 120 nM. Thus, (±)-**7e** was roughly equipotent to memoquin,[56] about 50-fold more potent than *bis*(7)-tacrine[62] and other huprine-based hybrids.[40] Very interestingly, the BACE-1 inhibitory activity of (±)-**7e** seems to be slightly higher than that of the Lilly's BACE-1 inhibitor LY2811376, a very promising anti-Alzheimer drug candidate whose Phase I clinical trials were recently discontinued due to toxicity issues unrelated to BACE-1 inhibition,[59] even though a head-to-head test in the same assay conditions would be required to confirm that point. Thus, the combination of huprine Y and rhein in a new hybrid molecule with a proper linker chain led to a significant enlargement of the activity profile, namely the strong inhibitory activity on BACE-1 that is not present in any of the parent compounds.

The preceding findings made it worth to determine the binding mode of the hybrids to BACE-1. In a first step, this was accomplished by examining the druggable pockets present in the enzyme in order to determine their ability to accommodate the huprine and hydroxyanthraquinone moities (see Experimental Section). Among the seven druggable pockets

shared by the four X-ray structures explored with the MDpocket program (PDB entries 1M4H, 1SGZ, 2OHL and 3CIB), only two of them, namely BS1, which encompasses the catalytic site, and BS2, which includes subsites P5–P7 (Figure S3, Supporting Information), were found to be suitable for binding of the huprine and hydroxyanthraquinone moieties present in hybrids. Furthermore, the distance between the centroids of the most populated clusters of huprine and hydroxyanthraquinone in these pockets was comprised between 7 and 11 Å, thus satisfying the geometrical criteria required for the tether in the rhein–huprine hybrids. Accordingly, docking of (+)-**7h** and (–)-**7h** was performed by exploring the volume defined by both BS1 and BS2 sites. Even though this compound is not the most potent within the series, it was chosen due to the limited number of rotatable bonds, which thus makes it easier to perform a more exhaustive exploration of the binding mode and examine the potential interaction at the two pockets identified separately for huprine and hydroxyanthraquinone moieties. Calculations led to a clear binding mode, in which the huprine moiety is accommodated at the BS1 pocket, and the hydroxyanthraquinone moiety fills the BS2 site. The structural integrity of this binding mode was supported by the analysis of four independent 50 ns molecular dynamics simulations run for both (+)-**7h** and (–)-**7h** bound to the enzyme (Figure 2). The huprine moiety remains tightly bound to BS1 in all cases, as expected from the electrostatic stabilization between the protonated aminoquinoline system and the catalytic dyad (Asp32 and Asp228), whereas the bicyclic system of the huprine moiety fills the hydrophobic pocket formed by residues Leu30, Phe108, Ile110 and Ile118 from subsites P2 and P3. On the other hand, the hydroxyanthraquinone moiety in (+)-**7h** exhibits a common binding mode, which involves the electrostatic interaction with Lys321, hydrogen bonds with the backbone of Phe322 and the side chain of Asn233, and hydrophobic contacts with Val309. For (–)-**7h**, the results show that, besides the preceding binding mode, the

hydroxyanthraquinone moiety can adopt an alternative arrangement, which mainly involves the direct electrostatic interaction with Arg307. On the basis of these findings, it is reasonable to expect that the larger flexibility afforded by the linker in **7e** will facilitate a proper accommodation to both BS1 and BS2 in BACE-1, thus explaining the increase in BACE-1 inhibitory activity compared to **7h**. Overall, this analysis suggests that BS2 may be exploited to find novel moieties leading to enhanced binding affinity and hence to hybrid compounds with more potent inhibitory activity against BACE-1.

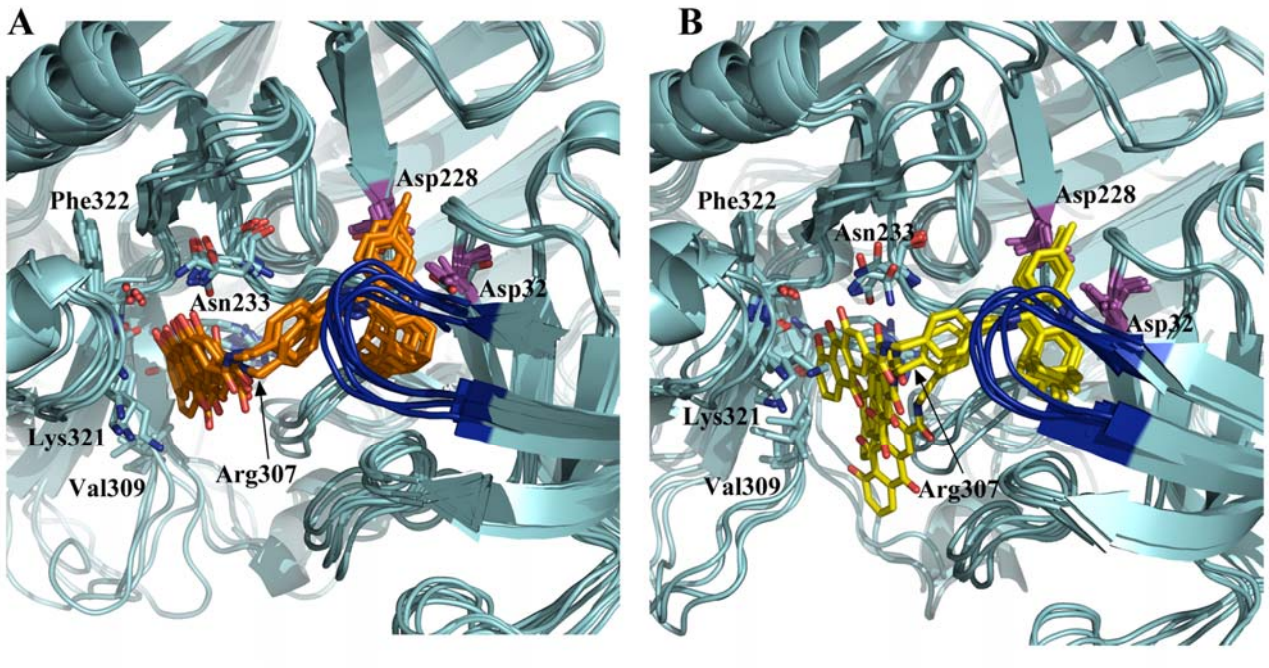

Figure 2. Superposition of the last snapshots sampled in four independent MD simulations of hybrid compounds (A) (+)-**7h** (shown as orange sticks) and (B) (–)-**7h** (shown as yellow sticks) bound to BACE-1 (shown as cyan cartoon). Selected residues that mediate the binding of the hybrids are shown as sticks, and the "flap" loop is shown in blue.

***In Vitro* Biological Profiling of Enantiopure Rhein–Huprine Hybrids (+)- and (–)-7e.** After the *in vitro* biological profiling of the racemic rhein–huprine hybrids, (±)-**7e** emerged as the most interesting member of the series, mainly by virtue of its outstanding BACE-1 inhibitory potency, but also because it was one of the most potent compounds of the series for hAChE, hBChE, AChE-induced and self-induced Aβ aggregation. To further optimize the lead of the series, the two enantiomers of **7e** were synthesized separately (see above) and subjected to *in vitro* biological profiling with the aim of unveiling potential enantioselective interactions with the different targets.

In agreement with the stereoselective interaction of the parent huprine Y, the levorotatory rhein–huprine hybrid (–)-**7e** was far more potent hAChE inhibitor than its enantiomer (+)-**7e**, with an enantioselectivity (1200-fold) somewhat more pronounced than that found for the parent huprine Y (430-fold) (Table 1), in agreement with the docking calculations (Figure 1). To further confirm the inhibition mechanism, a kinetic study of the interaction of (–)-**7e** with hAChE was also carried out. The mode of inhibition of (–)-**7e** was determined with the aid of Lineweaver-Burk double reciprocal plot. The interception of the lines in the Lineweaver-Burk plot above the x-axis (Figure 3) demonstrated that (–)-**7e** acts as a mixed-type inhibitor of hAChE.

The inhibitor dissociation constants K_i and K'_i, which denote the dissociation constant for the enzyme–inhibitor and enzyme–substrate–inhibitor complexes respectively (see Experimental Section), were estimated and resulted to be 2.65 and 3.41 nM, respectively.

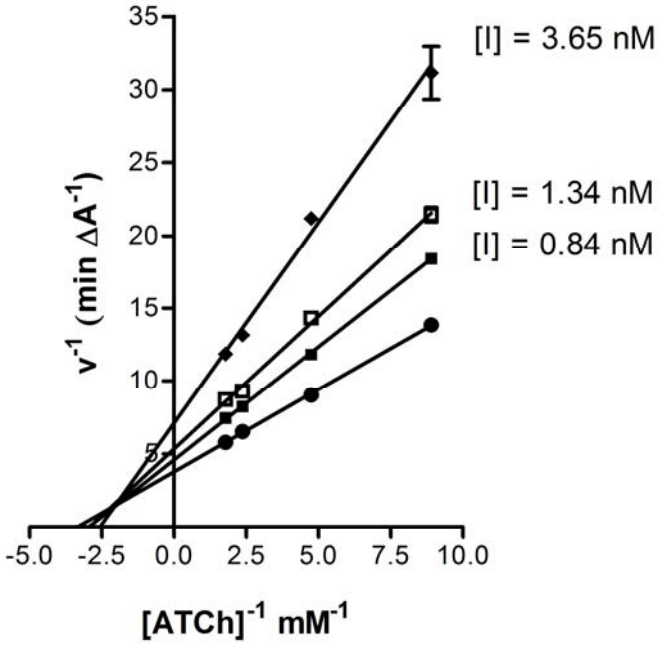

Figure 3. Kinetic study on the mechanism of AChE inhibition by (–)-**7e**. Overlaid Lineweaver–Burk reciprocal plots of AChE initial velocity at increasing substrate concentration (ATCh, 0.56–0.11 mM) in the absence and in the presence (0.84–3.65 nM) of (–)-**7e** are shown. Lines were derived from a weighted least-squares analysis of the data points.

Contrary to the inhibition of hAChE by the enantiomers of huprines, for hBChE inhibition the eutomer is the dextrorotatory (7*R*,11*R*)-enantiomer, (+)-**4**. Thus, not unexpectedly, for hBChE inhibition, the rhein–huprine hybrid (+)-**7e** was 2-fold more potent than (–)-**7e**, the enantioselectivity being quite similar to that found for huprine Y (1.3-fold) (Table 1).

In contrast to hAChE and hBChE inhibition and in agreement with the idea that the enantioselective inhibition of the cholinesterase catalytic activity is related to the interaction with CAS, no enantioselectivity was found in the inhibition by (+)- and (–)-**7e** of the AChE-induced aggregation of Aβ40 (37–38% inhibition at 100 μM). Similarly, no differences were highlighted

for the inhibition of the self-induced aggregation of Aβ42 (38–43% inhibition at 10 μM), and hBACE-1 activity (IC_{50} 80 nM in both enantiomers) by (+)- and (–)-**7e**.

***In Vitro* Blood–Brain Barrier Permeation Assay.** CNS drugs must be able to efficiently cross the blood–brain barrier (BBB). However, cell permeability and brain penetration constitute a major hurdle in the development of some classes of anti-Alzheimer drugs, particularly in BACE-1 inhibitors and in Aβ and tau aggregation inhibitors.[4,31,60,64] Moreover, compounds designed by combination of two pharmacophoric moieties, such as the novel rhein–huprine hybrids, usually have molecular weights over 500, which might challenge their ability to cross cell membranes.[65,66] However, different families of anti-Alzheimer hybrid compounds with molecular weights over 500 have shown good oral availability and/or brain permeability in *ex vivo* and *in vivo* studies in mice.[12,40,67,68] Even though the potential of a CNS drug to enter into the brain also depends on a low P-glycoprotein efflux liability,[69,70] a good brain permeability is a necessary requirement. In this work, the brain permeability of the novel rhein–huprine hybrids has been predicted through the widely known parallel artificial membrane permeation assay (PAMPA-BBB).[71] The *in vitro* permeability (P_e) of racemic rhein–huprine hybrids through a lipid extract of porcine brain was determined using phosphate-buffered saline (PBS)/EtOH 70:30. Assay validation was carried out by comparing the experimental and literature permeability values of 14 commercial drugs (Table S1, Supporting Information), which gave a good linear correlation: P_e (exp) = 1.4525 P_e (lit) – 0.4926 (R^2 = 0.9199). Using this equation and the limits established by Di et al. for BBB permeation,[71] the following ranges of permeability were established: P_e (10^{-6} cm s^{-1}) > 5.3 for compounds with high BBB permeation (CNS+); P_e (10^{-6} cm s^{-1}) < 2.4 for compounds with low BBB permeation (CNS–); and 5.3 > P_e (10^{-6} cm s^{-1}) > 2.4 for compounds with uncertain BBB permeation (CNS+/–). All the tested

rhein–huprine hybrids were predicted to be able to cross BBB, their measured P_e values being far above the threshold for high BBB permeation (Table 1), as it is also the case for the parent huprine Y, (±)**-4**, but not for rhein, **3**, for which an uncertain BBB permeability was predicted. Indeed, rhein is therapeutically used against arthritis in the form of the more lipophilic and cell permeable doubly acetylated prodrug diacerein.

Inhibition of Aβ42 and Tau Aggregation in Intact *Escherichia coli* Cells. The aggregation of two amyloidogenic proteins, namely Aβ and tau, plays a pivotal role in the pathological network of AD. Protein aggregation also occurs during the production of heterologous proteins in bacteria, leading to the formation of insoluble inclusion bodies (IBs). Because IBs contain highly ordered amyloid-like structures and their formation seems to share mechanistic features with amyloid self-assembly, they have been recently proposed as a model to study amyloid aggregation.[72,73] We have recently developed a methodology that allows a fast, simple, and inexpensive evaluation of the anti-aggregating activity of putative inhibitors, which is based on the *in vivo* staining with thioflavin S of IBs in intact *E. coli* cells that overexpress a given amyloidogenic protein in the presence and absence of the inhibitors, and monitoring of the corresponding changes in the fluorescence of thioflavin S.[74] The applicability of this method to the screening of both Aβ42 and tau aggregation inhibitors has been recently demonstrated.[74] Worthy of note, the Aβ42 anti-aggregating activities determined through this method for a number of known active and inactive inhibitors were very similar to those previously reported in *in vitro* assays using synthetic peptides, thereby validating this methodology.[74] A potential limitation of this method lies in the fact that only compounds that are membrane permeable can be detected, whereas potential hits that are active as aggregation inhibitors but unable to cross biological membranes would remain undetected. In the light of the results obtained in the

PAMPA-BBB assays this should not be an issue for the novel rhein–huprine hybrids, which were tested for their ability to inhibit both Aβ42 and tau aggregation in intact *E. coli* cells (Table 2).

Table 2. Inhibitory Activities of the Hydrochlorides of Rhein–Huprine Hybrids and Reference Compounds Toward Aβ42 and Tau Aggregation in Intact *E. coli* Cells[a]

compd	Aβ42 aggregation (% inhibition)[b]	tau aggregation (% inhibition)[b]
(±)-**7a**	68.0 ± 0.8	43.7 ± 1.1
(±)-**7b**	68.4 ± 8.9	30.9 ± 3.1
(±)-**7c**	63.2 ± 9.8	52.0 ± 1.1
(±)-**7d**	50.2 ± 5.6	29.2 ± 1.3
(±)-**7e**	47.9 ± 14.5	29.6 ± 8.5
(+)-**7e**	58.6 ± 7.1	24.9 ± 0.4
(–)-**7e**	47.2 ± 5.1	34.3 ± 0.1
(±)-**7f**	43.3 ± 4.1	57.1 ± 1.9
(±)-**7g**	40.7 ± 2.2	46.3 ± 0.7
(±)-**7h**	57.9 ± 0.0	23.1 ± 5.1
3	49.9 ± 6.4	40.8 ± 0.7
(±)-**4**	na[c]	na[c]

[a] Values are expressed as mean ± standard error of the mean (SEM) of four independent experiments (n=4). [b] % inhibition with inhibitor at 10 μM. [c] Not active.

All the rhein–huprine hybrids exhibited a moderately potent Aβ42 anti-aggregating activity in *E. coli* cells, with percentages of inhibition in the range 41–68% at 10 μM, and, hence, with IC_{50} values below 10 μM in most cases (Table 2). Some clear SAR trends became apparent, namely a higher Aβ42 anti-aggregating activity for the hybrids with the shortest oligomethylene linkers

and for the dextrorotatory over the levorotatory enantiomer of **7e**. The presence of an aromatic ring within the linker seemed not to be detrimental for Aβ42 anti-aggregating activity, hybrid (±)-**7h** displaying a notable 58% inhibition at 10 μM, albeit slightly lower than that of the oligomethylene-linked hybrid of similar tether length, (±)-**7b**. Interestingly, the Aβ42 anti-aggregating activities measured for the rhein–huprine hybrids in intact *E. coli* cells were of similar magnitude than those determined in the *in vitro* assay, albeit somewhat higher in most cases. Regarding the parent compounds, huprine Y was found to be essentially inactive in *E. coli* as it was in the *in vitro* assay, whereas rhein, which could not be evaluated *in vitro* for solubility problems under the assay conditions, was found to exhibit an interesting 50% inhibition at 10 μM in *E. coli* cells.

In agreement with our design strategy, the parent hydroxyanthraquinone derivative rhein was found to be active as inhibitor of tau aggregation in intact *E. coli* cells (41% inhibition at 10 μM), and this was also the case for the novel rhein–huprine hybrids (23–57% inhibition at 10 μM), but not for the parent huprine Y, which was inactive, as expected (Table 2). For the inhibitory activity on tau aggregation, the presence of an aromatic ring within the linker seemed to be detrimental and the levorotatory enantiomer of **7e** was more potent than (+)-**7e**. However, a clear SAR trend regarding the length of the linker could not be derived.

The dual Aβ42 and tau anti-aggregating action of the novel rhein–huprine hybrids seems very promising for anti-Alzheimer drug candidates. These results are also important in the context of the treatment of amyloidoses in general, insofar as they support the increasingly accepted notion that all diseases that involve the pathological aggregation of a particular protein might share common mechanisms and common therapeutic interventions.[75,76] Indeed, other examples of

compounds able to inhibit the aggregation of several amyloidogenic proteins have been reported.[40,75,77]

Protection Against the Synaptic Failure Induced by Aβ Oligomers in Hippocampal Slices of C57bl6 Mice. In the light of the outstanding multi-target pharmacological profile found *in vitro* and in *E. coli* cells for the enantiopure rhein–huprine hybrids (+)- and (–)-**7e**, involving the modulation of crucial targets of the pathological network of AD, these compounds were selected as leads for further pharmacological characterization.

Even though all aggregated forms of Aβ are likely pathological,[78] it has been reported that Aβ oligomers (Aβ-o) cause an impairment of synaptic functions observed in AD patients and mouse models of AD.[79] Because the target of Aβ-o is located at the postsynaptic region,[80,81] processes associated to synaptic plasticity as long-term potentiation (LTP) are critically altered, leading to diminished synaptic strength and efficacy. These dysfunctions are correlated with reduction in the levels of synaptic proteins that participate in events associated with learning and memory such as glutamatergic receptors and scaffold proteins.[82] To further assess the disease-modifying effects of the rhein–huprine hybrids (+)- and (–)-**7e**, their potential protective effect on synaptic integrity was assessed in hippocampal slices of 2-month-old C57bl6 male mice incubated with Aβ42 oligomers.

Electrophysiological Assays. Firstly, electrophysiological registers of the hippocampal slices were used to evaluate synaptic transmission through the LTP. Hippocampal slices were incubated with Aβ42 oligomers (1 μM) 10 min prior and 10 min after LTP induction. No induction of LTP was observed in hippocampal slices incubated either with Aβ42 oligomers alone or with Aβ42 oligomers and (–)-**7e** (10 μM) (Figure 4A, white circles and light grey circles, respectively). On the contrary, treatment with (+)-**7e** (10 μM) led to a 200% LTP

induction (Figure 4A, dark grey circles), similarly to the effect found in the control slices treated only with artificial cerebrospinal fluid (ACSF). In Figure 4B, the quantification at min 60 of the field excitatory postsynaptic potentials (fEPSP) are shown. Treatment with (+)-**7e** led to a 200% magnitude response when compared to slices treated either with Aβ42 oligomers alone or with Aβ42 oligomers and (–)-**7e**. These results indicate that (+)-**7e** protects against the synaptic failure induced by acute treatments with Aβ42 oligomers, within the context of LTP induction.

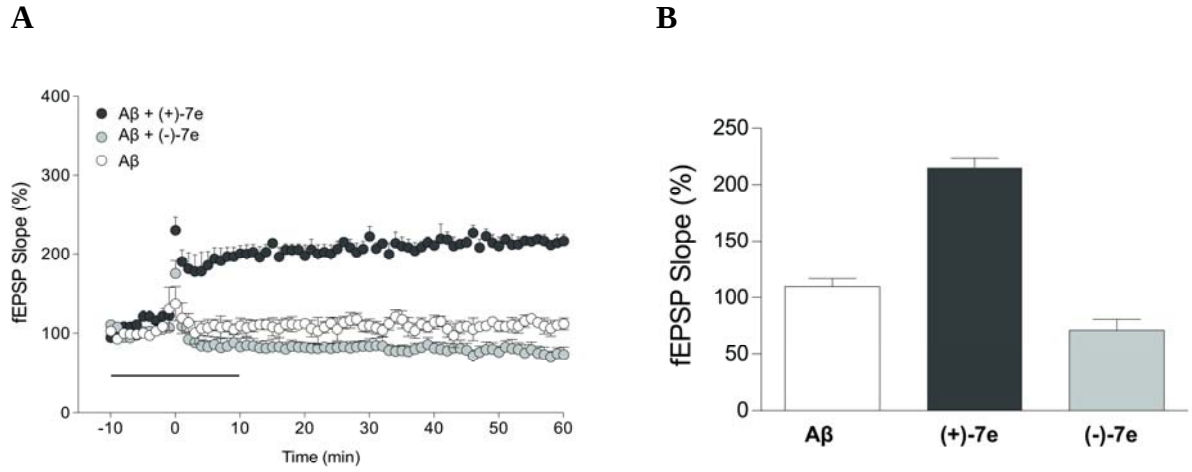

Figure 4. Electrophysiological assays in hippocampal slices of 2-month-old C57bl6 mice incubated with Aβ oligomers (1 μM) and (+)- or (–)-**7e** (10 μM). (A) Electrophysiological registers. (B) Quantification of field excitatory postsynaptic potentials (fEPSP).

Synaptic Protein Levels. Changes in the synaptic protein levels of hippocampal slices of 2-month-old C57bl6 mice treated with Aβ42 oligomers and different concentrations of (+)- and (–)-**7e** (1–100 μM) for 1 h were studied by densitometric analysis of western blots gels. Treatment of the hippocampal slices with Aβ42 oligomers (Figure 5, black bars) produced a decrease in the levels of the postsynaptic proteins GluA2 (a subunit of the AMPA receptor) and PSD95 (postsynaptic density protein 95, a scaffold protein within the postsynaptic density), and of the

presynaptic proteins synapsin (SYN) and the vesicular glutamate transporter 1 (VGlut1) in comparison with control slices (Figure 5, white bars), whereas the levels of the presynaptic protein synaptophysin (SYP) remained unchanged. In hippocampal slices co-treated with (–)-**7e** (Figure 5A) a neuroprotective effect was observed. Evident increases in the levels of GluA2 and PSD95 were observed at 10 and 100 μM, and in the levels of VGlut1 for every used concentration of (–)-**7e**, whereas increases in the levels of SYN and SYP were found only at the highest assayed concentration or were not observed. Co-treatment with (+)-**7e** produced increases, albeit more modest, in the levels of GluA2, PSD95 and SYN with every used concentration, whereas it had no effect on the levels of VGlut1 and SYP. Thus, both (+)- and (–)-**7e** exert a protective effect on synaptic proteins related with the stability of the synapses and the synaptic plasticity in the hippocampus.

Prevention of the Aβ-o-induced loss of synaptic proteins by treatment of hippocampal slices of 2-month-old C57bl6 mice with (+)-**7e** is in agreement with the results found in the electrophysiological assays and with the anti-amyloid activities found in the *in vitro* and in *E. coli* assays, namely its potent BACE-1 and Aβ aggregation inhibitory activities. Thus, the protective effects of (+)-**7e** and also (–)-**7e** on synaptic integrity might be ascribed to a reduction of the amount of Aβ aggregated species or to a reduction of Aβ production through the inhibition of APP processing, although participation of alternative or additional mechanisms can not be ruled out. For example, it has been reported that the increased levels of neurotransmitter acetylcholine due to AChE inhibition may promote changes in synaptic plasticity improving LTP.[83,84] Indeed, (–)-**7e**, the eutomer for hAChE inhibition, seems to be more potent regarding the preservation of synaptic proteins, even though it does not improve LTP. Different mechanisms are likely involved in the neuroprotective effect shown by (+)- and (–)-**7e**.

A

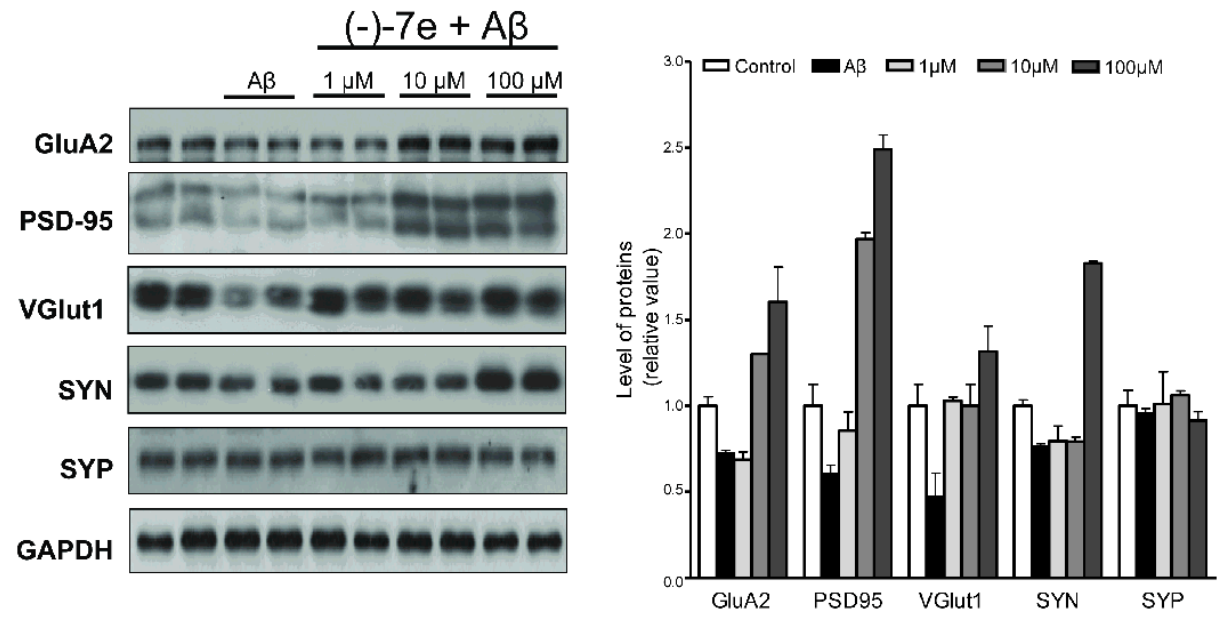

B

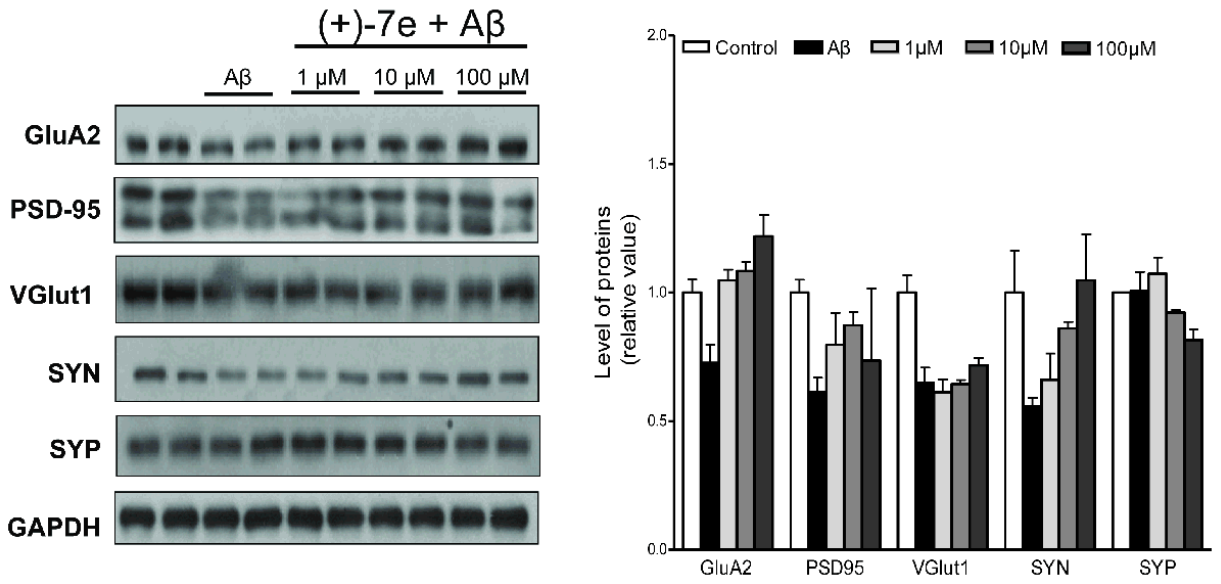

Figure 5. Synaptic protein levels of hippocampal slices of 2-month-old C57bl6 mice incubated with Aβ oligomers and (–)-**7e** (A) or (+)-**7e** (B).

***In Vivo* Aβ Lowering Effect.** Among the different interesting biological activities found *in vitro*, in *E. coli*, and *ex vivo* for the enantiopure rhein–huprine hybrids (+)-**7e** and (–)-**7e,** likely the most notable effect is the potent inhibition of BACE-1 (IC_{50} 80 nM). To gain further insight into the relevance of this activity, we have determined the *in vivo* effects of (+)-**7e** and (–)-**7e** on the level of total soluble Aβ oligomers, thought to be involved in synapse destruction and memory impairment in AD.[85] To this end, we used a well-established animal model of AD, namely the double transgenic mice APP-PS1 (see Experimental Section). This aggressive model of AD has been characterized both in the generation of senile plaques in the brain and in their behavioral changes,[86] describing the age at which these animals exhibit early senile plaques and cognitive impairment from 7 months of age, which occur mainly in the cortex and hippocampus.[86] 6- and 10-month-old APP-PS1 mice were treated with 2 mg/kg of (+)-**7e** or (–)-**7e** intraperitoneally three times per week for 4 weeks to evaluate the effects of these compounds on the production and aggregation of Aβ species in two different stages of the AD model; initial and severe, respectively. The soluble protein fraction from hippocampus homogenates of control and treated APP-PS1 mice was separated in tris-tricine gels, each lane being a different mouse, and specific mouse anti-β peptide 6E10 antibody was used, followed by immunoblot analysis.

Young (7-month-old after the treatment; n=3 control; n=3 (+)-**7e** treated; and n=2 (–)-**7e** treated APP-PS1 mice) and aged (11-month-old after the treatment; n=3 control; n=3 (+)-**7e** treated; and n=3 (–)-**7e** treated APP-PS1 mice) APP-PS1 mice exhibit several forms of Aβ peptides, including hexamers (ca. 24 kDa) and higher levels of Aβ dodecamers (ca. 56 kDa). Interestingly, young and aged APP-PS1 mice treated with (+)-**7e** showed a significant decrease in the levels of dodecamers, whereas only in young mice a reduction in the levels of hexamers was observed (Figures 6 and 7). In addition, young APP-PS1 mice treated with (–)-**7e** showed a

tendency toward decreased levels of both oligomeric species, whereas aged APP-PS1 mice treated with (–)-**7e** showed a diminution in the levels of dodecamers, without altering the levels of hexamers (Figures 6 and 7). The results observed in 11-month-old mice might be due to the high load of Aβ present in aging APP-PS1 mice. However the reduction in the levels of dodecamers, considered to be synaptotoxic, is very important, because it might be indicative of a reversion in the neurodegenerative process observed in the animal. More studies are necessary to corroborate this possibility. Together, these results suggest that rhein–huprine hybrids (+)-**7e** and (–)-**7e** either could favor the formation of senile plaques and the decrease of the soluble Aβ forms or prevent the APP processing and the subsequent aggregation, through inhibition of BACE-1. To corroborate the last hypothesis, the levels of APP protein were analyzed in the same gel described before where each lane represents an independent animal. The results showed that in young and aged APP-PS1 mice treated with (+)-**7e** and (–)-**7e** the levels of mature APP (ca. 100 KDa) are increased (Figures 6 and 7), indicating that these rhein–huprine hybrids are able to prevent APP processing, Aβ production and aggregation.

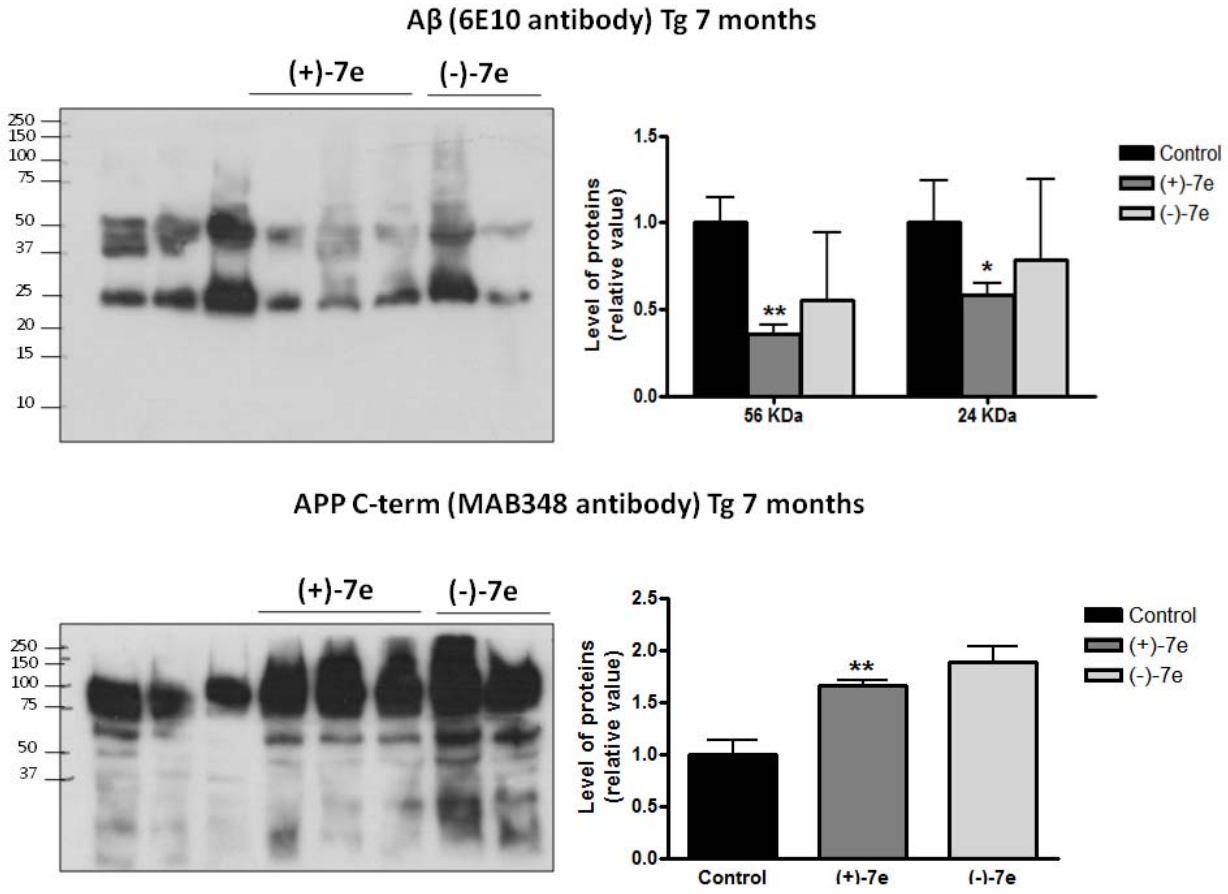

Figure 6. Soluble Aβ and APP protein levels of hippocampal samples from 7-month-old APP-PS1 mice treated with (–)-**7e** or (+)-**7e** for 4 weeks. Lanes 1-3 show hippocampus lysates from control mice (n=3), lanes 4-6 show hippocampus lysates from (+)-**7e** treated mice (n=3) and lanes 7-8 show hippocampus lysates from (–)-**7e** treated mice (n=2), each lane being an independent animal.

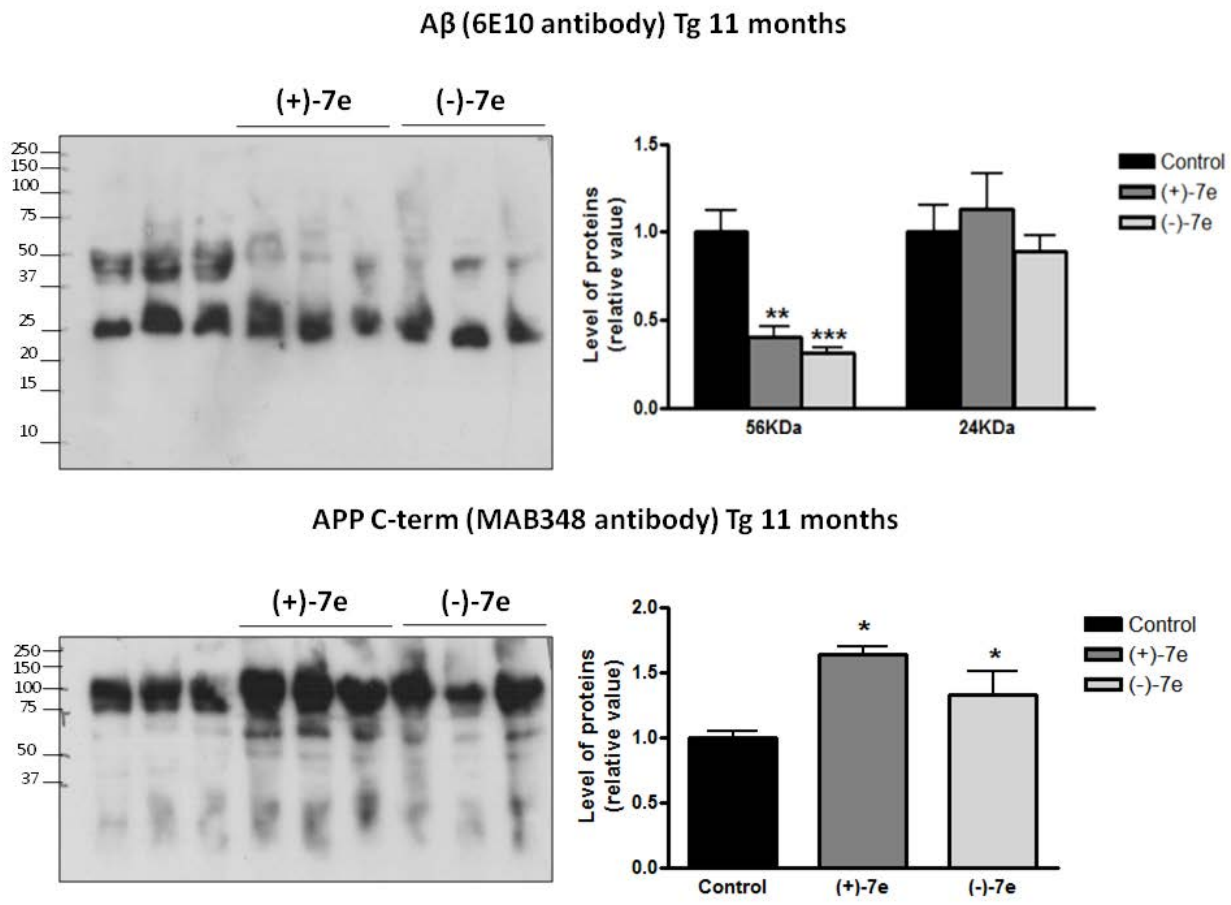

Figure 7. Soluble Aβ and APP protein levels of hippocampal samples from 11-month-old APP-PS1 mice treated with (–)-**7e** or (+)-**7e** for 4 weeks. Lanes 1-3 show hippocampus lysates from control mice (n=3), lanes 4-6 show hippocampus lysates from (+)-**7e** treated mice (n=3) and lanes 7-9 show hippocampus lysates from (–)-**7e** treated mice (n=3), each lane being an independent animal.

CONCLUSIONS

We have synthesized a series of racemic and enantiopure hybrid compounds that combine a unit of the hydroxyanthraquinone drug rhein and a unit of the potent AChE's CAS inhibitor huprine Y, connected through penta- to undeca-methylene or 1,4-phenylene-bis(methylene)

linkers. These hybrids were purportedly designed to exhibit a multi-target profile of interest for the efficient management of AD, which included the inhibitory actions expected for dual binding site inhibitors of AChE against the catalytic and the Aβ-proaggregating activities of this enzyme and the tau anti-aggregating effect known for some hydroxyanthraquinone compounds similar to rhein. In agreement with the design rationale, the novel rhein–huprine hybrids are endowed with very potent hAChE inhibitory activity and moderately potent inhibitory activities against hAChE-induced and self-induced aggregation of Aβ and against hBChE. Far beyond our expectations, some rhein–huprine hybrids additionally display a very potent BACE-1 inhibitory activity. Of note, these hybrids have been predicted to be able to cross BBB using an artificial membrane model, likely having the ability to exert the same actions *in vivo*. Both cell permeability and the Aβ anti-aggregating activity found *in vitro* for the rhein–huprine hybrids, as well as their expected tau anti-aggregating activity, have been confirmed by some assays based on the direct thioflavin S staining of IBs in intact *E. coli* cells that were genetically altered to overexpress Aβ42 and tau protein. On the basis of the biological profiling *in vitro* and in *E. coli*, (+)- and (–)-**7e** have been selected as lead rhein–huprine hybrids and their protective effects against the synaptic failure induced by Aβ oligomers in hippocampal slices of 2-month-old C57bl6 mice have been assessed. These studies have shown that both hybrids prevent the loss of synaptic proteins. Additionally, the beneficial effects of (+)-**7e** on synaptic integrity were apparent in the context of LTP induction. Finally, *in vivo* experiments with transgenic APP-PS1 mice have shown that (+)- and (–)-**7e** are able to lower the levels of hippocampal total soluble Aβ and increase the levels of APP both in initial and advanced stages of this AD model, thus suggesting a reduction of APP processing, as expected from their potent BACE-1 inhibitory activity. Overall, the novel rhein–huprine hybrids (+)- and (–)-**7e** emerge as very promising

multi-target anti-Alzheimer drug candidates with potential to positively modify the underlying mechanisms of this disease.

EXPERIMENTAL SECTION

Chemistry. Melting points were determined in open capillary tubes with a MFB 595010M Gallenkamp melting point apparatus. 400 MHz ^{1}H/100.6 MHz ^{13}C NMR spectra, and 500 MHz 1H/125.7 MHz ^{13}C NMR spectra were recorded on Varian Mercury 400, and Varian Inova 500 spectrometers, respectively. The chemical shifts are reported in ppm (δ scale) relative to internal tetramethylsilane, and coupling constants are reported in Hertz (Hz). Assignments given for the NMR spectra of the new compounds have been carried out on the basis of DEPT, COSY ^{1}H/^{1}H (standard procedures), and COSY ^{1}H/^{13}C (gHSQC or gHMBC sequences) experiments. The *syn* (*anti*) notation of the protons at position 13 of the huprine moiety of the hybrids means that the corresponding proton at position 13 is on the same (different) side of the quinoline moiety with respect to the cyclohexene ring. IR spectra were run on a Perkin-Elmer Spectrum RX I spectrophotometer. Absorption values are expressed as wave-numbers (cm^{-1}); only significant absorption bands are given. Optical rotations were measured on a Perkin-Elmer model 241 polarimeter. The specific rotation has not been corrected for the presence of solvent of crystallization. Column chromatography was performed on silica gel 60 AC.C (40–60 mesh, SDS, ref 2000027). Thin-layer chromatography was performed with aluminum-backed sheets with silica gel 60 F_{254} (Merck, ref 1.05554), and spots were visualized with UV light and 1% aqueous $KMnO_4$. NMR spectra of all of the new compounds were performed at the Centres Científics i Tecnològics of the University of Barcelona (CCiTUB), while elemental analyses and high resolution mass spectra were carried out at the Mycroanalysis Service of the IIQAB (CSIC,

Barcelona, Spain) with a Carlo Erba 1106 analyzer, and at the CCiTUB with a LC/MSD TOF Agilent Technologies spectrometer, respectively. The synthetic procedures for the preparation of the intermediate nitriles **5a**–**h** and amines **5a**–**h** are exemplified through the synthesis of **5a** and **6a**. The synthesis of the rest of nitriles and amines is included in the Supporting Information. The analytical samples of all of the rhein–huprine hybrids which were subjected to pharmacological evaluation possess a purity ≥95% as evidenced by their elemental analyses.

(±)-5-[(3-Chloro-6,7,10,11-tetrahydro-9-methyl-7,11-methanocycloocta[*b*]quinolin-12-yl)amino]pentanenitrile [(±)-5a]. A suspension of (±)-huprine Y, (±)-**4** (300 mg, 1.06 mmol) and finely powdered KOH (85% purity, 139 mg, 2.11 mmol), and 4 Å molecular sieves in anhyd DMSO (6 mL) was stirred, heating every 10 min approximately with a heat gun for 1 h and at rt one additional hour, and then treated with 5-bromovaleronitrile (0.15 mL, 208 mg, 1.28 mmol). The reaction mixture was stirred at rt overnight, diluted with 5N NaOH (25 mL) and extracted with EtOAc (3×40 mL). The combined organic extracts were washed with H_2O (3×50 mL), dried over anhyd Na_2SO_4, and evaporated under reduced pressure to give a yellow oil (469 mg), which was purified by column chromatography (40–60 μm silica gel, CH_2Cl_2/MeOH/50% aq. NH_4OH mixtures, gradient elution). On elution with CH_2Cl_2/50% aq. NH_4OH 100:0.2, the *N*,*N*-dialkylated derivative (±)-**8a** (78 mg, 16% yield) was isolated as a yellow oil. On elution with CH_2Cl_2/MeOH/50% aq. NH_4OH 99:1:0.2, nitrile (±)-**5a** (273 mg, 70% yield) was isolated as a beige solid; $R_{f[(\pm)\text{-}\mathbf{5a}]}$ 0.50; $R_{f[(\pm)\text{-}\mathbf{8a}]}$ 0.77 (CH_2Cl_2/MeOH/50% aq. NH_4OH 9:1:0.05).

A solution of (±)-**5a** (52 mg, 0.14 mmol) in CH_2Cl_2 (4.5 mL) was filtered through a 0.2 μm PTFE filter, treated with methanolic HCl (1.40N, 0.30 mL) and evaporated under reduced pressure. The resulting solid was washed with pentane (3×2 mL) to give, after drying at 65 ºC/2 Torr for 48 h, (±)-**5a**·HCl (58 mg) as a yellow solid: mp 181–183 °C (CH_2Cl_2/MeOH 94:6); IR

(KBr) *v* 3500–2500 (max at 3364, 3254, 3049, 3014, 2926, 2885, 2651, N-H, N^+-H and C-H st), 2243 (CN st), 1635, 1629, 1602, 1582, 1570, 1562 (ar-C-C and ar-C-N st) cm^{-1}; ^1H NMR (400 MHz, CD_3OD) δ 1.59 (s, 3H, 9'-CH_3), 1.79 (tt, $J \approx J' \approx 7.2$ Hz, 2H, 3-H_2), 1.93 (d, J=17.6 Hz, 1H, 10'-H_{endo}), superimposed in part 1.92–1.98 (m, 1H, 13'-H_{syn}), 2.01 (tt, $J \approx J' \approx 7.2$ Hz, 2H, 4-H_2), 2.09 (dm, J=12.8 Hz, 1H, 13'-H_{anti}), 2.56 (t, J=7.2 Hz, 2H, 2-H_2), superimposed in part 2.53–2.60 (m, 1H, 10'-H_{exo}), 2.77 (m, 1H, 7'-H), 2.88 (ddd, J=18.0 Hz, $J'=J''$=1.6 Hz, 1H, 6'-H_{endo}), 3.22 (dd, J=18.0 Hz, J'=5.2 Hz, 1H, 6'-H_{exo}), 3.47 (m, 1H, 11'-H), 4.03 (t, J= 7.6 Hz, 2H, 5-H_2), 4.85 (s, NH and $^+$NH), 5.59 (br d, J=4.4 Hz, 1H, 8'-H), 7.57 (dd, J=9.2 Hz, J'=2.0 Hz, 1H, 2'-H), 7.78 (d, $J \approx$2.0 Hz, 1H, 4'-H), 8.40 (d, $J \approx$9.2 Hz, 1H, 1'-H); ^{13}C NMR (100.6 MHz, CD_3OD) δ 17.1 (CH_2, C2), 23.4 (CH_3, 9'-CH_3), 23.9 (CH_2, C3), 27.3 (CH, C11'), 27.9 (CH, C7'), 29.3 (CH_2, C13'), 30.3 (CH_2, C4), 36.1 (CH_2), 36.2 (CH_2) (C6', C10'), 48.8 (CH_2, C5), 115.8 (C, C12a'), 117.9 (C, C11a'), 119.2 (CH, C4'), 120.9 (C, CN), 125.1 (CH, C8'), 126.8 (CH, C2'), 129.4 (CH, C1'), 134.6 (C, C9'), 140.3 (C, C3'), 141.0 (C, C4a'), 151.5 (C, C5a'), 157.0 (C, C12'). HRMS (ESI) calcd for ($C_{22}H_{24}{}^{35}ClN_3 + H^+$): 366.1732, found 366.1729.

A solution of (±)-**8a** (78 mg, 0.17 mmol) in CH_2Cl_2 (4.5 mL) was filtered through a 0.2 μm PTFE filter, treated with methanolic HCl (0.65N, 0.64 mL) and evaporated under reduced pressure. The resulting solid was washed with pentane (3×2 mL) to give, after drying at 65 ºC/2 Torr for 48 h, (±)-**8a**·HCl (80 mg) as a yellow solid: mp 196–198 ºC (CH_2Cl_2/MeOH 88:12); IR (KBr) *v* 3500–2450 (max at 3430, 3044, 2919, 2875, 2464, N^+-H and C-H st), 2243 (CN st), 1632, 1604, 1574 (ar-C-C and ar-C-N st) cm^{-1}; ^1H NMR (400 MHz, CD_3OD) δ 1.59 (s, 3H, 9'-CH_3), 1.65 (tt, $J \approx J' \approx 7.2$ Hz, 4H, 3-H_2), 1.72–1.98 (complex signal, 4H, 4-H_2), 2.00 (br d, J=17.6 Hz, 1H, 10'-H_{endo}), superimposed in part 2.06 (dm, $J \approx$12.8 Hz, 1H, 13'-H_{syn}), 2.12 (dm, J=12.8 Hz, 1H, 13'-H_{anti}), 2.48 (t, J=7.2 Hz, 4H, 2-H_2), 2.69 (dd, J=17.6 Hz, J'=5.6 Hz, 1H, 10'-H_{exo}),

2.82 (m, 1H, 7'-H), 3.17 (ddd, J=18.0 Hz, $J'\approx J''\approx$1.8 Hz, 1H, 6'-H_{endo}), 3.39 (dd, J=18.0 Hz, J'=5.6 Hz, 1H, 6'-H_{exo}), superimposed in part 3.73 (m, 1H, 11'-H), 3.73 (ddd, J=13.6 Hz, J'=9.6 Hz, J''=5.6 Hz, 2H) and 3.80 (ddd, J=13.6 Hz, J'=9.2 Hz, J''=6.0 Hz, 2H) (5-H_2), 4.84 (s, $^{+}$NH), 5.68 (br d, J=4.4 Hz, 1H, 8'-H), 7.72 (dd, J=9.2 Hz, J'=2.4 Hz, 1H, 2'-H), 7.99 (d, J=2.4 Hz, 1H, 4'-H), 8.26 (d, J=9.2 Hz, 1H, 1'-H); ^{13}C NMR (100.6 MHz, CD_3OD) δ 17.1 (CH_2, C2), 23.3 (CH_3, 9'-CH_3), 23.9 (CH_2, C3), 27.6 (CH, C7'), 28.6 (CH_2, C13'), 28.9 (CH_2, C4), 29.7 (CH, C11'), 37.7 (CH_2, C6'), 38.7 (CH_2, C10'), 55.1 (CH_2, C5), 120.0 (CH, C4'), 120.9 (C, CN), 125.5 (C, C12a'), 125.7 (CH, C8'), 192.2 (CH, C2'), 130.1 (CH, C1'), 132.5 (C, C11a'), 134.3 (C, C9'), 140.36 (C), 140.43 (C) (C3', C4a'), 157.6 (C, C5a'), 163.9 (C, C12'); HRMS (ESI) calcd for ($C_{27}H_{31}{}^{35}ClN_4 + H^+$) 447.2310, found 447.2309.

(±)-*N*-(3-Chloro-6,7,10,11-tetrahydro-9-methyl-7,11-methanocycloocta[*b*]quinolin-12-yl)pentane-1,5-diamine [(±)-6a]. To a suspension of $LiAlH_4$ (0.17 g, 4.47 mmol) in anhyd Et_2O (63 mL), nitrile (±)-**5a** (0.76 g, 2.08 mmol) was added, and the reaction mixture was stirred at rt overnight. The resulting mixture was treated with wet Et_2O (200 mL) and evaporated under reduced pressure. The solid was suspended in CH_2Cl_2, filtered through Celite® and evaporated under reduced pressure, to give amine (±)-**6a** (750 mg, 98% yield) as a yellow oil; R_f 0.03 (CH_2Cl_2/MeOH/50% aq. NH_4OH 9:1:0.05).

A solution of (±)-**6a** (50 mg, 0.14 mmol) in CH_2Cl_2 (3.5 mL) was filtered through a 0.2 μm PTFE filter, treated with methanolic HCl (1.4N, 0.87 mL), and evaporated under reduced pressure. The resulting solid was washed with pentane (3×2 mL) to give, after drying at 65 ºC/2 Torr for 48 h, (±)-**6a**·2HCl (54 mg) as a yellow solid: mp 193–194 ºC (CH_2Cl_2/MeOH 80:20); IR (KBr) ν 3500–2500 (max at 3396, 3253, 2925, 2856, N-H, N^+-H and C-H st), 1628, 1583, 1570, 1558 (ar-C-C and ar-C-N st) cm^{-1}; ^{1}H NMR (400 MHz, CD_3OD) δ 1.55 (tt, $J\approx J'\approx$7.6 Hz, 2H, 3-

H_2), 1.59 (s, 3H, 9'-CH_3), 1.76 (m, 2H, 4-H_2), 1.90–2.02 (complex signal, 4H, 10'-H_{endo}, 13'-H_{syn}, 2-H_2), 2.09 (dm, J=12.8 Hz, 1H, 13'-H_{anti}), 2.57 (ddm, J=17.6 Hz, J'=6.0 Hz, 1H, 10'-H_{exo}), 2.78 (m, 1H, 7'-H), 2.87 (br d, J=18.0 Hz, 1H, 6'-H_{endo}), 2.97 (t, J=7.6 Hz, 2H, 5-H_2), 3.21 (dd, J=18.0 Hz, J'=5.6 Hz, 1H, 6'-H_{exo}), 3.49 (m, 1H, 11'-H), 4.01 (t, $J\approx$7.6 Hz, 2H, 1-H_2), 4.85 (s, NH and $^{+}$NH), 5.59 (br d, J=4.4 Hz, 1H, 8'-H), 7.57 (dd, J=9.2 Hz, J'=2.0 Hz, 1H, 2'-H), 7.78 (d, J=2.0 Hz, 1H, 4'-H), 8.41 (d, J=9.2 Hz, 1H, 1'-H); ^{13}C NMR (100.6 MHz, CD_3OD) δ 23.5 (CH_3, 9'-CH_3), 24.7 (CH_2, C3), 27.3 (CH, C11'), 27.9 (CH, C7'), 28.2 (CH_2, C4), 29.3 (CH_2, C13'), 30.8 (CH_2, C2), 36.0 (CH_2), 36.2 (CH_2) (C6', C10'), 40.5 (CH_2, C5), 49.4 (CH_2, C1), 115.7 (C, C12a'), 117.8 (C, C11a'), 119.2 (CH, C4'), 125.1 (CH, C8'), 126.8 (CH, C2'), 129.4 (CH, C1'), 134.6 (C, C9'), 140.3 (C, C3'), 141.0 (C, C4a'), 151.4 (C, C5a'), 156.9 (C, C12'); HRMS (ESI) calcd for ($C_{22}H_{28}{}^{35}ClN_3 + H^+$) 370.2045, found 370.2041.

(±)-*N*-{5-[(3-Chloro-6,7,10,11-tetrahydro-9-methyl-7,11-methanocycloocta[*b*]quinolin-12-yl)amino]pentyl}-9,10-dihydro-4,5-dihydroxy-9,10-dioxoanthracene-2-carboxamide [(±)-7a]. A suspension of rhein, **3** (477 mg, 1.68 mmol), in anhyd CH_2Cl_2 (6 mL) was cooled to 0 ºC with an ice bath, and treated dropwise with freshly distilled Et_3N (0.47 mL, 341 mg, 3.38 mmol) and $ClCO_2Et$ (0.16 mL, 182 mg, 1.68 mmol). The resulting solution was stirred at 0 ºC for 30 min and treated with a solution of amine (±)-**6a** (621 mg, 1.68 mmol) in anhyd CH_2Cl_2 (6 mL). The reaction mixture was stirred at rt for 3 days, diluted with 10% aq. Na_2CO_3 (50 mL), the phases were separated and the aqueous phase was extracted with CH_2Cl_2 (3×35 mL). The combined organic extracts were dried over anhyd Na_2SO_4 and evaporated under reduced pressure, to give a red solid (770 mg), which was purified by column chromatography (40–60 µm silica gel, CH_2Cl_2/MeOH/50% aq. NH_4OH mixtures, gradient elution). On elution with

CH_2Cl_2/MeOH/50% aq. NH_4OH 99:1:0.2, hybrid (±)-**7a** (140 mg, 13% yield) was isolated as a red solid; R_f 0.45 (CH_2Cl_2/MeOH/50% aq. NH_4OH 9:1:0.05).

A solution of hybrid (±)-**7a** (79 mg, 0.12 mmol) in CH_2Cl_2 (4 mL) was filtered through a 0.2 μm PTFE filter, treated with methanolic HCl (1.4N, 0.26 mL) and evaporated under reduced pressure. The resulting solid was washed with pentane (3×2 mL) to give, after drying at 65 ºC/2 Torr for 48 h, (±)-**7a**·HCl (80 mg) as a yellow solid: mp 213–215 °C (CH_2Cl_2/MeOH 94:6); IR (KBr) ν 3500–2500 (max at 3224, 3047, 3005, 2923, 2852, O-H, N-H, N^+-H and C-H st), 1669, 1628, 1582, 1565 (C=O, ar-C-C and ar-C-N st) cm^{-1}; ^1H NMR (500 MHz, CD_3OD) δ 1.54–1.64 (complex signal, 2H, 3'-H_2), superimposed in part 1.59 (s, 3H, 9"-CH_3), 1.77 (tt, $J \approx J' \approx 7.0$ Hz, 2H, 2'-H_2), superimposed in part 1.90–2.00 (complex signal, 3H, 4'-H_2, 13"-H_{syn}), 1.94 (d, $J \approx 17.0$ Hz, 1H, 10"-H_{endo}), 2.08 (br d, J=12.5 Hz, 1H, 13"-H_{anti}), 2.56 (br dd, J=17.0 Hz, J'=4.0 Hz, 1H, 10"-H_{exo}), 2.77 (m, 1H, 7"-H), 2.84 (d, J=17.5 Hz, 1H, 6"-H_{endo}), 3.18 (dd, J=17.5 Hz, J'=5.5 Hz, 1H, 6"-H_{exo}), 3.42–3.52 (complex signal, 3H, 1'-H_2, 11"-H), 4.00 (dt, $J=J'$=7.5 Hz, 2H, 5'-H_2), 4.87 (s, NH, $^+$NH and OH), 5.58 (br d, J=4.5 Hz, 1H, 8"-H), 7.35 (dd, J=7.5 Hz, J'=2.0 Hz, 1H, 6-H), 7.47 (br d, J=8.5 Hz, 1H, 2"-H), 7.62 (br s, 2H, 3-H, 4"-H), 7.76 (d, J=7.5 Hz, 1H, 8-H), 7.78 (dd, $J=J'$=7.5 Hz, 1H, 7-H), 8.04 (s, 1H, 1-H), 8.34 (d, J=8.5 Hz, 1H, 1"-H); ^{13}C NMR (125.7 MHz, CD_3OD) δ 23.5 (CH_3, 9"-CH_3), 25.1 (CH_2, C3'), 27.3 (CH, C11"), 27.9 (CH, C7"), 29.3 (CH_2, C13"), 29.9 (CH_2, C2'), 31.0 (CH_2, C4'), 36.1 (CH_2, C6"), 36.2 (CH_2, C10"), 40.7 (CH_2, C1'), 49.5 (CH_2, C5'), 115.7 (C, C12a"), 117.0 (C, C10a), 117.6 (C, C11a"), 118.6 (C, C4a), 118.8 (CH, C1), 119.1 (CH, C4"), 120.9 (CH, C8), 123.7 (CH, C3), 125.1 (CH, C8"), 125.8 (CH, C6), 126.7 (CH, C2"), 129.3 (CH, C1"), 134.6 (C, C9"), 134.8 (C, C8a), 135.2 (C, C9a), 138.8 (CH, C7), 140.2 (C, C3"), 140.9 (C, C4a"), 143.4 (C, C2), 151.4 (C, C5a"), 156.7 (C, C12"), 163.4 (C, C4), 163.7 (C, C5), 167.3 (C, CONH), 182.2 (C, C9), 193.7 (C, C10);

HRMS (ESI) calcd for ($C_{37}H_{34}{}^{35}ClN_3O_5$ + H^+) 636.2260, found 636.2255. Anal. ($C_{37}H_{34}ClN_3O_5 \cdot HCl \cdot 1.5H_2O$) C, H, N, Cl.

(±)-*N*-{6-[(3-Chloro-6,7,10,11-tetrahydro-9-methyl-7,11-methanocycloocta[*b*]quinolin-12-yl)amino]hexyl}-9,10-dihydro-4,5-dihydroxy-9,10-dioxoanthracene-2-carboxamide

[(±)-7b]. It was prepared as described for (±)-**7a**. From rhein, **3** (1.19 g, 4.18 mmol), and amine (±)-**6b** (1.60 g, 4.18 mmol), a red solid (2.00 g) was obtained and purified by column chromatography (40–60 μm silica gel, hexane/EtOAc/MeOH/Et_3N mixtures, gradient elution). On elution with hexane/EtOAc/MeOH/Et_3N 10:90:0:0.2 to 0:80:20:0.2, hybrid (±)-**7b** (647 mg, 24% yield) was isolated as a red solid; R_f 0.54 (CH_2Cl_2/MeOH/50% aq. NH_4OH 9:1:0.05).

(±)-7b·HCl: mp 203–205 °C (CH_2Cl_2/MeOH 89:11); IR (KBr) ν 3500–2500 (max at 3228, 3042, 2927, 2859, 2722, O-H, N-H, N^+-H and C-H st), 1627, 1586, 1570 (C=O, ar-C-C and ar-C-N st) cm^{-1}; ^1H NMR (500 MHz, CD_3OD) δ 1.49–1.56 (complex signal, 4H, 3'-H_2, 4'-H_2), 1.59 (s, 3H, 9"-CH_3), 1.70 (tt, $J \approx J' \approx 6.7$ Hz, 2H, 2'-H_2), superimposed in part 1.87–1.94 (complex signal, 3H, 5'-H_2, 13"-H_{syn}), superimposed in part 1.94 (br d, J=17.5 Hz, 1H, 10"-H_{endo}), 2.07 (dm, J=12.0 Hz, 1H, 13"-H_{anti}), 2.54 (br dd, $J \approx 17.5$ Hz, $J' \approx 3.5$ Hz, 1H, 10"-H_{exo}), 2.77 (m, 1H, 7"-H), 2.82 (br d, J=18.0 Hz, 1H, 6"-H_{endo}), 3.17 (dd, J=18.0 Hz, J'=5.0 Hz, 1H, 6"-H_{exo}), 3.39–3.49 (complex signal, 3H, 1'-H_2, 11"-H), 3.96 (dt, $J = J' = 6.7$ Hz, 2H, 6'-H_2), 4.84 (s, NH, $^+$NH and OH), 5.58 (br d, J=5.0 Hz, 1H, 8"-H), 7.35 (dd, J=7.5 Hz, J'=1.5 Hz, 1H, 6-H), 7.46 (d, $J \approx 9.0$ Hz, 1H, 2"-H), 7.60 (s, 1H, 4"-H), 7.64 (s, 1H, 3-H), superimposed in part 7.75 (d, J=8.0 Hz, 1H, 8-H), superimposed in part 7.77 (dd, $J \approx J' \approx 8.0$ Hz, 1H, 7-H), 8.07 (s, 1H, 1-H), 8.32 (d, $J \approx 9.0$ Hz, 1H, 1"-H); ^{13}C NMR (125.7 MHz, CD_3OD) δ 23.4 (CH_3, 9"-CH_3), 27.2 (CH, C11"), 27.3 ($2CH_2$, C3', C4'), 27.9 (CH, C7"), 29.3 (CH_2, C13"), 30.0 (CH_2, C2'), 31.1 (CH_2, C5'), 36.1 ($2CH_2$, C6", C10"), 40.7 (CH_2, C1'), 49.5 (CH_2, C6'), 115.7 (C, C12a"), 117.0 (C, C10a),

117.7 (C, C11a"), 118.6 (C, C4a), 118.8 (CH, C1), 119.1 (CH, C4"), 120.9 (CH, C8), 123.7 (CH, C3), 125.1 (CH, C8"), 125.8 (CH, C6), 126.6 (CH, C2"), 129.4 (CH, C1"), 134.6 (C, C9"), 134.8 (C, C8a), 135.3 (C, C9a), 138.8 (CH, C7), 140.2 (C, C3"), 141.0 (C, C4a"), 143.6 (C, C2), 151.3 (C, C5a"), 156.8 (C, C12"), 163.4 (C, C4), 163.8 (C, C5), 167.3 (C, CONH), 182.2 (C, C9), 193.8 (C, C10); HRMS (ESI) calcd for ($C_{38}H_{36}{}^{35}ClN_3O_5$ + H^+) 650.2416, found 650.2414. Anal. ($C_{38}H_{36}ClN_3O_5 \cdot HCl \cdot 1.25H_2O$) C, H, N, Cl.

(±)-*N*-{7-[(3-Chloro-6,7,10,11-tetrahydro-9-methyl-7,11-methanocycloocta[*b*]quinolin-12-yl)amino]heptyl}-9,10-dihydro-4,5-dihydroxy-9,10-dioxoanthracene-2-carboxamide [(±)-7c]. It was prepared as described for (±)-**7a**. From rhein, **3** (1.43 g, 5.04 mmol), and amine (±)-**6c** (2.00 g, 5.04 mmol), a red solid (2.20 g) was obtained and purified by column chromatography (40–60 μm silica gel, hexane/EtOAc/MeOH/Et_3N mixtures, gradient elution). On elution with hexane/EtOAc/MeOH/Et_3N 40:60:0:0.2 to 0:80:20:0.2, hybrid (±)-**7c** (864 mg, 26% yield) was isolated as a red solid; R_f 0.48 (CH_2Cl_2/MeOH/50% aq. NH_4OH 9:1:0.05).

(±)-7c·HCl: mp 202–203 °C (EtOAc/CH_2Cl_2/MeOH 75:19:6); IR (KBr) ν 3500–2500 (max at 3048, 2926, 2855, 2742, O-H, N-H, N^+-H and C-H st), 1654, 1628, 1593, 1583, 1569, 1546 (C=O, ar-C-C and ar-C-N st) cm^{-1}; ^1H NMR (500 MHz, CD_3OD) δ 1.49 (complex signal, 6H, 3'-H_2, 4'-H_2, 5'-H_2), 1.58 (s, 3H, 9"-CH_3), 1.69 (tt, $J \approx J' \approx 6.5$ Hz, 2H, 2'-H_2), superimposed in part 1.87–1.94 (complex signal, 3H, 6'-H_2, 13"-H_{syn}), superimposed in part 1.94 (br d, $J \approx 18.0$ Hz, 1H, 10"-H_{endo}), 2.07 (dm, J=12.0 Hz, 1H, 13-H_{anti}), 2.53 (br dd, J=18.0 Hz, J'=5.0 Hz, 1H, 10-H_{exo}), 2.75 (m, 1H, 7"-H), 2.79 (br d, $J \approx 18.0$ Hz, 1H, 6"-H_{endo}), 3.14 (dd, $J \approx 18.0$ Hz, J'=5.5 Hz, 1H, 6"-H_{exo}), 3.37–3.48 (complex signal, 3H, 1'-H_2, 11"-H), 3.92 (dt, J=7.5 Hz, J'=4.0 Hz, 2H, 7'-H_2), 4.84 (s, NH, $^+$NH and OH), 5.58 (br d, J=5.0 Hz, 1H, 8"-H), 7.36 (dd, J=8.5 Hz, J'=1.0 Hz, 1H, 6-H), 7.44 (dd, $J \approx 9.0$ Hz, J'=2.0 Hz, 1H, 2"-H), 7.59 (d, J=2.0 Hz, 1H, 4"-H),

7.66 (d, *J*≈2.0 Hz, 1H, 3-H), 7.73 (dd, *J*=7.5 Hz, *J'*≈1.0 Hz, 1H, 8-H), 7.78 (dd, *J*≈*J'*≈7.5 Hz, 1H, 7-H), 8.09 (d, *J*=2.0 Hz, 1H, 1-H), 8.26 (d, *J*=9.0 Hz, 1H, 1"-H); ^{13}C NMR (125.7 MHz, CD_3OD) δ 23.4 (CH_3, 9"-CH_3), 27.3 (CH, C11"), 27.6 (CH_2), 27.7 (CH_2) (C4', C5'), 27.9 (CH, C7"), 29.3 (CH_2, C13"), 29.7 (CH_2), 29.9 (CH_2) (C2', C3'), 31.1 (CH_2, C6'), 36.0 (CH_2), 36.1 (CH_2) (C6", C10"), 41.0 (CH_2, C1'), 49.7 (CH_2, C7'), 115.6 (C, C12a"), 117.1 (C, C10a), 117.6 (C, C11a"), 118.6 (C, C4a), 118.7 (CH, C1), 119.2 (CH, C4"), 120.9 (CH, C8), 123.7 (CH, C3), 125.1 (CH, C8"), 125.8 (CH, C6), 126.6 (CH, C2"), 129.3 (CH, C1"), 134.6 (C, C9"), 134.8 (C, C8a), 135.3 (C, C9a), 138.8 (CH, C7), 140.2 (C, C3"), 141.0 (C, C4a"), 143.7 (C, C2), 151.3 (C, C5a"), 156.6 (C, C12"), 163.5 (C, C4), 163.8 (C, C5), 167.4 (C, CONH), 182.2 (C, C9), 193.6 (C, C10); HRMS (ESI) calcd for ($C_{39}H_{38}{}^{35}ClN_3O_5$ + H^+) 664.2573 found 664.2569. Anal. ($C_{39}H_{38}ClN_3O_5 \cdot HCl \cdot 0.5H_2O$) C, H, N, Cl.

(±)-*N*-{8-[(3-Chloro-6,7,10,11-tetrahydro-9-methyl-7,11-methanocycloocta[*b*]quinolin-12-yl)amino]octyl}-9,10-dihydro-4,5-dihydroxy-9,10-dioxoanthracene-2-carboxamide [(±)-7d]. It was prepared as described for (±)-**7a**. From rhein, **3** (213 mg, 0.75 mmol), and amine (±)-**6d** (307 mg, 0.75 mmol), a red solid (740 mg) was obtained and purified by column chromatography (40–60 μm silica gel, CH_2Cl_2/MeOH/50% aq. NH_4OH mixtures, gradient elution). On elution with CH_2Cl_2/MeOH/50% aq. NH_4OH 98:2:0.2 to 80:20:0.2, hybrid (±)-**7d** (80 mg, 16% yield) was isolated as a red solid; R_f 0.30 (CH_2Cl_2/MeOH/50% aq. NH_4OH 9:1:0.05).

(±)-7d·HCl: mp 180–182 °C (EtOAc/CH_2Cl_2/MeOH 66:17:17); IR (KBr) ν 3500–2500 (max at 3222, 3047, 3007, 2924, 2852, 2640, O-H, N-H, N^+-H and C-H st), 1766, 1674, 1628, 1607, 1582, 1566, 1522 (C=O, ar-C-C and ar-C-N st) cm^{-1}; ^{1}H NMR (500 MHz, CD_3OD) δ 1.44 (complex signal, 8H, 3'-H_2, 4'-H_2, 5'-H_2, 6'H_2), 1.59 (s, 3H, 9"-CH_3), 1.67 (tt, *J*≈*J'*≈7.0 Hz, 2H,

2'-H_2), superimposed in part 1.86 (tt, $J \approx J' \approx 7.0$ Hz, 2H, 7'-H_2), superimposed 1.85−1.94 (m, 1H, 13"-H_{syn}), superimposed in part 1.93 (br d, $J \approx 18.0$ Hz, 1H, 10"-H_{endo}), 2.06 (dm, $J = 12.0$ Hz, 1H, 13"-H_{anti}), 2.53 (br dd, $J \approx 18.0$ Hz, $J' = 4.5$ Hz, 1H, 10"-H_{exo}), 2.75 (m, 1H, 7"-H), 2.82 (br d, $J = 18.0$ Hz, 1H, 6"-H_{endo}), 3.13 (dd, $J = 18.0$ Hz, $J' = 5.0$ Hz, 1H, 6"-H_{exo}), 3.39–3.47 (complex signal, 3H, 1'-H_2, 11"-H), 3.87 (dt, $J \approx J' \approx 6.0$ Hz, 2H, 8'-H_2), 4.86 (s, NH, $^{+}$NH and OH), 5.58 (br d, $J = 5.0$ Hz, 1H, 8"-H), 7.26 (d, $J = 8.5$ Hz, 1H, 6-H), 7.35 (d, $J \approx 9.0$ Hz, 1H, 2"-H), 7.54 (s, 1H, 4"-H), 7.58 (s, 1H, 3-H), superimposed in part 7.57−7.61 (m, 1H, 8-H), 7.69 (dd, $J \approx J' \approx 8.0$ Hz, 1H, 7-H), 7.97 (s, 1H, 1-H), 8.19 (d, $J = 9.0$ Hz, 1H, 1"-H); ^{13}C NMR (125.7 MHz, CD_3OD) δ 23.5 (CH_3, 9"-CH_3), 27.2 (CH, C11"), 27.5 (CH_2), 27.6 (CH_2), (C5', C6'), 27.8 (CH, C7"), 29.3 (CH_2, C13"), 29.86 (CH_2), 29.92 (CH_2), 30.0 (CH_2) (C2', C3', C4'), 31.1 (CH_2, C7'), 36.0 (2CH_2, C6", C10"), 41.0 (CH_2, C1'), 49.7 (CH_2, C8'), 115.4 (C, C12a"), 116.7 (C, C10a), 117.5 (C, C11a"), 118.3 (C, C4a), 118.8 (CH, C1), 119.0 (CH, C4"), 120.8 (CH, C8), 123.7 (CH, C3), 125.1 (CH, C8"), 125.8 (CH, C6), 126.6 (CH, C2"), 129.2 (CH, C1"), 134.4 (C, C9"), 134.6 (C, C8a), 134.9 (C, C9a), 138.8 (CH, C7), 140.1 (C, C3"), 140.8 (C, C4a"), 143.6 (C, C2), 151.1 (C, C5a"), 156.5 (C, C12"), 163.3 (C, C4), 163.5 (C, C5), 167.1 (C, CONH), 181.8 (C, C9), 193.4 (C, C10); HRMS (ESI) calcd for ($C_{40}H_{40}{}^{35}ClN_3O_5$ + H^+) 678.2729, found 678.2734. Anal. ($C_{40}H_{40}ClN_3O_5 \cdot HCl \cdot H_2O$) C, H, N, Cl.

(±)-*N*-{9-[(3-Chloro-6,7,10,11-tetrahydro-9-methyl-7,11-methanocycloocta[*b*]quinolin-12-yl)amino]nonyl}-9,10-dihydro-4,5-dihydroxy-9,10-dioxoanthracene-2-carboxamide [(±)-7e]. It was prepared as described for (±)-**7a**. From rhein, **3** (213 mg, 0.75 mmol), and amine (±)-**6e** (321 mg, 0.75 mmol), a red solid (550 mg) was obtained and purified by column chromatography (40–60 μm silica gel, hexane/EtOAc/MeOH/Et_3N mixtures, gradient elution).

On elution with hexane/EtOAc/MeOH/Et_3N 20:80:0:0.2 to 0:80:20:0.2, hybrid (±)-**7e** (118 mg, 23% yield) was isolated as a red solid; R_f 0.33 (CH_2Cl_2/MeOH/50% aq. NH_4OH 9:1:0.05).

(±)-7e·HCl: mp 192−193 °C (EtOAc/CH_2Cl_2/MeOH 70:15:15); IR (KBr) ν 3500−2500 (max at 3401, 2925, 2853, O-H, N-H, N^+-H and C-H st), 1628, 1584, 1566, 1524 (C=O, ar-C-C and ar-C-N st) cm^{-1}; ^1H NMR (500 MHz, CD_3OD) δ 1.41 (complex signal, 10H, 3'-H_2, 4'-H_2, 5'-H_2, 6'H_2, 7'-H_2), 1.59 (s, 3H, 9"-CH_3), superimposed in part 1.64 (m, 2H, 2'-H_2), superimposed in part 1.66 (tt, J≈J'≈6.0 Hz, 2H, 8'-H_2), superimposed 1.84−1.94 (m, 1H, 13"-H_{syn}), superimposed in part 1.92 (br d, J=17.0 Hz, 1H, 10"-H_{endo}), 2.06 (dm, J≈10.5 Hz, 1H, 13"-H_{anti}), 2.53 (dm, J≈17.0 Hz, 1H, 10"-H_{exo}), 2.76 (m, 1H, 7"-H), superimposed in part 2.79 (br d, J≈18.0 Hz, 1H, 6"-H_{endo}), 3.14 (dd, J=18.0 Hz, J'=3.5 Hz, 1H, 6"-H_{exo}), 3.38–3.42 (complex signal, 3H, 1'-H_2, 11"-H), 3.86−3.96 (m, 2H, 9'-H_2), 4.85 (s, NH, $^+$NH and OH), 5.58 (br d, J=4.0 Hz, 1H, 8"-H), 7.31 (d, J=8.5 Hz, 1H, 6-H), 7.38 (d, J=8.5 Hz, 1H, 2"-H), 7.57 (s, 1H, 4"-H), 7.63 (s, 1H, 3-H), superimposed in part 7.64 (d, J=7.0 Hz, 1H, 8-H), 7.72 (dd, J≈J'≈8.0 Hz, 1H, 7-H), 8.04 (s, 1H, 1-H), 8.20 (d, J=8.5 Hz, 1H, 1"-H), 8.82 (br s, 1H, CONH); ^{13}C NMR (125.7 MHz, CD_3OD) δ 23.5 (CH_3, 9"-CH_3), 27.2 (CH, C11"), 27.5 (CH_2), 27.6 (CH_2) (C6', C7'), 27.8 (CH, C7"), 29.3 (CH_2, C13"), 29.7 ($2CH_2$), 30.0 (CH_2), 30.1 (CH_2) (C2', C3', C4', C5'), 31.2 (CH_2, C8'), 36.0 ($2CH_2$, C6", C10"), 41.0 (CH_2, C1'), 49.6 (CH_2, C9'), 115.4 (C, C12a"), 116.8 (C, C10a), 117.5 (C, C11a"), 118.4 (C, C4a), 118.8 (CH, C1), 119.1 (CH, C4"), 120.8 (CH, C8), 123.7 (CH, C3), 125.1 (CH, C8"), 125.8 (CH, C6), 126.6 (CH, C2"), 129.2 (CH, C1"), 134.6 (2C, C8a, C9"), 135.1 (C, C9a), 138.7 (CH, C7), 140.2 (C, C3"), 140.8 (C, C4a"), 143.7 (C, C2), 151.0 (C, C5a"), 156.6 (C, C12"), 163.4 (C, C4), 163.6 (C, C5), 167.3 (C, CONH), 182.0 (C, C9), 193.5 (C, C10); HRMS (ESI) calcd for ($C_{41}H_{42}{}^{35}ClN_3O_5$ + H^+) 692.2886, found 692.2873. Anal. ($C_{41}H_{42}ClN_3O_5$·1.3HCl·1.25H_2O) C, H, N, Cl.

(−)-*N*-{9-[(3-Chloro-6,7,10,11-tetrahydro-9-methyl-7,11-methanocycloocta[*b*]quinolin-12-yl)amino]nonyl}-9,10-dihydro-4,5-dihydroxy-9,10-dioxoanthracene-2-carboxamide [(−)-7e]. It was prepared as described for (±)-**7a**. From rhein, **3** (422 mg, 1.49 mmol), and amine (−)-**6e** (632 mg, 1.49 mmol), a red solid (1.10 g) was obtained and purified by column chromatography (40–60 μm silica gel, CH_2Cl_2/MeOH/50% aq. NH_4OH mixtures, gradient elution). On elution with CH_2Cl_2/MeOH/50% aq. NH_4OH 99:1:0.2, hybrid (−)-**7e** (101 mg, 10% yield) was isolated as a red solid; R_f 0.33 (CH_2Cl_2/MeOH/50% aq. NH_4OH 9:1:0.05).

(−)-7e·HCl: $[\alpha]^{20}_D$=−154 (*c*=0.10, MeOH); mp 168–170 °C (CH_2Cl_2/MeOH 83:17); IR (KBr) *ν* 3500–2500 (max at 3226, 3048, 3002, 2925, 2853, 2743, O-H, N-H, N^+-H and C-H st), 1766, 1705, 1675, 1629, 1604, 1582, 1566, 1524, 1509 (C=O, ar-C-C and ar-C-N st) cm^{-1}; the ^1H NMR and ^{13}C NMR spectra were identical to those of (±)-**7e**; HRMS (ESI) calcd for ($C_{41}H_{42}{}^{35}ClN_3O_5 + H^+$) 692.2886; found 692.2891. Anal. ($C_{41}H_{42}ClN_3O_5 \cdot HCl \cdot H_2O$) C, H, N, Cl.

(+)-*N*-{9-[(3-Chloro-6,7,10,11-tetrahydro-9-methyl-7,11-methanocycloocta[*b*]quinolin-12-yl)amino]nonyl}-9,10-dihydro-4,5-dihydroxy-9,10-dioxoanthracene-2-carboxamide [(+)-7e]. It was prepared as described for (±)-**7a**. From rhein, **3** (477 mg, 1.68 mmol), and amine (+)-**6e** (715 mg, 1.68 mmol), a red solid (1.50 g) was obtained and purified by column chromatography (40–60 μm silica gel, CH_2Cl_2/MeOH/50% aq. NH_4OH mixtures, gradient elution). On elution with CH_2Cl_2/MeOH/50% aq. NH_4OH 99:1:0.2, hybrid (+)-**7e** (191 mg, 16% yield) was isolated as a red solid; R_f 0.33 (CH_2Cl_2/MeOH/50% aq. NH_4OH 9:1:0.05).

(+)-7e·HCl: $[\alpha]^{20}_D$=+154 (*c*=0.10, MeOH); mp 164–165 °C (CH_2Cl_2/MeOH 88:12); IR (KBr) *ν* 3500–2500 (max at 3226, 3049, 2926, 2852, O-H, N-H, N^+-H and C-H st), 1763, 1739, 1723, 1710, 1656, 1629, 1583, 1566, 1555, 1537, 1511, 1501 (C=O, ar-C-C and ar-C-N st) cm^{-1}; the ^1H NMR and ^{13}C NMR spectra were identical to those of (±)-**7e**; HRMS (ESI) calcd for

($C_{41}H_{42}{}^{35}ClN_3O_5$ + H^+) 692.2886, found 692.2877. Anal. ($C_{41}H_{42}ClN_3O_5 \cdot 1.25HCl \cdot 0.75H_2O$) C, H, N, Cl.

(±)-*N*-{10-[(3-Chloro-6,7,10,11-tetrahydro-9-methyl-7,11-methanocycloocta[*b*]quinolin-12-yl)amino]decyl}-9,10-dihydro-4,5-dihydroxy-9,10-dioxoanthracene-2-carboxamide [(±)-7f]. It was prepared as described for (±)-**7a**. From rhein, **3** (344 mg, 1.21 mmol), and amine (±)-**6f** (530 mg, 1.21 mmol), a red solid (900 mg) was obtained and purified by column chromatography (40–60 μm silica gel, CH_2Cl_2/MeOH/50% aq. NH_4OH mixtures, gradient elution). On elution with CH_2Cl_2/MeOH/50% aq. NH_4OH 99:1:0.2, hybrid (±)-**7f** (115 mg, 13% yield) was isolated as a red solid; R_f 0.53 (CH_2Cl_2/MeOH/50% aq. NH_4OH 9:1:0.05).

(±)-7f·HCl: mp 171–173 °C (EtOAc/CH_2Cl_2/MeOH 72:14:14); IR (KBr) *ν* 3500–2500 (max at 3229, 3049, 3002, 2925, 2852, O-H, N-H, N^+-H and C-H st), 1767, 1739, 1715, 1675, 1629, 1604, 1583, 1567, 1524 (C=O, ar-C-C and ar-C-N st) cm^{-1}; ^1H NMR (500 MHz, CD_3OD) *δ* 1.34−1.44 (complex signal, 12H, 3'-H_2, 4'-H_2, 5'-H_2, 6'H_2, 7'-H_2, 8'-H_2), 1.58 (s, 3H, 9"-CH_3), 1.66 (tt, $J \approx J' \approx 7.0$ Hz , 2H, 2'-H_2), 1.83 (tt, $J \approx J' \approx 7.0$ Hz, 2H, 9'-H_2), superimposed 1.90−1.93 (m, 1H, 13"-H_{syn}), superimposed in part 1.92 (br d, J=17.0 Hz, 1H, 10"-H_{endo}), 2.06 (dm, $J \approx 12.0$ Hz, 1H, 13"-H_{anti}), 2.52 (br dd, $J \approx 17.0$ Hz, $J' \approx$ 4.3 Hz, 1H, 10"-H_{exo}), 2.75 (m, 1H, 7"-H), 2.82 (br d, J=18.0 Hz, 1H, 6"-H_{endo}), 3.15 (dd, $J \approx 18.0$ Hz, J'=5.3 Hz, 1H, 6"-H_{exo}), 3.38–3.45 (complex signal, 3H, 1'-H_2, 11"-H), 3.87 (dt, $J \approx J' \approx 6.5$ Hz, 2H, 10'-H_2), 4.85 (s, NH, $^+$NH and OH), 5.57 (br d, J=5.5 Hz, 1H, 8"-H), 7.27 (dd, J=8.5 Hz, J'=1.0 Hz, 1H, 6-H), 7.39 (dd, J=9.5 Hz, J'=1.5 Hz, 1H, 2"-H), superimposed in part 7.59 (s, 1H, 4"-H), 7.60 (d, J=1.5 Hz, 1H, 3-H), 7.63 (dd, J=7.5 Hz, J'=1.0 Hz, 1H, 8-H), 7.70 (dd, $J \approx J' \approx 8.0$ Hz, 1H, 7-H), 8.01 (d, J=1.5 Hz, 1H, 1-H), 8.21 (d, J=9.5 Hz, 1H, 1"-H); ^{13}C NMR (125.7 MHz, CD_3OD) *δ* 23.5 (CH_3, 9"-CH_3), 27.2 (CH, C11"), 27.7 ($2CH_2$), 27.8 (CH + CH_2) (C6', C7', C8', C7"), 29.3 (CH_2, C13"), 30.03

(CH_2), 30.05 (CH_2), 30.22 (CH_2), 30.25 (CH_2) (C2', C3', C4', C5'), 31.2 (CH_2, C9'), 36.0 ($2CH_2$, C6", C10"), 41.1 (CH_2, C1'), 49.6 (CH_2, C10'), 115.5 (C, C12a"), 116.8 (C, C10a), 117.5 (C, C11a"), 118.4 (C, C4a), 118.9 (CH, C1), 119.1 (CH, C4"), 120.9 (CH, C8), 123.7 (CH, C3), 125.1 (CH, C8"), 125.8 (CH, C6), 126.7 (CH, C2"), 129.3 (CH, C1"), 134.6 (2C, C8a, C9"), 135.0 (C, C9a), 138.7 (CH, C7), 140.2 (C, C3"), 140.8 (C, C4a"), 143.7 (C, C2), 151.0 (C, C5a"), 156.6 (C, C12"), 163.3 (C, C4), 163.6 (C, C5), 167.2 (C, CONH), 181.9 (C, C9), 193.5 (C, C10); HRMS (ESI) calcd for ($C_{42}H_{44}{}^{35}ClN_3O_5$ + H^+) 706.3042, found 706.3038. Anal. ($C_{42}H_{44}ClN_3O_5 \cdot HCl \cdot 0.5H_2O$) C, H, N, Cl.

(±)-*N*-{11-[(3-Chloro-6,7,10,11-tetrahydro-9-methyl-7,11-methanocycloocta[*b*]quinolin-12-yl)amino]undecyl}-9,10-dihydro-4,5-dihydroxy-9,10-dioxoanthracene-2-carboxamide [(±)-7g]. It was prepared as described for (±)-**7a**. From rhein, **3** (491 mg, 1.73 mmol), and amine (±)-**6g** (785 mg, 1.73 mmol), a red solid (1.60 g) was obtained and purified by column chromatography (40–60 μm silica gel, CH_2Cl_2/MeOH/50% aq. NH_4OH mixtures, gradient elution). On elution with CH_2Cl_2/MeOH/50% aq. NH_4OH 99:1:0.2, hybrid (±)-**7g** (338 mg, 27% yield) was isolated as a red solid; R_f 0.50 (CH_2Cl_2/MeOH/50% aq. NH_4OH 9:1:0.05).

(±)-7g·HCl: mp 171–172 °C (EtOAc/CH_2Cl_2/MeOH 60:20:20); IR (KBr) ν 3500–2500 (max at 3226, 3048, 3007, 2924, 2852, 2645, O-H, N-H, N^+-H and C-H st), 1765, 1675, 1628, 1607, 1583, 1567, 1522 (C=O, ar-C-C and ar-C-N st) cm^{-1}; ^1H NMR (500 MHz, CD_3OD) δ 1.33−1.43 (complex signal, 14H, 3'-H_2, 4'-H_2, 5'-H_2, 6'H_2, 7'-H_2, 8'-H_2, 9'-H_2), 1.58 (s, 3H, 9"-CH_3), 1.66 (tt, $J \approx J' \approx 7.0$ Hz, 2H, 2'-H_2), 1.82 (tt, $J \approx J' \approx 17.0$ Hz, 2H, 10'-H_2), superimposed 1.89−1.93 (m, 1H, 13"-H_{syn}), superimposed in part 1.91 (br d, J=17.0 Hz, 1H, 10"-H_{endo}), 2.05 (dm, $J \approx 10.5$ Hz, Hz, 1H, 13"-H_{anti}), 2.52 (br dd, $J \approx 17.0$ Hz, $J' \approx 4.5$ Hz, 1H, 10"-H_{exo}), 2.75 (m, 1H, 7"-H), 2.82 (br d, J=18.0 Hz, 1H, 6"-H_{endo}), 3.14 (dd, $J \approx 18.0$ Hz, J'=5.5 Hz, 1H, 6"-H_{exo}), superimposed in

part 3.37 (m, 1H, 11”-H), superimposed in part 3.40 (tt, $J \approx J' \approx 7.0$ Hz, 2H, 1’-H_2), 3.86 (dt, $J \approx J' \approx 7.0$ Hz, 2H, 11’-H_2), 4.85 (s, NH, $^{+}$NH and OH), 5.57 (br d, J=5.5 Hz, 1H, 8”-H), 7.23 (dd, J=8.5 Hz, J'=1.0 Hz, 1H, 6-H), 7.37 (dd, J=9.0 Hz, $J' \approx 1.5$ Hz, 1H, 2”-H), superimposed in part 7.57 (d, J=1.5 Hz, 1H, 4”-H), superimposed in part 7.58 (d, J=2.0 Hz, 1H, 3-H), superimposed in part 7.58 (dd, J=8.0 Hz, J'=1.0 Hz, 1H, 8-H), 7.67 (dd, $J \approx J' \approx 8.0$ Hz, 1H, 7-H), 7.97 (d, J=1.5 Hz, 1H, 1-H), 8.20 (d, J=9.0 Hz, 1H, 1”-H); ^{13}C NMR (125.7 MHz, CD_3OD) δ 23.5 (CH_3, 9”-CH_3), 27.2 (CH, C11”), 27.7 (CH_2), 27.82 (CH, C7”), 27.83 ($2CH_2$) (C7’, C8’, C9’, C7”), 29.3 (CH_2, C13”), 30.1 ($2CH_2$), 30.2 (CH_2), 30.36 (CH_2), 30.40 (CH_2) (C2’, C3’, C4’, C5’, C6’), 31.2 (CH_2, C10’), 36.0 ($2CH_2$, C6”, C10”), 41.2 (CH_2, C1’), 49.6 (CH_2, C11’), 115.4 (C, C12a”), 116.7 (C, C10a), 117.5 (C, C11a”), 118.3 (C, C4a), 118.9 (CH, C1), 119.1 (CH, C4”), 120.8 (CH, C8), 123.7 (CH, C3), 125.1 (CH, C8”), 125.8 (CH, C6), 126.6 (CH, C2”), 129.3 (CH, C1”), 134.5 (C, C9”), 134.6 (C, C8a), 134.9 (C, C9a), 138.7 (CH, C7), 140.2 (C, C3”), 140.8 (C, C4a”), 143.7 (C, C2), 151.0 (C, C5a”), 156.6 (C, C12”), 163.3 (C, C4), 163.5 (C, C5), 167.1 (C, CONH), 181.8 (C, C9), 193.4 (C, C10); HRMS (ESI) calcd for ($C_{43}H_{46}{}^{35}ClN_3O_5 + H^+$) 720.3199, found 720.3195. Anal. ($C_{43}H_{46}ClN_3O_5 \cdot HCl \cdot 0.5H_2O$) C, H, N, Cl.

(±)-*N*-{4-{[(3-Chloro-6,7,10,11-tetrahydro-9-methyl-7,11-methanocycloocta[*b*]quinolin-12-yl)amino]methyl}benzyl}-9,10-dihydro-4,5-dihydroxy-9,10-dioxoanthracene-2-carboxamide [(±)-7h]. It was prepared as described for (±)-**7a**. From rhein, **3** (548 mg, 1.93 mmol), and amine (±)-**6h** (780 mg, 1.93 mmol), a red solid (1.07 g) was obtained and purified by column chromatography (40–60 μm silica gel, hexane/EtOAc/Et_3N mixtures, gradient elution). On elution with hexane/EtOAc/Et_3N 40:60:0.2, hybrid (±)-**7h** (113 mg, 9% yield) was isolated as a red solid; R_f 0.57 (CH_2Cl_2/MeOH/50% aq. NH_4OH 9:1:0.05).

(±)-7h·HCl: mp 129–130 °C (EtOAc/CH_2Cl_2/MeOH 66:17:17); IR (KBr) *v* 3500–2500 (max at 3245, 3055, 2925, 2852, 2790, O-H, N-H, N^+-H and C-H st), 1705, 1673, 1629, 1607, 1583, 1560, 1516 (C=O, ar-C-C and ar-C-N st) cm^{-1}; ^1H NMR (400 MHz, CD_3OD) δ 1.59 (s, 3H, 9”-CH_3), superimposed 1.92–1.98 (m, 1H, 13”-H_{syn}), 1.97 (br d, *J*=16.8 Hz, 1H, 10”-H_{endo}), 2.08 (dm, *J*=12.4 Hz, 1H, 13”-H_{anti}), 2.53 (br dd, *J*≈16.8 Hz, *J’*≈5.0 Hz, 1H, 10”-H_{exo}), 2.78 (m, 1H, 7”-H), 2.86 (br d, *J*=18.0 Hz, 1H, 6”-H_{endo}), 3.20 (dd, *J*≈18.0 Hz, *J’*=5.6 Hz, 1H, 6”-H_{exo}), 3.47 (m, 1H, 11”-H), 4.60 (s, 2H, C*H*$_2$NH), 4.85 (s, NH, $^+$NH and OH), 5.18 (s, 2H, C*H*$_2$NHCO), 5.59 (m, 1H, 8”-H), 7.28 (dd, *J*=9.2 Hz, *J’*=2.0 Hz, 1H, 2”-H), 7.34 (dd, *J*=8.0 Hz, *J’*=2.0 Hz, 1H, 6-H), 7.41 (d, *J*=8.4 Hz, 2H) and 7.47 (d, *J*=8.4 Hz, 2H) [2’(6’)-H_2, 3’(5’)-H_2], 7.67 (d, *J*=2.0 Hz, 1H) and 7.69 (d, *J*=2.0 Hz, 1H) (3-H, 4”-H), 7.76 (dd, *J*≈*J’*≈7.2 Hz, 1H, 7-H), 7.79 (dd, *J*=7.2 Hz, *J’*=2.0 Hz, 1H, 8-H), 8.15 (d, *J*≈2.0 Hz, 1H, 1-H), 8.21 (d, *J*=9.2 Hz, 1H, 1”-H); ^{13}C NMR (125.7 MHz, CD_3OD) δ 23.5 (CH_3, 9”-CH_3), 27.5 (CH, C11”), 27.8 (CH, C7”), 29.3 (CH_2, C13”), 36.0 (CH_2, C6”), 36.2 (CH_2, C10”), 44.3 (CH_2, CH_2NH), 51.9 (CH_2, *C*H_2NHCO), 115.4 (C, C12a”), 116.9 (C, C10a), 118.2 (C, C11a”), 118.5 (C, C4a), 118.8 (CH, C1), 119.0 (CH, C4”), 120.9 (CH, C8), 123.7 (CH, C3), 125.0 (CH, C8”), 125.8 (CH, C6), 126.6 (CH, C2”), 128.1 (CH), 129.8 (CH) [C2’(6’), C3’(5’)], 129.3 (CH, C1”), 134.6 (C, C9”), 134.7 (C, C8a), 135.0 (C, C9a), 137.8 (C) and 139.2 (C) (C1’, C4’), 138.8 (CH, C7), 140.2 (C, C3”), 140.7 (C, C4a”), 143.1 (C, C2), 151.6 (C, C5a”), 157.1 (C, C12”), 163.3 (C, C4), 163.6 (C, C5), 167.1 (C, CONH), 182.0 (C, C9), 193.5 (C, C10); HRMS (ESI) calcd for ($C_{40}H_{32}{}^{35}ClN_3O_5$ + H^+) 670.2103, found 670.2104. Anal. ($C_{40}H_{32}ClN_3O_5$·1.1HCl·1.4H_2O) C, H, N, Cl.

***In Vitro* Biological Studies. AChE and BChE Inhibition Assay.** Human recombinant AChE (Sigma, Milan, Italy) inhibitory activity was evaluated spectrophotometrically by the method of Ellman *et al*.[46] Initial rate assays were performed at 37 ºC with a Jasco V-530 double beam

spectrophotometer. Stock solutions of the tested compounds (1 mM) were prepared in MeOH and diluted in MeOH. The assay solution consisted of a 0.1 M potassium phosphate buffer, pH 8.0, with the addition of 340 μM 5,5'-dithiobis(2-nitrobenzoic acid) (DTNB, used to produce the yellow anion of 5-thio-2-nitrobenzoic acid), 0.02 unit/mL hAChE and 550 μM substrate (acetylthiocholine iodide). Assay solutions with and without inhibitor were preincubated at 37 ºC for 20 min followed by the addition of substrate. Blank solutions containing all components except hAChE were prepared in parallel to account for the non-enzymatic hydrolysis of the substrate. Five increasing concentrations of the inhibitor were used, able to give an inhibition of the enzymatic activity in the range of 20–80%. The results were plotted by placing the percentage of inhibition in function of the decimal log of the final inhibitor concentration. Linear regression and IC_{50} values were calculated using Microcal Origin 3.5 software (Microcal Software, Inc).

Human serum BChE inhibitory activities were also evaluated spectrophotometrically by the method of Ellman *et al.*[46] The reactions took place in a final volume of 300 μL of 0.1 M phosphate-buffered solution pH 8.0, containing hBChE (0.02 u/mL) and 333 μM DTNB solution. Inhibition curves were performed in duplicates using at least 10 increasing concentrations of inhibitor and preincubated for 20 min at 37 ºC. One duplicate sample without inhibitor was always present to yield 100% of BChE activity. Then substrate butyrylthiocholine iodide (300 μM, Sigma-Aldrich) was added and the reaction was developed for 5 min at 37 ºC. The color production was measured at 414 nm using a labsystems Multiskan spectrophotometer. Data from concentration–inhibition experiments of the inhibitors were calculated by non-linear regression analysis, using the GraphPad Prism program package (GraphPad Software; San

Diego, USA), which gave estimates of the IC_{50} values. Results are expressed as mean ± S.E.M. of at least 4 experiments performed in duplicate.

Kinetic Analysis of AChE Inhibition. To assess the mechanism of action of hybrid (–)-**7e**, reciprocal plots of 1/velocity versus 1/[Substrate] were constructed at relatively low concentration of substrate (0.562–0.112 mM) by using Ellman's method[46] and human recombinant AChE (Sigma, Milan, Italy). Three concentrations of inhibitor were selected for this study: 0.84, 1.34, 3.65 nM. The plots were assessed by a weighted least-squares analysis that assumed the variance of the velocity (v) to be a constant percentage of v for the entire data set. Data analysis was performed with GraphPad Prism 4.03 software (GraphPad Software Inc.).

Calculation of the inhibitor constant (K_i) value was carried out by re-plotting slopes of lines from the Lineweaver-Burk plot *versus* the inhibitor concentration and K_i was determined as the intersect on the negative x-axis. K'_i (dissociation constant for the enzyme–substrate–inhibitor complex) value was determined by plotting the apparent $1/v_{max}$ *versus* inhibitor concentration.[87]

AChE-Induced Aβ40 Aggregation Inhibition Assay.[49] Thioflavin T (Basic Yellow 1), human recombinant AChE lyophilized powder, and 1,1,1,3,3,3-hexafluoro-2-propanol (HFIP) were purchased from Sigma Chemicals. Buffers and other chemicals were of analytical grade. Absolute DMSO over molecular sieves was from Fluka. Water was deionised and doubly distilled. Aβ40, supplied as trifluoroacetate salt, was purchased from Bachem AG (Germany). Aβ40 (2 mg mL^{-1}) was dissolved in HFIP, lyophilized and then resolubilized in DMSO to get a 2.3 mM Aβ40 solution. 1 mM solutions of tested inhibitors were prepared by dissolution in MeOH.

Aliquots of 2 μL Aβ40 peptide were incubated for 24 h at room temperature in 0.215 M sodium phosphate buffer (pH 8.0) at a final concentration of 230 μM. For co-incubation

experiments aliquots (16 μL) of hAChE (final concentration 2.30 μM, Aβ/AChE molar ratio 100:1) and AChE in the presence of 2 μL of the tested inhibitor (final inhibitor concentration 100 μM) in 0.215 M sodium phosphate buffer pH 8.0 solution were added. Blanks containing Aβ40 alone, human recombinant AChE alone, and Aβ40 plus tested inhibitors in 0.215 M sodium phosphate buffer (pH 8.0) were prepared. The final volume of each vial was 20 μL. Each assay was run in duplicate. To quantify amyloid fibril formation, the thioflavin T fluorescence method was then applied.[88] The fluorescence intensities due to β-sheet conformation were monitored for 300 s at λ_{em}=490 nm (λ_{exc}=446 nm). The percent inhibition of the AChE-induced aggregation due to the presence of the tested compound was calculated by the following expression: 100 – ($IF_i/IF_o \times 100$) where IF_i and IF_o are the fluorescence intensities obtained for Aβ plus AChE in the presence and in the absence of inhibitor, respectively, minus the fluorescence intensities due to the respective blanks.

Aβ42 Self-Aggregation Inhibition Assay. As reported in a previously published protocol,[58] HFIP pretreated Aβ42 samples (Bachem AG, Switzerland) were first solubilized with a CH_3CN/0.3 mM Na_2CO_3/250 mM NaOH (48.4:48.4:3.2) mixture to obtain a 500 μM solution. Experiments were performed by incubating the peptide in 10 mM phosphate buffer (pH = 8.0) containing 10 mM NaCl, at 30 °C for 24 h (final Aβ concentration 50 μM) with and without inhibitor (10 μM, Aβ/inhibitor = 5/1). Blanks containing the tested inhibitors were also prepared and tested. To quantify amyloid fibrils formation, the thioflavin T fluorescence method was used.[88] After incubation, samples were diluted to a final volume of 2.0 mL with 50 mM glycine–NaOH buffer (pH 8.5) containing 1.5 μM thioflavin T. A 300-second-time scan of fluorescence intensity was carried out (λ_{exc}=446 nm; λ_{em}=490 nm, FP-6200 fluorometer, Jasco Europe), and values at plateau were averaged after subtracting the background fluorescence of

1.5 μM thioflavin T solution. The fluorescence intensities were compared and the percent inhibition due to the presence of the inhibitor was calculated by the following formula: 100 – ($IF_i/IF_o \times 100$) where IF_i and IF_o are the fluorescence intensities obtained for Aβ42 in the presence and in the absence of inhibitor, respectively.

BACE-1 Inhibition Assay. β-Secretase (BACE-1, Sigma) inhibition studies were performed by employing a peptide mimicking APP sequence as substrate (Methoxycoumarin-Ser-Glu-Val-Asn-Leu-Asp-Ala-Glu-Phe-Lys-dinitrophenyl, M-2420, Bachem, Germany). The following procedure was employed: 5 μL of test compounds (or DMSO, if preparing a control well) were pre-incubated with 175 μL of enzyme (in 20 mM sodium acetate pH 4.5 containing CHAPS 0.1% w/v) for 1 h at room temperature. The substrate (3 μM, final concentration) was then added and left to react for 15 min. The fluorescence signal was read at λ_{em}=405 nm (λ_{exc}=320 nm). The DMSO concentration in the final mixture was maintained below 5% (v/v) to guarantee no significant loss of enzyme activity. The fluorescence intensities with and without inhibitor were compared and the percent inhibition due to the presence of test compounds was calculated. The background signal was measured in control wells containing all the reagents, except BACE-1 and subtracted. The % inhibition due to the presence of increasing test compound concentration was calculated by the following expression: 100 – ($IF_i/IF_o \times 100$) where IF_i and IF_o are the fluorescence intensities obtained for BACE-1 in the presence and in the absence of inhibitor, respectively. Inhibition curves were obtained by plotting the % inhibition versus the logarithm of inhibitor concentration in the assay sample, when possible. The linear regression parameters were determined and the IC_{50} extrapolated (GraphPad Prism 4.0, GraphPad Software Inc.). To demonstrate inhibition of BACE-1 activity a peptido-mimetic inhibitor (β-secretase inhibitor IV, Calbiochem) was serially diluted into the reactions' wells (IC_{50} = 13.0 ± 0.1 nM).

BBB Permeation Assay. The brain penetration of the synthesized hybrids was assessed using the parallel artificial membrane permeation assay for blood-brain barrier described by Di *et al.*[71] The *in vitro* permeability (P_e) of fourteen commercial drugs through lipid extract of porcine brain membrane together with that of the test compounds was determined. Commercial drugs and synthesized hybrids were tested using a mixture of PBS/EtOH 70:30. Assay validation was made by comparing the experimental permeability of the different compounds with the literature values of the commercial drugs, which showed a good correlation: P_e (exp) = 1.4525 P_e (lit) – 0.4926 (R^2 = 0.9199). From this equation and taking into account the limits established by Di *et al.* for BBB permeation, we established the following ranges of permeability: compounds of high BBB permeation (CNS+): P_e (10^{-6} cm s^{-1}) > 5.3; compounds of low BBB permeation (CNS–): P_e (10^{-6} cm s^{-1}) < 2.4, and compounds of uncertain BBB permeation (CNS+/–): 5.3 > P_e (10^{-6} cm s^{-1}) > 2.4.

Aβ42 Aggregation Inhibition Assay in Intact Escherichia coli Cells Overexpressing Aβ42 and Tau. Cloning and overexpression of Aβ42 peptide: *Escherichia coli* competent cells BL21 (DE3) were transformed with the pET28a vector (Novagen, Inc., Madison, WI, USA) carrying the DNA sequence of Aβ42. Because of the addition of the initiation codon ATG in front of both genes, the overexpressed peptide contains an additional methionine residue at its N terminus. For overnight culture preparation, 10 mL of lysogeny broth (LB) medium containing 50 μg·mL^{-1} of kanamycin were inoculated with a colony of BL21 (DE3) bearing the plasmid to be expressed at 37 °C. After overnight growth, the OD600 was usually 2–2.5. For expression of Aβ42 peptide, 20 μL of overnight culture were transferred into eppendorf tubes of 1.5 mL containing 980 μL of LB medium with 50 μg·mL–1 of kanamycin, 1 mM of isopropyl 1-thio-β-D-galactopyranoside (IPTG) and 10 μM of each hybrid 7 or reference compound to be tested in DMSO. The samples

were grown for 24 h at 37 °C and 1400 rpm using a Thermomixer (Eppendorf, Hamburg, Germany). In the negative control (without drug) the same amount of DMSO was added in the sample.

Cloning and overexpression of tau protein: *E. coli* BL21 (DE3) competent cells were transformed with pTARA containing the RNA-polymerase gen of T7 phage (T7RP) under the control of the promoter PBAD. *E. coli* BL21 (DE3) with pTARA competent cells were transformed with pRKT42 vector encoding four repeats of tau protein in two inserts. For overnight culture preparation, 10 mL of M9 medium containing 0.5% of glucose, 50 $\mu g \cdot mL^{-1}$ of ampicillin and 12.5 $\mu g \cdot mL^{-1}$ of chloramphenicol were inoculated with a colony of BL21 (DE3) bearing the plasmids to be expressed at 37 °C. After overnight growth, the OD600 was usually 2–2.5. For expression of tau protein, 20 μL of overnight culture were transferred into eppendorf tubes of 1.5 mL containing 980 μL of M9 medium containing 0.25% of arabinose, 0.5% of glucose, 50 $\mu g \cdot mL^{-1}$ of ampicillin and 12.5 $\mu g \cdot mL^{-1}$ of chloramphenicol and 10 μM of each hybrid **7** or reference compound to be tested in DMSO. The samples were grown for 24 h at 37 °C and 1400 rpm using a Thermomixer (Eppendorf, Hamburg, Germany). In the negative control (without drug) the same amount of DMSO was added in the sample.

Thioflavin-S (Th-S) steady-state fluorescence: Th-S (T1892) and other chemical reagents were purchased from Sigma (St. Louis, MO). Th-S stock solution (250 mM) was prepared in double-distilled water purified through a Milli-Q system (Millipore, USA). Fluorescent spectral scans of Th-S were analyzed using an Aminco Bowman Series 2 luminescence spectrophotometer (Aminco-Bowman AB2, SLM Aminco, Rochester, NY, USA). For the fluorescence assay, 25 μM of Th-S (20 μL of Th-S in 180 μL of sample) were added to samples and spectra were recorded after 15 min equilibration at 37 ºC. Excitation and emission slit widths of 5 nm were

used. Finally, the fluorescence emission at 520 nm, when exciting at 440 nm, was recorded. In order to normalize the Th-S fluorescence as a function of the bacterial concentration, OD600 was obtained using a Shimadzu UV-2401 PC UV–Vis spectrophotometer (Shimadzu, Japan). Note that the fluorescence normalization has been carried out considering as 100% the Th-S fluorescence of the bacterial cells expressing the peptide or protein in the absence of drug and 0% the Th-S fluorescence of the bacterial cells non-expressing the peptide or protein.

***Ex Vivo* Studies in C57bl6 Mice. Electrophysiological Assays in Hippocampal Slices Incubated with Aβ Oligomers.** Hippocampal slices were prepared according to standard procedures previously described.[89,90] Briefly, transverse slices (350 μm) from the dorsal hippocampus were cut under cold artificial cerebrospinal fluid (ACSF, in mM: 124 NaCl, 2.6 $NaHCO_3$, 10 D-glucose, 2.69 KCl, 1.25 KH_2PO_4 2.5 $CaCl_2$, 1.3 $MgSO_4$, and 2.60 $NaHPO_4$) using a Vibratome (Leica VT 1000s, Germany) and incubated in ACSF for 1 h at room temperature. In all experiments, 10 μM picrotoxin (PTX) was added to suppress inhibitory GABAA transmission. Slices were transferred to an experimental chamber (2 mL), superfused (3 mL/min, at 20–22 ºC) with gassed ACSF and visualized by trans-illumination with a binocular microscope (MSZ-10, Nikon, Melville, NY). To evoke field excitatory postsynaptic potentials (fEPSPs), we stimulated with bipolar concentric electrodes (Platinum/Iridium, 125 μm OD diameter, FHC Inc., Bowdoin, ME) generated by a stimulator (Axon 700b, Molecular Devices, Sunnyvale, CA) and connected to an isolation unit (Isoflex, AMPI, Jerusalem, Israel). The stimulation was in the Stratum Radiatum within 100-200 μm from the recording site. The paired pulse facilitation index was calculated by ((R2–R1)/R1), where R1 and R2 were the peak amplitudes of the first and second fEPSP respectively. To generate LTP we used Theta Burst Stimulation (TBS) consisting of 5 trains of stimulus with an inter-train interval of 20 s. Each

train consisted of 10 bursts at 5 Hz and each burst having 4 pulses at 100 Hz. To generate LTD we used Low Frequency Stimulation (LFS) consisting in 900 paired pulses at 1 Hz. Recordings were filtered at 2.0-3.0 kHz, sampled at 4.0 kHz using an A/D converter, and stored with pClamp 10 (Molecular Devices). Evoked postsynaptic responses were analyzed off-line, using an analysis software (pClampfit, Molecular Devices), which allowed visual detection of events, computing only those events that exceeded an arbitrary threshold.

Determination of Synaptic Protein Levels in Hippocampal Slices Incubated with Aβ Oligomers. Immunoblotting: The hippocampus of C57bl6 mice were dissected on ice and immediately frozen at –150 ºC or processed. Briefly, hippocampal tissue was homogenized in RIPA buffer (50 mM Tris-Cl, pH 7.5, 150 mM NaCl, 1% NP-40, 0.5% sodium deoxycholate, and 1% SDS) supplemented with a protease inhibitor cocktail (Sigma-Aldrich P8340) and phosphatase inhibitors (50 mM NaF, 1 mM Na_3VO_4 and 30 μM $Na_4P_2O_7$) using a Potter homogenizator and then passed sequentially through different caliber syringes. Protein samples were centrifuged at 14000 rpm at 4 ºC twice for 10 min. Protein concentration was determined using the BCA Protein Assay Kit (Pierce Biotechnology, Rockford, IL). 20 and 40 μg of hippocampal samples were resolved by 10% SDS-PAGE, transferred to a PVDF membrane. The reactions were followed by incubation with primary antibodies, secondary antibodies anti-mouse, anti-goat or anti-rabbit IgG peroxidase conjugated (Pierce) and developed using an ECL kit (Western Lightning Plus ECL, PerkinElmer).

***In Vivo* Studies in APP-PS1 Mice.**

Animals and Treatment. APPswe/PSEN1ΔE9 (APP-PS1) mice, which express the Swedish mutation of APP (K595N/M596L) and PS1 with the deletion of exon 9 were obtained from The Jackson Laboratory (Bar Harbor, ME; mice stock #004462). All animals were housed in

temperature- and light-controlled rooms, with food and water *ad libitum* during the treatment. Six and ten month-old mice were treated and handled according to the National Institutes of Health guidelines (NIH, Baltimore, MD). Treatments were performed by intra-peritoneal (i.p.) injection of 2.0 mg/kg enantiopure rhein–huprine hybrids (+)-**7e** or (–)-**7e** with saline solution as vehicle, three times per week during 4 weeks. Transgenic control animals were injected only with the vehicle.

Immunoblotting. The hippocampus from control or treated APP-PS1 mice were dissected on ice and immediately frozen at –150 ºC or processed has detailed previously.[90,91] Briefly, hippocampus were homogenized in RIPA buffer (50 mM Tris-Cl, pH 7.5, 150 mM NaCl, 1% NP-40, 0.5% sodium deoxycholate, and 1% SDS) supplemented with a protease inhibitor cocktail (Sigma-Aldrich P8340) and phosphatase inhibitors (50 mM NaF, 1 mM Na_3VO_4 and 30 μM $Na_4P_2O_7$) using a Potter homogenizator and then passed sequentially through different caliber syringes. Protein samples were centrifuged at 14000 rpm at 4 ºC twice for 20 min. Protein concentration was determined using the BCA Protein Assay Kit (Pierce Biotechnology, Rockford, IL).

Aβ detection. For the detection of soluble Aβ peptides, samples from hippocampus were centrifugated to 20.000g for 1 h and the protein concentration from supernatant was determined using the BCA Protein Assay Kit (Pierce Biotechnology, Rockford, IL). 80 μg of proteins were resolved in 17.5% SDS polyacrylamide Tris-tricine gels, followed by immunoblotting on PVDF membranes using mouse anti-Aβ protein 6E10 (Covance). To analyze the levels of APP the antibody MAB348 (Millipore) was utilized. Band intensities were visualized by ECL kit (Western Lightning Plus ECL, PerkinElmer), scanned and densitometrically quantified using ImageJ software.[85,92]

Docking in AChE. AChE models were built up from the human recombinant AChE structure 3LII.[93] The structure was refined by addition of missing hydrogen atoms, removal of non-standard residues and generation of disulfide bonds Cys69–Cys96, Cys257–272 and Cys405–Cys524. Since the fragment between residues Gly264 and Pro258 is not observed in the X-ray structure, it was modeled from the equivalent fragment of *Torpedo californica* AChE (*Tc*AChE). Finally, the enzyme was modeled in its physiological active form with neutral His447 and neutral Glu334, which together with Ser203 forms the catalytic triad. We considered the standard ionization state at phisiological pH for the rest of ionizable residues with exception of Glu450, which was modeled in its neutral state.

The binding mode of (–)-**7h** and (+)-**7h** to AChE was explored by means of docking calculations performed with rDock, whose reliability in predicting binding mode for dual site inhibitors of AChE has been largely demonstrated in previous studies.[94] The orientation of Tyr337 residue was modified to mimic the conformation of the equivalent residue Phe330 in the complex between *Tc*AChE and (–)-huprine X (PDB 1E66).[39] To explore the binding at the PAS, three different AChE models differing in the orientation of Trp286 were built. The side chain of Trp286 was oriented following the three orientations found in X-ray structures deposited in the Protein Data Bank, which can be characterized by dihedral angles χ_1 (N–C_α–C_β–C_γ) and χ_2 (C_α–C_β–C_γ–$C_{\delta 2}$) close to i) –60 and –80, ii) –120 and +50, and iii) –160 and –120 degrees. PDB structures 1N5R (AChE–propidium complex), 2CKM (AChE–*bis*(7)-tacrine complex) and 1Q83 (AChE–*syn*-TZ2PA6 complex), respectively, are representative cases of these orientations and were used to generate the corresponding models. The docking volume was defined as the space covered by the catalytic, midgorge and peripheral sites and each compound was subjected to 100 docking runs and solutions clustered according to the RMSD among its heavy atoms using a

threshold of 2.0 Å, selecting the best ranked pose to be representative of the cluster. The resulting binding modes were analyzed by visual inspection in conjunction with the docking scores.

Docking and molecular dynamics in BACE-1. In order to explore the binding mode of rhein–huprine hybrids, druggable pockets were identified using the MDpocket program.[95] Calculations were performed for X-ray structures 1M4H, 1SGZ, 2OHL and 3CIB chosen to account for structural variability in the flexible 'flap' loop located over the catalytic site and of certain regions (loops 9–12 and 263–268) and side chains in the peptide binding groove. The structures were refined by addition of missing hydrogen atoms, removal of non-standard residues and generation of disulfide bonds Cys155–Cys359, Cys217–Cys382 and Cys269–Cys319. Only druggable pockets that shared α-spheres in at least three different structures were retained and ranked according to druggability criteria.[96]

GLIDE[97] was used to explore the preferred binding sites of the huprine and hydroxyanthraquinone moieties (obtained by replacing the methylene chain by a methyl group) to the druggable sites and to explore the binding mode of compound **7h**. The docking cavity was defined as a 13824Å^3 cube whose center was located among residues Gly13, Leu30, Tyr71, Ile110, Trp115 and Gly230. Three different protonation states were considered for the catalytic diad (Asp32, Asp228), including the doubly deprotonated form and the two single deprotonated forms. Default settings were used and the best poses were clustered according to the RMSD between its heavy atoms, with a threshold of 2.0 Å and subsequently evaluated using the Glide-XP scoring function.

The binding modes proposed for (–)-**7h** and (+)-**7h** were assessed by means of Molecular Dynamics (MD) using GPU-accelerated PMEMD[98] module from the AMBER12 software

package.[99] The Parm99SB[100] force field was used for the protein and the gaff force field[101] was used to assign parameters to both ligands. Na^+ cations added to neutralize the system were treated according with Joung and Cheatham parameters.[102] The ligands charge distribution were determined from a fit to the HF/6-31G(d) electrostatic potential obtained with Gaussian09[103] using the RESP[104] protocol as implemented in the Antechamber module of AmberTools12 software package.

Each system comprised around 46000 atoms, including the protein–ligand complex and 8 Na^+ cations solvated on a truncated octahedral box of 13000 TIP3P water molecules.[105] The geometry of the system was minimized in four steps. First, water molecules were refined though 4500 steepest descent algorithm followed by 10500 steps of conjugate gradient. Then, protein and ligand hydrogen atoms positions were optimized using 500 steps of steepest descent and 4500 of conjugate gradient. Next the ligand, water molecules and counterions were further optimized with 2000 steps of steepest descent and 6000 of conjugate gradient and, at the last step, the whole system was optimized with 2500 steps of steepest descent and 4500 of conjugate gradient. At this point, 5 different replicas for each ligand were generated by randomly assigning different sets of velocities to the initial coordinates, all fitting a Maxwell distribution for a temperature of 50K. For each one of the replicas, thermalization was performed in the canonical ensemble during five 25 ps steps, using a time step of 1 fs and increasing the temperature from 50 to 298 K. Concomitantly, the inhibitor and the residues in the binding site were restrained during thermalization using a variable restraint force that was decreased sequentially from 5 kcal mol^{-1} $Å^{-2}$ to 0 kcal mol^{-1} $Å^{-2}$ using increments of 1 kcal mol^{-1} $Å^{-2}$ within the different thermalization stages. Prior to the production runs, a short 1 ns simulation in the isothermal-isobaric ensemble was performed in other to reach a stable density value of 1003 kg m^{-3}. Production runs consisted

of 50 ns trajectories (accounting for a global simulation time of 200 ns per ligand) using SHAKE for bonds involving hydrogen atoms, allowing for a timestep of 2 fs, in conjunction with periodic boundary conditions at constant volume and temperature (298 K; Langevin thermostat with a collision frequency of 3 ps^{-1}), particle mesh Ewald for long-range electrostatic interactions, and a cutoff of 10 Å for nonbonded interactions.

ASSOCIATED CONTENT

Supporting Information. Synthetic procedures and chemical characterization of intermediate nitriles **5a**–**h**, and amines **6a**–**h**, additional figures of the molecular modeling studies on AChE and BACE-1, additional data of PAMPA-BBB studies. This material is available free of charge via the Internet at http://pubs.acs.org.

AUTHOR INFORMATION

Corresponding Author

*Phone: +34-934024533. Fax: +34-934035941. E-mail: dmunoztorrero@ub.edu.

Present Addresses

Δ E.V.: Drug Discovery Unit, College of Life Sciences, University of Dundee, Dundee, DD1 5EH, UK.

Notes

The authors declare no competing financial interest.

ACKNOWLEDGMENTS

This work was supported by Ministerio de Ciencia e Innovación (MICINN) (CTQ2011-22433, SAF2009-10553, SAF2011-27642, start-up grant of the Ramón y Cajal program for R.S.), Generalitat de Catalunya (GC) (2009SGR1396, 2009SGR249), University of Bologna, Italian Ministry of Education (MIUR, FFO - Fondo Finanziamento Ordinario) and Uni-Rimini S.p.A., and CONICYT-PFB (12/2007). Fellowships from GC to E.V. and I.S., from FIS to J.J.-J., from CONICYT to C.T.R., a contract from the Ramón y Cajal program of MICINN to R.S., and the ICREA support to F.J.L. are gratefully acknowledged. The Center for Scientific and Academic Services of Catalonia (CESCA) is acknowledged for providing access to computational facilities.

ABBREVIATIONS USED

Aβ, β-Amyloid peptide; Aβ-o, Aβ oligomers; AChE, acetylcholinesterase; AChEI, AChE inhibitor; ACSF, artificial cerebrospinal fluid; AD, Alzheimer's disease; APP, amyloid precursor protein; BBB, blood–brain barrier; BACE-1, β-site APP cleaving enzyme 1; BChE, butyrylcholinesterase; CAS, catalytic anionic site; CNS, central nervous system; DTNB, 5,5'-dithiobis(2-nitrobenzoic acid); fEPSP, field excitatory postsynaptic potentials; hAChE, human acetylcholinesterase; hBChE, human butyrylcholinesterase; HFIP, 1,1,1,3,3,3-hexafluoro-2-propanol; IBs, inclusion bodies; LTP, long-term potentiation; PAS, peripheral anionic site; PBS, phosphate-buffered saline; SYN, synapsin; SYP, synaptophysin; *Tc*AChE, *Torpedo californica* acetylcholinesterase.

REFERENCES

(1) Batsch, N. L.; Mittelman, M. S. World Alzheimer Report 2012. Overcoming the stigma of dementia, London: Alzheimer's Disease International, 2012 (http://www.alz.co.uk).

(2) Hardy, J.; Selkoe, D. J. The amyloid hypothesis of Alzheimer's disease: progress and problems on the road to therapeutics. *Science* **2002**, *297*, 353–356.

(3) Kung, H. F. The β-amyloid hypothesis in Alzheimer's disease: seeing is believing. *ACS Med. Chem. Lett.* **2012**, *3*, 265–267.

(4) Citron, M. Alzheimer's disease: strategies for disease modification. *Nat. Rev. Drug Discovery* **2010**, *9*, 387–398.

(5) Pimplikar, S. W. Reassessing the amyloid cascade hypothesis of Alzheimer's disease. *Int. J. Biochem. Cell Biol.* **2009**, *41*, 1261–1268.

(6) Cavalli, A.; Bolognesi, M. L. Minarini, A, ; Rosini, M.; Tumiatti, V.; Recanatini, M.; Melchiorre, C. Multi-target-directed ligands to combat neurodegenerative diseases. *J. Med. Chem.* **2008**, *51*, 347–372.

(7) Bajda, M.; Guzior, N.; Ignasik, M.; Malawska, B. Multi-target-directed ligands in Alzheimer's disease treatment. *Curr. Med. Chem.* **2011**, *18*, 4949–4975.

(8) Geldenhuys, W. J.; Van der Schyf, C. J. Rationally designed multi-targeted agents against neurodegenerative diseases. *Curr. Med. Chem.* **2013**, *20*, 1662–1672.

(9) Chen, X.; Decker, M. Multi-target compounds acting in the central nervous system designed from natural products. *Curr. Med. Chem.* **2013**, *20*, 1673–1685.

(10) Russo, P.; Frustaci, A.; Del Bufalo, A.; Fini, M.; Cesario, A. Multitarget drugs of plants origin acting on Alzheimer's disease. *Curr. Med. Chem.*, **2013**, *20*, 1686–1693.

(11) For recent examples see references 11–15. Butini, S.; Brindisi, M.; Brogi, S.; Maramai, S.; Guarino, E.; Panico, A.; Saxena, A.; Chauhan, V.; Colombo, R.; Verga, L.; De Lorenzi, E.; Bartolini, M.; Andrisano, V.; Novellino, E.; Campiani, G.; Gemma, S. Multifunctional cholinesterase and amyloid beta fibrillization modulators. Synthesis and biological investigation. *ACS Med. Chem. Lett.* **2013**, *4*, in press (DOI: 10.1021/ml4002908).

(12) Capurro, V.; Busquet, P.; Lopes, J. P.; Bertorelli, R.; Tarozzo, G.; Bolognesi, M. L.; Piomelli, D.; Reggiani, A.; Cavalli, A. Pharmacological characterization of memoquin, a multi-target compound for the treatment of Alzheimer's disease. *PLoS One* **2013**, *8*, e56870.

(13) Kochi, A.; Eckroat, T. J.; Green, K. D.; Mayhoub, A. S.; Lim, M. H.; Garneau-Tsodikova, S. A novel hybrid of 6-chlorotacrine and metal–amyloid-β modulator for inhibition of acetylcholinesterase and metal-induced amyloid-β aggregation. *Chem. Sci.* **2013**, *4*, 4137–4145.

(14) Xie, S.-S.; Wang, X.-B.; Li, J.-Y.; Yang, L.; Kong, L.-Y. Design, synthesis and evaluation of novel tacrine-coumarin hybrids as multifunctional cholinesterase inhibitors against Alzheimer's disease. *Eur. J. Med. Chem.* **2013**, *64*, 540–553.

(15) Prinz, M.; Parlar, S.; Bayraktar, G.; Alptüzün, V.; Erciyas, E.; Fallarero, A.; Karlsson, D.; Vuorela, P.; Burek, M.; Förster, C.; Turunc, E.; Armagan, G.; Yalcin, A.; Schiller, C.; Leuner, K.; Krug, M.; Sotriffer, C. A.; Holzgrabe, U. 1,4-Substituted 4-(1H)-pyridylene-

hydrazone-type inhibitors of AChE, BChE, and amyloid-β aggregation crossing the blood–brain barrier. *Eur. J. Pharm. Sci.* **2013**, *49*, 603–613.

(16) Viayna, E.; Sabate, R.; Muñoz-Torrero, D. Dual inhibitors of β-amyloid aggregation and acetylcholinesterase as multi-target anti-Alzheimer drug candidates. *Curr. Top. Med. Chem.* **2013**, *13*, 1820–1842.

(17) Inestrosa, N. C.; Alvarez, A.; Pérez, C. A.; Moreno, R. D.; Vicente, M.; Linker, C.; Casanueva, O. I.; Soto, C.; Garrido, J. Acetylcholinesterase accelerates assembly of amyloid-β-peptides into Alzheimer's fibrils: possible role of the peripheral site of the enzyme. *Neuron* **1996**, *16*, 881–891.

(18) Alvarez, A.; Alarcón, R.; Opazo, C.; Campos, E. O.; Muñoz, F. J.; Calderón, F. H.; Dajas, F.; Gentry, M. K.; Doctor, B. P.; De Mello, F. G.; Inestrosa, N. C. Stable complexes involving acetylcholinesterase and amyloid-β-peptide change the biochemical properties of the enzyme and increase the neurotoxicity of Alzheimer's fibrils. *J. Neurosci.* **1998**, *18*, 3213–3223.

(19) De Ferrari, G. V.; Canales, M. A.; Shin, I.; Weiner, L. M.; Silman, I.; Inestrosa, N. C. A structural motif of acetylcholinesterase that promotes amyloid beta-peptide fibril formation. *Biochemistry* **2001**, *40*, 10447–10457.

(20) Sussman, J. L.; Harel, M.; Frolow, F.; Oefner, C.; Goldman, A.; Toker, L.; Silman, I. Atomic structure of acetylcholinesterase from *Torpedo californica*: a prototypic acetylcholine-binding protein. *Science* **1991**, *253*, 872–879.

(21) Du, D.-M.; Carlier, P. R. Development of bivalent acetylcholinesterase inhibitors as potential therapeutic drugs for Alzheimer's disease. *Curr. Pharm. Des.* **2004**, *10*, 3141–3156.

(22) Recanatini, M.; Valenti, P. Acetylcholinesterase inhibitors as a starting point towards improved Alzheimer's disease therapeutics. *Curr. Pharm. Des.* **2004**, *10*, 3157–3166.

(23) Castro, A.; Martinez, A. Targeting beta-amyloid pathogenesis through acetylcholinesterase inhibitors. *Curr. Pharm. Des.* **2006**, *12*, 4377–4387.

(24) Li, W. M.; Kan, K. K. W.; Carlier, P. R.; Pang, Y. P.; Han, Y. F. East meets West in the search for Alzheimer's therapeutics - Novel dimeric inhibitors from tacrine and huperzine A. *Curr. Alzheimer Res.* **2007**, *4*, 386–396.

(25) Holzgrabe, U.; Kapková, P.; Alptüzün, V.; Scheiber, J.; Kugelmann, E. Targeting acetylcholinesterase to treat neurodegeneration. *Expert Opin. Ther. Targets* **2007**, *11*, 161–179.

(26) Musial, A.; Bajda, M.; Malawska, B. Recent developments in cholinesterases inhibitors for Alzheimer's disease treatment. *Curr. Med. Chem.* **2007**, *14*, 2654–2679.

(27) Haviv, H.; Wong, D. M.; Silman, I.; Sussman, J. L. Bivalent ligands derived from huperzine A as acetylcholinesterase inhibitors. *Curr. Top. Med. Chem.* **2007**, *7*, 375–387.

(28) Muñoz-Torrero, D. Acetylcholinesterase inhibitors as disease-modifying therapies for Alzheimer's disease. *Curr. Med. Chem.* **2008**, *15*, 2433–2455.

(29) Rampa, A.; Belluti, F.; Gobbi, S.; Bisi, A. Hybrid-based multi-target ligands for the treatment of Alzheimer's disease. *Curr. Top. Med. Chem.* **2011**, *11*, 2716–2730.

(30) Pickhardt, M.; Gazova, Z.; von Bergen, M.; Khlistunova, I.; Wang, Y.; Hascher, A.; Mandelkow, E.-M.; Biernat, J.; Mandelkow, E. Anthraquinones inhibit tau aggregation and dissolve Alzheimer's paired helical filaments *in vitro* and in cells. *J. Biol. Chem.* **2005**, *280*, 3628–3635.

(31) Bulic, B.; Pickhardt, M.; Schmidt, B.; Mandelkow, E.-M.; Waldmann, H.; Mandelkow, E. Development of tau aggregation inhibitors for Alzheimer's disease. *Angew. Chem. Int. Ed.* **2009**, *48*, 1740–1752.

(32) Yang, X.; Sun, G.; Yang, C.; Wang, B. Novel rhein analogues as potential anticancer agents. *ChemMedChem* **2011**, *6*, 2294–2301.

(33) Shi, D.-H.; Huang, W.; Li, C.; Wang, L.-T.; Wang, S.-F. Synthesis, biological evaluation and molecular modeling of aloe-emodin derivatives as new acetylcholinesterase inhibitors. *Bioorg. Med. Chem.* **2013**, *21*, 1064–1073.

(34) Orhan, I.; Tosun, F.; Şener, B. Coumarin, anthroquinone and stilbene derivatives with anticholinesterase activity. *Z. Naturforsch.* **2008**, *63c*, 366–370.

(35) Guo, J.-P.; Yu, S.; McGeer, P. L. Simple in vitro assay to identify amyloid-*β* aggregation blockers for Alzheimer's disease therapy. *J. Alzheimer's Dis.* **2010**, *19*, 1359–1370.

(36) Camps, P.; Contreras, J.; Font-Bardia, M.; Morral, J.; Muñoz-Torrero, D.; Solans, X. Enantioselective synthesis of tacrine–huperzine A hybrids. Preparative chiral MPLC separation of their racemic mixtures and absolute configuration assignments by X-ray diffraction analysis. *Tetrahedron: Asymmetry* **1998**, *9*, 835–849.

(37) Camps, P.; El Achab, R.; Morral, J.; Muñoz-Torrero, D.; Badia, A.; Baños, J. E.; Vivas, N. M.; Barril, X.; Orozco, M.; Luque, F. J. New tacrine–huperzine A hybrids (huprines): Highly potent tight-binding acetylcholinesterase inhibitors of interest for the treatment of Alzheimer's disease. *J. Med. Chem.* **2000**, *43*, 4657–4666.

(38) Camps, P.; Cusack, B.; Mallender, W. D.; El Achab, R.; Morral, J.; Muñoz-Torrero, D.; Rosenberry, T. L. Huprine X is a novel high-affinity inhibitor of acetylcholinesterase that is of interest for the treatment of Alzheimer's disease. *Mol. Pharmacol.* **2000**, *57*, 409–417.

(39) Dvir, H.; Wong, D. M.; Harel, M.; Barril, X.; Orozco, M.; Luque, F. J.; Muñoz-Torrero, D.; Camps, P.; Rosenberry, T. L.; Silman, I.; Sussman, J. L. 3D Structure of *Torpedo californica* acetylcholinesterase complexed with huprine X at 2.1 Å resolution: Kinetic and molecular dynamics correlates. *Biochemistry* **2002**, *41*, 2970–2981.

(40) Galdeano, C.; Viayna, E.; Sola, I.; Formosa, X.; Camps, P.; Badia, A.; Clos, M. V.; Relat, J.; Ratia, M.; Bartolini, M.; Mancini, F.; Andrisano, V.; Salmona, M.; Minguillón, C.; González-Muñoz, G. C.; Rodríguez-Franco, M. I.; Bidon-Chanal, A.; Luque, F. J.; Muñoz-Torrero, D. Huprine–tacrine heterodimers as anti-amyloidogenic compounds of potential interest against Alzheimer's and prion diseases. *J. Med. Chem.* **2012**, *55*, 661–669.

(41) Camps, P.; Formosa, X.; Galdeano, C.; Muñoz-Torrero, D.; Ramírez, L.; Gómez, E.; Isambert, N.; Lavilla, R.; Badia, A.; Clos, M. V.; Bartolini, M.; Mancini, F.; Andrisano, V.; Arce, M. P.; Rodríguez-Franco, M. I.; Huertas, O.; Dafni, T.; Luque, F. J. Pyrano[3,2-

c]quinoline–6-chlorotacrine hybrids as a novel family of acetylcholinesterase- and *β*-amyloid-directed anti-Alzheimer compounds. *J. Med. Chem.* **2009**, *52*, 5365–5379.

(42) Best, M.; Gifford, A. N.; Kim, S. W.; Babst, B.; Piel, M.; Rösch, F.; Fowler, J. S. Rapid radiosynthesis of [^{11}C] and [^{14}C]azelaic, suberic, and sebacic acids for *in vivo* mechanistic studies of systemic acquired resistance in plants. *J. Labelled Compd. Radiopharm.* **2012**, *55*, 39–43.

(43) Taber, D. F.; Kong, S. Alkylation of acetonitrile. *J. Org. Chem.* **1997**, *62*, 8575–8576.

(44) Lethesh, K. C.; Van Hecke, K.; Van Meervelt, L.; Nockemann, P.; Kirchner, B.; Zahn, S.; Parac-Vogt, T. N.; Dehaen, W.; Binnemans, K. Nitrile-functionalized pyridinium, pyrrolidinium, and piperidinium ionic liquids. *J. Phys. Chem. B* **2011**, *115*, 8424–8438.

(45) Lane, R. M.; Potkin, S. G.; Enz, A. Targeting acetylcholinesterase and butyrylcholinesterase in dementia. *Int. J. Neuropsychopharmacol.* **2006**, *9*, 101–124.

(46) Ellman, G. L.; Courtney, K. D.; Andres, V., Jr.; Featherstone, R. M. A new and rapid colorimetric determination of acetylcholinesterase activity. *Biochem. Pharmacol.* **1961**, *7*, 88–95.

(47) Rydberg, E. H.; Brumshtein, B.; Greenblatt, H. M.; Wong, D. M.; Shaya, D.; Williams, L. D.; Carlier, P. R.; Pang, Y.-P.; Silman, I.; Sussman, J. L. Complexes of alkylene-linked tacrine dimers with *Torpedo californica* acetylcholinesterase: Binding of bis(5)-tacrine produces a dramatic rearrangement in the active site gorge. *J. Med. Chem.* **2006**, *49*, 5491–5500.

(48) Bolognesi, M. L.; Cavalli, A.; Valgimigli, L.; Bartolini, M.; Rosini, M.; Andrisano, V.; Recanatini, M.; Melchiorre, C. Multi-target-directed drug design strategy: from a dual binding site acetylcholinesterase inhibitor to a trifunctional compound against Alzheimer's disease. *J. Med. Chem.* **2007**, *50*, 6446–6449.

(49) Bartolini, M.; Bertucci, C.; Cavrini, V.; Andrisano, V. β-Amyloid aggregation induced by human acetylcholinesterase: Inhibition studies. *Biochem. Pharmacol.* **2003**, *65*, 407–416.

(50) Rouleau, J.; Iorga, B. I.; Guillou, C. New potent human acetylcholinesterase inhibitors in the tetracyclic triperpene series with inhibitory potency on amyloid β aggregation. *Eur. J. Med. Chem.* **2011**, *46*, 2193–2205.

(51) Mohamed, T.; Yeung, J. C. K.; Rao, P. P. N. Development of 2-substituted-*N*-(naphth-1-ylmethyl) and *N*-benzhydrylpyrimidin-4-amines as dual cholinesterase and Aβ-aggregation inhibitors: synthesis and biological evaluation. *Bioorg. Med. Chem. Lett.* **2011**, *21*, 5881–5887.

(52) Bolognesi, M. L.; Bartolini, M.; Mancini, F.; Chiriano, G.; Ceccarini, L.; Rosini, M.; Milelli, A.; Tumiatti, V.; Andrisano, V.; Melchiorre, C. Bis(7)-tacrine derivatives as multitarget-directed ligands: focus on anticholinesterase and antiamyloid activities. *ChemMedChem* **2010**, *5*, 1215–1220.

(53) Minarini, A.; Milelli, A.; Tumiatti, V.; Rosini, M.; Simoni, E.; Bolognesi, M. L.; Andrisano, V.; Bartolini, M.; Motori, E.; Angeloni, C.; Hrelia, S. Cystamine-tacrine dimer: a new multi-target-directed ligand as potential therapeutic agent for Alzheimer's disease treatment. *Neuropharmacology* **2012**, *62*, 997–1003.

(54) Rizzo, S.; Bisi, A.; Bartolini, M.; Mancini, F.; Belluti, F.; Gobbi, S.; Andrisano, V.; Rampa, A. Multi-target strategy to address Alzheimer's disease: design, synthesis and biological evaluation of new tacrine-based dimers. *Eur. J. Med. Chem.* **2011**, *46*, 4336–4343.

(55) Belluti, F.; Bartolini, M.; Bottegoni, G.; Bisi, A.; Cavalli, A.; Andrisano, V.; Rampa, A. Benzophenone-based derivatives: a novel series of potent and selective dual inhibitors of acetylcholinesterase and acetylcholinesterase-induced beta-amyloid aggregation. *Eur. J. Med. Chem.* **2011**, *46*, 1682–1693.

(56) Cavalli, A.; Bolognesi, M. L.; Capsoni, S.; Andrisano, V.; Bartolini, M.; Margotti, E.; Cattaneo, A.; Recanatini, M.; Melchiorre, C. A small molecule targeting the multifactorial nature of Alzheimer's disease. *Angew. Chem. Int. Ed.* **2007**, *46*, 3689–3692.

(57) Muñoz-Ruiz, P.; Rubio, L.; García-Palomero, E.; Dorronsoro, I.; del Monte-Millán, M.; Valenzuela, R.; Usán, P.; de Austria, C.; Bartolini, M.; Andrisano, V.; Bidon-Chanal, A.; Orozco, M.; Luque, F. J.; Medina, M.; Martínez, A. Design, synthesis, and biological evaluation of dual binding site acetylcholinesterase inhibitors: New disease-modifying agents for Alzheimer's disease. *J. Med. Chem.* **2005**, *48*, 7223–7233.

(58) Bartolini, M.; Bertucci, C.; Bolognesi, M. L.; Cavalli, A.; Melchiorre, C.; Andrisano, V. Insight into the kinetic of amyloid beta (1–42) peptide self-aggregation: Elucidation of inhibitors' mechanism of action. *ChemBioChem* **2007**, *8*, 2152–2161.

(59) May, P. C.; Dean, R. A.; Lowe, S. L.; Martenyi, F.; Sheehan, S. M.; Boggs, L. N.; Monk, S. A.; Mathes, B. M.; Mergott, D. J.; Watson, B. M.; Stout, S. L.; Timm, D. E.; Smith LaBell, E.; Gonzales, C. R.; Nakano, M.; Jhee, S. S.; Yen, M.; Ereshefsky, L.; Lindstrom, T. D.; Calligaro, D. O.; Cocke, P. J.; Hall, D. G.; Friedrich, S.; Citron, M.; Audia, J. E. Robust central reduction of amyloid-*β* in humans with an orally available, non-peptidic *β*-secretase inhibitor. *J. Neurosci.* **2011**, *31*, 16507–16516.

(60) Butini, S.; Brogi, S.; Novellino, E.; Campiani, G.; Ghosh, A. K.; Brindisi, M.; Gemma, S. The structural evolution of β-secretase inhibitors: a focus on the development of small-molecule inhibitors. *Curr. Top. Med. Chem.* **2013**, *13*, 1787–1807.

(61) Galdeano, C.; Viayna, E.; Arroyo, P.; Bidon-Chanal, A.; Blas, J. R.; Muñoz-Torrero, D.; Luque, F. J. Structural determinants of the multifunctional profile of dual binding site acetylcholinesterase inhibitors as anti-Alzheimer agents. *Curr. Pharm. Design* **2010**, *16*, 2818–2836.

(62) Fu, H.; Li, W.; Luo, J.; Lee, N. T. K.; Li, M.; Tsim, K. W. K.; Pang, Y.; Youdim, M. B. H.; Han, Y. Promising anti-Alzheimer's dimer bis(7)-tacrine reduces β-amyloid generation by directly inhibiting BACE-1 activity. *Biochem. Biophys. Res. Commun.* **2008**, *366*, 631–636.

(63) Hanessian, S.; Yun, H.; Hou, Y.; Yang, G.; Bayrakdarian, M.; Therrien, E.; Moitessier, N.; Roggo, S.; Veenstra, S.; Tintelnot-Blomley, M.; Rondeau, J.-M.; Ostermeier, C.; Strauss, A.; Ramage, P.; Paganetti, P.; Neumann, U.; Betschart, C. Structure-based design, synthesis, and memapsin 2 (BACE) inhibitory activity of carbocyclic and heterocyclic peptidomimetics. *J. Med. Chem.* **2005**, *48*, 5175–5190.

(64) Ballatore, C.; Brunden, K. R.; Piscitelli, F.; James, M. J.; Crowe, A.; Yao, Y.; Hyde, E.; Trojanowski, J. Q. ; Lee, V. M.-Y. ; Smith, III, A. B. Discovery of brain-penetrant, orally bioavailable aminothienopyridazine inhibitors of Tau aggregation. *J. Med. Chem.* **2010**, *53*, 3739–3747.

(65) Lipinski, C. A.; Lombardo, F.; Dominy, B. W.; Feeney, P. J. Experimental and computational approaches to estimate solubility and permeability in drug discovery and development settings. *Adv. Drug Delivery Rev.* **1997**, *23*, 3–25.

(66) Morphy, R.; Rankovic, Z. Designing multiple ligands – medicinal chemistry strategies and challenges. *Curr. Pharm. Des.* **2009**, *15*, 587–600.

(67) García-Palomero, E.; Muñoz, P.; Usan, P.; Garcia, P.; De Austria, C.; Valenzuela, R.; Rubio, L.; Medina, M.; Martínez, A. Potent β-Amyloid Modulators. *Neurodegener. Dis.* **2008**, *5*, 153–156.

(68) Spuch, C.; Antequera, D.; Fernandez-Bachiller, M. I.; Rodríguez-Franco, M. I.; Carro, E. A new tacrine–melatonin hybrid reduces amyloid burden and behavioral deficits in a mouse model of Alzheimer's disease. *Neurotox. Res.* **2010**, *17*, 421–431.

(69) Efremov, I. V.; Vajdos, F. F.; Borzilleri, K. A.; Capetta, S.; Chen, H.; Dorff, P. H.; Dutra, J. K.; Goldstein, S. W.; Mansour, M.; McColl, A.; Noell, S.; Oborski, C. E.; O'Connell, T. N.; O'Sullivan, T. J.; Pandit, J.; Wang, H.; Wei, B.; Withka, J. M. Discovery and optimization of a novel spiropyrrolidine inhibitor of *β*-secretase (BACE1) through fragment-based drug design. *J. Med. Chem.* **2012**, *55*, 9069–9088.

(70) Lu, K.; Jiang, Y.; Chen, B.; Eldemenky, E. M.; Ma, G.; Packiarajan, M.; Chandrasena, G.; White, A. D.; Jones, K. A.; Li, B.; Hong, S.-P. Strategies to lower the Pgp efflux liability in a series of potent indole azetidine MCHR1 antagonists. *Bioorg. Med. Chem. Lett.* **2011**, *21*, 5310−5314.

(71) Di, L.; Kerns, E. H.; Fan, K.; McConnell, O. J.; Carter, G. T. High throughput artificial membrane permeability assay for blood−brain barrier. *Eur. J. Med. Chem.* **2003**, *38*, 223−232.

(72) Ami, D.; Natalello, A.; Lotti, M.; Doglia, S. M. Why and how protein aggregation has to be studied *in vivo*. *Microb. Cell Fact.* **2013**, *12*, 17.

(73) Villar-Piqué, A.; Ventura, S. Modeling amyloids in bacteria. *Microb. Cell Fact.* **2012**, *11*, 166.

(74) Pouplana, S.; Espargaró, A.; Galdeano, C.; Viayna, E.; Sola, I.; Ventura, S.; Muñoz-Torrero, D.; Sabate, R. Thioflavin-S staining of bacterial inclusion bodies for the fast, simple, and inexpensive screening of amyloid aggregation inhibitors. *Curr. Med. Chem.* **2014**, *21*, in press.

(75) Porat, Y.; Abramowitz, A.; Gazit, E. Inhibition of amyloid fibril formation by polyphenols: structural similarity and aromatic interactions as a common inhibition mechanism. *Chem. Biol. Drug Des.* **2006**, *67*, 27−37.

(76) Zhang, H.-Y. Same causes, same cures. *Biochem. Biophys. Res. Commun.* **2006**, *351*, 578−581.

(77) Narlawar, R.; Pickhardt, M.; Leuchtenberger, S.; Baumann, K.; Krause, S.; Dyrks, T.; Weggen, S.; Mandelkow, E.; Schmidt, B. Curcumin-derived pyrazoles and isoxazoles: Swiss army knives or blunt tools for Alzheimer's disease? *ChemMedChem* **2008**, *3*, 165–172.

(78) LaFerla, F. M. Pathways linking Aβ and tau pathologies. *Biochem. Soc. Trans.* **2010**, *38*, 993–995.

(79) Shankar, G. M.; Walsh, D. M. Alzheimer's disease: synaptic dysfunction and Aβ. *Mol Neurodegener*. **2009**, *4*, 48.

(80) Lacor, P. N.; Buniel, M. C.; Chang, L.; Fernandez, S. J.; Gong, Y.; Viola, K. L.; Lambert, M. P.; Velasco, P. T.; Bigio, E. H.; Finch, C. E.; Krafft, G. A.; Klein, W. L. Synaptic targeting by Alzheimer's-related amyloid beta oligomers. *J. Neurosci.* **2004**, *24*, 10191–10200.

(81) Walsh, D. M.; Klyubin, I.; Fadeeva, J. V.; Cullen, W. K.; Anwyl, R.; Wolfe, M. S.; Rowan, M. J.; Selkoe, D. J. Naturally secreted oligomers of amyloid β protein potently inhibit hippocampal long-term potentiation *in vivo*. *Nature* **2002**, *416*, 535–539.

(82) Serrano-Pozo, A.; Frosch, M. P.; Masliah, E.; Hyman, B. T. Neuropathological alterations in Alzheimer disease. *Cold Spring Harb. Perspect. Med.* **2011**, 1:a006189.

(83) Alkondon, M.; Albuquerque, E. X.; Pereira, E. F. R. Acetylcholinesterase inhibition reveals endogenous nicotinic modulation of glutamate inputs to CA1 stratum radiatum interneurons in hippocampal slices. *Neurotoxicology* **2013**, *36*, 72–81.

(84) Ye, L.; Qi, J. S.; Qiao, J. T. Long-term potentiation in hippocampus of rats is enhanced by endogenous acetylcholine in a way that is independent of N-methyl-D-aspartate receptors. *Neurosci. Lett.* **2001**, *300*, 145–148.

(85) Ardiles, A. O.; Tapia-Rojas, C. C.; Mandal, M.; Alexandre, F.; Kirkwood, A.; Inestrosa, N. C.; Palacios, A. G. Postsynaptic dysfunction is associated with spatial and object recognition memory loss in a natural model of Alzheimer's disease. *Proc. Natl. Acad. Sci. U. S. A.* **2012**, *109*, 13835–13840.

(86) Garcia-Alloza, M.; Robbins, E. M.; Zhang-Nunes, S. X.; Purcell, S. M.; Betensky, R. A.; Raju, S.; Prada, C.; Greenberg, S. M.; Bacskai, B. J.; Frosch, M. P. Characterization of amyloid deposition in the APPswe/PS1dE9 mouse model of Alzheimer disease. Neurobiol. Dis. **2006**, *24*, 516–524.

(87) Silverman R. B. The organic chemistry of enzyme-catalyzed reactions. Academic Press, San. Diego, 2000.

(88) Naiki, H.; Higuchi, K.; Nakakuki, K.; Takeda, T. Kinetic analysis of amyloid fibril polymerization in vitro. *Lab Invest* **1991**, *65*, 104–110.

(89) Varela-Nallar, L.; Alfaro, I. E.; Serrano, F. G.; Parodi, J.; Inestrosa, N. C. Wingless-type family member 5a (Wnt-5a) stimulates synaptic differentiation and function of glutamatergic synaptses. *Proc. Natl. Acad. Sci. U.S.A.* **2010**, *107*, 21164–21169.

(90) Inestrosa, N. C.; Carvajal, F. J.; Zolezzi, J. M.; Tapia-Rojas, C.; Serrano, F.; Karmelic, D.; Toledo, E. M.; Toro, A.; Toro, J.; Santos, M. J. Peroxisome proliferator reduce spatial

(91) Carvajal, F. J.; Zolezzi, J. M.; Tapia-Rojas, C.; Godoy, J. A.; Inestrosa, N. C. Tetrahydrohyperforin decreases cholinergic markers associated with amyloid-β plaques, 4-hydroxynonenal formation, and caspase-3 activation in AβPP/PS1 mice. *J. Alzheimers Dis.* **2013**, *36*, 99–118.

(92) Dinamarca, M. C.; Sagal, J. P.; Quintanilla, R. A.; Godoy, J. A.; Arrázola, M. S.; Inestrosa, N. C. Amyloid-β-acetylcholinesterase complexes potentiate neurodegenerative changes induced by the Aβ peptide. Implications for the pathogenesis of Alzheimer's disease. *Mol. Neurodegener.* **2010**, *5*, 4.

(93) Dvir, H.; Silman, I.; Harel, M.; Rosenberry, T. L.; Sussman, J. L. Acetylcholinesterase: From 3D structure to function. *Chem.-Biol. Interact.* **2010**, *187*, 10–22.

(94) Morley, S. D.; Afshar, M. Validation of an empirical RNA-ligand scoring function for fast flexible docking using RiboDock. *J. Comput.-Aided Mol. Des.* **2004**, *18*, 189–208.

(95) Schmidtke, P.; Bidon-Chanal, A.; Luque, F. J.; Barril, X. MDpocket: Open source cavity detection and characterization on molecular dynamics trajectories. *Bioinformatics* **2011**, *27*, 3276–3285.

(96) Schmidtke, P.; Barril, X. Understanding and predicting druggability. A high-throughput method for detection of drug binding sites. *J. Med. Chem.* **2010**, *53*, 5858–5867.

(97) Friesner, R. A.; Murphy, R. B.; Repasky, M. P.; Frye, L. L.; Greenwood, J. R.; Halgren,T. A.; Sanschagrin, P. C.; Mainz, D. T. Extra precision Glide: Docking and

(98) Salomon-Ferrer, R.; Goetz, A. W.; Poole, D.; Le Grand, S.; Walker, R. C. Routine microsecond molecular dynamics simulations with AMBER on GPUs. 2. Explicit solvent Particle Mesh Ewald, *J. Chem. Theory Comput.* **2013**, *9*, 3878–3888.

(99) Case, D. A.; Darden, T. A.; Cheatham, III, T. E.; Simmerling, C. L.; Wang, J.; Duke, R. E.; Luo, R.; Walker, R. C.; Zhang, W.; Merz, K. M.; Roberts, B.; Hayik, S.; Roitberg, A.; Seabra, G.; Swails, J.; Goetz, A. W.; Kolossváry, I.; Wong, K. F.; Paesani, F.; Vanicek, J.; Wolf, R. M.; Liu, J.; Wu, X.; Brozell, S. R.; Steinbrecher, T.; Gohlke, H.; Cai, Q.; Ye, X.; Wang, J.; Hsieh, M.-J.; Cui, G.; Roe, D. R.; Mathews, D. H.; Seetin, M. G.; Salomon-Ferrer, R.; Sagui, C.; Babin, V.; Luchko, T.; Gusarov, S.; Kovalenko, A.; Kollman, P. A. (2012), *AMBER 12*, University of California, San Francisco.

(100) Hornak, V.; Abel, R.; Okur, A.; Strockbine, B.; Roitberg, A.; Simmerling, C. Comparison of multiple Amber force fields and development of improved protein backbone parameters. *Proteins* **2006**, *65*, 712–725.

(101) Wang, J. M.; Wolf, R. M.; Caldwell, J. W.; Kollman, P. A.; Case, D. A. Development and testing of a general amber force field, *J. Comput. Chem.* **2005**, *26*, 1157–1174.

(102) Joung, I. S.; Cheatham, T. E. Molecular dynamics simulations of the dynamic and energetic properties of alkali and halide ions using water-model-specific ion parameters, *J. Phys. Chem. B* **2009**, *113*, 13279–13290.

(103) Gaussian 09, Revision C.01; Frisch, M. J.; Trucks, G. W.; Schlegel, H. B.; Scuseria, G. E.; Robb, M. A.; Cheeseman, J. R.; Scalmani, G.; Barone, V.; Mennucci, B.; Petersson, G. A.; Nakatsuji, H.; Caricato, M.; Li, X.; Hratchian, H. P.; Izmaylov, A. F.; Bloino, J.; Zheng, G.; Sonnenberg, J. L.; Hada, M.; Ehara, M.; Toyota, K.; Fukuda, R.; Hasegawa, J.; Ishida, M.; Nakajima, T.; Honda, Y.; Kitao, O.; Nakai, H.; Vreven, T.; Montgomery, J. A., Jr.; Peralta, J. E.; Ogliaro, F.; Bearpark, M.; Heyd, J. J.; Brothers, E.; Kudin, K. N.; Staroverov, V. N.; Kobayashi, R.; Normand, J.; Raghavachari, K.; Rendell, A.; Burant, J. C.; Iyengar, S. S.; Tomasi, J.; Cossi, M.; Rega, N.; Millam, J. M.; Klene, M.; Knox, J. E.; Cross, J. B.; Bakken, V.; Adamo, C.; Jaramillo, J.; Gomperts, R.; Stratmann, R. E.; Yazyev, O.; Austin, A. J.; Cammi, R.; Pomelli, C.; Ochterski, J. W.; Martin, R. L.; Morokuma, K.; Zakrzewski, V. G.; Voth, G. A.; Salvador, P.; Dannenberg, J. J.; Dapprich, S.; Daniels, A. D.; Farkas, Ö.; Foresman, J. B.; Ortiz, J. V.; Cioslowski, J.; Fox, D. J. Gaussian, Inc., Wallingford CT, 2009.

(104) Bayly, C. I.; Cieplak, P.; Cornell, W.; Kollman, P. A. A well-behaved electrostatic potential based method using charge restraints for deriving atomic charges: the RESP model. *J. Phys. Chem.* **1993**, *97*, 10269–10280.

(105) Jorgensen, W. L.; Chandrasekhar, J.; Madura, J. D.; Impey, R. W.; Klein, M. L. Comparison of simple potential functions for simulating liquid water. *J. Chem. Phys.* **1983**, *79*, 926–935.

TOC graphic

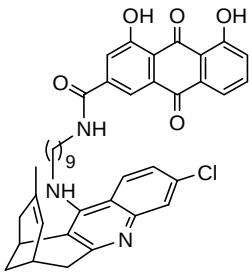

In vitro

hAChE IC_{50} 2.39 nM **hBChE IC_{50} 513 nM**

BACE-1 IC_{50} 80 nM **PAMPA-BBB: CNS+**

43% inhibition of Aβ42 aggregation at 10 μM

***In vivo* (intact *E. coli* cells)**

47% inhibition of Aβ42 aggregation at 10 μM

34% inhibition of tau aggregation at 10 μM

***Ex vivo* (mouse hippocampal slices)**

Prevention of Aβ-induced loss of synaptic proteins

(GluA2, PSD95, VGlut1, SYN)

***In vivo* (APP-PS1 mice)**

central Aβ lowering effect

SUPPORTING INFORMATION

Synthesis and multi-target biological profiling of a novel family of rhein derivatives as disease-modifying anti-Alzheimer agents

Elisabet Viayna,[†,‡,Δ] Irene Sola,[†,‡] Manuela Bartolini,[§] Angela De Simone,[¶] Cheril Tapia-Rojas,[#] Felipe G. Serrano,[#] Raimon Sabaté,[⊥,//] Jordi Juárez-Jiménez,[‡,⊥] Belén Pérez,[◊] F. Javier Luque,[‡,⊥] Vincenza Andrisano,[¶] M. Victòria Clos,[◊] Nibaldo C. Inestrosa,[#] and Diego Muñoz-Torrero[,†,‡]*

[†] Laboratori de Química Farmacèutica (Unitat Associada al CSIC), Facultat de Farmàcia, Universitat de Barcelona, Av. Joan XXIII 27-31, E-08028, Barcelona, Spain

[‡] Institut de Biomedicina (IBUB), Universitat de Barcelona, Barcelona, Spain

[§] Department of Pharmacy and Biotechnology, Alma Mater Studiorum University of Bologna, Via Belmeloro 6, I-40126, Bologna, Italy

[¶] Department for Life Quality Studies, University of Bologna, Corso d'Augusto 237, I-47921-Rimini, Italy

[#] Centro de Envejecimiento y Regeneración (CARE), Departamento de Biología Celular y Molecular, Facultad de Ciencias Biológicas, Pontificia Universidad Católica de Chile, Alameda 340, 8331150-Santiago, Chile

[⊥] Departament de Fisicoquímica, Facultat de Farmàcia, Universitat de Barcelona, Barcelona, Spain

[||] Institut de Nanociència i Nanotecnologia (IN^{2}UB), Universitat de Barcelona, Barcelona, Spain

[◊] Departament de Farmacologia, de Terapèutica i de Toxicologia, Institut de Neurociències, Universitat Autònoma de Barcelona, E-08193, Bellaterra, Barcelona, Spain

[Δ] Present address of E.V.: Drug Discovery Unit, College of Life Sciences, University of Dundee, Dundee, DD1 5EH, UK

TABLE OF CONTENTS

Synthetic procedures for intermediates **5a**–**h** and **6a**–**h** S3

Figure S1. Superposition of (–)-**7h** and huprine X in AChE S23

Figure S2. Superposition of (–)-**7h** and *bis*(7)-tacrine in AChE S24

Figure S3. Representation of BS1 and BS2 sites in BACE-1 S25

Table S1. PAMPA-BBB assay results of commercial drugs for assay validation S26

References S27

Appendix (elemental analysis data) S28

Synthetic Procedures for Intermediates 5a–h and 6a–h

(±)-5-[(3-Chloro-6,7,10,11-tetrahydro-9-methyl-7,11-methanocycloocta[*b*]quinolin-12-yl)amino]pentanenitrile [(±)-5a]. A suspension of (±)-huprine Y, (±)-**4** (300 mg, 1.06 mmol) and finely powdered KOH (85% purity, 139 mg, 2.11 mmol), and 4 Å molecular sieves in anhyd DMSO (6 mL) was stirred, heating every 10 min approximately with a heat gun for 1 h and at rt one additional hour, and then treated with 5-bromovaleronitrile (0.15 mL, 208 mg, 1.28 mmol). The reaction mixture was stirred at rt overnight, diluted with 5N NaOH (25 mL) and extracted with EtOAc (3×40 mL). The combined organic extracts were washed with H_2O (3×50 mL), dried over anhyd Na_2SO_4, and evaporated under reduced pressure to give a yellow oil (469 mg), which was purified by column chromatography (40–60 μm silica gel, CH_2Cl_2/MeOH/50% aq. NH_4OH mixtures, gradient elution). On elution with CH_2Cl_2/50% aq. NH_4OH 100:0.2, the *N*,*N*-dialkylated derivative (±)-**8a** (78 mg, 16% yield) was isolated as a yellow oil. On elution with CH_2Cl_2/MeOH/50% aq. NH_4OH 99:1:0.2, nitrile (±)-**5a** (273 mg, 70% yield) was isolated as a beige solid; R_f[(±)-**5a**] 0.50; R_f[(±)-**8a**] 0.77 (CH_2Cl_2/MeOH/50% aq. NH_4OH 9:1:0.05).

A solution of (±)-**5a** (52 mg, 0.14 mmol) in CH_2Cl_2 (4.5 mL) was filtered through a 0.2 μm PTFE filter, treated with methanolic HCl (1.40N, 0.30 mL) and evaporated under reduced pressure. The resulting solid was washed with pentane (3×2 mL) to give, after drying at 65 ºC/2 Torr for 48 h, (±)-**5a**·HCl (58 mg) as a yellow solid: mp 181−183 °C (CH_2Cl_2/MeOH 94:6); IR (KBr) ν 3500–2500 (max at 3364, 3254, 3049, 3014, 2926, 2885, 2651, N-H, N^+-H and C-H st), 2243 (CN st), 1635, 1629, 1602, 1582, 1570, 1562 (ar-C-C and ar-C-N st) cm^{-1}; ^1H NMR (400 MHz, CD_3OD) δ 1.59 (s, 3H, 9'-CH_3), 1.79 (tt, $J \approx J' \approx 7.2$ Hz, 2H, 3-H_2), 1.93 (d, J=17.6 Hz, 1H, 10'-H_{endo}), superimposed in part 1.92–1.98 (m, 1H, 13'-H_{syn}), 2.01 (tt, $J \approx J' \approx 7.2$ Hz, 2H, 4-H_2), 2.09

(dm, *J*=12.8 Hz, 1H, 13'-H_{anti}), 2.56 (t, *J*=7.2 Hz, 2H, 2-H_2), superimposed in part 2.53–2.60 (m, 1H, 10'-H_{exo}), 2.77 (m, 1H, 7'-H), 2.88 (ddd, *J*=18.0 Hz, *J'*=*J"*=1.6 Hz, 1H, 6'-H_{endo}), 3.22 (dd, *J*=18.0 Hz, *J'*=5.2 Hz, 1H, 6'-H_{exo}), 3.47 (m, 1H, 11'-H), 4.03 (t, *J*= 7.6 Hz, 2H, 5-H_2), 4.85 (s, NH and $^{+}$NH), 5.59 (br d, *J*=4.4 Hz, 1H, 8'-H), 7.57 (dd, *J*=9.2 Hz, *J'*=2.0 Hz, 1H, 2'-H), 7.78 (d, *J*≈2.0 Hz, 1H, 4'-H), 8.40 (d, *J*≈9.2 Hz, 1H, 1'-H); ^{13}C NMR (100.6 MHz, CD_3OD) δ 17.1 (CH_2, C2), 23.4 (CH_3, 9'-CH_3), 23.9 (CH_2, C3), 27.3 (CH, C11'), 27.9 (CH, C7'), 29.3 (CH_2, C13'), 30.3 (CH_2, C4), 36.1 (CH_2), 36.2 (CH_2) (C6', C10'), 48.8 (CH_2, C5), 115.8 (C, C12a'), 117.9 (C, C11a'), 119.2 (CH, C4'), 120.9 (C, CN), 125.1 (CH, C8'), 126.8 (CH, C2'), 129.4 (CH, C1'), 134.6 (C, C9'), 140.3 (C, C3'), 141.0 (C, C4a'), 151.5 (C, C5a'), 157.0 (C, C12'). HRMS (ESI) calcd for ($C_{22}H_{24}{}^{35}ClN_3$ + H^+): 366.1732, found 366.1729.

A solution of (±)-**8a** (78 mg, 0.17 mmol) in CH_2Cl_2 (4.5 mL) was filtered through a 0.2 μm PTFE filter, treated with methanolic HCl (0.65N, 0.64 mL) and evaporated under reduced pressure. The resulting solid was washed with pentane (3×2 mL) to give, after drying at 65 ºC/2 Torr for 48 h, (±)-**8a**·HCl (80 mg) as a yellow solid: mp 196–198 ºC (CH_2Cl_2/MeOH 88:12); IR (KBr) *ν* 3500–2450 (max at 3430, 3044, 2919, 2875, 2464, N^+-H and C-H st), 2243 (CN st), 1632, 1604, 1574 (ar-C-C and ar-C-N st) cm^{-1}; ^{1}H NMR (400 MHz, CD_3OD) δ 1.59 (s, 3H, 9'-CH_3), 1.65 (tt, *J*≈*J'*≈7.2 Hz, 4H, 3-H_2), 1.72–1.98 (complex signal, 4H, 4-H_2), 2.00 (br d, *J*=17.6 Hz, 1H, 10'-H_{endo}), superimposed in part 2.06 (dm, *J*≈12.8 Hz, 1H, 13'-H_{syn}), 2.12 (dm, *J*=12.8 Hz, 1H, 13'-H_{anti}), 2.48 (t, *J*=7.2 Hz, 4H, 2-H_2), 2.69 (dd, *J*=17.6 Hz, *J'*=5.6 Hz, 1H, 10'-H_{exo}), 2.82 (m, 1H, 7'-H), 3.17 (ddd, *J*=18.0 Hz, *J'*≈*J"*≈1.8 Hz, 1H, 6'-H_{endo}), 3.39 (dd, *J*=18.0 Hz, *J'*=5.6 Hz, 1H, 6'-H_{exo}), superimposed in part 3.73 (m, 1H, 11'-H), 3.73 (ddd, *J*=13.6 Hz, *J'*=9.6 Hz, *J"*=5.6 Hz, 2H) and 3.80 (ddd, *J*=13.6 Hz, *J'*=9.2 Hz, *J"*=6.0 Hz, 2H) (5-H_2), 4.84 (s, $^{+}$NH), 5.68 (br d, *J*=4.4 Hz, 1H, 8'-H), 7.72 (dd, *J*=9.2 Hz, *J'*=2.4 Hz,

1H, 2'-H), 7.99 (d, *J*=2.4 Hz, 1H, 4'-H), 8.26 (d, *J*=9.2 Hz, 1H, 1'-H); ^{13}C NMR (100.6 MHz, CD_3OD) δ 17.1 (CH_2, C2), 23.3 (CH_3, 9'-CH_3), 23.9 (CH_2, C3), 27.6 (CH, C7'), 28.6 (CH_2, C13'), 28.9 (CH_2, C4), 29.7 (CH, C11'), 37.7 (CH_2, C6'), 38.7 (CH_2, C10'), 55.1 (CH_2, C5), 120.0 (CH, C4'), 120.9 (C, CN), 125.5 (C, C12a'), 125.7 (CH, C8'), 192.2 (CH, C2'), 130.1 (CH, C1'), 132.5 (C, C11a'), 134.3 (C, C9'), 140.36 (C), 140.43 (C) (C3', C4a'), 157.6 (C, C5a'), 163.9 (C, C12'); HRMS (ESI) calcd for ($C_{27}H_{31}{}^{35}ClN_4$ + H^+) 447.2310, found 447.2309.

(±)-6-[(3-Chloro-6,7,10,11-tetrahydro-9-methyl-7,11-methanocycloocta[*b*]quinolin-12-yl)amino]hexanenitrile [(±)-5b]. It was prepared as described for (±)-**5a**. From (±)-huprine Y, (±)-**4** (1.50 g, 5.28 mmol) and 6-bromohexanenitrile (0.77 mL, 1.02 g, 5.80 mmol), a yellow oil (2.88 g) was obtained and purified by column chromatography (40–60 μm silica gel, CH_2Cl_2/50% aq. NH_4OH 100:0.2), to afford (±)-**5b** (1.26 g, 63% yield) as a yellow solid; R_f 0.77 (CH_2Cl_2/MeOH/50% aq. NH_4OH 9:1:0.05).

(±)-5b·HCl: mp 143–145 °C (CH_2Cl_2/MeOH 92:8); IR (KBr) *v* 3500–2500 (max at 3398, 3245, 3048, 2924, 2853, 2734, N-H, N^+-H and C-H st), 2242 (CN st), 1724, 1618, 1572 (ar-C-C and ar-C-N st) cm^{-1}; ^{1}H NMR (400 MHz, CD_3OD) δ 1.59 (s, 3H, 9'-CH_3), superimposed in part 1.54–1.62 (m, 2H, 4-H_2), 1.71 (m, 2H, 3-H_2), superimposed in part 1.91 (tt, *J*≈*J'*≈7.6 Hz, 2H, 5-H_2), superimposed 1.90–1.95 (m, 1H, 10'-H_{endo}), superimposed in part 1.92–1.98 (dm, *J*≈12.8 Hz, 1H, 13'-H_{syn}), 2.09 (dm, *J*≈12.8 Hz, 1H, 13'-H_{anti}), 2.48 (t, *J*≈7.2 Hz, 2H, 2-H_2), 2.56 (dm, *J*≈17.2 Hz, 1H, 10'-H_{exo}), 2.77 (m, 1H, 7'-H), 2.87 (ddd, *J*=17.6 Hz, *J'*=*J"*=1.6 Hz, 1H, 6'-H_{endo}), 3.21 (dd, *J*=17.6 Hz, *J'*≈5.6 Hz, 1H, 6'-H_{exo}), 3.46 (m, 1H, 11'-H), 4.01 (t, *J*≈7.6 Hz, 2H, 6-H_2), 4.85 (s, NH and $^+$NH), 5.59 (br d, *J*=4.4 Hz, 1H, 8'-H), 7.57 (dd, *J*=9.2 Hz, *J'*=2.0 Hz, 1H, 2'-H), 7.77 (d, *J*=2.0 Hz, 1H, 4'-H), 8.40 (d, *J*≈9.2 Hz, 1H, 1'-H); ^{13}C NMR (100.6 MHz,

CD_3OD) δ 17.2 (CH_2, C2), 23.4 (CH_3, 9'-CH_3), 26.0 (CH_2, C3), 26.8 (CH_2, C4), 27.3 (CH, C11'), 27.9 (CH, C7'), 29.3 (CH_2, C13'), 30.5 (CH_2, C5), 36.0 (CH_2), 36.2 (CH_2) (C6', C10'), 49.4 (CH_2, C6), 115.7 (C, C12a'), 117.8 (C, C11a'), 119.2 (CH, C4'), 121.0 (C, CN), 125.1 (CH, C8'), 126.8 (CH, C2'), 129.4 (CH, C1'), 134.6 (C, C9'), 140.3 (C, C3'), 141.0 (C, C4a'), 151.4 (C, C5a'), 157.0 (C, C12'); HRMS (ESI) calcd for ($C_{23}H_{26}{}^{35}ClN_3 + H^+$) 380.1888, found 380.1889.

(±)-7-[(3-Chloro-6,7,10,11-tetrahydro-9-methyl-7,11-methanocycloocta[*b*]quinolin-12-yl)amino]heptanenitrile [(±)-5c]. It was prepared as described for (±)-**5a**. From (±)-huprine Y, (±)-**4** (2.00 g, 7.04 mmol) and 7-bromoheptanenitrile (1.21 mL, 1.53 g, 8.05 mmol), a yellow oil (3.50 g) was obtained and purified by column chromatography (40–60 μm silica gel, CH_2Cl_2/50% aq. NH_4OH 100:0.2), to afford (±)-**5c** (2.40 g, 87% yield) as a yellow solid; R_f 0.66 (CH_2Cl_2/MeOH/50% aq. NH_4OH 9:1:0.05).

(±)-5c·HCl: mp 125–126 °C (CH_2Cl_2/MeOH 94:6); IR (KBr) ν 3500–2500 (max at 3219, 3049, 2927, 2852, 2733, 2651, N-H, N^+-H and C-H st), 2242 (CN st), 1620, 1571 (ar-C-C and ar-C-N st) cm^{-1}; ^1H NMR (400 MHz, CD_3OD) δ 1.44–1.56 (complex signal, 4H, 4-H_2 and 5-H_2), 1.59 (s, 3H, 9'-CH_3), 1.62–1.70 (m, 2H, 3-H_2), 1.91 (tt, J=J'=7.2 Hz, 2H, 6-H_2), superimposed 1.86–1.98 (complex signal, 2H, 10'-H_{endo}, 13'-H_{syn}), 2.09 (dm, J=13.2 Hz, 1H, 13'-H_{anti}), 2.46 (t, J=7.2 Hz, 2H, 2-H_2), 2.56 (dm, J=17.6 Hz, 10'-H_{exo}), 2.77 (m, 1H, 7'-H), 2.87 (dm, J≈18.0 Hz, 1H, 6'-H_{endo}), 3.21 (dd, J=18.0 Hz, J'=5.6 Hz, 1H, 6'-H_{exo}), 3.46 (m, 1H, 11'-H), 3.99 (t, J≈7.2 Hz, 2H, 7-H_2), 4.85 (s, NH and $^+$NH), 5.59 (br d, J=4.4 Hz, 1H, 8'-H), 7.56 (dd, J=9.6 Hz, J'=2.0 Hz, 2'-H), 7.77 (d, J=2.0 Hz, 1H, 4'-H), 8.40 (d, J=9.6 Hz, 1H, 1'-H); ^{13}C NMR (100.6 MHz, CD_3OD) δ 17.2 (CH_2, C2), 23.4 (CH_3, 9'-CH_3), 26.3 (CH_2, C3), 27.0 (CH_2, C5), 27.3 (CH, C11'), 27.9 (CH, C7'), 29.3 (2CH_2, C4 and C13'), 31.0 (CH_2, C6), 36.0

(CH_2), 36.1 (CH_2), (C6', C10'), 49.6 (CH_2, C7), 115.7 (C, C12a'), 117.7 (C, C11a'), 119.2 (CH, C4'), 121.1 (C, CN), 125.1 (CH, C8'), 126.7 (CH, C2'), 129.5 (CH, C1'), 134.6 (C, C9'), 140.2 (C, C3'), 141.0 (C, C4a'), 151.3 (C, C5a'), 156.9 (C, C12'). HRMS (ESI) calcd for ($C_{24}H_{28}{}^{35}ClN_3 + H^+$) 394.2045, found 394.2049.

(±)-8-[(3-Chloro-6,7,10,11-tetrahydro-9-methyl-7,11-methanocycloocta[*b*]quinolin-12-yl)amino]octanenitrile [(±)-5d]. It was prepared as described for (±)-**5a**. From (±)-huprine Y·HCl, (±)-**4**·HCl (1.86 g, 5.81 mmol) and 8-bromooctanenitrile (1.39 g, 6.81 mmol), a yellow oil (2.30 g) was obtained and purified by column chromatography (40–60 μm silica gel, CH_2Cl_2/50% aq. NH_4OH 100:0.2), to afford (±)-**5d** (1.00 g, 42% yield) as a yellow solid; R_f 0.65 (CH_2Cl_2/MeOH/50% aq. NH_4OH 9:1:0.05).

(±)-5d·HCl: mp 130–131 °C (CH_2Cl_2/MeOH 81:19); IR (KBr) ν 3500–2500 (max at 3397, 3244, 3108, 3048, 3007, 2925, 2852, N-H, N^+-H and C-H st), 2242 (CN st), 1701, 1624, 1562 (ar-C-C and ar-C-N st) cm^{-1}; ^1H NMR (400 MHz, CD_3OD) δ 1.40–1.52 (complex signal, 6H, 4-H_2, 5-H_2 and 6-H_2), 1.58 (s, 3H, 9'-CH_3), 1.64 (tt, $J \approx J' \approx 7.6$ Hz, 2H, 3-H_2), superimposed in part 1.88 (tt, $J \approx J' \approx 7.2$ Hz, 2H, 7-H_2), superimposed in part 1.94 (br d, J=17.2 Hz, 1H, 10'-H_{endo}), superimposed 1.90–1.98 (m, 1H, 13'-H_{syn}), 2.08 (dm, J=12.4 Hz, 1H, 13'-H_{anti}), 2.44 (t, $J \approx 7.2$ Hz, 2H, 2-H_2), 2.56 (br dd, J=17.6 Hz, J'=4.4 Hz, 1H, 10'-H_{exo}), 2.77 (m, 1H, 7'-H), 2.89 (br d, J=18.0 Hz, 1H, 6'-H_{endo}), 3.21 (dd, J=18.0 Hz, J'=5.6 Hz, 1H, 6'-H_{exo}), 3.47 (m, 1H, 11'-H), 3.99 (t, J=7.2 Hz, 2H, 8-H_2), 4.85 (s, NH and $^+$NH), 5.58 (br d, J=5.2 Hz, 1H, 8'-H), 7.54 (dd, J=9.6 Hz, J'=1.6 Hz, 1H, 2'-H), 7.79 (d, J=1.6 Hz, 1H, 4'-H), 8.40 (d, J=9.6 Hz, 1H, 1'-H); ^{13}C NMR (100.6 MHz, CD_3OD) δ 17.3 (CH_2, C2), 23.5 (CH_3, 9'-CH_3), 26.3 (CH_2, C3), 27.2 (CH, C11'), 27.5 (CH_2, C6), 27.8 (CH, C7'), 29.3 (CH_2, C13'), 29.4 (CH_2), 29.6 (CH_2) (C4, C5), 31.1 (CH_2, C7), 36.0 (CH_2), 36.1 (CH_2) (C6', C10'), 49.6 (CH_2, C8), 115.6 (C,

C12a'), 117.6 (C, C11a'), 119.1 (CH, C4'), 121.2 (C, CN), 125.1 (CH, C8'), 126.6 (CH, C2'), 129.5 (CH, C1'), 134.5 (C, C9'), 140.1 (C, C3'), 140.9 (C, C4a'), 151.2 (C, C5a'), 156.9 (C, C12'); HRMS (ESI) calcd for ($C_{25}H_{30}{}^{35}ClN_3$ + H^+) 408.2201, found 408.2203.

(±)-9-[(3-Chloro-6,7,10,11-tetrahydro-9-methyl-7,11-methanocycloocta[*b*]quinolin-12-yl)amino]nonanenitrile [(±)-5e]. It was prepared as described for (±)-**5a**. From (±)-huprine Y·HCl, (±)-**4**·HCl (1.89 g, 5.91 mmol) and 9-bromononanenitrile (1.56 g, 7.16 mmol), a yellow oil (2.86 g) was obtained and purified by column chromatography (40–60 μm silica gel, CH_2Cl_2/50% aq. NH_4OH 100:0.2), to afford (±)-**5e** (1.65 g, 66% yield) as a yellow solid; R_f 0.56 (CH_2Cl_2/MeOH/50% aq. NH_4OH 9:1:0.05).

(±)-5e·HCl: mp 121–123 °C (CH_2Cl_2/MeOH 81:19); IR (KBr) ν 3500–2500 (max at 3228, 3108, 3048, 3001, 2926, 2854, 2745, N-H, N^+-H and C-H st), 2242 (CN st), 1718, 1630, 1582, 1569, 1501 (ar-C-C and ar-C-N st) cm^{-1}; ^1H NMR (400 MHz, CD_3OD) δ 1.32–1.50 (complex signal, 8H, 4-H_2, 5-H_2, 6-H_2 and 7-H_2), 1.59 (s, 3H, 9'-CH_3), superimposed in part 1.62 (tt, $J \approx J' \approx 7.2$ Hz, 2H, 3-H_2), superimposed in part 1.87 (tt, $J \approx J' \approx 7.2$ Hz, 2H, 8-H_2), superimposed in part 1.93 (br d, J=18.0 Hz, 1H, 10'-H_{endo}), superimposed 1.90–1.96 (m, 1H, 13'-H_{syn}), 2.08 (dm, J=12.4 Hz, 1H, 13'-H_{anti}), 2.43 (t, J=7.2 Hz, 2H, 2-H_2), 2.56 (dm, J=17.6 Hz, J'=4.8 Hz, 1H, 10'-H_{exo}), 2.77 (m, 1H, 7'-H), 2.88 (br d, J=17.6 Hz, 1H, 6'-H_{endo}), 3.21 (dd, $J \approx 17.6$ Hz, $J' \approx 5.6$ Hz, 1H, 6'-H_{exo}), 3.46 (m, 1H, 11'-H), 3.99 (t, J=7.2 Hz, 2H, 9-H_2), 4.85 (s, NH and $^+$NH), 5.59 (d, J=4.4 Hz, 1H, 8'-H), 7.55 (dd, J=9.6 Hz, J'=2.4 Hz, 1H, 2'-H), 7.78 (d, J=2.4 Hz, 1H, 4'-H), 8.40 (d, J=9.6 Hz, 1H, 1'-H); ^{13}C NMR (100.6 MHz, CD_3OD) δ 17.3 (CH_2, C2), 23.5 (CH_3, 9'-CH_3), 26.4 (CH_2, C3), 27.3 (CH, C11'), 27.7 (CH_2, C7), 27.8 (CH, C7'), 29.3 (CH_2, C13'), 29.6 (CH_2), 29.7 (CH_2), 30.0 (CH_2) (C4, C5, C6), 31.2 (CH_2, C8), 36.0

(CH_2), 36.1 (CH_2) (C6', C10'), 49.6 (CH_2, C9), 115.6 (C, C12a'), 117.6 (C, C11a'), 119.1 (CH, C4'), 121.2 (C, CN), 125.1 (CH, C8'), 126.6 (CH, C2'), 129.5 (CH, C1'), 134.5 (C, C9'), 140.2 (C, C3'), 141.0 (C, C4a'), 151.2 (C, C5a'), 156.9 (C, C12'); HRMS (ESI) calcd for ($C_{26}H_{32}{}^{35}ClN_3 + H^+$) 422.2358, found 422.2363.

(–)-9-[(3-Chloro-6,7,10,11-tetrahydro-9-methyl-7,11-methanocycloocta[*b*]quinolin-12-yl)amino]nonanenitrile [(–)-5e]. It was prepared as described for (±)-**5a**. From (–)-huprine Y, (–)-**4** (>99% ee, 1.50 g, 5.28 mmol) and 9-bromononanenitrile (1.39 g, 6.40 mmol), a yellow oil (2.20 g) was obtained and purified by column chromatography (40–60 μm silica gel, CH_2Cl_2/50% aq. NH_4OH 100:0.2), to afford (–)-**5e** (750 mg, 34% yield) as a yellow solid; R_f 0.56 (CH_2Cl_2/MeOH/50% aq. NH_4OH 9:1:0.05).

(–)-5e·HCl: $[\alpha]^{20}_D$ = –212 (*c*=0.10, MeOH); mp 106–107 °C (CH_2Cl_2/MeOH 89:11); IR (KBr) *v* 3500–2500 (max at 3341, 3136, 3064, 2928, 2858, 2671, N-H, N^+-H and C-H st), 2245 (CN st), 1605, 1573, 1525 (ar-C-C and ar-C-N st) cm^{-1}; the ^1H NMR and ^{13}C NMR spectra were identical to those of (±)-**5e**; HRMS (ESI) calcd for ($C_{26}H_{32}{}^{35}ClN_3 + H^+$) 422.2358, found 422.2362.

(+)-9-[(3-Chloro-6,7,10,11-tetrahydro-9-methyl-7,11-methanocycloocta[*b*]quinolin-12-yl)amino]nonanenitrile [(+)-5e]. It was prepared as described for (±)-**5a**. From (+)-huprine Y, (+)-**4** (>99% ee, 1.50 g, 5.28 mmol) and 9-bromononanenitrile (1.39 g, 6.40 mmol), a yellow oil (2.20 g) was obtained and purified by column chromatography (40–60 μm silica gel, CH_2Cl_2/50% aq. NH_4OH 100:0.2), to afford (+)-**5e** (929 mg, 42% yield) as a yellow solid; R_f 0.56 (CH_2Cl_2/MeOH/50% aq. NH_4OH 9:1:0.05).

(+)-5e·HCl: $[\alpha]^{20}_D$ = +213 (*c*=0.10, MeOH); mp 109–111 °C (CH_2Cl_2/MeOH 93:7); IR (KBr) *v* 3500–2500 (max at 3379, 3228, 3111, 3038, 3007, 2926, 2854, N-H, N^+-H

and C-H st), 2242 (CN st), 1627, 1620, 1576, 1558, 1542, 1522, 1511 (ar-C-C and ar-C-N st) cm^{-1}; the ^{1}H NMR and ^{13}C NMR spectra were identical to those of (±)-**5e**; HRMS (ESI) calcd for ($C_{26}H_{32}{}^{35}ClN_3 + H^+$) 422.2358, found 422.2356.

(±)-10-[(3-Chloro-6,7,10,11-tetrahydro-9-methyl-7,11-methanocycloocta[*b*]quinolin-12-yl)amino]decanenitrile [(±)-5f]. It was prepared as described for (±)-**5a**. From (±)-huprine Y, (±)-**4** (2.00 g, 7.04 mmol) and 10-bromodecanenitrile (87% purity, 2.15 g, 8.06 mmol), a yellow oil (2.84 g) was obtained and purified by column chromatography (40–60 μm silica gel, CH_2Cl_2/MeOH/50% aq. NH_4OH mixtures, gradient elution). On elution with CH_2Cl_2/50% aq. NH_4OH 100:0.2, (±)-**5f** (756 mg, 25% yield) was isolated as a yellow solid. On elution with CH_2Cl_2/MeOH/50% aq. NH_4OH 98:2:0.2, starting (±)-**4** (382 mg) was recovered; $R_{f[(\pm)\text{-}\mathbf{5f}]}$ 0.66 (CH_2Cl_2/MeOH/50% aq. NH_4OH 9:1:0.05).

(±)-5f·HCl: mp 129–130 °C (CH_2Cl_2/MeOH 89:11); IR (KBr) *v* 3500–2500 (max at 3229, 3105, 3047, 3007, 2926, 2853, 2740, 2640, N-H, N^+-H and C-H st), 2242 (CN st), 1630, 1582, 1549, 1511 (ar-C-C and ar-C-N st) cm^{-1}; ^{1}H NMR (400 MHz, CD_3OD) δ 1.35–1.45 (complex signal, 10H, 4-H_2, 5-H_2, 6-H_2, 7-H_2 and 8-H_2), 1.59 (s, 3H, 9'-CH_3), superimposed in part 1.61 (tt, $J \approx J' \approx 7.2$ Hz, 2H, 3-H_2), superimposed in part 1.87 (tt, $J \approx J' \approx 7.2$ Hz, 2H, 9-H_2), superimposed 1.85–1.96 (complex signal, 1H, 13'-H_{syn}), superimposed in part 1.94 (d, $J \approx 16.8$ Hz, 1H, 10'-H_{endo}), 2.09 (dm, $J = 12.8$ Hz, 1H, 13'-H_{anti}), 2.43 (t, $J \approx 7.0$ Hz, 2H, 2-H_2), 2.55 (dd, $J = 17.6$ Hz, $J' = 4.4$ Hz, 1H, 10'-H_{exo}), 2.77 (m, 1H, 7'-H), 2.88 (br d, $J = 17.6$ Hz, 1H, 6'-H_{endo}), 3.21 (dd, $J = 17.6$ Hz, $J' = 5.6$ Hz, 1H, 6'-H_{exo}), 3.46 (m, 1H, 11'-H), 3.98 (t, $J \approx 6.8$ Hz, 2H, 10-H_2), 4.85 (s, NH and $^+$NH), 5.59 (d, $J = 4.8$ Hz, 1H, 8'-H), 7.55 (dd, $J = 9.6$ Hz, $J' = 2.0$ Hz, 1H, 2'-H), 7.77 (d, $J = 2.0$ Hz, 1H, 4'-H), 8.40 (d, $J = 9.6$ Hz, 1H, 1'-H); ^{13}C NMR (100.6 MHz, CD_3OD) δ 17.3 (CH_2, C2), 23.5 (CH_3, 9'-CH_3), 26.4 (CH_2, C3), 27.3 (CH, C11'), 27.7 (CH_2, C8), 27.8 (CH,

C7'), 29.3 (CH_2, C13'), 29.6 (CH_2), 29.7 (CH_2), 30.1 (CH_2), 30.3 (CH_2) (C4, C5, C6, C7), 31.2 (CH_2, C9), 36.0 (CH_2), 36.1 (CH_2) (C6', C10'), 49.7 (CH_2, C10), 115.6 (C, C12a'), 117.6 (C, C11a'), 119.1 (CH, C4'), 121.2 (C, CN), 125.1 (CH, C8'), 126.6 (CH, C2'), 129.5 (CH, C1'), 134.5 (C, C9'), 140.2 (C, C3'), 141.0 (C, C4a'), 151.2 (C, C5a'), 156.9 (C, C12'); HRMS (ESI) calcd for ($C_{27}H_{34}{}^{35}ClN_3$ + H^+) 436.2514, found 436.2508.

(±)-11-[(3-Chloro-6,7,10,11-tetrahydro-9-methyl-7,11-methanocycloocta[*b*]quinolin-12-yl)amino]undecanenitrile [(±)-5g]. It was prepared as described for (±)-**5a**. From (±)-huprine Y, (±)-**4** (1.70 g, 5.99 mmol) and 11-bromoundecanenitrile (80% purity, 2.11 g, 6.86 mmol), a yellow oil (2.20 g) was obtained and purified by column chromatography (40–60 μm silica gel, CH_2Cl_2/50% aq. NH_4OH 100:0.2), to afford (±)-**5g** (1.09 g, 40% yield) as a yellow solid; R_f 0.62 (CH_2Cl_2/MeOH/50% aq. NH_4OH 9:1:0.05).

(±)-5g·HCl: mp 131–133 °C (CH_2Cl_2/MeOH 93:7); IR (KBr) ν 3500–2500 (max at 3395, 3231, 3111, 3048, 3012, 2925, 2853, 2742, 2645, N-H, N^+-H and C-H st), 2242 (CN st), 1628, 1582, 1559, 1542, 1521, 1507 (ar-C-C and ar-C-N st) cm^{-1}; ^1H NMR (400 MHz, CD_3OD) δ 1.27–1.44 (complex signal, 12H, 4-H_2, 5-H_2, 6-H_2, 7-H_2, 8-H_2 and 9-H_2), 1.59 (s, 3H, 9'-CH_3), superimposed in part 1.62 (tt, $J \approx J' \approx 7.2$ Hz, 2H, 3-H_2), superimposed in part 1.87 (tt, $J \approx J' \approx 7.2$ Hz, 2H, 10-H_2), superimposed 1.86–1.96 (complex signal, 1H, 13'-H_{syn}), superimposed in part 1.94 (d, $J \approx 17.2$ Hz, 1H, 10'-H_{endo}), 2.08 (dm, J=12.4 Hz, 1H, 13'-H_{anti}), 2.43 (t, $J \approx 7.0$ Hz, 2H, 2-H_2), 2.56 (dd, J=17.6 Hz, J'=4.4 Hz, 1H, 10'-H_{exo}), 2.77 (m, 1H, 7'-H), 2.88 (d, J=18.0 Hz, 1H, 6'-H_{endo}), 3.21 (dd, $J \approx 18.0$ Hz, J'=5.6 Hz, 1H, 6'-H_{exo}), 3.46 (m, 1H, 11'-H), 3.99 (t, $J \approx 6.6$ Hz, 2H, 11-H_2), 4.85 (s, NH and $^+$NH), 5.59 (br d, J=4.8 Hz, 1H, 8'-H), 7.54 (dd, J=9.6 Hz, J'=2.0 Hz, 1H, 2'-H), 7.79 (d, J=2.0 Hz, 1H, 4'-H), 8.40 (d, J=9.6 Hz, 1H, 1'-H); ^{13}C NMR

(100.6 MHz, CD_3OD) δ 17.3 (CH_2, C2), 23.5 (CH_3, 9'-CH_3), 26.4 (CH_2, C3), 27.3 (CH, C11'), 27.76 (CH_2, C9), 27.83 (CH, C7'), 29.3 (CH_2, C13'), 29.7 (CH_2), 29.8 (CH_2), 30.2 (CH_2), 30.3 (CH_2), 30.4 (CH_2) (C4, C5, C6, C7, C8), 31.2 (CH_2, C10), 36.0 (CH_2), 36.1 (CH_2) (C6', C10'), 49.6 (CH_2, C11), 115.6 (C, C12a'), 117.6 (C, C11a'), 119.1 (CH, C4'), 121.2 (C, CN), 125.1 (CH, C8'), 126.6 (CH, C2'), 129.5 (CH, C1'), 134.5 (C, C9'), 140.2 (C, C3'), 141.0 (C, C4a'), 151.2 (C, C5a'), 156.9 (C, C12'); HRMS (ESI) calcd for ($C_{28}H_{36}{}^{35}ClN_3 + H^+$) 450.2671, found 450.2664.

(±)-4-{[(3-Chloro-6,7,10,11-tetrahydro-9-methyl-7,11-methanocycloocta[*b*]quinolin-12-yl)amino]methyl}benzonitrile [(±)-5h].

1) Preparation of the imine (±)-4-{[(3-chloro-6,7,10,11-tetrahydro-9-methyl-7,11-methanocycloocta[*b*]quinolin-12-yl)imino]methyl}benzonitrile, (±)-9. A suspension of (±)-huprine Y, (±)-**4** (2.00 g, 7.04 mmol) and 4 Å molecular sieves in anhyd toluene (19 mL) was treated with freshly distilled morpholine (0.67 mL, 675 mg, 7.75 mmol) and *p*-cyanobenzaldehyde (1.80 g, 13.7 mmol). The reaction mixture was stirred under reflux for 48 h, concentrated under reduced pressure. The resulting solid residue was purified through column chromatography (40–60 μm silica gel, CH_2Cl_2), to afford (±)-**9** (2.20 g, 79% yield) as a yellow solid; R_f 0.17 (CH_2Cl_2).

A solution of (±)-**9** (100 mg, 0.25 mmol) in CH_2Cl_2 (6.6 mL) was filtered through a 0.2 μm PTFE filter and evaporated under reduced pressure. The resulting solid was washed with pentane (3×2 mL) to give, after drying at 65 ºC/2 Torr for 48 h, the analytical sample of (±)-**9** (94 mg) as a yellow solid: mp 208–210 °C (CH_2Cl_2); IR (KBr) ν 2225 (CN st), 1721, 1639, 1600, 1570, 1553, 1500, 1479, 1455 (ar-C-C and ar-C-N st) cm^{-1}; ^1H NMR (400 MHz, $CDCl_3$) δ 1.52 (s, 3H, 9'-CH_3), 1.85 (br d, J=17.2 Hz, 1H, 10'-H_{endo}), 1.95–1.97 (complex signal, 2H, 13'-H_{syn} and 13'-H_{anti}), 2.35 (dd, J=17.2 Hz, J'=4.6 Hz, 1H, 10'-H_{exo}), 2.78 (m, 1H, 7'-H), 3.12 (br d, J=18.0 Hz, 1H, 6'-

H_{endo}), 3.21 (dd, *J*≈18.0 Hz, *J'*=5.2 Hz, 1H, 6'-H_{exo}), 3.35 (m, 1H, 11'-H), 5.56 (br d, *J*=5.2 Hz, 1H, 8'-H), 7.31, (dd, *J*=9.2 Hz, *J'*=2.0 Hz, 1H, 2'-H), 7.47 (d, *J*=9.2 Hz, 1H, 1'-H), 7.86 [dt, *J*=8.0 Hz, *J'*=1.6 Hz, 2H, 2(6)-H], 8.00 (d, *J*=2.0 Hz, 2H, 4'-H), 8.12 [d, *J*≈8.0 Hz, 2H, 3(5)-H], 8.42 (s, 1H, C*H*N); ^{13}C NMR (100.6 MHz, $CDCl_3$) δ 23.4 (CH_3, 9'-CH_3), 28.1 (CH, C11'), 28.3 (CH, C7'), 28.6 (CH_2, C13'), 37.1 (CH_2, C10'), 40.0 (CH_2, C6'), 115.8 (C, C1), 117.8 (C, C12a'), 118.1 (C, CN), 122.9 (C, C11a'), 123.9 (CH, C1'), 125.3 (CH, C8'), 126.4 (CH, C2'), 127.3 (CH, C4'), 129.4 [CH, C3(5)], 132.3 (C, C9'), 132.8 [CH, C2(6)], 134.9 (C, C3'), 138.5 (C, C4), 147.2 (C, C4a'), 153.4 (C, C12'), 159.8 (C, C5a'), 162.1 (CH, CHN); HRMS (ESI) calcd for ($C_{25}H_{20}{}^{35}ClN_3 + H^+$) 398.1419, found 398.1426.

2) Reduction of imine (±)-9. A solution of (±)-**9** (2.30 g, 5.79 mmol) in glacial AcOH (40 mL) was treated with $NaBH_3CN$ (764 mg, 12.2 mmol) portionwise for 1 h. The reaction mixture was stirred at rt for 3 h, cooled to 0 ºC with an ice bath, treated with 10N NaOH until pH 14, and extracted with EtOAc (2×200 mL). The combined organic extracts were dried over anhyd Na_2SO_4 and concentrated under reduced pressure, to give (±)-**5h** (2.10 g, 91% yield) as a yellow solid; R_f 0.75 (CH_2Cl_2/MeOH/50% aq. NH_4OH 9:1:0.05).

A solution of (±)-**5h** (60 mg, 0.15 mmol) in CH_2Cl_2 (5 mL) was filtered through a 0.2 µm PTFE filter, treated with methanolic HCl (0.53N, 0.85 mL), and evaporated under reduced pressure. The resulting solid was washed with pentane (3×2 mL), to give, after drying at 65 ºC/2 Torr for 48 h, (±)-**5h**·HCl (62 mg) as a yellow solid: mp 217–218 °C (CH_2Cl_2/MeOH 85:15); IR (KBr) ν 3500–2500 (max at 3229, 3101, 3050, 2999, 2901, 2722, N-H, N^+-H and C-H st), 2226 (CN st), 1718, 1631, 1582, 1555, 1507 (ar-C-C and ar-C-N st) cm^{-1}; ^{1}H NMR (400 MHz, CD_3OD) δ 1.61 (s, 3H, 9'-CH_3), 1.98 (br d, *J*=17.6 Hz, 1H, 10-H_{endo}), superimposed 2.00 (m, 1H, 13'-H_{syn}), 2.10 (dm, *J*=12.4 Hz,

1H, 13'-H_{anti}), 2.57 (dd, *J*=18.0 Hz, *J'*=4.8 Hz, 1H, 10'-H_{exo}), 2.80 (m, 1H, 7'-H), 2.94 (br d, *J*=18.0 Hz, 1H, 6'-H_{endo}), 3.26 (dd, *J*=18.0 Hz, *J'*=5.4 Hz, 1H, 6'-H_{exo}), 3.53 (m, 1H, 11'-H), 4.85 (s, NH and $^{+}$NH), 5.28 (s, 2H, CH_2N), 5.61 (br d, *J*=4.8 Hz, 1H, 8'-H), 7.39, (dd, *J*=9.2 Hz, *J'*=2.0 Hz, 1H, 2'-H), 7.63 [d, *J*=8.8 Hz, 2H, 3(5)-H], 7.79 [complex signal, 3H, 4'-H, 2(6)-H], 8.10 (d, *J*=9.2 Hz, 1H, 1'-H); ^{13}C NMR (100.6 MHz, CD_3OD) δ 23.4 (CH_3, 9'-CH_3), 27.6 (CH, C11'), 27.8 (CH, C7'), 29.2 (CH_2, C13'), 36.2 (CH_2), 36.4 (CH_2) (C6', C10'), 112.8 (C, C1), 115.7 (C, CN), 118.7 (C, C12a'), 119.4 (CH + C, C4', C11a'), 125.1 (CH, C8'), 127.0 (CH, C2'), 128.7 [CH, C3(5)], 128.9 (CH, C1'), 134.0 [CH, C2(6)], 134.6 (C, C9'), 140.4 (C, C3'), 140.8 (C, C4a'), 144.6 (C, C4), 152.2 (C, C5a'), 157.4 (C, C12'); HRMS (ESI) calcd for ($C_{25}H_{22}{}^{35}ClN_3 + H^+$) 400.1575, found 400.1582.

(±)-*N*-(3-Chloro-6,7,10,11-tetrahydro-9-methyl-7,11-methanocycloocta[*b*]quinolin-12-yl)pentane-1,5-diamine [(±)-6a]. To a suspension of $LiAlH_4$ (0.17 g, 4.47 mmol) in anhyd Et_2O (63 mL), nitrile (±)-**5a** (0.76 g, 2.08 mmol) was added, and the reaction mixture was stirred at rt overnight. The resulting mixture was treated with wet Et_2O (200 mL) and evaporated under reduced pressure. The solid was suspended in CH_2Cl_2, filtered through Celite® and evaporated under reduced pressure, to give amine (±)-**6a** (750 mg, 98% yield) as a yellow oil; R_f 0.03 (CH_2Cl_2/MeOH/50% aq. NH_4OH 9:1:0.05).

A solution of (±)-**6a** (50 mg, 0.14 mmol) in CH_2Cl_2 (3.5 mL) was filtered through a 0.2 μm PTFE filter, treated with methanolic HCl (1.4N, 0.87 mL), and evaporated under reduced pressure. The resulting solid was washed with pentane (3×2 mL) to give, after drying at 65 ºC/2 Torr for 48 h, (±)-**6a**·2HCl (54 mg) as a yellow solid: mp 193–194 ºC (CH_2Cl_2/MeOH 80:20); IR (KBr) *v* 3500–2500 (max at 3396, 3253, 2925, 2856, N-H, N^+-H and C-H st), 1628, 1583, 1570, 1558 (ar-C-C and ar-C-N st) cm^{-1}; ^{1}H NMR (400

MHz, CD_3OD) δ 1.55 (tt, $J \approx J' \approx 7.6$ Hz, 2H, 3-H_2), 1.59 (s, 3H, 9'-CH_3), 1.76 (m, 2H, 4-H_2), 1.90–2.02 (complex signal, 4H, 10'-H_{endo}, 13'-H_{syn}, 2-H_2), 2.09 (dm, J=12.8 Hz, 1H, 13'-H_{anti}), 2.57 (ddm, J=17.6 Hz, J'=6.0 Hz, 1H, 10'-H_{exo}), 2.78 (m, 1H, 7'-H), 2.87 (br d, J=18.0 Hz, 1H, 6'-H_{endo}), 2.97 (t, J=7.6 Hz, 2H, 5-H_2), 3.21 (dd, J=18.0 Hz, J'=5.6 Hz, 1H, 6'-H_{exo}), 3.49 (m, 1H, 11'-H), 4.01 (t, $J \approx 7.6$ Hz, 2H, 1-H_2), 4.85 (s, NH and $^+$NH), 5.59 (br d, J=4.4 Hz, 1H, 8'-H), 7.57 (dd, J=9.2 Hz, J'=2.0 Hz, 1H, 2'-H), 7.78 (d, J=2.0 Hz, 1H, 4'-H), 8.41 (d, J=9.2 Hz, 1H, 1'-H); ^{13}C NMR (100.6 MHz, CD_3OD) δ 23.5 (CH_3, 9'-CH_3), 24.7 (CH_2, C3), 27.3 (CH, C11'), 27.9 (CH, C7'), 28.2 (CH_2, C4), 29.3 (CH_2, C13'), 30.8 (CH_2, C2), 36.0 (CH_2), 36.2 (CH_2) (C6', C10'), 40.5 (CH_2, C5), 49.4 (CH_2, C1), 115.7 (C, C12a'), 117.8 (C, C11a'), 119.2 (CH, C4'), 125.1 (CH, C8'), 126.8 (CH, C2'), 129.4 (CH, C1'), 134.6 (C, C9'), 140.3 (C, C3'), 141.0 (C, C4a'), 151.4 (C, C5a'), 156.9 (C, C12'); HRMS (ESI) calcd for ($C_{22}H_{28}{}^{35}ClN_3 + H^+$) 370.2045, found 370.2041.

(±)-*N*-(3-Chloro-6,7,10,11-tetrahydro-9-methyl-7,11-methanocycloocta[*b*]quinolin-12-yl)hexane-1,6-diamine [(±)-6b]. It was prepared as described for (±)-**6a**. From nitrile (±)-**5b** (1.26 g, 3.32 mmol), amine (±)-**6b** (1.23 g, 97% yield) was obtained as a yellow oil; R_f 0.02 (CH_2Cl_2/MeOH/50% aq. NH_4OH 9:1:0.05).

(±)-6b·2HCl: mp 180–181 ºC (CH_2Cl_2/MeOH 79:21); IR (KBr) ν 3500–2500 (max at 3403, 3240, 2926, 2852, N-H, N^+-H and C-H st), 1728, 1624, 1578 (ar-C-C and ar-C-N st) cm^{-1}; ^{1}H NMR (400 MHz, CD_3OD) δ 1.46–1.51 (complex signal, 4H, 3-H_2, 4-H_2), 1.59 (s, 3H, 9'-CH_3), 1.70 (tt, $J \approx J' \approx 7.4$ Hz, 2H, 5-H_2), 1.85–1.97 (complex signal, 4H, 2-H_2, 10'-H_{endo}, 13'-H_{syn}), 2.09 (dm, $J \approx 12.6$ Hz, 1H, 13'-H_{anti}), 2.56 (dd, J=17.6 Hz, J'=4.8 Hz, 1H, 10'-H_{exo}), 2.78 (m, 1H, 7'-H), 2.87 (dm, $J \approx 18.0$ Hz, 1H, 6'-H_{endo}), 2.94 (t, J=7.6 Hz, 2H, 6-H_2), 3.21 (dd, J=18.0 Hz, J'=5.6 Hz, 1H, 6'-H_{exo}), 3.47 (m, 1H, 11'-

H), 4.00 (t, *J*=7.6 Hz, 2H, 1-H_2), 4.85 (s, NH and $^{+}$NH), 5.59 (br d, *J*=4.4 Hz, 1H, 8'-H), 7.57 (dd, *J*=9.2 Hz, *J'*=2.4 Hz, 1H, 2'-H), 7.77 (d, *J*=2.4 Hz, 1H, 4'-H), 8.41 (d, *J*≈9.2 Hz, 1H, 1'-H); ^{13}C NMR (100.6 MHz, CD_3OD) δ 23.5 (CH_3, 9'-CH_3), 27.1 (CH_2, C3), 27.3 (CH, C11'), 27.4 (CH_2, C4), 27.9 (CH, C7'), 28.5 (CH_2, C5), 29.3 (CH_2, C13'), 31.1 (CH_2, C2), 36.08 (CH_2), 36.15 (CH_2) (C6', C10'), 40.6 (CH_2, C6), 49.5 (CH_2, C1), 115.7 (C, C12a'), 117.7 (C, C11a'), 119.2 (CH, C4'), 125.1 (CH, C8'), 126.7 (CH, C2'), 129.5 (CH, C1'), 134.6 (C, C9'), 140.2 (C, C3'), 141.0 (C, C4a'), 151.3 (C, C5a'), 156.9 (C, C12'); HRMS (ESI) calcd for ($C_{23}H_{30}{}^{35}ClN_3$ + H^+) 384.2201; found 384.2197.

(±)-*N*-(3-Chloro-6,7,10,11-tetrahydro-9-methyl-7,11-methanocycloocta[*b*]quinolin-12-yl)heptane-1,7diamine [(±)-6c]. It was prepared as described for (±)-**6a**. From nitrile (±)-**5c** (2.20 g, 5.60 mmol), amine (±)-**6c** (1.98 g, 89% yield) was obtained as a yellow oil; R_f 0.07 (CH_2Cl_2/MeOH/50% aq. NH_4OH 9:1:0.05).

(±)-6c·2HCl: mp 181–183 ºC (CH_2Cl_2/MeOH 75:25); IR (KBr) *v* 3500–2500 (max at 3233, 2927, 2877, 2849, 2782, N-H, N^+-H and C-H st), 1628, 1582, 1566, 1550, 1524, 1508, 1492, 1476 (ar-C-C and ar-C-N st) cm^{-1}; ^{1}H NMR (400 MHz, CD_3OD) δ 1.41–1.52 (complex signal, 6H, 3-H_2, 4-H_2, 5-H_2), 1.59 (s, 3H, 9'-CH_3), 1.68 (tt, *J*≈*J'*≈7.2 Hz, 2H, 6-H_2), 1.84–1.95 (complex signal, 4H, 10'-H_{endo}, 13'-H_{syn}, 2-H_2), 2.09 (dm, *J*=13.2 Hz, 1H, 13'-H_{anti}), 2.56 (dd, *J*=17.6 Hz, *J'*=4.8 Hz, 1H, 10'-H_{exo}), 2.77 (m, 1H, 7'-H), 2.87 (ddd, *J*=18.0 Hz, *J'*≈*J"*≈1.6 Hz, 1H, 6'-H_{endo}), superimposed in part 2.93 (t, *J*=7.6 Hz, 2H, 7-H_2), 3.21 (dd, *J*=18.0 Hz, *J'*=5.6 Hz, 1H, 6'-H_{exo}), 3.47 (m, 1H, 11'-H), 3.99 (t, *J*≈7.6 Hz, 2H, 1-H_2), 4.85 (s, NH and $^{+}$NH), 5.59 (br d, *J*=4.4 Hz, 1H, 8'-H), 7.56 (dd, *J*=9.6 Hz, *J'*=2.0 Hz, 1H, 2'-H), 7.78 (d, *J*=2.0 Hz, 1H, 4'-H), 8.41 (d, *J*=9.6 Hz, 1H, 1'-H); ^{13}C NMR (100.6 MHz, CD_3OD) δ 23.5 (CH_3, 9'-CH_3), 27.3 (CH,

C11'), 27.4 (CH_2, C5), 27.7 (CH_2, C4), 27.8 (CH, C7'), 28.5 (CH_2, C3), 29.3 (CH_2, C13'), 29.8 (CH_2, C2), 31.2 (CH_2, C6), 36.0 (CH_2), 36.1 (CH_2) (C6', C10'), 40.7 (CH_2, C7), 49.6 (CH_2, C1), 115.6 (C, C12a'), 117.6 (C, C11a'), 119.1 (CH, C4'), 125.1 (CH, C8'), 126.7 (CH, C2'), 129.5 (CH, C1'), 134.6 (C, C9'), 140.2 (C, C3'), 141.0 (C, C4a'), 151.3 (C, C5a'), 156.9 (C, C12'); HRMS (ESI) calcd for ($C_{24}H_{32}{}^{35}ClN_3$ + H^+) 398.2358, found 398.2357.

(±)-*N*-(3-Chloro-6,7,10,11-tetrahydro-9-methyl-7,11-methanocycloocta[*b*]quinolin-12-yl)octane-1,8-diamine [(±)-6d]. It was prepared as described for (±)-**6a**. From nitrile (±)-**5d** (1.09 g, 2.68 mmol), amine (±)-**6d** (1.14 g, quantitative) was obtained as a yellow oil; R_f 0.07 (CH_2Cl_2/MeOH/50% aq. NH_4OH 9:1:0.05).

(±)-6d·2HCl: mp 209–211 °C (CH_2Cl_2/MeOH 77:23); IR (KBr) *v* 3500–2500 (max at 3395, 3245, 2927, 2854, 2780, N-H, N^+-H and C-H st), 1628, 1583, 1524, 1508, 1501 (ar-C-C and ar-C-N st) cm^{-1}; ^1H NMR (400 MHz, CD_3OD) δ 1.40–1.48 (complex signal, 8H, 3-H_2, 4-H_2, 5-H_2, 6-H_2), 1.59 (s, 3H, 9'-CH_3), 1.66 (tt, $J \approx J' \approx 7.2$ Hz, 2H, 7-H_2), superimposed 1.84–1.95 (m, 1H, 13'-H_{syn}), superimposed in part 1.84–1.93 (tt, $J \approx J' \approx 7.2$ Hz, 2H, 2-H_2), superimposed in part 1.93 (br d, J=17.6 Hz, 1H, 10'-H_{endo}), 2.10 (dm, $J \approx 10.4$ Hz, 1H, 13'-H_{anti}), 2.56 (dd, J=17.6 Hz, J'=4.8 Hz, 1H, 10'-H_{exo}), 2.77 (m, 1H, 7'-H), superimposed in part 2.87 (ddd, $J \approx 17.6$ Hz, $J' \approx J'' \approx 1.6$ Hz, 1H, 6'-H_{endo}), 2.92 (tt, $J \approx J' \approx 7.6$ Hz, 2H, 8-H_2), 3.21 (dd, J=17.6 Hz, J'=5.6 Hz, 1H, 6'-H_{exo}), 3.46 (m, 1H, 11'-H), 3.99 (tt, $J \approx J' \approx 7.6$ Hz, 2H, 1-H_2), 4.85 (s, NH and $^+$NH), 5.59 (br d, J=4.8 Hz, 1H, 8'-H), 7.56 (dd, J=9.6 Hz, J'=2.0 Hz, 1H, 2'-H), 7.78 (d, J=2.0 Hz, 1H, 4'-H), 8.40 (d, $J \approx 9.6$ Hz, 1H, 1'-H); ^{13}C NMR (100.6 MHz, CD_3OD) δ 23.5 (CH_3, 9'-CH_3), 27.3 (CH, C11'), 27.4 (CH_2, C3), 27.8 (CH_2, C4), 27.9 (CH, C7'), 28.5 (CH_2, C5), 29.2 (CH_2, C13'), 30.1 ($2CH_2$, C6, C7), 31.3 (CH_2, C2), 36.0 (CH_2), 36.1 (CH_2) (C6', C10'),

40.7 (CH_2, C8), 49.7 (CH_2, C1), 115.6 (C, C12a'), 117.6 (C, C11a'), 119.1 (CH, C4'), 125.1 (CH, C8'), 126.7 (CH, C2'), 129.5 (CH, C1'), 134.5 (C, C9'), 140.2 (C, C3'), 141.0 (C, C4a'), 151.2 (C, C5a'), 156.9 (C, C12'); HRMS (ESI) calcd for ($C_{25}H_{34}{}^{35}ClN_3$ + H^+) 412.2514, found 412.2509.

(±)-*N*-(3-Chloro-6,7,10,11-tetrahydro-9-methyl-7,11-methanocycloocta[*b*]quinolin-12-yl)nonane-1,9-diamine [(±)-6e]. It was prepared as described for (±)-**6a**. From nitrile (±)-**5e** (1.60 g, 3.80 mmol), amine (±)-**6e** (1.39 g, 86% yield) was obtained as a yellow oil; R_f 0.10 (CH_2Cl_2/MeOH/50% aq. NH_4OH 9:1:0.05).

(±)-6e·2HCl: mp 169–171 °C (CH_2Cl_2/MeOH 81:19); IR (KBr) *v* 3500–2500 (max at 3397, 3245, 2925, 2853, 2795, N-H, N^+-H and C-H st), 1629, 1582, 1508 (ar-C-C and ar-C-N st) cm^{-1}; ^1H NMR (400 MHz, CD_3OD) δ 1.34–1.48 (complex signal, 10H, 3-H_2, 4-H_2, 5-H_2, 6-H_2, 7-H_2), 1.59 (s, 3H, 9'-CH_3), 1.66 (tt, $J \approx J' \approx 6.8$ Hz, 2H, 8-H_2), superimposed in part 1.87 (tt, $J \approx J' \approx 7.6$ Hz, 2H, 2-H_2), superimposed 1.83–1.96 (m, 1H, 13'-H_{syn}), superimposed in part 1.93 (br d, $J \approx 18.0$ Hz, 1H, 10'-H_{endo}), 2.09 (dm, J=14.8 Hz, 1H, 13'-H_{anti}), 2.56 (dd, J=18.0 Hz, J'=4.8 Hz, 1H, 10'-H_{exo}), 2.77 (m, 1H, 7'-H), superimposed in part 2.87 (ddd, J=17.6 Hz, $J' \approx J'' \approx 1.6$ Hz, 1H, 6'-H_{endo}), 2.91 (br t, J=7.2 Hz, 2H, 9-H_2), 3.21 (dd, J=17.6 Hz, J'=5.6 Hz, 1H, 6'-H_{exo}), 3.46 (m, 1H, 11'-H), 3.98 (tt, $J \approx J' \approx 7.2$ Hz, 2H, 1-H_2), 4.85 (s, NH and $^+$NH), 5.59 (br d, J=4.8 Hz, 1H, 8'-H), 7.56 (dd, J=9.6 Hz, J'=2.0 Hz, 1H, 2'-H), 7.78 (d, J=2.0 Hz, 1H, 4'-H), 8.40 (d, J=9.6 Hz, 1H, 1'-H); ^{13}C NMR (100.6 MHz, CD_3OD) δ 23.5 (CH_3, 9'-CH_3), 27.3 (CH, C11'), 27.5 (CH_2, C3), 27.8 (CH + CH_2, C7', C4), 28.6 (CH_2, C5), 29.3 (CH_2, C13'), 30.1 (CH_2), 30.2 (CH_2), 30.4 (CH_2) (C6, C7, C8), 31.3 (CH_2, C2), 36.0 (CH_2), 36.1 (CH_2) (C6', C10'), 40.8 (CH_2, C9), 49.7 (CH_2, C1), 115.6 (C, C12a'), 117.6 (C, C11a'), 119.1 (CH, C4'), 125.1 (CH, C8'), 126.6 (CH, C2'), 129.5 (CH, C1'), 134.5 (C, C9'), 140.2

(C, C3'), 141.0 (C, C4a'), 151.2 (C, C5a'), 156.9 (C, C12'); HRMS (ESI) calcd for ($C_{26}H_{36}{}^{35}ClN_3 + H^+$) 426.2671, found 426.2664.

(–)-*N*-(3-Chloro-6,7,10,11-tetrahydro-9-methyl-7,11-methanocycloocta[*b*]quinolin-12-yl)nonane-1,9-diamine [(–)-6e]. It was prepared as described for (±)-**6a**. From nitrile (–)-**5e** (664 mg, 1.58 mmol), amine (–)-**6e** (652 mg, 97% yield) was obtained as a yellow oil; R_f 0.10 (CH_2Cl_2/MeOH/50% aq. NH_4OH 9:1:0.05).

(–)-6e·2HCl: $[\alpha]^{20}_D$=–170 (*c*=0.10, MeOH); mp 126–128 °C (CH_2Cl_2/MeOH 81:19); IR (KBr) *v* 3500–2500 (max at 3251, 2923, 2853, N-H, N^+-H and C-H st), 1629, 1582, 1512, 1501 (ar-C-C and ar-C-N st) cm^{-1}; the ^1H NMR and ^{13}C NMR spectra were identical to those of (±)-**6e**; HRMS (ESI) calcd for ($C_{26}H_{36}{}^{35}ClN_3 + H^+$) 426.2671, found 426.2656.

(+)-*N*-(3-Chloro-6,7,10,11-tetrahydro-9-methyl-7,11-methanocycloocta[*b*]quinolin-12-yl)nonane-1,9-diamine [(+)-6e]. It was prepared as described for (±)-**6a**. From nitrile (+)-**5e** (499 mg, 1.18 mmol), amine (+)-**6e** (429 mg, 86% yield) was obtained as a yellow oil; R_f 0.10 (CH_2Cl_2/MeOH/50% aq. NH_4OH 9:1:0.05).

(+)-6e·2HCl: $[\alpha]^{20}_D$=+186 (*c*=0.10, MeOH); mp 127–128 °C (CH_2Cl_2/MeOH 65:35); IR (KBr) *v* 3500–2500 (max at 3250, 2922, 2853, N-H, N^+-H and C-H st), 1629, 1582, 1512 (ar-C-C and ar-C-N st) cm^{-1}; the ^1H NMR and ^{13}C NMR spectra were identical to those of (±)-**6e**; HRMS (ESI) calcd for ($C_{26}H_{36}{}^{35}ClN_3 + H^+$) 426.2671, found 426.2668.

(±)-*N*-(3-Chloro-6,7,10,11-tetrahydro-9-methyl-7,11-methanocycloocta[*b*]quinolin-12-yl)decane-1,10-diamine [(±)-6f]. It was prepared as described for (±)-**6a**. From nitrile (±)-**5f** (645 mg, 1.48 mmol), amine (±)-**6f** (581 mg,

90% yield) was obtained as a yellow oil; R_f 0.06 (CH_2Cl_2/MeOH/50% aq. NH_4OH 9:1:0.05).

(±)-6f·2HCl: mp 179–180 °C (CH_2Cl_2/MeOH 82:18); IR (KBr) *v* 3500–2500 (max at 3382, 3235, 2997, 2926, 2853, 2790, N-H, N^+-H and C-H st), 1630, 1582, 1512 (ar-C-C and ar-C-N st) cm^{-1}; ^1H NMR (400 MHz, CD_3OD) δ 1.30–1.46 (complex signal, 12H, 3-H_2, 4-H_2, 5-H_2, 6-H_2, 7-H_2, 8-H_2), 1.58 (s, 3H, 9'-CH_3), 1.66 (tt, $J \approx J' \approx 7.2$ Hz, 2H, 9-H_2), superimposed in part 1.87 (tt, $J \approx J' \approx 7.6$ Hz, 2H, 2-H_2), superimposed 1.83–1.96 (m, 1H, 13'-H_{syn}), superimposed in part 1.94 (br d, $J \approx 17.6$ Hz, 1H, 10'-H_{endo}), 2.08 (dm, $J \approx 12.4$ Hz, 1H, 13'-H_{anti}), 2.56 (dd, $J = 17.6$ Hz, $J' = 4.4$ Hz, 1H, 10'-H_{exo}), 2.77 (m, 1H, 7'-H), superimposed in part 2.88 (d, $J = 18.0$ Hz, 6'-H_{endo}), superimposed in part 2.91 (tt, $J \approx J' \approx 7.8$ Hz, 2H, 10-H_2), 3.21 (dd, $J = 18.0$ Hz, $J' = 5.6$ Hz, 1H, 6'-H_{exo}), 3.47 (m, 1H, 11'-H), 3.99 (tt, $J \approx J' \approx 7.2$ Hz, 2H, 1-H_2), 4.85 (s, NH and $^+$NH), 5.59 (br d, $J = 4.8$ Hz, 1H, 8'-H), 7.55 (dd, $J = 9.6$ Hz, $J' \approx 2.0$ Hz, 1H, 2'-H), 7.80 (d, $J = 2.0$ Hz, 1H, 4'-H), 8.40 (d, $J = 9.6$ Hz, 1H, 1'-H); ^{13}C NMR (100.6 MHz, CD_3OD) δ 23.5 (CH_3, 9'-CH_3), 27.3 (CH, C11'), 27.5 (CH_2, C3), 27.8 (CH + CH_2, C7', C4), 28.6 (CH_2, C5), 29.3 (CH_2, C13'), 30.2 (CH_2), 30.3 (CH_2), 30.4 (CH_2), 30.5 (CH_2) (C6, C7, C8, C9), 31.3 (CH_2, C2), 36.0 (CH_2), 36.1 (CH_2) (C6', C10'), 40.8 (CH_2, C10), 49.7 (CH_2, C1), 115.6 (C, C12a'), 117.6 (C, C11a'), 119.1 (CH, C4'), 125.1 (CH, C8'), 126.6 (CH, C2'), 129.5 (CH, C1'), 134.5 (C, C9'), 140.2 (C, C3'), 141.0 (C, C4a'), 151.2 (C, C5a'), 156.9 (C, C12'); HRMS (ESI) calcd for ($C_{27}H_{38}{}^{35}ClN_3 + H^+$) 440.2827, found 440.2820.

(±)-*N*-(3-Chloro-6,7,10,11-tetrahydro-9-methyl-7,11-methanocycloocta[*b*]quinolin-12-yl)undecane-1,11-diamine [(±)-6g]. It was prepared as described for (±)-**6a**. From nitrile (±)-**5g** (1.05 g, 2.33 mmol), amine (±)-**6g** (849 mg, 81% yield) was obtained as a yellow oil; R_f 0.05 (CH_2Cl_2/MeOH/50% aq. NH_4OH 9:1:0.05).

(±)-6g·2HCl: mp 164–165 °C (CH_2Cl_2/MeOH 79:21); IR (KBr) *v* 3500–2500 (max at 3385, 3232, 3043, 2924, 2852, 2790, 2651, N-H, N^+-H and C-H st), 1630, 1582, 1512 (ar-C-C and ar-C-N st) cm^{-1}; ^1H NMR (400 MHz, CD_3OD) δ 1.26–1.44 (complex signal, 14H, 3-H_2, 4-H_2, 5-H_2, 6-H_2, 7-H_2, 8-H_2, 9-H_2), 1.58 (s, 3H, 9'-CH_3), 1.67 (tt, $J \approx J' \approx 6.8$ Hz, 2H, 10-H_2), superimposed in part 1.87 (tt, $J \approx J' \approx 7.2$ Hz, 2H, 2-H_2), superimposed 1.81–1.93 (m, 1H, 13'-H_{syn}), superimposed in part 1.94 (br d, J=17.2 Hz, 1H, 10'-H_{endo}), 2.08 (dm, J = 12.4 Hz, 1H, 13'-H_{anti}), 2.56 (dd, J=17.2 Hz, J'=4.4 Hz, 1H, 10'-H_{exo}), 2.77 (m, 1H, 7'-H), superimposed in part 2.91 (d, J=17.6, Hz, 6'-H_{endo}), superimposed in part 2.93 (tt, $J \approx J' \approx 7.6$ Hz, 2H, 11-H_2), 3.21 (dd, J=17.6 Hz, J'=5.6 Hz, 1H, 6'-H_{exo}), 3.49 (m, 1H, 11'-H), 3.99 (tt, $J \approx J' \approx 7.2$ Hz, 2H, 1-H_2), 4.85 (s, NH and $^+$NH), 5.58 (br d, J=5.2 Hz, 1H, 8'-H), 7.53 (dd, $J \approx 9.6$ Hz, J'=2.0 Hz, 1H, 2'-H), 7.82 (d, J=2.0 Hz, 1H, 4'-H), 8.40 (d, J=9.6 Hz, 1H, 1'-H); ^{13}C NMR (100.6 MHz, CD_3OD) δ 23.5 (CH_3, 9'-CH_3), 27.3 (CH, C11'), 27.5 (CH_2, C3), 27.8 (CH + CH_2, C7', C4), 28.5 (CH_2, C5), 29.3 (CH_2, C13'), 30.2 (CH_2), 30.3 (CH_2), 30.47 (CH_2), 30.51 (CH_2), 30.6 (CH_2) (C6, C7, C8, C9, C10), 31.2 (CH_2, C2), 36.0 (CH_2), 36.1 (CH_2) (C6', C10'), 40.8 (CH_2, C11), 49.6 (CH_2, C1), 115.6 (C, C12a'), 117.6 (C, C11a'), 119.1 (CH, C4'), 125.1 (CH, C8'), 126.6 (CH, C2'), 129.5 (CH, C1'), 134.5 (C, C9'), 140.1 (C, C3'), 140.9 (C, C4a'), 151.2 (C, C5a'), 156.9 (C, C12'); HRMS (ESI) calcd for ($C_{28}H_{40}{}^{35}ClN_3$ + H^+) 454.2984; found 454.2969.

(±)-4-{[(3-Chloro-6,7,10,11-tetrahydro-9-methyl-7,11-methanocycloocta[*b*]quinolin-12-yl)amino]methyl}benzylamine [(±)-6h]. It was prepared as described for (±)-**6a**. From nitrile (±)-**5h** (370 mg, 0.93 mmol), amine (±)-**6h** (352 mg, 94% yield) was obtained as a yellow oil; R_f 0.11 (CH_2Cl_2/MeOH/50% aq. NH_4OH 9:1:0.05).

(±)-6h·2HCl: mp 151–152 °C (CH_2Cl_2/MeOH 75:25); IR (KBr) *v* 3500–2500 (max at 3390, 3245, 3043, 3002, 2899, 2795, 2609, N-H, N^+-H and C-H st), 1715, 1700, 1631, 1583, 1517 (ar-C-C and ar-C-N st) cm^{-1}; ^1H NMR (400 MHz, CD_3OD) δ 1.61 (s, 3H, 9'-CH_3), superimposed in part 2.00 (br d, *J*=18.4 Hz, 1H, 10'-H_{endo}), superimposed 1.96–2.00 (m, 1H, 13'-H_{syn}), 2.10 (dm, *J*=12.4 Hz, 1H, 13'-H_{anti}), 2.57 (dd, *J*≈18.4 Hz, *J'*≈4.8 Hz, 1H, 10'-H_{exo}), 2.80 (m, 1H, 7'-H), 2.82 (dm, *J*=18.0 Hz, 1H, 6'-H_{endo}), 3.25 (dd, *J*=18.0 Hz, *J'*=5.8 Hz, 1H, 6'-H_{exo}), 3.54 (m, 1H, 11'-H), 4.14 (s, 2H, CH_2NH_2), 4.85 (s, NH and $^+$NH), 5.25 (s, 2H, CH_2NH), 5.61 (br d, *J*=4.8 Hz, 1H, 8'-H), 7.34 (dd, *J*=9.2 Hz, *J'*=2.4 Hz, 1H, 2'-H), 7.50–7.57 [complex signal, 4H, 2(6)-H_2 and 3(5)-H_2), 7.78 (d, *J*=2.4 Hz, 1H, 4'-H), 8.21 (d, *J*=9.2 Hz, 1H, 1'-H); ^{13}C NMR (100.6 MHz, CD_3OD) δ 23.5 (CH_3, 9'-CH_3), 27.6 (CH, C11'), 27.9 (CH, C7'), 29.3 (CH_2, C13'), 36.1 (CH_2), 36.3 (CH_2) (C6', C10'), 43.9 (CH_2, CH_2NH), 51.7 (CH_2, CH_2NH_2), 115.6 (C, C12a'), 118.4 (C, C11a'), 119.3 (CH, C4'), 125.1 (CH, C8'), 126.7 (CH, C2'), 128.5 [CH, C2(6)], 129.3 (CH, C1'), 130.9 [CH, C3(5)], 134.2 (C), 134.6 (C), 140.0 (C) (C1, C4, C9'), 140.3 (C, C3'), 140.9 (C, C4a'), 151.9 (C, C5a'), 157.3 (C, C12'); HRMS (ESI) calcd for ($C_{25}H_{26}{}^{35}ClN_3 + H^+$) 403.1575, found 403.1578.

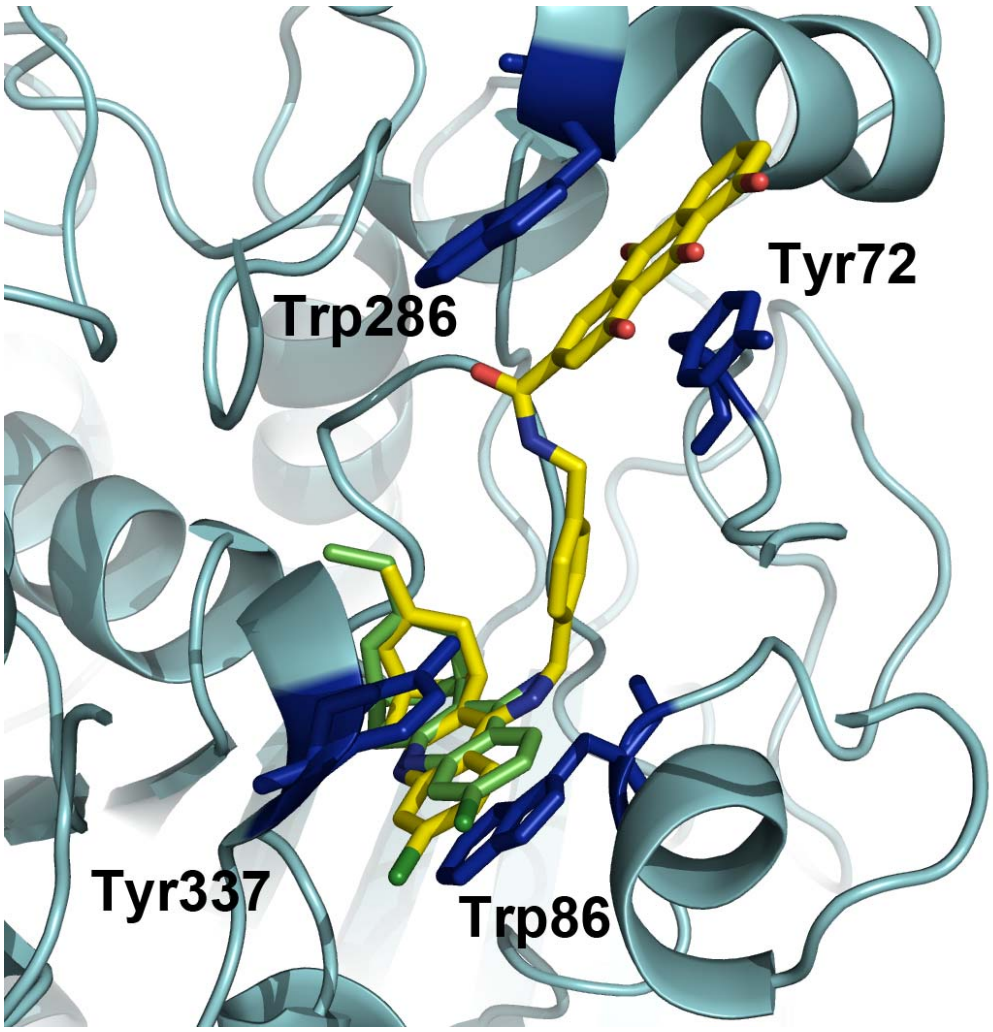

Figure S1. Superposition of hybrid (–)-**7h** (bound to human AChE; shown as yellow sticks) and huprine X (bound to *Torpedo californica* AChE; shown as green sticks).

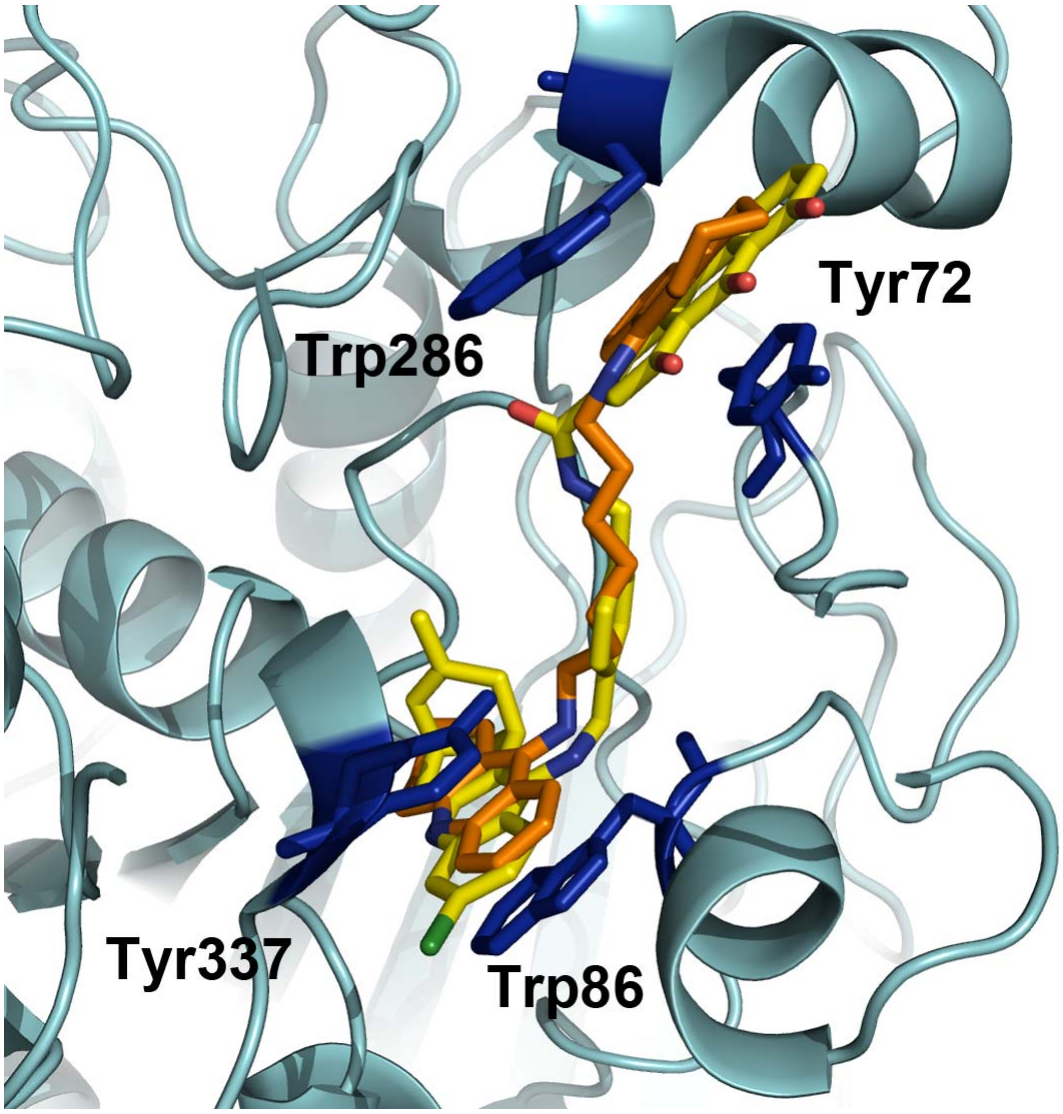

Figure S2. Superposition of hybrid (–)-**7h** (bound to human AChE; shown as yellow sticks) and *bis*(7)-tacrine (bound to *Torpedo californica* AChE; shown as orange sticks).

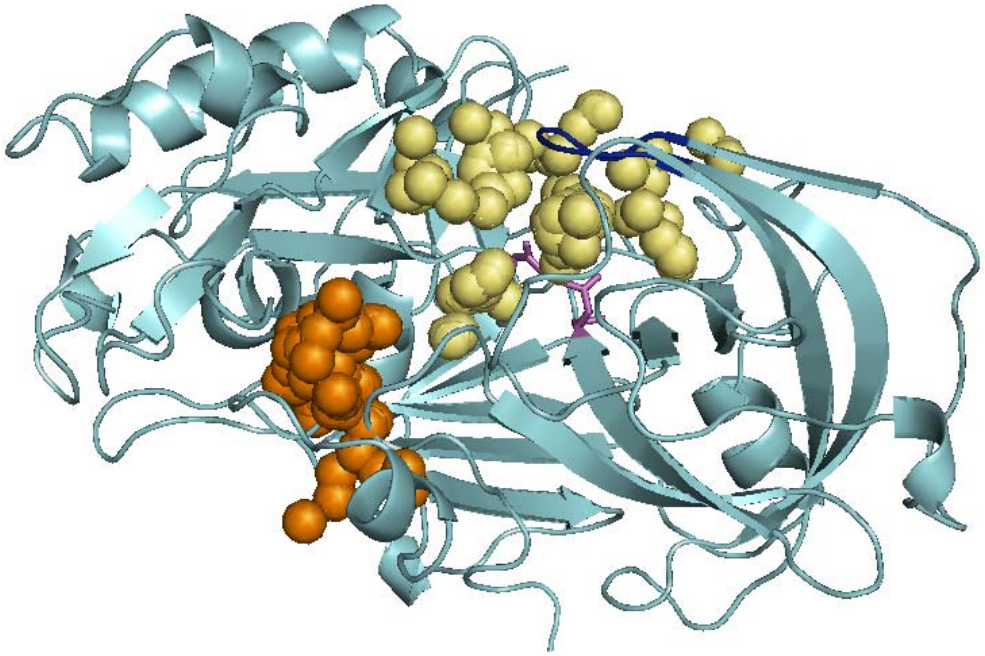

Figure S3. Representation of the two druggable sites in BACE-1 (shown as cyan cartoon) obtained from the analysis of MDpocket suitable to accommodate the huprine and hydroxyanthraquinone moieties present in the hybrids. The first binding site (BS1; yellow spheres) encompasses the catalytic site, including Asp32 and Asp228 (shown as magenta sticks) and is shaped by the β-hairpin loop commonly known as the "flap" (shown in blue). The second binding site (BS2; orange spheres) encompasses the exosites P5–P7 reported by Turner et al.[1]

BBB Permeation Assay.

Table S1. Literature and Experimental Permeability (*Pe* 10^{-6} cm s^{-1}) Values in the PAMPA-BBB Assay of 14 Commercial Drugs Used for Assay Validation.

Compound	**Bibliography value**[a]	**Experimental value (n=3) ± S.D.**
Verapamil	16	23.4 ± 3.21
Testosterone	17	22.6 ± 2.10
Costicosterone	5.1	8.02 ± 0.90
Clonidine	5.3	7.7 ± 0.5
Ofloxacin	0.8	0.08 ± 0.01
Lomefloxacin	1.1	0.70 ± 0.08
Progesterone	9.3	16.8 ± 0.03
Promazine	8.8	13.8 ± 0.4
Imipramine	13	12.3 ± 0.1
Hydrocortisone	1.9	1.52 ± 0.21
Piroxicam	2.5	1.92 ± 0.29
Desipramine	12	17.8 ± 0.1
Cimetidine	0.0	0.7 ± 0.03
Norfloxacin	0.1	0.9 ± 0.02

[a] From ref. 2.

References

1. Turner, R. T., III; Hong, L.; Koelsch, G.; Ghosh, A. K.; Tang, J. Structural locations and functional roles of new subsites S5, S6, and S7 in memapsin 2 (β-secretase). *Biochemistry* **2005**, *44*, 105–112.

2. Di, L.; Kerns, E. H.; Fan, K.; McConnell, O. J.; Carter, G. T. High throughput artificial membrane permeability assay for blood-brain barrier. *Eur. J. Med. Chem.* **2003**, *38*, 223–232.

Appendix (elemental analysis data)

Compound	**Molecular Formula**	**Calculated**				**Found**			
		C	H	N	Cl	C	H	N	Cl
(±)-**7a**·HCl·1.5H_2O	$C_{37}H_{34}ClN_3O_5$·HCl·1.5H_2O	63.52	5.47	6.01	10.13	63.39	5.72	5.64	10.91
(±)-**7b**·HCl·1.25H_2O	$C_{38}H_{36}ClN_3O_5$·HCl·1.25H_2O	64.36	5.61	5.93	10.00	64.52	5.55	5.83	10.50
(±)-**7c**·HCl·0.5H_2O	$C_{39}H_{38}ClN_3O_5$·HCl·0.5H_2O	66.01	5.68	5.92	9.99	66.26	5.64	5.90	9.63
(±)-**7d**·HCl·H_2O	$C_{40}H_{40}ClN_3O_5$·HCl·H_2O	65.57	5.92	5.73	9.68	65.52	5.86	5.83	9.35
(±)-**7e**·1.3HCl·1.25H_2O	$C_{41}H_{42}ClN_3O_5$·1.3HCl·1.25H_2O	64.61	6.06	5.51	10.70	64.51	6.00	6.10	10.97
(–)-**7e**·HCl·H_2O	$C_{41}H_{42}ClN_3O_5$·HCl·H_2O	65.95	6.07	5.63	9.50	65.50	6.07	5.20	9.91
(+)-**7e**·1.25HCl·0.75H_2O	$C_{41}H_{42}ClN_3O_5$·1.25HCl·0.75H_2O	65.54	6.00	5.59	10.62	65.79	6.28	5.80	10.89
(±)-**7f**·HCl·0.5H_2O	$C_{42}H_{44}ClN_3O_5$·HCl·0.5H_2O	67.11	6.17	5.59	9.43	66.76	6.26	5.27	9.91
(±)-**7g**·HCl·0.5H_2O	$C_{43}H_{46}ClN_3O_5$·HCl·0.5H_2O	67.44	6.32	5.49	9.26	67.52	6.46	5.30	9.51
(±)-**7h**·1.1HCl·1.4H_2O	$C_{40}H_{32}ClN_3O_5$·1.1HCl·1.4H_2O	65.32	4.92	5.71	10.12	65.32	5.06	6.09	10.15

5. B.

Curr. Alzheimer Res. **2016**, *13*, 1017

Rhein-huprine derivatives reduce cognitive impairment, synaptic failure and amyloid pathology in AβPPswe/PS-1 mice of different ages.

**Felipe G. Serrano[1], Cheril Tapia-Rojas[1], Francisco J. Carvajal[2], Pedro Cisternas[1], Elisabet Viayna[3,4], Irene Sola[3,4], Diego Muñoz-Torrero[3,4] and Nibaldo C. Inestrosa[1,2,5,6]*

[1]Centro de Envejecimiento y Regeneración (CARE)
[2]Departamento de Biología Celular y Molecular
Facultad de CienciasBiológicas,
Pontificia Universidad Católica de Chile,
Santiago,
[3]Laboratori de Química Farmacèutica (Unitat Associada al CSIC),
Facultat de Farmàcia,
Universitat de Barcelona,
Spain
[4]Institut de Biomedicina (IBUB),
Universitat de Barcelona,
Spain
[5]Center of Healthy Brain Aging, School of Psychiatry,
Faculty of Medicine,
University of New South Wales,
Sydney, Australia
[6]Centro de Excelencia en Biomedicina de Magallanes (CEBIMA),
Universidad de Magallanes,
Punta Arenas,
Chile

Running title: Novel family of rhein derivatives recovers memory and LTP

To whom correspondence should be addressed: Dr. Nibaldo C. Inestrosa

CARE Biomedical Center, P. Catholic University of Chile, Postal code 8331150, PO Box 114-D, Santiago, Chile. Tel.: +56 2 6862722; Fax: +56 2 6862959; E-mail: ninestrosa@bio.puc.cl.

Abstract

Alzheimer's disease (AD) is a neurodegenerative disorder in which the amyloid-β (Aβ) peptide plays a key role in synaptic impairment and memory decline associated with neuronal dysfunction and intra-neuronal accumulation of hyperphosphorylated *tau* protein. Two novel enantiopure rhein-huprine hybrids ((+)-1 and (–)-1) exhibit potent inhibitory effects against human acetylcholinesterase (AChE), butyrylcholinesterase (BuChE), BACE-1 and both Aβ and *tau* antiaggregation activity *in vitro* and reduction on the amyloid precursor protein (APP) processing *in vivo*. Interestingly, in this work, we observed beneficial effects with both (+)- and (–)-1 in the reversion of the neuropathology presented in the AβPPswe/PS-1 Alzheimer´s model, including a reduction in the Aβ levels, *tau* phosphorylation and memory impairment with both treatments. Also, in young transgenic mice that present early symptoms of synaptic failure and memory loss, we found a protection of cognitive functions, including long-term potentiation (LTP) and a reduction of the neuro-inflammation by both (+)- and (–)-1. Furthermore, animals with an advanced disease (11month-old) present an exacerbate neurodegeneration that is reversed only with the dextrorotatory enantiomer. These studies indicated that rhein-huprine derivatives with multiple properties might have interesting therapeutic potential for AD.

Keywords: Rhein-huprine hybrids, LTP, AD animals model, memory, amyloid β peptide, *tau.*

Introduction

Alzheimer's disease (AD) is the most common type of dementia, which is associated with extracellular deposition of the amyloid-β peptide (Aβ) and intra-neuronal accumulation of hyperphosphorylated *tau* protein [1; 2]. The increase in the deposition of Aβ aggregates depend of the levels and processing of the amyoid precursor protein (APP) by enzymes such as β-secretase (BACE-1) and γ-secretase [3]. Additionally, the aggregation of Aβ into oligomers and fibrils in the brain could be modified by different factors, which contribute to the acceleration of the formation of toxic aggregates facilitating the appearance of the disease. One of these enzymes is acetylcholinesterase (AChE), which participates in the structure and function of cholinergic synapses regulating the hydrolysis of the neurotransmitter acetylcholine in both the central and peripheral nervous system [4; 5]. AChE participates in a non-cholinergic mechanism related to AD by an acceleration in the aggregation of the Aβ assembly into Alzheimer-type aggregates *in vitro* [6-9], increasing its neurotoxicity and contributing to events associated to synaptic dysfunction, *tau* phosphorylation and aggregation, neuro-inflammation and oxidative stress, which eventually triggers neuronal cell death and cognitive deficit [10-12]. Several AChE inhibitors such as tacrine, donepezil, rivastigmine, and galantamine plus the NMDA antagonist memantine were developed to hit neurotransmitter deficits, particularly cholinergic and glutamatergic transmission, however, their results are regarded as merely symptomatic [13]. Butyrylcholinesterase (BChE) shares many structural and physicochemical properties with acetylcholinesterase and in normal cerebral cortex contains low amounts of BChE, most of which is located in deep cortical neurons and neuroglia, but at present, the biological function of BChE is unclear [14]. Otherwise, the *in*

vitro action of BChE is related to an inverse effect compared with AChE that is consistent with an arrest on fibril amyloid formation [15]. However, it is not clear whether butyrylcholinesterase would also affect Aβ oligomers formation.

Disappointingly, a number of drug candidates that were developed to address the underlying mechanisms of AD, especially by hitting a single target associated with Aβ biology, have recently failed to show efficacy over placebo in advanced clinical trials. The lack of efficacy of these drug candidates has been ascribed, at least in part, to the fact that AD pathology cannot be reversed if the effort is concentrated only in one biological target. Within this context, the use of multi-target drugs might provide new opportunities to help in the reduction of the neurodegenerative changes observed in AD [16].

We have recently developed a new family of rhein-huprine derivatives, which were rationally designed to simultaneously hit several important targets within the AD pathological network, namely Aβ and tau aggregation and AChE [17]. In this context, we previously found that rhein-huprine derivatives induce a reduction in the Aβ levels in a transgenic AD animal model accompanied by an increase in the levels of mature amyloid precursor protein (APP), which efficiently protect against the Aβ-induced synaptic dysfunction. Additionally, in an *in vitro* model of hippocampal slices, the co-incubation of rhein-huprine derivatives with Aβ-oligomers protects the induction of long-term potentiation (LTP) consistent with a recovery of synaptic proteins [17].

Indeed, biological profiling performed *in vitro* and in intact *Escherichia coli* cells have shown that these compounds, and particularly the two selected leads, the enantiomers (–)-(7*S*,11*S*)- and (+)-(7*R*,11*R*)-1 (Figure 1), exhibit a very promising multi-target profile, which encompasses a high inhibitory potency against human AChE and BChE, a dual Aβ

and tau anti-aggregating activity, and very interestingly a potent inhibitory activity against BACE-1. Moreover, using an artificial membrane model assay (PAMPA-BBB) these compounds have been predicted to be able to cross the blood–brain barrier, and, therefore, to reach their multiple targets in central nervous system. A first evidence of a disease-modifying effect of compounds (–)- and (+)-1, resulting from their multi-target profile, has been obtained in some *ex vivo* experiments, where these compounds exerted a protective effect against the synaptic dysfunction induced by Aβ oligomers in hippocampal slices from 2-month-old C57bl6 mice. The protective effect of (–)- and (+)-1 on synaptic integrity was apparent in terms of induction of long-term potentiation (LTP), in the case of (+)-1, and preservation of the levels of synaptic proteins, more evident in the case of (–)-1. At this point of development, *in vivo* efficacy studies in an appropriate animal model of AD would be essential to definitively prove the disease-modifying potential of compounds (–)- and (+)-1 and eventually to select one of them as the most adequate candidate for further development.

In the present study, we have designed a set of studies to determine the potential effect of the rhein-huprine hybrids (+)- and (–)-1 in AβPP and PS-1 mutant transgenes (AβPP/PS1) mice model of AD. Previous evidences *in vitro* indicate a protection with (+)- and (–)-1 against Aβ oligomers present in the same transgenic model, inducing a reduction in soluble Aβ by treatment with (+)-1 [17]. Here in, we study the effect of rhein-huprine hybrids (+)- and (–)-1 in young and aged transgenic mice (7-month- and 11-month-old mice, respectively) on spatial memory, LTP, *tau* phosphorylation and neuropathology. We have observed a recovery of all these features, as well as a reduction in neuro-inflammation in both groups of animals. In addition, in aged transgenic mice we observed

a decrease in the levels of amyloid 1-42 peptide and amyloid 42/40 ratio in the hippocampus of animals treated with hybrids (+)-1, accompanied of a decrease in the deposits of Aβ and senile plaques. Interestingly, our results suggest that (+)-1 might provide beneficial effects for the treatment of AD.

Material and Methods

Animals, drugs and treatment: AβPPswe/PS-1 double transgenic mice, which express the mutant APPswe (K595N/M596L) and PSEN1ΔE9, the deletion of the exon 9 under the control of the mouse prion promoter [18], were obtained from the Jackson Laboratory (Bar Harbor, ME, Stock no 004462).

Rhein-huprine hybrids (+)-(7*R*,11*R*)- and (–)-(7*S*,11*S*)-*N*-{9-[(3-chloro-6,7,10,11-tetrahydro-9-methyl-7,11-methanocycloocta[*b*]quinolin-12-yl)amino]nonyl}-9,10-dihydro-4,5-dihydroxy-9,10-dioxoanthracene-2-carboxamide, i.e. (+)- and (–)-1, were prepared as previously reported [17].

Experimental design comprised 6 groups. Treatment started when a group of mice were 6 month-old and another set was 10 month-old and continued for 4 weeks (so, at the end of the treatment, mice were 7 and 11 month-old, respectively). Each set comprised three experimental groups: AβPPswe/PS-1 Control, AβPPswe/PS-1 + (–)-1and AβPPswe/PS-1 + (+)-1. The treatment consisted of intraperitoneal injection (i.p.) of 2.0 mg/kg enantiopurerhein-huprine hybrids (+)- or (–)-1 with saline solution as vehicle, three times per week during 4 weeks. Transgenic control animals were injected only with the vehicle.

Primary antibodies used: Rabbit anti-GFAP (DAKO, Carpinteria, CA), mouse anti-Aβ (4G8, Chemicon, Temecula, CA), AT8 Anti-Phospho-PHF-tau pSer202+Thr205 clone AT8, (MN1020, Thermo scientific), anti-PHF1: We would like to thank Dr Peter Davies (Department of Pathology, Albert Einstein College of Medicine, NY, USA) for his kindly gift of the mouse anti-tau antibody epitope PHF-1. Anti-Tau (phospho-S235) antibody (ab30664) Abcam and Anti-tau (phospho T231) antibody (ab30665) Abcam.

Slice Preparation and Electrophysiology: Hippocampal slices were prepared according to standard procedures previously described [19]. Briefly, transverse slices (350 µm) from the dorsal hippocampus were cut under cold artificial cerebrospinal fluid (ACSF, in mM: 124 NaCl, 2.6 $NaHCO_3$, 10 D-glucose, 2.69 KCl, 1.25 KH_2PO_4 2.5 $CaCl_2$, 1.3 $MgSO_4$, and 2.60 $NaHPO_4$) using a Vibratome (Leica VT 1000s, Germany) and incubated in ACSF for 1 h at room temperature. In all experiments, 10 µM picrotoxin (PTX) was added to suppress inhibitory GABAA transmission. Slices were transferred to an experimental chamber (2 mL), superfused (3 mL/min, at 20-22ºC) with gassed ACSF and visualized by trans-illumination with a binocular microscope (MSZ-10, Nikon, Melville, NY). To evoke field excitatory postsynaptic potentials (fEPSPs), we stimulated with bipolar concentric electrodes (Platinum/Iridium, 125 µm OD diameter, FHC Inc., Bowdoin, ME) generated by a stimulator (Axon 700b, Molecular Devices, Sunnyvale, CA) and connected to an isolation unit (Isoflex, AMPI, Jerusalem, Israel). The stimulation was in the Stratum Radiatum within 100-200 µm from the recording site. To generate LTP we used Theta Burst Stimulation (TBS) consisting of 5 trains of stimulus with an inter-train interval of 20 s. Each train consisted of 10 bursts at 5 Hz and each burst having 4 pulses at 100 Hz. Recordings were filtered at 2.0-3.0 kHz, sampled at 4.0 kHz using an A/D converter, and stored with pClamp 10 (Molecular Devices). Evoked postsynaptic responses were analyzed off-line, using an analysis software (pClampfit, Molecular Devices), which allowed visual detection of events, computing only those events that exceeded an arbitrary threshold[19].

Immunoblotting: The hippocampus from treated or control mice were dissected on ice and immediately frozen at -150ºC or processed as detailed previously (Carvajal et al., 2013; Inestrosa et al., 2011). Briefly, slices were homogenized in RIPA buffer (50mMTris-Cl, pH

7.5, 150mMNaCl, 1% NP-40, 0.5% sodium deoxycholate, and 1% SDS) supplemented with a protease inhibitor cocktail (Sigma-Aldrich P8340) and phosphatase inhibitors (50mMNaF, 1mM Na_3VO_4 and 30μM $Na_4P_20_7$) using a Potter homogenizer and then passed sequentially through different caliber syringes. Protein samples were centrifuged at 14000 rpm at 4º C twice for 15 min. Protein concentration was determined using the BCA Protein Assay Kit (Pierce Biotechnology, Rockford, IL). 20 and 40 Micrograms samples were resolved by 10% SDS-PAGE and transferred to a PVDF membrane. The reactions were followed by incubation with anti-mouse, anti-goat or anti-rabbit IgG peroxidase conjugated antibody (Pierce, Rockford, IL) and developed using an ECL kit (Western Lightning Plus ECL, PerkinElmer).

Determination of Aβ peptides levels: For determinate the concentration of Aβ peptides, Sandwich Enzyme-linked Immunosorbent Assay specific for Aβ1-40 and Aβ1-42 were used as previously described (EZBRAIN40, EZBRAIN42; EMD Millipore Corporation, Billerica, MA) [20]. Briefly, hippocampal homogenates of control or treated transgenic mice were diluted to 0,2 μg/μl in homogenization buffer containing protease inhibitors. 50 μl of crude homogenate were performed to measure Aβ1-40 and Aβ1-42 levels according to the manufacturer's instructions. Plates were read at 450 nm and 590nm on a Metertech 960 ELISA Analyzer.

Behavioral test: Memory flexibility test: The Morris water maze (MWM) was performed as previously described in our laboratory [21]. Briefly, mice were trained in a circular water maze of 1.2 m diameter (opaque water, 50 cm deep, 19–21 ºC, 9 cm platform 1cm below water, maximum trial duration 60 s, 10 s on platform at the end of trials). Each animal was trained for one pseudo-random location of the platform per day, for 4 days, with a new

platform location each day. Training was conducted up to 10 trials per day, until the criterion of 3 successive trials with an escape latency of <20s was met. On completion of testing, the mouse was removed from the maze, dried and returned to its cage. The animals were tested for the next location on the following day. Data were collected using a video tracking system for water maze (HVS Imagen, Sheffield, UK).

Immunohistochemical procedures: Perfusion, fixation and free-floating immunohistochemical procedures were performed as previously described[19]. Washing and dilution of immune-reagents were performed using 0.01 M PBS with 0.2% Triton X-100 (PBS-T) throughout experiments, with two PBS-T washes per antibody incubation. Sections were pretreated with 0.5% H_2O_2 for 30 min to reduce endogenous peroxidase activity followed by treatment with 3% bovine serum albumin (BSA) at room temperature for 1 h to avoid non-specific binding. Primary antibodies (anti-Aβ, clone 4G8 and anti-GFAP) were incubated overnight at 4°C. Detection of primary antibody was performed using the Pierce ABC Kit (Thermo Fisher Scientific Inc., Rockford, IL). Staining was developed by incubating for 15 min with 0.6% diaminobenzidine followed by the addition of H_2O_2 (0.01% final concentration). After immunostaining, all sections were mounted on gelatin-coated slides, air-dried, dehydrated and cover-slipped with Canada balsam (Merck, Darmstadt, Germany). Immunofluorescence was performed as previously described. The primary antibody used was mouse anti-4-HNE (Life Technologies, Carlsbad, CA) and rabbit anti-interleukin-6 (IL-6, DAKO, Carpinteria, CA). The slices were subsequently mounted on slides using mounting medium and analyzed using a Zeiss LSM 5 Pascal confocal microscope. The images were analyzed using ImageJ software (NIH).

Thioflavine-S (Th-S) staining: Th-S staining was developed on gelatin-coated slices as previously described [19]. After dehydration and rehydration in ethanol and xilol batteries, slices were incubated in distilled water for 10 min and then were immersed in the Th-S solution (0.1% ThS in 70% ethanol) for 5 min. Slices were then washed twice in 70% ethanol for 30 s and cover-slipped with antifade mounting medium in dark.

Image analysis: Stained brain sections were photographed using an Olympus BX51 microscope coupled to a Micro-publisher 3.3 RTV camera (QImaging). The luminescence of the incident light and the time of exposure were calibrated to assign pixel values ranging from 0 to 255 in RGB image (no-light to full-light transmission), which were used along all preparations. The images were loaded into ImageJ v.1.40g software (NIH) for analysis. Selection of areas for measurement was performed by manual threshold adjustment or by direct manual selection of ROIs in heterogeneous stains.

Statistical analysis: Results are expressed as mean ± standard error. Data were analyzed by one-way ANOVA, followed by Bonferroni's post hoc test. $p \leq 0.05$ was considered as statistically significant. Statistical analysis was performed using Prism software (GraphPad Software Inc.).

RESULTS

Rhein-huprine (+)- and (–)-1 prevent spatial memory loss in young and old AβPPswe/PS-1 mice.

Hippocampal function was evaluated by a variant of the MWM, called memory flexibility test, which measures episodic and spatial memory [21; 22]. In this task, mice are required to learn the location of a hidden platform in a pool based on external cues. For

this experiment, 6 month-old AβPPswe/PS-1 were injected i.p. with (+)- or (–)-1 (three times per week for 4 weeks) showing a recovery of cognitive functions associated to an improvement in the number of trials to locate the hidden platform in animals treated with (+)- or (–)-1 in young animals compared with AβPPswe/PS-1 control (Figure 2A). However, in old mice (11 month-old AβPPswe/PS-1, after treatment) we observed a recovery of cognitive functions only in those treated with (+)-1 while no changes in the numbers of trials to locate the hidden platform were found in the animals treated with the enantiomer (–)-1 in comparison with AβPPswe/PS-1 control mice (Figure 2B). These results indicate that (+)-1 and (–)-1 have beneficial effects against the cognitive impairment present in the AβPPswe/PS-1 mice in young transgenic mice while only the dextrorotatory enantiomer induces a recovery of spatial memory in mature AβPPswe/PS-1 mice.

Rhein-huprine (+)-1 treatment recovers the induction and maintenance of LTP in AβPP/PS1 mice

Prevention and protection of the hippocampal network performance by memory analysis in AβPPswe/PS-1 mice model of AD could be related with the maintenance of the synaptic function and the neurotransmission associated to synaptic plasticity, which in the presence of the Aβ oligomers become disrupted [23-25]. In this case, we used one kind of long lasting plasticity called LTP, which indicates a correlation with memory in different zones of the brain, and is the parameter used to assess the state of synaptic strength [26; 27]. The response generated was measured by the fEPSP slope in transgenic mice treated with compounds (+)-1 and (–)-1in the stratum radiatum of CA1 hippocampal slices. We generated LTP using TBS and we observed that AβPPswe/PS-1 mice control did not

generate LTP (Fig. 3A and B) that is consistent with previous reports [19; 28]. When we treated animals with (+)-1, it was possible to induce a persistent LTP (Figure 3A, grey circles) in young AβPPswe/PS-1 animals. However, in the animals treated with (–)-1, it was not possible to induce a LTP (Figure 3A, black). Additionally, in 11-month old AβPPswe/PS-1 mice, the treatment with (+)-1 allows the induction of a LTP in comparison with AβPPswe/PS-1 control mice, while (–)-1was not able to induce LTP compared with controls (Figure 3B, black and grey circles respectively). These evidences indicate that the treatment with compound (+)-1 promotes LTP induction and maintenance in an AβPPswe/PS-1 mice model of AD.

Rhein-huprine (+)-1 treatment reduces the levels of $A\beta_{1-42}$ peptides in aged AβPPswe/PS-1 mice.

In order to assess whether the improvement in mice spatial behavior was correlated with a change in AD neuropathological markers, we determined the levels of Aβ peptides in the brain of AβPPswe/PS-1 transgenic mice. For this propose, hippocampal lysates from control, (+)- and (–)-1 treated mice from aged transgenic animals were used to detect both, $A\beta_{1-42}$ and $A\beta_{1-40}$ levels by ELISA assay. The figure 4A show that concentration of $A\beta_{1-42}$ peptide decrease significantly in animals treated only with (+)-1 in comparison with control mice. The Figure 4B show the concentration of $A\beta_{1-40}$ peptide and not significant differences were observed between the experimental groups, however the (+)-1 treatment show a tendency to increase the account of this peptide. With these concentrations of $A\beta_{1-42}$ and $A\beta_{1-40}$ peptides we calculated the Aβ42/Aβ40 ratio (Figure 4C), an indicative of increased toxicity of pathological AD [29] and observed that aged transgenic AβPPswe

/PS-1 treated with (+)-1 compound decrease of significant manner this parameter. These results suggest that (+)-1 treatment decrease the concentration of toxic $A\beta_{1-42}$ peptide and this could decrease the severity of the pathology in the transgenic mice.

Rhein-huprine (+)- and (-)-1 treatments reduce the amount of amyloid plaques in AβPPswe/PS-1 mice.

Previously and in concordance with the change in the levels of Aβ peptides, we observed that 6 and 11 month-old AβPPswe /PS-1mice treated with compounds (+)- or (–)-1 for 4 weeks shown a decrease in the levels of soluble Aβ species, accompanied by an increase in the levels of mature amyloid precursor protein (APP) [17]. In addition, to evaluate whether (+)- and (–)-1 treatments affect the total load of amyloid deposits, brain slices obtained from AβPPswe/PS-1 control mice and AβPPswe/PS-1 treated with compounds (+)- or (–)-1 were analyzed by immunodetection using the anti-Aβ 6E10 antibody to detect Aβ aggregates and the total load of Aβ deposits. Brains from 7-month-old animals treated with both compounds showed a significant reduction in the percentage of the area of Aβ-positive aggregates present on the brain cortex (Figure 5A). However, only (+)-1 was able to diminish the Aβ-oligomers load in the hippocampus. As for the 11-month-old AβPPswe/PS-1mice (Figure 5B), in both treatments a reduction in total Aβ load in the cortex area was observed, while similar to the previous case, only (+)-1 shows a reduction in total load of Aβ in the hippocampus in comparison with the control condition.

To analyze whether the different compounds alter the amount of amyloid deposits present, brains slices of AβPPswe/PS-1 control, and (+)- and (–)-1treated animals were stained with Thioflavin-S (Th-S), a fluorescent dye that binds to the β-sheet of the amyloid aggregates,

changing its fluorescence properties [30; 31], and the positive (Th-S) area fractions were analyzed (Figure 6). The analysis showed a significant reduction in the Th-S positive area with both the (+)-1 and the (–)-1 treatments in the cortex of 7 month-old AβPPswe/PS-1. Interestingly, similar to the analysis of the Aβ burden obtained in the immunohistochemistry, only the treatment with (+)-1 induces a reduction in the Th-S positive area in the hippocampus in comparison with the vehicle treated animals (Figure 6A). Also, when we analyzed the amyloid burden in 11 month-old AβPPswe/PS-1 mice, we detected that both treatments induced a reduction of the Th-S positive area in the cortex, but in hippocampus only (+)-1 promoted a reduction in amyloid plaques (Figure 6B). Therefore, the treatment with both drugs induces a reduction in the neuropathological marker in cortex in different aged animals, but only (+)-1 was able to induce changes in the hippocampus, indicating a reduction in the total amount of Aβ aggregates.

Rhein-huprine (+)- and (–)-1 treatments reduce the phosphorylation of *tau* protein in AβPPswe/PS-1 11 month-old mice.

In addition, we examined the effect of the rhein-huprine hybrids over *tau* protein phosphorylation in AβPPswe/PS-1 mice at an advanced age (11-month-age) (Figure 7). The epitopes T231 and S235 have been associated previously with the triggering process of *tau* aggregation into neurofibrillary tangles [32]. In contrast, the AT8 and PHF-1 epitopes are associated with the process of aggregation and eventual accumulation of the paired-helical filaments that form the neurofibrillary tangles [33]. The figure 7A show western blot of three different conditions: control, (+)-1 and (–)-1 treated mice. The densitometric analysis shows that both treatments induce a decrease in the early phosphorylation of tau epitopes (Figure 7B). In the (+)-1 treated group we observed a significant decrease in the

phosphorylation of S235 epitope whereas the phosphorylation of the epitope T231 was decreased in (–)-1 treated mice. In contrast, the epitopes associated with the process of aggregation of tau protein AT8 and PHF1 only were decrease significantly in the (+)-1 treated group (Figure 7C). Therefore, these results suggest that rhein-huprine derivatives, in particular (+)-1 was able to revert the process of phosphorylation of the tau protein observed in AβPPswe/PS-1 old mice.

Rhein-huprine (+)- and (–)-1 treatments reduce the inflammatory reaction in the AβPPswe/PS-1 transgenic mice.

Neuro-inflammation was evaluated, mainly through astrogliosis, in the brain of control and (+)-1 and (–)-1treated APPswe-PS-1 mice through immunostaining with anti-GFAP, which labels the intermediate filaments of astrocytes. With this staining plus the evaluation of the amount of GFAP positive cells and the morphological changes, it is possible to evaluate the inflammatory state caused by toxic agents [34]. The analysis was performed through the detection of the occupied area by hyper-reactive astrocytes observed in 7- (Figure 8A) and 11- month-old transgenic animals treated with (+)- and (–)-1 (Figure 8B) in cortex and hippocampus respectively. In every case, a decrease in the inflammatory response indicates a recovery of the function with a stabilization of the cellular processes associated to the glia. Western blot analyses to GFAP and CD11b, a marker for microglial cells, were performed in aged transgenic animals treated with (+)- and (–)-1 (Figure 8C) and the densitometric analysis indicate that both (+)- and (–)-1 treatment are able to decrease the levels of inflammation markers (Figure 8D). Additionally, we evaluate Interleukin-6 (Il-6), a pro-inflammatory cytokine related with neuro-inflammation in AD and released by the

presence of Aβ [35-38] in our animal model. We do not observed variations in cortex or hippocampus in the control compared to the (+)- and (–)-1 treatment of 7-month old transgenic animals (Figure 8E). However, both cortex and hippocampus of control of 11-month old transgenic mice we observed an increase in the levels of Il-6 that are reduced with (+)- and (–)-1 treatments (Figure 8F). Additionally, we study the levels of 4-hydroxinonenal (4-HNE), and oxidative stress marker reported in our transgenic model [4]. In this context, we do not observed changes in cortex or hippocampus in levels of 4-HNE in 7-month old transgenic mice (Figure 9A), but in 11-month old transgenic mice we found a significant reduction in 4HNE only with the treatment of (+)-1 (Figure 9B). These evidences indicate a reduction of neuro-inflammation in 11-month old transgenic mice with rhein derivatives treatment.

Discussion

We have recently demonstrated the beneficial and protective *in vitro* and *ex vivo* effects of a novel class of synthetic compounds that combine a unit of the drug rhein and a unit of the potent *catalytic anionic site* (CAS) AChE inhibitor huprine Y, connected through linkers of different lengths. The rationale behind this design strategy was: i) that rhein might be endowed with tau anti-aggregating properties, as it had been reported for other structurally related hydroxyanthraquinone derivatives, and might confer that potential activity to its derivatives, ii) that the rhein-huprine hybrids might be able to simultaneously bind both the CAS and the *peripheral anionic site* (PAS) of AChE, which might result in a blockade of the AChE-induced aggregation of Aβ (see below) and a potent inhibition of AChE activity, and iii) that the expected multi-target profile of the rhein-huprine hybrids might enable an

AD-modifying effect associated with a reduction in the Aβ soluble levels and a protection of LTP in an *in vitro* condition [17], which had to be eventually assessed in *in vivo* efficacy studies in a well-established animal model of AD (Figure 10). Herein, we have studied the properties of the two leads of the series of rhein-huprine hybrids, i.e. the nonamethylene-linked derivatives (+)- and (–)-1, in an AβPPswe/PS-1 model of AD that presents a progressive neurodegeneration with the pass of time. This animal model features an increase in the amount of amyloid in the hippocampus and cortex [2; 18], which is associated with a reduction of synaptic functions and a progressive loss of synaptic plastic events such as LTP [39], which in turn, is a widely accepted model of learning and memory in the CA1 region of the hippocampus [40; 41]. In this context, an inhibition of the induction of LTP is related with a loss of cognitive process such as the spatial learning and memory [27; 42; 43]. Interestingly, we found that the treatment with rhein-huprine hybrids (+)- and (–)-1 reduce the cognitive damage and re-establish synaptic transmission processes such as LTP. In the present study we provided evidence that the rhein-huprine hybrids trigger a reduction of the toxic Aβ aggregates in the cortex, however, only (+)-1 was able to promote a selective effect in the hippocampal region both in $A\beta_{1-42}$ peptide concentration and in Aβ aggregates. The mechanisms associated to the recovery of synaptic and cognitive functions by the rhein-huprine hybrids are probably related to a reduction of the toxic amyloid and phosphorylated tau aggregates, as we have recently found in a simplified model of protein aggregation within intact *Escherichia coli* cells and AβPPswe/PS-1 model [17]. Very interestingly, we have found a very potent *in vitro* BACE-1 inhibitory activity for the rhein-huprine hybrids (+)- and (–)-1 (IC_{50} = 80 nM) [17], which complement a very interesting multi-target biological profile. BACE-1 inhibition should result *in vivo* in a

reduction of the formation of Aβ levels [3], and promotion of the recovery of the levels of APP, as we have certainly found in AβPPswe/PS-1 model of AD [17] This could be a explanation because we observed a decrease in the $A\beta_{1-42}$ concentration in the hippocampus and the change in the $A\beta_{42}/A\beta_{4o}$ ratio with (+)-1 treatment in aged transgenic mice. The most abundant amyloid peptides $A\beta_{1-42}$ and $A\beta_{1-40}$ are present under physiological conditions in the brain in an Aβ42/Aβ40 ratio of 1:9. This ratio is drastically altered by the increase in the $A\beta_{1-42}$ concentration in brains of patients with familial AD or mice model of AD and this has been shown to lead to increased synaptotoxicity [29]. In concordance with the anterior, in our studies the reduction of Aβ is related with a protection *in vitro* of the induction of LTP by co-incubations of the Aβ oligomers with rhein-huprine hybrids [17]. Interestingly, in 7 month-old APPswe/PS-1 we observed a protection and induction of LTP with both treatments. However, only (+)-1 protects the induction and maintenance of LTP while (–)-1was not able to recover the loss of LTP observed in 11 month-old APPswe/PS-1 transgenic mice. Our results therefore indicate that a recovery of synaptic function by compound (+)-1 is associated with the LTP recovery and the concomitant recovery of the cognitive processes in AβPPswe/PS-1 in different ages. The reduction in the soluble Aβ levels with a concomitant increase in the levels of its precursor APP and a restitution of the LTP *in vitro,* previously observed [17] was replicable in our *in vivo* model. Interestingly, another property of the rhein-huprine hybrids is associated with a potent AChE inhibitory activity, resulting from a dual binding to CAS and PAS, which may contribute with a reduction in the activity of a non-cholinergic pathway associated to processes of self-aggregation of Aβ [4]. In this context, AChE is considered as a nucleation factor for the Aβ aggregation and an accelerating factor for the assembly of $A\beta_{1-40}$ into Alzheimer's fibrils [7;

9]. These previous reports indicate that AChE acts as a chaperone promoting the assembly of $A\beta_{1-40}$ aggregates by a mechanism that involves the PAS of the enzyme, located at the rim of the active site gorge of AChE [9]. The AChE-induced Aβ aggregation is sensitive to PAS ligands such as propidium, and this effect is partially inhibited by anti-AChE agents that bind both to the catalytic and the peripheral sites, such as physostigmine, donepezil, and xanthostigmine derivates [44]. Blockade of the peripheral anionic site by specific inhibitors has emerged as an alternative disease-modifying strategy for AD. Based on these assumptions, dual binding site AChE inhibitors have emerged as a valuable tool in order to achieve a disease-modifying approach [13; 45]. In this context, *in vitro* biological assays as well as molecular modeling studies demonstrate that rhein-huprine hybrids induce an inhibition of the AChE activity by simultaneous blockade of CAS and PAS. Additionally, we previously report the effect of rhein-huprine derivatives in BChE but all the derivatives turned out to be selective for hAChE over hBChE inhibition [17]. Besides of these hybrids to exhibit a moderately potent hBChE inhibitory activity, with IC_{50} values in the submicromolar to low micromolar range [17], the most potent hBChE inhibitor of the series was not used in this investigation. However, is necessary realizing more studies about the effect of the rhein–huprine hybrids in BChE in our animal model of AD.

Therefore, we found that the reduction in the amount of amyloid detected at the level of Th-S represents a correlate with a reduction in the aggregation of the amyloid species in both the cortex and the hippocampus, determining a decrease in the synaptic damage, a situation which has repercussions in the reduction of the cognitive deficit observed in the animals after the treatment with the rhein-huprine derivatives. Certain reports indicated that the interaction between Aβ oligomers and *tau* could promote the damage and increase cell

death in the brain [46]. Combining this idea with the amyloid cascade hypothesis, it is suggested that Aβ formation is a critical step in driving AD pathogenesis and that Aβ formation could coexist with the action generated by *tau*, increasing dysregulation signals in AD [47]. In the present study, we demonstrated that *tau* phosphorylation at the PHF-1, AT-8, T231 and S235 sites are reduced. This reduction in the phosphorylated state of tau is consistent with the tau anti-aggregating effect found for these drugs in the *E. coli* model [17] and with a recovery of cognitive function and a protection of LTP induction in the CA1 regions of hippocampus in AβPPswe/PS-1 mice.

According to the amyloid hypothesis, the production, aggregation and accumulation of the Aβ peptide is the main responsible factor of AD [48], therefore, this could be a key event that triggers the synaptic failure, oxidative stress and neuro-inflammation observed in the present study. Interestingly, we observed that rhein-huprine hybrids, in particular (+)-1 also decrease the levels of phosphorylated *tau* protein, a hallmark of AD. Furthermore, the AChE associated to amyloid plaques showed changes in biochemical and pharmacological properties, as well as an increase in the neurotoxicity of the AChE–Aβ complexes. For example, tetrahydrohyperforin, an hyperforin derivative releases AChE from the Aβ aggregates and inhibit AChE–Aβ interactions *in vitro* and *in vivo*, thereby preventing the development of the disease in a transgenic mice model of AD [4; 10]. Considering previous evidence *in vitro* and the results obtained in young and mature AβPPswe/PS-1 mice, it is apparent that the rhein-huprine hybrids act as an anti-β-amyloidogenic agents both *in vitro* and *in vivo* and are amenable to further development [49] as potential treatments for neurodegenerative diseases such as AD (Figure 10).

ACKNOWLEDGMENTS

This work was supported by grants PFB 12/2007 from the Basal Centre for Excellence in Science and Technology, FONDECYT 1120156 to N.C.I. and by grants CTQ2011-22433 and 2009SGR1396 from Ministerio de Ciencia e Innovación and Generalitat de Catalunya (GC), respectively, to D.M.-T. Pre-doctoral fellowships from CONICYT to F.G.S and C.T.R, from the VRI of the Catholic University of Chile to F.J.C., and from GC to E.V. and I.S. are gratefully acknowledged.

Abbreviations: APP = Amyloid Precursor Protein; PS-1 = Presenilin-1; Aβ = Amyloid β-peptide; GFAP = Glial Fibrillary Acidic Protein; MWM = Morris Water Maze; LTP = Long-Term Potentiation; CNS = Central Nervous System; BSA = Bovine Serum Albumin; ACSF = Artificial Cerebrospinal Fluid; fEPSP = field Excitatory Post-Synaptic Potential; TBS = Theta Burst Stimulation.

CONFLICT OF INTEREST STATEMENT

The authors declare that they have no competing interests.

L**egends to the Figures**

Fig. 1. Chemical structure of huprine-rhein hybrids (+)- and (–)-1.

Fig. 2. Rhein-huprine hybrids (+)- and (–)-1recover the cognitive functions in an AD mouse model of different ages. (A) Behavioral performance in the memory flexibility test. 7-Month-old AβPP/PS1 mice treated with control vehicle solution (Control AβPP/PS1 , white squares),(+)-1 (AβPP/PS1 (+)-1, black squares) or (–)-1 (AβPP/PS1 (–)-1, grays quares). (B) Behavioral performance in the memory flexibility test. 12-Month-old AβPP/PS1 mice treated with control vehicle solution (Control AβPP/PS1, white squares), (+)-1 (AβPP/PS1 (+)-1, black squares) or (–)-1 (AβPP/PS1 (–)-1, gray squares). n≥ 4 per treatment *p<0.05.

Fig. 3.Rhein-huprine hybrids (+)- and (–)-1 recover LTP inyoung and old AβPP/PS1 mice.(A) LTP generated by TBS in hippocampal CA1 in AβPP/PS1 slices from 7-month-old mice treated with rhein-huprine hybrids (+)- and (–)-1 (AβPP/PS1 (+)-1 and AβPP/PS1 (–)-1, black and gray circles, respectively) shows a recovery in the capacity to induce LTP in comparison with AβPP/PS1 control (white circles). (B) LTP generated by TBS in hippocampal CA1 in AβPP/PS1 slices from 11-month-old mice treated with rhein-huprine hybrids (+)- and (–)-1 (AβPP/PS1 (+)-1 and AβPP/PS1 (–)-1), black and gray circles, respectively) shows a recovery in the capacity to induce LTP only with the treatment of rhein-huprine hybrids (+)-1 in comparison with AβPP/PS1 control (white circles). The dots and bars are mean ± SE from 7 different slices, n=3 * p< 0.05.

Fig. 4. Rhein-huprine hybrid (+)-1 reduces the $A\beta_{1-42}$ peptide concentration and the Aβ42/Aβ40 ratio in the hippocampus of old AβPP/PS1 mice. (A) $A\beta_{1-42}$ concentration in the hippocampus of control, rhein-huprine hybrids (+)- and (–)-1 treated mice measuring

by ELISA assay. (B) $A\beta_{1-40}$ concentration in the hippocampus of control, (+)- and (–)-1 treated mice measuring by ELISA assay. (C) Aβ42/Aβ40 ratio of control, rhein-huprine hybrids (+)- and (–)-1 treatment. n≥3 in control and (+)-1 mice, n=1 in (-)-1 mice *p<0.05.

Fig. 5. Rhein-huprine hybrids (+)- and (–)-1 reduce the Aβ-burden in the brain of young and old AβPP/PS1 mice. (A) Representative staining against Aβ by 4G8 antibody used to detect amyloid deposits of transgenic mice in the cortex and hippocampus of 7-month-old AβPP/PS1 mice with vehicle (white bars) and rhein-huprine hybrids (+)- and (–)-1 treatment (black and gray bars, respectively), picture at 10x. (B) Representative staining against Aβ by 4G8 antibody used to detect amyloid deposits of transgenic mice in the cortex and hippocampus of 11-month-old AβPP/PS1 mice with vehicle (white bars) and rhein-huprine hybrids (+)- and (–)-1 treatment (black and gray bars, respectively), picture at 10x. Graph represents normalized densitometry analysis profile of the slot intensity for each treatment, n≥3 *p<0.05; **p<0.01; *** p<0.001.

Fig. 6. Rhein-huprine hybrids (+)- and (–)-1 reduce the Aβ amount of aggregates in the brain of young and old AβPP/PS1 mice. (A) Representative Th-S staining used to detect amyloid deposits of transgenic mice in the cortex and hippocampus of 7-month-old AβPP/PS1 mice with vehicle (white bars) and rhein-huprine hybrids (+)- and (–)-1 treatment (black and gray bars). Amyloid burden was quantified with the Th-S staining and number of amyloid plaques per area in cortex and hippocampus, respectively, picture at 10x. (B) Representative Th-S staining used to detect amyloid deposits of transgenic mice in the cortex and hippocampus of 11-month-old AβPP/PS1 mice with vehicle (white bars) and rhein-huprine hybrids (+)- and (–)-1 treatment (black and gray bars respectively),

picture at 10x. Graph represents normalized densitometry analysis profile of the slot intensity for each treatment, n≥3 *p<0.05; **p<0.01; *** p<0.001.

Fig. 7. Rhein-huprine hybrids (+)- and (–)-1 reduce tau phosphorylation in the brains of 11 mont-old AβPPswe/PS1 mice. (A) Immunoblot of hippocampus homogenates from mature (11-month-old) AβPPswe/PS-1 control (white bars) and (+)- and (–)-1 treated mice (black and gray bars respectively) using the PHF-1, AT8, T231 and S235 antibodies. (A, B) Graph corresponds to the densitometric analysis of bands normalized against a loading control and compared with AβPPswe/PS-1 control and (+)- and (–)-1 treated mice. n≥3. * p<0.05; ** p<0.01; *** p<0.001.

Fig. 8. Rhein-huprine hybrids (+)- and (–)-1 reduce the neuroinflammation in the brain of young and old AβPP/PS1 mice. (A) Representative GFAP area fraction ((GFAP area/total field area)*100) in cortex and hippocampus of 7-month-old AβPP/PS1 mice with vehicle (white bars) and rhein-huprine hybrids (+)- and (–)-1 treatment (black and gray bars). (B) Representative GFAP area fraction ((GFAP area/total field area)*100) in cortex and hippocampus of 11-month-old AβPP/PS1 mice with vehicle (white bars) and rhein-huprine hybrids (+)- and (–)-1 treatment (black and gray bars), picture at 10x.Graph represents normalized densitometry analysis profile of the slot intensity for each treatment. (C) Immunoblot of hippocampus homogenates from mature (11-month-old) AβPPswe/PS-1 control (white bars) and (+)- and (–)-1 treated mice (black and gray bars respectively) using the GFAP and CD11b antibodies. (D) Graph corresponds to the densitometric analysis of bands normalized against a loading control and compared with AβPPswe/PS-1 control and (+)- and (–)-1 treated mice. * p<0.05; ** p<0.01; *** p<0.001.

Fig. 9. Rhein-huprine hybrids (+)- and (–)-1 reduces oxidative damage in the brain of young and old AβPP/PS1 mice. (A) Representative 4-HNE in cortex and hippocampus of 7-month-old AβPP/PS1 mice with vehicle (white bars) and rhein-huprine hybrids (+)- and (–)-1 treatment (black and gray bars). * $p<0.05$; ** $p<0.01$; *** $p<0.001$.

Fig. 10. Mechanism proposed to the effect of rhein-huprine hybrids (+)- and (–)-1. The rhein-huprine hybrids might be able to simultaneously bind both the CAS and the *peripheral anionic site* (PAS) of AChE, which might result in a blockade of the AChE-induced aggregation of Aβ. Additionally, rhein-huprine hybrids might able to inhibit the activity of BACE1, which result in a reduction in the amyloid toxic deposit inducing a reduction of inflammation. These cascades of events prevent and recover synaptic and cognitive processes in young and old AD mice model.

References

[1] Querfurth HW, LaFerla FM. Alzheimer's disease. N Engl J Med 362(4): 329-44.(2010).
[2] Serrano-Pozo A, Frosch MP, Masliah E, Hyman BT. Neuropathological alterations in Alzheimer disease. Cold Spring Harb Perspect Med 1(1): a006189.(2011).
[3] O'Brien RJ, Wong PC. Amyloid precursor protein processing and Alzheimer's disease. Annu Rev Neurosci 34: 185-204.(2011).
[4] Carvajal FJ, Inestrosa NC. Interactions of AChE with Abeta Aggregates in Alzheimer's Brain: Therapeutic Relevance of IDN 5706. Frontiers in molecular neuroscience 4: 19.(2011).
[5] Picciotto MR, Higley MJ, Mineur YS. Acetylcholine as a neuromodulator: cholinergic signaling shapes nervous system function and behavior. Neuron 76(1): 116-29.(2012).
[6] Inestrosa NC, Dinamarca MC, Alvarez A. Amyloid-cholinesterase interactions. Implications for Alzheimer's disease. FEBS J 275(4): 625-32.(2008).
[7] Inestrosa NC, Sagal JP, Colombres M. Acetylcholinesterase interaction with Alzheimer amyloid beta. Subcell Biochem 38: 299-317.(2005).
[8] Alvarez A, Opazo C, Alarcon R, Garrido J, Inestrosa NC. Acetylcholinesterase promotes the aggregation of amyloid-beta-peptide fragments by forming a complex with the growing fibrils. J Mol Biol 272(3): 348-61.(1997).
[9] Inestrosa NC, Alvarez A, Perez CA, Moreno RD, Vicente M, Linker C*, et al.* Acetylcholinesterase accelerates assembly of amyloid-beta-peptides into Alzheimer's fibrils: possible role of the peripheral site of the enzyme. Neuron 16(4): 881-91.(1996).
[10] Dinamarca MC, Arrazola M, Toledo E, Cerpa WF, Hancke J, Inestrosa NC. Release of acetylcholinesterase (AChE) from beta-amyloid plaques assemblies improves the spatial memory impairments in APP-transgenic mice. Chem Biol Interact 175(1-3): 142-9.(2008).
[11] Reyes AE, Chacon MA, Dinamarca MC, Cerpa W, Morgan C, Inestrosa NC. Acetylcholinesterase-Abeta complexes are more toxic than Abeta fibrils in rat hippocampus: effect on rat beta-amyloid aggregation, laminin expression, reactive astrocytosis, and neuronal cell loss. Am J Pathol 164(6): 2163-74.(2004).
[12] Chacon MA, Reyes AE, Inestrosa NC. Acetylcholinesterase induces neuronal cell loss, astrocyte hypertrophy and behavioral deficits in mammalian hippocampus. J Neurochem 87(1): 195-204.(2003).
[13] Colombres M, Sagal JP, Inestrosa NC. An overview of the current and novel drugs for Alzheimer's disease with particular reference to anti-cholinesterase compounds. Curr Pharm Des 10(25): 3121-30.(2004).
[14] Lockridge O, Schopfer LM, Winger G, Woods JH. Large Scale Purification of Butyrylcholinesterase from Human Plasma Suitable for Injection into Monkeys; a Potential New Therapeutic for Protection against Cocaine and Nerve Agent Toxicity. The journal of medical, chemical, biological, and radiological defense 3: nihms5095.(2005).
[15] Diamant S, Podoly E, Friedler A, Ligumsky H, Livnah O, Soreq H. Butyrylcholinesterase attenuates amyloid fibril formation in vitro. Proceedings of the National Academy of Sciences of the United States of America 103(23): 8628-33.(2006).
[16] Citron M. Alzheimer's disease: strategies for disease modification. Nature reviews Drug discovery 9(5): 387-98.(2010).
[17] Viayna E, Sola I, Bartolini M, De Simone A, Tapia-Rojas C, Serrano FG*, et al.* Synthesis and multitarget biological profiling of a novel family of rhein derivatives as disease-modifying anti-Alzheimer agents. Journal of medicinal chemistry 57(6): 2549-67.(2014).

[18] Garcia-Alloza M, Robbins EM, Zhang-Nunes SX, Purcell SM, Betensky RA, Raju S*, et al.* Characterization of amyloid deposition in the APPswe/PS1dE9 mouse model of Alzheimer disease. Neurobiol Dis 24(3): 516-24.(2006).
[19] Inestrosa NC, Carvajal FJ, Zolezzi JM, Tapia-Rojas C, Serrano F, Karmelic D*, et al.* Peroxisome proliferators reduce spatial memory impairment, synaptic failure, and neurodegeneration in brains of a double transgenic mice model of Alzheimer's disease. J Alzheimers Dis 33(4): 941-59.(2013).
[20] Mufson EJ, He B, Nadeem M, Perez SE, Counts SE, Leurgans S*, et al.* Hippocampal proNGF signaling pathways and beta-amyloid levels in mild cognitive impairment and Alzheimer disease. Journal of neuropathology and experimental neurology 71(11): 1018-29.(2012).
[21] Toledo EM, Inestrosa NC. Activation of Wnt signaling by lithium and rosiglitazone reduced spatial memory impairment and neurodegeneration in brains of an APPswe/PSEN1DeltaE9 mouse model of Alzheimer's disease. Mol Psychiatry 15(3): 272-85, 28.(2010).
[22] Chen G, Chen KS, Knox J, Inglis J, Bernard A, Martin SJ*, et al.* A learning deficit related to age and beta-amyloid plaques in a mouse model of Alzheimer's disease. Nature 408(6815): 975-9.(2000).
[23] Shankar GM, Li S, Mehta TH, Garcia-Munoz A, Shepardson NE, Smith I*, et al.* Amyloid-beta protein dimers isolated directly from Alzheimer's brains impair synaptic plasticity and memory. Nat Med 14(8): 837-42.(2008).
[24] Selkoe DJ. Soluble oligomers of the amyloid beta-protein impair synaptic plasticity and behavior. Behav Brain Res 192(1): 106-13.(2008).
[25] Walsh DM, Klyubin I, Fadeeva JV, Cullen WK, Anwyl R, Wolfe MS*, et al.* Naturally secreted oligomers of amyloid beta protein potently inhibit hippocampal long-term potentiation in vivo. Nature 416(6880): 535-9.(2002).
[26] Whitlock JR, Heynen AJ, Shuler MG, Bear MF. Learning induces long-term potentiation in the hippocampus. Science 313(5790): 1093-7.(2006).
[27] Morris RG, Anderson E, Lynch GS, Baudry M. Selective impairment of learning and blockade of long-term potentiation by an N-methyl-D-aspartate receptor antagonist, AP5. Nature 319(6056): 774-6.(1986).
[28] Vargas JY, Fuenzalida M, Inestrosa NC. In vivo activation of Wnt signaling pathway enhances cognitive function of adult mice and reverses cognitive deficits in an Alzheimer's disease model. The Journal of neuroscience : the official journal of the Society for Neuroscience 34(6): 2191-202.(2014).
[29] Pauwels K, Williams TL, Morris KL, Jonckheere W, Vandersteen A, Kelly G*, et al.* Structural basis for increased toxicity of pathological abeta42:abeta40 ratios in Alzheimer disease. The Journal of biological chemistry 287(8): 5650-60.(2012).
[30] Kitazawa M, Medeiros R, Laferla FM. Transgenic mouse models of Alzheimer disease: developing a better model as a tool for therapeutic interventions. Curr Pharm Des 18(8): 1131-47.(2012).
[31] Lesne S, Koh MT, Kotilinek L, Kayed R, Glabe CG, Yang A*, et al.* A specific amyloid-beta protein assembly in the brain impairs memory. Nature 440(7082): 352-7.(2006).
[32] Sengupta A, Kabat J, Novak M, Wu Q, Grundke-Iqbal I, Iqbal K. Phosphorylation of tau at both Thr 231 and Ser 262 is required for maximal inhibition of its binding to microtubules. Archives of biochemistry and biophysics 357(2): 299-309.(1998).

[33] Zheng-Fischhofer Q, Biernat J, Mandelkow EM, Illenberger S, Godemann R, Mandelkow E. Sequential phosphorylation of Tau by glycogen synthase kinase-3beta and protein kinase A at Thr212 and Ser214 generates the Alzheimer-specific epitope of antibody AT100 and requires a paired-helical-filament-like conformation. European journal of biochemistry / FEBS 252(3): 542-52.(1998).
[34] Moore AH, O'Banion MK. Neuroinflammation and anti-inflammatory therapy for Alzheimer's disease. Adv Drug Deliv Rev 54(12): 1627-56.(2002).
[35] Gitter BD, Cox LM, Rydel RE, May PC. Amyloid beta peptide potentiates cytokine secretion by interleukin-1 beta-activated human astrocytoma cells. Proceedings of the National Academy of Sciences of the United States of America 92(23): 10738-41.(1995).
[36] Millington C, Sonego S, Karunaweera N, Rangel A, Aldrich-Wright JR, Campbell IL*, et al.* Chronic neuroinflammation in Alzheimer's disease: new perspectives on animal models and promising candidate drugs. BioMed research international 2014: 309129.(2014).
[37] Breitner JC. The role of anti-inflammatory drugs in the prevention and treatment of Alzheimer's disease. Annual review of medicine 47: 401-11.(1996).
[38] Bauer J, Strauss S, Schreiter-Gasser U, Ganter U, Schlegel P, Witt I*, et al.* Interleukin-6 and alpha-2-macroglobulin indicate an acute-phase state in Alzheimer's disease cortices. FEBS letters 285(1): 111-4.(1991).
[39] Selkoe DJ. Alzheimer's disease is a synaptic failure. Science 298(5594): 789-91.(2002).
[40] Ashe KH. Learning and memory in transgenic mice modeling Alzheimer's disease. Learn Mem 8(6): 301-8.(2001).
[41] Martin SJ, Grimwood PD, Morris RG. Synaptic plasticity and memory: an evaluation of the hypothesis. Annu Rev Neurosci 23: 649-711.(2000).
[42] Caroni P, Donato F, Muller D. Structural plasticity upon learning: regulation and functions. Nature reviews Neuroscience 13(7): 478-90.(2012).
[43] Morris RG, Garrud P, Rawlins JN, O'Keefe J. Place navigation impaired in rats with hippocampal lesions. Nature 297(5868): 681-3.(1982).
[44] Belluti F, Rampa A, Piazzi L, Bisi A, Gobbi S, Bartolini M*, et al.* Cholinesterase inhibitors: xanthostigmine derivatives blocking the acetylcholinesterase-induced beta-amyloid aggregation. Journal of medicinal chemistry 48(13): 4444-56.(2005).
[45] Bartolini M, Bertucci C, Cavrini V, Andrisano V. beta-Amyloid aggregation induced by human acetylcholinesterase: inhibition studies. Biochemical pharmacology 65(3): 407-16.(2003).
[46] Morris M, Maeda S, Vossel K, Mucke L. The many faces of tau. Neuron 70(3): 410-26.(2011).
[47] Selkoe D, Mandelkow E, Holtzman D. Deciphering Alzheimer disease. Cold Spring Harb Perspect Med 2(1): a011460.(2012).
[48] Hardy J, Selkoe DJ. The amyloid hypothesis of Alzheimer's disease: progress and problems on the road to therapeutics. Science 297(5580): 353-6.(2002).
[49] Munoz-Torrero D. Complexity against complexity: multitarget drugs. Current medicinal chemistry 20(13): 1621-2.(2013).

Figure 1

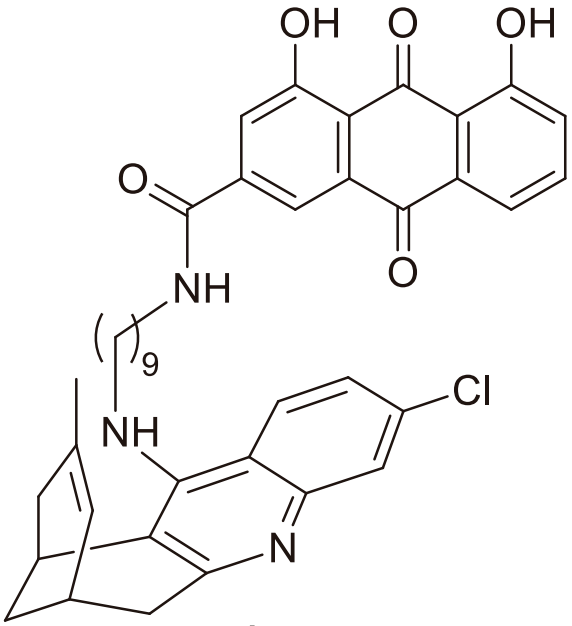

(+)-**1**

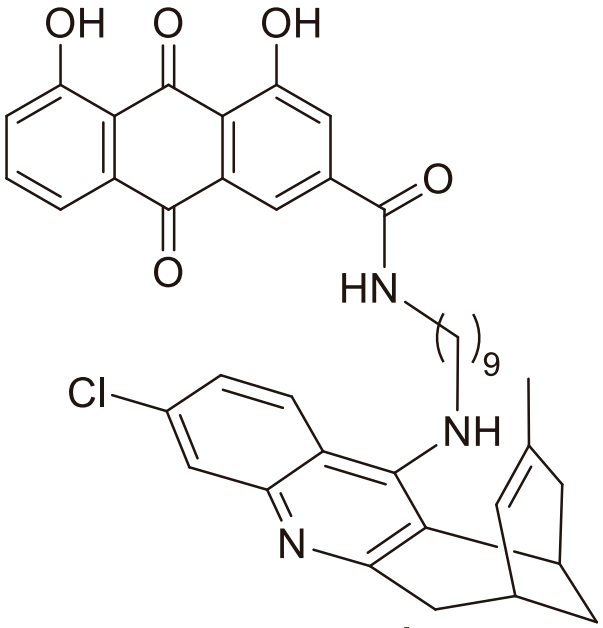

(–)-**1**

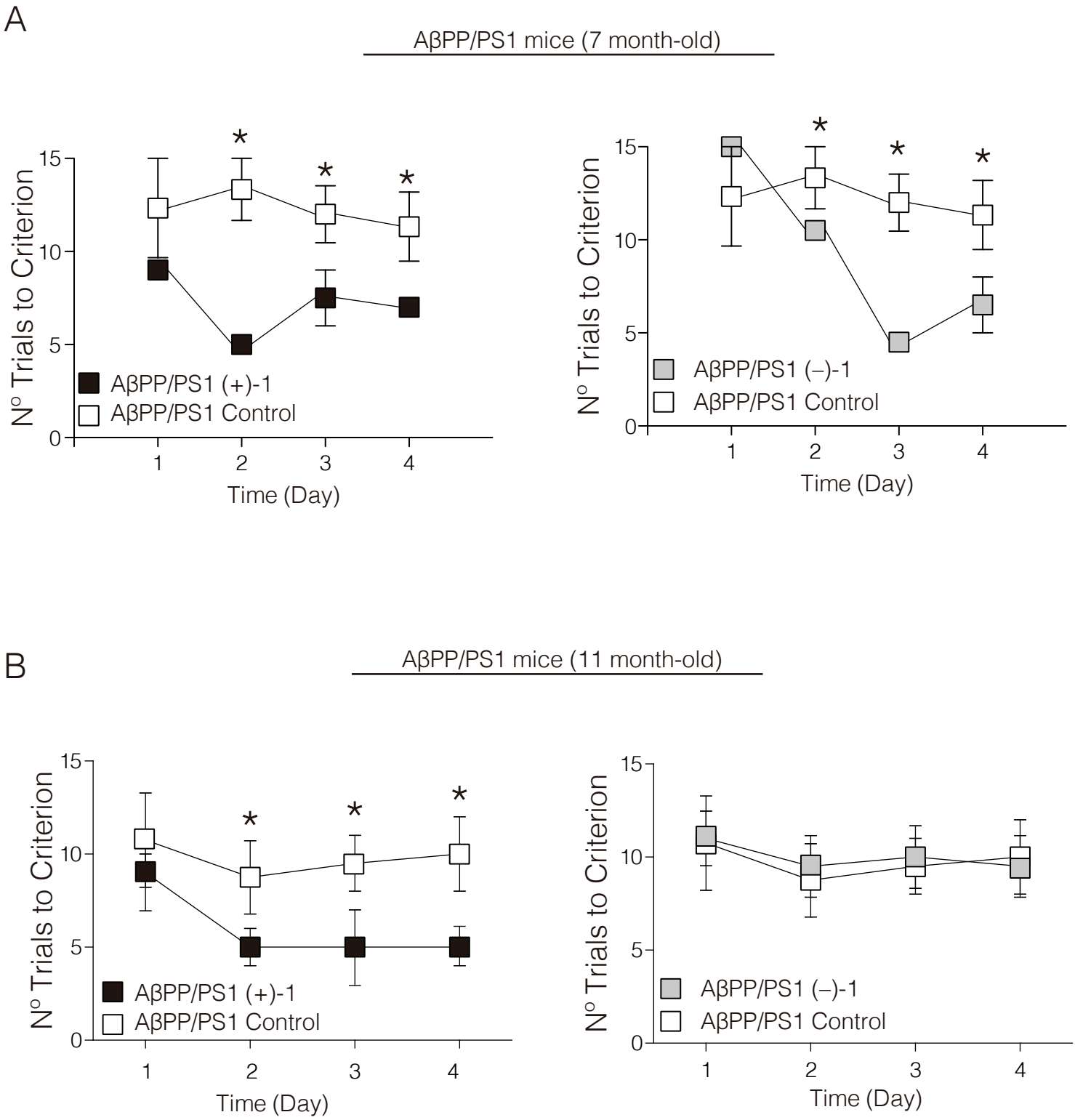
A
AβPP/PS1 mice (7 month-old)
N° Trials to Criterion
15
10
5
0
1
2
3
4
Time (Day)
AβPP/PS1 (+)-1
AβPP/PS1 Control
AβPP/PS1 (–)-1
AβPP/PS1 Control
*
B
AβPP/PS1 mice (11 month-old)

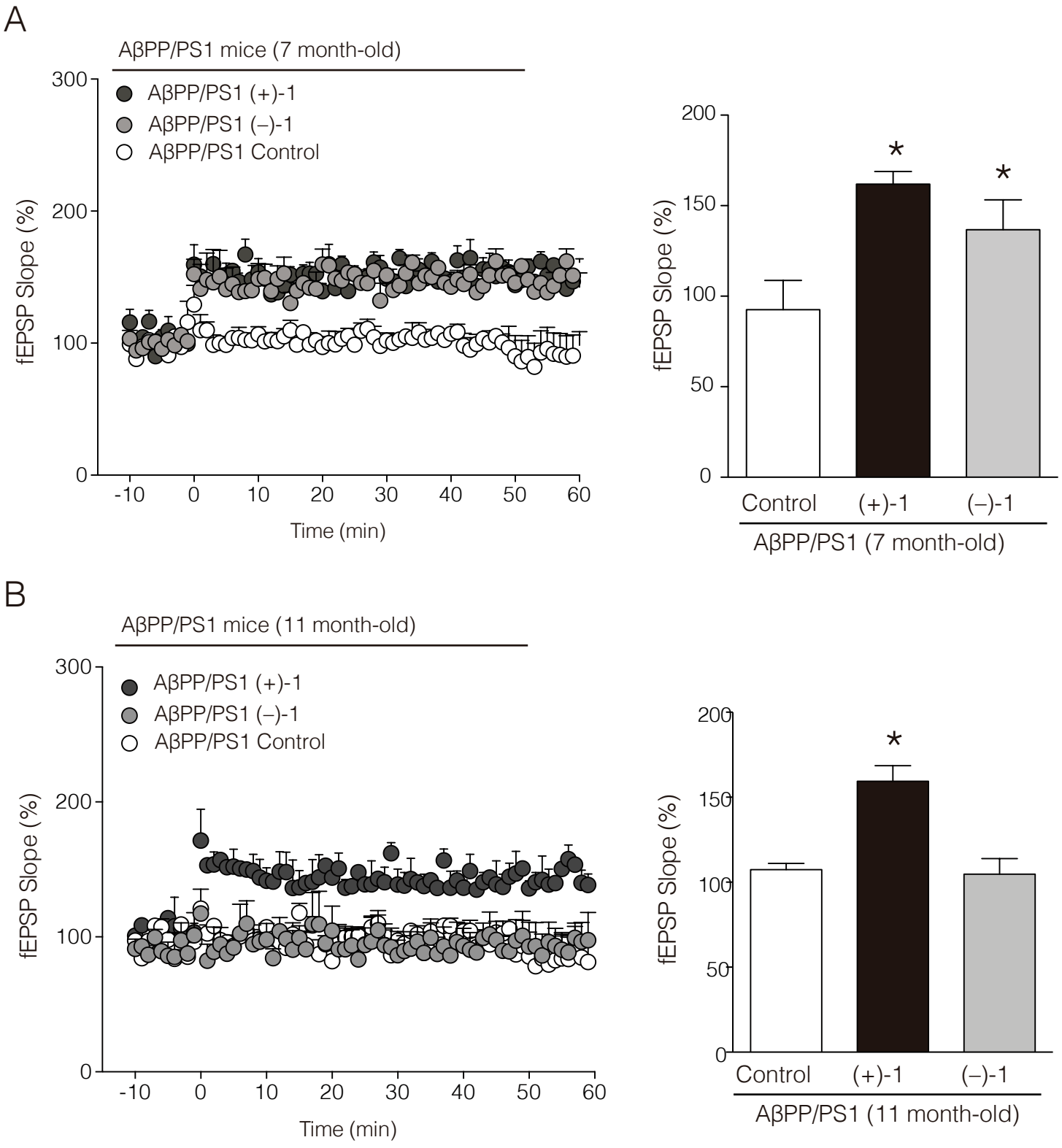
A
AβPP/PS1 mice (7 month-old)
AβPP/PS1 (+)-1
AβPP/PS1 (–)-1
AβPP/PS1 Control
fEPSP Slope (%)
Time (min)
Control
(+)-1
(–)-1
AβPP/PS1 (7 month-old)
B
AβPP/PS1 mice (11 month-old)
AβPP/PS1 (+)-1
AβPP/PS1 (–)-1
AβPP/PS1 Control
fEPSP Slope (%)
Time (min)
Control
(+)-1
(–)-1
AβPP/PS1 (11 month-old)

A

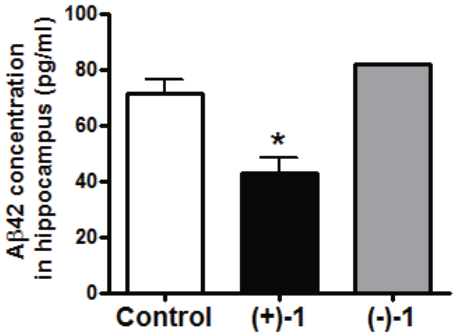
Aβ42 concentration in hippocampus (pg/ml)
100
80
60
40
20
0
*
Control
(+)-1
(-)-1

B

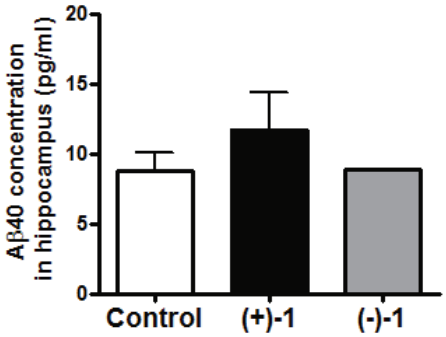
Aβ40 concentration in hippocampus (pg/ml)
20
15
10
5
0
Control
(+)-1
(-)-1

C

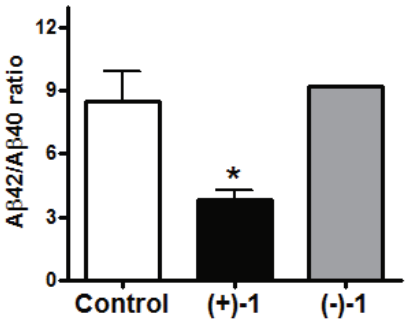
Aβ42/Aβ40 ratio
12
9
6
3
0
*
Control
(+)-1
(-)-1

Figure 5

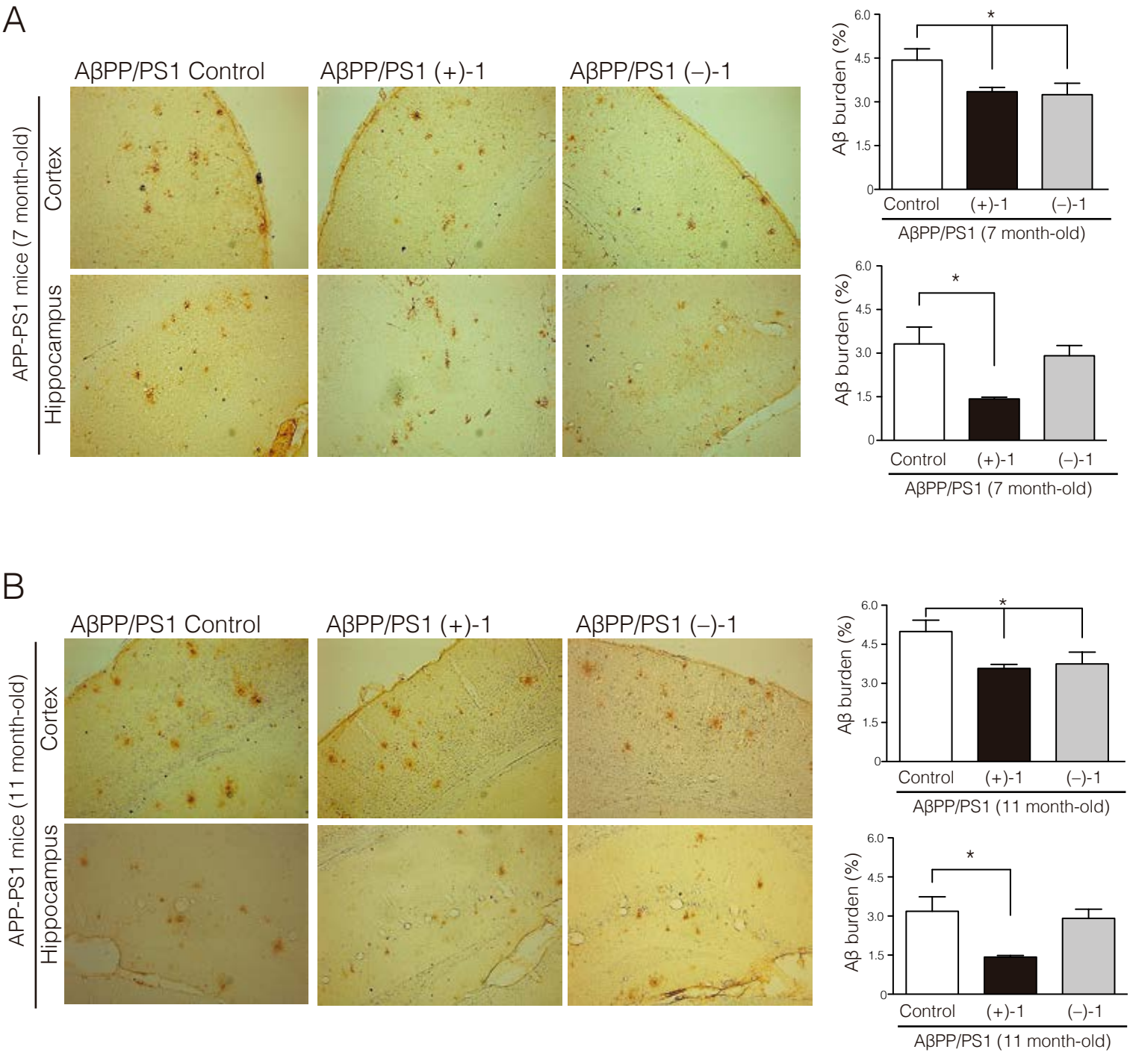
A
AβPP/PS1 Control
AβPP/PS1 (+)-1
AβPP/PS1 (–)-1
APP-PS1 mice (7 month-old)
Cortex
Hippocampus
Aβ burden (%)
6.0
4.5
3.0
1.5
0
*
Control
(+)-1
(–)-1
AβPP/PS1 (7 month-old)
B
AβPP/PS1 Control
AβPP/PS1 (+)-1
AβPP/PS1 (–)-1
APP-PS1 mice (11 month-old)
Cortex
Hippocampus
Aβ burden (%)
Control
(+)-1
(–)-1
AβPP/PS1 (11 month-old)

Figure 6

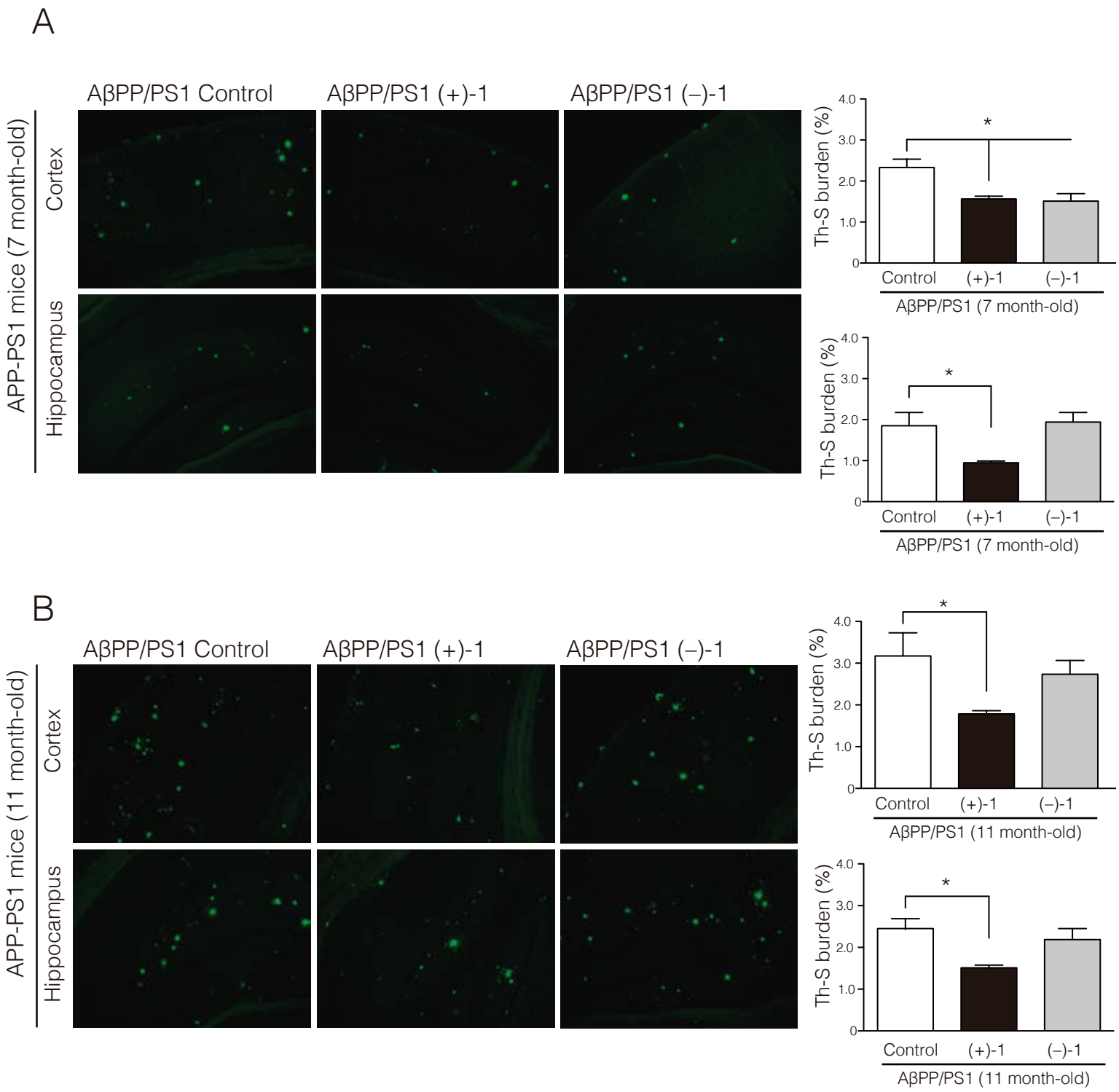
A
AβPP/PS1 Control
AβPP/PS1 (+)-1
AβPP/PS1 (–)-1
APP-PS1 mice (7 month-old)
Cortex
Hippocampus
Th-S burden (%)
4.0
3.0
2.0
1.0
0
*
Control
(+)-1
(–)-1
AβPP/PS1 (7 month-old)
B
AβPP/PS1 Control
AβPP/PS1 (+)-1
AβPP/PS1 (–)-1
APP-PS1 mice (11 month-old)
Cortex
Hippocampus
Th-S burden (%)
Control
(+)-1
(–)-1
AβPP/PS1 (11 month-old)

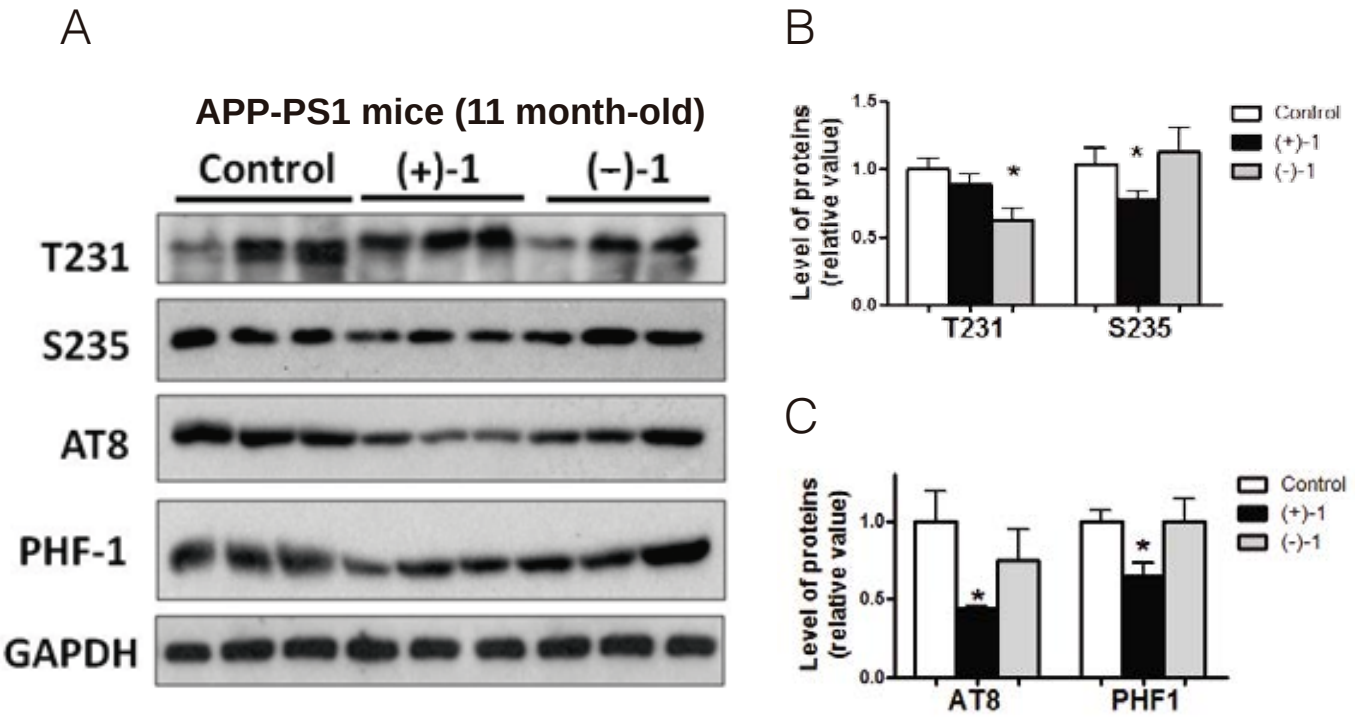
A
APP-PS1 mice (11 month-old)
Control
(+)-1
(−)-1
T231
S235
AT8
PHF-1
GAPDH
B
Level of proteins (relative value)
1.5
1.0
0.5
0.0
*
*
T231
S235
Control
(+)-1
(-)-1
C
Level of proteins (relative value)
1.0
0.5
0.0
*
*
AT8
PHF1
Control
(+)-1
(-)-1

Figure 8

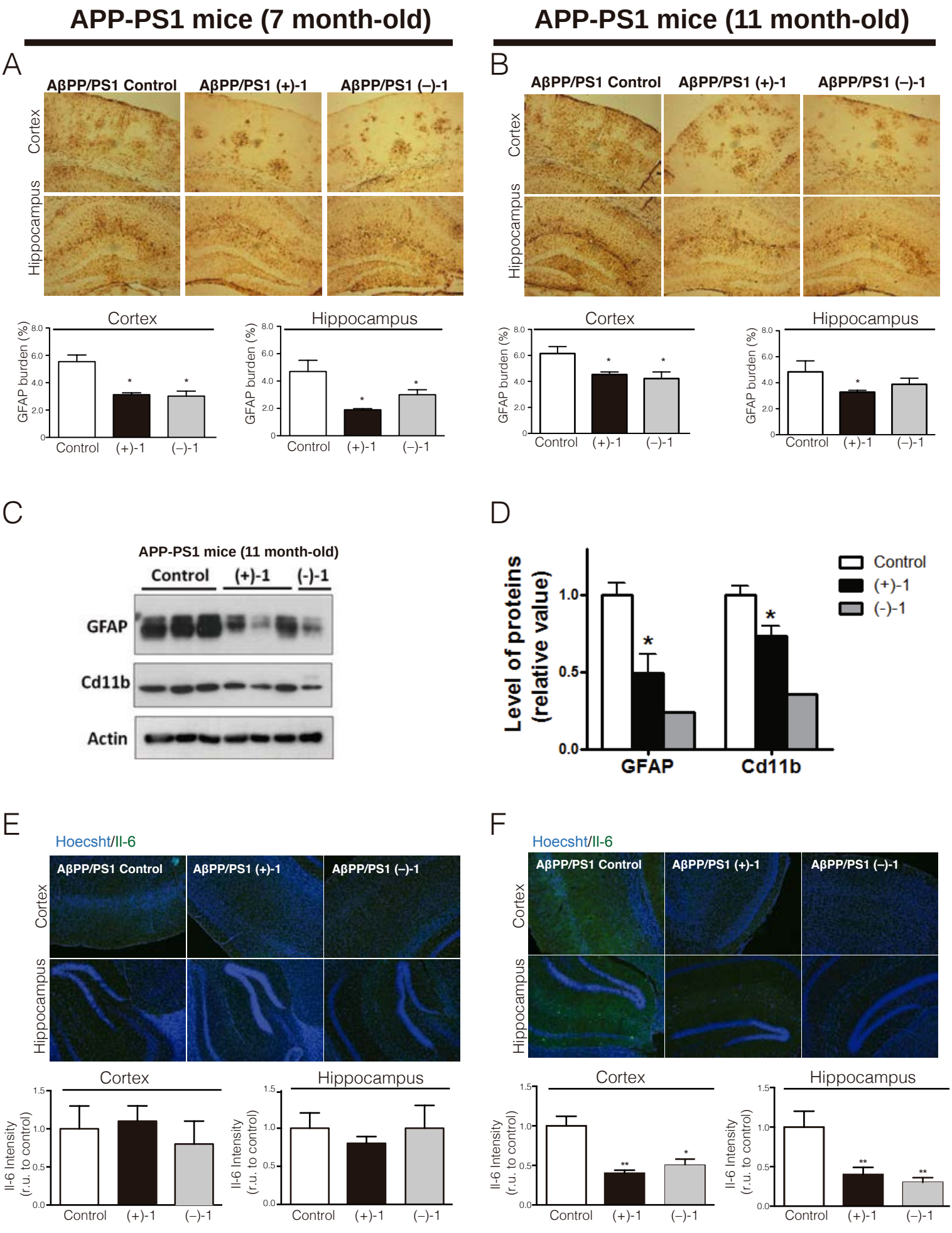
APP-PS1 mice (7 month-old)
APP-PS1 mice (11 month-old)
A
B
AβPP/PS1 Control
AβPP/PS1 (+)-1
AβPP/PS1 (–)-1
Cortex
Hippocampus
GFAP burden (%)
Control
(+)-1
(–)-1
C
APP-PS1 mice (11 month-old)
Control
(+)-1
(-)-1
GFAP
Cd11b
Actin
D
Level of proteins (relative value)
Control
(+)-1
(-)-1
GFAP
Cd11b
E
F
Hoecsht/Il-6
Il-6 Intensity (r.u. to control)

Figure 9

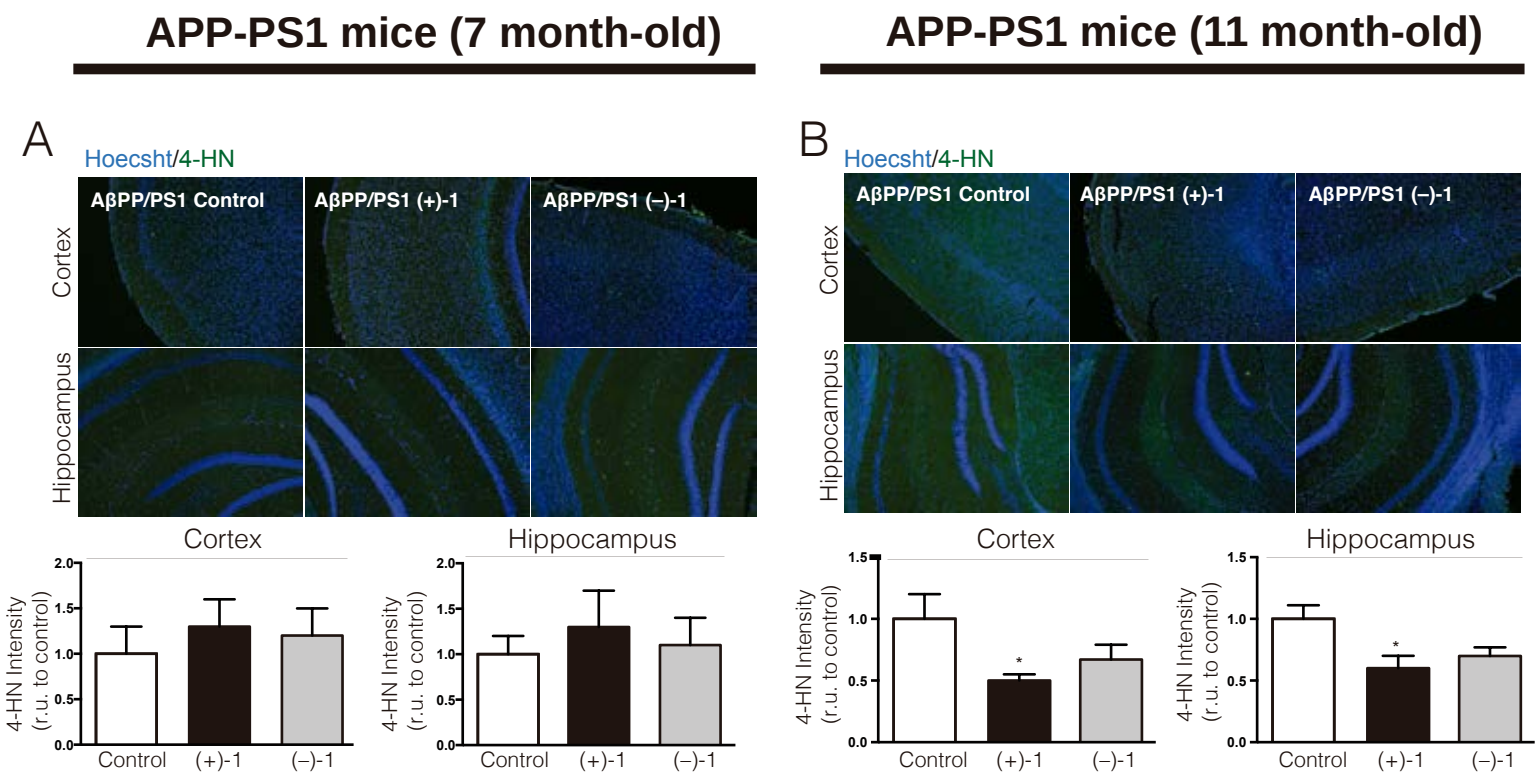
APP-PS1 mice (7 month-old)
APP-PS1 mice (11 month-old)
A
B
Hoecsht/4-HN
AβPP/PS1 Control
AβPP/PS1 (+)-1
AβPP/PS1 (–)-1
Cortex
Hippocampus
4-HN Intensity (r.u. to control)
Control
(+)-1
(–)-1
*

Figure 10

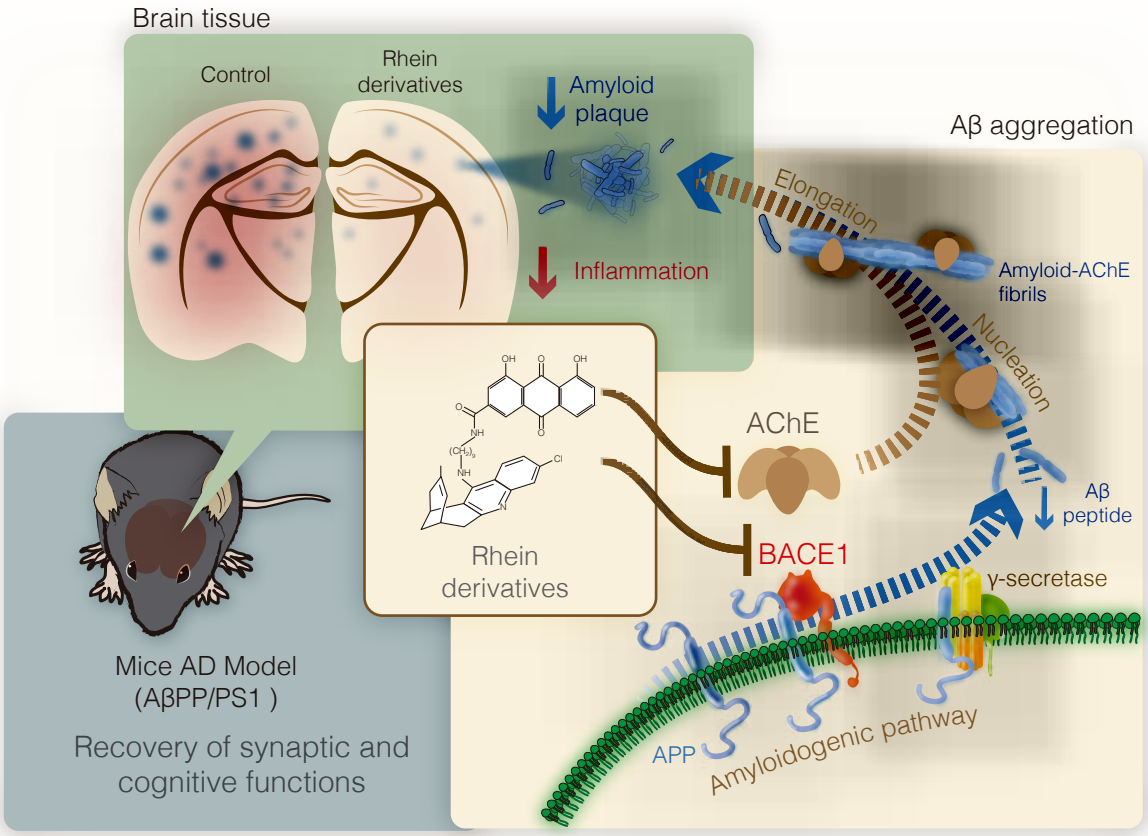
Brain tissue
Control
Rhein derivatives
Amyloid plaque
Inflammation
Aβ aggregation
Elongation
Amyloid-AChE fibrils
Nucleation
AChE
Aβ peptide
BACE1
γ-secretase
APP
Amyloidogenic pathway
Rhein derivatives
Mice AD Model (AβPP/PS1)
Recovery of synaptic and cognitive functions

5. C.

J. Med. Chem. **2015**, *58*, 6018

Novel levetiracetam derivatives that are effective against the Alzheimer-like phenotype in mice: Synthesis, *in vitro*, *ex vivo* and *in vivo* efficacy studies

Irene Sola,[†,‡] *Ester Aso,*[§,#,‡] *Daniela Frattini,*[†] *Irene López-González,* [§,#] *Alba Espargaró,*[¶] *Raimon Sabaté,*[¶] *Ornella Di Pietro,*[†] *F. Javier Luque,*[//] *M. Victòria Clos,*[⊥] *Isidro Ferrer,*[*,§,#] *and Diego Muñoz-Torrero*[*,†]

[†] Laboratori de Química Farmacèutica (Unitat Associada al CSIC), Facultat de Farmàcia, and Institut de Biomedicina (IBUB), Universitat de Barcelona, Av. Joan XXIII 27-31, E-08028, Barcelona, Spain

[§] Institut de Neuropatologia, Servei d'Anatomia Patològica, IDIBELL-Hospital Universitari de Bellvitge, Universitat de Barcelona, L'Hospitalet de Llobregat, Spain

[#] CIBERNED, Centro de Investigación Biomédica en Red de Enfermedades Neurodegenerativas, Instituto Carlos III, Spain

[¶] Departament de Fisicoquímica, Facultat de Farmàcia, and Institut de Nanociència i Nanotecnologia (IN^{2}UB), Universitat de Barcelona, Barcelona, Spain

[||]Departament de Fisicoquímica, Facultat de Farmàcia (Campus Torribera), and IBUB, Universitat de Barcelona, Prat de la Riba 171, E-08921, Santa Coloma de Gramenet, Spain

[⊥] Departament de Farmacologia, de Terapèutica i de Toxicologia, Institut de Neurociències, Universitat Autònoma de Barcelona, E-08193, Bellaterra, Barcelona, Spain

ABSTRACT: We have synthesized a series of heptamethylene-linked levetiracetam–huprine and levetiracetam–(6-chloro)tacrine hybrids to hit amyloid, tau and cholinergic pathologies as well as β-amyloid (Aβ)-induced epileptiform activity, some of the mechanisms that eventually lead to cognitive deficits in Alzheimer's disease patients. These hybrids are potent inhibitors of human acetylcholinesterase and butyrylcholinesterase *in vitro* and moderately potent Aβ42 and tau anti-aggregating agents in a simple *E. coli* model of amyloid aggregation. *Ex vivo* determination of the brain acetylcholinesterase inhibitory activity of these compounds after intraperitoneal injection to C57BL6J mice has demonstrated their ability to enter the brain. The levetiracetam−huprine hybrid **10** significantly reduced the incidence of epileptic seizures, cortical amyloid burden and neuroinflammation in APP/PS1 mice after a four-week treatment with a 5 mg/kg dose. Moreover, the hybrid **10** rescued transgenic mice from cognitive deficits, thereby emerging as an interesting disease-modifying anti-Alzheimer drug candidate.

INTRODUCTION

Alzheimer's disease (AD) is the most prevalent neurodegenerative disorder. It affects over 35 million people worldwide and this figure will grow exponentially in the upcoming years along with demographic changes.[1] Currently there exists no therapy that can halt or slow AD progression, so that this disease inexorably leads to the death of the patient. Consequently, the increasing prevalence of AD is being accompanied with increasing mortality figures, in sharp contrast to other major causes of death such as cardiovascular disease or cancer, for which the number of associated deaths has been decreasing in the past decade.[2]

Only five drugs have been approved so far for the treatment of AD, namely the acetylcholinesterase (AChE) inhibitors tacrine, donepezil, rivastigmine and galantamine and the glutamate NMDA receptor antagonist memantine.[3] These drugs were developed to alleviate the cognitive and functional decline associated to neurotransmitter deficits that appear long after the initiation of the neurodegenerative process, and, hence, they are regarded as mainly symptomatic treatments. An efficient management of AD relies heavily on the development of novel drugs that can address the earliest disease mechanisms as well as on the parallel discovery of suitable biomarkers and techniques that allow an early diagnosis, thereby enabling the use of putative disease-modifying drugs in the most appropriate time. i.e. when neurodegeneration is not too widespread. Two proteins, β-amyloid peptide (Aβ) and tau, are widely thought to be at the root of the pathogenesis of AD, even though it is not clear whether or not their appearance is a cause or a consequence of the disease. Particularly, huge economic and research investments have focused on the development of disease-modifying drug candidates that address the biology of the 39–43 amino acid peptide Aβ.[4,5] However these endeavors have so far failed to derive any new approved drug.[3] Indeed, it has been suggested that the formation and subsequent aggregation of

Aβ might not be the sole cause of the disease but just one of the main components of a pathological network, where hyperphosphorylation and aggregation of protein tau, synaptic dysfunction or neuroinflammation, among others, would be also key players.[6]

This conception of AD has prompted the development of an important number of compounds purposely designed to simultaneously hit several of the key biological targets or events of the AD pathological network.[7–19] In most cases, anti-Alzheimer multitarget compounds are designed to hit Aβ formation and/or aggregation and the enzyme AChE,[20,21] which besides its cholinergic function, has been reported to be able to interact with Aβ, thereby promoting its aggregation.[22,23]

It has been recently suggested that aberrant neuronal network activity might be another key component of the AD network,[24] which has been associated to elevated levels of Aβ and causally linked to Aβ-induced synaptic and cognitive deficits.[25] Indeed, the incidence of epileptic seizures or epileptiform activity is increased in AD patients relative to the general population,[24,26] especially in those individuals with early-onset AD, which is characterized by mutations in some deterministic genes encoding proteins involved in the production of Aβ, namely amyloid precursor protein (APP) and the enzymes involved in the APP cleavage presenilin 1 and presenilin 2. Increased incidence of epileptic seizures also occurs in other conditions which are associated with elevated levels of Aβ such as patients with Down syndrome, which feature three copies of chromosome 21, where the APP gene is located, and the incidence is still higher in individuals with Down syndrome that develop AD.[27] Also, transgenic mouse models of AD that overexpress human mutated APP show epileptiform activity along with synaptic and cognitive deficits.[28] Very interestingly, chronic treatment with the antiepileptic drug levetiracetam (**1**, Figure 1) can effectively suppress aberrant network activity and improve memory performance in patients with amnestic mild cognitive impairment (aMCI)[29] as well as in hAPPJ20 and

APP/PS1 mouse models of AD,[30,31] thereby highlighting the critical therapeutic potential of targeting excess neuronal network activity, especially in combination with other copathogenic factors that fuel the progression of AD such as Aβ and tau aggregation and accumulation.[32]

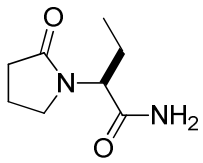

1, **levetiracetam**

Figure 1. Structure of levetiracetam.

We have recently developed several structural families of anti-Alzheimer hybrid compounds that contain the structure of 6-chlorotacrine (9-amino-6-chloro-1,2,3,4-tetrahydroacridine) or the high affinity AChE inhibitor huprine Y,[33–36] structurally related to tacrine, which exhibit a common multitarget biological profile encompassing inhibition of the aggregation of Aβ42 and tau and inhibition of both cholinesterases, i.e. AChE and butyrylcholinesterase (BChE), apart from modulation of other specific targets or pathological events.[37–39]

Herein, we describe the synthesis and biological evaluation of a series of hybrid compounds that feature the 2-(2-oxopyrrolidin-1-yl)butyramide moiety of levetiracetam linked to a tacrine, 6-chlorotacrine or huprine Y unit as novel multitarget anti-Alzheimer leads with potential to modify AD progression. The biological profiling of the novel compounds includes: i) the *in vitro* assessment of their human AChE and BChE inhibitory activity; ii) the evaluation of their inhibitory activity against both Aβ42 and tau aggregation in intact *Escherichia coli* cells overexpressing these proteins, as a simple *in vivo* model of amyloid aggregation; iii) the *ex vivo* evaluation of their brain AChE inhibitory activity after intraperitoneal injection in C57BL6J

mice, as an indirect proof of their brain penetration; iv) a preliminary assessment of their acute toxicity in C57BL6J mice; and v) the *in vivo* efficacy studies after chronic administration to transgenic APP/PS1 mice, a well-established mouse model of AD, encompassing the evaluation of their effect on cognition, spontaneous epileptic seizures, cortical soluble Aβ40 and Aβ42 levels, cortical Aβ burden, and gliosis around Aβ plaques.

RESULTS AND DISCUSSION

Chemistry. In this work, we envisaged first the straightforward synthesis of hybrids (±)-**5** and (±)-**6** (Scheme 1), which bear a tacrine or a 6-chlorotacrine unit linked to the racemic form of **1** (etiracetam), as well as the synthesis of the enantiopure hybrids (*S*)-**5**, featuring the (*S*)-eutomer form of etiracetam as an antiepileptic drug (levetiracetam), and its enantiomer (*R*)-**5** (Scheme 1), to assess potential enantioselective interactions with the targets to be evaluated *in vitro*, due to the levetiracetam moiety. The eutomer for AChE inhibition of huprine Y and other huprine-based hybrids previously developed in our group is the (7*S*,11*S*)-enantiomer, whereas the opposite trend or no enantioselectivity has been found for their interaction with other targets of interest such as BChE or Aβ and tau aggregation.[34,37,40] In this light, we also planned the synthesis of enantiopure levetiracetam–huprine hybrids **10** and **11** (Scheme 2), featuring the (*S*)-form of **1** and either a (7*S*,11*S*)- or (7*R*,11*R*)-huprine moiety. In all cases, an heptamethylene chain was chosen as the linker between the two pharmacophoric moieties because it should enable the hybrids to span the whole length of the active site gorge of AChE, one of their putative targets, thereby leading to high inhibitory potencies, as it has been reported for a number of tacrine-based dimeric and hybrid compounds.[41,42] Indeed, other heptamethylene-linked

huprine-based hybrids recently developed in our group have been consistently found to be among the most potent AChE inhibitors of the corresponding structural families.[37,40]

Scheme 1. Synthesis of the levetiracetam–tacrine hybrids (±)-5, (*S*)-5, (*R*)-5 and (±)-6[a]

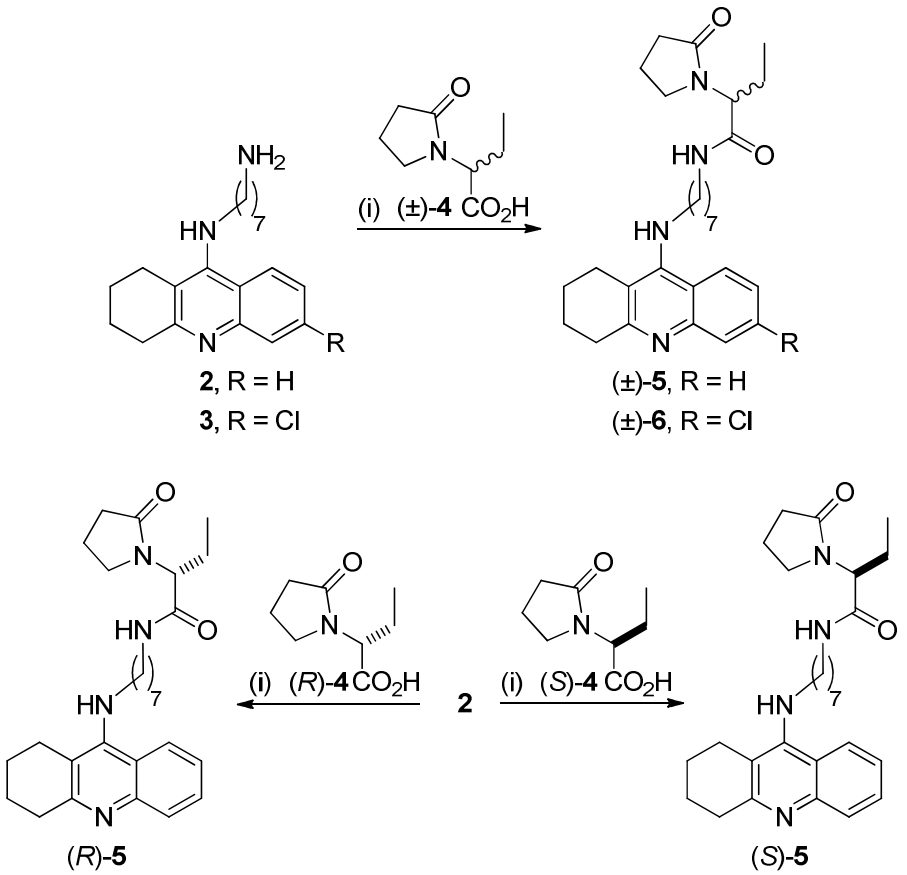

[a]Reagents and conditions: (i) (±)-**4**, (*S*)-**4** or (*R*)-**4** (1 equiv), $ClCO_2Et$ (1 equiv), Et_3N (2 equiv), CH_2Cl_2, 0 ºC, 30 min; then, amine **2** or **3** (1 equiv), CH_2Cl_2, rt, 3 days, 93% [(±)-**5**], 60% [(*S*)-**5**], 27% [(*R*)-**5**], 78% [(±)-**6**].

The synthesis of hybrids (±)-**5** and (±)-**6** was carried out by treatment of the readily available racemic 2-(2-oxopyrrolidin-1-yl)butyric acid, (±)-**4**,[43] with 1 equiv of ethyl chloroformate and 2 equiv of Et_3N in CH_2Cl_2, followed by reaction of the resulting mixed anhydride with 1 equiv of

the known 7-aminoheptyltacrines **2**[44] and **3**[45] at room temperature for 3 days, followed by silica gel column chromatography purification of the crude products (Scheme 1).

Enantiopure carboxylic acids (*S*)-**4** or (*R*)-**4** were prepared through a methodology previously developed in our group, based on the resolution of the racemic acid (±)-**4** through formation and silica gel column chromatography separation of its diastereomeric esters with (*S*)-*N*-phenylpantolactam followed by separate hydrolysis with LiOH / H_2O_2 in THF.[43] Coupling of aminoheptyltacrine **2** with carboxylic acids (*S*)-**4** and (*R*)-**4** under the same reaction conditions used for the racemic compound, afforded in moderate yields the enantiopure hybrids (*S*)-**5** and (*R*)-**5**, respectively (Scheme 1).

The synthesis of enantiopure hybrids **10** and **11** was undertaken starting from enantiopure huprines (7*S*,11*S*)-**7** and (7*R*,11*R*)-**7**, which are readily available even at multigram amounts by chromatographic resolution.[33,46] Alkylation of (7*S*,11*S*)-**7** and (7*R*,11*R*)-**7** with 7-bromoheptanenitrile in the presence of NaOH in DMSO afforded in moderate yields the novel enantiopure nitriles (7*S*,11*S*)-**8** and (7*R*,11*R*)-**8**, which were subsequently reduced to the novel amines (7*S*,11*S*)-**9** and (7*R*,11*R*)-**9** upon treatment with $LiAlH_4$ in Et_2O (Scheme 2). Treatment of the mixed anhydride derived from carboxylic acid (*S*)-**4** and ethylchloroformate with amines (7*S*,11*S*)-**9** and (7*R*,11*R*)-**9** afforded the enantiopure levetiracetam–huprine hybrids (2*S*,7"'*S*,11"'*S*)-**10** and (2*S*,7"'*R*,11"'*R*)-**11** in moderate yields, after silica gel column chromatography purification.

Scheme 2. Synthesis of the levetiracetam–huprine hybrids (2*S*,7'''*S*,11'''*S*)-10 and (2*S*,7'''*R*,11'''*R*)-11[a]

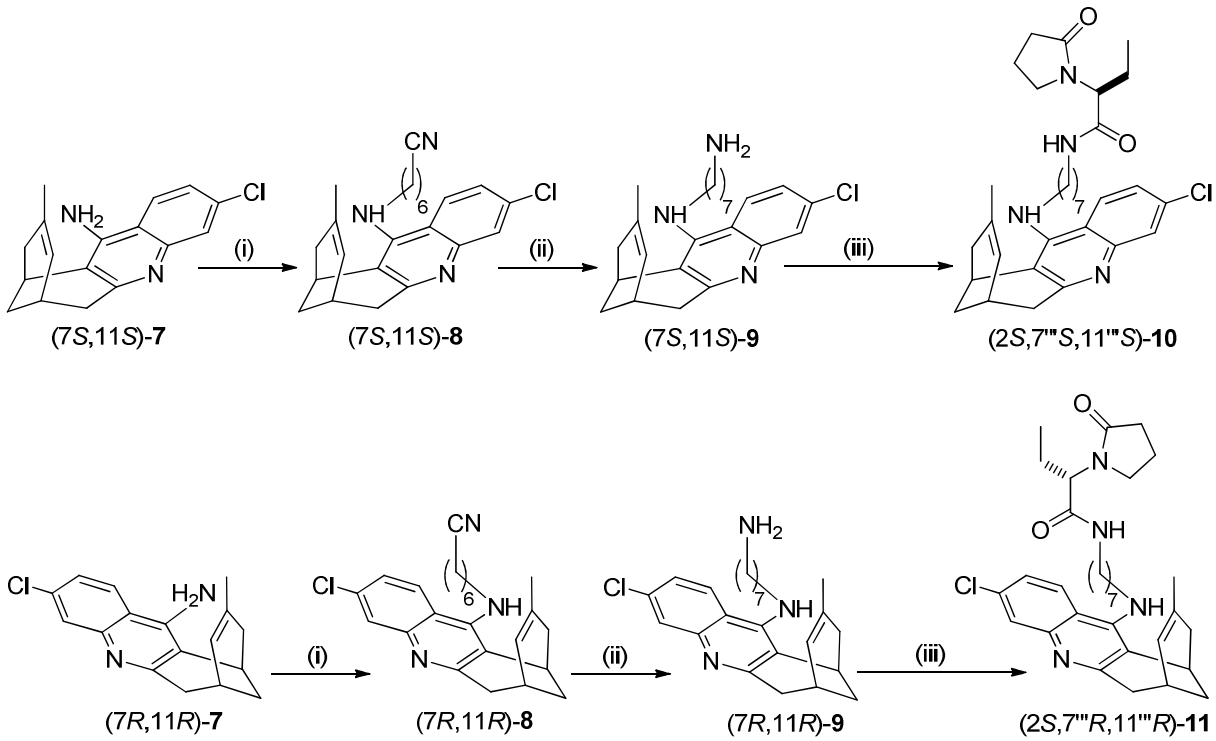

[a]Reagents and conditions: (i) NaOH (3.3 equiv) 4 Å molecular sieves, DMSO, rt, 2 h; then 7-bromoheptanenitrile (1.2 equiv), DMSO, rt, overnight, 52% [(7*S*,11*S*)-**8**], 55% [(7*R*,11*R*)-**8**]; (ii) $LiAlH_4$ (6 equiv), Et_2O, 0 ºC to rt, 20 h at rt, 91% [(7*S*,11*S*)-**9**], 45% [(7*R*,11*R*)-**9**]; (iii) (*S*)-**4** (1 equiv), $ClCO_2Et$ (1 equiv), Et_3N (2 equiv), CH_2Cl_2, 0 ºC, 30 min; then, amine (7*S*,11*S*)-**9** or (7*R*,11*R*)-**9** (1 equiv), CH_2Cl_2, rt, 3 days, 30% (**10**), 56% (**11**).

The novel levetiracetam-based hybrids were converted into their hydrochloride salts for their chemical characterization and biological profiling.

***In Vitro* Inhibition of Human Cholinesterases**. Together with AChE, BChE is partly responsible for the hydrolysis of the neurotransmitter acetylcholine. Unlike AChE, whose brain levels are significantly reduced when AD progresses, the levels of BChE remain the same or may

be even increased.[47] Thus, dual inhibition of AChE and BChE is increasingly pursued in the search for novel AD treatments.[48] Accordingly, the inhibitory activity of the novel levetiracetam-based hybrids **5**, **6**, **10** and **11** and of the reference compounds (*S*)-**1**, tacrine, 6-chlorotacrine and (7*S*,11*S*)- and (7*R*,11*R*)-huprine Y against human recombinant AChE (hAChE) and human serum BChE (hBChE) was evaluated by the method of Ellman *et al.*[49] The marketed anti-Alzheimer reversible AChE inhibitors donepezil and galantamine were also evaluated as reference compounds.

All the levetiracetam-based hybrids turned out to be very potent inhibitors of hAChE, with IC_{50} values in the low nanomolar range (Table 1). Indeed, in agreement with the expected binding of these hybrids along the active site gorge of AChE, the hybridization strategy led to increased hAChE inhibitory potencies of hybrids **5**, **6** and **11** relative to their parent compounds tacrine, 6-chlorotacrine, (7*R*,11*R*)-huprine Y, and levetiracetam, which, to our surprise, exhibited an outstanding two-digit nanomolar hAChE inhibitory activity (Table 1). The sole exception was the levetiracetam–huprine hybrid **10**, which, despite its remarkable IC_{50} value of 4.2 nM, was still 6-fold less potent than its highly potent parent compound (7*S*,11*S*)-huprine Y, as we have also found for other (7*S*,11*S*)-huprine Y-based hybrids.[37,40] All of the hybrids were found to be much more potent than galantamine and two of them, **6** and **10**, also 2–3-fold more potent than donepezil. The order of hAChE inhibitory potencies found for the hybrids (**6** ≈ **10** > **5** > **11**) is consistent with the known positive effect of the chlorine atom at position 6 of the tacrine unit,[50,51] the levetiracetam–6-chlorotacrine hybrid **6** being 10-fold more potent than the levetiracetam–tacrine hybrid **5**, and with the higher potency of (7*S*,11*S*)-huprine derivatives relative to the (7*R*,11*R*)-counterparts,[34,37,40] hybrid **10** being 13-fold more potent than **11**. Regarding the influence of the stereochemistry of the levetiracetam moiety on hAChE inhibitory

activity, the levetiracetam–tacrine hybrid (*R*)-**5** was found to be 3-fold more potent than its enantiomer.

Like the reference compounds, including **1**, all of the novel levetiracetam-based hybrids were also found to be potent hBChE inhibitors, exhibiting two- to three-digit nanomolar IC_{50} values (Table 1), and hence, displaying an interesting dual AChE / BChE inhibitory activity. The known SAR trends for BChE inhibition regarding the presence of a chlorine atom at position 6 of the tacrine unit or at the equivalent position 3 of the huprine moiety and the enantiopreference of the huprine moiety are just the opposite than for AChE inhibition. Indeed, it is well-known that introduction of a chlorine atom at position 6 of the tacrine unit is somewhat detrimental for the interaction with BChE due to steric hindrance effects at the enzyme active site[52,53] and that (7*R*,11*R*)-huprine derivatives are more potent hBChE inhibitors than their (7*S*,11*S*)-counterparts.[34,37,40] Thus, the order of potencies for hBChE inhibition of the levetiracetam-based hybrids (**5** > **11** > **6** > **10**) is consistent with the expected SAR trends, with the levetiracetam–tacrine hybrid **5** being 4-fold more potent than the levetiracetam–6-chlorotacrine hybrid **6**, and with hybrid **11** being 4-fold more potent than **10**. Additionally, it was found that for BChE inhibition the stereochemistry of the levetiracetam moiety did not seem to play a significant role, with hybrids (*S*)-**5** and (*R*)-**5** being roughly equipotent.

Table 1. Inhibitory Activities of the Hydrochlorides of Levetiracetam-Based Hybrids and Reference Compounds toward AChE, BChE and Aβ42, and Tau Aggregation[a]

compd	hAChE IC_{50} (nM)[a]	hBChE IC_{50} (nM)[a]	Aβ42 aggregation (% inhibition)[b]	tau aggregation (% inhibition)[b]
(±)-**5**	30.7 ± 6.9	21.8 ± 0.5	13.8 ± 2.3	12.8 ± 1.2
(*S*)-**5**	89.9 ± 8.3	12.2 ± 1.0	12.6 ± 1.9	14.9 ± 1.6
(*R*)-**5**	26.2 ± 1.7	17.5 ± 3.4	<10[c]	<10[d]
(±)-**6**	3.1 ± 0.2	135 ± 19	24.0 ± 0.9	34.0 ± 1.6
(2*S*,7"'*S*,11"'*S*)-**10**	4.2 ± 0.2	232 ± 9	36.4 ± 2.5	54.1 ± 1.1
(2*S*,7"'*R*,11"'*R*)-**11**	56.0 ± 7.1	58 ± 10	26.0 ± 3.0	49.5 ± 2.8
(*S*)-Levetiracetam	75.7 ± 5.5	241 ± 50	<10[e]	<10[f]
Tacrine	317 ± 15.3	24.5 ± 0.6	<10[g]	<10[g]
6-Chlorotacrine	5.9 ± 0.6	114 ± 4	<10[h]	<10[i]
(7*S*,11*S*)-**7**	0.74 ± 0.06	222 ± 17	22.6 ± 2.9	33.3 ± 2.3
(7*R*,11*R*)-**7**	321 ± 16	170 ± 17	24.2 ± 1.2	31.3 ± 1.0
Donepezil	10.4 ± 0.5	nd[j]	nd[j]	nd[j]
Galantamine	735 ± 95	nd[j]	nd[j]	nd[j]

[a] IC_{50} inhibitory concentration (nM) of human recombinant AChE or human serum BChE. Values are expressed as mean ± standard error of the mean (SEM) of at least three experiments (n=3), each performed in duplicate. [b] % inhibition of Aβ42 and tau aggregation in intact *E. coli* cells with inhibitor at 20 μM. Values are expressed as mean ± SEM of four independent experiments (n=4). [c] 2% inhibition. [d] 8.7% inhibition. [e] 9.1% inhibition. [f] 1.3% inhibition. [g] No inhibiton was observed. [h] 2.3% inhibition. [i] 3.0% inhibition. [j] Not determined.

Binding Mode within hAChE: Docking Studies. A dual site binding of hybrid **10** to hAChE has been suggested by docking calculations (see Experimental Section for details). As expected, the huprine moiety was positioned filling the catalytic site and the tether was aligned along the gorge, whereas the levetiracetam moiety was bound to the peripheral anionic site (PAS), at the

entrance of the active site gorge, filling the space located around Trp286 and Tyr72 (Figure 2). While for PAS binders containing aromatic rings (e.g., propidium) the stacking against Trp286 seems to be the major binding contribution, the analysis of the best poses of **10** suggests that the major contribution to the binding of its levetiracetam moiety comes from Tyr72, since the formation of a hydrogen bond between the hydroxyl group of Tyr72 and the amide NH/C=O groups of this moiety leads to two distinct arrangements in the PAS.

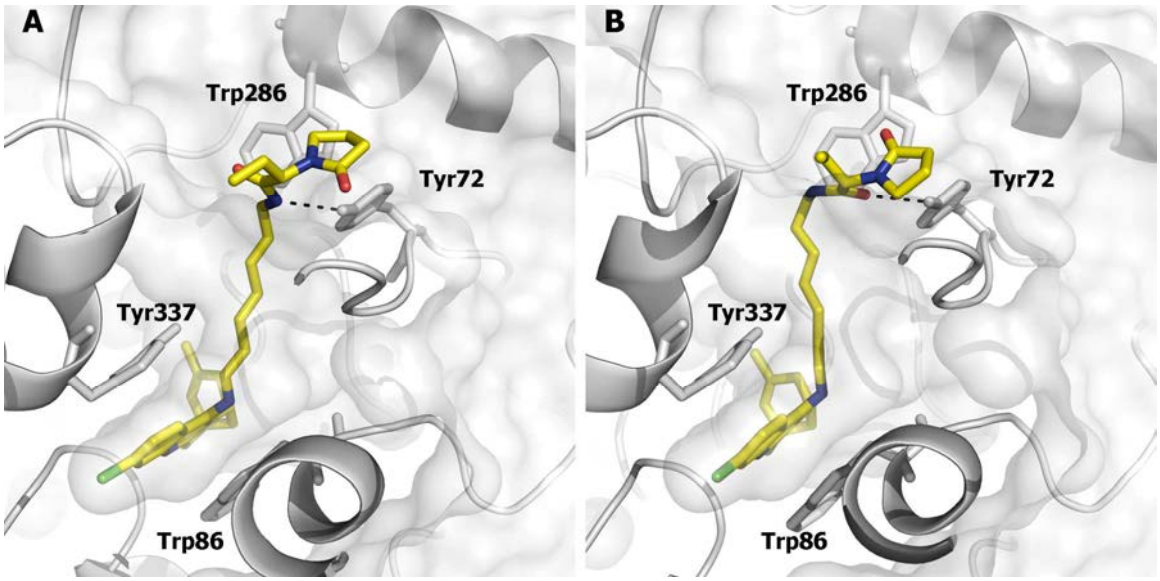

Figure 2. Representation of the binding mode of hybrid **10** in hAChE. The huprine moiety fills the catalytic binding site, and the levetiracetam moiety is bound to the PAS, where the hydroxyl group of Tyr72 can form a hydrogen bond with either the (A) NH or (B) carbonyl group of the amide function.

Inhibition of Aβ42 and Tau Aggregation in Intact *Escherichia coli* Cells. Besides the aggregation of Aβ42, it is also widely accepted that aggregation of another amyloidogenic protein, namely tau protein, plays a pivotal role in AD network. Thus, a dual inhibition of Aβ42 and tau aggregation might be of utmost importance for effectively preventing or halting

neurodegeneration.[54,55] We have recently found that several classes of 6-chlorotacrine- and huprine-based hybrid compounds exhibit such a dual Aβ42 and tau anti-aggregating profile in a simple *in vivo* model of protein aggregation, namely in intact *E. coli* cells that overexpress these proteins.[37–39] To assess whether the novel levetiracetam–tacrine, levetiracetam–6-chlorotacrine and levetiracetam–huprine hybrids shared this dual anti-aggregating profile, they were subjected to the *E. coli* assay, which is based on monitoring the changes in the fluorescence of thioflavin S after *in vivo* staining of the amyloid-containing insoluble inclusion bodies[56] that are formed upon expression and subsequent aggregation of the heterologous proteins in the bacteria.[57]

In contrast with the rather low anti-aggregating activity found for racemic and enantiopure tacrine-based hybrids **5** and **6**, especially in the case of (*R*)-**5**, the levetiracetam–huprine hybrids **10** and **11** exhibited a moderately potent Aβ42 and tau anti-aggregating activity, with percentages of inhibition around 30% and 50%, respectively, at 20 μM (Table 1). These hybrids, and especially **10**, were clearly more potent than all the reference compounds, including both enantiomers of huprine Y, which displayed significant anti-aggregating properties (around 20% and 30% for Aβ42 and tau aggregation, respectively).

Like Aβ, tau seems also to induce synaptic and neuronal network impairments, whereas reduction of tau pathology has been reported to prevent spontaneous epileptiform activity and to rescue hAPP mice from synaptic and cognitive deficits.[58] Thus, the dual effect of some of the novel levetiracetam-based hybrids on amyloid and tau pathology might well complement their expected *in vivo* effects on epileptiform activity and cognition due to the presence of the levetiracetam pharmacophore.

Brain Penetration and Preliminary Acute Toxicity Studies in C57BL6J Mice. An efficient brain penetration is a condition *sine qua non* for central nervous system drugs, including anti-Alzheimer drugs. Hybrid compounds resulting from pharmacophore combination approaches tend to be large molecules with molecular weights often exceeding 500, as it is the case for the levetiracetam–huprine hybrids **10** and **11**, which might challenge their ability to cross cell membranes.[59,60] Therefore, an assessment of the ability of the novel hybrids to cross the blood–brain barrier (BBB) was deemed necessary before progressing into *in vivo* efficacy studies.

To this end, we carried out the *ex vivo* determination of the brain AChE activity at two different times after intraperitoneal (ip) injection of 2.5 mg/kg of the levetiracetam-based hybrids **5**, **6**, **10** and **11** to C57BL6J mice. Ten min after administration of hybrids **5**, **6**, **10** and **11** mouse brain AChE activity had been inhibited by 19%, 31%, 16% and 18% relative to untreated control animals, respectively, whereas the inhibitory activities decreased to 8%, 0%, 7% and 1%, respectively, when the determination was carried out 20 min after administration. In the case of hybrid **10**, a dose of 5 mg/kg was also tested, which led to a remarkable 43% inhibition of C57BL6J mouse brain AChE 10 min after administration. The significant inhibition of mouse brain AChE after ip administration of the levetiracetam-based hybrids clearly demonstrates their ability to cross the BBB *in vivo*.

To adjust the dose for the *in vivo* efficacy studies, a preliminary assessment of acute toxicity effects of the novel hybrids was carried out. We examined the general health of C57BL6/J mice at different times (5 min, 10 min, 20 min, 30 min, 45 min, 1 h, 3 h, and 24 h) after acute administration of increasing doses of the compounds (1.25, 2.5, 5 and 10 mg/kg). No clinical

signs were observed at any dose except a reduced activity and ptosis from 10 min to 45 min in those animals receiving the highest dose (10 mg/kg) of the compounds.

With the results obtained in C57BL6J mice, a dose of 5 mg/kg of the levetiracetam-based hybrids was selected for the *in vivo* efficacy studies.

***In Vivo* Efficacy Studies in APP/PS1 mice.** After having demonstrated the ability of the levetiracetam-based hybrids to inhibit hAChE and hBChE *in vitro* and Aβ42 and tau aggregation in the *E. coli* model and to cross the BBB *in vivo*, it remained to be determined whether this multitarget profile might lead *in vivo* to a reduction of the Alzheimer-like phenotype, including cognitive deficits, amyloid pathology and neuroinflammation. Particularly, we were very intrigued to see any potential reduction of epileptiform activity or seizures that might be ascribed to the presence of the levetiracetam pharmacophoric moiety of the hybrids and might be involved in their putative disease-modifying effects. Thus, we performed a chronic *in vivo* efficacy study using a well-established mouse model of AD, namely transgenic APP/PS1 mice. Levetiracetam-based hybrids **5**, **6**, **10** and **11** at a dose of 5 mg/kg or vehicle were administered ip once daily for 4 weeks to 5 month-old transgenic mice (pre-symptomatic phase, n = 6–10 per group). Hybrids and vehicle were also administered using the same protocol to wild-type (C57BL6J) littermates (n = 6–11 per group), to enable the confirmation of the AD-like phenotype of APP/PS1 mice by comparison between both genotypes and to evaluate the chronic toxicity of the compounds in both healthy and AD-like mice. During the daily manipulation, the general health status of animals was monitored and their body weight, spontaneous seizures leading to convulsions and abnormal behavior were recorded. After a 2-day washout period, animals were subjected to behavioral evaluation. At the end of the behavioral testing, the animals were sacrificed and their

brains collected and processed for the quantification of cortical soluble Aβ40 and Aβ42 levels, cortical amyloid burden and gliosis associated with Aβ deposition.

Effect of the Levetiracetam-Based Hybrids on Epileptic Seizures and General Health. Some lines of hAPP mice have convulsive seizures although such events appear not to be very frequent in most hAPP mice.[24] Indeed, during the 4-week-treatment period, only 8 spontaneous seizures episodes were recorded in vehicle-treated APP/PS1 mice out of a total number of events of 330 (number of animals × days of observation), whereas none of the wild-type animals suffered any spontaneous seizure during the observation period. Notwithstanding the relatively low incidence of epileptic seizures in the vehicle-treated transgenic control group, a lower number of seizures was found in the APP/PS1 mice treated with all the levetiracetam-based hybrids, i.e. 4 episodes / 300 events and 4 episodes / 180 events in animals treated with the racemic compounds **5** and **6**, respectively, and only 1 episode / 329 events and 2 episodes / 180 events in the animals treated with the enantiopure compounds **10** and **11**, respectively, which feature the eutomeric form of levetiracetam as an antiepileptic [(*S*)-levetiracetam]. The χ^2 test revealed a significant reduction in the frequency of spontaneous convulsions in APP/PS1 mice treated with the levetiracetam-huprine hybrid **10** ($\chi^2_{(1)}$= 5.3880, $p < 0.05$), but not in the other compounds, when compared to vehicle-treated littermates.

The mechanism of antiepileptic action of levetiracetam, by modulation of synaptic vesicle protein SV2A[61] or by inhibition of presynaptic Ca_V channels,[62] has been reported that might result in altered cholinergic neurotransmission.[62] Also, a wide range of behavioral adverse effects has been reported to occur in up to 16% of patients treated with levetiracetam.[63] These adverse effects might negatively impact the disease process. However, no significant body weight loss or

other clinical signs were recorded in any of the wild-type or APP/PS1 mice treated with the novel levetiracetam-based hybrids, apart from the above-mentioned seizures, suggesting lack of side-effects related to the chronic administration of the hybrid compounds in both healthy and AD-like animals.

Behavioral Evaluation of Cognitive Performance. The effects of the levetiracetam-based hybrids on cognition were evaluated through the two-object recognition test. After 2 days of training in which mice were allowed first to explore the apparatus and then to explore two identical objects placed at the end of the arms of the maze during 9 minutes each session, one of the two familiar objects was replaced by a novel object and the time spent exploring the two objects was recorded. The object recognition index (RI) was calculated as the difference between the time spent exploring the novel (T_N) and the familiar object (T_F), divided by the total time spent exploring the two objects [$RI = (T_N–T_F)/(T_N+T_F)$]. Low RI values are indicative of memory impairment.

APP/PS1 mice treated with vehicle and hybrids **6** and **11** exhibited low RI values and, hence, memory impairment in the two-object recognition test at six months of age (end of treatment and beginning of the symptomatic phase in APP/PS1 mice) when compared to corresponding WT littermates ($p < 0.01$, Figure 3). Interestingly, APP/PS1 mice treated with hybrids **5** and **10** exhibited significantly increased recognition indices when compared to vehicle-treated animals ($p < 0.05$ in both cases). Thus, the levetiracetam–tacrine hybrid **5** and the levetiracetam–huprine hybrid **10** were able to prevent the memory impairment in APP/PS1 mice when administered at the pre-symptomatic stage. It is worth noting that the effective dose of hybrids **5** and **10** used in the present study (5 mg/kg/day) is much lower than the levetiracetam doses reported to be

effective in previous studies (50–75 mg/kg/day) by using similar animal models of AD,[30,31] thereby suggesting that the new compounds may exhibit a better therapeutic profile than levetiracetam itself.

The cognition enhancing effects of hybrids **5** and **10** seem to be independent from their acute cholinesterase inhibitory activities. On the one hand, the results obtained in the behavioral test do not correlate with the *in vitro* anticholinesterasic potencies of the different hybrids. On the other hand, and more importantly, taking into account that the behavioral test was carried out four days after stopping compound treatments (2 days of washout period + 2 days of the training phase), it seems very likely that the cognition improvement found in APP/PS1 mice treated with hybrids **5** and **10** is not a mere result of an acute cholinergic action but rather it reflects long-lasting molecular modifications.

In the light of the positive effect observed at the cognitive level in animals treated with hybrids **5** and **10** and the absence of any positive effect in animals treated with the other two compounds, further molecular studies were performed only on brain samples obtained from animals treated with **5** and **10**.

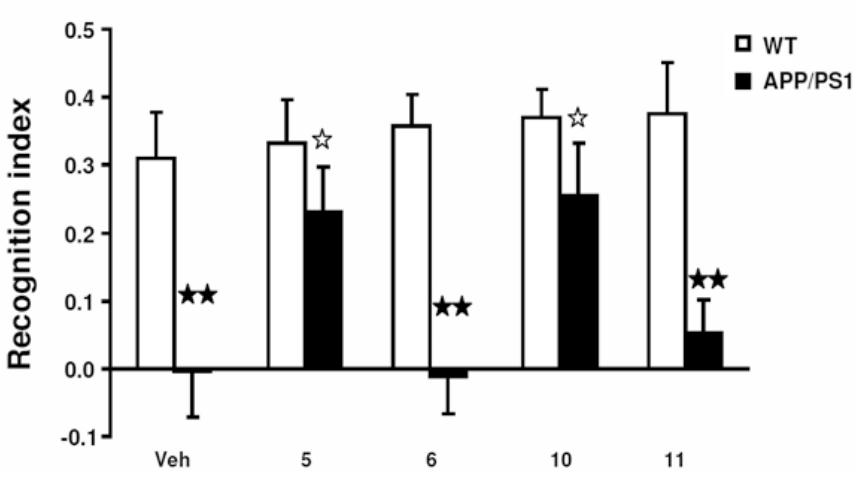

Figure 3. Memory performance in the two-object recognition test of wild-type (WT) and APP/PS1 mice after chronic treatment with the novel levetiracetam-based hybrids **5**, **6**, **10** and **11** (5 mg/kg/day, 4 weeks, ip). APP/PS1 mice chronically treated with vehicle (Veh), **6** and **11** exhibit a significant reduction in the recognition index when compared to corresponding wild-type littermates. In contrast, chronic administration of **5** and **10** induces memory improvement in APP/PS1 mice, as demonstrated by the significant increase in the recognition index compared to transgenic mice treated with vehicle. ★★ $p < 0.01$ genotype effect; ☆ $p < 0.05$ compared to vehicle.

Effect of the Levetiracetam-Based Hybrids on Amyloid Burden and Soluble Aβ Levels. Aβ burden was quantified by immunohistochemical determination in the main regions of Aβ deposition in the neocortex of APP/PS1 mice treated with vehicle or hybrids **5** and **10**. Also, to assess whether the positive effects of these compounds on cognition arise from a reduction in the production of Aβ, the levels of soluble Aβ40 and Aβ42, two of the most toxic forms of Aβ peptide, were also quantified in the soluble fractions from cortex homogenates of APP/PS1 mice treated with these hybrids.

Chronic treatment with the levetiracetam–huprine hybrid **10** reduced the Aβ burden in the cortex of APP/PS1 mice when compared to vehicle-treated animals ($p < 0.05$), whereas no significant modifications in the cortical Aβ burden were observed after chronic treatment with the levetiracetam–tacrine hybrid **5** (Figure 4A).

Cortical soluble Aβ40 and Aβ42 levels were not significantly modified by chronic treatment with these compounds, in spite of a tendency to decrease both peptides in APP/PS1 mice treated with the levetiracetam–huprine hybrid **10** (Figure 4B).

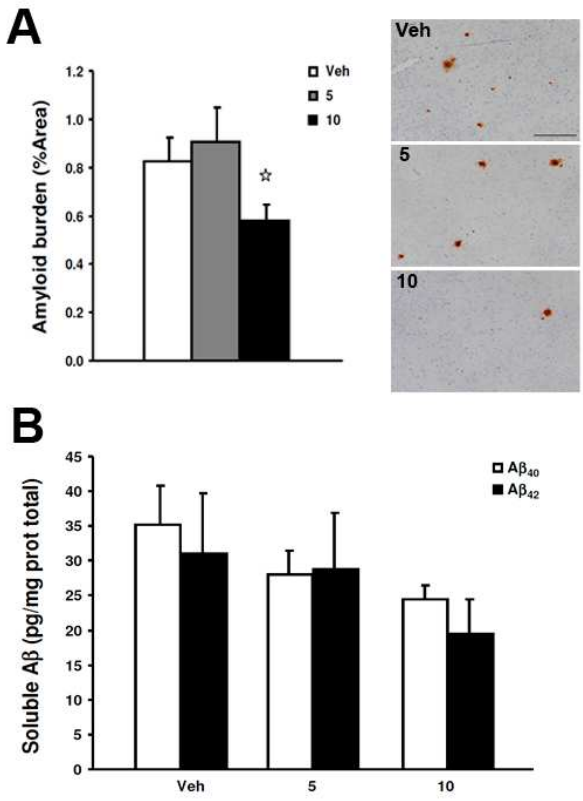

Figure 4. (A) Left: Aβ burden was significantly reduced in cortex of APP/PS1 mice treated with hybrid **10**. Right: Representative images of Aβ immunoreactivity in cortical sections of APP/PS1 mice subjected to chronic treatment with vehicle (Veh), **5** and **10**. Scale bar represents 200 µm. (B) Soluble Aβ40 and Aβ42 levels were not significantly modified by chronic treatment with **5** or **10** in cortical homogenates from APP/PS1 mice, despite a tendency to decrease both peptides in mice treated with **10**. Data are expressed as the mean values ± SEM. ☆ $p < 0.05$ compared to vehicle.

The levetiracetam–huprine hybrid **10** was the most potent Aβ42 and tau anti-aggregating compound of the series in the assay in *E. coli* cells (Table 1). The anti-aggregating action of **10** seems to operate also in APP/PS1 mice, thereby accounting for the significant reduction of amyloid burden in the transgenic mice treated with this compound.

Effect of the Levetiracetam-Based Hybrids on Gliosis Associated with Aβ Deposition. The effects of the chronic treatment with hybrids **5** and **10** on the astrocytic and microglial responses to Aβ deposition in the neocortex of APP/PS1 mice were evaluated by glial and Aβ double immunofluorescence and densitometric quantification of GFAP and Iba1 protein expression levels around Aβ plaques. These assays revealed that chronic treatment with the levetiracetam–huprine hybrid **10** produced a significant reduction of GFAP positive astrocytes around Aβ plaques in APP/PS1 mice ($p < 0.01$, Figure 5A, B). In a similar way, the number of Iba1 positive microglial cells associated with Aβ plaques was significantly reduced by hybrid **10** ($p < 0.01$) in comparison to vehicle-treated APP/PS1 animals (Figure 5A, C), a tendency also observed in transgenic mice treated with hybrid **5**. These results are compatible with an anti-inflammatory effect of hybrid **10**, and likely **5**, considering the role of glial cells in the inflammatory processes occurring in AD.[64]

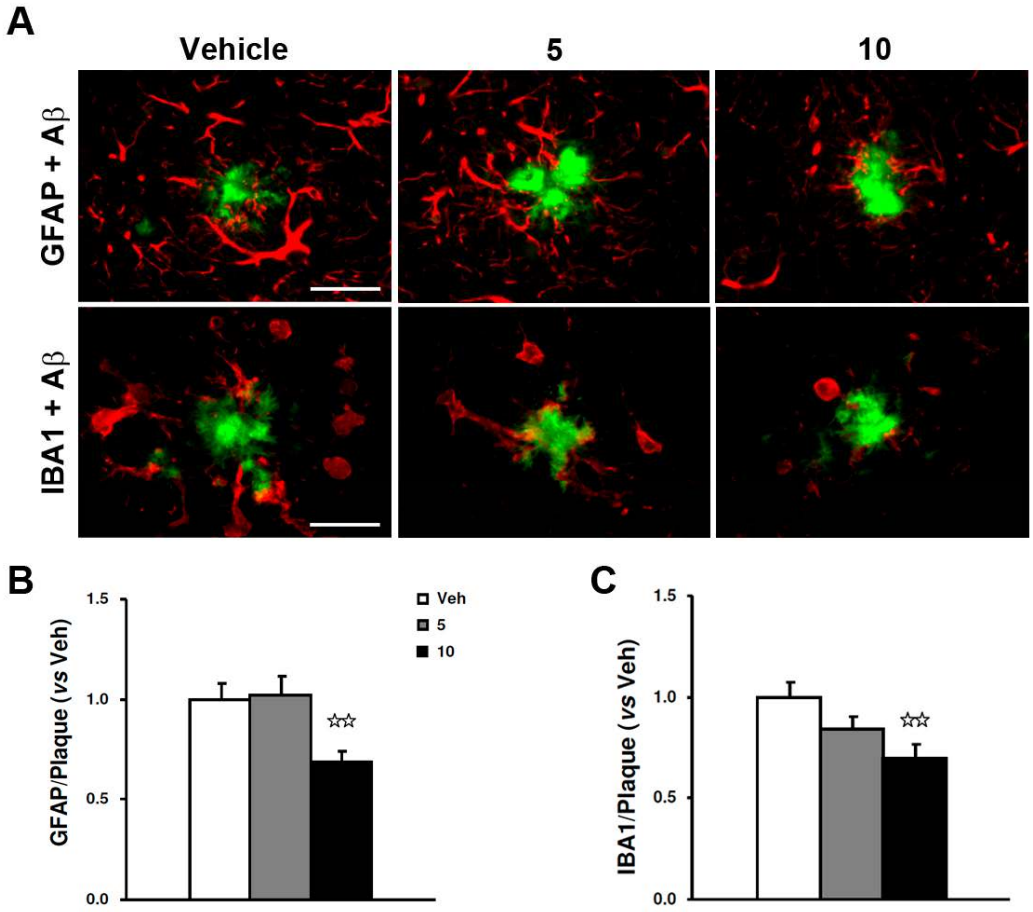

Figure 5. (A) Representative images of double GFAP (upper panels, red) or Iba1 (lower panels, red) and Aβ (green) immunoreactivity in cortical sections of APP/PS1 mice chronically treated with vehicle (Veh), **5** and **10**. Scale bars represent 50 µm. Quantification of the glial staining around the Aβ plaques reveals a significant reduction of the astroglial (B) and microglial (C) response in APP/PS1 mice chronically treated with hybrid **10**. Data are expressed as the mean values ± SEM. ☆☆ $p < 0.01$ compared to vehicle.

CONCLUSIONS

High levels of Aβ seem to be responsible for eliciting epileptiform activity and seizures in transgenic mouse models of AD that express human mutated APP, even at the early stages of the disease process.[26] This Aβ-induced aberrant neuronal network activity seems to be one of the mechanisms by which Aβ exerts its toxic effects to synapses, eventually leading to cognitive deficits, thereby constituting a prime target for AD drug discovery. The therapeutic potential of targeting aberrant neuronal network activity has been demonstrated with the antiepileptic drug levetiracetam, **1**, which can effectively suppress epileptiform activity and improve cognition in patients with aMCI[29] and in different hAPP mouse models of AD.[30,31] In this work, we have designed and synthesized a series of heptamethylene-linked hybrid compounds that combine the structure of **1** with the structure of a potent inhibitor of AChE such as tacrine, 6-chlorotacrine or huprine Y, as a novel class of multitarget anti-Alzheimer compounds that might be endowed with the positive effects of **1** against Aβ-induced epileptiform activity and with a common pattern of inhibitory activities against AChE, BChE, and Aβ42 and tau aggregation found for other structurally related 6-chlorotacrine- and huprine-based hybrids.[37–39] In agreement with the design rationale, the novel levetiracetam-based hybrids are very potent dual inhibitors of hAChE and hBChE *in vitro* and some of them, especially the enantiopure levetiracetam–huprine hybrid **10**, also moderately potent dual Aβ42 and tau anti-aggregating agents in a simple *in vivo* model of amyloid aggregation in intact *E. coli* cells. The brain penetration of the levetiracetam-based hybrids has been demonstrated by acute ip administration of these compounds to C57BL6J mice and subsequent *ex vivo* determination of their inhibitory activity against AChE from brain homogenates of the treated mice. After a preliminary assessment of the acute toxicity of the novel hybrids in C57BL6J mice, a dose of 5 mg/kg was considered to be safe and was selected

for a chronic *in vivo* efficacy study in transgenic APP/PS1 mice. Very interestingly, the number of epileptic seizures registered during the chronic treatment was lower in all of the group of transgenic mice treated with the novel hybrids relative to the control transgenic group treated with vehicle, even though only for the group treated with the levetiracetam–huprine hybrid **10** the reduction of the incidence of epileptic seizures was statistically significant. Hybrids **5** and **10** led to a clear cognitive improvement in APP/PS1 mice after four days without receiving the compounds, with these results being indicative of a disease-modifying effect, independent from their anti-cholinesterasic acute action. Moreover, cortical amyloid burden and neuroinflammation around Aβ plaques were significantly reduced in transgenic animals treated with **10**, without altering the levels of soluble Aβ40 and Aβ42, but not in animals treated with **5**, which has discouraged us from testing *in vivo* any of its enantiomers. Likely, the anti-aggregating effect found in *E. coli* for **10** also operates in transgenic mice, accounting for its positive effects on amyloid burden and cognition, but it seems also quite reasonable that an effect against the aberrant neuronal network activity of transgenic mice, due to the presence of the levetiracetam pharmacophore, might be also contributing to the disease-modifying effect of this compound that results in a significant reduction of epileptic seizures and in cognitive improvement. Indeed, the cognitive enhancing effects reported for **1** seem to arise only from the supression of the epileptiform activity, inasmuch as it did not alter either soluble Aβ levels or Aβ deposition.[30] In the case of the levetiracetam–huprine hybrid **10**, its putative effect on epileptiform activity is complemented with a direct effect on amyloid and tau pathologies, neuroinflammation and cholinesterases, thereby emerging as a very promising disease-modifying anti-Alzheimer drug candidate.

EXPERIMENTAL SECTION

Chemistry. Melting points were determined in open capillary tubes with a MFB 595010M Gallenkamp melting point apparatus. 400 MHz ^{1}H/100.6 MHz ^{13}C NMR spectra were recorded on a Varian Mercury 400 spectrometer. The chemical shifts are reported in ppm (δ scale) relative to residual solvent signals (CD_3OD at 3.31 and 49.0 ppm in the ^{1}H and ^{13} C NMR spectra, respectively), and coupling constants are reported in Hertz (Hz). The *syn* (*anti*) notation of the protons at position 13 of the huprine moiety of hybrids (2*S*,7"'*S*,11"'*S*)-**10** and (2*S*,7"'*R*,11"'*R*)-**11** means that the corresponding proton at position 13 is on the same (different) side of the quinoline moiety with respect to the cyclohexene ring. IR spectra were run on a Perkin-Elmer Spectrum RX I spectrophotometer. Absorption values are expressed as wave-numbers (cm^{-1}); only significant absorption bands are given. Optical rotations were measured on a Perkin-Elmer model 241 polarimeter. The specific rotation has not been corrected for the presence of solvent of crystallization. Column chromatography was performed on silica gel 60 AC.C (40–60 mesh, SDS, ref 2000027). Thin-layer chromatography was performed with aluminum-backed sheets with silica gel 60 F_{254} (Merck, ref 1.05554), and spots were visualized with UV light and 1% aqueous $KMnO_4$. NMR spectra of all of the new compounds were performed at the Centres Científics i Tecnològics of the University of Barcelona (CCiTUB), while elemental analyses and high resolution mass spectra were carried out at the Mycroanalysis Service of the IIQAB (CSIC, Barcelona, Spain) with a Carlo Erba 1106 analyzer, and at the CCiTUB with a LC/MSD TOF Agilent Technologies spectrometer, respectively. The analytical samples of all of the levetiracetam-based hybrids which were subjected to pharmacological evaluation possess a purity ≥95% as evidenced by their elemental analyses [(±)-**5**, and (±)-**6**] or by HPLC

measurements [(*S*)-**5**, (*R*)-**5**, **10**, and **11**]. The enantiopurity of the levetiracetam–tacrine hybrids (*S*)-**5** and (*R*)-**5** was confirmed by chiral HPLC, carried out with a Perkin-Elmer model 200 chromatograph equipped with a variable λ UV detector, using a CHIRALPAK® IC column, a mixture of heptane/ *i*-PrOH / diethylamine 55:45:0.1 as the eluent, flow 1 mL/min, λ = 235 nm; (*R*)-**5**, retention time = 35.99 min; (*S*)-**5**, retention time = 55.90 min. The enantio- and diastereo-purity of the levetiracetam–huprine hybrids (2*S*,7"'*S*,11"'*S*)-**10** and (2*S*,7"'*R*,11"'*R*)-**11** was confirmed by chiral HPLC, using the above described equipment and conditions, but with a mixture of heptane/ *i*-PrOH / diethylamine 63:37:0.1 as the eluent; (2*S*,7"'*R*,11"'*R*)-**11**, retention time = 34.65 min; (2*S*,7"'*S*,11"'*S*)-**10**, retention time = 36.36 min.

(±)-*N*-{7-[(1,2,3,4-Tetrahydroacridin-9-yl)amino]heptyl}-2-(2-oxopyrrolidin-1-yl)butanamide [(±)-5]. A solution of (±)-2-(2-oxopyrrolidin-1-yl)butanoic acid, [(±)-**4**] (445 mg, 2.60 mmol) in anhyd CH_2Cl_2 (26 mL) was cooled to 0 ºC with an ice bath, and treated dropwise with anhyd Et_3N (0.72 mL, 525 mg, 5.20 mmol) and $ClCO_2Et$ (0.25 mL, 282 mg, 2.60 mmol). The resulting mixture was stirred at 0 ºC for 30 min and treated with a solution of amine **2** (810 mg, 2.60 mmol) in anhyd CH_2Cl_2 (20 mL). The reaction mixture was stirred at rt for 3 days and treated with 10% aq Na_2CO_3 (150 mL). The phases were separated and the aqueous phase was extracted with CH_2Cl_2 (3 × 150 mL). The combined organic extracts were dried over anhyd Na_2SO_4 and evaporated under reduced pressure to give a crude product (1.25 g), which was subjected to column chromatography [40–60 µm silica gel, CH_2Cl_2/MeOH/50% aq NH_4OH mixtures]. On elution with CH_2Cl_2/MeOH/50% aq NH_4OH 99.8:0.2:0.2 to 98:2:0.2, levetiracetam–tacrine hybrid (±)-**5** (1.12 g, 93% yield) was isolated as a yellowish solid; R_f 0.52 (CH_2Cl_2/MeOH/50% aq. NH_4OH 9:1:0.05).

A solution of (±)-**5** (1.12 g, 2.41 mmol) in CH_2Cl_2 (60 mL) was filtered through a 0.2 µm NYL filter, treated with methanolic HCl (0.55 N, 19.7 mL) and evaporated under reduced pressure. The resulting solid was washed with pentane (3×5 mL) to give, after drying at 40 ºC/30 Torr for 48 h, (±)-**5**·HCl (641 mg) as a very hygroscopic yellowish solid: mp 55–58 °C; IR (KBr) *ν* 3500–2500 (max at 3243, 3060, 2928, 2854, N–H, N^+–H and C–H st), 1654, 1633, 1580, 1572, 1522 (C=O, Ar–C–C and Ar–C–N st) cm^{-1}; ^{1}H NMR (400 MHz, CD_3OD) *δ* 0.89 (dd, *J* = *J'* = 7.2 Hz, 3H, 4-H_3), 1.25–1.53 (complex signal, 8H, 2"-H_2, 3"-H_2, 4"-H_2, 5"-H_2), 1.70 (ddq, *J* = 14.4 Hz, *J'* = 9.6 Hz, *J"* = 7.2 Hz, 1H, 3-H_a), 1.79–2.08 (complex signal, 9H, 3-H_b, 4'-H_2, 6"-H_2, 2"'-H_2, 3"'-H_2), 2.40 (m, 2H, 3'-H_2), 2.71 (br t, *J* = 5.6 Hz, 2H, 1"'-H_2), 3.02 (br t, *J* = 6.0 Hz, 2H, 4"'-H_2), 3.16 (td, *J* = 7.2 Hz, *J'* = 5.6 Hz, 2H, 1"-H_2), 3.46 (m, 1H) and 3.56 (m, 1H) (5'-H_2), 3.95 (t, *J* = 7.6 Hz, 2H, 7"-H_2), 4.40 (dd, *J* = 9.6 Hz, *J'* = 6.4 Hz, 1H, 2-H), 4.85 (s, NH, $^+$NH), 7.59 (ddd, *J* = 8.4 Hz, *J'* = 6.8 Hz, *J"* = 1.6 Hz, 1H, 7"'-H), 7.76 (br d, *J* = 8.4 Hz, 1H, 5"'-H), 7.85 (ddd, *J* = 8.4 Hz, *J'* = 6.8 Hz, *J"* = 1.2 Hz, 1H, 6"'-H), 7.97 (br signal, 1H, NHCO), 8.40 (br d, *J* = 8.4 Hz, 1H, 8"'-H); ^{13}C NMR (100.6 MHz, CD_3OD) *δ* 11.0 (CH_3, C4), 19.2 (CH_2, C3), 21.8 (CH_2, C3"'), 23.0 (CH_2, C2"'), 23.2 (CH_2, C4'), 24.9 (CH_2, C1"'), 27.6 (CH_2, C5"), 27.7 (CH_2, C3"), 29.3 (CH_2, C4"'), 29.8 (CH_2, C4"), 30.2 (CH_2, C2" major rotamer), 30.7 (CH_2, C2" minor rotamer), 31.4 (CH_2, C6"), 32.0 (CH_2, C3'), 40.2 (CH_2, C1" minor rotamer), 40.3 (CH_2, C1" major rotamer), 45.4 (CH_2, C5'), 49.1 (CH_2, C7"), 57.97 (CH, C2 minor rotamer), 58.01 (CH, C2 major rotamer), 112.8 (C) and 117.0 (C) (C8a"', C9a"'), 120.1 (CH, C5"'), 126.3 (CH, C7"'), 126.5 (CH, C8"'), 134.1 (CH, C6"'), 139.8 (C, C10a"'), 151.7 (C, C4a"'), 158.0 (C, C9"'), 172.4 (C, C1 minor rotamer), 172.5 (C, C1 major rotamer), 178.4 (C, C2'); HRMS (ESI) calcd for ($C_{28}H_{40}N_4O_2$ + H^+): 465.3224, found 465.3212. Anal. ($C_{28}H_{40}N_4O_2$·HCl·1.25H_2O) C, H, N, Cl. HPLC purity 95%.

(*S*)-*N*-{7-[(1,2,3,4-Tetrahydroacridin-9-yl)amino]heptyl}-2-(2-oxopyrrolidin-1-yl)butanamide [(*S*)-5]. It was prepared as described for (±)-**5**. From acid (*S*)-**4** (159 mg, 0.93 mmol), and amine **2** (291 mg, 0.93 mmol), a crude product (732 mg) was obtained and purified by column chromatography (40–60 μm silica gel, CH_2Cl_2/MeOH/50% aq NH_4OH mixtures, gradient elution). On elution with CH_2Cl_2/MeOH/50% aq NH_4OH 99.8:0.2:0.2 to 99.6:0.4:0.2, impure levetiracetam–tacrine hybrid (*S*)-**5** (568 mg) was isolated; R_f 0.52 (CH_2Cl_2/MeOH/50% aq. NH_4OH 9:1:0.05).

A solution of impure (*S*)-**5** (568 mg) in CH_2Cl_2 (40 mL) was filtered through a 0.2 μm NYL filter, treated with methanolic HCl (0.55 N, 11 mL) and evaporated under reduced pressure. The resulting solid was taken in MeOH (0.75 mL) and precipitated from EtOAc (4 mL). The solid was washed with pentane (3×5 mL) to give, after drying at 40 ºC/30 Torr for 48 h, pure (*S*)-**5**·HCl (281 mg, 60% yield) as a very hygroscopic yellowish solid: $[\alpha]^{20}_D$ = –36 (*c* = 0.46, MeOH); mp 49–51 °C; IR (ATR) *v* 3500–2500 (max at 3232, 3055, 2924, 2850, N–H, N^+–H and C–H st), 1657, 1650, 1632, 1580, 1573, 1523 (C=O, Ar–C–C and Ar–C–N st) cm^{-1}; the ^1H and ^{13}C NMR spectra of (*S*)-**5**·HCl were identical to those of the racemic compound (±)-**5**; HRMS (ESI) calcd for ($C_{28}H_{40}N_4O_2 + H^+$): 465.3224,, found 465.3223. HPLC purity 96%.

(*R*)-*N*-{7-[(1,2,3,4-Tetrahydroacridin-9-yl)amino]heptyl}-2-(2-oxopyrrolidin-1-yl)butanamide [(*R*)-5]. It was prepared as described for (±)-**5**. From acid (*R*)-**4** (128 mg, 0.75 mmol), and amine **2** (232 mg, 0.75 mmol), a crude product (295 mg) was obtained and purified by column chromatography (40–60 μm silica gel, CH_2Cl_2/MeOH/50% aq NH_4OH mixtures, gradient elution). On elution with CH_2Cl_2/MeOH/50% aq NH_4OH 99:1:0.2, levetiracetam–tacrine hybrid (*R*)-**5** (93 mg, 27% yield) was isolated as a yellowish solid; R_f 0.52 (CH_2Cl_2/MeOH/50% aq. NH_4OH 9:1:0.05).

(*R*)-**5**·HCl: $[\alpha]^{20}_{D}$ = +32 (*c* = 1.25, MeOH); mp 61–63 °C; IR (ATR) *v* 3500–2500 (max at 3256, 3115, 3048, 2927, 2846, N–H, N^{+}–H and C–H st), 1659, 1651, 1633, 1568, 1524 (C=O, Ar–C–C and Ar–C–N st) cm^{-1}; the ^{1}H and ^{13}C NMR spectra of (*R*)-**5**·HCl were identical to those of the racemic compound (±)-**5**; HRMS (ESI) calcd for ($C_{28}H_{40}N_4O_2$ + H^{+}): 465.3224, found 465.3224. HPLC purity >99%.

(±)-*N*-{7-[(6-Chloro-1,2,3,4-tetrahydroacridin-9-yl)amino]heptyl}-2-(2-oxopyrrolidin-1-yl)butanamide [(±)-6]. It was prepared as described for (±)-**5**. From acid (±)-**4** (298 mg, 1.74 mmol), and amine **3** (602 mg, 1.74 mmol), a crude product (892 mg) was obtained and purified by column chromatography (40–60 μm silica gel, CH_2Cl_2/MeOH/50% aq NH_4OH mixtures, gradient elution). On elution with CH_2Cl_2/MeOH/50% aq NH_4OH 99.8:0.2:0.2 to 99:1:0.2, levetiracetam–chlorotacrine hybrid (±)-**6** (677 mg, 78% yield) was isolated; R_f 0.65 (CH_2Cl_2/MeOH/50% aq. NH_4OH 9:1:0.05).

(±)-6·HCl: mp 65–68 °C; IR (KBr) *v* 3500–2500 (max at 3251, 3050, 2928, 2854, 2802, 2749, N–H, N^{+}–H and C–H st), 1659, 1652, 1632, 1601, 1573, 1538, 1519 (C=O, Ar–C–C and Ar–C–N st) cm^{-1}; ^{1}H NMR (400 MHz, CD_3OD) δ 0.89 (dd, *J* = *J'* = 7.2 Hz, 3H, 4-H_3), 1.25–1.54 (complex signal, 8H, 2"-H_2, 3"-H_2, 4"-H_2, 5"-H_2), 1.70 (ddq, *J* = 14.4 Hz, *J'* = 9.6 Hz, *J"* = 7.2 Hz, 1H, 3-H_a), 1.79–2.10 (complex signal, 9H, 3-H_b, 4'-H_2, 6"-H_2, 2"'-H_2, 3"'-H_2), 2.40 (m, 2H, 3'-H_2), 2.68 (m, 2H, 1"'-H_2), 3.00 (t, *J* = 5.6 Hz, 2H, 4"'-H_2), 3.15 (br t, *J* = 7.2 Hz, 2H, 1"-H_2), 3.46 (m, 1H) and 3.57 (m, 1H) (5'-H_2), 3.94 (t, *J* = 7.6 Hz, 2H, 7"-H_2), 4.40 (dd, *J* = 9.6 Hz, *J'* = 6.4 Hz, 1H, 2-H), 4.85 (s, NH, $^{+}$NH), 7.57 (dd, *J* = 9.2 Hz, *J'* = 2.0 Hz, 1H, 7"'-H), 7.78 (d, *J* = 2.0 Hz, 1H, 5"'-H), 7.58 (br signal, 1H, NHCO), 8.39 (d, *J* = 9.2 Hz, 1H, 8"'-H); ^{13}C NMR (100.6 MHz, CD_3OD) δ 11.0 (CH_3, C4), 19.2 (CH_2, C3), 21.8 (CH_2, C3"'), 22.9 (CH_2, C2"'), 23.2 (CH_2, C4'), 24.8 (CH_2, C1"'), 27.6 (CH_2, C5"), 27.7 (CH_2, C3"), 29.4 (CH_2, C4"'),

29.8 (CH_2, C4”), 30.2 (CH_2, C2” major rotamer), 30.7 (CH_2, C2” minor rotamer), 31.3 (CH_2, C6”), 32.0 (CH_2, C3’), 40.2 (CH_2, C1” major rotamer), 40.3 (CH_2, C1” minor rotamer), 45.4 (CH_2, C5’), 49.2 (CH_2, C7”), 58.0 (CH, C2), 113.4 (C, C9a”’), 115.5 (C, C8a”’), 119.2 (CH, C5”’), 126.7 (CH, C7”’), 128.8 (CH, C8”’), 140.0 (C, C6”’), 140.6 (C, C10a”’), 152.2 (C, C4a”’), 157.8 (C, C9”’), 172.4 (C, C1 major rotamer), 172.5 (C, C1 minor rotamer), 178.4 (C, C2’); HRMS (ESI) calcd for ($C_{28}H_{39}{}^{35}ClN_4O_2$ + H^+): 499.2834, found 499.2827. Anal. ($C_{28}H_{39}ClN_4O_2 \cdot HCl \cdot H_2O$) C, H, N, Cl. HPLC purity >99%.

(7*S*,11*S*)-7-[(3-Chloro-6,7,10,11-tetrahydro-9-methyl-7,11-methanocycloocta[*b*]quinolin-12-yl)amino]heptanenitrile [(7*S*,11*S*)-8]. A suspension of (7*S*,11*S*)-huprine Y, (7*S*,11*S*)-**7** (1.00 g, 3.52 mmol) and finely powdered NaOH (0.46 g, 11.6 mmol), and 4 Å molecular sieves in anhyd DMSO (15 mL) was stirred, heating every 10 min approximately with a heat gun for 1 h and at rt one additional hour, and then treated with a solution of 7-bromoheptanenitrile (90% purity reagent, 0.61 mL, 0.77 g, 4.05 mmol) in anhyd DMSO (1 mL) dropwise for 30 min. The reaction mixture was stirred at rt overnight, diluted with aq 2 N NaOH (50 mL), and extracted with EtOAc (3 × 75 mL). The combined organic extracts were washed with H_2O and aq 5 N NaOH (6 × 100 mL), dried over anhyd Na_2SO_4, and evaporated under reduced pressure to give a yellow oily residue (953 mg), which was purified by column chromatography (40–60 µm silica gel, CH_2Cl_2/MeOH/50% aq. NH_4OH mixtures, gradient elution). On elution with CH_2Cl_2/MeOH/50% aq. NH_4OH 97.5:2.5:0.2, nitrile (7*S*,11*S*)-**8** (514 mg, 52% yield) was isolated as a yellowish solid; R_f 0.80 (CH_2Cl_2/MeOH/50% aq. NH_4OH 9:1:0.05).

A solution of (7*S*,11*S*)-**8** (40 mg, 0.10 mmol) in CH_2Cl_2 (3 mL) was filtered through a 0.2 µm NYL filter, treated with methanolic HCl (0.53 N, 0.58 mL) and evaporated under reduced pressure. The resulting solid was washed with pentane (3×5 mL) to give, after drying at 65 ºC/30

Torr for 48 h, (7*S*,11*S*)-**8**·HCl (43 mg) as a yellowish solid: $[\alpha]^{20}_{D} = -203$ (*c* = 1, MeOH); mp 98–102 °C; IR (KBr) *v* 3500–2500 (max at 3229, 3044, 2928, 2905, 2865, 2759, N–H, N^{+}–H and C–H st), 2234 (CN st), 1630, 1582, 1567, 1513 (Ar–C–C and Ar–C–N st) cm^{-1}; the ^{1}H and ^{13}C NMR spectra of (7*S*,11*S*)-**8**·HCl were identical to those reported for the racemic compound;[37] HRMS (ESI) calcd for ($C_{24}H_{28}{}^{35}ClN_3 + H^{+}$): 394.2045, found 394.2049.

(7*R*,11*R*)-7-[(3-Chloro-6,7,10,11-tetrahydro-9-methyl-7,11-methanocycloocta[*b*]quinolin-12-yl)amino]heptanenitrile [(7*R*,11*R*)-8]. It was prepared as described for (7*S*,11*S*)-**8**. From (7*R*,11*R*)-**7** (1.00 g, 3.52 mmol) and 7-bromoheptanenitrile (90% purity reagent, 0.61 mL, 0.77 g, 4.05 mmol), a yellow oily residue (780 mg) was obtained and purified by column chromatography (40–60 µm silica gel, CH_2Cl_2/MeOH/50% aq NH_4OH mixtures, gradient elution). On elution with CH_2Cl_2/MeOH/50% aq NH_4OH 100:0:0.2 to 95:5:0.2, nitrile (7*R*,11*R*)-**8** (755 mg, 55% yield) was isolated as a yellowish solid; R_f 0.80 (CH_2Cl_2/MeOH/50% aq. NH_4OH 9:1:0.05).

(7*R*,11*R*)-**8**·HCl: $[\alpha]^{20}_{D} = +234$ (*c* = 0.52, MeOH); mp 107–110 °C; IR (KBr) *v* 3500–2500 (max at 3229, 3044, 2925, 2854, 2775, N–H, N^{+}–H and C–H st), 2242 (CN st), 1631, 1581, 1560, 1513 (Ar–C–C and Ar–C–N st) cm^{-1}; the ^{1}H and ^{13}C NMR spectra of (7*R*,11*R*)-**8**·HCl were identical to those reported for the racemic compound;[37] HRMS (ESI) calcd for ($C_{24}H_{28}{}^{35}ClN_3 + H^{+}$): 394.2045, found 394.2046.

(7*S*,11*S*)-*N*-(3-Chloro-6,7,10,11-tetrahydro-9-methyl-7,11-methanocycloocta[*b*]quinolin-12-yl)heptane-1,7-diamine [(7*S*,11*S*)-9]. A solution of nitrile (7*S*,11*S*)-**8** (474 mg, 1.20 mmol) in anhyd Et_2O (22 mL) was cooled to 0 ºC and treated dropwise with a 4 M solution of $LiAlH_4$ in Et_2O (0.90 mL, 3.60 mmol). The reaction mixture was stirred at rt for 20 h and then treated dropwise with H_2O and 5 N NaOH and extracted with EtOAc (3 × 100 mL). The combined

organic extracts were washed with H_2O (3 × 100 mL), dried over anhyd Na_2SO_4, and evaporated under reduced pressure to furnish amine (7*S*,11*S*)-**9** (432 mg, 91% yield) as a yellowish oil; R_f 0.16 (CH_2Cl_2/MeOH/50% aq. NH_4OH 9:1:0.05).

A solution of (7*S*,11*S*)-**9** (40 mg, 0.10 mmol) in CH_2Cl_2 (10 mL) was filtered through a 0.2 µm PTFE filter, treated with methanolic HCl (0.53 N, 1.71 mL), and evaporated under reduced pressure. The resulting solid was washed with pentane (3×2 mL) to give, after drying at 65 ºC/30 Torr for 48 h, (7*S*,11*S*)-**9**·2HCl (45 mg) as a yellow solid: $[\alpha]^{20}_D = -197$ (*c* = 1.14, MeOH); mp 176–180 °C; IR (KBr) *v* 3500–2500 (max at 3250, 2891, 2870, N–H, N^+–H and C–H st), 1629, 1580, 1548, 1538, 1514 (Ar–C–C and Ar–C–N st) cm^{-1}; the ^1H and ^{13}C NMR spectra of (7*S*,11*S*)-**9**·2HCl were identical to those reported for the racemic compound;[37] HRMS (ESI) calcd for ($C_{24}H_{32}{}^{35}ClN_3 + H^+$): 398.2358, found 398.2356.

(7*R*,11*R*)-*N*-(3-Chloro-6,7,10,11-tetrahydro-9-methyl-7,11-methanocycloocta[*b*]quinolin-12-yl)heptane-1,7-diamine [(7*R*,11*R*)-9]. It was prepared as described for (7*S*,11*S*)-**9**. From nitrile (7*R*,11*R*)-**8** (599 mg, 1.52 mmol), a yellow oily residue (445 mg) was obtained and purified by column chromatography (40–60 µm silica gel, CH_2Cl_2/MeOH/50% aq NH_4OH mixtures, gradient elution). On elution with CH_2Cl_2/MeOH/50% aq NH_4OH 99.8:0.2:1 to 99:1:1, amine (7*R*,11*R*)-**9** (270 mg, 45% yield) was isolated as a yellowish oil; R_f 0.16 (CH_2Cl_2/MeOH/50% aq. NH_4OH 9:1:0.05).

(7*R*,11*R*)-**9**·2HCl: $[\alpha]^{20}_D = +176$ (*c* = 1.08, MeOH); mp 179–183 °C; IR (KBr) *v* 3500–2500 (max at 3240, 2923, 2849, 2802, N–H, N^+–H and C–H st), 1629, 1581, 1551, 1513 (Ar–C–C and Ar–C–N st) cm^{-1}; the ^1H and ^{13}C NMR spectra of (7*R*,11*R*)-**9**·2HCl were identical to those reported for the racemic compound;[37] HRMS (ESI) calcd for ($C_{24}H_{32}{}^{35}ClN_3 + H^+$): 398.2358, found 398.2356.

(2*S*,7"'*S*,11"'*S*)-*N*-{7-[(3-Chloro-6,7,10,11-tetrahydro-9-methyl-7,11-methanocycloocta[*b*]quinolin-12-yl)amino]heptyl}-2-(2-oxopyrrolidin-1-yl)butanamide [(2*S*,7"'*S*,11"'*S*)-10]. It was prepared as described for (±)-**5**. From acid (*S*)-**4** (169 mg, 0.99 mmol), and amine (7*S*,11*S*)-**9** (392 mg, 0.99 mmol), a crude product (681 mg) was obtained. After two consecutive column chromatography purifications (40–60 µm silica gel, CH_2Cl_2/MeOH/50% aq NH_4OH mixtures and hexane/EtOAc/Et_3N mixtures, gradient elution), levetiracetam–huprine hybrid (2*S*,7"'*S*,11"'*S*)-**10** (30 mg on elution with CH_2Cl_2/MeOH/50% aq NH_4OH 99.95:0.05:0.2 + 131 mg on elution with hexane/EtOAc/Et_3N 30:70:0.2 to 10:90:0.2, 30% total yield) was isolated as a yellowish solid; R_f 0.71 (CH_2Cl_2/MeOH/50% aq. NH_4OH 9:1:0.05).

(2*S*,7"'*S*,11"'*S*)-**10**·HCl: $[\alpha]^{20}_D$ = –195 (*c* = 0.80, MeOH); mp 96–99 °C; IR (KBr) *v* 3500–2500 (max at 3249, 3055, 2925, 2854, 2786, N–H, N^+–H and C–H st), 1656, 1649, 1633, 1581, 1565, 1518 (C=O, Ar–C–C and Ar–C–N st) cm^{-1}; ^1H NMR (400 MHz, CD_3OD) δ 0.89 (dd, *J* = *J*' = 7.2 Hz, 3H, 4-H_3), 1.24–1.54 (complex signal, 8H, 2"-H_2, 3"-H_2, 4"-H_2, 5"-H_2), 1.58 (s, 3H, 9"'-CH_3), 1.70 (ddq, *J* = 14.4 Hz, *J*' = 9.6 Hz, *J*" = 7.2 Hz, 1H, 3-H_a), 1.80–2.11 (complex signal, 7H, 3-H_b, 4'-H_2, 6"-H_2, 13"'-H_{syn}, 13"'-H_{anti}), overimposed in part 1.93 (br d, *J* = 17.6 Hz, 1H, 10"'-H_{endo}), 2.40 (m, 2H, 3'-H_2), 2.55 (br dd, *J* = 17.6 Hz, *J*' = 4.8 Hz, 1H, 10"'-H_{exo}), 2.77 (m, 1H, 7"'-H), 2.88 (br d, *J* = 18.0 Hz, 1H, 6"'-H_{endo}), 3.16 (td, *J* = 6.8 Hz, *J*' = 6.0 Hz, 2H, 1"-H_2), overimposed in part 3.21 (dd, *J* = 18.0 Hz, *J*' = 5.2 Hz, 1H, 6"'-H_{exo}), overimposed 3.42–3.49 (m, 1H, 11"'-H), 3.46 (m, 1H) and 3.57 (m, 1H) (5'-H_2), 3.98 (t, *J* = 7.6 Hz, 2H, 7"-H_2), 4.41 (dd, *J* = 9.6 Hz, *J*' = 6.4 Hz, 1H, 2-H), 4.85 (s, NH, $^+$NH), 5.59 (br d, *J* = 4.8 Hz, 1H, 8"'-H), 7.55 (dd, *J* = 9.6 Hz, *J*' = 1.6 Hz, 1H, 2"'-H), 7.78 (d, *J* = 1.6 Hz, 1H, 4"'-H), 7.99 (m, 1H, NHCO), 8.40 (d, *J* = 9.6 Hz, 1H, 1"'-H); ^{13}C NMR (100.6 MHz, CD_3OD) δ

11.0 (CH_3, C4), 19.2 (CH_2, C3), 23.2 (CH_2, C4'), 23.5 (CH_3, 9"'-CH_3), 27.3 (CH, C11"'), 27.7 (2 CH_2, C3", C5"), 27.8 (CH, C7"'), 29.3 (CH_2, C13"'), 29.8 (CH_2, C4"), 30.2 (CH_2, C2" major rotamer), 30.7 (CH_2, C2" minor rotamer), 31.2 (CH_2, C6"), 32.0 (CH_2, C3'), 36.0 (CH_2) and 36.1 (CH_2) (C6"', C10"'), 40.2 (CH_2, C1" minor rotamer), 40.3 (CH_2, C1" major rotamer), 45.4 (CH_2, C5'), 49.6 (CH_2, C7"), 57.96 (CH, C2 minor rotamer), 58.00 (CH, C2 major rotamer), 115.6 (C, C12a"'), 117.6 (C, C11a"'), 119.1 (CH, C4"'), 125.1 (CH, C8"'), 126.7 (CH, C2"'), 129.5 (CH, C1"'), 134.5 (C, C9"'), 140.2 (C, C3"'), 141.0 (C, C4a"'), 151.2 (C, C5a"'), 156.9 (C, C12"'), 172.36 (C, C1 minor rotamer), 172.44 (C, C1 major rotamer), 178.4 (C, C2'); HRMS (ESI) calcd for ($C_{32}H_{43}{}^{35}ClN_4O_2 + H^+$): 551.3147, found 551.3135; HPLC purity 96%.

(2*S*,7"'*R*,11"'*R*)-*N*-{7-[(3-Chloro-6,7,10,11-tetrahydro-9-methyl-7,11-methanocycloocta[*b*]quinolin-12-yl)amino]heptyl}-2-(2-oxopyrrolidin-1-yl)butanamide [(2*S*,7"'*R*,11"'*R*)-11]. It was prepared as described for (±)-**5**. From acid (2*S*)-**4** (99 mg, 0.58 mmol), and amine (7*R*,11*R*)-**9** (230 mg, 0.58 mmol), a crude product (343 mg) was obtained and purified by column chromatography (40–60 µm silica gel, CH_2Cl_2/MeOH/50% aq NH_4OH mixtures, gradient elution). On elution with CH_2Cl_2/MeOH/50% aq NH_4OH 99.95:0.05:0.2, levetiracetam–huprine hybrid (2*S*,7"'*R*,11"'*R*)-**11** (176 mg, 56% yield) was isolated as a yellowish solid; R_f 0.70 (CH_2Cl_2/MeOH/50% aq. NH_4OH 9:1:0.05).

(2*S*,7"'*R*,11"'*R*)-**11**·HCl: $[\alpha]^{20}_D$ = +152 (*c* = 0.48, MeOH); mp 102–105 °C; IR (KBr) *v* 3500–2500 (max at 3256, 3055, 2925, 2854, 2796, N–H, N^+–H and C–H st), 1657, 1649, 1630, 1581, 1565, 1514 (C=O, Ar–C–C and Ar–C–N st) cm^{-1}; ^1H NMR (400 MHz, CD_3OD) δ 0.89 (dd, *J* = *J*' = 7.2 Hz, 3H, 4-H_3), 1.25–1.54 (complex signal, 8H, 2"-H_2, 3"-H_2, 4"-H_2, 5"-H_2), 1.58 (s, 3H, 9"'-CH_3), 1.70 (ddq, *J* = 14.4 Hz, *J*' = 9.6 Hz, *J*" = 7.2 Hz, 1H, 3-H_a), 1.80–2.12 (complex signal, 7H, 3-H_b, 4'-H_2, 6"-H_2, 13"'-H_{syn}, 13"'-H_{anti}), overimposed in part 1.93 (br d, *J*

= 17.6 Hz, 1H, 10”’-H_{endo}), 2.40 (m, 2H, 3’-H_2), 2.55 (br dd, *J* = 17.6 Hz, *J’* = 4.0 Hz, 1H, 10”’-H_{exo}), 2.77 (m, 1H, 7”’-H), 2.88 (br d, *J* = 18.0 Hz, 1H, 6”’-H_{endo}), 3.16 (td, *J* = *J’* = 6.4 Hz, 2H, 1”-H_2), overimposed in part 3.21 (dd, *J* = 18.0 Hz, *J’* = 5.2 Hz, 1H, 6”’-H_{exo}), overimposed in part 3.45 (m, 1H, 11”’-H), 3.46 (m, 1H) and 3.57 (m, 1H) (5’-H_2), 3.98 (t, *J* = 7.2 Hz, 2H, 7”-H_2), 4.41 (dd, *J* = 9.6 Hz, *J’* = 6.4 Hz, 1H, 2-H), 4.86 (s, NH, $^+$NH), 5.59 (br d, *J* = 4.4 Hz, 1H, 8”’-H), 7.56 (dd, *J* = 9.2 Hz, *J’* = 2.0 Hz, 1H, 2”’-H), 7.78 (d, *J* = 2.0 Hz, 1H, 4”’-H), 7.99 (m, 1H, NHCO), 8.40 (d, *J* = 9.2 Hz, 1H, 1”’-H); ^{13}C NMR (100.6 MHz, CD_3OD) δ 11.0 (CH_3, C4), 19.2 (CH_2, C3), 23.2 (CH_2, C4’), 23.5 (CH_3, 9”’-CH_3), 27.3 (CH, C11”’), 27.7 (2 CH_2, C3”, C5”), 27.8 (CH, C7”’), 29.3 (CH_2, C13”’), 29.8 (CH_2, C4”), 30.2 (CH_2, C2” major rotamer), 30.7 (CH_2, C2” minor rotamer), 31.2 (CH_2, C6”), 32.0 (CH_2, C3’), 36.0 (CH_2) and 36.1 (CH_2) (C6”’, C10”’), 40.2 (CH_2, C1” minor rotamer), 40.3 (CH_2, C1” major rotamer), 45.4 (CH_2, C5’), 49.6 (CH_2, C7”), 57.96 (CH, C2 minor rotamer), 58.00 (CH, C2 major rotamer), 115.6 (C, C12a”’), 117.6 (C, C11a”’), 119.1 (CH, C4”’), 125.1 (CH, C8”’), 126.7 (CH, C2”’), 129.5 (CH, C1”’), 134.5 (C, C9”’), 140.2 (C, C3”’), 141.0 (C, C4a”’), 151.2 (C, C5a”’), 156.9 (C, C12”’), 172.4 (C, C1 minor rotamer), 172.5 (C, C1 major rotamer), 178.4 (C, C2’); HRMS (ESI) calcd for ($C_{32}H_{43}{}^{35}ClN_4O_2 + H^+$): 551.3147, found 551.3138; HPLC purity 95%.

***In Vitro* Biological Studies. AChE and BChE Inhibition Assay.** Human recombinant AChE (Sigma-Aldrich) and human serum BChE (Sigma-Aldrich) inhibitory activities were evaluated spectrophotometrically by the method of Ellman *et al.*[49] The reactions took place in a final volume of 300 μL of 0.1 M phosphate-buffered solution pH 8.0, containing hAChE or hBChE (0.02 u/mL) and 333 μM 5,5'-dithiobis(2-nitrobenzoic) acid (DTNB; Sigma-Aldrich) solution used to produce the yellow anion of 5-thio-2-nitrobenzoic acid. Inhibition curves were performed in duplicate using at least 10 increasing concentrations of inhibitors and preincubated for 20 min

at 37 ºC before adding the substrate.[65] One duplicate sample without inhibitor was always present to yield 100% of AChE or BChE activities. Then substrates, acetylthiocholine iodide (450 μM; Sigma-Aldrich) or butyrylthiocholine iodide (300 μM; Sigma-Aldrich), were added and the reaction was developed for 5 min at 37 ºC. Colour production was measured at 414 nm using a labsystems Multiskan spectrophotometer.

Data from concentration–inhibition experiments of the inhibitors were calculated by non-linear regression analysis, using the GraphPad Prism program package (GraphPad Software; San Diego, USA), which gave estimates of the IC_{50} (concentration of drug producing 50% of enzyme activity inhibition). Results are expressed as mean ± S.E.M. of at least 4 experiments performed in duplicate.

Aβ42 and Tau Aggregation Inhibition Assay in *Escherichia coli* Cells Overexpressing Aβ42 and Tau. Cloning and overexpression of Aβ42 peptide: *Escherichia coli* competent cells BL21 (DE3) were transformed with the pET28a vector (Novagen, Inc., Madison, WI, USA) carrying the DNA sequence of Aβ42. Because of the addition of the initiation codon ATG in front of both genes, the overexpressed peptide contains an additional methionine residue at its N terminus. For overnight culture preparation, 10 mL of M9 minimal medium containing 50 $\mu g \cdot mL^{-1}$ of kanamycin were inoculated with a colony of BL21 (DE3) bearing the plasmid to be expressed at 37 °C. For expression of the Aβ42 peptide, the required volume of overnight culture to obtain 1:500 dilution was added into fresh M9 minimal medium containing 50 $\mu g \cdot mL^{-1}$ of kanamycin and 250 μM of Th-S. The bacterial culture was grown at 37 ºC and 250 rpm. When the cell density reached OD_{600} = 0.6, 980 μL of culture were transferred into eppendorf tubes of 1.5 mL with 10 μL of each compound to be tested in DMSO and 10 μL of isopropyl 1-thio-β-D-galactopyranoside (IPTG) at 100 mM. The final concentration of drug was fixed at 20 μM. The

samples were grown overnight at 37 °C and 1400 rpm using a Thermomixer (Eppendorf, Hamburg, Germany). As negative control (maximal amyloid presence) the same amount of DMSO without drug was added in the sample. In parallel, non-induced samples (in absence of IPTG) were also prepared and used as positive controls (non-amyloid presence). In addition, these samples were used to assess the potential intrinsic toxicity of the compounds and to confirm the correct bacterial growth.

Cloning and overexpression of tau protein: *E. coli* BL21 (DE3) competent cells were transformed with pTARA containing the RNA-polymerase gen of T7 phage (T7RP) under the control of the promoter PBAD. *E. coli* BL21 (DE3) with pTARA competent cells were transformed with pRKT42 vector encoding four repeats of tau protein in two inserts. For overnight culture preparation, 10 mL of M9 medium containing 0.5% of glucose, 50 $\mu g \cdot mL^{-1}$ of ampicillin and 12.5 $\mu g \cdot mL^{-1}$ of chloramphenicol were inoculated with a colony of BL21 (DE3) bearing the plasmids to be expressed at 37 °C. For expression of tau protein, the required volume of overnight culture to obtain 1:500 dilution was added into fresh M9 minimal medium containing 0.5% of glucose, 50 $\mu g \cdot mL^{-1}$ of ampicillin, 12.5 $\mu g \cdot mL^{-1}$ of chloramphenicol, and 250 μM of Th-S. The bacterial culture was grown at 37 ºC and 250 rpm. When the cell density reached OD_{600} = 0.6, 980 μL of culture were transferred into eppendorf tubes of 1.5 mL with 10 μL of each compound to be tested in DMSO and 10 μL of arabinose at 25%. The final concentration of drug was fixed at 20 μM. The samples were grown overnight at 37 °C and 1400 rpm using a Thermomixer (Eppendorf, Hamburg, Germany). As negative control (maximal presence of tau) the same amount of DMSO without drug was added in the sample. In parallel, non-induced samples (in absence of arabinose) were also prepared and used as positive controls

(absence of tau). In addition, these samples were used to assess the potential intrinsic toxicity of the compounds and to confirm the correct bacterial growth.

Thioflavin-S (Th-S) steady-state fluorescence: Th-S (T1892) and other chemical reagents were purchased from Sigma (St. Louis, MO). Th-S stock solution (2500 mM) was prepared in double-distilled water purified through a Milli-Q system (Millipore, USA). For the fluorescence assay, the Th-S spectra were measured on an Aminco Bowman Series 2 luminescence spectrophotometer (Aminco-Bowman AB2, SLM Aminco, Rochester, NY, USA) from 460 to 600 nm at 25 °C using an excitation wavelength of 440 nm and slit widths of 4 nm. The emission at 485 nm (Th-S peak fluorescence in presence of amyloids) was recorded. In order to normalize the Th-S fluorescence as a function of the bacterial concentration, OD_{600} was obtained using a Shimadzu UV-2401 PC UV–Vis spectrophotometer (Shimadzu, Japan). Note that the fluorescence normalization was carried out considering as 100% the Th-S fluorescence of the bacterial cells expressing the peptide or protein in the absence of drug and 0% the Th-S fluorescence of the bacterial cells non-expressing the peptide or protein.

***Ex Vivo* BBB Permeation Studies and Acute Administration in C57BL/6J Mice.** The capability of the novel levetiracetam-based hybrid compounds to cross the BBB was evaluated e*x vivo*. The compounds at a dose of 2.5 mg/kg and 5 mg/kg were administered intraperitoneally to C57BL/6J mice and 10 or 20 minutes after administration their brains were collected (n = 3, each group). Brains were homogenized in 0.5 volumes of phosphate buffer 0.1 M (pH 8.0) with 0.7% triton at 4 ºC. Just before analyzing the enzymatic activity, 100 µL of homogenate were diluted 2.5 times in 0.1 M phosphate-buffered solution (pH 8.0). The inhibitory effect of the novel compounds on AChE activity was evaluated spectrophotometrically at 25 °C by the method of Ellman *et al.*,[49] modified according to Lassiter *et al*.[66] The reaction took place in a

final volume of 300 µL of 0.1 M phosphate-buffered solution (pH 8.0) containing 100 µL of diluted homogenate and 333 µM DTNB solution. To avoid interferences between AChE and BChE activities, 100 µM ISO-OMPA (specific BChE inhibitor) was present in the incubation medium. Prior to the addition of the substrate acetylthiocholine, a pre-incubation period of 5 min was used to eliminate the endogenous acetylcholine present in the homogenates. The reaction was started by the addition of acetylthiocholine iodide (450 µM) and the absorbance at 414 nm was evaluated 2 min after the substrate addition.

Percent of inhibition was calculated by comparing AChE activity in brain of the drug-treated mice with activity from untreated controls. This protocol was approved by the Animals Ethics Committee of the Universitat Autònoma de Barcelona and complies with the current laws of Spain, which are in accordance with the European Communities Council Directive 2010/63/EU. All efforts were made to minimize animal suffering and to reduce the number of animals used.

Increasing amounts of the novel levetiracetam-based hybrid compounds (1.25, 2.5, 5 and 10 mg/kg ip) were acutely administered to C57BL/6J mice and the state of general health was assessed at 5 min, 10 min, 20 min, 30 min, 45 min, 1 h, 3 h and 24 h after administration (n = 3, each group).

***In Vivo* Efficacy Studies in APP/PS1 Mice. Animals.** The experiments were carried out on male AßPP/PS1 mice and wild-type littermates that were 5 month-old at the beginning of the study. The generation of mice expressing the human mutated forms APPswe and PS1dE9 (AßPP/PS1) has been already described.[67] Animals were maintained under standard animal housing conditions in a normal 12-h dark-light cycle with free access to food and water. Animal procedures were conducted according to ethical guidelines (European Community Council Directive 2010/63/EU) and approved by the local ethical committee (Universitat de Barcelona).

Chronic Treatment. The novel levetiracetam-based hybrid compounds (5 mg/kg) were dissolved in 1% DMSO and 90% saline and were injected intraperitoneally (i.p.) in a volume of 10 mL/kg body weight. Animals were treated once daily for 4 weeks with the compounds or the corresponding vehicle (wild-type, n = 6–11; APP/PS1, n = 6–10, each group). During the daily manipulation, the health status of animals was monitored and body weight, spontaneous seizures leading to convulsions and abnormal behavior of mice were recorded. After 2 days of washout period, animals were subjected to behavioral evaluation.

Behavioral Evaluation of Cognitive Performance. The two-object recognition test was performed in a V-maze because it improves the exploration time of the animals with respect to a classical open field. On day 1, mice were habituated for 9 min, allowing them to freely explore the apparatus. On the second day, mice were placed for 9 min in the maze, where two identical objects were situated at the end of the arms, and the time that the mice spent exploring each object was recorded. Then, 24 h after the training session, animals were placed again in the V-maze where one of the two familiar objects was replaced by a novel object. The time that the animals spent exploring the two objects was recorded and an object recognition index (RI) was calculated as the difference between the time spent exploring the novel (T_N) and the familiar object (T_F), divided by the total time spent exploring the two objects [$RI = (T_N–T_F)/(T_N+T_F)$]. Animals exhibiting memory impairments revealed a lower object recognition index.

Tissue Collection. At the end of the behavioral testing, the animals were sacrificed and their brains were removed. One brain hemisphere was dissected on ice, immediately frozen and stored at –80 ºC until processing for protein quantification. The other brain hemisphere was fixed in 4% paraformaldehyde and processed for immunohistochemistry.

Aβ Immunohistochemistry. Tissue samples were embedded in paraffin and coronal sections (4 μm) were cut with a microtome. De-waxed sections were incubated with 98% formic acid (3 min) and then treated with citrate buffer (20 min) to enhance antigenicity. Then, the endogenous peroxidases were blocked by incubation in 10% MeOH–1% H_2O_2 solution (15 min). Sections were blocked with 3% normal horse serum solution and then incubated at 4 ºC overnight with the primary antibody against Aβ (1:50, Dako, Clone 6F/3D). Sections were subsequently rinsed and incubated with biotinylated secondary antibody (Dako), followed by EnVision+ system peroxidase (Dako) and finally with the chromogen diaminobenzidine and H_2O_2. Some sections were incubated without the primary antibody. No immunostaining was detected in these sections. Sections were lightly counterstained with haematoxylin. After staining, the sections were dehydrated and cover-slipped for microscopic observation. The Aβ burden in neocortex was calculated as the percentage of the Aβ deposition area with respect to the total area in 9 representative pictures in each animal, corresponding to the main regions where Aβ deposition is observed in AβPP/PS1 mice. Sections from all the AβPP/PS1 animals were evaluated by using the Analysis tool of the software Adobe® Photoshop® CS4.

Aβ Soluble Quantification: Enzyme-Linked Immunosorbent Assay (ELISA). Fresh-frozen mouse brain cortex was homogenized in 4 volumes (wt:vol) of TBS extraction buffer (140 mM NaCl, 3 mM KCl, 25 mM Tris (pH 7.4), 5 mM EDTA, and protease inhibitor cocktail (Roche Molecular Systems, Pleasanton, CA, USA). Homogenate was spun 100,000 g × 1 h and the supernatant was saved as the soluble fraction for Aβ quantification. $A\beta_{40}$ and $A\beta_{42}$ Human ELISA kits (Invitrogen™ Corporation, Camarillo, CA, USA) were used to quantify the levels of $A\beta_{40}$ and $A\beta_{42}$ peptides in the brain soluble fractions. Quantitative determination was carried out according to the manufacturer's instructions. $A\beta_{40}$ and $A\beta_{42}$ levels were normalized to the total

amount of protein from each individual sample (BCA method, Thermo Fisher Scientific, Wilmington, DE, USA).

Glial and Aβ Double-Immunofluorescence. De-waxed sections were stained with a saturated solution of Sudan black B (Merck) for 30 min to block the autofluorescence of lipofuscin granules present in cell bodies, then rinsed in 70% EtOH and washed in distilled water. The sections were treated with 98% formic acid (3 min) and with citrate buffer to enhance antigenicity, and then incubated at 4 ºC overnight with combinations of primary antibodies against Aβ (1:50, Dako) and GFAP (1:250, Dako, Denmark) or Iba1 (1:250, Wako, USA). After washing, the sections were incubated with Alexa488 or Alexa546 (1:400, Molecular Probes) fluorescence secondary antibodies against the corresponding host species. After washing, the sections were mounted in Immuno-Fluore Mounting medium (ICN Biomedicals, USA), sealed, and dried overnight. Sections were examined with an Olympus BX51 microscope.

Densitometric Quantification of Glia Around Aβ Plaques. Astrocytic and microglial responses to Aβ deposition were evaluated by densitometric quantification of GFAP and Iba1 protein expression levels around Aβ plaques, respectively. The GFAP and Iba1 immunostaining was in reference to the Aβ plaque area in 5 representative pictures taken from the neocortex of each animal (n=5 per group) using the software Adobe® Photoshop® CS4.

Statistical Analyses. Data were analyzed by two-way ANOVA with genotype and treatment as between factors, followed by Tukey's *post hoc* test. Aβ and glia quantifications were analyzed by one-way ANOVA followed by Tukey's *post hoc* test. The frequency of spontaneous seizures was analysed by Pearson's chi-squared test (χ^2). In all the experiments, the significance level was set at $p < 0.05$.

Molecular Modeling. The X-ray crystallographic structure of the recombinant human acetylcholinesterase (PDB ID: 3LII)[68] was used for docking calculations. *N*-acetyl-D-glucosamine and sulfate anions were removed, hydrogen atoms were added, and the missing loop defined by residues 259–263 was rebuilt from the X-ray structure of hAChE complexed with huprine W (PDB ID: 4BDT).[69] The enzyme was modeled in its physiological active form with neutral His447 and deprotonated Glu334, which together with Ser203 form the catalytic triad. PROPKA3[70] was used to assign the protonation state of ionizable residues at neutral pH, suggesting that residues Glu285, Glu450 and Glu452 were protonated. Finally, three disulfide bridges (residues 69–96, 257–272 and 409–529) were defined. Since Trp286 can adopt three main conformations in the peripheral binding site,[71] three models were built up by re-orienting the side chain of Trp286 as found in the X-ray structures of the AChE complexes with propidium, *bis*(7)-tacrine and *syn*-TZ2PA6 (PDB ID: 1N5R, 2CKM and 1Q83, respectively).

Docking was performed using the rDock program,[72] which was successful in predicting the binding mode of a variety of AChE inhibitors to the enzyme gorge.[71] A cavity of radius 17 Å, centered on a superligand containing huprine X, donepezil and propidium (as found in the X-ray structures 1E66, 1EVE and 1N5R)[36,73,74] was used to define the docking volume. Since huprine X and propidium are bound to the catalytic and peripheral binding sites, and donepezil is aligned along the gorge, this definition guarantees the exploration of the binding mode along the whole volume accessible for binding. Docking calculations were performed separately for the three models of the human enzyme (see above). Conformational flexibility around rotatable bonds of the ligand was allowed, whereas adjustments of other residues in the binding site were accounted for indirectly by rescaling (by a factor of 0.9) the van der Waals volume of atoms. Each

compound was subjected to 100 docking runs and the poses were sorted according to its docking score. The top 50 best scored poses were clustered and further analyzed by visual inspection.

AUTHOR INFORMATION

Corresponding Authors

* For D.M.-T.: phone: +34-934024533; E-mail: dmunoztorrero@ub.edu.

* For I.F.: phone: +34-932607452; E-mail: 8082ifa@gmail.com.

Author Contributions

‡ These authors contributed equally.

Notes

The authors declare no competing financial interest.

ACKNOWLEDGMENTS

This work was supported by Ministerio de Ciencia e Innovación (MICINN) (CTQ2011-22433, SAF2009-10553, start-up grant of the Ramón y Cajal program for R.S.), Ministerio de Economía y Competitividad (MINECO) (SAF2014-57094-R), Instituto de Salud Carlos III (ISCIII) (FIS PI14/00757) and Generalitat de Catalunya (GC) (2014SGR52, 2014SGR938, 2014SGR1189). Fellowships from GC to I.S. and from Lifelong Learning Programme/Erasmus to D.F., a contract from the Ramón y Cajal program of MICINN to R.S. (RYC-2011-07987), and a contract from the Juan de la Cierva program of MINECO to A.E. (JCI-2012-12193) are gratefully acknowledged. We thank Arnau Novell for his assistance in the chiral HPLC analyses of the enantiopure hybrids.

ABBREVIATIONS USED

Aβ, β-Amyloid peptide; AChE, acetylcholinesterase; AD, Alzheimer's disease; aMCI, amnestic mild cognitive impairment; APP, amyloid precursor protein; BBB, blood–brain barrier; BChE, butyrylcholinesterase; DTNB, 5,5'-dithiobis(2-nitrobenzoic acid); hAChE, human acetylcholinesterase; hBChE, human butyrylcholinesterase; ip, intraperitoneal; PAS, peripheral anionic site; RI, recognition index; Veh, vehicle; WT, wild-type.

REFERENCES

(1) Prince, M.; Bryce, R.; Albanese, E.; Wimo, A.; Ribeiro, W.; Ferri, C. P. The global prevalence of dementia: A systematic review and metaanalysis. *Alzheimer's Dementia* **2013**, *9*, 63–75.

(2) Alzheimer's Association. 2015 Alzheimer's disease facts and figures. www.alz.org. Accessed on March 26th 2015.

(3) Schneider, L. S.; Mangialasche, F.; Andreasen, N.; Feldman, H.; Giacobini, E.; Jones, R.; Mantua, V.; Mecocci, P.; Pani, L.; Winblad, B.; Kivipelto, M. Clinical trials and late-stage drug development for Alzheimer's disease: an appraisal from 1984 to 2014. *J. Intern. Med.* **2014**, *275*, 251–283.

(4) Hardy, J.; Selkoe, D. J. The amyloid hypothesis of Alzheimer's disease: progress and problems on the road to therapeutics. *Science* **2002**, *297*, 353–356.

(5) Mucke, L.; Selkoe, D. J. Neurotoxicity of amyloid-β protein: Synaptic and network dysfunction. *Cold Spring Harb. Perspect. Med.* **2012**, *2***,** a006338.

(6) Pimplikar, S. W. Reassessing the amyloid cascade hypothesis of Alzheimer's disease. *Int. J. Biochem. Cell Biol.* **2009**, *41*, 1261–1268.

(7) For reviews see references 7–12. Cavalli, A.; Bolognesi, M. L. Minarini, A, ; Rosini, M.; Tumiatti, V.; Recanatini, M.; Melchiorre, C. Multi-target-directed ligands to combat neurodegenerative diseases. *J. Med. Chem.* **2008**, *51*, 347–372.

(8) Guzior, N.; Wieckowska, A.; Panek, D.; Malawska, B. Recent development of multifunctional agents as potential drug candidates for the treatment of Alzheimer's disease. *Curr. Med. Chem.* **2015**, *22*, 373–404.

(9) Geldenhuys, W. J.; Van der Schyf, C. J. Rationally designed multi-targeted agents against neurodegenerative diseases. *Curr. Med. Chem.* **2013**, *20*, 1662–1672.

(10) Chen, X.; Decker, M. Multi-target compounds acting in the central nervous system designed from natural products. *Curr. Med. Chem.* **2013**, *20*, 1673–1685.

(11) Carreiras, M. C.; Mendes, E.; Perry, M. J.; Francisco, A. P.; Marco-Contelles, J. The multifactorial nature of Alzheimer's disease for developing potential therapeutics. *Curr. Top. Med. Chem.* **2013**, *13*, 1745–1770.

(12) Rampa, A.; Gobbi, S.; Belluti, F.; Bisi, A. Emerging targets in neurodegeneration: New opportunities for Alzheimer's disease treatment? *Curr. Top. Med. Chem.* **2013**, *13*, 1879–1904.

(13) For recent examples see references 13–19. Prati, F.; De Simone, A.; Bisignano, P.; Armirotti, A.; Summa, M.; Pizzirani, D.; Scarpelli, R.; Perez, D. I.; Andrisano, V.; Perez-Castillo, A.; Monti, B.; Massenzio, F.; Polito, L.; Racchi, M.; Favia, A. D.; Bottegoni, G.;

Martinez, A.; Bolognesi, M. L.; Cavalli, A. Multitarget drug discovery for Alzheimer's disease: Triazinones as BACE-1 and GSK-3β inhibidors. *Angew. Chem., Int. Ed.* **2015**, *54*, 1578-1582.

(14) Rochais, C.; Lecoutey, C.; Gaven, F.; Giannoni, P.; Hamidouche, K.; Hedou, D.; Dubost, E.; Genest, D.; Yahiaoui, S.; Freret, T.; Bouet, V.; Dauphin, F.; Sopkova de Oliveira Santos, J.; Ballandonne, C.; Corvaisier, S.; Malzert-Fréon, A.; Legay, R.; Boulouard, M.; Claeysen, S.; Dallemagne, P. Novel multitarget-directed ligands (MTDLs) with acetylcholinesterase (AChE) inhibitory and serotonergic subtype 4 receptor (5-HT_4R) agonist activities as potential agents against Alzheimer's disease: The design of donecopride. *J. Med. Chem.* **2015**, *58*, 3172–3187.

(15) Guzior, N.; Bajda, M.; Skrok, M.; Kurpiewska, K.; Lewinski, K.; Brus, B.; Pislar, A.; Kos, J.; Gobec, S.; Malawska, B. Development of multifunctional, heterodimeric isoindoline-1,3-dione derivatives as cholinesterase and β-amyloid aggregation inhibitors with neuroprotective properties. *Eur. J. Med. Chem.* **2015**, *92*, 738–749.

(16) Xie, S.-S.; Lan, J.-S.; Wang, X.-B.; Jiang, N.; Dong, G.; Li, Z.-R.; Wang, K. D. G.; Guo, P.-P.; Kong, L.-Y. Multifunctional tacrine–trolox hybrids for the treatment of Alzheimer's disease with cholinergic, antioxidant, neuroprotective and hepatoprotective properties. *Eur. J. Med. Chem.* **2015**, *93*, 42–50.

(17) Sang, Z.; Qiang, X.; Li, Y.; Yuan, W.; Liu, Q.; Shi, Y.; Wei, A.; Luo, Y.; Tan, Z.; Deng, Y. Design, synthesis and evaluation of scutellarein-O-alkylamines as multifunctional agents for the treatment of Alzheimer's disease. *Eur. J. Med. Chem.* **2015**, *94*, 348–366.

(18) Benchekroun, M.; Bartolini, M.; Egea, J.; Romero, A.; Soriano, E.; Pudlo, M.; Luzet, V.; Andrisano, V.; Jimeno. M.-L.; López, M. G.; Wehle, S.; Gharbi, T.; Refouvelet, B.; de Andrés, L.; Herrera-Arozamena, C.; Monti, B.; Bolognesi, M. L.; Rodríguez-Franco, M. I.; Decker, M.; Marco-Contelles, J.; Ismaili, L. Novel tacrine-grafted Ugi adducts as multipotent anti-Alzheimer drugs: A synthetic renewal in tacrine–ferulic acid hybrids, *ChemMedChem* **2015**, *10*, 523–539.

(19) Liu, Q.; Qiang, X.; Li, Y.; Sang, Z.; Li, Y.; Tan, Z.; Deng, Y. Design, synthesis and evaluation of chromone-2-carboxamidoalkylbenzylamines as multifunctional agents for the treatment of Alzheimer's disease. *Bioorg. Med. Chem.* **2015**, *23*, 911–923.

(20) Brogi, S.; Butini, S.; Maramai, S.; Colombo, R.; Verga, L.; Lanni, C.; De Lorenzi, E.; Lamponi, S.; Andreassi, M.; Bartolini, M.; Andrisano, V.; Novellino, E.; Campiani, G.; Brindisi, M.; Gemma, S. Disease-modifying anti-Alzheimer's drugs: Inhibitors of human cholinesterases interfering with β-amyloid aggregation. *CNS Neurosci. Ther.* **2014**, *20*, 624–632.

(21) Viayna, E.; Sabate, R.; Muñoz-Torrero, D. Dual inhibitors of β-amyloid aggregation and acetylcholinesterase as multi-target anti-Alzheimer drug candidates. *Curr. Top. Med. Chem.* **2013**, *13*, 1820–1842.

(22) Inestrosa, N. C.; Alvarez, A.; Pérez, C. A.; Moreno, R. D.; Vicente, M.; Linker, C.; Casanueva, O. I.; Soto, C.; Garrido, J. Acetylcholinesterase accelerates assembly of amyloid-β-peptides into Alzheimer's fibrils: possible role of the peripheral site of the enzyme. *Neuron* **1996**, *16*, 881–891.

(23) De Ferrari, G. V.; Canales, M. A.; Shin, I.; Weiner, L. M.; Silman, I.; Inestrosa, N. C. A structural motif of acetylcholinesterase that promotes amyloid beta-peptide fibril formation. *Biochemistry* **2001**, *40*, 10447–10457.

(24) Palop, J. J.; Mucke, L. Epilepsy and cognitive impairments in Alzheimer disease. *Arch. Neurol.* **2009**, *66*, 435–440.

(25) Palop, J. J.; Mucke, L. Amyloid-β–induced neuronal dysfunction in Alzheimer's disease: from synapses toward neural networks. *Nat. Neurosci.* **2010**, *13*, 812–818.

(26) Vossel, K. A.; Beagle, A. J.; Rabinovici, G. D.; Shu, H.; Lee, S. E.; Naasan, G.; Hegde, M.; Cornes, S. B.; Henry, M. L.; Nelson, A. B.; Seeley, W. W.; Geschwind, M. D.; Gorno-Tempini, M. L.; Shih, T.; Kirsch, H. E.; Garcia, P. A.; Miller, B. L.; Mucke, L. Seizures and epileptiform activity in the early stages of Alzheimer disease. *JAMA Neurol.* **2013**, *70*, 1158–1166.

(27) McCarron, M.; Gill, M.; McCallion, P.; Begley, C. Health co-morbidities in ageing persons with Down syndrome and Alzheimer's dementia. *J. Intellect. Disabil. Res.* **2005**, *49*, 560–566.

(28) Palop, J. J.; Chin, J.; Roberson, E. D.; Wang, J.; Thwin, M. T.; Bien-Ly, N.; Yoo, J.; Ho, K. O.; Yu, G. Q.; Kreitzer, A.; Finkbeiner, S.; Noebels, J. L.; Mucke, L. Aberrant excitatory neuronal activity and compensatory remodeling of inhibitory hippocampal circuits in mouse models of Alzheimer's disease. *Neuron* **2007**, *55*, 697–711.

(29) Bakker, A.; Krauss, G. L.; Albert, M. S.; Speck, C. L.; Jones, L. R.; Stark, C. E.; Yassa, M. A.; Bassett, S. S.; Shelton, A. L.; Gallagher, M. Reduction of hippocampal

hyperactivity improves cognition in amnestic mild cognitive impairment. *Neuron* **2012**, *74*, 467–474.

(30) Sanchez, P. E.; Zhu, L.; Verret, L.; Vossel, K. A.; Orr, A. G.; Cirrito, J. R.; Devidze, N.; Ho, K.; Yu, G.-Q.; Palop, J. J.; Mucke, L. Levetiracetam suppresses neuronal network dysfunction and reverses synaptic and cognitive deficits in an Alzheimer's disease model. *Proc. Natl. Acad. Sci. U. S. A.* **2012**, *109*, E2895–E2903.

(31) Shi, J.-Q.; Wang, B.-R.; Tian, Y.-Y.; Xu, J.; Gao, L.; Zhao, S.-L.; Jiang, T.; Xie, H.-G.; Zhang, Y.-D. Antiepileptics topiramate and levetiracetam alleviate behavioral deficits and reduce neuropathology in APPswe/PS1dE9 transgenic mice. *CNS Neurosci. Ther.* **2013**, *19*, 871–881.

(32) Mucke, L.; Selkoe, D. J. Neurotoxicity of amyloid-β protein: Synaptic and network dysfunction. *Cold Spring Harb. Perspect. Med.* **2012**, *2***,** a006338.

(33) Camps, P.; Contreras, J.; Font-Bardia, M.; Morral, J.; Muñoz-Torrero, D.; Solans, X. Enantioselective synthesis of tacrine–huperzine A hybrids. Preparative chiral MPLC separation of their racemic mixtures and absolute configuration assignments by X-ray diffraction analysis. *Tetrahedron: Asymmetry* **1998**, *9*, 835–849.

(34) Camps, P.; El Achab, R.; Morral, J.; Muñoz-Torrero, D.; Badia, A.; Baños, J. E.; Vivas, N. M.; Barril, X.; Orozco, M.; Luque, F. J. New tacrine–huperzine A hybrids (huprines): Highly potent tight-binding acetylcholinesterase inhibitors of interest for the treatment of Alzheimer's disease. *J. Med. Chem.* **2000**, *43*, 4657–4666.

(35) Camps, P.; Cusack, B.; Mallender, W. D.; El Achab, R.; Morral, J.; Muñoz-Torrero, D.; Rosenberry, T. L. Huprine X is a novel high-affinity inhibitor of acetylcholinesterase that is of interest for the treatment of Alzheimer's disease. *Mol. Pharmacol.* **2000**, *57*, 409–417.

(36) Dvir, H.; Wong, D. M.; Harel, M.; Barril, X.; Orozco, M.; Luque, F. J.; Muñoz-Torrero, D.; Camps, P.; Rosenberry, T. L.; Silman, I.; Sussman, J. L. 3D Structure of *Torpedo californica* acetylcholinesterase complexed with huprine X at 2.1 Å resolution: Kinetic and molecular dynamics correlates. *Biochemistry* **2002**, *41*, 2970–2981.

(37) Viayna, E.; Sola, I.; Bartolini, M.; De Simone, A.; Tapia-Rojas, C.; Serrano, F. G.; Sabaté, R.; Juárez-Jiménez, J.; Pérez, B.; Luque, F. J.; Andrisano, V.; Clos, M. V.; Inestrosa, N. C.; Muñoz-Torrero, D. Synthesis and multitarget biological profiling of a novel family of rhein derivatives as disease-modifying anti-Alzheimer agents. *J. Med. Chem.* **2014**, *57*, 2549–2567.

(38) Di Pietro, O.; Pérez-Areales, F. J.; Juárez-Jiménez, J.; Espargaró, A.; Clos, M. V.; Pérez, B.; Lavilla, R.; Sabaté, R.; Luque, F. J.; Muñoz-Torrero, D. Tetrahydrobenzo[*h*][1,6]naphthyridine-6-chlorotacrine hybrids as a new family of anti-Alzheimer agents targeting β-amyloid, tau, and cholinesterase pathologies. *Eur. J. Med. Chem.* **2014**, *84*, 107–117.

(39) Pérez-Areales, F. J.; Di Pietro, O.; Espargaró, A.; Vallverdú-Queralt, A.; Galdeano, C.; Ragusa, I. M.; Viayna, E.; Guillou, C.; Clos, M. V.; Pérez, B.; Sabaté, R.; Lamuela-Raventós, R. M.; Luque, F. J.; Muñoz-Torrero, D. Shogaol–huprine hybrids: Dual

antioxidant and anticholinesterase agents with β-amyloid and tau anti-aggregating properties. *Bioorg. Med. Chem.* **2014**, *22*, 5298–5307.

(40) Galdeano, C.; Viayna, E.; Sola, I.; Formosa, X.; Camps, P.; Badia, A.; Clos, M. V.; Relat, J.; Ratia, M.; Bartolini, M.; Mancini, F.; Andrisano, V.; Salmona, M.; Minguillón, C.; González-Muñoz, G. C.; Rodríguez-Franco, M. I.; Bidon-Chanal, A.; Luque, F. J.; Muñoz-Torrero, D. Huprine–tacrine heterodimers as anti-amyloidogenic compounds of potential interest against Alzheimer's and prion diseases. *J. Med. Chem.* **2012**, *55*, 661–669.

(41) Pang, Y.-P.; Quiram, P.; Jelacic, T.; Hong, F.; Brimijoin, S. Highly potent, selective, and low cost bis-tetrahydroaminacrine inhibitors of acetylcholinesterase. *J. Biol. Chem.* **1996**, *271*, 23646–23649.

(42) Li, W. M.; Kan, K. K. W.; Carlier, P. R.; Pang, Y. P.; Han, Y. F. East meets West in the search for Alzheimer's therapeutics - Novel dimeric inhibitors from tacrine and huperzine A. *Curr. Alzheimer Res.* **2007**, *4*, 386–396.

(43) Boschi, F.; Camps, P.; Comes-Franchini, M.; Muñoz-Torrero, D.; Ricci, A.; Sánchez, L. A synthesis of levetiracetam based on (*S*)-*N*-phenylpantolactam as a chiral auxiliary. *Tetrahedron: Asymmetry* **2005**, *16*, 3739–3745.

(44) Carlier, P. R.; Chow, E. S.-H.; Han, Y.; Liu, J.; El Yazal, J.; Pang, Y.-P. Heterodimeric tacrine-based acetylcholinesterase inhibitors: Investigating ligand–peripheral site interactions. *J. Med. Chem.* **1999**, *42*, 4225–4231.

(45) Muñoz-Ruiz, P.; Rubio, L.; García-Palomero, E.; Dorronsoro, I.; del Monte-Millán, M.; Valenzuela, R.; Usán, P.; de Austria, C.; Bartolini, M.; Andrisano, V.; Bidon-Chanal, A.; Orozco, M.; Luque, F. J.; Medina, M.; Martínez, A. Design, synthesis, and biological evaluation of dual binding site acetylcholinesterase inhibitors: New disease-modifying agents for Alzheimer's disease. *J. Med. Chem.* **2005**, *48*, 7223–7233.

(46) Sola, I.; Viayna, E.; Gómez, T.; Galdeano, C.; Cassina, M.; Camps, P.; Romeo, M.; Diomede, L.; Salmona, M.; Franco, P.; Schaeffer, M.; Colantuono, D.; Robin, D.; Brunner, D.; Taub, N.; Hutter-Paier, B.; Muñoz-Torrero, D. Multigram synthesis and *in vivo* efficacy studies of a novel multitarget anti-Alzheimer compound. *Molecules* **2015**, *20*, 4492–4515.

(47) Lane, R. M.; Potkin, S. G.; Enz, A. Targeting acetylcholinesterase and butyrylcholinesterase in dementia. *Int. J. Neuropsychopharmacol.* **2006**, *9*, 101–124.

(48) Macdonald. I. R.; Rockwood, K.; Martin, E.; Darvesh, S. Cholinesterase inhibition in Alzheimer's disease: Is specificity the answer? *J. Alzheimer's Dis.* **2014**, *42*, 379–384.

(49) Ellman, G. L.; Courtney, K. D.; Andres, V., Jr.; Featherstone, R. M. A new and rapid colorimetric determination of acetylcholinesterase activity. *Biochem. Pharmacol.* **1961**, *7*, 88–95.

(50) Recanatini, M.; Cavalli, A.; Belluti, F.; Piazzi, L.; Rampa, A.; Bisi, A.; Gobbi, S.; Valenti, P.; Andrisano, V.; Bartolini, M., Cavrini, V. SAR of 9-amino-1,2,3,4-tetrahydroacridine-based acetylcholinesterase inhibitors: Synthesis, enzyme inhibitory

activity, QSAR, and structure-based CoMFA of tacrine analogues. *J. Med. Chem.* **2000**, *43*, 2007–2018.

(51) Wlodek, S. T.; Antosiewicz, J.; McCammon, J. A.; Straatsma, T. P.; Gilson, M. K.; Briggs, J. M.; Humblet, C.; Sussman, J. L. Binding of tacrine and 6-chlorotacrine by acetylcholinesterase. *Biopolymers* **1996**, *38*, 109–117.

(52) Savini, L.; Gaeta, A.; Fattorusso, C.; Catalanotti, B.; Campiani, G.; Chiasserini, L.; Pellerano, C.; Novellino, E.; McKissic, D.; Saxena, A. Specific targeting of acetylcholinesterase and butyrylcholinesterase recognition sites. Rational design of novel, selective, and highly potent cholinesterase inhibitors. *J. Med. Chem.* **2003**, *46*, 1–4.

(53) Elsinghorst, P. W.; Cieslik, J. S.; Mohr, K.; Tränkle, C.; Gütschow, M. First gallamine–tacrine hybrid: Design and characterization at cholinesterases and the M_2 muscarinic receptor. *J. Med. Chem.* **2007**, *50*, 5685–5695.

(54) Medina, M.; Avila, J. New perspectives on the role of tau in Alzheimer's disease. Implicactions for therapy. *Biochem. Pharmacol.* **2014**, *88*, 540–547.

(55) Lansdall, C. J. An effective treatment for Alzheimer's disease must consider both amyloid and tau. *Biosci. Horiz.* **2014**, *7*, hzu002.

(56) Villar-Piqué, A.; Ventura, S. Modeling amyloids in bacteria. *Microb. Cell Fact.* **2012**, *11*, 166.

(57) Pouplana, S.; Espargaró, A.; Galdeano, C.; Viayna, E.; Sola, I.; Ventura, S.; Muñoz-Torrero, D.; Sabate, R. Thioflavin-S staining of bacterial inclusion bodies for the fast,

simple, and inexpensive screening of amyloid aggregation inhibitors. *Curr. Med. Chem.* **2014**, *21*, 1152–1159.

(58) Roberson, E. D.; Halabisky, B.; Yoo, J. W.; Yao, J.; Chin, J.; Yan, F.; Wu, T.; Hamto, P.; Devidze, N.; Yu, G.-Q.; Palop, J. J.; Noebels, J. L.; Mucke, L. Amyloid-*β*/Fyn–induced synaptic, network, and cognitive impairments depend on tau levels in multiple mouse models of Alzheimer's disease. *J. Neurosci.* **2011**, *31*, 700–711.

(59) Lipinski, C. A.; Lombardo, F.; Dominy, B. W.; Feeney, P. J. Experimental and computational approaches to estimate solubility and permeability in drug discovery and development settings. *Adv. Drug Delivery Rev.* **1997**, *23*, 3–25.

(60) Morphy, R.; Rankovic, Z. Designing multiple ligands – medicinal chemistry strategies and challenges. *Curr. Pharm. Des.* **2009**, *15*, 587–600.

(61) Lynch, B. A.; Lambeng, N.; Nocka, K.; Kensel-Hammes, P.; Bajjalieh, S. M.; Matagne, A.; Fuks, B. The synaptic vesicle protein SV2A is the binding site for the antiepileptic drug levetiracetam. *Proc. Natl. Acad. Sci. U.S.A.* **2004**, *101*, 9861–9866.

(62) Vogl, C.; Mochida, S.; Wolff, C.; Whalley, B. J.; Stephens, G. J. The synaptic vesicle glycoprotein 2A ligand levetiracetam inhibits presynaptic Ca^{2+} channels through an intracellular pathway. *Mol. Pharmacol.* **2012**, *82*, 199–208.

(63) Farooq, M. U.; Bhatt, A.; Majid, A.; Gupta, R.; Khasnis, A.; Kassab, M. Y. Levetiracetam for managing neurologic and psychiatric disorders. *Am. J. Health Syst. Pharm.* **2009**, *66*, 541–561.

(64) Ferrer, I. Defining Alzheimer as a common age-related neurodegenerative process not inevitably leading to dementia. *Prog. Neurobiol.* **2012**, *97*, 38–51.

(65) Viayna, E.; Gómez, T.; Galdeano, C.; Ramírez, L.; Ratia, M.; Badia, A.; Clos, M. V.; Verdaguer, E.; Junyent, F.; Camins, A.; Pallàs, M.; Bartolini, M.; Mancini, F.; Andrisano, V.; Arce, M. P.; Rodríguez-Franco, M. I.; Bidon-Chanal, A.; Luque, F. J.; Camps, P.; Muñoz-Torrero, D. Novel huprine derivatives with inhibitory activity toward β-amyloid aggregation and formation as disease-modifying anti-Alzheimer drug candidates. *ChemMedChem* **2010**, *5*, 1855–1870.

(66) Lassiter, T. L.; Marshall, R. S.; Jackson, L. C.; Hunter, D. L.; Vu, J. T.; Padilla, S. Automated measurement of acetylcholinesterase activity in rat peripheral tissues. *Toxicology* **2003**, *186*, 241–253.

(67) Borchelt, D. R.; Ratovitski, T.; van Lare, J.; Lee, M. K.; Gonzales, V.; Jenkins, N. A.; Copeland, N. G.; Price, D. L.; Sisodia, S. S. Accelerated amyloid deposition in the brains of transgenic mice coexpressing mutant presenilin 1 and amyloid precursor proteins. *Neuron* **1997**, *19*, 939–945.

(68) Dvir, H.; Silman, I.; Harel, M.; Rosenberry, T. L.; Sussman, J. L. Acetylcholinesterase: from 3D structure to function. *Chem. Biol. Interact.* **2010**, *187*, 10–22.

(69) Nachon, F.; Carletti, E.; Ronco, C.; Trovaslet, M.; Nicolet, Y.; Jean, L.; Renard, P.-Y. Crystal structures of human cholinesterases in complex with huprine W and tacrine: Elements of specificity for anti-Alzheimer's drugs targeting acetyl- and butyrylcholinesterase. *Biochem. J.* **2013**, *453*, 393–399.

(70) Olsson, M. H. M.; Sondergard, C. R.; Rostkowski, M.; Jensen, J. H. PROPKA3: Consistent treatment of internal and surface residues in empirical pKa predictions. *J. Chem. Theory Comput*. **2011**, *7*, 525–537.

(71) Camps, P.; Formosa, X.; Galdeano, C.; Muñoz-Torrero, D.; Ramírez, L.; Gómez, E.; Isambert, N.; Lavilla, R.; Badia, A.; Clos, M. V.; Bartolini, M.; Mancini, F.; Andrisano, V.; Arce, M. P.; Rodríguez-Franco, M. I.; Huertas, O.; Dafni, T.; Luque, F. J. Pyrano[3,2-*c*]quinoline–6-chlorotacrine hybrids as a novel family of acetylcholinesterase- and β-amyloid-directed anti-Alzheimer compounds. *J. Med. Chem*. **2009**, *52*, 5365–5379.

(72) Ruiz-Carmona, S.; Alvarez-García, D.; Foloppe, N.; Garmendia-Doval, A. B.; Juhos, S.; Schmidtke, P.; Barril, X.; Hubbard, R. E.; Morley, S. D. rDock: A fast, versatile and open source code for docking ligands to proteins and nucleic acids. *PLOS Comput. Biol*. **2014**, *10*, e1003571.

(73) Kryger, G.; Silman, I.; Sussman, J. L. Structure of acetylcholinesterase complexed with E2020 (Aricept): Implications for the design of new anti-Alzheimer drugs, *Structure* **1999**, *7*, 297–307.

(74) Bourne, Y.; Taylor, P.; Radic, Z.; Marchot, P. Structural insights into ligand interactions at the acetycholinesterase peripheral anionic site. *EMBO J.* **2003**, *22*, 1–12.

TOC graphic

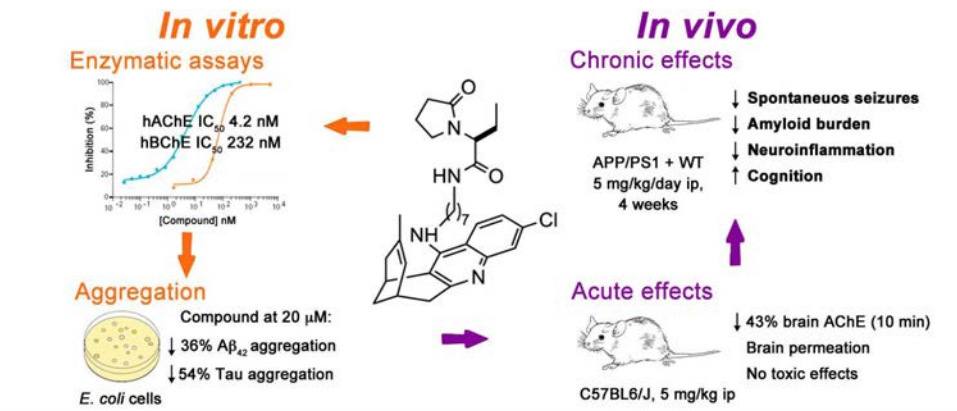
In vitro
Enzymatic assays
hAChE IC50 4.2 nM
hBChE IC50 232 nM
Inhibition (%)
[Compound] nM
Aggregation
Compound at 20 μM:
↓ 36% Aβ42 aggregation
↓ 54% Tau aggregation
E. coli cells
HN
O
N
NH
Cl
In vivo
Chronic effects
APP/PS1 + WT
5 mg/kg/day ip,
4 weeks
↓ Spontaneuos seizures
↓ Amyloid burden
↓ Neuroinflammation
↑ Cognition
Acute effects
↓ 43% brain AChE (10 min)
Brain permeation
No toxic effects
C57BL6/J, 5 mg/kg ip

CHAPTER 6

Exploitation of the huprine scaffold for HAT drug development

6.1. Drug repurposing strategy from anti-Alzheimer compounds to antiprotozoal agents

At a first glance, drug discovery approaches for AD and NTD may appear antithetical. But both diseases are major health problems and leading causes of death worldwide, with no efficient drug available that can change the prognosis of these diseases or lead to a dramatic recovery. In this light, links in methodology and meaning become clear, but these do not appear to be the only connecting links between both diseases.

An increasing number of publications claim the use of the multitarget approach for the development of novel drugs to efficiently tackle both diseases.[405] In this light, "privileged structures" could offer a viable starting point in the search for novel MTDL because of their inherent affinity for various targets.[406] Within this context, quinoline derivatives have been reported as a major class of privileged motifs which are in fact commonly found in the drug discovery field of AD and NTD. This trait can be related to their ability to form a range of π–π-stacking interactions with nucleic acid bases, aromatic amino acids, and porphyrines by means of its aromatic core structure (**Figure 6.1**).[176]

For instance, clioquinol (**35**, **Figure 6.1**), an 8-hydroxyquinoline, is a good example of a potential anti-AD drug.[186] **35** has a moderate chelating affinity for Cu and Zn and inhibits metal-induced Aβ aggregation and reactive oxygen species generation *in vitro* and in AD transgenic mice,[407,408] and has shown activity in reducing Aβ levels and improving behavioral deficits in mouse models of Aβ pathology.[409] Furthermore, hybrid compounds consisting of tacrine or other quinoline scaffolds have been also designed as potential multitarget anti-AD drug candidates, for example *bis*(7)-tacrine (**8, Figure 6.1**).

On the other hand, the prototype of quinolines for its use in the treatment of protozoan diseases is chloroquine (**29**, **Figure 6.1**), the first synthetic antimalarial drug, which was developed in the 1950s. Various other 8-substituted quinolines were registered as antimalarials, including primaquine, mefloquine, and amodiaquine (**see section 3.3**). Moreover, a very active

[176] Bongarzone, S.; Bolognesi, M. L. *Expert Opin. Drug Discov.* **2011**, *6*, 251−268.
[186] Adlard, P. A.; Cherny, R. A.; Finkelstein, D. I. *et al. Neuron.* **2008**, *59*, 43−55.
[405] Prati, F.; Uliassi, E.; Bolognesi, M. L. *Med. Chem. Commun*. **2014**, *5*, 853–861.
[406] Morphy, R.; Kay, C.; Rankovic, Z. *Drug Discov. Today*, **2004**, *9*, 641–651.
[407] Cherny, R. A.; Atwood, C. S.; Xilinas, M. E. *et al. Neuron* **2001**, *30*, 665−676.
[408] Ritchie, C. W.; Bush, A. I.; Mackinnon, A. *et al*. *Arch. Neurol.* **2003**, *60*, 1685−1691.
[409] LeVine H. 3rd.; Ding, Q.; Walker, J. A. *et al*. *Neurosci. Lett.* **2009**, *465*, 99−103.

area of quinoline research involves identifying 'dual inhibitors' or 'double drugs' that will potentially inhibit multiple targets within *P. falciparum*.[195,196] New antimalarial therapies based on these multitarget drugs may have higher efficacy and reduced likelihood of development of resistance with respect to those based on single-target drugs. Particularly, a number of 4-amino-7-chloroquinolines and other aminoquinoline derivatives have been recently synthesized and found to be active against *T. brucei* and/or *P. falciparum*,[189,190,203,204] the causative agents of HAT and malaria, respectively, which is of great interest because both diseases often affect overlapping populations in developing countries, and thus development of compounds endowed with dual trypanocidal and antiplasmodial activity may become a feasible economic therapeutic strategy.[410]

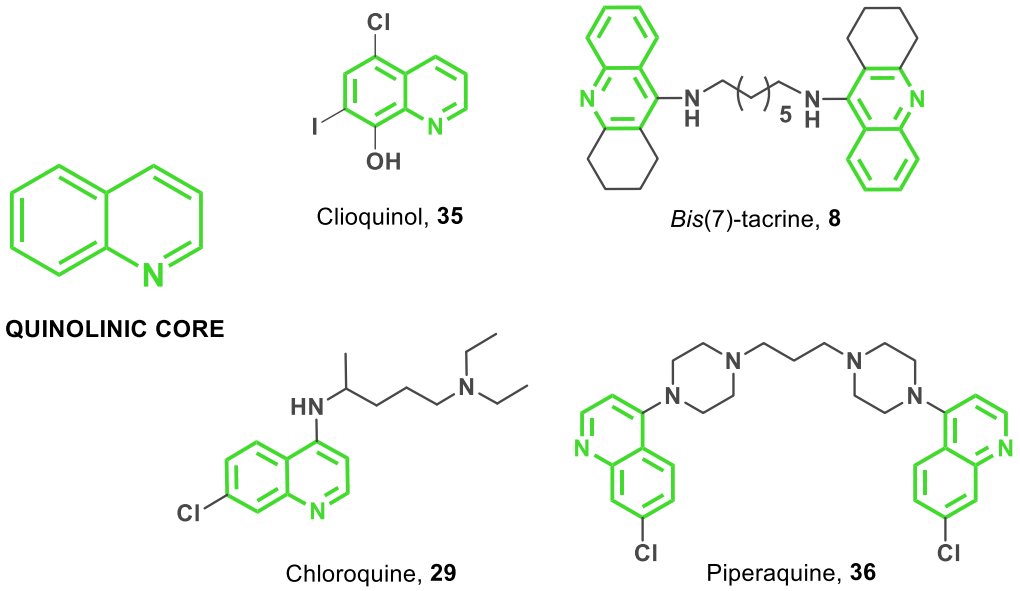

Figure 6.1. Anti-Alzheimer compounds (**8** and **35**) and antiprotozoal agents (**29** and **36**) bearing a quinolinic core within their structure.

Within these findings in mind, our research group decided to assess the antiprotozoal activity of huprines, a structural class of compounds featuring a 4-aminoquinoline moiety, which, as we have previously seen, had been initially developed as brain permeable inhibitors of the AChE enzyme for its use in AD chemotherapy (see **section *1.3.1.3***). After an exhaustive evaluation of

[189] Musonda, C. C.; Gut, J.; Rosenthal, P. J. *et al. Bioorg. Med. Chem.* **2006**, *14*, 5605–5615.
[190] Musonda, C. C.; Yardley, V.; de Souza, R. C. C. *et al. Org. Biomol. Chem.* **2008**, *6*, 4446–4451.
[195] Kouznetsov, V. V.; Gomez-Barrio, A. *Eur. J. Med. Chem.* **2009**, *44*, 3091−3113.
[196] Muregi, F. W.; Ishih, A. *Drug Dev. Res.* **2010**, 71, 20−32.
[203] Upadhayaya, R. S.; Dixit, S. S.; Földesi, A. *et al. Bioorg. Med. Chem. Lett*. **2013**, *23*, 2750−2758.
[204] Rashad, A. A.; Jones, A. J.; Avery, V. M. *et al*. *ACS Med. Chem. Lett*. **2014**, *5*, 496−500.
[410] Chibale, K. *Pure Appl. Chem.* **2005**, *77*, 1957−1964.

more than 30 huprines, we found them to be moderately potent and selective trypanocidal agents, with a few also being active against the chloroquine-resistant K1 strain of *P. falciparum*.[202,206] In fact, huprine Y (**11**, **Figure 6.2**) exhibited the most potent activity against *T. brucei* and one of the best selectivity indices over rat myoblast L6 cells, besides a proven ability of crossing BBB which is considered an appealing property given the lack of a satisfying treatment for late-stage HAT, but it was essentially devoid of antiplasmodial activity.[206]

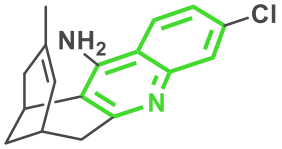

Huprine Y, **11**

T. brucei IC_{50} = 0.61 µM
T. brucei IC_{90} = 2.94 µM
rat L6 cells IC_{50} = 7.80 µM
SI = 13
hAChE IC_{50} = 0.61 nM

Figure 6.2. Huprine Y (**11**) and its biological profiling.

The lack of potency of huprines against *P. falciparum* was rather striking because their close structural similarity with chloroquine, the most used antimalarial compound for centuries and considered to be the pharmocophoric moiety responsible for the inhibition of dimerization and crystallization of free haem, generated during the digestion of hemoglobin in the host erythrocytes, into nontoxic insoluble haemozoin, which results in increased levels of toxic haem, and ultimately in parasite death.[190,411,412] Hence we hypothesized that the lack of antimalarial activity of huprines might be ascribed to the inability to hit the biological target of chloroquine. For this reason, we focused our next projects in the hit-to-lead optimization of huprines towards its trypanocidal activity.

6.2. Hit-to-lead optimization by huprine dimerization

Given the fact that molecular dimerization had been reported to increase antiprotozoal activity and/or overcome drug resistance, mainly in the malaria field due to a more efficient trapping in the acidic digestive vacuole of the parasite and prevention of heme polymerization,[179,413] our next aim was to explore the dimerization strategy on the huprine scaffold in order to identify

[179] Kaur, K.; Jain, M.; Reddy, R. P. *et al*. *Eur. J. Med. Chem.* **2010**, *45*, 3245–3264.
[190] Musonda, C. C.; Yardley, V.; de Souza, R. C. C. *et al. Org. Biomol. Chem.* **2008**, *6*, 4446–4451.
[202] Oluwafemi, A. J.; Okanla, E. O.; Camps, P. *et al. Nat. Prod. Commun.* **2009**, *4*, 193–198.
[206] Defaux, J.; Sala, M.; Formosa, X. *et al. Bioorg. Med. Chem.* **2011**, *19*, 1702–1707.
[411] Egan, T. J. *Drug Des. Rev. Online* **2004**, *1*, 93–110.
[412] Onyeibor, O.; Croft, S. L.; Dodson, H. I. *et al. J. Med. Chem*. **2005**, *48*, 2701−2709.
[413] Girault, S.; Grellier, P.; Berecibar, A. *et al. J. Med. Chem*. **2000**, *43*, 2646−2654.

compounds with more favourable trypanocidal/cytotoxic and trypanocidal/anticholinesterase activity ratios than monomeric huprines.

For that purpose, we envisaged the preparation of several homo- and hetero-dimers containing at least one huprine or a closely related 4-aminoquinoline moiety, with the two constituting units connected through linkers of different chemical nature and length.

In the event, as we will discuss below, this approach proved to be successful in the pursuit of a trypanocidal potency improvement. For instance, the novel dodecamethylene-linked *bis*(+)-huprine Y, **101d**, (**Figure 6.3**) achieved a three-fold enhancement of the selectivity of the parent huprine Y, **11**, (**SI= 13, Figure 6.2**) against *T. brucei.* Interestingly, the lead heterodimeric compounds **102d** and **103d** comprising also two quinoline moieties connected in both cases with a nonamethylene linker, achieved a greater trypanocidal potency and selectivity than **101d** (**Figure 6.3**).

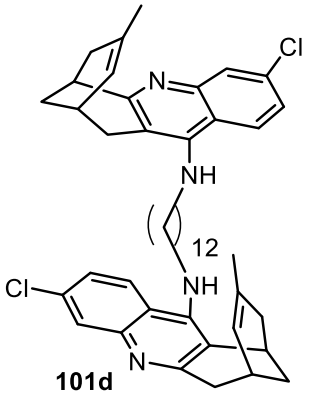

101d

T. brucei IC_{50} = 0.76 ± 0.03 μM
T. brucei IC_{90} = 0.99 ± 0.05 μM
L6 cells IC_{50} = 28.5 ± 2.9 μM
SI = 37.5

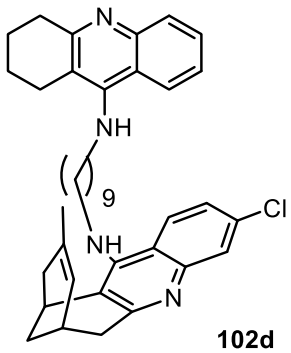

102d

T. brucei IC_{50} = 0.21 ± 0.03 μM
T. brucei IC_{90} = 0.45 ± 0.02 μM
L6 cells IC_{50} = 7.15 ± 0.30 μM
SI = 34

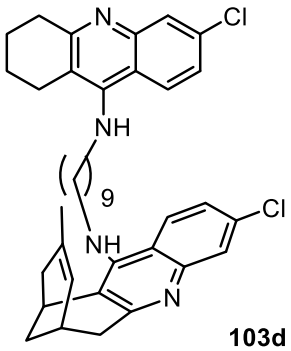

103d

T. brucei IC_{50} = 0.24 ± 0.04 μM
T. brucei IC_{90} = 0.52 ± 0.01 μM
L6 cells IC_{50} = 40 ± 5.1 μM
SI = 167

Figure 6.3. Lead huprine-based homo- and heterodimeric compounds **101d** and **102**,**103d** belonging to the next projects described below.

6.2.1. Bis(+)-Huprines (*Bioorg. Med. Chem. Lett*. **2014**, *24*, 5435)

A novel series of homodimers of huprines named as *bis*-huprines was prepared through a straightforward route and later evaluated against *T. brucei* and *P. falciparum*. The cytotoxicity of this series was also assessed using rat skeletal myoblast L6 cells, besides their AChE inhibition.

6.2.1.1. Preparation of bis(+)-huprines (+)-101a–e

The synthesis of this short series of compounds was carried out by a one-pot double nucleophilic substitution reaction with 2 equiv. of (+)-(7*R*,11*R*)-huprine Y, (+)-**11**, and 1 equiv. of the corresponding α,ω-dihaloalkane, **104a**–**e**, using KOH as the base in DMSO at r. t. for three days. All homodimers were isolated after silica gel column chromatography of the crude products, albeit in low yields, due to the formation of β-elimination byproducts (+)-**105** in different proportions (**Scheme 6.1**). β-Elimination byproducts (+)-**105a**–**d** could not be isolated.

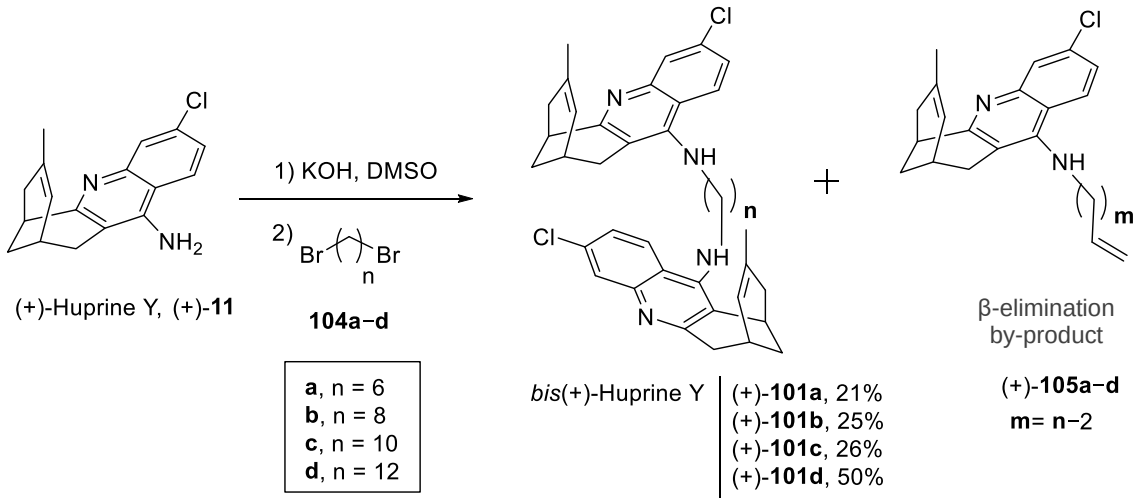

Scheme 6.1. One-pot synthesis of oligomethylene-linked *bis*(+)-huprines (+)-**101a**–**d**.

During the formation of the *p*-phenylene-bis(methylene)-linked *bis*(+)-huprine (+)-**101**e, a significant percentage of monoalkylation byproduct, (+)-**105e**, was also isolated (**Scheme 6.2**).

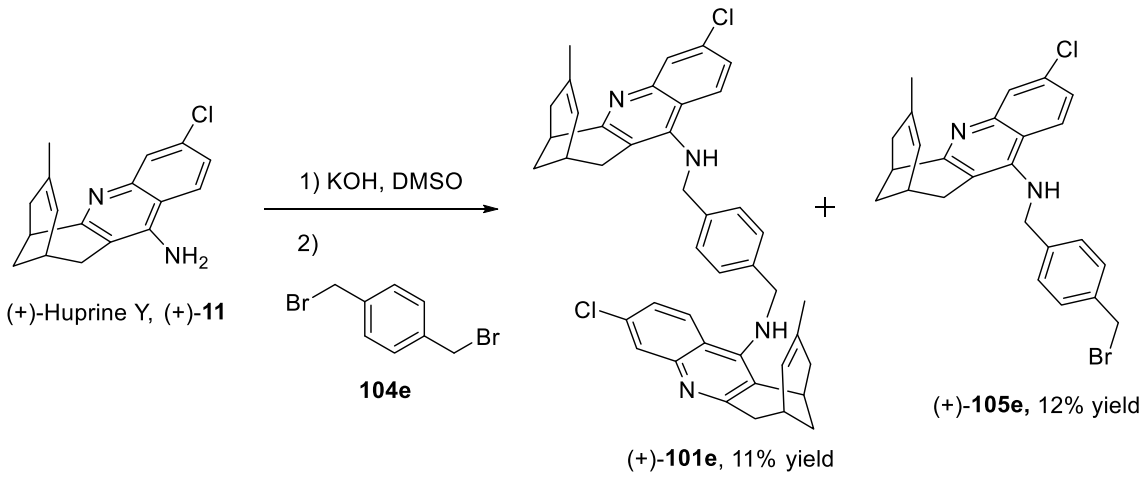

Scheme 6.2. Obtention of *p*-phenylene-bis(methylene)-linked *bis*(+)-huprine (+)-**101e**.

6.2.1.2. Pharmacological evaluation of bis(+)-huprines (+)-101a–e

The antitrypanosomal and cytotoxic activities of bis(+)-huprines were assessed by the group of Dr. John M. Kelly (London School of Hygiene and Tropical Medicine, UK). The antimalarial activity of these compounds was determined by the group of Dr. Colin W. Wright (University of Bradford, UK). The AChE inhibitory activity and brain permeability were determined by Drs. M. Victòria Clos and Belén Pérez (Universitat Autònoma de Barcelona).

All *bis*(+)-huprines, (+)-**101a**–**e**, showed similar *in vitro* potencies against cultured bloodstream forms of *T. brucei* in spite of the structural differences between them, with IC_{50} values in the range 0.50–0.89 μM and IC_{90} values around 1 μM, significantly lower than that of the parent huprine Y (IC_{90} = 2.94 μM).

Bis(+)-huprines (+)-**101a**–**e** were also evaluated against the chloroquine-resistant K1 strain of *P. falciparum*, but despite the moderate antiplasmodial activity displayed by some huprines,[206] all this series of compounds exhibited very low inhibitory potencies (IC_{50} > 6–7 μM), similar to that found for the parent huprine Y (IC_{50} > 10 μM).

Moreover, they displayed a modest toxicity against the mammalian L6 cells, exhibiting IC_{50} values in the range 1.6–28.5 μM. In this case, a clear structure–cytotoxicity trend was found, with cytotoxicity decreasing with increased tether length and with the presence of a benzene ring within the linker. Thus, the longest homologue (+)-**101d** and the *p*-phenylene-bis(methylene)-linked *bis*(+)-huprine (+)-**101e** displayed the highest selectivity indices for trypanocidal over cytotoxic activity (SI = 37.5 and 28.2, respectively).

Their inhibitory activity against human recombinant AChE (hAChE) was also evaluated by the method of Ellman,[414] because huprine Y was originally designed as AChE inhibitor and thus *bis*(+)-huprines might also exert toxicity issues arising from this anticholinesterasic effect. Although all tested compounds, (+)-**101a**–**d**, were 30 to 700-fold less potent hAChE inhibitors (hAChE IC_{50} = 17.5−431 nM) than racemic huprine Y (hAChE IC_{50} = 0.61 nM), they still were more potent anticholinesterase than trypanocidal agents (2–29-fold). The favourable, but not sufficient, reduction of the anticholinesterasic effect seems likely to arise as a consequence of using the dextrorrotatory form of huprine Y, (+)-**11**, for the preparation of this series, which is

[206] Defaux, J.; Sala, M.; Formosa, X. *et al. Bioorg. Med. Chem.* **2011**, *19*, 1702–1707.
[414] Ellman, G. L.; Courtney, K. D.; Andres, V., Jr. *et al*. *Biochem. Pharmacol*. **1961**, *7*, 88−95.

well established to be the huprine distomer in terms of AChE inhibition. [201,404]

Finally, the *in vitro* permeation through the blood-brain barrier (BBB) was also assessed using the PAMPA-BBB assay, because crossing BBB is a necessary condition for drug candidates of HAT given the lack of a satisfying treatment against late-stage disease, when parasite invade human CNS and produces a host of symptoms including psychiatric, motor and sensorial disorders along with abnormal reflexes, and eventually death if untreated.[135] In fact, all the *bis*-huprines were predicted to have the ability to cross the BBB with permeabilities clearly above the threshold established for high BBB permeation [P_e (10^{-6} cm s^{-1}) > 5.1],[366] which might seem unlikely in the light of their elevated molecular weights, as it is claimed in different studies like the Lipinski rule of 5.[415]

6.2.2. Huprine-based heterodimers (*Bioorg. Med. Chem*. **2015**, *23*, 5156)

Taking into account the improved trypanocidal/anticholinesterase activity ratio and selectivity over L6 cells of *bis*(+)-huprines, relative to monomeric huprine Y, we turned our attention to an in-depth exploration of heterodimeric structures. To start with, we firstly performed an screening against cultured bloodstream forms of *T. brucei* and *P. falciparum* and rat myoblast L6 cells of a small in-house library of brain permeable huprine- or tacrine-based heterodimeric compounds, belonging to three distinct structural classes (**series I–III, Figure 6.4**), which had been previously developed in our research group as AChE inhibitors of potential interest for the treatment of AD in the framework of the PhD Theses of Dr. Carles Galdeano and Dr. Elisabet Viayna.[88b, 89b,d]

Secondly, the synthesis of novel heterodimeric compounds based on the most promising series above mentioned and subsequent evaluation of their *T. brucei*, *P. falciparum*, rat myoblast L6 cell and human AChE inhibitory activities and brain permeability were also devised.

[88b] Galdeano, C.; Viayna, E.; Sola I. *et al. J. Med. Chem*. **2012**, *55*, 661−669.
[89] b) Camps, P.; Formosa, X.; Galdeano, C. *et al. J. Med. Chem*. **2008**, *51*, 3558−3598. d) Viayna, E.; Gómez, T.; Galdeano, C. *et al. ChemMedChem* **2010**, *5*, 1855−1870.
[135] Atouguia, J. L. M.; Kennedy, P. G. E.; Davis, L. E. Butterworth-Heinemann, Oxford, **2000**, 321−372.
[201] Camps, P.; El Achab, R.; Morral, J. *et al. J. Med. Chem.* **2000**, *43*, 4657–4666.
[366] Di, L.; Kerns, E. H.; Fan, K. *et al*. *Eur. J. Med. Chem*. **2003**, *38*, 223−232.
[404] Camps, P.; Contreras, J.; Font-Bardia, M. *et al. Tetrahedron: Asymmetry* **1998**, *9*, 835−849.
[415] Doak, B. C.; Zheng, J.; Dobritzsch, D. *et al*. *J. Med. Chem.* **2016**, *59*, 2312−2327.

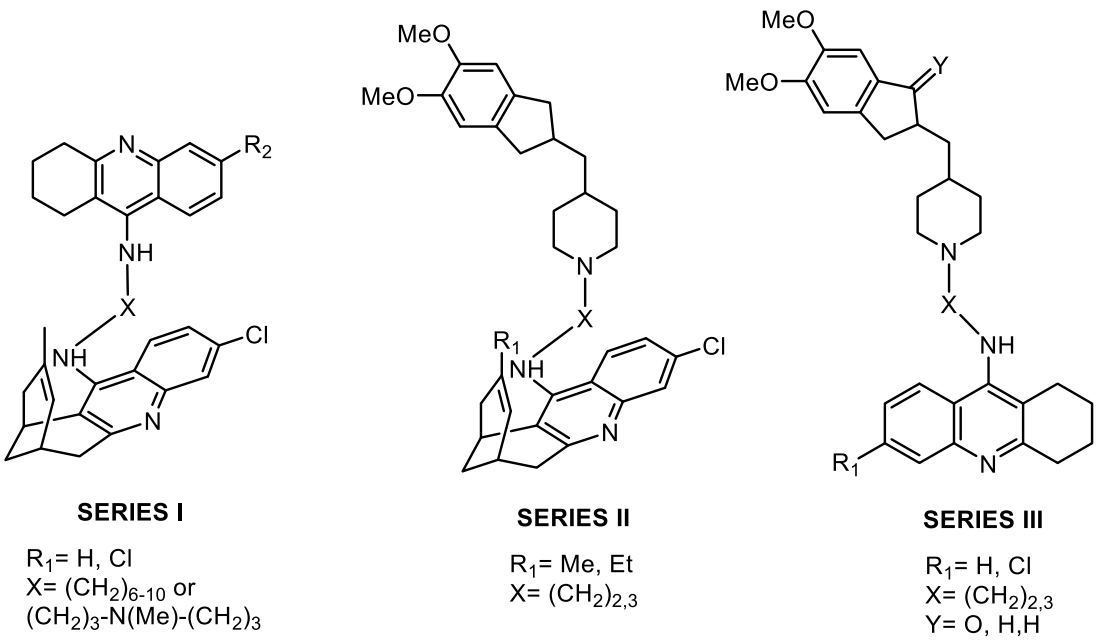

Figure 6.4. General structure of series **I**–**III**.

Finally, assessment of the putative biological targets in *T. brucei* and *P. falciparum* of selected hits of the different series and monomeric huprine Y was carried out by *in vitro* evaluation of their inhibitory activity against *T. brucei* trypanothione reductase and β-haematin formation.

6.2.2.1. Preparation of huprine-based heterodimers

Hereafter, I will describe briefly the synthesis that was used for the obtention of selected compounds belonging to series **I**–**III**.

The group of 14 different *bis*(4-aminoquinolines) heterodimers belonging to series **I** had been prepared through an easy methodology that consists of a nucleophilic substitution of the corresponding α,ω-dibromoalkanes, **108a**–**f**, with the readily accessible tacrine or 6-chlorotacrine, **2** or **109**,[416] in the presence of KOH in DMSO[84a] to afford bromoalkyltacrines, **106a**–**f** and **107a**–**f**, in moderate yields, followed by a second alkylation with racemic or enantiopure huprine Y, (±)-, (+)-, or (−)-**11**,[404] under the same basic conditions. Finally, the desired racemic, (±)-**102a**–**f** and (±)-**103a**–**f**, and the enantiopure heterodimers, (+)- and (−)-**102b**, were isolated in moderate to good yields after silica gel column chromatography purification of the crude products (**Scheme 6.3**).[88b]

[84a] Pang, Y. P.; Quiram, P.; Jelacic, T. *et al*. *J. Biol. Chem*. **1996**, *271*, 23646−23649.
[88b] Galdeano, C.; Viayna, E.; Sola I. *et al. J. Med. Chem*. **2012**, *55*, 661−669.
[404] Camps, P.; Contreras, J.; Font-Bardia, M. *et al. Tetrahedron: Asymmetry* **1998**, *9*, 835−849.
[416] Gregor, V. E.; Emmerling, M. R.; Lee, C. *et al*. *Bioorg. Med. Chem. Lett*. **1992**, *2*, 861−864.

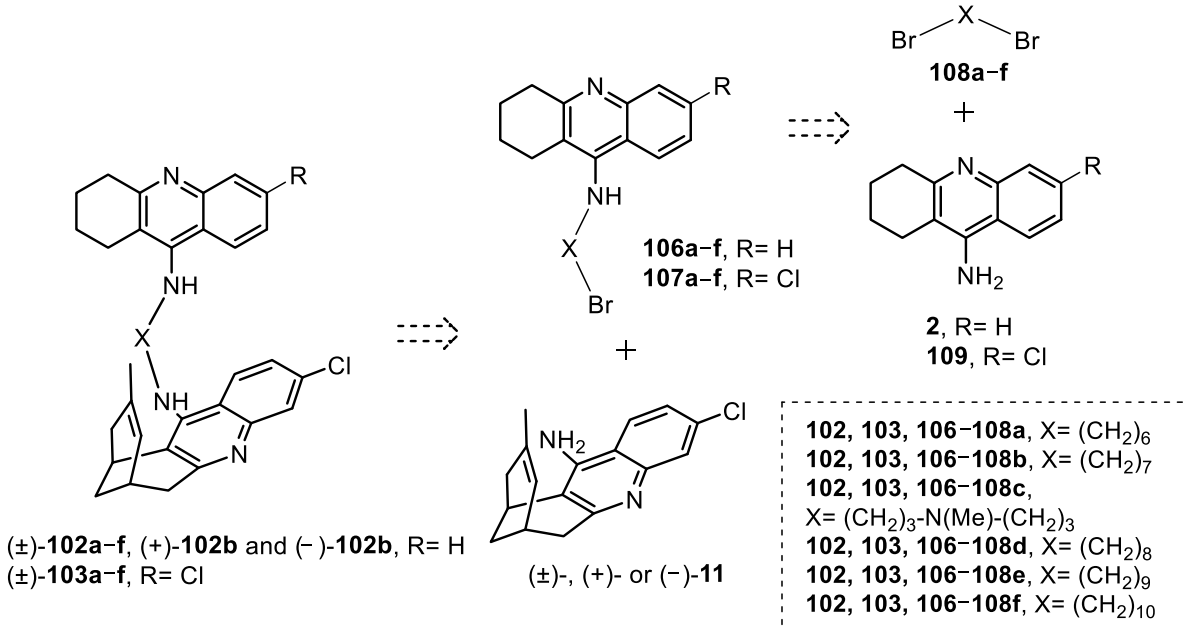

Scheme 6.3. Retrosynthesis of huprine–tacrine heterodimers series **I** (**102**–**103**).

Alternative procedures based on the high-temperature nucleophilic aromatic substitution of 4-chloroquinoline derivatives with α,ω-diaminoalkanes[403] or Pd-catalyzed amination reactions[417,418] were discarded because they required the use of a not readily available huprine-related 4-chloroquinoline precursor,[419] as it also happens for the synthesis of series **II**.

The synthesis of series **II** compounds was carried out through a three-step sequence involving alkylation of 2-cloroethanol, **114a**, or 3-chloro-1-propanol, **114b**, with the donepezil-based fragment, **115**, which in turn could be easily accessed from indanone **116**, followed by transformation of the alcohols **113a,b** into the chloroderivatives **112a,b** and their subsequent alkylation with the corresponding racemic or enantiopure huprine, (±)- or (−)-**11** (**Scheme 6.4**).[89d]

[89d] Viayna, E.; Gómez, T.; Galdeano, C. *et al. ChemMedChem* **2010**, *5*, 1855–1870.
[403] Carlier, P. R.; Chow, E. S. H.; Han, Y. *et al*. *J. Med. Chem.* **1999**, *42*, 4225–4231.
[417] Ma, M.; Mehta, J.; Williams, L. D. *et al*. *Tetrahedron Lett*. **2011**, *52*, 16–919.
[418] Ronco, C.; Jean, L.; Outaabout, H. *et al*. *Eur. J. Org. Chem*. **2011**, 302–310.
[419] Camps, P.; Formosa, X.; Muñoz-Torrero, D. *et al*. *J. Med. Chem.* **2005**, *48*, 1701–1704.

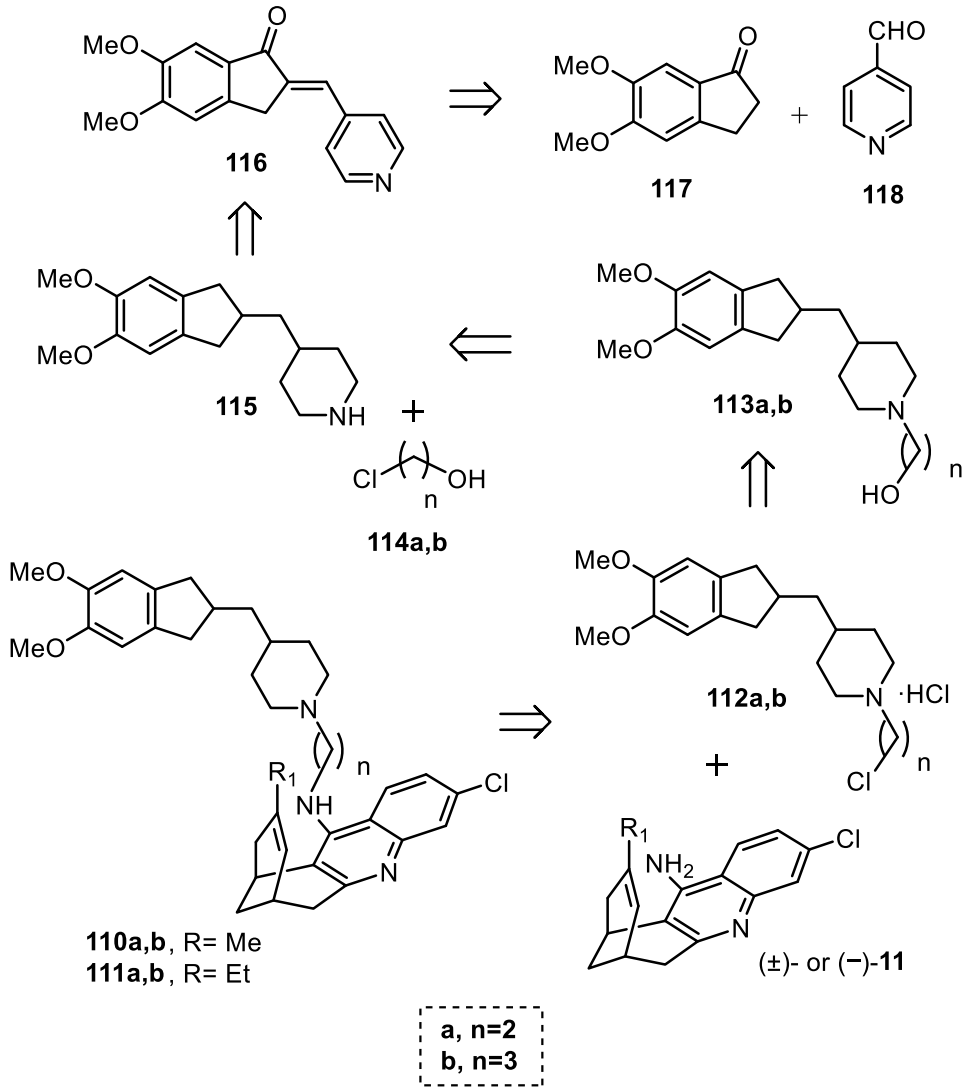

Scheme 6.4. Retrosynthesis of the huprine−donepezil heterodimers series **II** (**110**−**111**).

On the other hand, preparation of the eight selected compounds belonging to series **III** had been performed by amination of 4-chloroquinolines, **89** or **90**,[420,421] derived from tacrine or 6-chlorotacrine, respectively, with 2-aminoethanol, **129a**, or 3-amino-1-propanol, **129b**, followed by conversion of the alcohols **127** and **128** into the mesylates **125** and **126,** and final reaction with the known piperidines, **123** or **124**, easily accessible from the indanone **116** using different hydrogenation reaction conditions (**Scheme 6.5**).[89b]

[89b] Camps, P.; Formosa, X.; Galdeano, C. T. *et al. J. Med. Chem*. **2008**, *51*, 3558−3598.
[420] Hu, M. K.; Lu, C. F. *Tetrahedron Lett.* **2000**, *41*, 1815–1818.
[421] Michalson, E. T.; D'Andrea, S.; Freeman, J. P. *et al*. *Heterocycles* **1990**, *30*, 415–425.

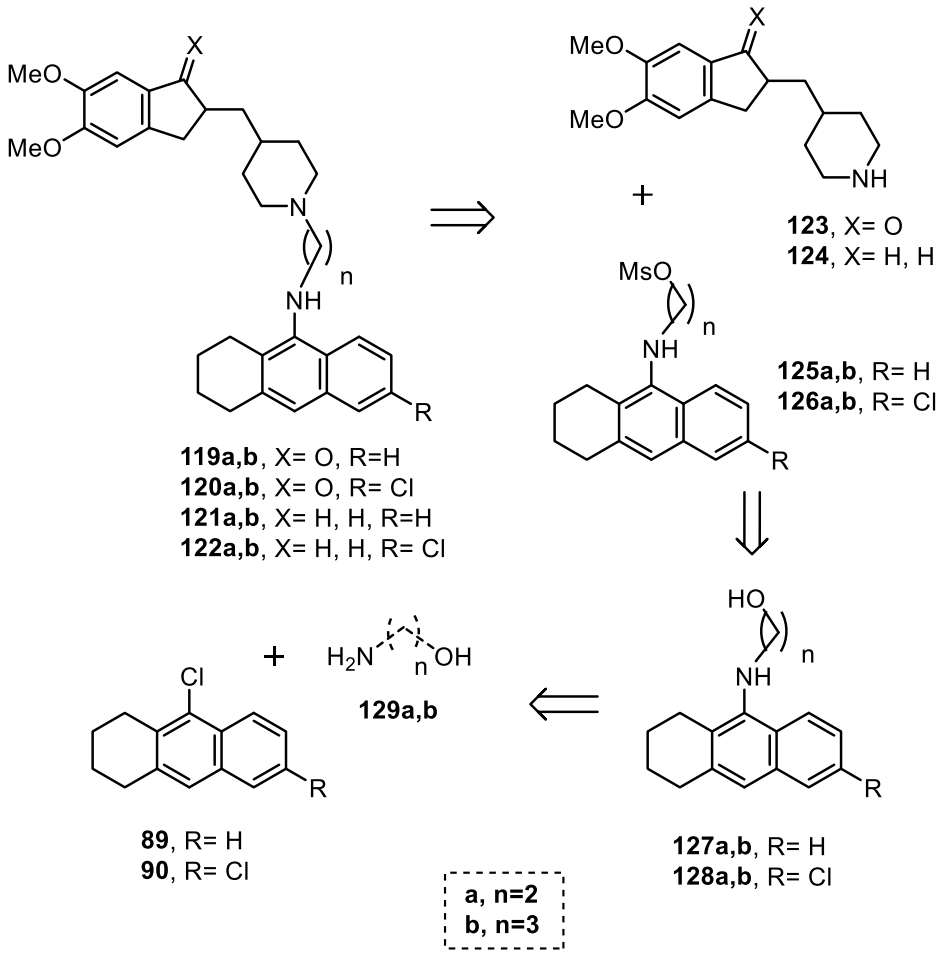

Scheme 6.5. Retrosynthesis of the (6-chloro)tacrine−donepezil heterodimers series **III** (**119**−**122**).

After a phenotypic screening of the above described 21 compounds, huprine−tacrine heterodimers belonging to series **I** showed the most interesting activities as we will later see in detail, particularly those compounds with longer linkers. For this reason, in the context of the present PhD Thesis we envisaged the preparation of six novel hybrids containing a deca- or dodecamethylene linker, connecting tacrine or 6-clorotacrine, **2** or **109**, to the known huprine Y, **11**, or a modified huprine, **130**, without chlorine in the aromatic system, because removal of the chlorine atom at position 3 of the huprine moiety is known to decrease AChE inhibitory activity.[201]

[201] Camps, P.; El Achab, R.; Morral, J. *et al. J. Med. Chem.* **2000**, *43*, 4657–4666.

The preparation of these novel heterodimers of series **I** involved an initial alkylation of **2** or **109** with 1,10-dibromodecane, **108f**, or 1,12-dibromododecane, **108g**, in the presence of KOH in DMSO to afford the previously described 10-bromodecyltacrines **106f** and **107f** and the novel 12-bromododecyltacrines **106g** and **107g** in moderate yields (30−39%). Posterior alkylation of huprines **11** or **130** with **106f,g** or **107f,g** at r. t. for 4 days gave rise to the novel heterodimers **102g**, **103g**, **131f,g**, and **132f,g** in moderate to good yields (45−88%) after silica gel column chromatography purification of the crude products (**Scheme 6.6**).

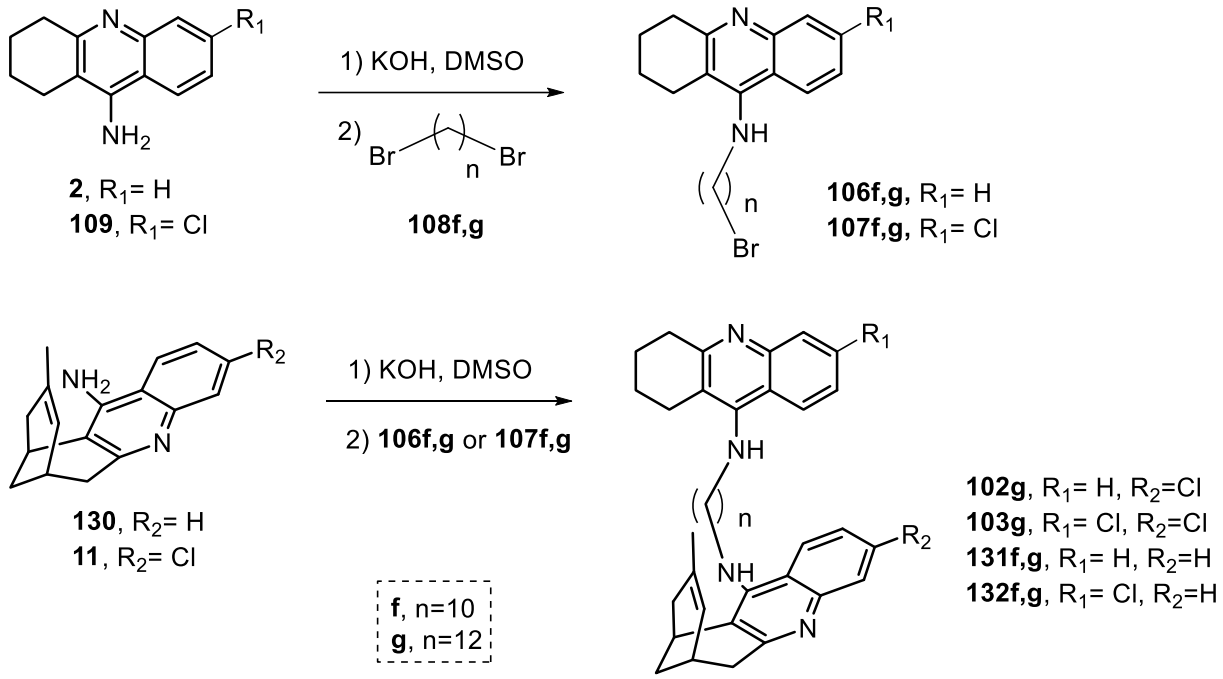

Scheme 6.6. Synthesis of novel heterodimers **102g**, **103g**, **131f,g**, and **132f,g** bearing a unit of tacrine, **2**, or 6-chlorotacrine, **109**, connected to huprine **11** or **130**.

6.2.2.2. Phenotypic screening of huprine-based heterodimers and mechanistic studies

The antitrypanosomal and cytotoxic activities of the huprine- and tacrine-based heterodimers were assessed by the group of Dr. John M. Kelly (London School of Hygiene and Tropical Medicine, UK), whereas the studies about their potential trypanocidal mechanism was carried out by the group of Dr. Alan H. Fairlamb (University of Dundee, UK). The determination of the antimalarial activity of these compounds and the mechanism that might account for that activity was determined by the group of Dr. Colin W. Wright (University of Bradford, UK). The AChE

inhibitory activity and brain permeability were determined by Drs. M. Victòria Clos and Belén Pérez (Universitat Autònoma de Barcelona).

All of the tested compounds were evaluated *in vitro* against cultured bloodstream forms of *T. brucei*, the chloroquine-resistant K1 strain of *P. falciparum*, and rat skeletal myoblast L6 cells, in order to assess their putative dual trypanocidal/antiplasmodial and cytotoxic activities, respectively. The activity data of the heterodimers are listed in the published paper. In summary, the entire set of screened compounds exhibited submicromolar IC_{50} values against *T. brucei* (IC_{50} = 0.12−0.97 μM) and submicromolar to low micromolar IC_{90} values (IC_{90} = 0.17−2.39 μM). The vast majority were more potent trypanocidal agents than the parent huprine Y, **11**, (IC_{50} = 0.61 and IC_{90} = 2.94 μM). A small part of these compounds also exhibited submicromolar IC_{50} values against *P. falciparum* (IC_{50} = 0.35−0.83 μM), and increased potency compared to the reference antimalarial compound chloroquine (IC_{50} = 0.93 μM).

Additionaly, the novel six huprine-tacrine heterodimers, **102g**, **103g**, **131f,g**, and **132f,g**, were also evaluated *in vitro* against hAChE by the method of Ellman et al.,[414] and their brain permeation was also assessed by the PAMPA-BBB assay.[366] All of the novel compounds resulted to retain high AChE inhibitory potency (IC_{50} = 1.48−10.1 nM) with a significant 2−16-fold reduction in comparison with their parent molecule, huprine Y, **11** (IC_{50} = 0.61 nM), and all they had good BBB permeability, but regrettably also exhibited unfavourable selectivity indices. Interestingly, substitution of the huprine Y unit of heterodimers of series **I** by a 3-unsubstituted huprine moiety, **130**, led in general to slightly increased trypanocidal potencies, especially if IC_{90} values are taken into account (IC_{50} = 0.24−0.55 μM and IC_{90} = 0.31−0.75 μM). Indeed, the novel heterodimer **131g** exhibited the lowest IC_{90} value (0.28 μM) amongst all the heterodimers of series **I**. Unlike most previously screened heterodimers of series **I**, the novel **102g**, **103g**, **131f,g**, and **132f,g** were found to be essentially inactive or only moderately potent antiplasmodial compounds, displaying one-digit micromolar activities in the best cases. In particular, homologation of the tether chain to a dodecamethylene linker and removal of the chlorine atom of huprine were detrimental for antiplasmodial activity.

Furthermore, a determination of the trypanocidal and antiplasmodial mode of action of some selected heterodimeric compounds of series **I**–**III** was performed. On the one hand, the

[366] Di, L.; Kerns, E. H.; Fan, K. *et al*. *Eur. J. Med. Chem*. **2003**, *38*, 223−232.
[414] Ellman, G. L.; Courtney, K. D.; Andres, V., Jr. *et al*. *Biochem. Pharmacol*. **1961**, *7*, 88−95.

evaluation of trypanothione reductase (TryR) activity was carried out, since it is unique and essential to *Trypanosoma* parasites and thus constitute a valuable target for HAT drug discovery programs.[422,423] Moreover, several precedents prompted us to determine wether TryR was a biological target for our heterodimers of series **I**–**III**, since a number of quinoline or aminoacridine derivatives have been reported to be TryR inhibitors,[423,424,425,426] and different classes of dimeric structures have also led to increased potency,[427,428,429] which might be related to the presence of two interacting binding sites in the large active site of TryR. Therefore, three selected compounds, **102d**, **110b**, and **120b**, were studied and they exhibited submicromolar to low micromolar IC_{50} values for TryR inhibition, and particularly **102d** turned out to be the most potent, with a 6−8-fold increased potency (IC_{50} = 0.87 μM) relative to the parent huprine **11** (IC_{50} = 5.00 μM) and the hit heterodimers of the other series (**110b**, IC_{50} = 4.88 μM and **120b**, IC_{50} = 7.39 μM). However, no correlation was found between the trypanocidal and TryR inhibitory activities of these compounds, because all displayed more potent trypanocidal than TryR inhibitory activity (6−62-fold), which might suggest that the trypanocidal potency of these heterodimers can only partly be ascribed to inhibition of TryR or that they might be selectively concentrated into the cell or metabolically activated, as it has been hypothesized for other reported compounds.[430]

Some heterodimers of series **I**–**III** were suprisingly quite potent antiplasmodial activity, although huprine Y, **11**, and *bis*-huprines (+)-**101a–e** had been found to be totally inactive against *P. falciparum*, which led us to study whether the selected heterodimers (**102d**, **110b**, and **120b**) were also able to inhibit the formation of β-haematin, which is identical to haemozoin, the target of the antimalarial drug chloroquine.[431,432] All the tested heterodimers exhibited haem polymerization inhibitory activity (HPIA) comparably to that seen with chloroquine, whereas huprine Y and tetracycline, the negative controls, showed no inhibition. Particularly, heterodimer **102d** was equipotent to chloroquine, and heterodimers **110b** and **120b** were slightly less potent (3- and 4-fold). In this case, these results correlate well with their phenotypic

[422] Eberle, C.; Burkhard, J. A.; Stump, B. *et al. ChemMedChem* **2009**, *4*, 2034−2044.
[423] Krauth-Siegel, R. L.; Inhoff, O. *Parasitol. Res*. **2003**, *90*, S77−85.
[424] Spinks, D.; Shanks, E. J.; Cleghorn, L. A. T. *et al. ChemMedChem* **2009**, *4*, 2060−2069.
[425] Chibale, K.; Haupt, H.; Kendrick, H. *et al. Bioorg. Med. Chem. Lett.* **2001**, *11*, 2655−2657.
[426] Saravanamuthu, A.; Vickers, T. J.; Bond, C. S. *et al. J. Biol. Chem.* **2004**, *279*, 29493−29500.
[427] Bonnet, B.; Soullez, D.; Davioud-Charvet, E. *et al. Bioorg. Med. Chem.* **1997**, *5*, 1249−1256.
[428] Girault, S.; Baillet, S.; Horvath, D. *et al. Eur. J. Med. Chem.* **1997**, *32*, 39−52.
[429] Girault, S.; Davioud-Charvet, T. E.; Maes, L.*et al. Bioorg. Med. Chem*. **2001**, *9*, 837−846.
[430] Walton, J. G. A.; Jones, D. C.; Kiuru, P. *et al. ChemMedChem* **2011**, *6*, 321−328.
[431] Basilico, N.; Pagani, E.; Monti, D. *et al*. *Antimicrob. Chemother.* **1998**, *42*, 55−60.
[432] Parapini, S.; Basilico, N.; Pasini, E. *et al*. *Exp. Parasitol*. **2000**, *96*, 249−256.

activities, so that we can conclude that their antiplasmodial potency seems to arise from an inhibition of the haem detoxification process.

6.3. Hit-to-lead optimization by side chain modification (*Bioorg. Med. Chem*. **2016**, in press)

As a further part of our ongoing research work in HAT field, we decided to explore the introduction of a side chain at the exocyclic primary amino group of huprine, with the aim of optimizing the antitrypanosomal activity profile with regard to the parent huprine Y and the huprine homo- and heterodimers.

In this light, we envisaged first the screening against cultured bloodstream forms of *T. brucei* and rat myoblast L6 cells of a small in-house library of 16 *N*-alkylhuprines functionalized either with a cyano or an amino group at the end of an oligomethylene chain, containing in some cases a *p*-phenylene ring (**77a–h**, **76a–h**, and **133**) (**Figure 6.5**).

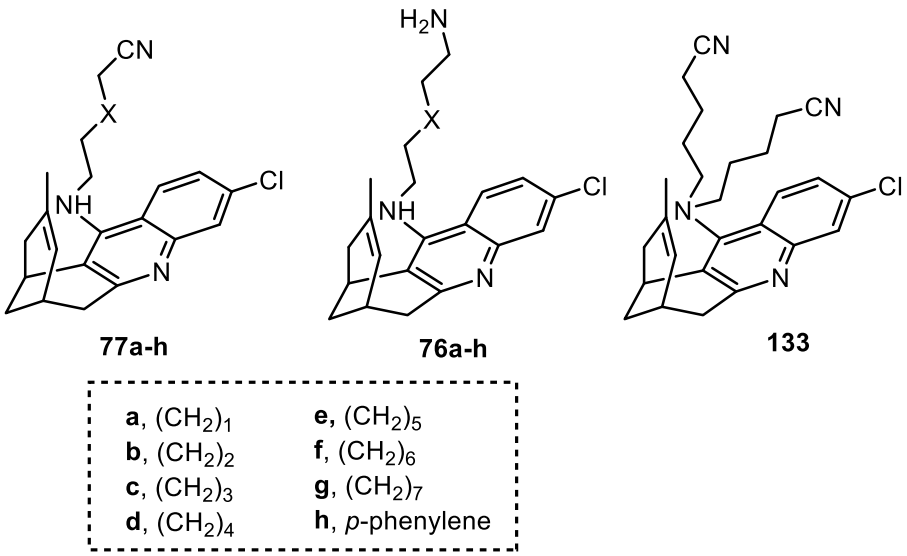

Figure 6.5. Small in-house library based on *N*-ω-cyanoalkyl- and *N*-ω-aminoalkyl huprines.

On the basis of the structure–activity data from the screened *N*-alkylated huprines, we undertook the synthesis of a second generation of modified side chain analogs, involving the preparation of novel *N*-cyano, *N*-amino, and *N*-guanidinoalkylated derivatives of huprine (**134b,e**), tacrine (**135, 137**, and **139c,f**), or 6-chlorotacrine (**136, 138**, and **140c,f**), and the preparation of the *N*-piperidinopropyl and *N*-morpholinopropyl substituted huprines, **141** and **142** (**Figure 6.6**).

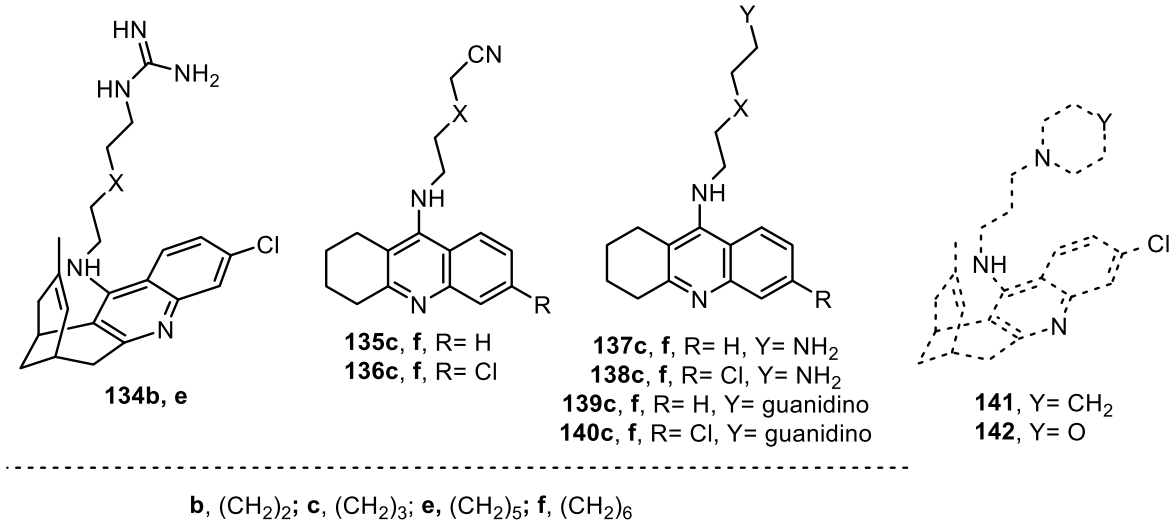

Figure 6.6. General structures of second generation *N*-ω-cyanoalkyl-, *N*-ω-aminoalkyl, and *N*-ω-guanidinoalkyl 4-aminoquinoline derivatives.

Afterwards, we assessed the novel compounds against *T. brucei* and rat myoblast L6 cells, AChE[414] and their BBB permeability[366] was also determined.

6.3.1. Synthesis of ω-cyanoalkyl-, ω-aminoalkyl-, and ω-guanidinoalkylhuprine (tacrine) derivatives

The known set of *N*-alkylhuprine derivatives, **77a–h**, had been previously reported by us as intermediate products during the formation of rhein−huprine hybrids, a family of potential anti-Alzheimer compounds. As a reminder, they were prepared through an easy one to two-step sequence, involving either a nucleophilic substitution of the corresponding ω-bromoalkanenitrile **78a–g** at the exocyclic amino group of huprine Y unit to afford **77a–g** (**Scheme 5.2, section 5.2.1**), or a reductive amination process to obtain compound 7**7h**, which contains a *p*-phenylene ring within the tether chain (**Scheme 5.3**). Then, all cyano derivatives were reduced by treatment with $LiAlH_4$ to afford the desired aminoalkylhuprines **76a–h** (**Scheme 5.4**)**.**

For the preparation of the novel *N*-guanidinoalkylhuprines (**134b,e**) a straightforward synthesis was carried out by treatment of the previously described amine precursors, **76b** and **76e** with commercially available 1*H*-pyrazole-1-carboxamidine hydrochloride under reflux of anhydrous CH_3CN (**Scheme 6.7**).

[366] Di, L.; Kerns, E. H.; Fan, K. *et al*. *Eur. J. Med. Chem*. **2003**, *38*, 223−232.
[414] Ellman, G. L.; Courtney, K. D.; Andres, V., Jr. *et al*. *Biochem. Pharmacol*. **1961**, *7*, 88−95.

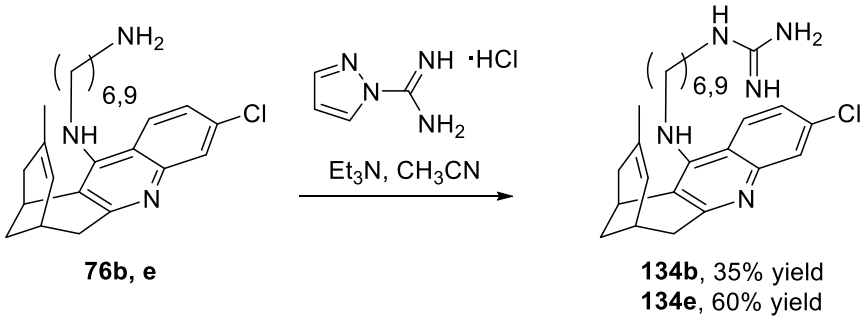

76b, e

134b, 35% yield
134e, 60% yield

Scheme 6.7. Synthesis of *N*-guanidinoalkylhuprines **134b**,**e**.

N-Cyanoalkyl derivatives **135c**,**f** and **136c**,**f** were synthesized in moderate to excellent yields (38−94%) by alkylation of readily accessible tacrine (**2**) or 6-chlorotacrine (**109**)[416] with 7-bromoheptanenitrile and 9-bromononanenitrile, **78c and 78f**[433,434,435] in the presence of KOH in DMSO. Subsequent reaction with $LiAlH_4$ gave the known primary amines **137c**,**f** and **138c**,**f**,[86,403] which were then treated with 1*H*-pyrazole-1-carboxamidine hydrochloride, as described above, to provide *N*-guanidinoalkyl compounds, **139c**,**f** and **140c**,**f**, in moderate to good yields (60–76%) (**Scheme 6.8**).

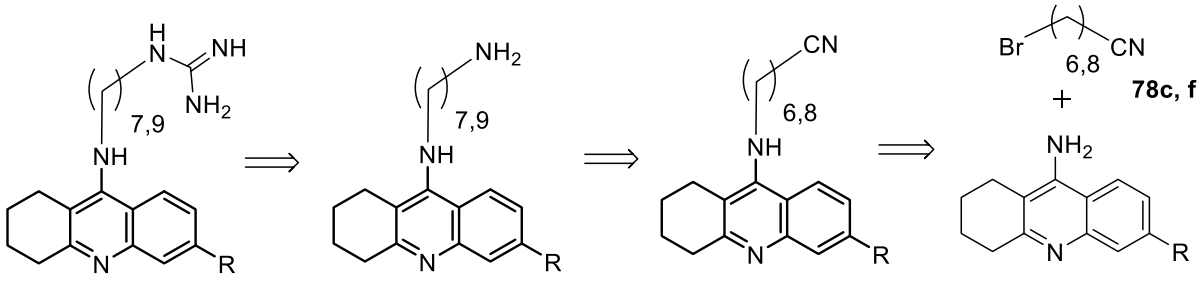

139c, f, R = H
140c, f, R = Cl

137c, f, R = H
138c, f, R = Cl

135c, f, R = H
136c, f, R = Cl

2, R = H
109, R = Cl

Scheme 6.8. Retrosynthesis of the *N*-cyanoalkyl-, *N*-aminoalkyl-, and *N*-guanidinoalkyl-tacrine or 6-chlorotacrine derivatives.

The synthesis of the novel *N*-piperidino- and *N*-morpholinopropyl substituted huprines, **141** and **142**, was carried out by reaction of racemic huprine, (±)-**11,** with commercially available 1-(3-chloropropyl)piperidine hydrochloride, **143**, or the readily accesible 3-morpholinopropyl

[86] Muñoz-Ruiz, P.; Rubio, L.; García-Palomero, E. *et al. J. Med. Chem*. **2005**, *48*, 7223−7233.
[403] Carlier, P. R.; Chow, E. S. H.; Han, Y. *et al. J. Med. Chem.* **1999**, *42*, 4225−4231.
[416] Gregor, V. E.; Emmerling, M. R.; Lee, C. *et al*. *Bioorg. Med. Chem. Lett*. **1992**, *2*, 861−864.
[433] Best, M.; Gifford, A. N.; Kim, S. W. *et al. J. Labelled Compd. Radiopharm*. **2012**, *55*, 39−43.
[434] Taber, D. F.; Kong, S. *J. Org. Chem.* **1997**, *62*, 8575−8576.
[435] Lethesh, K. C.; Van Hecke, K.; Van Meervelt, L. *et al. J. Phys. Chem. B* **2011**, *115*, 8424−8438.

methanesulfonate, **144,**[89b,436] under similar conditions as for the other alkylation reactions, followed by silica gel column chromatography purification of the reaction crudes (**Scheme 6.9**).

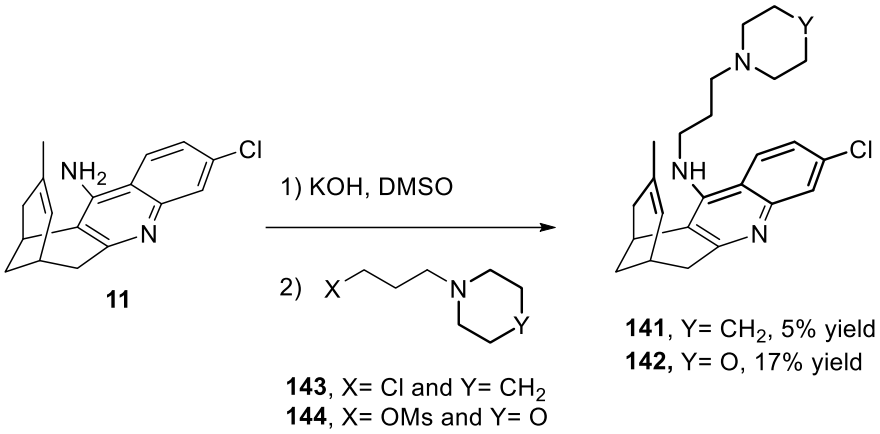

Scheme 6.9. Preparation of *N*-piperidinopropyl (**141**) and *N*-morpholinopropyl (**142**) substituted huprines.

6.3.2. Pharmacological evaluation

The antitrypanosomal and cytotoxic activities of the modified side chain 4-aminoquinoline derivatives were assessed by the group of Dr. John M. Kelly (London School of Hygiene and Tropical Medicine, UK). The AChE inhibitory activity and brain permeability were determined by Drs. M. Victòria Clos and Belén Pérez (Universitat Autònoma de Barcelona).

The first set of screened *N*-alkylhuprines turned out to be moderate trypanocidal agents with IC_{50} values in the submicromolar to micromolar range (IC_{50} = 0.32−3.33 μM), emerging *N*-cyanooctyl- and *N*-cyanononylhuprines, **77e** and **77f**, as the compounds with the best trypanocidal profile (**77e**: IC_{50} = 0.32 μM, IC_{90} = 0.42 μM and SI_{Tb} = 25.1; **77f**: IC_{50} = 0.46 μM, IC_{90} = 0.61 μM and SI_{Tb} = 10.4). Overall, replacement of nitrile by an amino group gave rise to lower activities in most cases, except for amine **76h** containing an aromatic ring within the linker, which was 2-fold more potent (IC_{50} = 0.92 μM, IC_{90} = 1.44 μM) than the cyano precursor **77h** (IC_{50} = 1.86 μM, IC_{90} = 3.39 μM). Moreover, the presence of two side chains was found to be deleterious for antitrypanosomal activity, being compound **133** essentially inactive.

Given the fact the introduction of an 8−9-carbon length side chain provided the optimal substitution pattern, we selected hexa- to nonamethylene linkers for the second generation of

[89b] Camps, P.; Formosa, X.; Galdeano, C. *et al. J. Med. Chem*. **2008**, *51*, 3558−3598.
[436] Chang, C. S.; Su, C. C.; Zhuang, J. R. *et al*. *J. Mol. Catal. B-Enzym.* **2004**, *30*, 151–157.

huprine-like derivatives. The novel compounds displayed antitrypanosomal activity, with IC_{50} values in the range of 0.12–7.92 μM and IC_{90} values of 0.25–12.2 μM, being most of them less potent than huprine Y, **11** (IC_{50} = 0.61 μM and IC_{90} = 2.94 μM) and *N*-cyanoalkylhuprine **77e** (IC_{50} = 0.32 μM and IC_{90} = 0.42 μM). Interestingly, *N*-guanidinononyltacrine **139f** turned out to be 2−5-fold more potent than **11** and **77e** when considering their IC_{50} values and 2–12-fold with respect to IC_{90} values (**139f**, IC_{50} = 0.12 μM and IC_{90} = 0.25 μM)**.** Overall, an outstanding improvement was observed with the replacement of an amino by a guanidino group, with all the guanidine compounds, **134**, **139**, and **140** being 1.5–34-fold more potent than their amine precursors.

On the other hand, the novel compounds bearing a piperidinopropyl, **141**, or morpholinopropyl group, **142**, showed a moderate growth inhibitory activity (IC_{50}= 0.83 and 1.75 μM, respectively).

All the tested compounds displayed a clear ability to cross BBB, according to the results of the PAMPA-BBB assay, with the exception of aminoalkyl huprine **77g**, for which an uncertain BBB permeation was predicted. Again, all these huprine and tacrine derivatives were found to be more potent AChE inhibitors than antitrypanosomal agents, despite being all of them 2 to 3-orders of magnitude less potent anticholinesterase inhibitors than huprine Y (**11**, IC_{50} = 0.61 nM), with IC_{50} values in the range of 16 to 158 nM. Furthermore, all of them showed low selectivity for *T. brucei* vs mammalian cells, exhibiting selectivity indices (SI_{Tb}) in the range of 2.3 to 33, with the exception of compound **139f** which stood out as the best trypanocidal agent with the highest selectivity index (SI = 133 nM) as well as the best trypanocidal inhibitory activity (IC_{50} = 120 nM). In fact, **139f** was chosen to perform *in vivo* efficacy studies in infected mice. Unfortunately, preliminary studies with male Balb/c mice to set the dose of compound **139f** showed evident signs of neurotoxicity, after intraperitoneal injection of a dose of 20 mg/kg of **139f**, which precluded the planned efficacy studies.

In summary, homodimerization, heterodimerization, and side chain modification of the 4-aminoquinoline derivatives huprine and tacrine have successfully led to increased antitrypanosomal potencies, and, in some cases, to significant antimalarial activity and favourable selectivity indices. Even though the AChE inhibitory activity has been greatly reduced with respect to the parent huprine, all the new derivatives still retain a significant activity, which might result in unwanted cholinergically mediated side effects. Maybe, these side effects account for the *in vivo* neurotoxicity observed for the lead **139f**. Thus, further efforts in this structural class should mainly address novel modifications that can be accompanied by a dramatic reduction of the AChE inhibitory.

6. A.

Bioorg. Med. Chem. Lett. **2014**, *24*, 5435

Graphical Abstract

To create your abstract, type over the instructions in the template box below.
Fonts or abstract dimensions should not be changed or altered.

Synthesis and antiprotozoal activity of oligomethylene- and *p*-phenylene-*bis*(methylene)-linked *bis*(+)-huprines

Leave this area blank for abstract info.

Irene Sola, Albert Artigas, Martin C. Taylor, Stephen Y. Gbedema, Belén Pérez, M. Victòria Clos, Colin W. Wright, John M. Kelly, Diego Muñoz-Torrero

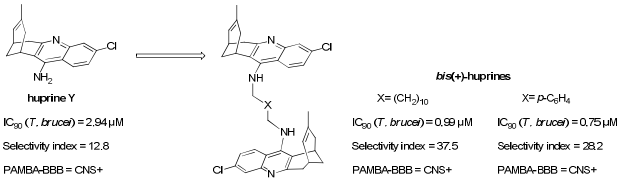

Bioorganic & Medicinal Chemistry Letters
journal homepage: www.elsevier.com

Synthesis and antiprotozoal activity of oligomethylene- and *p*-phenylene-*bis*(methylene)-linked *bis*(+)-huprines

Irene Sola[a], Albert Artigas[a], Martin C. Taylor[b], Stephen Y. Gbedema[c,d], Belén Pérez[e], M. Victòria Clos[e], Colin W. Wright[c], John M. Kelly[b], Diego Muñoz-Torrero[a,*]

[a] *Laboratori de Química Farmacèutica (Unitat Associada al CSIC), Facultat de Farmàcia, and Institut de Biomedicina (IBUB), Universitat de Barcelona, Av. Joan XXIII 27-31, 08028-Barcelona, Spain*
[b] *Department of Pathogen Molecular Biology, London School of Hygiene and Tropical Medicine, Keppel Street, London WC1E 7HT, United Kingdom*
[c] *Bradford School of Pharmacy, University of Bradford, West Yorkshire BD7 1 DP, United Kingdom*
[d] *Department of Pharmaceutics, Kwame Nkrumah University of Science and Technology, Kumasi, Ghana*
[e] *Departament de Farmacologia, de Terapèutica i de Toxicologia, Universitat Autònoma de Barcelona, 08193-Bellaterra, Barcelona, Spain*

ARTICLE INFO

Article history:
Received
Revised
Accepted
Available online

Keywords:
Molecular dimerization
Trypanocidal agents
Antimalarial agents
Bis(4-aminoquinolines)
Brain permeability

ABSTRACT

We have synthesized a series of dimers of (+)-(7*R*,11*R*)-huprine Y and evaluated their activity against *Trypanosoma brucei*, *Plasmodium falciparum*, rat myoblast L6 cells and human acetylcholinesterase (hAChE), and their brain permeability. Most dimers have more potent and selective trypanocidal activity than huprine Y and are brain permeable, but they are devoid of antimalarial activity and remain active against hAChE. Lead optimization will focus on identifying compounds with a more favourable trypanocidal/anticholinesterase activity ratio.

In the last few years, implementation of prevention and control measures has significantly reduced the burden of tropical protozoan diseases such as human African trypanosomiasis (HAT or sleeping sickness) and malaria. However, approximately 70 million people remain at risk of HAT, and in the case of malaria, half of the world's population live in countries where the disease is endemic. Thus, these parasitic infections continue to pose a serious health threat, especially in developing regions.[1,2]

The causative agents of HAT and malaria are the single-celled parasites *Trypanosoma brucei gambiense* or *T. brucei rhodesiense*, and several species of the genus *Plasmodium*, amongst which, *P. falciparum* is the most common and deadly. The parasites are transmitted through the bite of infected insects, namely *Glossina* flies (tsetse flies) for HAT and *Anopheles* mosquitoes for malaria.

In HAT, following an initial hemolymphatic phase, parasites can cross the blood–brain barrier (BBB) and infect the central nervous system (CNS), leading to severe neurological symptoms. Without treatment, death is inevitable when the disease has reached this late stage. In malaria, the parasites multiply initially ~~in the liver~~, and then in the bloodstream. In severe cases, they can become sequestered within brain capillaries, particularly in children, causing the so-called cerebral malaria, frequently with fatal consequences.

Current options to reduce the burden of HAT and malaria are far from ideal.[3-5] There is no licensed vaccine for either infection, with vector control and public health measures being the main means of prevention. Currently registered drugs are problematic, with toxicity and resistance being major problems. For example, although five drugs have been approved for the treatment of HAT (pentamidine, suramin, melarsoprol, nifurtimox and eflornithine), their activity can be stage and/or species specific, they display a range of toxic side effects, and require strict and complicated parenteral administration regimens.[6] This type of specialized infrastructure is often unavailable in the poor rural settings where HAT is endemic. Drug resistance continues to emerge and undermine clinical effectiveness. Increased resistance has been observed for the trypanocidal agent melarsoprol. In the case of malaria, chloroquine is no longer widely effective and rising resistance against the current front line drug artemisinin is a potential threat to global health. Overall, there is an acute need to

* Corresponding author. Tel.: +34-934024533; fax: +34-934035941; e-mail: dmunoztorrero@ub.edu (D. Muñoz-Torrero)

develop novel drugs for HAT and malaria that can circumvent the limitations of existing therapies.

Several approaches have been proposed to speed up the antiprotozoal drug pipeline. These include high-throughput screening of large compound libraries, new strategies to functionally validate novel druggable targets involved in key steps of the parasite life-cycle,[7-10] or the simultaneous inhibition of two or more key biological targets with combination therapies or multitarget-directed ligands.[11-13] Increasingly, the search for novel antiprotozoal agents also involves the repositioning of existing drugs registered for other applications[14] or the synthesis of new chemical entities endowed with antiprotozoal activity.[15-17]

In recent years, new compounds bearing the 4-amino-7-chloroquinoline core of chloroquine, or other aminoquinoline moieties, have been assessed as novel trypanocidal or antimalarial agents, or as dual agents endowed with both activities.[18-21] The development of single molecules that have potency against different protozoan diseases (such as HAT and malaria) has been regarded as an feasible approach, with potential economic savings.[22] We recently reported that the aminoquinoline derivatives huprines, a structural class initially developed as inhibitors of the enzyme acetylcholinesterase, are moderately effective and selective trypanocidal agents, with some also being active against a chloroquine-resistant strain of *P. falciparum*.[23,24] In particular, the 4-amino-7-chloroquinoline derivative **1** (huprine Y, Scheme 1) exhibited the lowest IC_{50} value of the series against *T. brucei* (IC_{50} = 0.61 µM; IC_{90} = 2.94 µM), with one of the best selectivity indices over rat myoblast L6 cells (SI = 13) among the entire set of tested huprines.[23]

Molecular dimerization of compounds with known antiprotozoal activity constitutes a strategy that can be used to overcome drug resistance.[25] This approach has proven successful for dimers of 4-aminoquinolines, in which the two constituting units were connected through linkers of different length or containing different functional groups.[26-29]

Here, we report the synthesis of dimers of huprine Y, in which the two huprine moieties have been connected through oligomethylene linkers of different length, or with a *p*-phenylene-*bis*(methylene) tether. To this end, enantiopure (+)-(7*R*,11*R*)-huprine Y [(7*R*,11*R*)-**1**, Scheme 1], the least active enantiomer in terms of acetylcholinesterase (AChE) inhibition activity,[30-32] has been used. The dimeric *bis*(+)-huprines have been tested against cultured bloodstream forms of *T. brucei* and *P. falciparum*, and their cytotoxicity against mammalian cells, inhibitory activity against human AChE, and brain permeability have been assessed.

The synthesis of hexa-, octa-, deca-, and dodeca-methylene linked *bis*-huprines (+)-**2a**–**d** and the *p*-phenylene-*bis*(methylene)-linked *bis*-huprine (+)-**2e** was carried out by reaction of 2 equivalents of (+)-(7*R*,11*R*)-huprine Y with 1 equivalent of the corresponding α,ω-dihaloalkane, using KOH as the base in DMSO at room temperature for three days (Scheme 1). After silica gel column chromatography purification, *bis*(+)-huprines (+)-**2a**–**d** were obtained in moderate yields (21–50% yields, whereas (+)-**2e** was obtained in a lower yield (11%) along with the byproduct resulting from the monoalkylation of (+)-**1** (12% yield).

Bis-huprines (+)-**2a**–**e** were converted into the corresponding dihydrochlorides for their chemical characterization (specific rotation, melting point, IR, ^{1}H and ^{13}C NMR, HRMS, and elemental analysis) and biological profiling.[33]

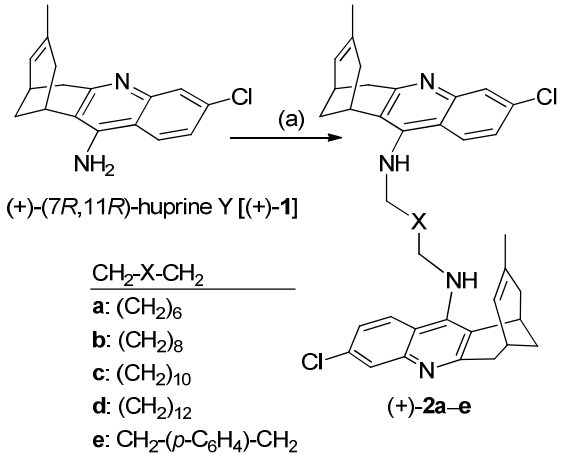

Scheme 1. Reagents and conditions: (a) (+)-**1** (2 equiv.), KOH, DMSO, 2 h; then, α,ω-dihaloalkane (1 equiv.) in DMSO, rt, 3 days.

Bis-huprines (+)-**2a**–**e** were first tested *in vitro* against cultured bloodstream forms of *T. brucei*. All of the *bis*-huprines exhibited IC_{50} values in the range 0.50–0.89 µM. Their IC_{90} values of around 1 µM (0.73–1.09 µM) (Table 1), were significantly lower than the parent huprine Y (IC_{90} = 2.94 µM). Given the narrow range of potencies of the different *bis*-huprines, the length of the linker or the presence of a benzene ring within the linker do not seem to have a strong influence on the trypanocidal activity of *bis*(+)-huprines. Thus, the increased trypanocidal potency of *bis*-huprines, relative to huprine Y, might be ascribed to the dimerization strategy, even though the mechanisms responsible for inhibition of trypanosome growth or for the enhanced activity are not known.

Bis-huprines (+)-**2a**–**e** were also evaluated against the chloroquine-resistant K1 strain of *P. falciparum*. Even though some huprines have been reported to exhibit moderately potent antiplasmodial properties,[23] huprine Y did not exhibit significant activity (IC_{50} > 10 µM). Huprine Y bears the 4-amino-7-chloroquinoline moiety, thought to be an antimalarial pharmacophore responsible for inhibition of heme dimerization.[20,34] Since dimerization of other 4-aminoquinoline compounds increased antiplasmodial potency and/or overcame the chloroquine resistance mechanism,[26-29] we hypothesized that dimerization of huprine Y to *bis*-huprines (+)-**2a**–**e** might also enhance activity. However, no noticeably increased antiplasmodial potency was observed for the dimeric compounds, which exhibited IC_{50} values > 5 µg/mL (i.e. > 6–7 µM), much higher than that of artemisinin (IC_{50} = 91 nM) used in this assay as a positive control. The improvement of potency against chloroquine resistant strains of *P. falciparum* of other *bis*(4-aminoquinoline) derivatives relative to the corresponding monomeric compounds has been ascribed mainly to the doubling of the number of protonatable nitrogen atoms in the dimers, which might lead to more efficient trapping in the acidic digestive vacuole of the parasite and prevention of heme polymerization.[25,29] The failure of *bis*-huprines to show antiplasmodial activity might be indicative of the fact that these compounds cannot hit the biological target of chloroquine and other 4-aminoquinoline derivatives despite their structural similarity. Indeed, we have recently found that the parent huprine Y, unlike chloroquine, shows no inhibition of β-haematin formation, whereas several huprine analogues that possess antiplasmodial activity are effective inhibitors of β-haematin formation (unpublished results).

Table 1
Trypanocidal, cytotoxic and hAChE inhibitory activity of *bis*-huprines (+)-**2a**–**e**[a]

Compd	*T. brucei* IC_{50} µM	*T. brucei* IC_{90} µM	L6 cells IC_{50} µM	SI[b]	hAChE IC_{50} nM
(+)-**2a**	0.89 ± 0.02	1.09 ± 0.01	1.61 ± 0.07	1.8	192 ± 18
(+)-**2b**	0.52 ± 0.01	0.74 ± 0.02	4.92 ± 0.15	9.5	72.5 ± 8.3
(+)-**2c**	0.50 ± 0.01	0.73 ± 0.01	7.71 ± 0.70	15.4	17.5 ± 3.8
(+)-**2d**	0.76 ± 0.03	0.99 ± 0.05	28.5 ± 2.9	37.5	431 ± 22
(+)-**2e**	0.57 ± 0.02	0.75 ± 0.02	16.1 ± 0.3	28.2	nd[c]
1	0.61 ± 0.03[d]	2.94 ± 0.20[d]	7.80 ± 0.47[d]	12.8	0.61 ± 0.03[e]

[a] *In vitro* activity against bloodstream form of *T. brucei* (pH 7.4) and rat myoblast L6 cells expressed at the concentration that inhibited growth by 50% (IC_{50}) and 90% (IC_{90}, for trypanocidal activity). Data are the mean of triplicate experiments ± SEM.

[b] SI: Selectivity index is the ratio of cytotoxic to trypanocidal IC_{50} values.

[c] Not determined.

[d] Taken from ref. 23.

[e] Taken from ref 35.

The cytotoxicity of *bis*-huprines was assessed *in vitro* using rat skeletal myoblast L6 cells. These compounds displayed a modest toxicity against the mammalian cells, exhibiting IC_{50} values in the range 1.6–28.5 µM (Table 1). A clear structure-cytotoxicity trend was found, with cytotoxicity decreasing with increased tether length and with the presence of a benzene ring within the linker. Thus, the dodecamethylene-linked *bis*-huprine (+)-**2d** was found to be 18-, 6-, and 4-fold less cytotoxic than the hexa-, octa-, and deca-methylene counterparts (+)-**2a**, (+)-**2b**, and (+)-**2c**, respectively, whereas the *p*-phenylene-*bis*(methylene)-linked *bis*-huprine (+)-**2e** was 10-fold less cytotoxic than the oligomethylene-linked *bis*-huprine with a similar tether length, (+)-**2a.** Thus, the longest homologue (+)-**2d** and the *p*-phenylene-*bis*(methylene)-linked *bis*-huprine (+)-**2e** displayed the highest selectivity indices for trypanocidal over cytotoxic activity (SI = 37.5 and 28.2, respectively).

Bis-huprines possess two units of (+)-huprine Y, which is the distomer for AChE inhibition. Even though the dextrorotatory enantiomers of huprine Y and some hybrid derivatives are less potent AChE inhibitors than the racemic mixtures and the levorotatory counterparts, they typically exhibit activities in the nanomolar to low micromolar range.[32,35] To assess potential toxicity issues arising from AChE inhibition by *bis*-huprines, their inhibitory activity against human recombinant AChE (hAChE) was evaluated by the method of Ellman.[36] As expected, *bis*-huprines (+)-**2a**-**d** are 30-700-fold less potent hAChE inhibitors than racemic huprine Y, but they exhibit more potent anticholinesterase than trypanocidal activity (2-29-fold), with IC_{50} values for hAChE inhibition in the two-three digit nanomolar range (Table 1). The least active compound against hAChE is (+)-**2d**, which is the dimer with the best selectivity index for trypanocidal over cytotoxic activity. However, even in this case, its 2-fold higher anticholinesterase activity could still be a concern in terms of further development.

Permeability across the BBB is a necessary condition for drug candidates against HAT that are to be effective against late-stage disease, when the CNS is invaded by the parasite.

Table 2
BBB predicted permeabilities of *bis*-(+)-huprines (+)-**2a**–**e** and parent huprine Y

Compd	P_e (10^{-6} cm s^{-1})[a]	Prediction
(+)-**2a**	11.1 ± 0.3	CNS+
(+)-**2b**	13.9 ± 1.0	CNS+
(+)-**2c**	8.7 ± 1.5	CNS+
(+)-**2d**	17.4 ± 0.7	CNS+
(+)-**2e**	8.3 ± 0.6	CNS+
huprine Y, **1**	23.8 ± 2.7[b]	CNS+

[a] Values are expressed as mean ± SD of three independent experiments.

[b] Taken from ref. 32.

The BBB permeability of *bis*-huprines (+)-**2a**–**e** was assessed *in vitro* through the widely used parallel artificial membrane permeability assay (PAMPA-BBB), using a lipid extract of porcine brain as the artificial membrane.[37] Assay validation was performed by comparing the experimentally observed permeabilities [P_e (exp)] of fourteen marketed drugs with the permeabilities reported in the literature [P_e (lit)], which provided a good linear correlation: P_e (exp) = 1.4974 P_e (lit) – 0.8434 (R^2 = 0.9428). Taking into account this equation and the limits established by Di *et al.*,[35] three ranges of BBB permeation were established: high BBB permeation (CNS+) for those compounds with P_e (10^{-6} cm s^{-1}) > 5.1; low BBB permeation (CNS–) for those compounds with P_e (10^{-6} cm s^{-1}) < 2.1; and uncertain BBB permeation (CNS±) for those compounds with 5.1 > P_e (10^{-6} cm s^{-1}) > 2.1. All the *bis*-huprines exhibited permeabilities clearly above the threshold established for high BBB permeation (Table 2), even though they seem to be less permeable than monomeric huprine Y. This may arise because they are dibasic compounds and will mostly be in the diprotonated form, whereas monomeric huprine, with only one basic nitrogen atom, will be monoprotonated under the assay conditions.

In summary, we report the synthesis of a series of dimeric *bis*(4-aminoquinoline) derivatives, which are composed of two units of (+)-(7*R*,11*R*)-huprine Y connected through oligomethylene linkers of different length or a *p*-phenylene-*bis*(methylene) linker. We also describe the assessment of the different *bis*(+)-huprines on the growth of bloodstream forms of *T. brucei* and *P. falciparum*, and of rat skeletal myoblast L6 cells, as well as their hAChE inhibitory activity and BBB permeability. All of the *bis*(+)-huprines exhibited potent trypanocidal activity, with IC_{50} and IC_{90} values in the submicromolar range. However, they did not exhibit significant antiplasmodial activity, and, conversely, they were found to potently inhibit hAChE. As trypanocidal agents, *bis*(+)-huprines are more potent than monomeric huprine Y and some of them, particularly the dodecamethylene- and *p*-phenylene-*bis*(methylene)-linked dimers (+)-**2d** and (+)-**2e**, are less cytotoxic and, hence, more selective for *T. brucei* over rat L6 cells growth inhibition than huprine Y. All the *bis*(+)-huprines have been predicted to have the ability to cross the BBB, thereby being potentially useful for the treatment of late-stage HAT. Overall, *bis*(+)-huprines (+)-**2d** and (+)-**2e** emerge as interesting lead compounds for further trypanocidal drug development. Future research should focus not only on increasing trypanocidal potency, but decreasing cytotoxicity and AChE inhibitory activity.

Acknowledgments

This work was supported by Ministerio de Ciencia e Innovación (MICINN) (CTQ2011-22433) and Generalitat de Catalunya (GC) (2014SGR52). JMK acknowledges funding support from the Wellcome Trust (Grant number WT084175). A fellowship from GC to I.S. is gratefully acknowledged. SYG is grateful to the Commonwealth Scholarship Secretariat, UK, and to the Government of Ghana for financial support.

Supplementary data

Supplementary data (synthetic procedures and chemical characterization of *bis*(+)-huprines and biological methods) associated with this article can be found, in the online version, at http://dx.doi.org/10.1016/...

References and notes

1. Simarro, P. P.; Cecchi, G.; Franco, J. R.; Paone, M.; Diarra, A.; Ruiz-Postigo, J. A.; Fevre, E. M.; Mattioli, R. C.; Jannin, J. G. *PLoS Negl. Trop. Dis.* **2012**, *6*, e1859.
2. World Health Organization. World Malaria Report 2013.
3. Espuelas, S.; Plano, D.; Nguewa, P.; Font, M.; Palop, J. A.; Irache, J. M.; Sanmartín, C. *Curr. Med. Chem.* **2012**, *19*, 4259.
4. Hu, L.; Patel, A.; Bondada, L.; Yang, S.; Wang, M. Z.; Munde, M.; Wilson, W. D.; Wenzler, T.; Brun, R.; Boykin, D. W. *Bioorg. Med. Chem.* **2013**, *21*, 6732.
5. Faist, J.; Seebacher, W.; Kaiser, M.; Brun, R.; Saf, R.; Weis, R. *Bioorg. Med. Chem.* **2013**, *21*, 4988.
6. Phillips, M. A. *Mol. Microbiol.* **2012**, *86*, 10.
7. Fairlamb, A. H. *Nature* **2012**, *482*, 167.
8. Alsford, S.; Eckert, S.; Baker, N.; Glover, L.; Sanchez-Flores, A.; Leung, K. F.; Turner, D. J.; Field, M. C.; Berriman, M.; Horn, D. *Nature* **2012**, *482*, 232.
9. Gilbert, I. H. *J. Med. Chem.* **2013**, *56*, 7719.
10. Spinks, D.; Shanks, E. J.; Cleghorn, L. A. T.; McElroy, S.; Jones, D.; James, D.; Fairlamb, A. H.; Frearson, J. A.; Wyatt, P. G.; Gilbert, I. H. *ChemMedChem* **2009**, *4*, 2060.
11. Belluti, F.; Uliassi, E.; Veronesi, G.; Bergamini, C.; Kaiser, M.; Brun, R.; Viola, A.; Fato, R.; Michels, P. A. M.; Krauth-Siegel, R. L.; Cavalli, A.; Bolognesi, M. L. *ChemMedChem* **2014**, *9*, 371.
12. Njogu, P. M.; Chibale, K. *Curr. Med. Chem.* **2013**, *20*, 1715.
13. Prati, F.; Uliassi, E.; Bolognesi, M. L. *MedChemComm* **2014**, *5*, 853.
14. Njoroge, M.; Njuguna, N. M.; Mutai, P.; Ongarora, D. S. B.; Smith, P. W.; Chibale, K. *Chem. Rev.* **2014**, in press, DOI: 10.1021/cr500098f.
15. Persch, E.; Bryson, S.; Todoroff, N. K.; Eberle, C.; Thelemann, J.; Dirdjaja, N.; Kaiser, M.; Weber, M.; Derbani, H.; Brun, R.; Schneider, G.; Pai, E. F.; Krauth-Siegel, R. L.; Diederich, F. *ChemMedChem* **2014**, *9*, 1880.
16. Stich, A.; Ponte-Sucre, A.; Holzgrabe, U. *Lancet Infect. Dis.* **2013**, *13*, 733.
17. Ferrins, L.; Rahmani, R.; Baell, J. B. *Future Med. Chem.* **2013**, *5*, 1801.
18. Upadhayaya, R. S.; Dixit, S. S.; Földesi, A.; Chattopadhyaya, J. *Bioorg. Med. Chem. Lett.* **2013**, *23*, 2750.
19. Rashad, A. A.; Jones, A. J.; Avery, V. M.; Baell, J.; Keller, P. A. *ACS Med. Chem. Lett.* **2014**, *5*, 496.
20. Musonda, C. C.; Yardley, V.; Carvalho de Souza, R. C.; Ncokazi, K.; Egan, T. J.; Chibale, K. *Org. Biomol. Chem.* **2008**, *6*, 4446.
21. Musonda, C. C.; Gut, J.; Rosenthal, P. J.; Yardley, V.; Carvalho de Souza, R. C.; Chibale, K. *Bioorg. Med. Chem.* **2006**, *14*, 5605.
22. Chibale, K. *Pure Appl. Chem.* **2005**, *77*, 1957.
23. Defaux, J.; Sala, M.; Formosa, X.; Galdeano, C.; Taylor, M. C.; Alobaid, W. A. A.; Kelly, J. M.; Wright, C. W.; Camps, P.; Muñoz-Torrero, D. *Bioorg. Med. Chem.* **2011**, *19*, 1702.
24. Oluwafemi, A. J.; Okanla, E. O.; Camps, P.; Muñoz-Torrero, D.; Mackey, Z. B.; Chiang, P. K.; Seville, S.; Wright, C. W. *Nat. Prod. Commun.* **2009**, *4*, 193.
25. Kaur, K.; Jain, M.; Reddy, R. P.; Jain, R. *Eur. J. Med. Chem.* **2010**, *45*, 3245.
26. Girault, S.; Grellier, P.; Berecibar, A.; Maes, L.; Lemière, P.; Muray, E.; Davioud-Charvet, E.; Sergheraert, C. *J. Med. Chem.* **2001**, *44*, 1658.
27. Ayad, F.; Tilley, L.; Deady, L. W. *Bioorg. Med. Chem. Lett.* **2001**, *11*, 2075.
28. Cowman, A. F.; Deady, L. W.; Deharo, E.; Desneves, J.; Tilley, L. *Aust. J. Chem.* **1997**, *50*, 1091.
29. Girault, S.; Grellier, P.; Berecibar, A.; Maes, L.; Mouray, E.; Lemière, P.; Debreu, M.-A.; Davioud-Charvet, E.; Sergheraert, C. *J. Med. Chem.* **2000**, *43*, 2646.
30. Camps, P.; Contreras, J.; Font-Bardia, M.; Morral, J.; Muñoz-Torrero, D.; Solans, X. *Tetrahedron: Asymmetry* **1998**, *9*, 835.
31. Camps, P.; El Achab, R.; Morral, J.; Muñoz-Torrero, D.; Badia, A.; Baños, J. E.; Vivas, N. M.; Barril, X.; Orozco, M.; Luque, F. J. *J. Med. Chem.* **2000**, *43*, 4657.
32. Viayna, E.; Sola, I.; Bartolini, M.; De Simone, A.; Tapia-Rojas, C.; Serrano, F. G.; Sabaté, R.; Juárez-Jiménez, J.; Pérez, B.; Luque, F. J.; Andrisano, V.; Clos, M. V.; Inestrosa, N. C.; Muñoz-Torrero, D. *J. Med. Chem.* **2014**, *57*, 2549.
33. The synthetic procedure for the preparation of *bis*(+)-huprines is exemplified by the synthesis and chemical characterization of (+)-**2d**: (+)-*N,N'-bis*[(7*R*,11*R*)-3-chloro-6,7,10,11-tetrahydro-9-methyl-7,11-methanocicloocta[*b*]quinolin-12-yl]-1,12-dodecanediamine. A suspension of (+)-huprine Y, (+)-**1** (500 mg, 1.76 mmol, 2 equiv) and finely powdered KOH (85% purity, 347 mg, 5.26 mmol, 6 equiv), and 4 Å molecular sieves (approx. 1 g) in anhydrous DMSO (10 mL) was stirred, heating every 10 min approximately with a heat gun for 1 h and at rt one additional hour, and then treated with a solution of 1,12-dibromododecane (289 mg, 0.88 mmol, 1 equiv) in DMSO (4 mL) dropwise for 30 min. The reaction mixture was stirred at room temperature for 3 days, diluted with 5N NaOH (100 mL) and H_2O (50 mL), and extracted with EtOAc (2×200 mL). The combined organic extracts were washed with H_2O (2×50 mL), dried over anhydrous Na_2SO_4, and evaporated under reduced pressure to give a yellow oil (614 mg), which was purified through column chromatography (40–60 µm silica gel, CH_2Cl_2/50% aq. NH_4OH 100:0.2), to afford *bis*-huprine (+)-**2d** (323 mg, 50% yield); R_f 0.75 (CH_2Cl_2/MeOH/50% aq. NH_4OH 9:1:0.05). A solution of (+)-**2d** (223 mg, 0.30 mmol) in CH_2Cl_2 (4 mL) was filtered through a 0.2 µm PTFE filter, treated with methanolic HCl (0.43 N, 4.2 mL) and evaporated under reduced pressure. The resulting solid was washed with pentane (3×2 mL) to give, after drying at 65 ºC/2 Torr for 48 h, (+)-**2d**·2HCl (199 mg) as a yellowish solid: $[\alpha]_D^{20}$ = + 239 (MeOH, *c* = 0.6); mp 179–181 °C; IR (KBr) ν 3500–2500 (max at 3208, 3050, 3002, 2924, 2849, 2733, N-H, N^+-H and C-H st), 1631, 1582, 1567, 1514 (ar-C-C and ar-C-N st) cm^{-1}; ^{1}H NMR (400 MHz, CD_3OD) δ 1.22–1.48 [complex signal, 16H, 3(10)-H_2, 4(9)-H_2, 5(8)-H_2, 6(7)-H_2], 1.58 [s, 6H, 9'(9")-CH_3], 1.80–1.94 [complex signal, 6H, 2(11)-H_2, 13'(13")-H_{syn}], 1.93 [d, *J* = 17.6 Hz, 2H, 10'(10")-H_{endo}], 2.08 [br d, *J* = 12.4 Hz, 2H, 13'(13")-H_{anti}], 2.55 [dd, *J* = 17.6 Hz, *J'* = 4.4 Hz, 2H, 10'(10")-H_{exo}], 2.77 [m, 2H, 7'(7")-H], 2.87 [d, *J* = 17.6 Hz, 2H, 6'(6")-H_{endo}], 3.21 [dd, *J* = 17.6 Hz, *J'* = 5.2 Hz, 2H, 6'(6")-H_{exo}], 3.45 [m, 2H, 11'(11")-H], 3.98 [t, *J* = 6.8 Hz, 4H, 1(12)-H_2], 4.85 (s, NH, NH^+), 5.58 [br d, *J* = 4.0 Hz, 2H, 8'(8")-H], 7.54 [dd, *J* = 9.2 Hz, *J'* = 1.2 Hz, 2H, 2'(2")-H], 7.77 [br s, 2H, 4'(4")-H], 8.39 [d, *J* = 9.2 Hz, 2H, 1'(1")-H]; ^{13}C NMR (100.6 MHz, CD_3OD) δ 23.5 [CH_3, 9'(9")-CH_3], 27.3 [CH, C11'(11")], 27.83 [CH_2, C3(10)], 27.85 [CH, C7'(7")], 29.3 [CH_2, C13'(13")], 30.3 (CH_2) and 30.6 ($2CH_2$) [C4(9), C5(8), C6(7)], 31.2 [CH_2, C2(11)], 36.0 [CH_2, C10'(10")], 36.1 [CH_2, C6'(6")], 49.7 [CH_2, C1(12)], 115.6 (C) and 117.6 (C) [C11a'(11a"), C12a'(12a")], 119.1 [CH, C4'(4")], 125.2 [CH, C8'(8")], 126.6 [CH, C2'(2")], 129.5 [CH, C1'(1")], 134.5 [C, C9'(9")], 140.2 [C, C3'(3")], 141.0 [C, C4a'(4a")], 151.2 [C, C5a'(5a")], 156.9 [C, C12'(12")]. HRMS (ESI) calcd for ($C_{46}H_{56}{}^{35}Cl_2N_4$ + H^+): 735.3955, found 735.3960. Anal. calcd for ($C_{46}H_{56}Cl_2N_4$·2HCl·1.25H_2O): C 66.46%, H 7.34%, N 6.74%; found: C 66.63%, H 7.66%, N 6.23%.
34. Egan, T. J. *Drug Des. Rev.* **2004**, *1*, 93.
35. Viayna, E.; Gómez, T.; Galdeano, C.; Ramírez, L.; Ratia, M.; Badia, A.; Clos, M. V.; Verdaguer, E.; Junyent, F.; Camins, A.; Pallàs, M.; Bartolini, M.; Mancini, F.; Andrisano, V.; Arce, M. P.; Rodríguez-Franco, M. I.; Bidon-Chanal, A.; Luque, F. J.; Camps, P.; Muñoz-Torrero, D. *ChemMedChem* **2010**, *5*, 1855.
36. Ellman, G. L.; Courtney, K. D.; Andres, V. Jr.; Featherstone, R. M. *Biochem. Pharmacol.* **1961**, *7*, 88.
37. Di, L.; Kerns, E. H.; Fan, K.; McConnell, O. J.; Carter, G. T. *Eur. J. Med. Chem.* **2003**, *38*, 223.

6. B.

Bioorg. Med. Chem. **2015**, *23*, 5156

Bioorganic & Medicinal Chemistry
journal homepage: www.elsevier.com

Synthesis, biological profiling and mechanistic studies of 4-aminoquinoline-based heterodimeric compounds with dual trypanocidal-antiplasmodial activity

Irene Sola[a], Sílvia Castellà[a], Elisabet Viayna[a], Carles Galdeano[a], Martin C. Taylor[b], Stephen Y. Gbedema[c,d], Belén Pérez[e], M. Victòria Clos[e], Deuan C. Jones[f], Alan H. Fairlamb[f], Colin W. Wright[c], John M. Kelly[b], Diego Muñoz-Torrero[a,*1]

[a] *Laboratori de Química Farmacèutica (Unitat Associada al CSIC), Facultat de Farmàcia, and Institut de Biomedicina (IBUB), Universitat de Barcelona, Av. Joan XXIII, 27-31, E-08028, Barcelona, Spain*
[b] *Department of Pathogen Molecular Biology, London School of Hygiene and Tropical Medicine, Keppel Street, London WC1E 7HT, United Kingdom*
[c] *Bradford School of Pharmacy, University of Bradford, West Yorkshire BD7 1 DP, United Kingdom*
[d] *Department of Pharmaceutics, Kwame Nkrumah University of Science and Technology, Kumasi, Ghana*
[e] *Departament de Farmacologia, de Terapèutica i de Toxicologia, Universitat Autònoma de Barcelona, 08193-Bellaterra, Barcelona, Spain*
[f] *Division of Biological Chemistry & Drug Discovery, College of Life Sciences, University of Dundee, Dundee DD1 5EH, United Kingdom*

ARTICLE INFO

Article history:
Received
Received in revised form
Accepted
Available online

Keywords:
Molecular hybridization
Trypanocidal agents
Antimalarial agents
Trypanothione reductase inhibitors
Inhibitors of β-haematin formation
Brain permeability

ABSTRACT

Dual submicromolar trypanocidal-antiplasmodial compounds have been identified by screening and chemical synthesis of 4-aminoquinoline-based heterodimeric compounds of three different structural classes. In *Trypanosoma brucei*, inhibition of the enzyme trypanothione reductase seems to be involved in the potent trypanocidal activity of these heterodimers, although it is probably not the main biological target. Regarding antiplasmodial activity, the heterodimers seem to share the mode of action of the antimalarial drug chloroquine, which involves inhibition of the haem detoxification process. Interestingly, all of these heterodimers display good brain permeabilities, thereby being potentially useful for late stage human African trypanosomiasis. Future optimization of these compounds should focus mainly on decreasing cytotoxicity and acetylcholinesterase inhibitory activity.

1. Introduction

Human African trypanosomiasis (HAT or sleeping sickness), one of the 17 so-called neglected tropical diseases, and malaria have an enormous health and socioeconomic impact in the developing world.[1-3] Notwithstanding a wide-scale reduction in the number of infected people over recent years due to public health campaigns, HAT and malaria are still leading causes of morbidity and death and of loss of productivity especially in sub-Saharan Africa.[1,4-6] Malaria annually kills more than 600,000 people.[3] The numbers dying from trypanosomiasis have recently been reduced to around 10,000, but the disease retains the potential for major epidemic outbreaks, and it has a devastating impact on domestic livestock.

HAT and malaria are caused by protozoan parasites of the genera *Trypanosoma* and *Plasmodium*, which are transmitted to humans through the bite of blood-feeding infected tsetse flies and female *Anopheles* mosquitoes, respectively. The most common form of HAT in humans, accounting for nearly 95% of cases, is caused by *Trypanosoma brucei gambiense*, which results in a chronic infection that can last for years. A less common form of the disease with a more acute clinical presentation is caused by the subspecies *Trypanosoma brucei rhodesiense*. In the case of malaria, five species of *Plasmodium* can cause the disease, *Plasmodium falciparum* being the most common and deadly.

HAT begins with a hemolymphatic stage, where the parasite multiplies within the blood, lymph and subcutaneous tissue, and which is characterized by the appearance of nonspecific symptoms such as fever and headache. Invasion of the central nervous system (CNS) by the parasite, after crossing the blood–brain barrier (BBB), leads to the late-stage meningoencephalitic disease. This gives rise to severe neurological symptoms such as psychiatric, motor and sleep disturbances and loss of consciousness. Without treatment, this results in coma and death.

*[1] Corresponding autor. Tel.: +34-934024533.
E-mail address: dmunoztorrero@ub.edu (D. Muñoz-Torrero).

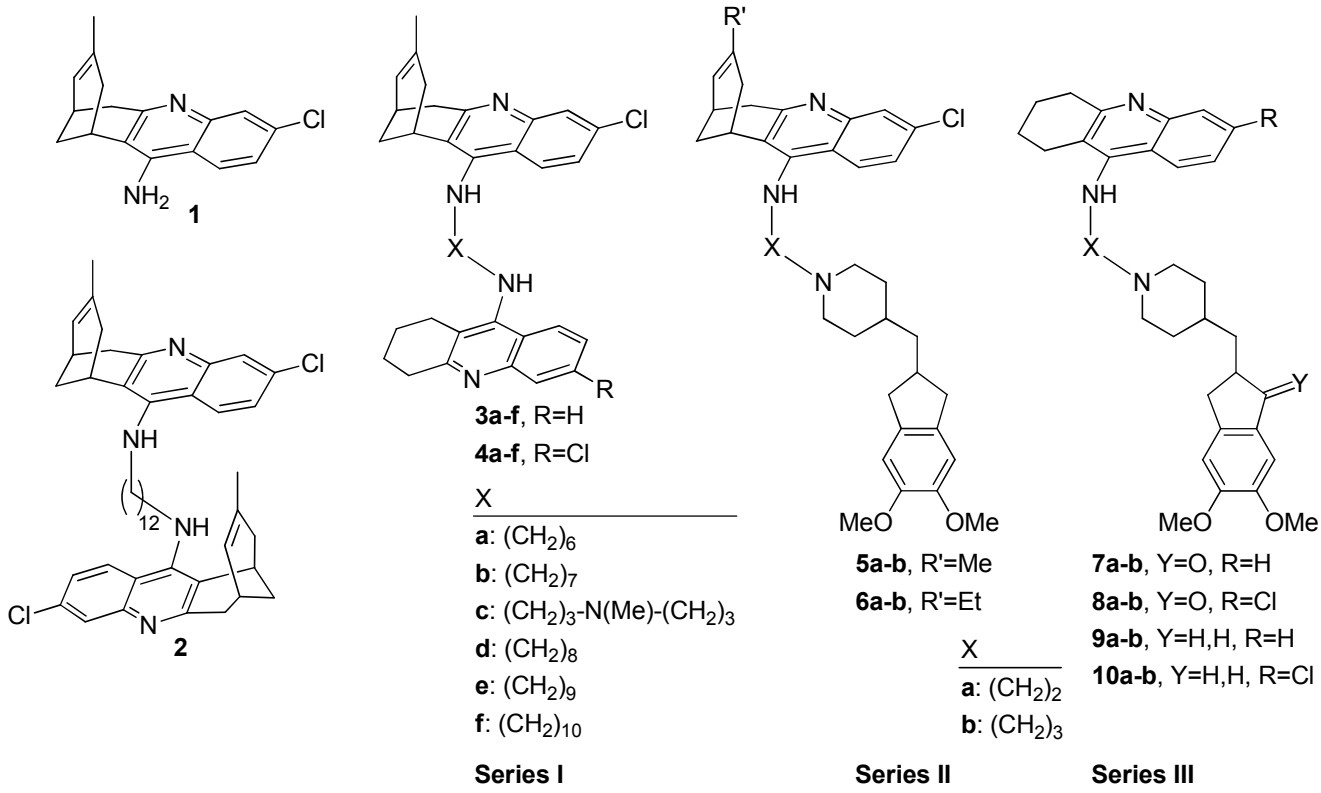

Figure 1. Structures of huprine Y, **1**, bis(4-aminoquinoline) homodimer **2** and bis- or mono-(4-aminoquinoline)-based heterodimers of series **I**-**III**

In malaria, the parasites initially infect the liver, and are then released into the bloodstream. The disease may progress to a severe form, where parasites can become sequestered within brain capillaries, particularly in children, evolving to cerebral malaria and eventually to coma and death.

Vector control and public health interventions remain the main options for prevention, as no licensed vaccine for either infection is available. Worryingly, current chemotherapy against HAT and malaria suffers from serious limitations.[1,4,7-9] Although five trypanocidal drugs are currently in use (pentamidine, suramin, melarsoprol, nifurtimox and eflornithine), they are generally effective against only one stage of the disease. In addition, they are relatively expensive, require long-lasting parenteral administration which is often impracticable in poor rural settings, display toxicity and parasite resistance has frequently emerged. In the case of the arsenical melarsoprol,[10] the latter two issues have challenged its widespread, safe and efficacious use.[11,12] The emergence of resistance is the reason that chloroquine, after decades of being the mainstay for malaria treatment, is no longer widely used. Resistance is also beginning to threaten the effectiveness of the current first-line treatments, based on artemisinin.[1]

In this context, it is critically important to ensure that the trypanocidal and antimalarial drug development pipelines are continuously replenished with novel candidates that are devoid of the important flaws of existing drugs. The requirement is for new non toxic and inexpensive chemical entities that are effective against resistant parasite strains and are brain permeable, so that they may be useful against malaria and both disease stages of HAT. Intensive research efforts involving phenotypic whole-cell screening of chemical libraries or newly synthesized compounds,[13-16] identification of novel key biological targets and subsequent target-based screening or rational design campaigns,[17-21] development of multitarget-directed ligands,[22-24] or drug repurposing programs[1] are being carried out in the pursuit of novel antiprotozoal compounds.

Because HAT and malaria often affect overlapping populations, development of compounds endowed with dual trypanocidal and antiplasmodial activity can be regarded a feasible economic therapeutic strategy.[25] A number of 4-amino-7-chloroquinolines and other aminoquinoline derivatives have been recently synthesized and found to be active against *T. brucei* and/or *P. falciparum*.[26-29] This prompted us to assess the antiprotozoal activity of huprines, a novel structural class of compounds featuring a 4-aminoquinoline moiety, which had been initially developed as brain permeable inhibitors of the enzyme acetylcholinesterase (AChE). Huprines in general turned out to be moderately potent and selective trypanocidal agents, with a few also being active against the chloroquine-resistant K1 strain of *P. falciparum*.[30,31] The so-called huprine Y (**1**, Fig. 1) exhibited the most potent activity against *T. brucei* (IC_{50} = 0.61 μM; IC_{90} = 2.94 μM) and one of the best selectivity indices over rat myoblast L6 cells (SI = 13), but it was essentially devoid of antiplasmodial activity.[30]

Next, we turned our attention to the molecular dimerization of huprine Y because this approach had been successfully applied to other 4-aminoquinoline derivatives to overcome drug resistance.[32-36] One of the most interesting huprine dimers was the novel dodecamethylene-linked bis(4-aminoquinoline) compound **2** (Fig. 1), which tripled the potency and selectivity of the parent huprine Y against *T. brucei*, but remained inactive against *P. falciparum*.[37]

The lack of potency of huprine Y and bis-huprines against *P. falciparum* was rather striking because: i) the huprine Y unit contains the 4-amino-7-chloroquinoline moiety of chloroquine,

which is considered to be the pharmocophoric moiety responsible for the inhibition of heme dimerization by the antimalarial drug,[28,38] and ii) in other bis(4-aminoquinoline) derivatives dimerization had been reported to increase antiplasmodial potency relative to the 4-aminoquinoline monomeric parent compounds due to the doubling of the number of protonatable nitrogen atoms. This enabled a more efficient trapping of the dimeric compounds in the acidic digestive vacuole of *P. falciparum*, and hence, a more efficient inhibition of heme dimerization.[32,35] We hypothesized that neither huprine Y nor bis-huprines were able to hit the biological target of chloroquine and other bis(4-aminoquinoline) derivatives, despite their structural similarity.

To explore further the dimerization strategy, and to discover new hits with dual trypanocidal-antiplasmodial activity, we report here: i) the screening against cultured bloodstream forms of *T. brucei* and *P. falciparum* and rat myoblast L6 cells of a small in-house library of brain permeable 4-aminoquinoline-based heterodimeric compounds, belonging to three distinct structural classes (series **I-III**, Fig. 1); ii) the synthesis of novel 4-aminoquinoline-based heterodimeric compounds based on the most promising series and evaluation of their *T. brucei*, *P. falciparum*, rat myoblast L6 cell and human AChE inhibitory activities and brain permeability; and iii) the assessment of the putative biological targets in *T. brucei* and *P. falciparum* of selected hits of the different series and monomeric huprine Y by the *in vitro* evaluation of their inhibitory activity against *T. brucei* trypanothione reductase and β-haematin formation.

2. Results and discussion

2.1. Screening of trypanocidal, antiplasmodial and cytotoxic activity of 4-aminoquinoline-based heterodimeric compounds of series I-III

The heterodimers of series **I-III** (Fig. 1) were recently developed by us as inhibitors of the enzyme AChE, of potential interest for the treatment of Alzheimer's disease.[39-41] The high AChE inhibitory activity displayed by these heterodimers (IC_{50} values in the low nanomolar range) is a drawback for antiprotozoal drug development. However, the presence of one or two 4-aminoquinoline moieties in the structures of these heterodimers, and the fact that all of them had been found to be brain permeable, encouraged us to screen them as potential hits applicable to both stages of HAT. Derivatives that displayed promise could then be further optimized in terms of trypanocidal/anticholinesterase activity ratio.

Heterodimers of series **I** are a group of 14 racemic or enantiopure bis(4-aminoquinoline) derivatives that contain a unit of huprine Y and a unit of the structurally related tacrine (heterodimers **3a-f**) or 6-chlorotacrine (heterodimers **4a-f**), connected through linkers of different length and nature (hexa- to deca-methylene or 4-methyl-4-azaheptamethylene), which are di- or tri-protonated at physiological or acidic pH. The antiprotozoal activity of heterodimers of series **I** was assessed *in vitro* against cultured bloodstream forms of *T. brucei* and the chloroquine-resistant K1 strain of *P. falciparum* and their cytotoxicity determined against rat skeletal myoblast L6 cells. All of the heterodimers of series **I** were found to be potent trypanocidal agents, exhibiting IC_{50} and IC_{90} values in the 0.15-0.56 μM and 0.29-0.79 μM range, respectively (Table 1). The main structural feature influencing their trypanocidal potency was the length of the linker. Indeed, the trypanocidal potency seemed to increase with increased length of the tether, both in heterodimers containing an unsubstituted tacrine moiety (heterodimers **3**) and in those bearing a 6-chlorotacrine unit (heterodimers **4**). Thus, the trypanocidal activity peaks in the octa- and deca-methylene heterodimers **3d**, **4d**, **3f** and **4f** that are more than 3-fold more potent than their hexamethylene-linked counterparts. In contrast, the presence of a third protonatable nitrogen atom within the linker did not seem to have a significant influence on trypanocidal potency, heterodimers **3c** and **4c** being roughly equipotent to heptamethylene-linked heterodimers **3b** and **4b**, which have an equivalent tether length. Also, the presence or absence of a chlorine atom at the tacrine unit does not have much effect on trypanocidal activity, heterodimers **3a-f** being essentially equipotent to **4a-f**. Finally, there did not seem to be enantioselectivity in the trypanocidal activity of these heterodimers, as enantiopure heterodimers (7*R*,11*R*)-**3b** and (7*S*,11*S*)-**3b** and racemic **3b** display essentially the same potency. Of note, all of the heterodimers of series **I** are more potent than monomeric huprine Y (up to 4-fold when considering IC_{50} values and up to 10-fold when considering IC_{90} values). Overall, heterodimerization here results in increased trypanocidal potency, similar to the homodimerization strategy leading to bis-huprines such as **2**.[37]

Strikingly, unlike the parent huprine Y and homodimerization leading to bis-huprines, which were inactive against *P. falciparum*, heterodimerization resulted in moderately potent antiplasmodial activities, with most heterodimers of series **I** exhibiting IC_{50} values in the submicromolar range (Table 1). Very interestingly, seven of these heterodimers were even 2-3-fold more potent than the reference compound chloroquine against a chloroquine-resistant strain of malaria. Some clear structure-activity relationship trends were found for this activity in heterodimers of series **I**. Thus, the presence of an unsubstituted tacrine unit and increased tether lengths were the structural features leading to higher antiplasmodial potencies. The presence of a tertiary amino group within the linker only influenced antiplasmodial activity in the subseries bearing a chlorosubstituted tacrine unit. As with trypanocidal activity, essentially no enantioselectivity was observed for antiplasmodial activity, with enantiomeric (7*R*,11*R*)-**3b** and (7*S*,11*S*)-**3b** and racemic **3b** displaying roughly the same potencies.

With the exceptions of the nonamethylene-linked heterodimers **3e** and **4e**, which displayed a similar or a 5-fold lower cytotoxicity relative to the parent huprine Y, the rest of heterodimers of series **I** were more cytotoxic than huprine Y. Thus, heterodimers **3e** and **4e** showed the best selectivity indices against *T. brucei* (SI = 34 and 167, respectively), but only **3e** had a favourable selectivity index in the case of *P. falciparum* (SI = 20), thereby emerging as the most interesting dual acting trypanocidal-antiplasmodial heterodimer of the series.

Heterodimers of series **II** are a group of 5 racemic or enantiopure compounds that contain a unit of huprine Y or its 9-ethyl analogue, connected through an ethylene or trimethylene linker to a piperidine ring substituted at position 4 with a (5,6-dimethoxyindan-2-yl)methyl group. They are diprotonated at physiological or acidic pH. Again, all of the heterodimers of this series display potent trypanocidal activities, with IC_{50} and IC_{90} values in the 0.17-0.49 μM and 0.35-1.33 μM range, respectively (Table 1). They were up to 4-fold more potent than the parent huprine Y based on IC_{50} values, and up to 8-fold based on IC_{90} values). The presence of a trimethylene linker seemed to have a positive effect on trypanocidal activity, whereas no clear trend was found regarding the presence of a methyl or an ethyl group at the huprine moiety. Also, there seems not to be any enantioselectivity in the trypanocidal action of these compounds, as enantiopure (7*S*,11*S*)-**6a** exhibits the same potency as the racemic compound.

Table 1
Trypanocidal, antiplasmodial and cytotoxic activity of 4-aminoquinoline–based heterodimeric compounds **3**-**10** and reference compounds **1** and chloroquine diphosphate[a]

Compd	X	R	R'	Y	*T. brucei* IC_{50} µM	*T. brucei* IC_{90} µM	*P. falciparum* IC_{50} µM	L6 cells IC_{50} µM	SI_{Tb}[b]	SI_{Pf}[b]
3a	$(CH_2)_6$	H			0.47 ± 0.05	0.66 ± 0.01	2.99 ± 0.85	1.17 ± 0.03	2.5	0.39
3b	$(CH_2)_7$	H			0.24 ± 0.04	0.43 ± 0.02	0.47 ± 0.36	<1.0	<4.2	<2.1
(7*R*,11*R*)-**3b**	$(CH_2)_7$	H			0.21 ± 0.03	0.42 ± 0.01	0.35 ± 0.15	0.73 ± 0.28	3.5	2.1
(7*S*,11*S*)-**3b**	$(CH_2)_7$	H			0.29 ± 0.04	0.49 ± 0.02	0.46 ± 0.19	<1.0	<3.4	<2.2
3c	$(CH_2)_3N(Me)(CH_2)_3$	H			0.32 ± 0.02	0.45 ± 0.01	0.43 ± 0.22	<1.0	<3.1	<2.3
3d	$(CH_2)_8$	H			0.15 ± 0.02	0.29 ± 0.01	0.39 ± 0.14	1.11 ± 0.15	7.4	2.8
3e	$(CH_2)_9$	H			0.21 ± 0.03	0.45 ± 0.02	0.35 ± 0.06	7.15 ± 0.30	34	20
3f	$(CH_2)_{10}$	H			0.14 ± 0.01	0.48 ± 0.02	nd	1.67 ± 0.04	12	nd
4a	$(CH_2)_6$	Cl			0.56 ± 0.03	0.79 ± 0.03	4.40 ± 1.38	1.10 ± 0.01	2.0	0.25
4b	$(CH_2)_7$	Cl			0.27 ± 0.06	0.43 ± 0.04	>6.88	<3.0	<11	<0.44
4c	$(CH_2)_3N(Me)(CH_2)_3$	Cl			0.28 ± 0.04	0.40 ± 0.01	0.52 ± 0.13	<1	<3.6	<1.9
4d	$(CH_2)_8$	Cl			0.17 ± 0.01	0.46 ± 0.02	>7.14	0.97 ± 0.13	5.7	<0.14
4e	$(CH_2)_9$	Cl			0.24 ± 0.04	0.52 ± 0.01	>6.82	40.0 ± 5.1	167	<5.9
4f	$(CH_2)_{10}$	Cl			0.17 ± 0.01	0.49 ± 0.02	2.10 ± 0.72	2.63 ± 0.16	15	1.3
5a	$(CH_2)_2$		Me		0.49 ± 0.12	1.18 ± 0.07	>7.01	6.76 ± 0.28	14	<1.0
5b	$(CH_2)_3$		Me		0.17 ± 0.01	0.35 ± 0.03	nd	2.06 ± 0.17	12	nd
6a	$(CH_2)_2$		Et		0.29 ± 0.03	0.70 ± 0.04	>7.14	3.55 ± 0.17	12	<0.50
(7*S*,11*S*)-**6a**	$(CH_2)_2$		Et		0.29 ± 0.02	0.72 ± 0.03	>7.05	6.29 ± 0.58	22	<0.89
(7*S*,11*S*)-**6b**	$(CH_2)_3$		Et		0.26 ± 0.03	1.33 ± 0.10	0.81 ± 0.20	2.15 ± 0.06	8.3	2.7
7a	$(CH_2)_2$	H		O	0.41 ± 0.03	0.88 ± 0.07	>8.15	<3.0	<7.3	<0.37
7b	$(CH_2)_3$	H		O	0.28 ± 0.02	0.62 ± 0.04	nd	<1.0	<3.6	nd
8a	$(CH_2)_2$	Cl		O	0.30 ± 0.03	0.68 ± 0.04	4.86 ± 3.30	<3.0	<10	<0.62
8b	$(CH_2)_3$	Cl		O	0.12 ± 0.01	0.17 ± 0.03	0.36 ± 0.07	0.57 ± 0.19	4.7	1.6
9a	$(CH_2)_2$	H		H,H	0.38 ± 0.04	0.79 ± 0.01	2.60 ± 1.91	<3.0	<7.9	<1.2
9b	$(CH_2)_3$	H		H,H	0.27 ± 0.03	0.66 ± 0.03	0.83 ± 0.44	<3.0	<11	<3.6
10a	$(CH_2)_2$	Cl		H,H	0.97 ± 0.11	2.39 ± 0.08	>7.72	2.42 ± 0.20	2.5	<0.31
10b	$(CH_2)_3$	Cl		H,H	0.34 ± 0.07	0.66 ± 0.04	6.04 ± 5.94	<3.0	<8.8	<0.5
1[c]					0.61 ± 0.03	2.94 ± 0.20	>10	7.80 ± 0.47	13	<0.78
chloroquine							0.93 ± 0.44			

[a] *In vitro* activity against bloodstream form of *T. brucei* (pH 7.4), *P. falciparum* (strain K1), and rat myoblast L6 cells expressed at the concentration that inhibited growth by 50% (IC_{50}) and 90% (IC_{90}, for trypanocidal activity). Data are the mean of triplicate experiments ± SEM.

[b] SI: Selectivity index is the ratio of cytotoxic to trypanocidal (SI_{Tb}) or antiplasmodial (SI_{Pf}) IC_{50} values.

[c] Activity values of reference compound **1** taken from ref. 30.

In sharp contrast with series **I**, most heterodimers of series **II** were essentially inactive against *P. falciparum*, with the sole exception of **6b** (IC_{50} = 0.81 µM, Table 1), which is roughly equipotent to the reference antimalarial drug chloroquine.

All of the heterodimers of series **II** turned out to be slightly more cytotoxic than the parent huprine Y. However, their superior trypanocidal potencies resulted in similar or even better selectivity indices against *T. brucei* than that of huprine Y (in almost all cases >10).

Heterodimers of series **III** form a group of 8 compounds that combine the 4-aminoquinoline unit of tacrine or 6-chlorotacrine with the 4-[(5,6-dimethoxyindan-2-yl)methyl]piperidine group that was also present in series **II** or with the indanone derivative thereof (Fig. 1). As with the other series, all of these heterodimers have trypanocidal activity at submicromolar concentrations (IC_{50} = 0.12-0.97 µM, IC_{90} = 0.17-2.39 µM, Table 1), and are more potent than huprine Y. The presence of an indanone system and a trimethylene linker are the structural features that lead to higher trypanocidal potencies. As for the influence of an unsubstituted or a 6-chloro-substituted tacrine unit, the former seems to be optimal for the indane derivatives and the latter for the indanone analogues.

Most heterodimers of series **III** are submicromolar or low micromolar antiplasmodial compounds, one of them, **8b**, being 3-fold more potent than chloroquine. As with trypanocidal activity, in general the antiplasmodial potency of these heterodimers

increased with the presence of an indanone system, a trimethylene linker and a tacrine or a 6-chlorotacrine unit for the indane or the indanone derivatives, respectively.

An important issue with heterodimers of series **III** was their cytotoxicity, which was greater than that of huprine Y and the other series of heterodimers: This resulted in poor selectivity indices against both *T. brucei* and *P. falciparum*.

Overall, all of the 27 screened 4-aminoquinoline-based heterodimers turned out to be more potent trypanocidal agents than huprine Y, and 10 of them (most belonging to series **I**) also exhibited more potent antiplasmodial activity than the antimalarial drug chloroquine. However, most heterodimers have marginal selectivity indices in terms of their trypanocidal and antiplasmodial activities. The most interesting hit is heterodimer **3e** (series **I**), with a balanced dual trypanocidal (IC_{50} = 0.21 µM) and antiplasmodial (IC_{50} = 0.35 µM) activity and selectivity indices of 34 and 20 for these activities over L6 cell cytotoxicity.

2.2. Synthesis of novel 4-aminoquinoline-based heterodimeric compounds

Based on: i) the most favourable dual trypanocidal/antiplasmodial profile of heterodimers of series **I**; ii) their easier and less expensive synthesis relative to heterodimers of series **II** and **III**; and iii) the trend towards increased trypanocidal and antiplasmodial potencies at increased tether lengths, we proceeded with the synthesis and biological profiling of the upper dodecamethylene-linked homologues of series **I** **3g** and **4g** (Scheme 1). In addition, because removal of the chlorine atom at position 3 of the huprine moiety is known to decrease AChE inhibitory activity,[42] we also undertook the synthesis and evaluation of the deca- and dodeca-methylene-linked heterodimers **16f-g** and **17f-g** bearing a 3-unsubstituted huprine moiety (Scheme 1).

The synthesis of the novel heterodimers of series **I** involved an initial alkylation of tacrine, **11**, or 6-chlorotacrine, **12**, with 1,10-dibromodecane or 1,12-dibromododecane in the presence of KOH in DMSO, which generated the known 10-bromodecyltacrines **13f**[39] and **14f**[39] and the novel 12-bromododecyltacrines **13g** and **14g** in moderate yields (30-39%) (Scheme 1). Subsequent alkylation of huprine Y, **1**, or its 3-unsubstituted derivative **15**, with the ω-haloalkyltacrines **13f-g** or **14f-g** under similar conditions at rt for 4 days, resulted in the novel heterodimers **3g**, **4g**, **16f-g** and **17f-g** in moderate to good yields (45-88%) after silica gel column chromatography purification of the reaction crudes. The novel heterodimers were converted into the corresponding dihydrochlorides for their chemical characterization (melting point, IR, ^{1}H and ^{13}C NMR, HRMS and elemental analysis) and biological profiling.

2.3. Biological profiling of the novel 4-aminoquinoline-based heterodimeric compounds

The putative dual trypanocidal/antiplasmodial and cytotoxic activities of the novel heterodimers **3g**, **4g**, **16f-g** and **17f-g** were evaluated *in vitro* against cultured bloodstream forms of *T. brucei*, the chloroquine-resistant K1 strain of *P. falciparum*, and rat skeletal myoblast L6 cells, respectively. Additionally, their inhibitory activity against human recombinant AChE was evaluated *in vitro* by the method of Ellman *et al.*[43] and their brain permeation assessed through the well-established parallel artificial membrane permeability assay (PAMPA-BBB).[44]

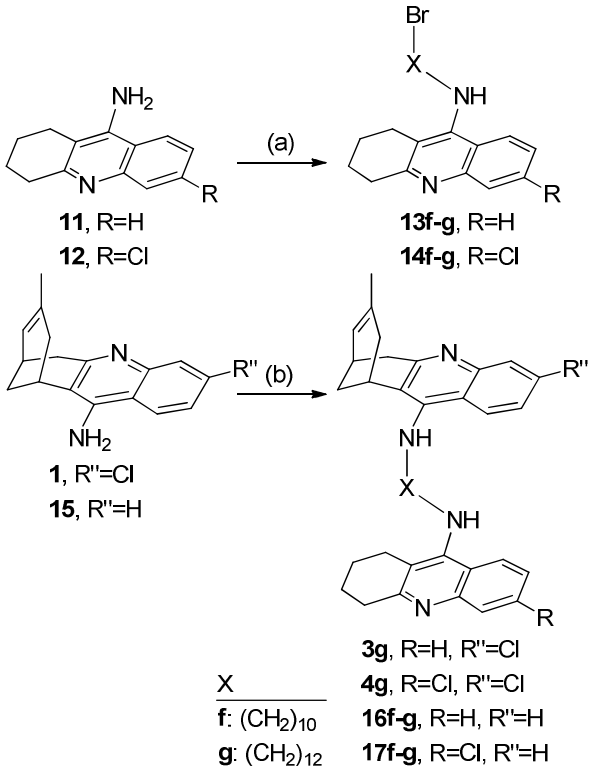

Scheme 1. Reagents and conditions: (a) **11** or **12**, KOH, DMSO, 2 h; then, 1,10-dibromodecane or 1,12-dibromododecane (1.2 eq), DMSO, rt, overnight; (b) **1** or **15**, KOH, DMSO, 2 h; then, **13f-g** or **14f-g** (1.2 eq), DMSO, rt, 4 days.

The activity data of the novel heterodimers are listed in Table 2, together with those of huprine Y, chloroquine, and **3e** (the heterodimer with the best selectivity index), as reference compounds. All of the novel heterodimers turned out to be more potent trypanocidal agents than the parent huprine (up to 3- and 10-fold when considering IC_{50} or IC_{90} values, respectively) (Table 2). Elongation of the tether chain from 10 methylenes in **3f** and **4f** to 12 methylenes in the novel heterodimers **3g** and **4g** resulted in a slightly decreased potency, so that the octa- and deca-methylene chains remained the optimal linkers for trypanocidal activity of huprine Y-based heterodimers of series **I**, as found in the initial screening experiments. Substitution of the huprine Y unit of heterodimers of series **I** by a 3-unsubstituted huprine moiety led in general to slightly increased trypanocidal potencies, especially if IC_{90} values are taken into account. Indeed, the novel heterodimer **16g** exhibited the lowest IC_{90} value (0.28 µM) amongst all the heterodimers of series **I**.

Unlike most previously screened heterodimers of series **I**, the novel heterodimers **3g**, **4g**, **16f-g** and **17f-g** were found to be essentially inactive or only moderately potent antiplasmodial compounds, displaying one-digit micromolar activities in the best cases (Table 2). Thus, homologation of the tether chain to a dodecamethylene linker and removal of the chlorine atom at position 3 of the huprine unit are detrimental for antiplasmodial activity.

Similar to most of the screened heterodimers of series **I**, the novel analogues had inadequate selectivity indices for both *T. brucei* and *P. falciparum* over rat L6 cells.

Table 2
Trypanocidal, antiplasmodial, cytotoxic, and anticholinesterase activity and BBB permeabilities of the novel 4-aminoquinoline–based heterodimeric compounds **3g**, **4g**, **16f-g**, and **17f-g** and reference compounds **1**, **3e**, and chloroquine diphosphate[a]

Compd	X	R	R"	*T. brucei*	*T. brucei*	*P. falciparum*	L6 cells	SI_{Tb}[b]	SI_{Pf}[b]	hAChE	*Pe* (10^{-6} cm s^{-6})[c]
				IC_{50} µM	IC_{90} µM	IC_{50} µM	IC_{50} µM			IC_{50} (nM)	(Prediction)
3g	$(CH_2)_{12}$	H	Cl	0.35 ± 0.01	0.52 ± 0.01	>6.9	1.04 ± 0.02	3.0	<0.15	1.92 ± 0.40	10.8 ± 1.0 (CNS+)
4g	$(CH_2)_{12}$	Cl	Cl	0.59 ± 0.05	0.77 ± 0.01	>6.6	5.58 ± 0.53	9.5	<0.85	3.46 ± 0.56	16.8 ± 0.3 (CNS+)
16f	$(CH_2)_{10}$	H	H	0.24 ± 0.01	0.31 ± 0.04	3.50 ± 2.29	<1	<4.2	<0.29	6.46 ± 1.43	6.3 ± 1.1 (CNS+)
16g	$(CH_2)_{12}$	H	H	0.21 ± 0.00	0.28 ± 0.01	>7.3	<1	<4.8	<0.14	10.1 ± 1.19	7.3 ± 0.7 (CNS+)
17f	$(CH_2)_{10}$	Cl	H	0.34 ± 0.02	0.43 ± 0.01	4.36 ± 2.82	1.11 ± 0.04	3.3	0.25	1.48 ± 0.24	17.2 ± 1.6 (CNS+)
17g	$(CH_2)_{12}$	Cl	H	0.55 ± 0.01	0.75 ± 0.01	>6.9	2.74 ± 0.29	5.0	<0.40	3.66 ± 0.33	11.0 ± 1.0 (CNS+)
1[d]				0.61 ± 0.03	2.94 ± 0.20	>10	7.80 ± 0.47	13	<0.78	0.61 ± 0.03[e]	23.8 ± 2.7 (CNS+)[f]
3e[g]	$(CH_2)_9$	H	Cl	0.21 ± 0.03	0.45 ± 0.02	0.35 ± 0.06	7.15 ± 0.30	34	20	3.53 ± 0.37	6.0 ± 0.3 (CNS+)
chloroquine						0.93 ± 0.44					

[a] *In vitro* activity against bloodstream form of *T. brucei* (pH 7.4), *P. falciparum* (strain K1), and rat myoblast L6 cells expressed at the concentration that inhibited growth by 50% (IC_{50}) and 90% (IC_{90}, for trypanocidal activity) and *in vitro* activity against human recombinant AChE expressed at the concentration that inhibited enzyme activity by 50% (IC_{50}). Data are the mean of triplicate experiments ± SEM.

[b] SI: Selectivity index is the ratio of cytotoxic to trypanocidal (SI_{Tb}) or antiplasmodial (SI_{Pf}) IC_{50} values.

[c] Permeability values from the PAMPA-BBB assay. Values are expressed as the mean ± SD of three independent experiments.

[d] Antiprotozoal and cytotoxic activity values of reference compound **1** taken from ref. 30.

[e] Taken from ref. 40.

[f] Taken from ref. 45.

[g] Taken from ref. 39.

To complete the biological profiling of the novel heterodimers, their brain permeation and human AChE inhibitory activities were assessed.

Brain permeation of the novel heterodimers was determined *in vitro* through the widely used PAMPA-BBB assay,[44] using a lipid extract of porcine brain as an artificial membrane model of the BBB. The heterodimerization strategy, as also found for homodimerization,[37] resulted in dibasic bis(4-aminoquinoline) derivatives that will be mostly diprotonated under the assay conditions, which could explain their lower permeabilities relative to the parent monobasic huprine Y (Table 2). However, all the heterodimers had permeabilities well above the threshold established for high BBB permeation (P_e (10^{-6} cm s^{-1}) > 5.1, CNS+, Table 2). As expected, elongation of the linker from 10 to 12 methylenes and the presence of a chlorine substituent at the huprine moiety led to increased lipophilicity, and, hence, increased brain permeability.

As expected, replacement of the 3-chlorosubstituted huprine Y unit in these heterodimers by a 3-unsubstituted huprine moiety resulted, in general, in a reduced inhibitory activity against human recombinant AChE. However, the reduction of this activity was very modest, so that the novel heterodimers **16f-g** and **17f-g** remained very active anticholinesterase compounds, as was the case for **3g**, **4g** (Table 2) and all of the screened heterodimers. These compounds are about 2 orders of magnitude more potent anticholinesterase than trypanocidal or antiplasmodial agents. The use of these compounds at concentrations required to produce trypanocidal and antiplasmodial activity could therefore result in a range of side effects arising from overactivation of the peripheral and central cholinergic neurotransmission system.

Thus, extension of series **I** with the novel heterodimers resulted in the identification of two of the most potent trypanocidal compounds of the series, **16f** and **16g**, the latter also displaying significant antiplasmodial activity. Reduction of their cytotoxicity and AChE inhibitory activities will need to be addressed in future development of this structural class.

2.4. Determination of the trypanocidal and antiplasmodial mode of action of 4-aminoquinoline-based heterodimeric compounds of series I-III

Identification of the biological target involved in the trypanocidal and antiplasmodial activity of the heterodimers of series **I-III** might enable further optimization of the initial hits through target-based screening, or by structure-based rational design of novel analogues, when 3D structures of the biological target are available.

2.4.1. Trypanothione reductase inhibitory activity

Trypanothione reductase (TryR) is an NADPH-dependent disulfide oxidoreductase enzyme that is involved in the protection of trypanosomatid parasites from oxidative damage. Because it is unique and essential to these parasites, TryR constitutes a valuable target for trypanocidal drug discovery programs.[46,47]

A number of quinoline or aminoacridine derivatives have been reported to be inhibitors of TryR.[20,46,48,49] In these compounds, the presence of a protonatable nitrogen atom seems to be crucial for the TryR inhibitory activity because it mimics the positively charged substrate, trypanothione disulfide. Interestingly, it has been reported that dimerization of several classes of compounds with known TryR inhibitory activity leads to increased

potency,[50-52] which might be related to the presence of two interacting binding sites in the large active site of TryR.[49]

These precedents prompted us to determine whether TryR was a biological target for aminoquinoline-based heterodimers of series **I-III**. The TryR inhibitory activity of selected compounds of these series, namely heterodimers **3d**, **5b** and **8b**, as well as the parent huprine Y, **1**, was determined through a described methodology based on the colorimetric reduction of 5,5'-dithiobis(2-nitrobenzoic) acid (DTNB) by dithiol trypanothione ($T[SH]_2$), the product of the reaction catalyzed by TryR.[53,54]

The four tested compounds exhibited submicromolar to low micromolar IC_{50} values for TryR inhibition (Table 3). The most potent compound turned out to be **3d** (series **I**) which was 6-8-fold more potent than the parent huprine and the heterodimers of the other series. Thus, as previously reported for other structural classes, dimerization of a 4-aminoquinoline motif in **3d** relative to huprine Y resulted in increased TryR inhibitory activity.

Of note, no correlation was found between the trypanocidal and TryR inhibitory activities of these compounds. Indeed, all the tested compounds displayed more potent trypanocidal than TryR inhibitory activity (6-62-fold). These results might suggest that either TryR is not the sole target of these compounds or that they might be selectively concentrated into the cell or metabolically activated, as suggested for other trypanocidal compounds.[55]

2.4.2. Inhibition of β-haematin formation

The 4-amino-7-chloroquinoline unit present in chloroquine and other antimalarial compounds is the pharmacophoric moiety responsible for the inhibition of dimerization and crystallization of free haem, generated during the digestion of hemoglobin in the host erythrocytes, into nontoxic insoluble haemozoin, which results in increased levels of toxic haem, and in parasite death.[28,56]

Huprine Y, **1**, and bis-huprine **2** contain the 4-amino-7-chloroquinoline moiety, but they are inactive against *P. falciparum*.[30,37] Surprisingly, many heterodimers of series **I-III**, which in most cases also feature one or two 4-amino-7-chloroquinoline motifs, have been found to be quite potent antiplasmodial compounds (Tables 1 and 2). In the light of these results, we assessed whether the antiplasmodial activity of these heterodimers relied on the same mechanism of action of chloroquine, by determining the inhibition of the formation of β-haematin, which is identical to haemozoin. Thus, the inhibitiory activity against β-haematin formation of heterodimers **3d**, **5b** and **8b** was evaluated following a described procedure,[57,58] and expressed as the 50% inhibitory concentration for β-haematin inhibition in equivalents of the tested compound relative to haemin ($BHIA_{50}$). The parent huprine Y and tetracycline were also evaluated as negative controls and chloroquine was used as a positive control. All the tested heterodimers inhibited β-haematin formation comparably to that seen with chloroquine, whereas huprine Y and tetracycline showed no inhibition (Table 3). Particularly, heterodimer **3d** (series **I**) was equipotent to chloroquine as an inhibitor of β-haematin formation (Table 3) and heterodimers **5b** and **8b** turned out to be slightly less potent (3- and 4-fold). Because the inhibitory activities of these heterodimers on β-haematin formation correlate well with their antiplasmodial activities, it might be that inhibition of β-haematin formation is an important mechanim by which they inhibit the growth of malaria parasites.

Table 3
Inhibitory activity of selected 4-aminoquinoline-based heterodimeric compounds and reference compounds **1**, tetracycline hydrochloride and chloroquine diphosphate against *T. brucei* trypanothione reductase and β-haematin formation[a]

Compd	*Tb* TryR[b]	$BHIA_{50}$[c]
	IC_{50} μM	
3d	0.87 ± 0.10	0.19 ± 0.02
5b	4.88 ± 0.44	0.42 ± 0.06
8b	7.39 ± 0.43	0.54 ± 0.08
1	5.00 ± 0.31	>4
tetracycline		>4
chloroquine		0.14 ± 0.05

[a] Values are expressed as the mean ± SD of three independent experiments.

[b] *In vitro* activity against recombinant *T. brucei* TryR expressed at the concentration that inhibited enzyme activity by 50% (IC_{50}).

[b] β-Haematin inhibitory activity in equivalents of drug relative to haemin causing 50% inhibition.

3. Conclusion

By phenotypic screening of a small library of 27 brain permeable 4-aminoquinoline-based heterodimeric compounds against bloodstream forms of *T. brucei* and the multidrug-resistant strain K1 of *P. falciparum*, we have identified a number of dual submicromolar trypanocidal-antiplasmodial compounds. Indeed, all of the tested compounds had submicromolar IC_{50} values against *T. brucei*, with the vast majority also displaying submicromolar IC_{90} values. They were all more potent trypanocidal agents than the parent huprine Y. One third of the compounds also exhibited submicromolar IC_{50} values against *P. falciparum*, and increased potency compared to the reference antimalarial compound chloroquine. In further studies with the most promising structural class (series **I**), to explore structure-activity relationships and to decrease the AChE inhibitory activity which was present in all the screened compounds, 6 novel heterodimers were synthesized and biologically evaluated. All of the novel compounds retained high trypanocidal potency and good BBB permeability. Some also displayed moderately potent antiplasmodial activity and AChE inhibitory activity, but had unfavourable selectivity indices.

Mechanistic studies have shown that the high trypanocidal activity of these heterodimers can only partly be ascribed to inhibition of the enzyme TryR, whereas their antiplasmodial activity seems to arise from an inhibition of the haem detoxification process, similar to the antimalarial drug chloroquine.

Heterodimer **3e** (series **I**) emerged as an interesting hit featuring balanced dual trypanocidal (IC_{50} = 0.21 μM) and antiplasmodial (IC_{50} = 0.35 μM) activity and selectivity indices of 34 and 20 over rat L6 cell cytotoxicity. Further optimization should focus on improving the selectivity indices and reducing the AChE inhibitory activities of these heterodimers.

4. Experimental

4.1. Chemistry

Melting points were determined in open capillary tubes with a MFB 595010M Gallenkamp melting point apparatus. 400 MHz ^{1}H / 100.6 MHz ^{13}C NMR spectra were recorded on a Varian Mercury 400 spectrometer at the Centres Científics i Tecnològics of the University of Barcelona (CCiTUB). The chemical shifts are reported in ppm (δ scale) and coupling constants are reported in Hertz (Hz). The *syn* (*anti*) notation of the protons at position 13 of the huprine moiety of the heterodimers means that the corresponding proton at position 13 is on the same (different) side of the quinoline moiety with respect to the cyclohexene ring. IR spectra were run on a Perkin-Elmer Spectrum RX I spectrophotometer, using KBr pellets. Absorption values are expressed as wave-numbers (cm^{-1}); only significant absorption bands are given. Column chromatography was performed on silica gel 60 AC.C (40–60 μM, SDS, ref 2000027). Thin-layer chromatography was performed with aluminum-backed sheets with silica gel 60 F_{254} (Merck, ref 1.05554), and spots were visualized with UV light and 1% aqueous solution of $KMnO_4$. Elemental analyses and high resolution mass spectra were carried out at the Mycroanalysis Service of the IIQAB (CSIC, Barcelona, Spain) with a Carlo Erba 1106 analyzer, and at the CCiTUB with a LC/MSD TOF Agilent Technologies spectrometer, respectively. The analytical samples of all of the heterodimers that were subjected to pharmacological evaluation were dried at 65 ºC / 2 Torr at least for 2 days (standard conditions) and possess a purity ≥95% as evidenced by their elemental analyses.

4.1.1. 9-(12-Bromododecyl)amino-1,2,3,4-tetrahydroacridine (13g)

A suspension of tacrine, **11** (3.00 g, 15.2 mmol, 1 eq), and finely powdered KOH (85% purity reagent, 1.60 g, 24.3 mmol, 1.6 eq) in anhydrous DMSO (37 mL) was stirred, heating every 10 min approximately with a heat gun for 1 h and at rt for an additional hour. This mixture was added dropwise during 1.5 h to a solution of 1,12-dibromododecane (5.98 g, 18.2 mmol, 1.2 eq) in anhydrous DMSO (20 mL), containing 4 Å molecular sieves. The reaction mixture was stirred at rt overnight, diluted with 10N NaOH (150 mL) and H_2O (200 mL) and extracted with EtOAc (3×200 mL). The combined organic extracts were washed with H_2O (2×200 mL), dried over anhydrous Na_2SO_4, and evaporated at reduced pressure to give a yellow oil (8.02 g), which was purified by column chromatography (40–60 μm silica gel, CH_2Cl_2/50% aq. NH_4OH 100:0.2), to afford bromoalkyl derivative **13g** (2.65 g, 40% yield); R_f 0.27 (CH_2Cl_2/MeOH/50% aq. NH_4OH 9:1:0.05).

A solution of **13g** (106 mg, 0.24 mmol) in MeOH (10 mL) was filtered through a 0.2 μm NYL filter and treated with 45% aq. HBr (0.50 mL, 4.14 mmol, 17 eq). The resulting solution was evaporated at reduced pressure and the solid was taken in MeOH (0.1 mL) and precipitated upon addition of AcOEt (1.2 mL). The precipitated solid was separated and washed with pentane (3×2 mL) to give, after drying under standard conditions, **13g**·HBr (49 mg) as a yellowish solid: mp 131–133 ºC; IR (KBr) ν 3500–2500 (max at 3255, 3044, 3004, 2915, 2846 and 2793, N^+–H, N–H, C–H st), 1629, 1605, 1588, 1573 and 1517 (Ar–C–C, Ar–C–N st) cm^{-1}; ^{1}H NMR (400 MHz, CD_3OD) δ 1.26–1.46 (complex signal, 16H, 3'-H_2, 4'-H_2, 5'-H_2, 6'-H_2, 7'-H_2, 8'-H_2, 9'-H_2, 10'-H_2), 1.78–1.88 (complex signal, 4H, 2'-H_2, 11'-H_2), 1.93–2.02 (complex signal, 4H, 2-H_2, 3-H_2), 2.71 (t, J = 5.6 Hz, 2H, 1-H_2), 3.02 (t, J = 5.6 Hz, 2H, 4-H_2), 3.43 (t, J = 6.6 Hz, 2H, 12'-H_2), 3.96 (t, J = 7.6 Hz, 2H, 1'-H_2), 4.85 (s, NH, NH^+), 7.59 (ddd, J = 8.4 Hz, J' = 6.8 Hz, J'' = 1.2 Hz, 1H, 7-H), 7.75 (dd, J = 8.4 Hz, J' = 1.2 Hz, 1H, 5-H), 7.85 (ddd, J = 8.4 Hz, J' = 6.8 Hz, J'' = 1.2 Hz, 1H, 6-H), 8.40 (br d, J = 8.4 Hz, 1H, 8-H); ^{13}C NMR (100.6 MHz, CD_3OD) δ 21.8 (CH_2, C3), 23.0 (CH_2, C2), 24.9 (CH_2, C1), 29.3 (CH_2, C4), 27.7 (CH_2), 29.1 (CH_2), 29.8 (CH_2), 30.2 (CH_2), 30.51 (3 CH_2) and 30.54 (CH_2) (C3', C4', C5', C6', C7', C8', C9', C10'), 31.5 (CH_2) and 34.0 (CH_2) (C2', C11'), 34.5 (CH_2, C12'), 49.2 (CH_2, C1'), 112.8 (C, C9a), 117.0 (C, C8a), 120.1 (CH, C5), 126.3 (CH, C7), 126.5 (CH, C8), 134.1 (CH, C6), 139.7 (C, C10a), 151.6 (C, C4a), 158.0 (C, C9); HRMS (ESI), calcd for [$C_{25}H_{37}BrN_2$ + H^+] 445.2213, found 445.2212.

4.1.2. 9-(12-Bromododecyl)amino-6-chloro-1,2,3,4-tetrahydroacridine (14g)

It was prepared as described for **13g**. Starting from 6-chlorotacrine, **12** (2.00 g, 8.60 mmol, 1 eq), and a solution of 1,12-dibromododecane (3.38 g, 10.3 mmol, 1.2 eq) in anhydrous DMSO (20 mL), a brown oil (4.70 g) was obtained and subjected to column chromatography purification (40–60 μm silica gel, CH_2Cl_2/MeOH/50% aq. NH_4OH mixtures, gradient elution). On elution with CH_2Cl_2/MeOH/50% aq. NH_4OH 100:0:0.2, bromoalkyl derivative **14g** (546 mg) was isolated. On elution with CH_2Cl_2/MeOH/50% aq. NH_4OH 100:0:0.2 to 90:10:0.2, a mixture of **14g** and starting **12** (2.60 g) was obtained. Column chromatography purification of this mixture (40–60 μm silica gel, CH_2Cl_2/50% aq. NH_4OH 100:0.2) afforded more **14g** (691 mg, 30% total yield); R_f 0.46 (CH_2Cl_2/MeOH/50% aq. NH_4OH 9:1:0.05).

A solution of **14g** (100 mg, 0.21 mmol) in MeOH (18 mL) was filtered through a 0.2 μm NYL filter and treated with 45% aq. HBr (0.5 mL, 4.14 mmol, 20 eq). The resulting solution was evaporated at reduced pressure and the solid was washed with pentane (3×2 mL) to give, after drying under standard conditions, **14g**·HBr (87 mg) as a beige solid: mp 122–124 ºC; IR (KBr) ν 3500–2500 (max at 3241, 3134, 3044, 2921, 2850 and 2791, N^+–H, N–H, C–H st), 1630, 1620, 1588, 1572, 1546 and 1521 (Ar–C–C, Ar–C–N st) cm^{-1}; ^{1}H NMR (400 MHz, CD3OD) δ 1.26–1.46 (complex signal, 16H, 3'-H_2, 4'-H_2, 5'-H_2, 6'-H_2, 7'-H_2, 8'-H_2, 9'-H_2, 10'-H_2), 1.78–1.88 (complex signal, 4H, 2'-H_2, 11'-H_2), 1.92–2.02 (complex signal, 4H, 2-H_2, 3-H_2), 2.68 (t, J = 6.0 Hz, 2H, 1-H_2), 3.00 (t, J = 5.6 Hz, 2H, 4-H_2), 3.43 (t, J = 6.6 Hz, 2H, 12'-H_2), 3.94 (t, J = 7.6 Hz, 2H, 1'-H_2), 4.85 (s, NH, NH^+), 7.56 (dd, J = 9.2 Hz, J' = 2.0 Hz, 1H, 7-H), 7.77 (d, J = 2.0 Hz, 1H, 5-H), 8.39 (d, J = 9.2 Hz, 1H, 8-H); ^{13}C NMR (100.6 MHz, CD_3OD) δ 21.8 (CH_2, C3), 22.9 (CH_2, C2), 24.7 (CH_2, C1), 29.3 (CH_2, C4), 27.7 (CH_2), 29.1 (CH_2), 29.8 (CH_2), 30.2 (CH_2) and 30.5 (4 CH_2) (C3', C4', C5', C6', C7', C8', C9', C10'), 31.3 (CH_2) and 34.0 (CH_2) (C2', C11'), 34.5 (CH_2, C12'), 49.2 (CH_2, C1'), 113.4 (C) and 115.4 (C) (C8a, C9a), 119.1 (CH, C5), 126.8 (CH, C7), 128.8 (CH, C8), 140.1 (C, C6), 140.5 (C, C10a), 152.1 (C, C4a), 157.9 (C, C9); HRMS (ESI), calcd for [$C_{25}H_{36}BrClN_2$ + H^+] 479.1823, found 479.1830.

4.1.3. 3-Chloro-6,7,10,11-tetrahydro-9-methyl-12-{{12-[(1,2,3,4-tetrahydroacridin-9-yl)amino]dodecyl}amino}-7,11-methanocycloocta[b]quinoline (3g)

A mixture of finely powdered KOH (85% purity reagent, 209 mg, 3.16 mmol, 3 eq), huprine **1** (300 mg, 1.05 mmol, 1 eq), 4 Å molecular sieves (approximately 690 mg) in dry DMSO (4 mL) was thoroughly stirred for 1 h heating with a heatgun every 10 min and for one additional hour at rt. The resulting mixture was added dropwise during 1 h to a mixture of bromoalkyltacrine **13g** (562 mg, 1.26 mmol, 1.2 eq) in dry DMSO (6 mL). The reaction mixture was vigorously stirred at rt for 4 days, diluted with 10 N NaOH (150 mL), H_2O (200 mL), and extracted with AcOEt

(3×200 mL). The combined organic extracts were washed with 1N NaOH (3×200 mL), dried with anhydrous Na_2SO_4 and evaporated at reduced pressure to give a brown oily residue (820 mg), which was subjected to column chromatography (40–60 mesh silica gel, CH_2Cl_2/50% aqueous NH_4OH 100:0.2), to afford heterodimer **3g** (507 mg, 71% yield) as a yellow oil; R_f 0.48 (CH_2Cl_2/MeOH/50% aq. NH_4OH 9:1:0.05).

A solution of **3g** (507 mg, 0.78 mmol) in CH_2Cl_2 (26 mL) was filtered through a 0.2 µm NYL filter, and treated with an excess of a methanolic solution of HCl (1.45 N, 4.9 mL, 7.10 mmol) and the resulting solution was concentrated in vacuo to dryness. The solid was taken in MeOH (1.5 mL) and precipitated upon addition of AcOEt (12 mL). The precipitated solid was separated, washed with pentane (3×2), and dried under standard conditions, to give **3g**·2HCl (362 mg) as a yellow solid: mp: 165-168 ºC; IR (KBr) ν 3500–2500 (max at 3380, 3234, 3108, 3048, 3007, 2923, 2850, and 2788, N^+–H, N–H, C–H st), 1632, 1583 and 1521 (Ar–C–C, Ar–C–N st) cm^{-1}; ^{1}H NMR (400 MHz, CD_3OD) δ 1.24–1.46 (complex signal, 16H, 3'-H_2, 4'-H_2, 5'-H_2, 6'-H_2, 7'-H_2, 8'-H_2, 9'-H_2, 10'-H_2), 1.57 (s, 3H, 9-CH_3), 1.78–2.00 (complex signal, 10H, 10-H_{endo}, 13-H_{syn}, 2'-H_2, 11'-H_2, 2"-H_2, 3"-H_2), 2.08 (dm, J = 12.4 Hz, 1H, 13-H_{anti}), 2.55 (br dd, J = 17.2 Hz, J' = 3.6 Hz, 1H, 10-H_{exo}), 2.70 (m, 2H, 1"-H_2), 2.76 (m, 1H, 7-H), 2.88 (d, J = 18.0 Hz, 1H, 6-H_{endo}), 3.02 (m, 2H, 4"-H_2), 3.20 (dd, J = 18.0 Hz, J' = 5.2 Hz, 1H, 6-H_{exo}), 3.46 (m, 1H, 11-H), 3.95 (t, J = 7.6 Hz, 2H) and 3.98 (t, J = 7.2 Hz, 2H) (1'-H_2, 12'-H_2), 4.85 (s, NH, NH^+), 5.58 (br d, J = 5.2 Hz, 1H, 8-H), 7.54 (br d, J = 9.2 Hz, 1H, 2-H), 7.57 (dd, J = 8.0 Hz, J' = 7.2 Hz, 1 H, 7"-H), 7.76–7.86 (complex signal, 3H, 4-H, 5"-H, 6"-H), 8.38 (d, J = 8.0 Hz, 1H) and 8.39 (d, J = 9.2 Hz, 1H) (1-H, 8''-H); ^{13}C NMR (100.6 MHz, CD_3OD) δ 21.8 (CH_2, C3"), 23.0 (CH_2, C2"), 23.5 (CH_3, 9-CH_3), 24.9 (CH_2, C1"), 27.3 (CH, C11), 27.7 (CH_2) and 27.77 (CH_2) (C3', C10'), 27.81 (CH, C7), 29.3 (2 CH_2, C13, C4"), 30.2 (CH_2), 30.3 (CH_2) and 30.6 (4 CH_2) (C4', C5', C6', C7', C8', C9'), 31.2 (CH_2) and 31.5 (CH_2) (C2', C11'), 36.0 (CH_2) and 36.1 (CH_2) (C6, C10), 49.1 (CH_2) and 49.6 (CH_2) (C1', C12'), 112.8 (C), 115.6 (C), 117.0 (C) and 117.6 (C) (C11a, C12a, C8a", C9a"), 119.1 (CH) and 120.1 (CH) (C4, C5"), 125.1 (CH, C8), 126.3 (CH, C7"), 126.5 (CH, C8"), 126.6 (CH, C2), 129.4 (CH, C1), 134.1 (CH, C6"), 134.5 (C, C9), 139.7 (C), 140.2 (C) and 141.0 (C) (C3, C4a, C10a"), 151.2 (C) and 151.6 (C) (C5a, C4a"), 156.8 (C), 158.0 (C) (C12, C9"); HRMS (ESI), calcd for [$C_{42}H_{53}{}^{35}ClN_4$ + H^+] 649.4032, found 649.4019; Anal. calcd. for $C_{42}H_{53}ClN_4$·2HCl·1.5H_2O: C, 67.32; H, 7.80; N, 7.48; Cl, 14.19. Found: C, 67.33; H, 7.88; N, 7.29; Cl, 14.47.

4.1.4. 3-Chloro-6,7,10,11-tetrahydro-9-methyl-12-{{12-[(6-chloro-1,2,3,4-tetrahydroacridin-9-yl)amino]dodecyl}amino}-7,11-methanocycloocta[b]quinoline (4g)

It was prepared as described for **3g**. Starting from huprine **1** (290 mg, 1.02 mmol, 1 eq), and a solution of of bromoalkyltacrine **14g** (587 mg, 1.22 mmol, 1.2 eq) in anhydrous DMSO (6 mL), a brown oily residue (1.20 g) was obtained and subjected to column chromatography purification (40–60 µm silica gel, CH_2Cl_2/50% aq. NH_4OH 100:0.2), to afford the heterodimer **4g** (311 mg, 45% yield) as a yellow oil; R_f 0.67 (CH_2Cl_2/MeOH/50% aq. NH_4OH 9:1:0.05).

A solution of **4g** (122 mg, 0.18 mmol) in CH_2Cl_2 (6 mL) was filtered through a 0.2 µm NYL filter, and treated with an excess of a methanolic solution of HCl (1.45 N, 1.1 mL, 1.59 mmol) and the resulting solution was concentrated in vacuo to dryness. The solid was taken in MeOH (0.5 mL) and precipitated upon addition of AcOEt (3 mL). The precipitated solid was separated, washed with pentane (3×2), and dried under standard conditions, to give **4g**·2HCl (49 mg) as a yellow solid: mp 178–181 ºC; IR (KBr) ν 3500–2500 (max at 3224, 3034, 2924, 2854 and 2786, N^+–H, N–H, C–H st), 1632, 1583, 1572, 1567, and 1519 (Ar–C–C, Ar–C–N st) cm^{-1}; ^{1}H NMR (400 MHz, CD_3OD) δ 1.24–1.46 (complex signal, 16H, 3'-H_2, 4'-H_2, 5'-H_2, 6'-H_2, 7'-H_2, 8'-H_2, 9'-H_2, 10'-H_2), 1.58 (s, 3H, 9-CH_3), 1.78–2.00 (complex signal, 10H, 10-H_{endo}, 13-H_{syn}, 2'-H_2, 11'-H_2, 2"-H_2, 3"-H_2), 2.08 (dm, J = 12.4 Hz, 1H, 13-H_{anti}), 2.55 (br dd, J = 17.2 Hz, J' = 4.4 Hz, 1H, 10-H_{exo}), 2.67 (m, 2H, 1"-H_2), 2.77 (m, 1H, 7-H), 2.87 (br d, J = 18.0 Hz, 1H, 6-H_{endo}), 3.00 (m, 2H, 4"-H_2), 3.20 (dd, J = 18.0 Hz, J' = 5.6 Hz, 1H, 6-H_{exo}), 3.45 (m, 1H, 11-H), 3.94 (t, J = 7.2 Hz, 2H) and 3.98 (t, J = 6.4 Hz, 2H) (1'-H_2,12'-H_2), 4.84 (s, NH, NH^+), 5.58 (br d, J = 4.4 Hz, 1H, 8-H), 7.52–7.58 (complex signal, 2H, 2-H, 7"-H), 7.78 (br s, 1H) and 7.79 (br s, 1H) (4-H, 5"-H), 8.38 (d, J = 9.2 Hz, 1H) and 8.39 (d, J = 9.2 Hz, 1H) (1-H, 8"-H); ^{13}C NMR (100.6 MHz, CD_3OD) δ 21.8 (CH_2, C3"), 22.8 (CH_2, C2"), 23.5 (CH_3, 9-CH_3), 24.7 (CH_2, C1"), 27.3 (CH, C11), 27.7 (CH_2) and 27.79 (CH_2), (C3', C10'), 27.81 (CH, C7), 29.3 (2 CH_2, C13, C4"), 30.2 (2 CH_2), 30.57 (2 CH_2) and 30.60 (2 CH_2) (C4', C5', C6', C7', C8', C9'), 31.2 (CH_2) and 31.3 (CH_2) (C2', C11'), 36.0 (CH_2) and 36.1 (CH_2, C6, C10), 49.2 (CH_2) and 49.6 (CH_2) (C1', C12'), 113.3 (C), 115.4 (C), 115.6 (C) and 117.6 (C) (C11a, C12a, C8a" and C9a"), 119.2 (2 CH, C4, C5"), 125.1 (CH, C8), 126.6 (CH) and 126.7 (CH) (C2, C7"), 128.7 (CH) and 129.4 (CH) (C1, C8"), 134.5 (C, C9), 140.1 (C) and 140.2 (C) (C3, C6") 140.5 (C) and 141.0 (C) (C4a, C10a"), 151.2 (C) and 152.1 (C) (C5a, C4a"), 156.9 (C), 157.8 (C) (C12, C9"); HRMS (ESI), calcd for [$C_{42}H_{52}{}^{35}Cl_2N_4$ + H^+] 683.3641, found 683.3622; Anal. calcd. for $C_{42}H_{52}Cl_2N_4$·2HCl·1.5H_2O: C, 64.37; H, 7.33; N, 7.15; Cl, 18.09. Found: C, 64.14; H, 7.20; N, 6.80; Cl, 17.71.

4.1.5. 6,7,10,11-Tetrahydro-9-methyl-12-{{10-[(1,2,3,4-tetrahydroacridin-9-yl)amino]decyl}amino}-7,11-methanocycloocta[b]quinoline (16f)

It was prepared as described for **3g**. Starting from huprine **15** (250 mg, 1.00 mmol, 1 eq), and a solution of of bromoalkyltacrine **13f** (551 mg, 1.32 mmol, 1.3 eq) in anhydrous DMSO (6 mL), a brown oily residue (1.04 g) was obtained and subjected to column chromatography purification (40–60 µm silica gel, CH_2Cl_2/MeOH/50% aq. NH_4OH mixtures, gradient elution). On elution with CH_2Cl_2/MeOH/50% aq. NH_4OH 100:0:0.2 to 95:5:0.2, the heterodimer **16f** (518 mg, 88% yield) was isolated as a yellow oil; R_f 0.44 (CH_2Cl_2/MeOH/50% aq. NH_4OH 9:1:0.05).

A solution of **16f** (518 mg, 0.88 mmol) in CH_2Cl_2 (25 mL) was filtered through a 0.2 µm NYL filter, and treated with an excess of a methanolic solution of HCl (1.70 N, 4.65 mL, 7.90 mmol) and the resulting solution was concentrated in vacuo to dryness. The solid was taken in MeOH (1.5 mL) and precipitated upon addition of AcOEt (11 mL). The precipitated solid was separated, washed with pentane (3×2), and dried under standard conditions, to give **16f**·2HCl (481 mg) as a yellow solid: mp 168–170 ºC; IR (KBr) ν 3500–2500 (max at 3380, 3237, 3120, 3055, 3013, 2925, 2852, and 2805, N^+–H, N–H, C–H st), 1633, 1585 and 1522 (Ar–C–C, Ar–C–N st) cm^{-1}; ^{1}H NMR (400 MHz, CD_3OD) δ 1.26–1.46 (complex signal, 12H, 3'-H_2, 4'-H_2, 5'-H_2, 6'-H_2, 7'-H_2, 8'-H_2), 1.57 (s, 3H, 9-CH_3), 1.78–2.00 (complex signal, 10H, 10-H_{endo}, 13-H_{syn}, 2'-H_2, 9'-H_2, 2"-H_2, 3"-H_2), 2.08 (dm, J = 12.4 Hz, 1H, 13-H_{anti}), 2.55 (br dd, J = 17.6 Hz, J' = 4.0 Hz, 1H, 10-H_{exo}), 2.70 (m, 2H, 1"-H_2), 2.76 (m, 1H, 7-H), 2.90 (d, J = 18.0 Hz, 1H, 6-H_{endo}), 3.02 (m, 2H, 4"-H_2), 3.21 (dd, J = 18.0 Hz, J' = 5.6 Hz, 1H, 6-H_{exo}), 3.47 (m, 1H, 11-H), 3.95 (t, J = 7.6 Hz, 2H) and 3.99 (t, J = 7.2 Hz, 2H) (1'-H_2, 10'-H_2), 4.85 (s, NH, NH^+), 5.58 (br d, J = 4.4 Hz, 1H, 8-H), 7.54–7.62 (complex

signal, 2H, 2-H, 7”-H), 7.76–7.86 (complex signal, 4H, 3-H, 4-H, 5”-H, 6”-H), 8.39 (d, *J* = 8.4 Hz, 1H) and 8.40 (d, *J* = 8.8 Hz, 1H) (1-H, 8”-H); ^{13}C NMR (100.6 MHz, CD_3OD) δ 21.9 (CH_2, C3”), 23.0 (CH_2, C2”), 23.5 (CH_3, 9-CH_3), 24.9 (CH_2, C1”), 27.3 (CH, C11), 27.7 (CH_2) and 27.8 (CH_2) (C3’, C8’), 27.9 (CH, C7), 29.3 (CH_2) and 29.4 (CH_2) (C13, C4”), 30.26 (CH_2), 30.29 (CH_2), 30.48 (CH_2) and 30.53 (CH_2) (C4’, C5’, C6’, C7’), 31.4 (CH_2) and 31.5 (CH_2) (C2’, C9’), 36.0 (CH_2) and 36.3 (CH_2) (C6, C10), 49.1 (CH_2) and 49.6 (CH_2) (C1’, C10’), 112.8 (C), 117.0 (C), 117.15 (C) and 117.21 (C) (C11a, C12a, C8a”, C9a”), 120.1 (2 CH, C4, C5”), 125.2 (CH, C8), 126.1 (CH, C1), 126.3 (CH, C7”), 126.5 (CH, C8”), 127.3 (CH, C2), 134.1 (CH, C6”), 134.2 (CH, C3), 134.5 (C, C9), 139.8 (C) and 140.2 (C) (C4a, C10a”), 150.7 (C) and 151.7 (C) (C5a, C4a”), 157.0 (C) and 158.0 (C) (C12, C9”); HRMS (ESI), calcd for [$C_{40}H_{50}N_4$ + H^+] 587.4108, found 587.4099; Anal. calcd. for $C_{40}H_{50}N_4 \cdot 2HCl \cdot 2H_2O$: C, 69.05; H, 8.11; N, 8.05; Cl, 10.19. Found: C, 68.68; H, 8.08; N, 7.76; Cl, 10.18.

4.1.6. 6,7,10,11-Tetrahydro-9-methyl-12-{{12-[(1,2,3,4-tetrahydroacridin-9-yl)amino]dodecyl}amino}-7,11-methanocycloocta[b]quinoline (16g)

It was prepared as described for **3g**. Starting from huprine **15** (300 mg, 1.20 mmol, 1 eq), and a solution of of bromoalkyltacrine **13g** (642 mg, 1.44 mmol, 1.2 eq) in anhydrous DMSO (6.5 mL), a brown oily residue (805 mg) was obtained and subjected to column chromatography purification (40–60 µm silica gel, CH_2Cl_2/MeOH/50% aq. NH_4OH mixtures, gradient elution. On elution with CH_2Cl_2/MeOH/50% aq. NH_4OH 99:1:0.2, the heterodimer **16g** (609 mg, 83% yield) was isolated as a yellow oil; R_f 0.53 (CH_2Cl_2/MeOH/50% aq. NH_4OH 9:1:0.05).

A solution of **16g** (609 mg, 0.99 mmol) in CH_2Cl_2 (33 mL) was filtered through a 0.2 µm NYL filter, and treated with an excess of a methanolic solution of HCl (1.45 N, 6.2 mL, 8.99 mmol) and the resulting solution was concentrated in vacuo to dryness. The solid was taken in MeOH (2 mL) and precipitated upon addition of AcOEt (14 mL). The precipitated solid was separated, washed with pentane (3×2), and dried under standard conditions, to give **16g**·2HCl (612 mg) as a yellow solid: mp 159–162 ºC; IR (KBr) *ν* 3500–2500 (max at 3386, 3236, 3114, 3054, 3007, 2923, 2851, and 2800, N^+–H, N–H, C–H st), 1633, 1585, 1568 and 1520 (Ar–C–C, Ar–C–N st) cm^{-1}; ^{1}H NMR (400 MHz, CD_3OD) δ 1.26–1.46 (complex signal, 16H, 3’-H_2, 4’-H_2, 5’-H_2, 6’-H_2, 7’-H_2, 8’-H_2, 9’-H_2, 10’-H_2), 1.58 (s, 3H, 9-CH_3), 1.78–2.02 (complex signal, 10H, 10-H_{endo}, 13-H_{syn}, 2’-H_2, 11’-H_2, 2”-H_2, 3”-H_2), 2.09 (dm, *J* = 12.8 Hz, 1H, 13-H_{anti}), 2.56 (br dd, *J* = 17.6 Hz, *J’* = 4.4 Hz, 1H, 10-H_{exo}), 2.70 (m, 2H, 1”-H_2), 2.77 (m, 1H, 7-H), 2.90 (br d, *J* = 18.0 Hz, 1H, 6-H_{endo}), 3.02 (m, 2H, 4”-H_2), 3.21 (dd, *J* = 18.0 Hz, *J’* = 5.6 Hz, 1H, 6-H_{exo}), 3.48 (m, 1H, 11-H), 3.95 (t, *J* = 7.6 Hz, 2H) and 4.00 (td, *J* = 6.8 Hz, *J’* = 3.2 Hz, 2H) (1’-H_2, 12’-H_2), 4.85 (s, NH, NH^+), 5.58 (br d, *J* = 4.4 Hz, 1H, 8-H), 7.54–7.61 (complex signal, 2H, 2-H, 7”-H), 7.76–7.87 (complex signal, 4H, 3-H, 4-H, 5”-H, 6”-H), 8.39 (d, *J* = 8.4 Hz, 1H) and 8.40 (d, *J* = 8.8 Hz, 1H) (1-H, 8”-H); ^{13}C NMR (100.6 MHz, CD_3OD) δ 21.9 (CH_2, C3”), 23.0 (CH_2, C2”), 23.5 (CH_3, 9-CH_3), 24.9 (CH_2, C1”), 27.3 (CH, C11), 27.7 (CH_2) and 27.8 (CH_2) (C3’, C10’), 27.9 (CH, C7), 29.3 (CH_2) and 29.4 (CH_2) (C13, C4”), 30.3 (2 CH_2), 30.59 (2 CH_2) and 30.62 (2 CH_2) (C4’, C5’, C6’, C7’, C8’, C9’), 31.4 (CH_2) and 31.5 (CH_2) (C2’, C11’), 36.0 (CH_2) and 36.3 (CH_2) (C6, C10), 49.1 (CH_2) and 49.6 (CH_2) (C1’, C12’), 112.8 (C), 117.0 (C), 117.15 (C) and 117.21 (C) (C11a, C12a, C8a” and C9a”), 120.1 (2 CH, C4, C5”), 125.2 (CH, C8), 126.1 (CH; C1), 126.3 (CH, C7”), 126.5 (CH, C8”), 127.3 (CH, C2), 134.1 (CH, C6”), 134.2 (CH, C3), 134.5 (C, C9), 139.8 (C) and 140.3 (C) (C4a, C10a”), 150.7 (C) and 151.6 (C) (C5a, C4a”), 157.0 (C) and 158.0 (C) (C12, C9”); HRMS (ESI), calcd for [$C_{42}H_{54}N_4$ + H^+] 615.4421, found 615.4423; Anal. calcd. for $C_{42}H_{54}N_4 \cdot 2HCl \cdot 2H_2O$: C, 69.69; H, 8.35; N, 7.74; Cl, 9.80. Found: C, 69.75; H, 8.40; N, 7.49; Cl, 9.62.

4.1.7. 6,7,10,11-Tetrahydro-9-methyl-12-{{10-[(6-chloro-1,2,3,4-tetrahydroacridin-9-yl)amino]decyl}amino}-7,11-methanocycloocta[b]quinoline (17f)

It was prepared as described for **3g**. Starting from huprine **15** (274 mg, 1.10 mmol, 1 eq), and a solution of of bromoalkyltacrine **14f** (596 mg, 1.32 mmol, 1.3 eq) in anhydrous DMSO (6 mL), a brown oily residue (810 mg) was obtained and subjected to column chromatography purification (40–60 µm silica gel, EtOAc/hexane/Et_3N mixtures, gradient elution). On elution with EtOAc/hexane/Et_3N 50:50:0.2 to 100:0:0.2, the heterodimer **17f** (477 mg, 70% yield) was isolated as a yellow oil; R_f 0.51 (CH_2Cl_2/MeOH/50% aq. NH_4OH 9:1:0.05).

A solution of **17f** (450 mg, 0.72 mmol) in CH_2Cl_2 (48 mL) was filtered through a 0.2 µm NYL filter, and treated with an excess of a methanolic solution of HCl (0.75 N, 9.0 mL, 6.75 mmol) and the resulting solution was concentrated in vacuo to dryness. The solid was taken in MeOH (1.5 mL) and precipitated upon addition of AcOEt (10 mL). The precipitated solid was separated, washed with pentane (3×2), and dried under standard conditions, to give **17f**·2HCl (351 mg) as a yellow solid: mp 176–178 ºC; IR (KBr) *ν* 3500–2500 (max at 3351, 3232, 3048, 3001, 2924, 2852, and 2792, N^+–H, N–H, C–H st), 1632, 1585, 1571 and 1519 (Ar–C–C, Ar–C–N st) cm^{-1}; ^{1}H NMR (400 MHz, CD_3OD) δ 1.28–1.46 (complex signal, 12H, 3’-H_2, 4’-H_2, 5’-H_2, 6’-H_2, 7’-H_2, 8’-H_2), 1.57 (s, 3H, 9-CH_3), 1.78–2.02 (complex signal, 10H, 10-H_{endo}, 13-H_{syn}, 2’-H_2, 9’-H_2, 2”-H_2, 3”-H_2), 2.08 (dm, *J* = 12.4 Hz, 1H, 13-H_{anti}), 2.56 (dm, *J* = 16.4 Hz, 1H, 10-H_{exo}), 2.68 (m, 2H, 1”-H_2), 2.77 (m, 1H, 7-H), 2.91 (d, *J* = 18.0 Hz, 1H, 6-H_{endo}), 3.01 (m, 2H, 4”-H_2), 3.21 (dd, *J* = 18.0 Hz, *J’* = 5.2 Hz, 1H, 6-H_{exo}), 3.48 (m, 1H, 11-H), 3.93 (t, *J* = 6.8 Hz, 2H) and 3.99 (t, *J* = 7.6 Hz, 2H) (1’-H_2, 10’-H_2), 4.85 (s, NH, NH^+), 5.58 (br d, *J* = 4.4 Hz, 1H, 8-H), 7.52–7.60 (complex signal, 2H, 2-H, 7”-H), 7.76–7.86 (complex signal, 3H, 3-H, 4-H, 5”-H), 8.38 (d, *J* = 8.8 Hz, 1H) and 8.39 (d, *J* = 8.0 Hz, 1H) (1-H, 8”-H); ^{13}C NMR (100.6 MHz, CD_3OD) δ 21.7 (CH_2, C3”), 22.9 (CH_2, C2”), 23.5 (CH_3, 9-CH_3), 24.8 (CH_2, C1”), 27.3 (CH, C11), 27.7 (CH_2) and 27.8 (CH_2) (C3’, C8’), 27.9 (CH, C7), 29.3 (CH_2) and 29.4 (CH_2) (C13, C4”), 30.2 (2 CH_2), 30.46 (CH_2) and 30.51 (CH_2) (C4’, C5’, C6’, C7’), 31.3 (CH_2) and 31.4 (CH_2) (C2’, C9’), 36.0 (CH_2) and 36.3 (CH_2) (C6, C10), 49.2 (CH_2) and 49.6 (CH_2) (C1’, C10’), 113.3 (C), 115.4 (C), 117.1 (C) and 117.2 (C) (C11a, C12a, C8a”, C9a”), 119.1 (CH) and 120.1 (C) (C4, C5”), 125.2 (CH, C8), 126.1 (CH, C1), 126.7 (CH, C7”), 127.3 (CH, C2), 128.8 (CH, C8”), 134.2 (CH, C3), 134.5 (C, C9), 140.0 (C), 140.2 (C) and 140.5 (C) (C4a, C6”, C10a”), 150.7 (C) and 152.1 (C) (C5a, C4a”), 157.0 (C) and 157.8 (C) (C12, C9”); HRMS (ESI), calcd for [$C_{40}H_{49}{}^{35}ClN_4$ + H^+] 621.3719, found 621.3717; Anal. calcd. for $C_{40}H_{49}ClN_4 \cdot 2HCl \cdot 2H_2O$: C, 65.79; H, 7.59; N, 7.67; Cl, 14.56. Found: C, 66.10; H, 7.35; N, 7.56; Cl, 14.59.

4.1.8. 6,7,10,11-Tetrahydro-9-methyl-12-{{12-[(6-chloro-1,2,3,4-tetrahydroacridin-9-yl)amino]dodecyl}amino}-7,11-methanocycloocta[b]quinoline (17g)

It was prepared as described for **3g**. Starting from huprine **15** (278 mg, 1.11 mmol, 1 eq), and a solution of of bromoalkyltacrine **14g** (639 mg, 1.33 mmol, 1.2 eq) in anhydrous DMSO (6 mL), a brown oily residue (1.30 g) was obtained and

subjected to column chromatography purification (40–60 μm silica gel, CH_2Cl_2/50% aq. NH_4OH 100:0.2), to afford the heterodimer **17g** (449 mg, 62% yield) as a yellow oil; R_f 0.58 (CH_2Cl_2/MeOH/50% aq. NH_4OH 9:1:0.05).

A solution of **17g** (143 mg, 0.22 mmol) in CH_2Cl_2 (7 mL) was filtered through a 0.2 μm NYL filter, and treated with an excess of a methanolic solution of HCl (1.45 N, 1.35 mL, 2.00 mmol) and the resulting solution was concentrated in vacuo to dryness. The resulting solid was washed with pentane (3×2), and dried under standard conditions, to give **17g**·2HCl (121 mg) as a yellow solid: mp 182–185 ºC; IR (KBr) *ν* 3500–2500 (max at 3366, 3240, 3050, 2922, 2852 and 2796, N^+–H, N–H, C–H st), 1631, 1584, 1572, 1567, and 1519 (Ar–C–C, Ar–C–N st) cm^{-1}; ^{1}H NMR (400 MHz, CD_3OD) δ 1.26–1.46 (complex signal, 16H, 3'-H_2, 4'-H_2, 5'-H_2, 6'-H_2, 7'-H_2, 8'-H_2, 9'-H_2, 10'-H_2), 1.58 (s, 3H, 9-CH_3), 1.78–2.00 (complex signal, 10H, 10-H_{endo}, 13-H_{syn}, 2'-H_2, 11'-H_2, 2"-H_2, 3"-H_2), 2.09 (dm, *J* = 13.2 Hz, 1H, 13-H_{anti}), 2.56 (dm, *J* = 15.6 Hz, 1H, 10-H_{exo}), 2.68 (m, 2H, 1"-H_2), 2.78 (m, 1H, 7-H), 2.89 (d, *J* = 17.6 Hz, 1H, 6-H_{endo}), 3.00 (m, 2H, 4"-H_2), 3.21 (dd, *J* = 17.6 Hz, *J'* = 4.8 Hz, 1H, 6-H_{exo}), 3.47 (m, 1H, 11-H), 3.94 (t, *J* = 6.8 Hz, 2H) and 3.99 (m, 2H) (1'-H_2, 12'-H_2), 4.85 (s, NH, NH^+), 5.59 (br d, *J* = 3.6 Hz, 1H, 8-H), 7.54–7.60 (complex signal, 2H, 2-H, 7"-H), 7.76 (d, *J* = 8.0 Hz, 1H, 4-H), 7.78 (br s, 1H, 5"-H), 7.84 (dd, *J* = 8.0 Hz, *J'* = 7.2 Hz, 1H, 3-H), 8.39 (d, *J* = 8.0 Hz, 1H) and superimposed in part 8.41 (d, *J* = 7.6 Hz, 1H) (1-H, 8"-H); ^{13}C NMR (100.6 MHz, CD_3OD) δ 21.8 (CH_2, C3"), 22.9 (CH_2, C2"), 23.5 (CH_3, 9-CH_3), 24.8 (CH_2, C1"), 27.3 (CH, C11), 27.7 (CH_2) and 27.88 (CH_2) (C3', C10'), 27.93 (CH, C7), 29.35 (CH_2) and 29.44 (CH_2) (C13, C4"), 30.3 (2 CH_2) and 30.7 (4 CH_2) (C4', C5', C6', C7', C8', C9'), 31.4 (CH_2) and 31.5 (CH_2) (C2', C11'), 36.0 (CH_2) and 36.3 (CH_2) (C6, C10), 49.3 (CH_2) and 49.7 (CH_2) (C1', C12'), 113.4 (C), 115.5 (C), 117.17 (C) and 117.25 (C) (C11a, C12a, C8a" and C9a"), 119.2 (CH) and 120.1 (CH) (C4, C5"), 125.2 (CH, C8), 126.2 (CH, C1), 126.8 (CH, C7"), 127.3 (CH, C2), 128.8 (CH, C8"), 134.2 (CH, C3), 134.5 (C, C9), 140.1 (C), 140.3 (C) and 140.6 (C) (C4a, C6", C10a"), 150.7 (C) and 152.1 (C) (C5a, C4a"), 157.1 (C) and 157.9 (C) (C12, C9"); HRMS (ESI), calcd for [$C_{42}H_{53}{}^{35}ClN_4$ + H^+] 649.4032, found 649.4022; Anal. calcd. for $C_{42}H_{53}ClN_4$·2HCl·2H_2O: C, 66.52; H, 7.84; N, 7.39; Cl, 14.03. Found: C, 66.95; H, 7.99; N, 6.97; Cl, 13.83.

Biological profiling

4.1.9. T. brucei culturing and evaluation of trypanocidal activity

Bloodstream form *T. brucei* (strain 221) was cultured at 37 ºC in modified Iscove's medium.[59] Trypanocidal activity was assessed by growing parasites in the presence of various concentrations of the 4-aminoquinoline-based heterodimeric compounds and determining the levels which inhibited growth by 50% (IC_{50}) and 90% (IC_{90}). *T. brucei* in the logarithmic phase of growth were diluted back to 2.5×10^4 mL^{-1} and aliquoted into 96-well plates. Heterodimeric compounds were then added at a range of concentrations and the plates incubated at 37 °C. Each drug concentration was tested in triplicate. Resazurin was added after 48 h and the plates incubated for a further 16 h and the plates then read in a Spectramax plate reader. Results were analysed using GraphPad Prism.

4.1.10. P. falciparum culturing and evaluation of antiplasmodial activity

Malaria parasites were maintained in human A^+ erythrocytes suspended in RPMI 1640 medium supplemented with A^+ serum and D-glucose according to previously published methods.[60,61] Cultures containing predominantly early ring stages were used for testing. Compounds were dissolved in DMSO and further diluted with RPMI 1640 medium (the final DMSO concentration did not exceed 0.5% which did not affect parasite growth). Two-fold serial dilutions were made in 96-well microtitre plates in duplicate and infected erythrocytes were added to give a final volume of 100 μL with haematocrit 2.5% and 1% parasitaemia. Chloroquine diphosphate was used as a positive control and uninfected and infected erythrocytes without compounds were included in each test. Plates were placed into a modular incubator gassed with nitrogen 93%, oxygen 3%, carbon dioxide 4% and incubated at 37 ºC for 48 h. Parasite growth was assessed by measuring lactate dehydrogenase activity.[62] The reagent used contained the following in each mL: acetylpyridine adenine dinucleotide (APAD), 0.74 mg; lithium lactate, 19.2 mg; diaphorase, 0.1 mg; triton X-100, 2 μL; and nitroblue tetrazolium, 1 mg. Fifty μL of this reagent was added to each well and mixed, and plates were incubated for 10–15 min at 37 ºC. Absorbances were read at 550 nm using a Dynatech Laboratories MRX microplate reader and % inhibition of growth was calculated by comparison with control values. IC_{50} values were determined using linear regression analysis (Microsoft Excel).

4.1.11. Cytotoxic activity against rat skeletal myoblast L6 cells

Cytotoxicity against mammalian cells was assessed using microtitre plates following a described procedure.[63] Briefly, L6 cells (a rat skeletal muscle line) were seeded at 1×10^4 mL^{-1} in 200 μL of growth medium containing different compound concentrations. The plates were incubated for 6 days at 37 °C and 20 μL resazurin was then added to each well. After a further 8 h incubation, the fluorescence was determined using a Spectramax plate reader.

4.1.12. Acetylcholinesterase inhibitory activity

The inhibitory activities of the novel 4-aminoquinoline-based heterodimeric compounds **3g**, **4g**, **16f-g**, and **17f-g** against human recombinant AChE (Sigma-Aldrich) were evaluated spectrophotometrically by the method of Ellman et al.[43] The reactions took place in a final volume of 300 μL of 0.1 M phosphate-buffered solution pH 8.0, containing hAChE (0.02 u/mL) and 333 μM 5,5'-dithiobis(2-nitrobenzoic) acid (DTNB; Sigma-Aldrich) solution used to produce the yellow anion of 5-thio-2-nitrobenzoic acid. Inhibition curves were performed in duplicates using at least 10 increasing concentrations of inhibitors and preincubated for 20 min at 37 ºC before adding the substrate. One duplicate sample without inhibitor was always present to yield 100% of AChE activity. Then, substrate acetylthiocholine iodide (450 μM; Sigma-Aldrich) was added and the reaction was developed for 5 min at 37 ºC. The colour production was measured at 414 nm using a labsystems Multiskan spectrophotometer.

Data from concentration–inhibition experiments of the compounds were calculated by non-linear regression analysis, using the GraphPad Prism program package (GraphPad Software; San Diego, USA), which gave estimates of the IC_{50} (concentration of drug producing 50% of enzyme activity inhibition). Results are expressed as mean ± S.E.M. of at least 4 experiments performed in duplicate.

4.1.13. Determination of brain permeability: PAMPA-BBB assay

The *in vitro* permeability (P_e) of the novel 4-aminoquinoline-based heterodimeric compounds **3g**, **4g**, **16f-g**, and **17f-g** and fourteen known drugs through lipid extract of porcine brain membrane was determined by using a parallel artificial membrane permeation assay,[44] using a mixture PBS:EtOH 70:30. Assay validation was made by comparison of the experimental P_e

values of the known drugs with their reported values, which showed a good correlation: P_e (exp) = 1.4974 P_e (lit) – 0.8434 (R^2 = 0.9428). From this equation and the limits established by Di *et al.* for BBB permeation,[44] three ranges of permeability were established: compounds of high BBB permeation (CNS+): P_e (10^{-6} cm s^{-1}) > 5.10; compounds of low BBB permeation (CNS–): P_e (10^{-6} cm s^{-1}) < 2.15; and compounds of uncertain BBB permeation (CNS±): 5.10 > P_e (10^{-6} cm s^{-1}) > 2.15.

Table 4
Reported and experimental permeability values (P_e 10^{-6} cm s^{-1}) of 14 commercial drugs used for the PAMPA-BBB assay validation

Compound	Literature value[a]	Experimental value[b]
Cimetidine	0.0	0.70 ± 0.03
Lomefloxacin	1.1	0.75 ± 0.02
Norfloxacin	0.1	0.90 ± 0.02
Ofloxacin	0.8	0.97 ± 0.01
Hydrocortisone	1.9	1.40 ± 0.05
Piroxicam	2.5	1.71 ± 0.02
Clonidine	5.3	6.50 ± 0.05
Corticosterone	5.1	6.70 ± 0.10
Imipramine	13	12.3 ± 0.10
Promazine	8.8	13.8 ± 0.30
Progesterone	9.3	16.8 ± 0.30
Desipramine	12	17.8 ± 0.10
Testosterone	17	24.0 ± 0.14
Verapamil	16	25.3 ± 0.78

[a] Taken from ref. 44.

[b] Values are expressed as the mean ± SD of three independent experiments.

4.1.14. Trypanothione reductase inhibitory activity

The TryR inhibitory activity of selected compounds was determined using the colorimetric reduction of DTNB by dithiol trypanothione ($T[SH]_2$).[53,54] The assay mixture consisted of: 40 mM HEPES pH 7.4, 1 mM EDTA, 6 µM trypanothione disulfide ($T[S]_2$), 50 µM DTNB, 2 mU mL^{-1} TryR and 150 µM NADPH. IC_{50} values were determined using 11 serial dilutions. Starting with 12 µL of a 10 mM DMSO solution of each compound, 6 µL was removed and added to another Eppendorf tube containing 6 µL of DMSO. The tube was sealed, mixed and then briefly centrifuged to ensure that the sample was at the bottom of the tube. This procedure was repeated 11 times to produce 12 serial two-fold dilutions. Assays were performed in triplicate, by adding 158.2 µL of reagents (TryR + trypanothione + DTNB in assay buffer) to 1.8 µL of the inhibitor solution, and finally 20 µL of NADPH solution to start the assay. Absorbance at 412 nm was monitored at 25 ºC for 15 min using a SpectraMax 340PC (Molecular Devices) plate reader. Data were inspected for linearity and IC_{50} values determined by nonlinear regression to the following four-paramenter equation: $y = (\text{range}/(1+x/IC_{50})^{\text{Slope factor}}) + \text{background}$. The choice of disulphide concentration represents [S] ≈ 2 × K_m for the recombinant *T. brucei* enzyme.

4.1.15. β-Haematin inhibitory activity

The quantitative β-haematin inhibitory activity (BHIA) assay is based on the differential solubility of haemin and β-haematin in DMSO (haemin is soluble while β-haematin is insoluble).[57,58] The method determines a 50% inhibitory concentration for β-haematin inhibition in equivalents of the compound under test with respect to haemin ($BHIA_{50}$). Drug samples were dissolved in DMSO (25%) to give concentrations of 32 mM. Fifty µL aliquots of DMSO (25%) were placed in wells of 96-well microplates and serial dilutions of drugs were made to give concentrations of 0.5–32 mM. Fifty µL haemin chloride (8 mM) in DMSO was then added to each well. Drug free controls were prepared by adding haemin chloride solution (50 µL) to 50 µL DMSO (25%) in place of drug solution; chloroquine diphosphate and tetracycline hydrochloride were used as positive and negative controls respectively. β-haematin formation was initiated by the addition of 100 µL of 8 M acetate buffer (pH 5.0) and the plates were then incubated at 37 ºC for 18 h.

Following incubation, microplates were inspected visually. In wells where β-haematin formation was strongly inhibited clumps of black precipitate consisting of drug-haem complex were observed with a clear supernatant whereas less or no inhibition was indicated by wells with a precipitate evenly distributed throughout. The minimum inhibitory concentration was taken to be the lowest concentration of drug that was see to produce clumps of precipitate. The quantitative estimation of β-haematin formation using methodology similar to that reported by Basilico *et al.*,[57] was carried out as follows. Samples were transferred to Eppendorf tubes, centrifuged and the supernatants discarded. DMSO (200 µL) was used to wash out any remaining precipitate from the microplate wells and then thoroughly mixed with the precipitate in the Eppendorf tubes. After centrifuging again, the supernatants were discarded. Insoluble β-haematin was then dissolved by adding 200 µL 0.1M NaOH and mixing thoroughly. Aliquots of 75 µL were transferred to a fresh microplate and optical densities read at 400 nm using a Dynatech Laboratories MRX microplate reader and percent inhibition of β-haematin compared to drug-free controls calculated using linear regression analysis. A minimum of three separate determinations was carried out for each compound except for inactive compounds in which two determinations were carried out.

Acknowledgments

This work was supported by Ministerio de Ciencia e Innovación (MICINN) (CTQ2011-22433) and Generalitat de Catalunya (GC) (2014SGR52). JMK acknowledges funding support from the Wellcome Trust (Grant number WT084175). A fellowship from GC to I.S. is gratefully acknowledged. SYG is grateful to the Commonwealth Scholarship Secretariat, UK, and to the Government of Ghana for financial support.

References and notes

1. Njoroge, M.; Njuguna, N. M.; Mutai, P.; Ongarora, D. S. B.; Smith, P. W.; Chibale, K. *Chem. Rev.* **2014**, in press, DOI: 10.1021/cr500098f.
2. Simarro, P. P.; Cecchi, G.; Franco, J. R.; Paone, M.; Diarra, A.; Ruiz-Postigo, J. A.; Fevre, E. M.; Mattioli, R. C.; Jannin, J. G. *PLoS Negl. Trop. Dis.* **2012**, *6*, e1859.
3. World Health Organization. World Malaria Report 2013.
4. Nagle, A. S.; Khare, S.; Kumar, A. B.; Supek, F.; Buchynskyy, A.; Mathison, C. J. N.; Chennamaneni, N. K.; Pendem, N.; Buckner, F. S.; Gelb, M. H.; Molteni, V. *Chem. Rev.* **2014**, in press, DOI: 10.1021/cr500365f.
5. Fevre, E. M.; Wissmann, B. V.; Welburn, S. C.; Lutumba, P. *PLoS Neglected Trop. Dis.* **2008**, *2*, e333.
6. Hotez, P. J.; Fenwick, A.; Savioli, L.; Molyneux, D. H. *Lancet* **2009**, *373*, 1570.
7. Espuelas, S.; Plano, D.; Nguewa, P.; Font, M.; Palop, J. A.; Irache, J. M.; Sanmartín, C. *Curr. Med. Chem.* **2012**, *19*, 4259.

8. Hu, L.; Patel, A.; Bondada, L.; Yang, S.; Wang, M. Z.; Munde, M.; Wilson, W. D.; Wenzler, T.; Brun, R.; Boykin, D. W. *Bioorg. Med. Chem.* **2013**, *21*, 6732.
9. Faist, J.; Seebacher, W.; Kaiser, M.; Brun, R.; Saf, R.; Weis, R. *Bioorg. Med. Chem.* **2013**, *21*, 4988.
10. Baker, N.; de Konng, H. P.; Maser, P.; Horn, D. *Trends Parasitol.* **2013**, *29*, 110.
11. Phillips, M. A. *Mol. Microbiol.* **2012**, *86*, 10.
12. Eperon, G.; Balasegaram, M.; Potet, J.; Mowbray, C.; Valverde, O.; Chappuis, F. *Expert Rev. Anti Infect. Ther.* **2014**, *12*, 1407.
13. Persch, E.; Bryson, S.; Todoroff, N. K.; Eberle, C.; Thelemann, J.; Dirdjaja, N.; Kaiser, M.; Weber, M.; Derbani, H.; Brun, R.; Schneider, G.; Pai, E. F.; Krauth-Siegel, R. L.; Diederich, F. *ChemMedChem* **2014**, *9*, 1880.
14. Stich, A.; Ponte-Sucre, A.; Holzgrabe, U. *Lancet Infect. Dis.* **2013**, *13*, 733.
15. Ferrins, L.; Rahmani, R.; Baell, J. B. *Future Med. Chem.* **2013**, *5*, 1801.
16. Tatipaka, H. B.; Gillespie, J. R.; Chaterjee, A. K.; Norcross, N. R.; Hulverson, M. A.; Ranade, R. M.; Nagendar, P.; Creason, S. A.; McQueen, J.; Duster, N. A.; Nagle, A.; Supek, F.; Molteni, V.; Wenzler, T.; Brun, R.; Glynne, R.; Buckner, F. S.; Gelb, M. H. *J. Med. Chem.* **2014**, *57*, 828.
17. Fairlamb, A. H. *Nature* **2012**, *482*, 167.
18. Alsford, S.; Eckert, S.; Baker, N.; Glover, L.; Sanchez-Flores, A.; Leung, K. F.; Turner, D. J.; Field, M. C.; Berriman, M.; Horn, D. *Nature* **2012**, *482*, 232.
19. Gilbert, I. H. *J. Med. Chem.* **2013**, *56*, 7719.
20. Spinks, D.; Shanks, E. J.; Cleghorn, L. A. T.; McElroy, S.; Jones, D.; James, D.; Fairlamb, A. H.; Frearson, J. A.; Wyatt, P. G.; Gilbert, I. H. *ChemMedChem* **2009**, *4*, 2060.
21. Urich, R.; Grimaldi, R.; Luksch, T.; Frearson, J. A.; Brenk, R.; Wyatt, P. G. *J. Med. Chem.* **2014**, *57*, 7536.
22. Belluti, F.; Uliassi, E.; Veronesi, G.; Bergamini, C.; Kaiser, M.; Brun, R.; Viola, A.; Fato, R.; Michels, P. A. M.; Krauth-Siegel, R. L.; Cavalli, A.; Bolognesi, M. L. *ChemMedChem* **2014**, *9*, 371.
23. Njogu, P. M.; Chibale, K. *Curr. Med. Chem.* **2013**, *20*, 1715.
24. Prati, F.; Uliassi, E.; Bolognesi, M. L. *MedChemComm* **2014**, *5*, 853.
25. Chibale, K. *Pure Appl. Chem.* **2005**, *77*, 1957.
26. Rashad, A. A.; Jones, A. J.; Avery, V. M.; Baell, J.; Keller, P. A. *ACS Med. Chem. Lett.* **2014**, *5*, 496.
27. Upadhayaya, R. S.; Dixit, S. S.; Földesi, A.; Chattopadhyaya, J. *Bioorg. Med. Chem. Lett.* **2013**, *23*, 2750.
28. Musonda, C. C.; Yardley, V.; Carvalho de Souza, R. C.; Ncokazi, K.; Egan, T. J.; Chibale, K. *Org. Biomol. Chem.* **2008**, *6*, 4446.
29. Musonda, C. C.; Gut, J.; Rosenthal, P. J.; Yardley, V.; Carvalho de Souza, R. C.; Chibale, K. *Bioorg. Med. Chem.* **2006**, *14*, 5605.
30. Defaux, J.; Sala, M.; Formosa, X.; Galdeano, C.; Taylor, M. C.; Alobaid, W. A. A.; Kelly, J. M.; Wright, C. W.; Camps, P.; Muñoz-Torrero, D. *Bioorg. Med. Chem.* **2011**, *19*, 1702.
31. Oluwafemi, A. J.; Okanla, E. O.; Camps, P.; Muñoz-Torrero, D.; Mackey, Z. B.; Chiang, P. K.; Seville, S.; Wright, C. W. *Nat. Prod. Commun.* **2009**, *4*, 193.
32. Kaur, K.; Jain, M.; Reddy, R. P.; Jain, R. *Eur. J. Med. Chem.* **2010**, *45*, 3245.
33. Girault, S.; Grellier, P.; Berecibar, A.; Maes, L.; Lemière, P.; Muray, E.; Davioud-Charvet, E.; Sergheraert, C. *J. Med. Chem.* **2001**, *44*, 1658.
34. Ayad, F.; Tilley, L.; Deady, L. W. *Bioorg. Med. Chem. Lett.* **2001**, *11*, 2075.
35. Girault, S.; Grellier, P.; Berecibar, A.; Maes, L.; Mouray, E.; Lemière, P.; Debreu, M.-A.; Davioud-Charvet, E.; Sergheraert, C. *J. Med. Chem.* **2000**, *43*, 2646.
36. Cowman, A. F.; Deady, L. W.; Deharo, E.; Desneves, J.; Tilley, L. *Aust. J. Chem.* **1997**, *50*, 1091.
37. Sola, I.; Artigas, A.; Taylor, M. C.; Gbedema, S. Y.; Pérez, B.; Clos, M. V.; Wright, C. W.; Kelly, J. M.; Muñoz-Torrero, D. *Bioorg. Med. Chem. Lett.* **2014**, *24*, 5435.
38. Egan, T. J. *Drug Des. Rev.* **2004**, *1*, 93.
39. Galdeano, C.; Viayna, E.; Sola, I.; Formosa, X.; Camps, P.; Badia, A.; Clos, M. V.; Relat, J.; Ratia, M.; Bartolini, M.; Mancini, F.; Andrisano, V.; Salmona, M.; Minguillón, C.; González-Muñoz, G. C.; Rodríguez-Franco, M. I.; Bidon-Chanal, A.; Luque, F. J.; Muñoz-Torrero, D. *J. Med. Chem.* **2012**, *55*, 661.
40. Viayna, E.; Gómez, T.; Galdeano, C.; Ramírez, L.; Ratia, M.; Badia, A.; Clos, M. V.; Verdaguer, E.; Junyent, F.; Camins, A.; Pallàs, M.; Bartolini, M.; Mancini, F.; Andrisano, V.; Arce, M. P.; Rodríguez-Franco, M. I.; Bidon-Chanal, A.; Luque, F. J.; Camps, P.; Muñoz-Torrero, D. *ChemMedChem* **2010**, *5*, 1855.
41. Camps, P.; Formosa, X.; Galdeano, C.; Gómez, T.; Muñoz-Torrero, D.; Scarpellini, M.; Viayna, E.; Badia, A.; Clos, M. V.; Camins, A.; Pallàs, M.; Bartolini, M.; Mancini, F.; Andrisano, V.; Estelrich, J.; Lizondo, M.; Bidon-Chanal, A.; Luque, F. J. *J. Med. Chem.* **2008**, *51*, 3588.
42. Camps, P.; El Achab, R.; Morral, J.; Muñoz-Torrero, D.; Badia, A.; Baños, J. E.; Vivas, N. M.; Barril, X.; Orozco, M.; Luque, F. J. *J. Med. Chem.* **2000**, *43*, 4657.
43. Ellman, G. L.; Courtney, K. D.; Andres, V. Jr.; Featherstone, R. M. *Biochem. Pharmacol.* **1961**, *7*, 88.
44. Di, L.; Kerns, E. H.; Fan, K.; McConnell, O. J.; Carter, G. T. *Eur. J. Med. Chem.* **2003**, *38*, 223.
45. Viayna, E.; Sola, I.; Bartolini, M.; De Simone, A.; Tapia-Rojas, C.; Serrano, F. G.; Sabaté, R.; Juárez-Jiménez, J.; Pérez, B.; Luque, F. J.; Andrisano, V.; Clos, M. V.; Inestrosa, N. C.; Muñoz-Torrero, D. *J. Med. Chem.* **2014**, *57*, 2549.
46. Eberle, C.; Burkhard, J. A.; Stump, B.; Kaiser, M.; Brun, R.; Krauth-Siegel, R. L.; Diederich, F. *ChemMedChem* **2009**, *4*, 2034.
47. Krauth-Siegel, M. L.; Inhoff, O. *Parasitol. Res.* **2003**, *90*, S77.
48. Chibale, K.; Haupt, H.; Kendrick, H.; Yardley, V.; Saravanamuthu, A.; Fairlamb, A. H.; Croft, S. L. *Bioorg. Med. Chem. Lett.* **2001**, *11*, 2655.
49. Saravanamuthu, A.; Vickers, T. J.; Bond, C. S.; Peterson, M. R.; Hunter, W. N.; Fairlamb, A. H. *J. Biol. Chem.* **2004**, *279*, 29493.
50. Bonnet, B.; Soullez, D.; Davioud-Charvet, E.; Landry, V.; Horvath, D.; Sergheraert, C. *Bioorg. Med. Chem.* **1997**, *5*, 1249.
51. Girault, S.; Baillet, S.; Horvath, D.; Lucas, V.; Davioud-Charvet, E.; Tartar, A.; Sergheraert, C. *Eur. J. Med. Chem.* **1997**, *32*, 39.
52. Girault, S.; Davioud-Charvet, T. E.; Maes, L.; Dubremetz, J. F.; Debreu, M. A.; Landry, V.; Sergheraert, C. *Bioorg. Med. Chem.* **2001**, *9*, 837.
53. Hamilton, C. J.; Saravanamuthu, A.; Eggleston, I. M.; Fairlamb, A. H. *Biochem. J.* **2003**, *369*, 529.
54. Richardson, J. L.; Nett, I. R. E.; Jones, D. C.; Yardley, M. H.; Gilbert, I. H.; Fairlamb, A. H. *ChemMedChem* **2009**, *4*, 1333.
55. Walton, J. G. A.; Jones, D. C.; Kiuru, P.; Durie, A. J.; Westwood, N. J.; Fairlamb, A. H. *ChemMedChem* **2011**, *6*, 321.
56. Onyeibor, O.; Croft, S. L.; Dodson, H. I.; Feiz-Haddad, M.; Kendrick, H.; Millington, N. J.; Parapini, S.; Phillips, R. M.; Seville, S.; Shnyder, S. D.; Taramelli, D.; Wright, C. W. *J. Med. Chem.* **2005**, *48*, 2701.
57. Basilico, N.; Pagani, E.; Monti, D.; Olliaro, P.; Taramelli, D. *J. Antimicrob. Chemother.* **1998**, *42*, 55.
58. Parapini, S.; Basilico, N.; Pasini, E.; Egan, T. J.; Olliaro, P.; Taramelli, D.; Monti, D. *Exp. Parasitol.* **2000**, *96*, 249.
59. Wilkinson, S. R.; Prathalingam, S. R.; Taylor, M. C.; Ahmed, A.; Horn, D.; Kelly, J. M. *Free Radical Biol. Med.* **2006**, *40*, 198.
60. Fairlamb, A. H.; Warhurst, D. C.; Peters, W. *Ann. Trop. Med. Parasitol.* **1985**, *79*, 379.
61. Trager, W.; Jensen, J. B. *Science* **1976**, *193*, 673.
62. Makler, M. T.; Ries, J. M.; Williams, J. A.; Bancroft, J. E.; Piper, R. C.; Gibbins, B. L.; Himrichs, D. J. *Am. J. Trop. Med. Hyg.* **1993**, *48*, 739.
63. Bot, C.; Hall, B. S.; Bashir, N.; Taylor, M. C.; Helsby, N. A.; Wilkinson, S. R. *Antimicrob. Agents Chemother.* **2010**, *54*, 4246.

6. C.

Bioorg. Med. Chem. **2016**, in press

Synthesis and biological evaluation of *N*-cyanoalkyl-, *N*-aminoalkyl-, and *N*-guanidinoalkyl-substituted 4-aminoquinoline derivatives as potent, selective, brain permeable antitrypanosomal agents

Irene Sola[a], Albert Artigas[a], Martin C. Taylor[b], F. Javier Pérez-Areales[a], Elisabet Viayna[a], M. Victòria Clos[c], Belén Pérez[c], Colin W. Wright[d], John M. Kelly[b], Diego Muñoz-Torrero[a,*]

[a] *Laboratory of Pharmaceutical Chemistry (CSIC Associated Unit), Faculty of Pharmacy and Food Sciences, and Institute of Biomedicine (IBUB), University of Barcelona, Av. Joan XXIII, 27-31, E-08028, Barcelona, Spain*

[b] *Department of Pathogen Molecular Biology, London School of Hygiene and Tropical Medicine, Keppel Street, London WC1E 7HT, United Kingdom*

[c] *Department of Pharmacology, Therapeutics and Toxicology, Institute of Neurosciences, Autonomous University of Barcelona, E-08193, Bellaterra, Barcelona, Spain*

[d] *Bradford School of Pharmacy, University of Bradford, West Yorkshire BD7 1 DP, United Kingdom*

* Corresponding author. Tel.: +34 934024533; fax: +34 934035941.

E-mail address: dmunoztorrero@ub.edu (D. Muñoz-Torrero).

ABSTRACT

Current drugs against human African trypanosomiasis (HAT) suffer from several serious drawbacks. The search for novel, effective, brain permeable, safe, and inexpensive antitrypanosomal compounds is therefore an urgent need. We have recently reported that the 4-aminoquinoline derivative huprine Y, developed in our group as an anticholinesterasic agent, exhibits a submicromolar potency against *Trypanosoma brucei* and that its homo- and hetero-dimerization can result in to up to three-fold increased potency and selectivity. As an alternative strategy towards more potent smaller molecule anti-HAT agents, we have explored the introduction of ω-cyanoalkyl, ω-aminoalkyl, or ω-guanidinoalkyl chains at the primary amino group of huprine or the simplified 4-aminoquinoline analogue tacrine. Here, we describe the evaluation of a small in-house library and a second generation of newly synthesized derivatives, which has led to the identification of 13 side chain modified 4-aminoquinoline derivatives with submicromolar potencies against *T. brucei*. Among these compounds, the guanidinononyltacrine analogue **15e** exhibits a 5-fold increased antitrypanosomal potency, 10-fold increased selectivity, and 100-fold decreased anticholinesterasic activity relative to the parent huprine Y. Its biological profile, lower molecular weight relative to dimeric compounds, reduced lipophilicity, and ease of synthesis, make it an interesting anti-HAT lead, amenable to further optimization to eliminate its remaining anticholinesterasic activity.

Keywords: 4-Aminoquinolines
Side chain modification
Guanidines
Antitrypanosomal agents
Brain permeability

1. Introduction

Human African trypanosomiasis (HAT or sleeping sickness) is one of the 17 infectious diseases grouped under the term *Neglected Tropical Diseases*, which inflict a devastating effect on the health and economy of nearly 150 countries.[1–4] HAT is caused by two subspecies of the protozoan parasite *Trypanosoma brucei*, which are transmitted to humans through the bite of tsetse flies in rural areas of sub-Saharan Africa. The two subspecies of this parasite lead to distinct disease courses and display different geographical distribution. Most cases of HAT occur in western and central Africa and are due to *T. brucei gambiense*, which causes a chronic infection that slowly progresses from an initial hemolymphatic stage, often asymptomatic, to a late stage, in which the parasites spread into the central nervous system. This produces severe neurological pathology, including sleep disruptions, which give rise to the common name of the disease. About 2–5% of HAT cases occur in southern and eastern Africa and are caused by *T. brucei rhodesiense*. This leads to an acute infection that rapidly progresses from early to late stage disease. With both forms of HAT, the absence of effective treatment in the late stage inexorably leads to coma and death.[5]

Over the last 15 years, because of public health measures, there has been considerable success combatting HAT, with the estimated numbers of those infected falling from 300,000 to less than 20,000.[6] However, the disease still occurs in 36 countries, with 65 million people at risk, and there is a constant potential for large epidemic outbreaks. Vaccines are not a realistic option for prevention of HAT because of antigenic variation in the parasite.[7] Chemotherapy is therefore of particular importance.[8] Unfortunately, the few drugs that have been approved for HAT (pentamidine and suramin for early stage HAT; melarsoprol and eflornithine, alone or in combination with nifurtimox, for late stage HAT) are unsatisfactory for several reasons, which include the occurrence of major side effects, high costs associated with parenteral administration and medical supervision, lack of brain permeability (in the case of pentamidine and suramin), which precludes their use in late stage HAT, and the increasing emergence of resistance.[9–11] Thus, the development of novel antitrypanosomal compounds that can overcome these issues is urgently needed.[3,12]

Repurposing of known drugs is being increasingly pursued for antitrypanosomal drug discovery, particularly because this strategy should be more rapid and less expensive than the development of new chemical entities.[4,13–15] Despite this, most research efforts to replenish the antitrypanosomal pipeline remain focussed on the development of novel

compounds, rationally designed or screened against one or several parasite biological targets[16–19] or, more often, arising from phenotypic whole cell screens of compound libraries.[20–26]

7-Chloro-4-aminoquinoline derivatives are within those structural classes that are being developed for the treatment of HAT.[27] We recently reported that huprine Y (**1**, Fig. 1), a 7-chloro-4-aminoquinoline derivative with potent acetylcholinesterase (AChE) inhibitory activity, developed in our group as an anti-Alzheimer drug candidate,[28] exhibited significant activity against *T. brucei* (IC_{50} = 0.61 μM, selectivity index (SI) over rat myoblast L6 cells = 13).[29,30] In 4-aminoquinoline-based antimalarials, both dimerization and side chain modification have been used to increase potency and overcome parasite resistance.[31–35] Interestingly, we have found that homodimerization of huprine Y (as in compound **2**,[36] Fig. 1) and heterodimerization with the 4-aminoquinoline derivative tacrine (as in compound **3**,[37] Fig. 1) also results in up to 3-fold increased potency and selectivity against *T. brucei*.

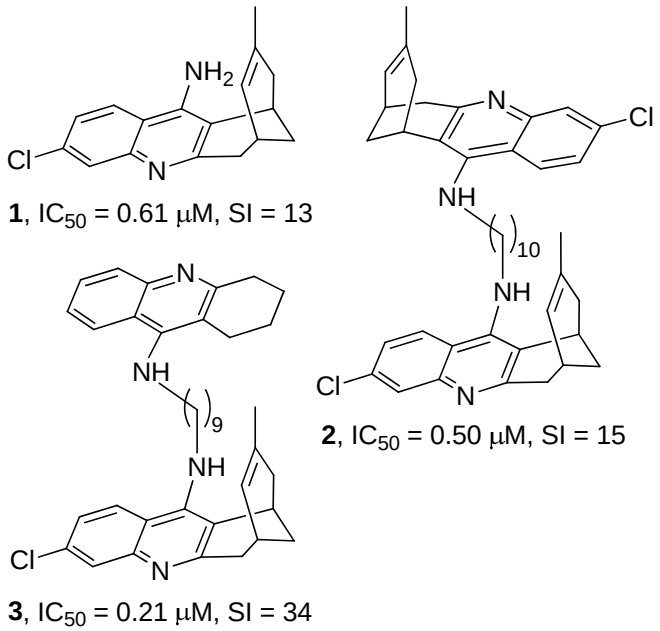

Fig. 1. Structures, trypanocidal (*T. brucei*) activities, and selectivity indices of huprine Y, **1**, and the oligomethylene-linked homo- and heterodimers **2** and **3**.

Modification of the side chain attached to the exocyclic amino group of 7-chloro-4-aminoquinoline derivatives has also been reported to lead to increased antitrypanosomal activity.[35] To explore further the structure–antitrypanosomal activity relationships

around the huprine scaffold, we report here: (i) the screening of a series of huprine derivatives, substituted at the exocyclic amino group with cyanoalkyl or aminoalkyl chains of different lengths and nature (nitriles **4a**-**h**, and amines **5a**-**h**, Fig. 2), against cultured bloodstream forms of *T. brucei*, rat skeletal myoblast L6 cells, and electric eel AChE, and the evaluation of their brain permeability using an *in vitro* artificial membrane assay (PAMPA-BBB); (ii) the synthesis and evaluation of the antitrypanosomal, cytotoxic, and anticholinesterasic activity and brain permeability of novel huprine and structurally related tacrine derivatives with other modified side chains terminating in cyano, primary or cyclic amino, or guanidino groups.

2. Results and discussion

2.1. Screening of the antitrypanosomal, cytotoxic, and anticholinesterasic activity and brain permeability of the ω-cyanoalkyl- and ω-aminoalkyl-huprines 4a–h and 5a–h

The ω-aminoalkyl-huprines **5a**–**h** (Fig. 2) were recently synthesized in our group as immediate precursors of a family of huprine-based anti-Alzheimer hybrid compounds.[38] We inferred that these compounds might be interesting antitrypanosomal leads based on two grounds. Firstly, aminoalkylhuprines **5a**–**h** should be diprotonated at physiological pH, like pentamidine and other antitrypanosomal dicationic compounds,[39,40] which seemed favourable for anti-HAT activity. Secondly, we expected that the substitution of one of the lipophilic 4-aminoquinoline moieties of bis(4-aminoquinoline) dimers, like **2** and **3** (Fig. 1), by a primary amino group in aminoalkylhuprines **5a**–**h** would result in a decreased AChE inhibitory activity, and hence, a lower risk of unwanted cholinergic side-effects. Indeed, this trend in AChE inhibitory activity has been reported for a family of dimeric tacrines,[41] and can be ascribed to a less efficient interaction with a secondary binding site of the enzyme AChE, the so-called peripheral anionic site, when the second 4-aminoquinoline moiety of the dimer, *bis*(7)tacrine, is substituted by a simple primary amino group.

Because some nitriles have been found to display antitrypanosomal activity,[9,42] we also envisaged the biological screening of the nitriles **4a**–**h** (Fig. 2), the synthetic precursors of amines **5a**–**h**.[38]

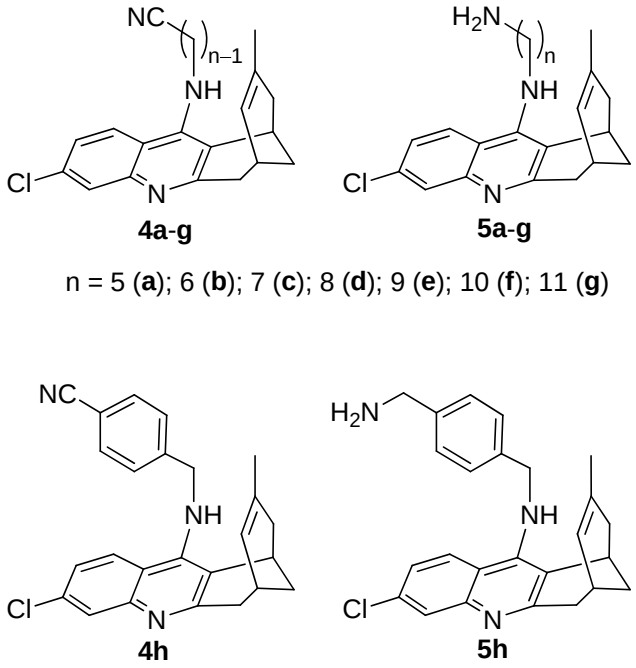

Fig. 2. Structures of cyanoalkyl- and aminoalkyl-huprines **4a**-**h** and **5a**-**h**.

The ω-cyanoalkyl-huprines **4a**–**h** and the ω-aminoalkyl-huprines **5a**–**h** were first screened against the bloodstream form of *T. brucei*, the clinically relevant form of the parasite,[43] using nifurtimox and huprine Y as reference compounds. These side chain modified huprine derivatives displayed low micromolar to submicromolar IC_{50} values, with all of them being more potent antitrypanosomal agents than nifurtimox, and a few being slightly more potent than, or equipotent to, the parent huprine Y (Table 1). Somewhat unexpectedly, nitriles were found to be in general more potent than the corresponding amines, especially those featuring hepta- to nona-methylene side chains (octa- to deca-methylene side chains in the amines), which were 4–8-fold more potent than their amine counterparts. A clear trend was found in the antitrypanosomal potency of nitriles **4a**–**h** regarding the length of the linker, with the potency increasing from n = 5 (**4a**) to n = 9 (**4e**), and then decreasing for the longer homologues **4f** and **4g**. For the amines, the highest potency was found for the heptamethylene-linked derivative **5c**. The presence of a *p*-phenylene ring in the side chain does not seem to be of particular relevance for the antitrypanosomal activity, with the *p*-phenylene-linked nitrile **4h** and amine **5h** being equipotent to nitrile **4a** and amine **5a** with a similar side chain length.

Table 1

Antitrypanosomal, cytotoxic, and anticholinesterasic activity and BBB permeability of cyanoalkylhuprines **4a**–**h** and aminoalkylhuprines **5a**–**h** and reference compounds **1** and nifurtimox.[a]

Compd	*T. brucei* IC_{50} (μM)	*T. brucei* IC_{90} (μM)	L6 cells IC_{50} (μM)	SI_{Tb}[b]	*Ee*AChE IC_{50} (nM)	P_e (10^{-6} cm s^{-1})[c] (prediction)
4a	2.13 ± 0.49	4.04 ± 0.06	20.3 ± 0.2	9.7	26.9 ± 1.1	[d]
4b	1.60 ± 0.13	3.21 ± 0.32	19.0 ± 0.3	11.9	31.1 ± 3.1	12.4 ± 0.6 (CNS+)
4c	0.86 ± 0.05	1.22 ± 0.03	11.6 ± 3.0	13.5	[d]	[d]
4d	0.62 ± 0.02	0.85 ± 0.01	7.65 ± 0.41	12.3	[d]	[d]
4e	0.32 ± 0.01	0.42 ± 0.01	8.04 ± 0.53	25.1	[d]	[d]
4f	0.46 ± 0.01	0.61 ± 0.01	4.79 ± 0.25	10.4	9.67 ± 0.89	11.3 ± 1.2 (CNS+)
4g	1.37 ± 0.06	1.91 ± 0.02	4.98 ± 0.21	3.6	[d]	16.2 ± 1.3 (CNS+)
4h	1.86 ± 0.08	3.39 ± 0.15	10.0 ± 0.8	5.4	158 ± 21	19.3 ± 1.2 (CNS+)
5a	0.92 ± 0.08	2.92 ± 0.43	3.82 ± 0.11	4.2	[d]	[d]
5b	2.03 ± 0.10	3.09 ± 0.21	4.78 ± 0.16	2.4	[d]	[d]
5c	0.68 ± 0.20	1.15 ± 0.05	4.33 ± 0.08	6.4	36.0 ± 3.5	7.6 ± 0.7 (CNS+)
5d	2.28 ± 0.29	4.28 ± 0.46	12.5 ± 3.3	5.5	17.3 ± 1.2	9.8 ± 0.6 (CNS+)
5e	2.61 ± 0.16	4.58 ± 0.31	13.6 ± 3.4	5.2	16.4 ± 1.8	7.1 ± 0.7 (CNS+)
5f	3.33 ± 0.10	4.33 ± 0.18	7.55 ± 0.19	2.3	20.3 ± 2.5	7.0 ± 0.3 (CNS+)
5g	1.79 ± 0.03	2.24 ± 0.04	8.06 ± 0.63	4.5	35.3 ± 3.9	4.0 ± 0.2 (CNS±)
5h	0.92 ± 0.03	1.44 ± 0.15	4.27 ± 0.13	4.6	[d]	11.7 ± 1.1 (CNS+)
1[e]	0.61 ± 0.03	2.94 ± 0.20	7.80 ± 0.47	13	0.30 ± 0.01	23.8 ± 2.7 (CNS+)[f]
nifurtimox	4.4 ± 0.7[g]		32.0 ± 1.1	7.3	[d]	[d]

[a] *In vitro* activity against bloodstream form of *T. brucei* (pH 7.4), rat myoblast L6 cells, and *Electrophorus electricus* AChE, expressed as the concentration that inhibited growth or enzyme activity by 50% (IC_{50}) and 90% (IC_{90}, for *T. brucei*). Data are the mean of triplicate experiments ± SEM.

[b] SI_{Tb}: selectivity index as the ratio of cytotoxic to anti-*T. brucei* IC_{50} values.

[c] Permeability values from the PAMPA-BBB assay. Values are expressed as the mean ± SD of three independent experiments.

[d] Not determined.

[e] Trypanocidal and cytotoxicity activity values taken from Ref. 29.

[f] Taken from Ref. 38.

[g] Taken from Ref. 44.

Thus, the most interesting side chain modified huprine derivative was nitrile **4e**, which, with an IC_{50} value against *T. brucei* of 320 nM (and an IC_{90} value of 420 nM), was 14-fold more potent than nifurtimox and 2-fold more potent than huprine Y (7-fold more potent than huprine Y in terms of the IC_{90} values), in agreement with the expected increase in antitrypanosomal potency upon modification of the side chain at the exocyclic amino group.

Interestingly, nitriles **4a**–**h** and amines **5a**–**h** turned out to be less toxic to rat skeletal myoblast L6 cells than to *T. brucei*, with nitriles **4a**–**h** being less cytotoxic than the corresponding amines **5a**–**h** (Table 1), especially nitrile **4e**, which displayed a selectivity index of 25, i.e. 2- and 3.5-fold more than that of the parent huprine Y and nifurtimox, respectively.

As expected, the introduction of the ω-cyanoalkyl and ω-aminoalkyl chains at the primary amino group of huprine Y led to a clear decrease in AChE inhibitory activity (up to 500-fold). Notwithstanding the lower AChE inhibitory potency relative to the parent huprine Y, nitriles **4a**–**h** and amines **5a**–**h** were more potent AChE inhibitors than would be desirable in antitrypanosomal agents, with nanomolar IC_{50} values for electric eel AChE inhibition (Table 1).

Because good brain penetration is necessary for the treatment of late-stage HAT, the brain permeability of nitriles **4a**–**h** and amines **5a**–**h** was assessed *in vitro* through the well-established parallel artificial membrane permeability assay (PAMPA-BBB).[45] As with the parent huprine Y, the permeabilities of most of these modified analogues, through the porcine brain lipid extract used as an artificial blood–brain barrier (BBB) model, were found to be above the threshold established for high BBB permeation (CNS+, P_e (10^{-6} cm s^{-1}) > 5.17, Table 1). Therefore, these compounds are predicted to be able to cross the BBB, with nitriles **4a**–**h** being more permeable than the corresponding amines (Table 1), probably due to the dicationic character of the latter at physiological pH.

Overall, the screening of this small in-house compound library pointed to neutral cyano or basic primary amino groups at the end of a side chain of 9 or 7 carbon atoms, respectively, as being favourable substitution patterns for potent, selective, and brain permeable antitrypanosomal agents.

2.2. Synthesis of novel side chain modified 4-aminoquinoline derivatives

Even though the ω-aminoalkyl-huprines **5a**–**h** turned out to be less potent antitrypanosomal agents than the corresponding nitriles **4a**–**h**, they still displayed a submicromolar antitrypanosomal potency in some cases, as well as some selectivity and brain permeability. Indeed, other classes of compounds, such as bis-guanidines and bis-amidines, are diprotonated at physiological pH, like aminoalkylhuprines **5a**–**h**, and exhibit potent antitrypanosomal activity,[40,46–49] and brain permeability.[40] To further extend the SAR around side chain modified huprine derivatives, we undertook the synthesis and biological profiling of novel dibasic huprine derivatives featuring a terminal guanidine (**6b** and **6e**, Scheme 1), piperidine (**7**, Scheme 2) or morpholine (**8**, Scheme 2) moiety, together with different side chain lengths.

In addition, to assess the role of the unsaturated methyl-substituted three-carbon bridge of the huprine moiety, we also synthesised a series of ω-cyanoalkyl-, ω-aminoalkyl-, and ω-guanidinoalkyl derivatives (**11c**, **11e**, **12c**–**e**, **13c**, **13e**, **14e**, **15c**, **15e**, **16e**, Scheme 3), in which the huprine core was substituted by the simpler, less lipophilic (by around 2 logP units), and easier-to-synthesize tricyclic core of the 4-aminoquinoline derivatives tacrine and 6-chlorotacrine (**9** and **10**, respectively, Scheme 3). These featured oligomethylene chains of lengths in the range that was found optimal for antitrypanosomal activity in the huprine series (n = 7–9).

Guanidinoalkyl huprines **6b** and **6e** were readily synthesized in moderate yield (30% and 59%, respectively) from the corresponding amines **5b** and **5e** upon reaction with 1*H*-pyrazole-1-carboxamidine hydrochloride in dry CH_3CN in the presence of Et_3N (Scheme 1).

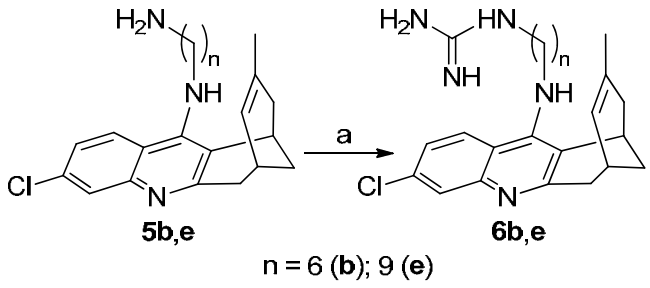

Scheme 1. Reagents and conditions: (a) 1*H*-pyrazole-1-carboxamidine hydrochloride, Et_3N, CH_3CN, reflux, overnight.

Likewise, the synthesis of the piperidinopropyl- and morpholinopropyl-huprines **7** and **8** only required one step, i.e. the alkylation of huprine Y, **1**, with the commercial 1-(3-chloropropyl)piperidine hydrochloride or the readily available 3-morpholinopropyl methanesulfonate,[50] after deprotonation of the primary amino group with KOH (Scheme 2).

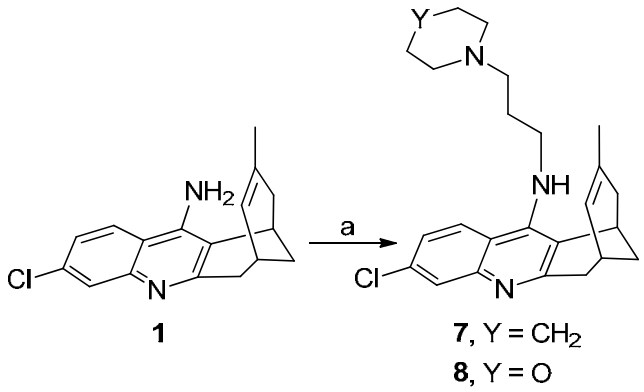

1 **7**, Y = CH_2 **8**, Y = O

Scheme 2. Reagents and conditions: (a) KOH, 4 Å molecular sieves, DMSO, rt, 2h; then, 1-(3-chloropropyl)piperidine hydrochloride or 3-morpholinopropyl methanesulfonate, DMSO, rt, overnight.

For the synthesis of the novel cyanoalkyl tacrines **11c**, **11e**, and **12c**–**e**, the known aminoalkyl tacrines **13c**,[41] **13e**,[51] and **14e**,[52] and the novel guanidinoalkyl tacrines **15c**, **15e**, and **16e**, we followed the same three-step protocol that we had used in the huprine series, based on the initial alkylation of tacrine or chlorotacrine with the corresponding ω-bromoalkanenitrile, followed by $LiAlH_4$ reduction of the cyano to a primary amino group, and final conversion of the amines into the guanidines upon treatment with 1*H*-pyrazole-1-carboxamidine hydrochloride (Scheme 3).

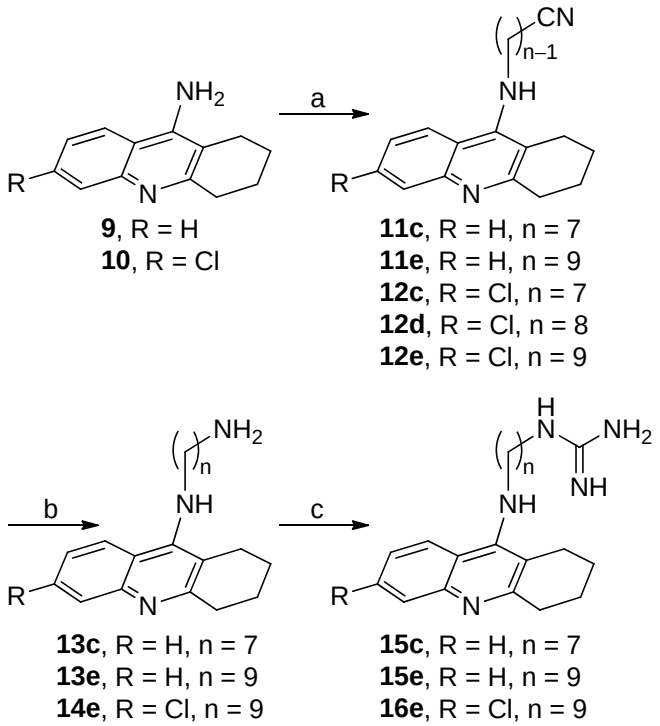

Scheme 3. Reagents and conditions: (a) KOH, 4 Å molecular sieves, DMSO, rt, 2h; then, ω-bromoalkanenitrile, DMSO, rt, overnight; (b) $LiAlH_4$, Et_2O, rt, overnight; (c) 1*H*-pyrazole-1-carboxamidine hydrochloride, Et_3N, CH_3CN, reflux, overnight.

All the target compounds were transformed into the corresponding hydrochloride or dihydrochloride salts, with which their chemical and biological characterization was performed.

2.3. Biological profiling of the novel side chain modified 4-aminoquinoline derivatives

The therapeutic potential of the second generation side chain modified huprine and tacrine derivatives was assessed by evaluation of their antitrypanosomal activity against cultured bloodstream forms of *T. brucei*, and by their brain permeability. Additionally, their potential toxicity was assessed by measuring their effect on the viability of rat L6 cells as a model of normal mammalian cells and by their AChE inhibitory activity.
We found several compounds that exhibited nanomolar antitrypanosomal IC_{50} and IC_{90} values, favourable selectivity indices, and brain permeability (Table 2).

Table 2

Antitrypanosomal, cytotoxic, and anticholinesterase activity and BBB permeability of the *N*-cyanoalkyl, *N*-aminoalkyl, and *N*-guanidinoalkyl 4-aminoquinoline derivatives **6b**,**e**, **7**, **8**, **11c**,**e**, **12c**–**e**, **13c**,**e**, **14e**, **15c**,**e**, and **16e** and reference compounds **1** and nifurtimox.[a]

Compd	*T. brucei* IC_{50} (μM)	*T. brucei* IC_{90} (μM)	L6 cells IC_{50} (μM)	SI_{Tb}[b]	*Ee*AChE IC_{50} (nM)	P_e (10^{-6} cm s^{-1})[c] (prediction)
6b	1.37 ± 0.02	1.54 ± 0.01	21.0 ± 1.6	15.3	11.8 ± 1.3	2.9 ± 0.4 (CNS±)
6e	0.33 ± 0.06	0.70 ± 0.09	10.9 ± 0.9	33	10.6 ± 0.8	5.4 ± 0.3 (CNS+)
7	0.83 ± 0.04	1.70 ± 0.21	2.40 ± 0.19	2.9	48.4 ± 2.7	5.9 ± 0.4 (CNS+)
8	1.75 ± 0.19	4.88 ± 0.27	14.3 ± 0.5	8.2	13.3 ± 0.8	15.0 ± 1.0 (CNS+)
11c	3.81 ± 1.13	10.3 ± 2.7	34.8 ± 1.6	9.1	53.9 ± 3.0	11.2 ± 0.2 (CNS+)
11e	0.98 ± 0.05	1.38 ± 0.09	5.73 ± 0.16	4.2	44.9 ± 1.6	7.6 ± 0.35 (CNS+)
12c	7.92 ± 0.17	12.2 ± 0.2	34.7 ± 0.6	4.4	[d]	16.7 ± 0.9 (CNS+)
12d	6.89 ± 0.13	8.75 ± 0.24	27.8 ± 1.6	4.0	46.0 ± 6.0	14.7 ± 0.8 (CNS+)
12e	1.57 ± 0.17	2.56 ± 0.07	8.00 ± 0.44	5.1	24.3 ± 4.5	5.4 ± 0.4 (CNS+)
13c	2.13 ± 0.05	3.12 ± 0.14	7.28 ± 0.86	3.4	23.9 ± 2.6	7.4 ± 0.1 (CNS+)
13e	4.07 ± 0.12	5.55 ± 0.10	16.6 ± 0.6	4.1	15.6 ± 1.5	6.9 ± 0.5 (CNS+)
14e	2.31 ± 0.36	4.88 ± 0.18	7.62 ± 0.81	3.3	14.5 ± 1.6	5.8 ± 0.3 (CNS+)
15c	0.85 ± 0.09	1.30 ± 0.20	< 1.20	< 1.4	23.9 ± 2.6	5.9 ± 0.3 (CNS+)
15e	0.12 ± 0.01	0.25 ± 0.04	15.9 ± 0.8	133	30.5 ± 1.9	6.5 ± 0.3 (CNS+)
16e	0.63 ± 0.08	0.96 ± 0.02	11.9 ± 1.2	19	16.4 ± 1.5	6.7 ± 0.4 (CNS+)
1[e]	0.61 ± 0.03	2.94 ± 0.20	7.80 ± 0.47	13	0.30 ± 0.01	23.8 ± 2.7 (CNS+)[f]
nifurtimox	4.4 ± 0.7[g]		32.0 ± 1.1	7.3	[d]	[d]

[a] *In vitro* activity against bloodstream form of *T. brucei* (pH 7.4), rat myoblast L6 cells, and *Electrophorus electricus* AChE, expressed as the concentration that inhibited growth or enzyme activity by 50% (IC_{50}) and 90% (IC_{90}, for *T. brucei*). Data are the mean of triplicate experiments ± SEM.

[b] SI_{Tb}: selectivity index as the ratio of cytotoxic to anti-*T. brucei* IC_{50} values.

[c] Permeability values from the PAMPA-BBB assay. Values are expressed as the mean ± SD of three independent experiments.

[d] Not determined.

[e] Trypanocidal and cytotoxicity activity values taken from Ref. 29.

[f] Taken from Ref. 38.

[g] Taken from Ref. 44.

With the huprine derivatives, we found that the introduction of a guanidine at the end of the side chain led to increased antitrypanosomal potencies relative to the corresponding primary amine counterparts, and to roughly equipotent activity relative to the nitriles. Thus, the novel guanidine **6e**, with a total of 9 carbon atoms in the side chain, displayed the same antitrypanosomal potency as the most active compound of the initially screened series, nitrile **4e** (IC_{50} 0.3 μM) (Table 2). The introduction of a piperidino or a morpholino substituent at the side chain of the huprine derivatives **7** and **8** did not seem to confer any particular contribution to the antitrypanosomal properties, with these compounds displaying similar activities to several of the aminoalkylhuprines.

The same trend observed with the huprine derivatives in regard of the terminal functionality and length of the side chain was found in the tacrine derivatives. The order of antitrypanosomal potencies was guanidines > nitriles > amines, with higher potencies for the guanidines and nitriles that have a total number of 9 carbon atoms in the side chain. Higher antitrypanosomal potencies were also found for those derivatives with an unsubstituted tacrine moiety. Thus, the nonamethylene-linked guanidine **15e** (IC_{50} 120 nM) was found to be the most potent side chain modified tacrine derivative (Table 2). With regard to the 4-aminoquinoline core, replacement of the huprine with the less complex tacrine moiety led, in general, to a drop in antitrypanosomal activity, with ω-aminoalkyl- and ω-cyanoalkyl (6-chloro)tacrines being 1–3-fold and 3–9-fold, respectively, less potent than the corresponding ω-aminoalkyl- and ω-cyanoalkyl huprine derivatives. A notable exception was the ω-guanidinononyl tacrine **15e**, which was 3-fold more potent than the ω-guanidinononyl huprine **6e**. Overall this was the most potent side chain modified 4-aminoquinoline derivative.

Interestingly, all the second generation side chain modified huprine and tacrine derivatives could be inferred to be capable of entering the central nervous system (with the sole exception of guanidine **6b**), on the basis of their measured PAMPA-BBB permeabilities. All of them, with the exception of **15c**, also turned out to be less toxic to mammalian L6 cells than to *T. brucei*, with selectivity indices ranging from 3 to 133 (Table 2). Unfortunately, as with the first generation of screened compounds, despite inhibiting AChE 35–180-fold less potently than the parent compound huprine Y, the anticholinesterasic activity of the second generation side chain modified huprine and tacrine derivatives was still not ideal. Their anticholinesterasic activity was 1–2 orders

of magnitude higher than their antitrypanosomal potencies, with the guanidinononyl tacrine **15e** being the best balanced compound (with the anticholinesterasic activity only 4-fold greater than that against typanosomes).

3. Conclusion

We recently found that both homodimerization and heterodimerization of the 4-aminoquinoline derivative huprine Y results in increased potency against *T. brucei* and improved selectivity over mammalian cells relative to the parent compound,[36,37] albeit at the expense of increasing lipophilicity and molecular weight. In this current paper, we have explored the effect on antitrypanosomal activity of the introduction of a side chain, featuring a terminal cyano, amino, or guanidino group, at the primary amino group of huprine Y or the simpler structurally related tacrine or 6-chlorotacrine, as an alternative approach to improve the antitrypanosomal profile. We found that the introduction of a guanidino or a cyano group at the end of a chain of nine carbon atoms was the best type of substitution to produce good antitrypanosomal activity in both the huprine and the tacrine series. The presence of the tetracyclic huprine core leads to higher antitrypanosomal potency in the cyanoalkyl derivatives, whereas the opposite trend was found for guanidinoalkyl derivatives, with the guanidinononyltacrine analogue **15e** being the most promising compound of the side chain modified 4-aminoquinoline derivatives. Overall, 13 out of the 31 side chain modified 4-aminoquinoline derivatives displayed submicromolar potencies against cultured bloodstream form *T. brucei* and good brain permeability. The antitrypanosomal potency of these compounds is greater than their toxicity to mammalian cells, but lower than their anticholinesterasic activity, which might result in undesirable cholinergic side effects.

Guanidinononyltacrine **15e** emerges as the most interesting antitrypanosomal lead of this class. It is endowed with potent (IC_{50} = 120 nM) and selective (SI = 133) activity against *T. brucei*, should be brain permeable, and has the least unfavourable antitrypanosomal/anticholinergic activity ratio. This compound has 5-fold increased antitrypanosomal potency, 10-fold increased selectivity index, and 100-fold decreased anticholinesterasic activity compared with the parent huprine Y, together with lower lipophilicity and molecular weight relative to huprine-based homo- and hetero-dimeric compounds. Our findings confirm that introduction of a conveniently functionalized side chain at the primary amino group of 4-aminoquinoline derivatives may be superior

to homo- and hetero-dimerization as a strategy to improve the potential anti-HAT therapeutic profile of this structural class.

4. Experimental

4.1. Chemistry. General methods

Melting points were determined in open capillary tubes with a MFB 595010M Gallenkamp melting point apparatus. 400 MHz ^{1}H/100.6 MHz ^{13}C NMR spectra were recorded on a Varian Mercury 400 spectrometer at the Centres Científics i Tecnològics of the University of Barcelona (CCiTUB). The chemical shifts are reported in ppm (δ scale) relative to solvent signals (CD_3OD at 3.31 and 49.0 ppm in the ^{1}H and ^{13} C NMR spectra, respectively), and coupling constants are reported in Hertz (Hz). The *syn* (*anti*) notation of the protons at position 13 of the huprine moiety of compounds **6b**,**e**, **7**, and **8** means that the corresponding proton at position 13 is on the same (different) side of the quinoline moiety with respect to the cyclohexene ring. IR spectra were run on a Perkin-Elmer Spectrum RX I spectrophotometer. Absorption values are expressed as wavenumbers (cm^{-1}); only significant absorption bands are given. Column chromatography was performed on silica gel 60 AC.C (35–70 mesh, SDS, ref 2000027). Thin-layer chromatography was performed with aluminum-backed sheets with silica gel 60 F_{254} (Merck, ref 1.05554), and spots were visualized with UV light and 1% aqueous solution of $KMnO_4$. High resolution mass spectra were carried out at the CCiTUB with a LC/MSD TOF Agilent Technologies spectrometer. The analytical samples of all of the compounds that were subjected to pharmacological evaluation were dried at 65 ºC / 2 Torr for at least 2 days (standard conditions). Nitriles **11c** and **12c** are protected in a patent of our group,[53] where, however, no NMR spectra data were given. A more consistent chemical characterization of these compounds is included in this section.

4.1.1. 1-{6-[(3-Chloro-6,7,10,11-tetrahydro-9-methyl-7,11-methanocycloocta[*b*]quinolin-12-yl)amino]hexyl}guanidine (6b)

To a solution of amine **5b** (462 mg, 1.20 mmol) in dry CH_3CN (5 mL), anhydrous Et_3N (0.5 mL, 363 mg, 3.59 mmol) and 1*H*-pyrazole-1-carboxamidine hydrochloride (172 mg, 1.17 mmol) were added. The reaction mixture was stirred under reflux overnight. The resulting precipitated solid was taken in CH_2Cl_2 (25 mL) and treated with 2 N NaOH (20 mL). The organic phase was washed with H_2O (3 × 20 mL), dried over

anhydrous Na_2SO_4, and concentrated under reduced pressure to afford guanidine **6b** (150 mg, 30% yield), as a brownish solid.

A solution of **6b** (150 mg, 0.39 mmol) in CH_2Cl_2 (10 mL) was treated with a methanolic solution of HCl (0.75 N, 4.2 mL, 3.15 mmol) and concentrated under reduced pressure. The resulting solid was taken in MeOH (0.25 mL) and precipitated by addition of EtOAc (1.4 mL). The precipitate was washed with pentane (3 × 2 mL) to give, after drying under standard conditions, **6b**·2HCl (37 mg) as a brownish hygroscopic solid; mp 166–168 ºC; IR (ATR) *ν* 3500–2500 (max at 3260, 3134, 2929, 2865, $^{+}$NH, NH, CH st), 1659, 1631, 1582, 1567, 1514 (C=N, Ar–C–C, Ar–C–N st) cm^{-1}; ^{1}H NMR (400 MHz, CD_3OD) δ 1.42–1.54 (complex signal, 4H, 3-H_2, 4-H_2), 1.58 (s, 3H, 9'-CH_3), superimposed in part 1.62 (tt, $J = J' = 6.8$ Hz, 2H, 2-H_2), superimposed in part 1.91 (tt, $J = J' = 7.2$ Hz, 2H, 5-H_2), 1.93 (br d, $J = 17.2$ Hz, 1H, 10'-H_{endo}), superimposed in part 1.94 (br d, $J = 12.8$ Hz, 1H, 13'-H_{syn}), 2.09 (dm, $J = 12.8$ Hz, 1H, 13'-H_{anti}), 2.56 (dd, $J = 17.2$ Hz, $J' = 4.4$ Hz, 1H, 10'-H_{exo}), 2.77 (m, 1H, 7'-H), 2.86 (br d, $J = 17.6$ Hz, 1H, 6'-H_{endo}), 3.19 (t, $J = 6.8$ Hz, 2H, 1-H_2), superimposed in part 3.20 (dd, $J = 17.6$ Hz, $J' = 5.2$ Hz, 1H, 6'-H_{exo}), 3.46 (m, 1H, 11'-H), 4.00 (t, $J = 7.2$ Hz, 2H, 6-H_2), 4.85 (s, $^{+}$NH, $^{+}$$NH_2$, NH, NH_2), 5.59 (br d, $J = 4.8$ Hz, 1H, 8'-H), 7.57 (dd, $J = 9.2$ Hz, $J' = 2.0$ Hz, 1H, 2'-H), 7.77 (d, $J = 2.0$ Hz, 1H, 4'-H), 8.41 (d, $J = 9.2$ Hz, 1H, 1'-H); ^{13}C NMR (100.6 MHz, CD_3OD) δ 23.5 (CH_3, 9'-CH_3), 27.26 (CH, C11'), 27.29 (CH_2), 27.4 (CH_2) (C3, C4), 27.8 (CH, C7'), 29.3 (CH_2, C13'), 29.8 (CH_2, C2), 31.2 (CH_2, C5), 36.0 (CH_2, C6'), 36.1 (CH_2, C10'), 42.4 (CH_2, C1), 49.5 (CH_2, C6), 115.6 (C, C12a'), 117.6 (C, C11a'), 119.1 (CH, C4'), 125.1 (CH, C8'), 126.7 (CH, C2'), 129.5 (CH, C1'), 134.6 (C, C9'), 140.2 (C, C3'), 141.0 (C, C4a'), 151.3 (C, C5a'), 156.8 (C, C12'), 158.6 (C, guanidine C=N); HRMS (ESI), calcd for ($C_{24}H_{32}{}^{35}ClN_5 + H^+$) 426.2419, found 426.2414.

4.1.2. 1-{9-[(3-Chloro-6,7,10,11-tetrahydro-9-methyl-7,11-methanocycloocta[*b*]quinolin-12-yl)amino]nonyl}guanidine (6e)

It was prepared as described for **6b**. From amine **5e** (50 mg, 0.12 mmol) and 1*H*-pyrazole-1-carboxamidine hydrochloride (21 mg, 0.14 mmol), a brownish solid residue (39 mg) was obtained. This crude product was taken in MeOH (2 mL) and eluted through a Dowex™ Marathon™ A OH^- anion exchange resin (5 g) using MeOH (500 mL) as the eluent, to provide **6e** (33 mg, 59% yield) as a brownish oil.

6e·2HCl: brownish solid; mp 210–211 ºC; IR (ATR) ν 3500–2500 (max at 3250, 3137, 2923, 2852, $^{+}$NH, NH, CH st), 1630, 1577, 1513 (C=N, Ar–C–C, Ar–C–N st) cm^{-1}; ^{1}H NMR (400 MHz, CD_3OD) δ 1.34–1.48 (complex signal, 10H, 3-H_2, 4-H_2, 5-H_2, 6-H_2, 7-H_2), superimposed in part 1.56 (m, 2H, 2-H_2), 1.59 (s, 3H, 9'-CH_3), 1.86 (tt, J = J' = 7.2 Hz, 2H, 8-H_2), 1.93 (br d, J = 17.6 Hz, 1H, 10'-H_{endo}), superimposed in part 1.94 (dm, J = 12.4 Hz, 1H, 13'-H_{syn}), 2.09 (dm, J = 12.4 Hz, 1H, 13'-H_{anti}), 2.55 (dd, J = 17.6 Hz, J' = 4.4 Hz, 1H, 10'-H_{exo}), 2.77 (m, 1H, 7'-H), 2.86 (br d, J = 18.0 Hz, 1H, 6'-H_{endo}), 3.16 (t, J = 7.2 Hz, 2H, 1-H_2), 3.21 (dd, J = 18.0 Hz, J' = 5.6 Hz, 1H, 6'-H_{exo}), 3.45 (m, 1H, 11'-H), 3.98 (t, J = 7.2 Hz, 2H, 9-H_2), 4.85 (s, $^{+}$NH, $^{+}NH_2$, NH, NH_2), 5.59 (br d, J = 4.4 Hz, 1H, 8'-H), 7.56 (dd, J = 9.2 Hz, J' = 2.4 Hz, 1H, 2'-H), 7.77 (d, J = 2.4 Hz, 1H, 4'-H), 8.40 (d, J = 9.2 Hz, 1H, 1'-H); ^{13}C NMR (100.6 MHz, CD_3OD) δ 23.5 (CH_3, 9'-CH_3), 27.3 (CH, C11'), 27.7 (CH_2), 27.8 [(CH, C7') + CH_2] (C3, C7), 29.3 (CH_2, C13'), 29.9 (CH_2, C2), 30.3 (2CH_2), 30.6 (CH_2) (C4, C5, C6), 31.3 (CH_2, C8), 36.0 (CH_2, C6'), 36.1 (CH_2, C10'), 42.5 (CH_2, C1), 49.6 (CH_2, C9), 115.7 (C, C12a'), 117.6 (C, C11a'), 119.1 (CH, C4'), 125.1 (CH, C8'), 126.6 (CH, C2'), 129.5 (CH, C1'), 134.5 (C, C9'), 140.3 (C, C3'), 141.0 (C, C4a'), 151.2 (C, C5a'), 156.9 (C, C12'), 158.6 (C, guanidine C=N); HRMS (ESI), calcd for ($C_{27}H_{38}{}^{35}ClN_5 + H^+$) 468.2889, found 468.2903.

4.1.3. 3-Chloro-6,7,10,11-tetrahydro-9-methyl-12-[(3-piperidinopropyl)amino]-7,11-methanocycloocta[*b*]quinoline (7)

A mixture of huprine Y, **1** (500 g, 1.76 mmol), finely powdered KOH (85% purity, 346 mg, 5.24 mmol), and 4 Å molecular sieves in anhydrous DMSO (4 mL) was stirred, heating every 10 min approximately with a heat gun for 1 h and at rt for an additional hour, and then treated with a solution of 1-(3-chloropropyl)piperidine hydrochloride (429 mg, 2.17 mmol) in anhydrous DMSO (2.5 mL). The reaction mixture was stirred at room temperature overnight, diluted with H_2O (50 mL) and extracted with CH_2Cl_2 (3 × 25 mL). The combined organic extracts were washed with H_2O (3 × 100 mL), dried over anhydrous Na_2SO_4, and evaporated at reduced pressure to give a yellowish solid (413 mg), which was purified by column chromatography (40–60 µm silica gel, CH_2Cl_2/MeOH/50% aq. NH_4OH mixtures, gradient elution). On elution with CH_2Cl_2/MeOH/50% aq. NH_4OH 99:1:0.4 , piperidinopropylhuprine **7** (35 mg, 5% yield) was isolated as a yellowish oil; R_f 0.38 (CH_2Cl_2/MeOH/50% aq. NH_4OH 9:1:0.1).

A solution of **7** (74 mg, 0.18 mmol) in CH_2Cl_2 (3 mL) was filtered through a 0.2 μm NYL filter, treated with HCl / Et_2O (2.36 N, 0.16 mL, 0.38 mmol), and evaporated under reduced pressure. The resulting solid was washed with pentane (3 × 2 mL) to give, after drying under standard conditions, **7**·2HCl (81 mg) as a pale yellow solid; mp 189–190 ºC (dec.); IR (ATR) *ν* 3500–2500 (max at 3370, 3261, 3070, 2932, $^{+}$NH, NH, CH st), 1630, 1580, 1513 (Ar–C–C, Ar–C–N st) cm^{-1}; ^{1}H NMR (400 MHz, CD_3OD) *δ* 1.59 (s, 3H, 9-CH_3), superimposed 1.86–1.96 [complex signal, 6H, piperidine 3(5)-H_2, piperidine 4-H_2], 1.93 (br d, *J* = 17.2 Hz, 1H, 10-H_{endo}), superimposed in part 1.97 (dm, *J* = 12.4 Hz, 1H, 13-H_{syn}), 2.10 (dm, *J* =12.4 Hz, 1H, 13-H_{anti}), 2.37 (tt, *J* = 7.6 Hz, *J'* = 7.2 Hz, 2H, 2'-H_2), 2.59 (dd, *J* = 17.2 Hz, *J'* = 4.8 Hz, 1H, 10-H_{exo}), 2.79 (m, 1H, 7-H), 2.89 (br d, *J* = 17.6 Hz, 1H, 6-H_{endo}), 2.90–3.06 [br signal, 2H, piperidine 2(6)-H_{ax}], 3.23 (dd, *J* = 17.6 Hz, *J'* = 5.6 Hz, 1H, 6-H_{exo}), 3.25 (t, *J* = 7.6 Hz, 2H, 3'-H_2), 3.53 (m, 1H, 11-H), 3.50–3.62 [br signal, 2H, piperidine 2(6)-H_{eq}], 4.08 (t, *J* = 7.2 Hz, 2H, 1'-H_2), 4.85 (s, $^{+}$NH, NH), 5.59 (br d, *J* = 4.8 Hz, 1H, 8-H), 7.61 (dd, *J* = 9.2 Hz, *J'* = 2.0 Hz, 1H, 2-H), 7.79 (d, *J* = 2.0 Hz, 1H, 4-H), 8.41 (d, *J* = 9.2 Hz, 1H, 1-H); ^{13}C NMR (100.6 MHz, CD_3OD) *δ* 22.7 (CH_2, piperidine C4), 23.4 (CH_3, 9-CH_3), 24.2 [2CH_2, piperidine C3(5)], 26.0 (CH_2, C2'), 27.3 (CH, C11), 27.8 (CH, C7), 29.2 (CH_2, C13), 36.1 (CH_2, C6), 36.3 (CH_2, C10), 46.5 (CH_2, C1'), 54.4 [2CH_2, piperidine C2(6)], 55.3 (CH_2, C3'), 115.8 (C, C12a), 118.3 (C, C11a), 119.2 (CH, C4), 125.1 (CH, C8), 127.1 (CH, C2), 129.2 (CH, C1), 134.6 (C, C9), 140.3 (C, C3), 140.9 (C, C4a), 151.8 (C, C5a), 156.8 (C, C12); HRMS (ESI), calcd for ($C_{25}H_{32}{}^{35}ClN_3 + H^+$) 410.2358, found 410.2365.

4.1.4. (±)-3-Chloro-6,7,10,11-tetrahydro-9-methyl-12-[(3-morpholinopropyl)amino]-7,11-methanocycloocta[*b*]quinoline (8)

It was prepared as described for **7**. From **1** (500 mg, 1.76 mmol) and 3-morpholinopropyl methanesulfonate (470 mg, 2.10 mmol), a brownish oily residue (543 mg) was obtained and purified by column chromatography (40–60 μm silica gel, CH_2Cl_2 / 50% aq. NH_4OH 100:0.4), to give morpholinopropylhuprine **8** (121 mg, 17% yield) as a yellow oil; R_f 0.42 (CH_2Cl_2/MeOH/50% aq. NH_4OH 9:1:0.1).
8·2HCl: pale yellow solid; mp 173–174 ºC (dec.); IR (ATR) *ν* 3500–2500 (max at 3384, 3225, 3109, 3048, 2922, 2790, 2728, 2683, 2610, $^{+}$NH, NH, CH st), 1631, 1582, 1563, 1512 (Ar–C–C, Ar–C–N st) cm^{-1}; ^{1}H NMR (400 MHz, CD_3OD) *δ* 1.59 (s, 3H), 1.93 (br

d, J = 17.2 Hz, 1H, 10-H_{endo}), superimposed in part 1.97 (dm, J = 12.8 Hz, 1H, 13-H_{syn}), 2.10 (dm, J = 12.8 Hz, 1H, 13-H_{anti}), 2.39 (tt, $J = J'$ = 7.2 Hz, 2H, 2'-H_2), 2.59 (dd, J = 17.2 Hz, J' = 4.8 Hz, 1H, 10-H_{exo}), 2.78 (m, 1H, 7-H), 2.89 (br d, J = 18.0 Hz, 1H, 6-H_{endo}), superimposed 3.12–3.22 (m, 2H, 3'-H_2), 3.23 (dd, J = 18.0 Hz, J' = 5.2 Hz, 1H, 6-H_{exo}), superimposed with the CD_3OD signal 3.28–3.36 [br signal, 2H, morpholine 3(5)-H_{ax}], 3.53 (m, 1H, 11-H), superimposed 3.46–3.58 (br signal, 2H, morpholine 3(5)-H_{eq}], 3.82–3.93 [br signal, 2H, morpholine 2(6)-H_{ax}], 4.02–4.08 [br signal, 2H, morpholine 2(6)-H_{eq}], 4.10 (t, J = 7.2 Hz, 2H, 1'-H_2), 4.85 (s, $^+$NH, NH), 5.59 (br d, J = 4.8 Hz, 1H, 8-H), 7.61 (dd, J = 9.6 Hz, J' = 2.0 Hz, 1H, 2-H), 7.79 (d, J = 2.0 Hz, 1H, 4-H), 8.41 (d, J = 9.6 Hz, 1H, 1-H); ^{13}C NMR (100.6 MHz, CD_3OD) δ 23.5 (CH_3, 9-CH_3), 25.7 (CH_2, C2'), 27.3 (CH, C11), 27.9 (CH, C7), 29.2 (CH_2, C13), 36.1 (CH_2, C6), 36.4 (CH_2, C10), 46.5 (CH_2, C1'), 53.3 [2CH_2, morpholine C3(5)], 55.6 (CH_2, C3'), 65.1 [2CH_2, morpholine C2(6)], 115.8 (C, C12a), 118.3 (C, C11a), 119.3 (CH, C4), 125.1 (CH, C8), 127.2 (CH, C2), 129.3 (CH, C1), 134.7 (C, C9), 140.3 (C, C3), 140.9 (C, C4a), 151.8 (C, C5a), 156.9 (C, C12); HRMS (ESI), calcd for ($C_{24}H_{30}{}^{35}ClN_3O$ + H^+) 412.2150, found 412.2164.

4.1.5. 7-[(1,2,3,4-Tetrahydroacridin-9-yl)amino]heptanenitrile (11c)[53]

A suspension of tacrine, **9** (1.70 g, 8.57 mmol) and finely powdered KOH (85% purity, 0.97 g, 14.7 mmol), and 4 Å molecular sieves in anhydrous DMSO (20 mL) was stirred, heating every 10 min approximately with a heat gun for 1 h and at room temperature one additional hour, and then treated with a solution of 7-bromoheptanenitrile (90% purity, 1.55 mL, 1.96 g, 9.28 mmol) in anhydrous DMSO (12 mL) dropwise during 30 minutes. The reaction mixture was stirred at room temperature overnight, diluted with 5 N NaOH (50 mL) and extracted with EtOAc (3 × 150 mL). The combined organic extracts were washed with H_2O (4 × 100 mL), dried over anhydrous Na_2SO_4, and evaporated under reduced pressure to give a crude product (2.53 g). Purification of this residue by column chromatography (40–60 µm silica gel, CH_2Cl_2/50% aq. NH_4OH 100:0.2) afforded a 85:15 mixture of the dialkylated byproduct and nitrile **11c** (190 mg) and pure nitrile **11c** (1.75 g, 66% isolated yield) as a yellow oil; R_f 0.77 (CH_2Cl_2/MeOH/50% aq. NH_4OH 9:1:0.05).

A solution of **11c** (79 mg, 0.26 mmol) in CH_2Cl_2 (15 mL) was filtered through a 0.2 µm NYL filter, treated with methanolic HCl (0.53 N, 2.15 mL, 1.14 mmol) and evaporated

under reduced pressure. The resulting solid was taken in MeOH (0.20 mL) and precipitated by addition of EtOAc (0.60 mL). The precipitate was washed with pentane (3 × 2 mL) to give, after drying under standard conditions, **11c**·HCl (39 mg) as a pale brown sticky solid; IR (ATR) *ν* 3500–2500 (max at 3237, 2932, 2860, 2770, $^{+}$NH, NH, CH st), 2242 (CN st), 1633, 1586, 1573, 1523 (Ar–C–C, Ar–C–N st) cm^{-1}; ^{1}H NMR (400 MHz, CD_3OD) *δ* 1.46–1.54 (complex signal, 4H, 4-H_2, 5-H_2), 1.66 (tt, *J* = 7.2 Hz, *J'* = 6.8 Hz, 2H, 3-H_2), 1.86 (tt, *J* = 7.2 Hz, *J'* = 6.8 Hz, 2H, 6-H_2), 1.94–2.02 (complex signal, 4H, 2'-H_2, 3'-H_2), 2.44 (t, *J* = 6.8 Hz, 2H, 2-H_2), 2.71 (br t, *J* = 5.6 Hz, 2H, 1'-H_2), 3.02 (br t, *J* = 6.0 Hz, 2H, 4'-H_2), 3.97 (t, *J* = 7.2 Hz, 2H, 7-H_2), 4.85 (s, $^{+}$NH, NH), 7.59 (dd, *J* = 8.4 Hz, *J'* = 7.6 Hz, 1H, 7'-H), 7.77 (d, *J* = 8.8 Hz, 1H, 5'-H), 7.85 (dd, *J* = 8.8 Hz, *J'* = 7.6 Hz, 1H, 6'-H), 8.40 (d, *J* = 8.4 Hz, 1H, 8'-H); ^{13}C NMR (100.6 MHz, CD_3OD) *δ* 17.2 (CH_2, C2), 21.8 (CH_2, C3'), 23.0 (CH_2, C2'), 24.9 (CH_2, C1'), 26.3 (CH_2, C3), 26.9 (CH_2, C5), 29.30 (CH_2), 29.33 (CH_2) (C4, C4'), 31.2 (CH_2, C6), 49.0 (CH_2, C7), 112.9 (C, C9a'), 117.1 (C, C8a'), 120.1 (CH, C5'), 121.1 (C, C1), 126.3 (CH, C7'), 126.5 (CH, C8'), 134.1 (CH, C6'), 139.8 (C, C10a'), 151.7 (C, C4a'), 158.0 (C, C9'); HRMS (ESI), calcd for ($C_{20}H_{25}N_3$ + H^+) 308.2121, found 308.2117.

4.1.6. 9-[(1,2,3,4-Tetrahydroacridin-9-yl)amino]nonanenitrile (11e)

It was prepared as described for **11c**. From **9** (500 mg, 2.52 mmol) and 9-bromononanenitrile (659 mg, 3.02 mmol), a yellowish oily residue (984 mg) was obtained and purified by column chromatography (40–60 μm silica gel, CH_2Cl_2/MeOH/50% aq. NH_4OH mixtures, gradient elution). On elution with CH_2Cl_2/MeOH/50% aq. NH_4OH 99.9:0.1:0.4 to 99.7:0.3:0.4, nitrile **11e** (272 mg, 32% yield) was isolated as a yellow oil; R_f 0.51 (CH_2Cl_2/MeOH/50% aq. NH_4OH 9:1:0.1).

11e·HCl: yellow sticky solid; IR (ATR) *ν* 3500–2500 (max at 3268, 2931, 2848, 2756, 2700, 2667, $^{+}$NH, NH, CH st), 2241 (CN st), 1630, 1590, 1572, 1522 (Ar–C–C, Ar–C–N st) cm^{-1}; ^{1}H NMR (400 MHz, CD_3OD) *δ* 1.34–1.48 (complex signal, 8H, 4-H_2, 5-H_2, 6-H_2, 7-H_2), 1.62 (tt, *J* = *J'* = 7.2 Hz, 2H, 3-H_2), 1.84 (tt, *J* = *J'* = 7.2 Hz, 2H, 8-H_2), 1.94–2.00 (complex signal, 4H, 2'-H_2, 3'-H_2), 2.42 (t, *J* = 7.2 Hz, 2H, 2-H_2), 2.71 (br t, *J* = 5.6 Hz, 2H, 1'-H_2), 3.02 (br t, *J* = 6.0 Hz, 2H, 4'-H_2), 3.96 (t, *J* = 7.2 Hz, 2H, 9-H_2), 4.85 (s, $^{+}$NH, NH), 7.59 (ddd, *J* = 8.4 Hz, *J'* = 7.2 Hz, *J"* = 1.2 Hz, 1H, 7'-H), 7.75 (br d, *J* = 7.6 Hz, 1H, 5'-H), 7.85 (ddd, *J* = 7.6 Hz, *J'* = 7.2 Hz, *J"* = 1.2 Hz, 1H, 6'-H),

8.40 (br d, J = 8.4 Hz, 1H, 8'-H); ^{13}C NMR (100.6 MHz, CD_3OD) δ 17.3 (CH_2, C2), 21.8 (CH_2, C3'), 23.0 (CH_2, C2'), 24.8 (CH_2, C1'), 26.3 (CH_2, C3), 27.5 (CH_2, C7), 29.3 (CH_2, C4'), 29.5 (CH_2), 29.6 (CH_2), 29.9 (CH_2) (C4, C5, C6), 31.4 (CH_2, C8), 49.1 (CH_2, C9), 112.8 (C, C9a'), 117.0 (C, C8a'), 120.1 (CH, C5'), 121.3 (C, C1), 126.3 (CH, C7'), 126.5 (CH, C8'), 134.1 (CH, C6'), 139.8 (C, C10a'), 151.7 (C, C4a'), 158.0 (C, C9'); HRMS (ESI), calcd for ($C_{22}H_{29}N_3 + H^+$) 336.2434, found 336.2436.

4.1.7. 7-[(6-Chloro-1,2,3,4-tetrahydroacridin-9-yl)amino]heptanenitrile (12c)[53]

It was prepared as described for **11c**. From 6-chlorotacrine, **10** (2.00 g, 8.59 mmol), and 7-bromoheptanenitrile (90% purity, 1.55 mL, 1.96 g, 9.28 mmol), a yellow oily residue (3.06 g) was obtained. Purification of this residue by column chromatography (40–60 µm silica gel, CH_2Cl_2/50% aq. NH_4OH 100:0.2) afforded a 87:13 mixture of dialkylated byproduct and nitrile **12c** (789 mg) and pure nitrile **12c** (2.06 g, 70% isolated yield) as a yellow oil; R_f 0.92 (CH_2Cl_2/MeOH/50% aq. NH_4OH 9:1:0.05).

12c·HCl: yellowish solid; mp 86–87 °C; IR (ATR) ν 3500–2500 (max at 3347, 3138, 3059, 2949, 2928, 2858, 2744, $^+$NH, NH, CH st), 2245 (CN st), 1639, 1605, 1573, 1524 (Ar–C–C, Ar–C–N st) cm^{-1}; ^{1}H NMR (400 MHz, CD_3OD) δ 1.46–1.54 (complex signal, 4H, 4-H_2, 5-H_2), 1.66 (tt, J = 7.2 Hz, J' = 6.8 Hz, 2H, 3-H_2), 1.87 (tt, J = J' = 7.2 Hz, 2H, 6-H_2), 1.92–2.02 (complex signal, 4H, 2'-H_2, 3'-H_2), 2.45 (t, J = 7.2 Hz, 2H, 2-H_2), 2.69 (br t, J = 6.0 Hz, 2H, 1'-H_2), 3.01 (br t, J = 5.6 Hz, 2H, 4'-H_2), 3.96 (t, J = 7.2 Hz, 2H, 7-H_2), 4.84 (s, $^+$NH, NH), 7.56 (dd, J = 9.2 Hz, J' = 2.4 Hz, 1H, 7'-H), 7.79 (d, J = 2.4 Hz, 1H, 5'-H), 8.39 (d, J = 9.2 Hz, 1H, 8'-H); ^{13}C NMR (100.6 MHz, CD_3OD) δ 17.2 (CH_2, C2), 21.7 (CH_2, C3'), 22.9 (CH_2, C2'), 24.8 (CH_2, C1'), 26.3 (CH_2, C3), 26.9 (CH_2, C5), 29.29 (CH_2), 29.34 (CH_2) (C4, C4'), 31.1 (CH_2, C6), 49.1 (CH_2, C7), 113.4 (C), 115.4 (C) (C8a', C9a'), 119.1 (CH, C5'), 121.2 (C, C1), 126.8 (CH, C7'), 128.8 (CH, C8'), 140.1 (CH, C6'), 140.5 (C, C10a'), 152.2 (C, C4a'), 157.8 (C, C9'); HRMS (ESI), calcd for ($C_{20}H_{24}{}^{35}ClN_3 + H^+$) 342.1732, found 342.1737.

4.1.8. 8-[(6-Chloro-1,2,3,4-tetrahydroacridin-9-yl)amino]octanenitrile (12d)

It was prepared as described for **11c**. From 6-chlorotacrine, **10** (1.00 g, 4.30 mmol), and 8-bromooctanenitrile (1.01 g, 4.95 mmol), a yellow oily residue (1.73 g) was obtained. Purification of this crude by column chromatography (40–60 µm silica gel, CH_2Cl_2/50%

aq. NH_4OH 100:0.4), nitrile **12d** (411 mg, 27% yield) as a yellow oil; R_f 0.80 (CH_2Cl_2/MeOH/50% aq. NH_4OH 9:1:0.1).

12d·HCl: yellowish solid; mp 210–213 °C; IR (ATR) *ν* 3500–2500 (max at 3251, 3052, 2934, 2853, 2711, $^+$NH, NH, CH st), 2246 (CN st), 1633, 1616, 1588, 1567, 1542, 1517 (Ar–C–C, Ar–C–N st) cm^{-1}; ^1H NMR (400 MHz, CD_3OD) δ 1.40–1.52 (complex signal, 6H, 4-H_2, 5-H_2, 6-H_2), 1.63 (tt, $J = J' = 7.2$ Hz, 2H, 3-H_2), 1.85 (tt, $J = J' = 7.2$ Hz, 2H, 7-H_2), 1.92–2.00 (complex signal, 4H, 2'-H_2, 3'-H_2), 2.43 (t, $J = 7.2$ Hz, 2H, 2-H_2), 2.68 (br t, $J = 6.0$ Hz, 2H, 1'-H_2), 3.00 (br t, $J = 6.0$ Hz, 2H, 4'-H_2), 3.95 (t, $J = 7.2$ Hz, 2H, 8-H_2), 4.85 (s, $^+$NH, NH), 7.57 (dd, $J = 9.2$ Hz, $J' = 2.0$ Hz, 1H, 7'-H), 7.77 (d, $J = 2.0$ Hz, 1H, 5'-H), 8.39 (d, $J = 9.2$ Hz, 1H, 8'-H); ^{13}C NMR (100.6 MHz, CD_3OD) δ 17.2 (CH_2, C2), 21.8 (CH_2, C3'), 22.9 (CH_2, C2'), 24.7 (CH_2, C1'), 26.3 (CH_2, C3), 27.4 (CH_2, C6), 29.36 (CH_2), 29.40 (CH_2) (C4, C4'), 29.5 (CH_2, C5), 31.2 (CH_2, C7), 49.2 (CH_2, C8), 113.4 (C), 115.5 (C) (C8a', C9a'), 119.2 (CH, C5'), 121.2 (C, C1), 126.8 (CH, C7'), 128.8 (CH, C8'), 140.1 (CH, C6'), 140.6 (C, C10a'), 152.2 (C, C4a'), 157.8 (C, C9'); HRMS (ESI), calcd for ($C_{21}H_{26}{}^{35}ClN_3 + H^+$) 356.1888, found 356.1878.

4.1.9. 9-[(6-Chloro-1,2,3,4-tetrahydroacridin-9-yl)amino]nonanenitrile (12e)

It was prepared as described for **11c**. From 6-chlorotacrine, **10** (500 mg, 2.15 mmol), and 9-bromononanenitrile (561 mg, 2.57 mmol), a yellow oily residue (849 mg) was obtained and purified by column chromatography (40–60 μm silica gel, CH_2Cl_2/MeOH/50% aq. NH_4OH mixtures, gradient elution). On elution with CH_2Cl_2/MeOH/50% aq. NH_4OH 100:0:0.4 to 99.8:0.2:0.4, nitrile **12e** (380 mg, 48% yield) was isolated as a yellow oil; R_f 0.82 (CH_2Cl_2/MeOH/50% aq. NH_4OH 9:1:0.1).

12e·HCl: yellowish solid; mp 176–177 ºC; IR (ATR) *ν* 3500–2500 (max at 3248, 3048, 2931, 2852, 2714, $^+$NH, NH, CH st), 2246 (CN st), 1632, 1589, 1566, 1523 (Ar–C–C, Ar–C–N st) cm^{-1}; ^1H NMR (400 MHz, CD_3OD) δ 1.36–1.50 (complex signal, 8H, 4-H_2, 5-H_2, 6-H_2, 7-H_2), 1.62 (tt, $J = J' = 7.2$ Hz, 2H, 3-H_2), 1.84 (tt, $J = J' = 7.2$ Hz, 2H, 8-H_2), 1.92–2.02 (complex signal, 4H, 2'-H_2, 3'-H_2), 2.43 (t, $J = 7.2$ Hz, 2H, 2-H_2), 2.68 (br t, $J = 6.0$ Hz, 2H, 1'-H_2), 3.00 (br t, $J = 6.4$ Hz, 2H, 4'-H_2), 3.95 (t, $J = 7.2$ Hz, 2H, 9-H_2), 4.85 (s, $^+$NH, NH), 7.56 (dd, $J = 9.2$ Hz, $J' = 2.0$ Hz, 1H, 7'-H), 7.78 (d, $J = 2.0$ Hz, 1H, 5'-H), 8.39 (d, $J = 9.2$ Hz, 1H, 8'-H); ^{13}C NMR (100.6 MHz, CD_3OD) δ 17.3 (CH_2, C2), 21.8 (CH_2, C3'), 22.9 (CH_2, C2'), 24.7 (CH_2, C1'), 26.4 (CH_2, C3), 27.6

(CH_2, C7), 29.3 (CH_2, C4'), 29.6 (CH_2), 29.7 (CH_2), 30.0 (CH_2) (C4, C5, C6), 31.3 (CH_2, C8), 49.2 (CH_2, C9), 113.4 (C), 115.5 (C) (C8a', C9a'), 119.2 (CH, C5'), 121.2 (C, C1), 126.8 (CH, C7'), 128.8 (CH, C8'), 140.1 (CH, C6'), 140.5 (C, C10a'), 152.1 (C, C4a'), 157.9 (C, C9'); HRMS (ESI), calcd for ($C_{22}H_{28}{}^{35}ClN_3 + H^+$) 370.2045, found 370.2037.

4.1.10. 1-{7-[(1,2,3,4-Tetrahydroacridin-9-yl)amino]heptyl}guanidine (15c)

It was prepared as described for **6b**. From amine **13c** (100 mg, 0.32 mmol) and 1*H*-pyrazole-1-carboxamidine hydrochloride (57 mg, 0.39 mmol), a brownish solid residue (87 mg) was obtained. This crude product was taken in MeOH (2 mL) and eluted through a Dowex™ Marathon™ A OH^- anion exchange resin (5 g) using MeOH (500 mL) as the eluent, to provide guanidine **15c** (81 mg, 72% yield) as a brownish oil.

15c·2HCl: brownish sticky solid; IR (ATR) *v* 3500–2500 (max at 3257, 3132, 2930, 2858, $^+$NH, NH, CH st), 1631, 1574, 1520 (C=N, Ar–C–C, Ar–C–N st) cm^{-1}; ^{1}H NMR (400 MHz, CD_3OD) δ 1.38−1.50 (complex signal, 6H, 3-H_2, 4-H_2, 5-H_2), 1.59 (tt, $J = J'$ = 6.8 Hz, 2H, 2-H_2), 1.86 (tt, $J = J'$ = 7.2 Hz, 2H, 6-H_2), 1.92–2.02 (complex signal, 4H, 2'-H_2, 3'-H_2), 2.71 (br t, J = 5.2 Hz, 2H, 1'-H_2), 3.02 (t, J = 5.6 Hz, 2H, 4'-H_2), 3.16 (t, J = 6.8 Hz, 2H, 1-H_2), 3.96 (t, J = 7.2 Hz, 2H, 7-H_2), 4.85 (s, $^+$NH, $^+NH_2$, NH, NH_2), 7.59 (ddd, J = 8.4 Hz, J'= 6.8 Hz, J'' = 1.6 Hz, 1H, 7'-H), 7.76 (dd, J = 8.4 Hz, J' = 1.6 Hz, 1H, 5'-H), 7.86 (ddd, J = 8.4 Hz, J' = 6.8 Hz, J'' = 1.2 Hz, 1H, 6'-H), 8.40 (br d, J = 8.4 Hz, 1H, 8'-H); ^{13}C NMR (100.6 MHz, CD_3OD) δ 21.8 (CH_2, C3'), 23.0 (CH_2, C2'), 24.9 (CH_2, C1'), 27.57 (CH_2), 27.63 (CH_2) (C3, C5), 29.3 (CH_2, C4'), 29.8 (CH_2), 29.9 (CH_2) (C2, C4), 31.5 (CH_2, C6), 42.4 (CH_2, C1), 49.1 (CH_2, C7), 112.8 (C, C9a'), 117.0 (C, C8a'), 120.1 (CH, C5'), 126.3 (CH, C7'), 126.5 (CH, C8'), 134.1 (CH, C6'), 139.8 (C, C10a'), 151.7 (C, C4a'), 158.0 (C, C9'), 158.5 (C, guanidine C=N); HRMS (ESI), calcd for ($C_{21}H_{31}N_5 + H^+$) 354.2652, found 354.2665.

4.1.11. 1-{9-[(1,2,3,4-Tetrahydroacridin-9-yl)amino]nonyl}guanidine (15e)

It was prepared as described for **6b**. From **13e**·HCl (47 mg, 0.12 mmol) and 1*H*-pyrazole-1-carboxamidine hydrochloride (21 mg, 0.14 mmol), a brownish solid residue (46 mg) was obtained. This crude product was taken in MeOH (2 mL) and eluted

through a Dowex™ Marathon™ A OH^- anion exchange resin (5 g) using MeOH (500 mL) as the eluent, to provide guanidine **15e** (35 mg, 76% yield) as a brownish oil.

15e·2HCl: brownish sticky solid; IR (ATR) *ν* 3500–2500 (max at 3256, 3132, 2926, 2852, $^+$NH, NH, CH st), 1661, 1631, 1575, 1521 (C=N, Ar–C–C, Ar–C–N st) cm^{-1}; ^1H NMR (400 MHz, CD_3OD) *δ* 1.34–1.48 (complex signal, 10H, 3-H_2, 4-H_2, 5-H_2, 6-H_2, 7-H_2), 1.58 (tt, *J* = *J'* = 6.8 Hz, 2H, 2-H_2), 1.84 (tt, *J* = *J'* = 7.2 Hz, 2H, 8-H_2), 1.94–2.00 (complex signal, 4H, 2'-H_2, 3'-H_2), 2.70 (br t, *J* = 6.0 Hz, 2H, 1'-H_2), 3.02 (br t, *J* = 6.4 Hz, 2H, 4'-H_2), 3.16 (t, *J* = 6.8 Hz, 2H, 1-H_2), 3.95 (t, *J* = 7.2 Hz, 2H, 9-H_2), 4.85 (s, $^+$NH, $^+NH_2$, NH, NH_2), 7.59 (ddd, *J* = 8.8 Hz, *J'* = 6.8 Hz, *J"* = 1.2 Hz, 1H, 7'-H), 7.76 (dd, *J* = 8.4 Hz, *J'* = 1.2 Hz, 1H, 5'-H), 7.85 (ddd, *J* = 8.4 Hz, *J'* = 6.8 Hz, *J"* = 1.2 Hz, 1H, 6'-H), 8.40 (br d, *J* = 8.8 Hz, 1H, 8'-H); ^{13}C NMR (100.6 MHz, CD_3OD) *δ* 21.8 (CH_2, C3'), 22.9 (CH_2, C2'), 24.9 (CH_2, C1'), 27.6 ($2CH_2$, C3, C7), 29.3 (CH_2, C4'), 29.8 (CH_2, C2), 30.1 ($2CH_2$), 30.4 (CH_2) (C4, C5, C6), 31.5 (CH_2, C8), 42.4 (CH_2, C1), 49.1 (CH_2, C9), 112.8 (C, C9a'), 116.9 (C, C8a'), 120.1 (CH, C5'), 126.3 (CH, C7'), 126.4 (CH, C8'), 134.1 (CH, C6'), 139.7 (C, C10a'), 151.6 (C, C4a'), 157.9 (C, C9'), 158.5 (C, guanidine C=N); HRMS (ESI), calcd for ($C_{23}H_{35}N_5 + H^+$) 382.2965, found 382.2975.

4.1.12. 1-{9-[(6-Chloro-1,2,3,4-tetrahydroacridin-9-yl)amino]nonyl}guanidine (16e)

It was prepared as described for **6b**. From **14e**·HCl (90 mg, 0.22 mmol) and 1*H*-pyrazole-1-carboxamidine hydrochloride (39 mg, 0.27 mmol), a brownish solid residue (81 mg) was obtained. This crude product was taken in MeOH (2 mL) and eluted through a Dowex™ Marathon™ A OH^- anion exchange resin (5 g) using MeOH (500 mL) as the eluent, to provide guanidine **16e** (61 mg, 67% yield) as a brownish oil.

16e·2HCl: brownish solid; mp 209–210 ºC; IR (ATR) *ν* 3500–2500 (max at 3253, 3126, 2928, 2855, $^+$NH, NH, CH st), 1631, 1572, 1514 (C=N, Ar–C–C, Ar–C–N st) cm^{-1}; ^1H NMR (400 MHz, CD_3OD) *δ* 1.38–1.52 (complex signal, 10H, 3-H_2, 4-H_2, 5-H_2, 6-H_2, 7-H_2), 1.60 (tt, *J* = *J'* = 6.8 Hz, 2H, 2-H_2), 1.86 (tt, *J* = *J'* = 7.2 Hz, 2H, 8-H_2), 1.92–2.02 (complex signal, 4H, 2'-H_2, 3'-H_2), 2.68 (br t, *J* = 6.0 Hz, 2H, 1'-H_2), 3.00 (br t, *J* = 6.0 Hz, 2H, 4'-H_2), 3.17 (t, *J* = 6.8 Hz, 2H, 1-H_2), 3.95 (t, *J* = 7.2 Hz, 2H, 9-H_2), 4.85 (s, $^+$NH, $^+NH_2$, NH, NH_2), 7.57 (dd, *J* = 9.2 Hz, *J'* = 2.4 Hz, 1H, 7'-H), 7.79 (d, *J* = 2.4 Hz, 1H, 5'-H), 8.40 (d, *J* = 9.2 Hz, 1H, 8'-H); ^{13}C NMR (100.6 MHz, CD_3OD) *δ* 21.8 (CH_2,

C3'), 22.9 (CH_2, C2'), 24.8 (CH_2, C1'), 27.5 (CH_2), 27.6 (CH_2) (C3, C7), 29.3 (CH_2, C4'), 29.7 ($2CH_2$), 29.8 ($2CH_2$) (C2, C4, C5, C6), 31.3 (CH_2, C8), 42.4 (CH_2, C1), 49.2 (CH_2, C9), 113.3 (C), 115.4 (C) (C8a', C9a'), 119.1 (CH, C5'), 126.8 (CH, C7'), 128.8 (CH, C8'), 140.0 (CH, C6'), 140.4 (C, C10a'), 152.1 (C, C4a'), 157.7 (C, C9'), 158.6 (C, guanidine C=N); HRMS (ESI), calcd for ($C_{23}H_{34}{}^{35}ClN_5 + H^+$) 416.2576, found 416.2589.

4.2. Biological assays

4.2.1. *T. brucei* culturing and evaluation of antitrypanosomal activity

Bloodstream form *T. brucei* (strain 221) was cultured at 37 ºC in modified Iscove's medium.[54] Trypanocidal activity was assessed by growing parasites in the presence of various concentrations of the novel compounds and determining the levels which inhibited growth by 50% (IC_{50}) and 90% (IC_{90}). *T. brucei* in the logarithmic phase of growth were diluted back to 2.5×10^4 mL^{-1} and aliquoted into 96-well plates. The compounds were then added at a range of concentrations and the plates incubated at 37 °C. Each drug concentration was tested in triplicate. Resazurin was added after 48 h and the plates incubated for a further 16 h and the plates then read in a Spectramax plate reader. Results were analysed using GraphPad Prism.

4.2.2. Cytotoxic activity against rat skeletal myoblast L6 cells

Cytotoxicity against mammalian cells was assessed using microtitre plates following a described procedure.[55] Briefly, rat skeletal muscle L6 cells were seeded at 1×10^4 mL^{-1} in 200 µL of growth medium containing different compound concentrations. The plates were incubated for 6 days at 37 ºC and 20 µL resazurin was then added to each well. After a further 8 h incubation, the fluorescence was determined using a Spectramax plate reader.

4.2.3. Acetylcholinesterase inhibitory activity

The inhibitory activity against *Electrophorus electricus* (Ee) AChE (Sigma-Aldrich) was evaluated spectrophotometrically by the method of Ellman *et al*.[56] The reactions took place in a final volume of 300 µL of 0.1 M phosphate-buffered solution pH 8.0, containing EeAChE (0.03 u/mL) and 333 µM 5,5'-dithiobis(2-nitrobenzoic) acid (DTNB; Sigma-Aldrich) solution used to produce the yellow anion of 5-thio-2-

nitrobenzoic acid. Inhibition curves were performed in duplicates using at least 10 increasing concentrations of inhibitors and preincubated for 20 min at 37 ºC before adding the substrate. One duplicate sample without inhibitor was always present to yield 100% of AChE activity. Then substrate, acetylthiocholine iodide (450 μM; Sigma-Aldrich), was added and the reaction was developed for 5 min at 37 ºC. The colour production was measured at 414 nm using a labsystems Multiskan spectrophotometer. Data from concentration–inhibition experiments of the inhibitors were calculated by non-linear regression analysis, using the GraphPad Prism program package (GraphPad Software; San Diego, USA), which gave estimates of the IC_{50} (concentration of drug producing 50% of enzyme activity inhibition). Results are expressed as mean ± S.E.M. of at least 4 experiments performed in duplicate.

4.2.4. Determination of brain permeability: PAMPA-BBB assay

The *in vitro* permeability (P_e) of the novel compounds and fourteen commercial drugs through lipid extract of porcine brain membrane was determined by using a parallel artificial membrane permeation assay.[45] Commercial drugs and the target compounds were tested using a mixture of PBS:EtOH 70:30. Assay validation was made by comparing experimental and described permeability values of the commercial drugs, which showed a good correlation: P_e (exp) = 1.6079 P_e (lit) – 1.2585 (R^2 = 0.9217). From this equation and the limits established by Di *et al.* for BBB permeation, three ranges of permeability were established: compounds of high BBB permeation (CNS+): P_e (10^{-6} cm s^{-1}) > 5.17; compounds of low BBB permeation (CNS–): P_e (10^{-6} cm s^{-1}) < 1.95; and compounds of uncertain BBB permeation (CNS±): 5.17 > P_e (10^{-6} cm s^{-1}) > 1.95.

Table 3

Reported and experimental permeabilities (P_e 10^{-6} cm s^{-1}) of 14 commercial drugs used for the PAMPA-BBB assay validation

Compd	Literature value[a]	Experimental value[b]
Cimetidine	0.0	0.7 ± 0.1
Lomefloxacin	1.1	0.7 ± 0.1
Norfloxazin	0.1	0.9 ± 0.1
Ofloxazin	0.8	1.0 ± 0.1

Hydrocortisone	1.9	1.4 ± 0.1
Piroxicam	2.5	2.2 ± 0.1
Clonidine	5.3	6.5 ± 0.1
Corticosterone	5.1	6.7 ± 0.1
Imipramine	13.0	12.3 ± 0.1
Promazine	8.8	13.8 ± 0.3
Progesterone	9.3	16.8 ± 0.3
Desipramine	12.0	17.8 ± 0.1
Testosterone	17.0	26.5 ± 0.4
Verapamil	16.0	28.4 ± 0.5

[a] Taken from Ref. 45.

[b] Values are expressed as the mean ± SD of three independent experiments.

Acknowledgments

This work was supported by Ministerio de Economía y Competitividad (MINECO) (SAF2014-57094-R) and Generalitat de Catalunya (GC) (2014SGR52). JMK acknowledges funding support from the Wellcome Trust (Grant number WT092573MA). Fellowships from GC to I.S., F.J.P.-A., and E.V. are gratefully acknowledged.

Supplementary data

Supplementary data associated with this article can be found, in the online version, at http://dx.doi.org/10.1016/j.bmc.

References

1. Centers for Disease Control and Prevention, Neglected Tropical Diseases, http://www.cdc.gov/globalhealth/ntd/. Accessed June 15th 2016.
2. Hotez, P. J.; Fenwick, A.; Savioli, L.; Molyneux, D. H. *Lancet* **2009**, *373*, 1570.
3. Chibale, K. *Bioorg. Med. Chem.* **2015**, *23*, 5085.
4. Njoroge, M.; Njuguna, N. M.; Mutai, P.; Ongarora, D. S. B.; Smith, P. W.; Chibale, K. *Chem. Rev.* **2014**, *114*, 11138.
5. Woodland, A.; Grimaldi, R.; Luksch, T.; Cleghorn, L. A. T.; Ojo, K. K.; Van Voorhis, W. C.; Brenk, R.; Frearson, J. A.; Gilbert, I. H.; Wyatt, P. G. *ChemMedChem* **2013**, *8*, 1127.

6. World Health Organization, Trypanosomiasis, human African (sleeping sickness), http://www.who.int/mediacentre/factsheets/fs259/en/, accessed on July 5th 2016.
7. Horn, D. *Molec. Biochem. Parasitol.* **2014**, *195*, 123.
8. Barrett, M. P.; Croft, S. L. *Br. Med. Bull.* **2012**, *104*, 175.
9. Mallari, J. P.; Shelat, A. A.; Obrien, T.; Caffrey, C. R.; Kosinski, A.; Connelly, M.; Harbut, M.; Greenbaum, D., McKerrow, J. H.; Guy, R. K. *J. Med. Chem.* **2008**, *51*, 545.
10. Clark, R. L.; Clements, C. J.; Barret, M. P.; Mackay, S. P.; Rathman, R. P.; Owusu-Dapaah, G.; Spencer, J.; Huggan, J. K. *Biooorg. Med. Chem.* **2012**, *20*, 6019.
11. Mäser, P.; Wittlin, S.; Rottmann, M.; Wenzler, T.; Kaiser, M.; Brun, R. *Curr. Opin. Pharmacol.* **2012**, *12*, 562.
12. Shi, P.-Y.; Smith, P. W.; Diagana, T. T. *ACS Infect. Dis.* **2015**, *1*, 76.
13. Carrillo, A. K.; Guiguemde, W. A.; Guy, R. K. *Bioorg. Med. Chem.* **2015**, *23*, 5151.
14. Amata, E.; Bland, N. D.; Hoyt, C. T.; Settimo, L.; Campbell, R. K.; Pollastri, M. P. *Bioorg. Med. Chem. Lett.* **2014**, *24*, 4084.
15. Nagle, A. S.; Khare, S.; Babu Kumar, A.; Supek, F.; Buchynskyy, A.; Mathison, C. J. N.; Kumar Chennamaneni, N.; Pendem, N.; Buckner, F. S.; Gelb, M. H.; Molteni, V. *Chem. Rev.* **2014**, *114*, 11305.
16. Prati, F.; Uliassi, E.; Bolognesi, M. L. *Med. Chem. Commun.* **2014**, *5*, 853.
17. Lizzi, F.; Veronesi, G.; Belluti, F.; Bergamini, C.; López-Sánchez, A.; Kaiser, M.; Brun, R.; Krauth-Siegel, R. L.; Hall, D. G.; Rivas, L.; Bolognesi, M. L. *J. Med. Chem.* **2012**, *55*, 10490.
18. Urich, R.; Grimaldi, R.; Luksch, T.; Frearson, J. A.; Brenk, R.; Wyatt, P. G. *J. Med. Chem.* **2014**, *57*, 7536.
19. Fairlamb, A. H. *Nature* **2012**, *482*, 167.
20. Patrick, D. A.; Wenzler, T.; Yang, S.; Weiser, P. T.; Wang, M. Z.; Brun, R.; Tidwell, R. R. *Bioorg. Med. Chem.* **2016**, *24*, 2451.
21. Cleghorn, L. A. T.; Albrecht, S.; Stojanovski, L.; Simeons, F. R. J.; Norval, S.; Kime, R.; Collie, I. T.; De Rycker, M.; Campbell, L.; Hallyburton, I.; Frearson, J. A.; Wyatt, P. G.; Read, K. D.; Gilbert, I. H. *J. Med. Chem.* **2015**, *58*, 7695.

22. Woodland, A.; Thompson, S.; Cleghorn, L. A. T.; Norcross, N.; De Rycker, M.; Grimaldi, R.; Hallyburton, I.; Rao, B.; Norval, S.; Stojanovski, L.; Brun, R.; Kaiser, M.; Frearson, J. A.; Gray, D. W.; Wyatt, P. G.; Read, K. D.; Gilbert, I. H. *ChemMedChem* **2015**, *10*, 1809.
23. Llurba-Montesino, N.; Kaiser, M.; Brun, R.; Schmidt, T. J. *Molecules* **2015**, *20*, 14118.
24. Annang, F.; Pérez-Moreno, G.; García-Hernández, R.; Cordon-Obras, C.; Martín, J.; Tormo, J. R.; Rodríguez, L.; de Pedro, N.; Gómez-Pérez, V.; Valente, M.; Reyes, F.; Genilloud, O.; Vicente, F.; Castanys, S.; Ruiz-Pérez, L. M.; Navarro, M.; Gamarro, F.; González-Pacanowska, D. *J. Biomol. Screening* **2015**, *20*, 82.
25. Tatipaka, H. B.; Gillespie, J. R.; Chatterjee, A. K.; Norcross, N. R.; Hulverson, M. A.; Ranade, R. M.; Nagendar, P.; Creason, S. A.; McQueen, J.; Duster, N. A.; Nagle, A.; Supek, F.; Molteni, V.; Wenzler, T.; Brun, R.; Glynne, R.; Buckner, F. S.; Gelb, M. H. *J. Med. Chem.* **2014**, *57*, 828.
26. Cavalli, A.; Lizzi, F.; Bongarzone, S.; Belluti, F.; Piazzi, L.; Bolognesi, M. L. *FEMS Immunol. Med. Microbiol.* **2010**, *58*, 51.
27. Singh Grewal, A.; Pandita, D.; Bhardwaj, S.; Lather, V. *Curr. Top. Med. Chem.* **2016**, *16*, 2245.
28. Camps, P.; El Achab, R.; Morral, J.; Muñoz-Torrero, D.; Badia, A.; Baños, J. E.; Vivas, N. M.; Barril, X.; Orozco, M.; Luque, F. J. *J. Med. Chem.* **2000**, *43*, 4657.
29. Defaux, J.; Sala, M.; Formosa, X.; Galdeano, C.; Taylor, M. C.; Alobaid, W. A. A.; Kelly, J. M.; Wright, C. W.; Camps, P.; Muñoz-Torrero, D. *Bioorg. Med. Chem.* **2011**, *19*, 1702.
30. Oluwafemi, A. J.; Okanla, E. O.; Camps, P.; Muñoz-Torrero, D.; Mackey, Z. B.; Chiang, P. K.; Seville, S.; Wright, C. W. *Nat. Prod. Commun.* **2009**, *4*, 193.
31. Kaur, K.; Jain, M.; Reddy, R. P.; Jain, R. *Eur. J. Med. Chem.* **2010**, *45*, 3245.
32. Gomes, A.; Pérez, B.; Alburquerque, I.; Machado, M.; Prudêncio, M.; Nogueira, F.; Teixeira, C.; Gomes, P. *ChemMedChem* **2014**, *9*, 305.
33. Ryckebusch, A.; Debreu-Fontaine, M.-A.; Mouray, E.; Grellier, P.; Sergheraert, C.; Melnyk, P. *Bioorg. Med. Chem. Lett.* **2005**, *15*, 297.
34. Ekoue-Kovi, K.; Yearick, K.; Iwaniuk, D. P.; Natarajan, J. K.; Alumasa, J.; de Dios, A. C.; Roepe, P. D.; Wolf, C. *Bioorg. Med. Chem.* **2009**, *17*, 270.

35. Musonda, C. C.; Gut, J.; Rosenthal, P. J.; Yardley, V.; Carvalho de Souza, R. C.; Chibale, K. *Bioorg. Med. Chem.* **2006**, *14*, 5605.
36. Sola, I.; Artigas, A.; Taylor, M. C.; Gbedema, S. Y.; Pérez, B.; Clos, M. V.; Wright, C. W.; Kelly, J. M.; Muñoz-Torrero, D. *Bioorg. Med. Chem. Lett.* **2014**, *24*, 5435.
37. Sola, I.; Castellà, S.; Viayna, E.; Galdeano, C.; Taylor, M. C.; Gbedema, S. Y.; Pérez, B.; Clos, M. V.; Jones, D. C.; Fairlamb, A. H.; Wright, C. W.; Kelly, J. M.; Muñoz-Torrero, D. *Bioorg. Med. Chem.* **2015**, *23*, 5156.
38. Viayna, E.; Sola, I.; Bartolini, M.; De Simone, A.; Tapia-Rojas, C.; Serrano, F. G.; Sabaté, R.; Juárez-Jiménez, J.; Pérez, B.; Luque, F. J.; Andrisano, V.; Clos, M. V.; Inestrosa, N. C.; Muñoz-Torrero, D. *J. Med. Chem.* **2014**, *57*, 2549.
39. Patrick, D. A.; Bakunov, S. A.; Bakunova, S. M.; Kumar, E. V. K. S.; Chen, H.; Kilgore Jones, S.; Wenzler, T.; Barzcz, T.; Werbovetz, K. A.; Brun, R.; Tidwell, R. R. *Eur. J. Med. Chem.* **2009**, *44*, 3543.
40. Wenzler, T.; Yang, S.; Patrick, D. A.; Braissant, O.; Ismail, M. A.; Tidwell, R. R.; Boykin, D. W.; Wang, M. Z.; Brun, R. *Antimicrob. Agents Chemother.* **2014**, *58*, 4452.
41. Carlier, P. R.; Chow, E. S.-H.; Han, Y.; Liu, J.; El Yazal, J.; Pang, Y.-P. *J. Med. Chem.* **1999**, *42*, 4225.
42. Löser, R.; Schilling, K.; Dimmig, E.; Gütschow, M. *J. Med. Chem.* **2005**, *48*, 7688.
43. Sykes, M. L.; Avery, V. M. *J. Med. Chem.* **2013**, *56*, 7727.
44. Havrylyuk, D.; Zimenkovsky, B.; Karpenko, O.; Grellier, P.; Lesyk, R. *Eur. J. Med. Chem.* **2014**, *85*, 245.
45. Di, L.; Kerns, E. H.; Fan, K.; McConnell, O. J.; Carter, G. T. *Eur. J. Med. Chem.* **2003**, *38*, 223.
46. Reid, C. M.; Ebikeme, C.; Barret. M. P.; Patzewitz, E.-M.; Müller, S.; Robins, D. J.; Sutherland, A. *Biooog. Med. Chem. Lett.* **2008**, *18*, 5399.
47. McKeever, C.; Kaiser, M.; Rozas, I. *J. Med. Chem.* **2013**, *56*, 700.
48. Gonzalez, J. L.; Stephens, C. E.; Wenzler, T.; Brun, R.; Tanious, F. A.; Wilson, W. D.; Barszcz, T.; Werbovetz, K. A.; Boykin, D. W. *Eur. J. Med. Chem.* **2007**, *42*, 552.
49. Arafa, R. K.; Wenzler, T.; Brun, R.; Chai, Y.; Wilson, W. D. *Eur. J. Med. Chem.* **2011**, *46*, 5852.

50. Anandan, S. K.; Webb, H. K.; Do, Z. N.; Gless, R. D. *Bioorg. Med. Chem. Lett.* **2009**, *19*, 4259.
51. Muñoz-Ruiz, P.; Rubio, L.; García-Palomero, E.; Dorronsoro, I.; del Monte-Millán, M.; Valenzuela, R.; Usán, P.; de Austria, C.; Bartolini, M.; Andrisano, V.; Bidon-Chanal, A.; Orozco, M.; Luque, F. J.; Medina, M.; Martínez, A. *J. Med. Chem.* **2005**, *48*, 7223.
52. Carlier, P. R.; Du, D.-M.; Han, Y.; Liu, J.; Pang, Y.-P. *Bioorg. Med. Chem. Lett.* **1999**, *9*, 2335.
53. Muñoz-Torrero, D.; Ferrer, I.; Sola, I.; Aso, E. EP 2818467 A1; WO 2014/206877 A1.
54. Wilkinson, S. R.; Prathalingam, S. R.; Taylor, M. C.; Ahmed, A.; Horn, D.; Kelly, J. M. *Free Radical Biol. Med.* **2006**, *40*, 198.
55. Bot, C.; Hall, B. S.; Bashir, N.; Taylor, M. C.; Helsby, N. A.; Wilkinson, S. R. *Antimicrob. Agents Chemother.* **2010**, *54*, 4246.
56. Ellman, G. L.; Courtney, K. D.; Andres Jr., V.; Featherstone, R. M. *Biochem. Pharmacol.* **1961**, *7*, 88.

Supplementary Material

Synthesis and biological evaluation of *N*-cyanoalkyl-, *N*-aminoalkyl-, and *N*-guanidinoalkyl-substituted 4-aminoquinoline derivatives as potent, selective, brain permeable antitrypanosomal agents

Irene Sola[a], Albert Artigas[a], Martin C. Taylor[b], F. Javier Pérez-Areales[a], Elisabet Viayna[a], M. Victòria Clos[c], Belén Pérez[c], Colin W. Wright[d], John M. Kelly[b], Diego Muñoz-Torrero[a,*]

[a] *Laboratory of Pharmaceutical Chemistry (CSIC Associated Unit), Faculty of Pharmacy and Food Sciences, and Institute of Biomedicine (IBUB), University of Barcelona, Av. Joan XXIII, 27-31, E-08028, Barcelona, Spain*

[b] *Department of Pathogen Molecular Biology, London School of Hygiene and Tropical Medicine, Keppel Street, London WC1E 7HT, United Kingdom*

[c] *Department of Pharmacology, Therapeutics and Toxicology, Institute of Neurosciences, Autonomous University of Barcelona, E-08193, Bellaterra, Barcelona, Spain*

[d] *Bradford School of Pharmacy, University of Bradford, West Yorkshire BD7 1 DP, United Kingdom*

* Corresponding author. Tel.: +34 934024533; fax: +34 934035941.

E-mail address: dmunoztorrero@ub.edu (D. Muñoz-Torrero).

Copies of ^{1}H and ^{13}C NMR spectra of the new compounds

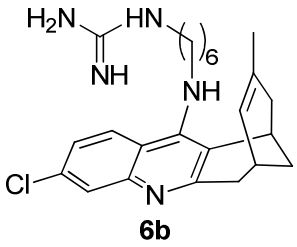

6b

^{1}H NMR (400 MHz, CD_3OD)

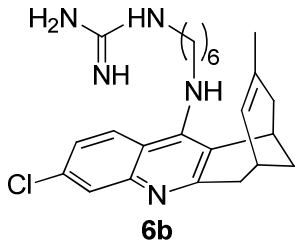

6b

^{13}C NMR (100.6 MHz, CD_3OD)

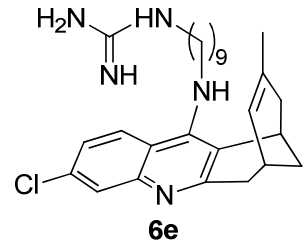

6e

^{1}H NMR (400 MHz, CD_3OD)

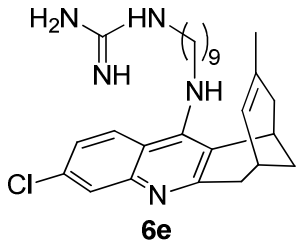

6e

^{13}C NMR (100.6 MHz, CD_3OD)

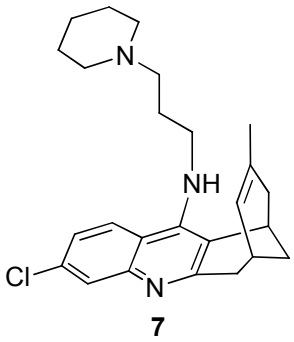

7

^{1}H NMR (400 MHz, CD_3OD)

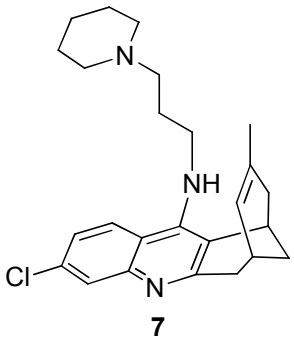

7

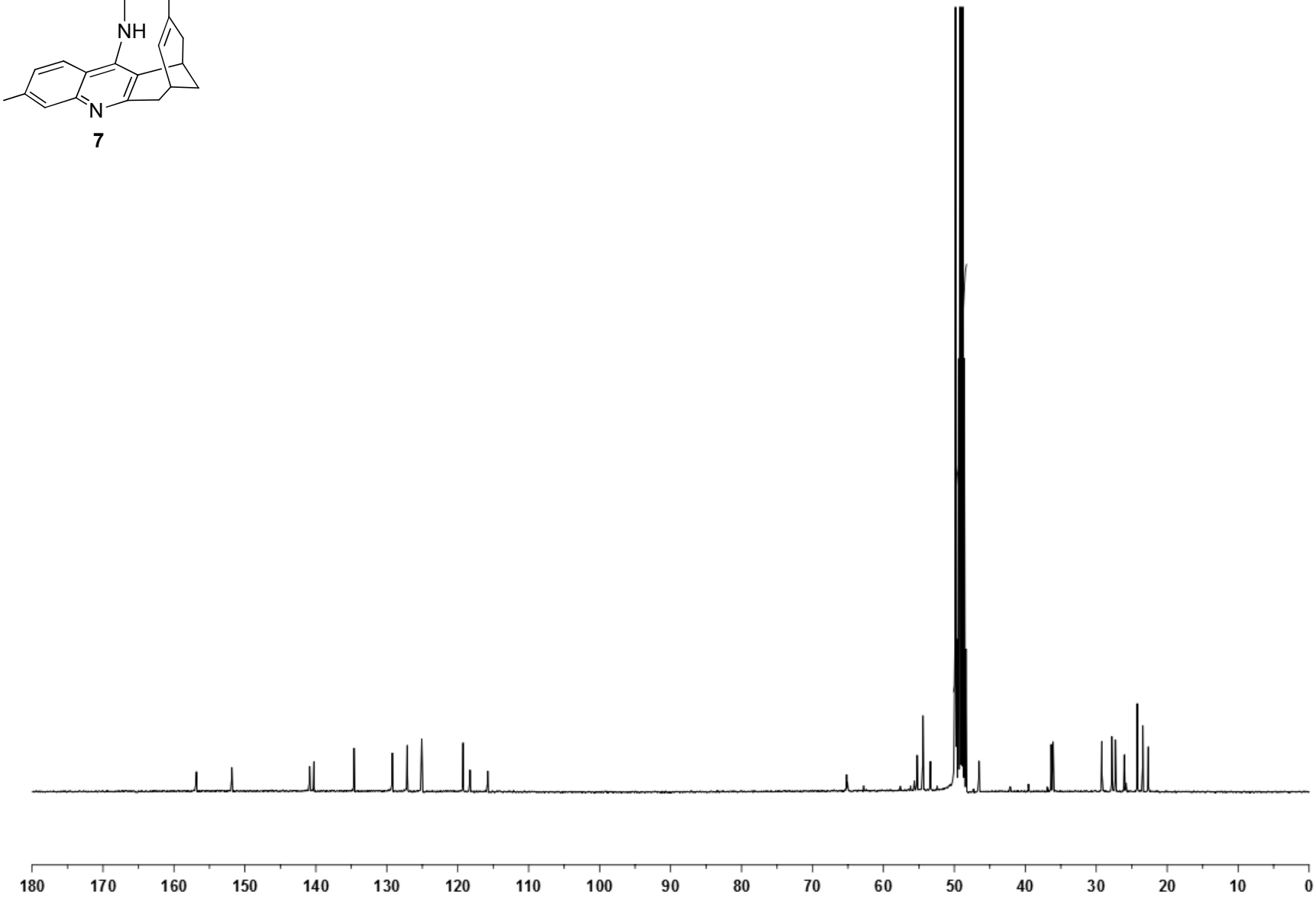

^{13}C NMR (100.6 MHz, CD_3OD)

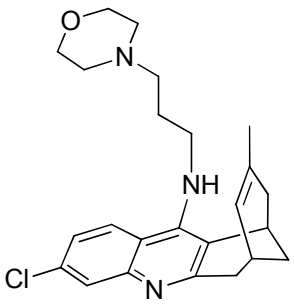

8

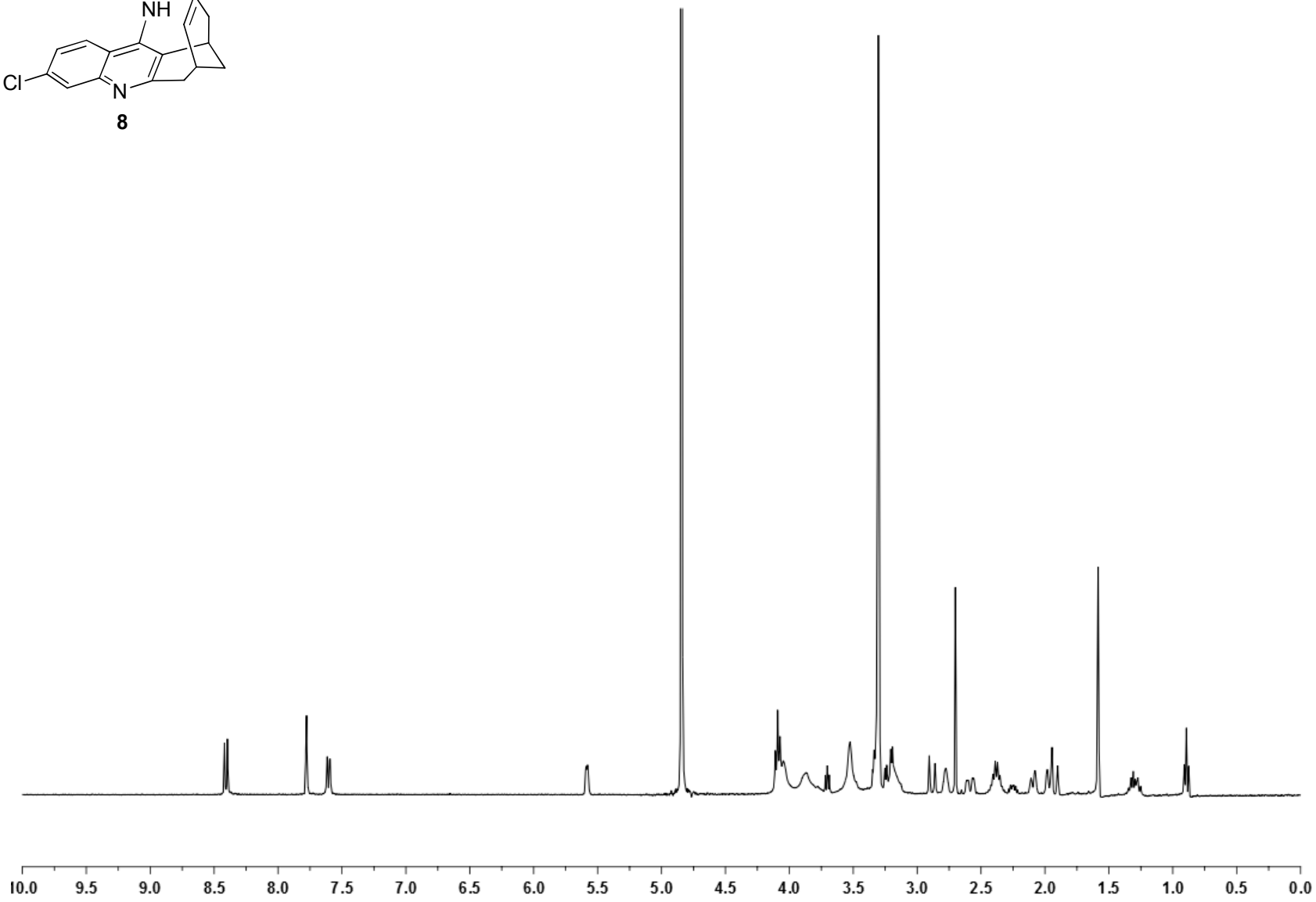

^{1}H NMR (400 MHz, CD_3OD)

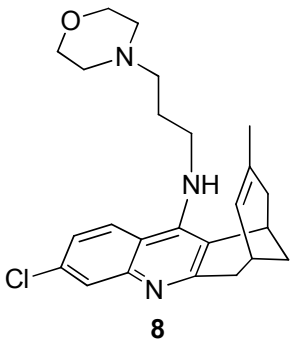

8

^{13}C NMR (100.6 MHz, CD_3OD)

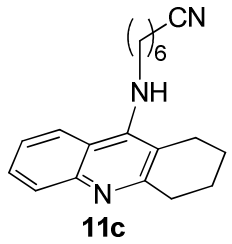

11c

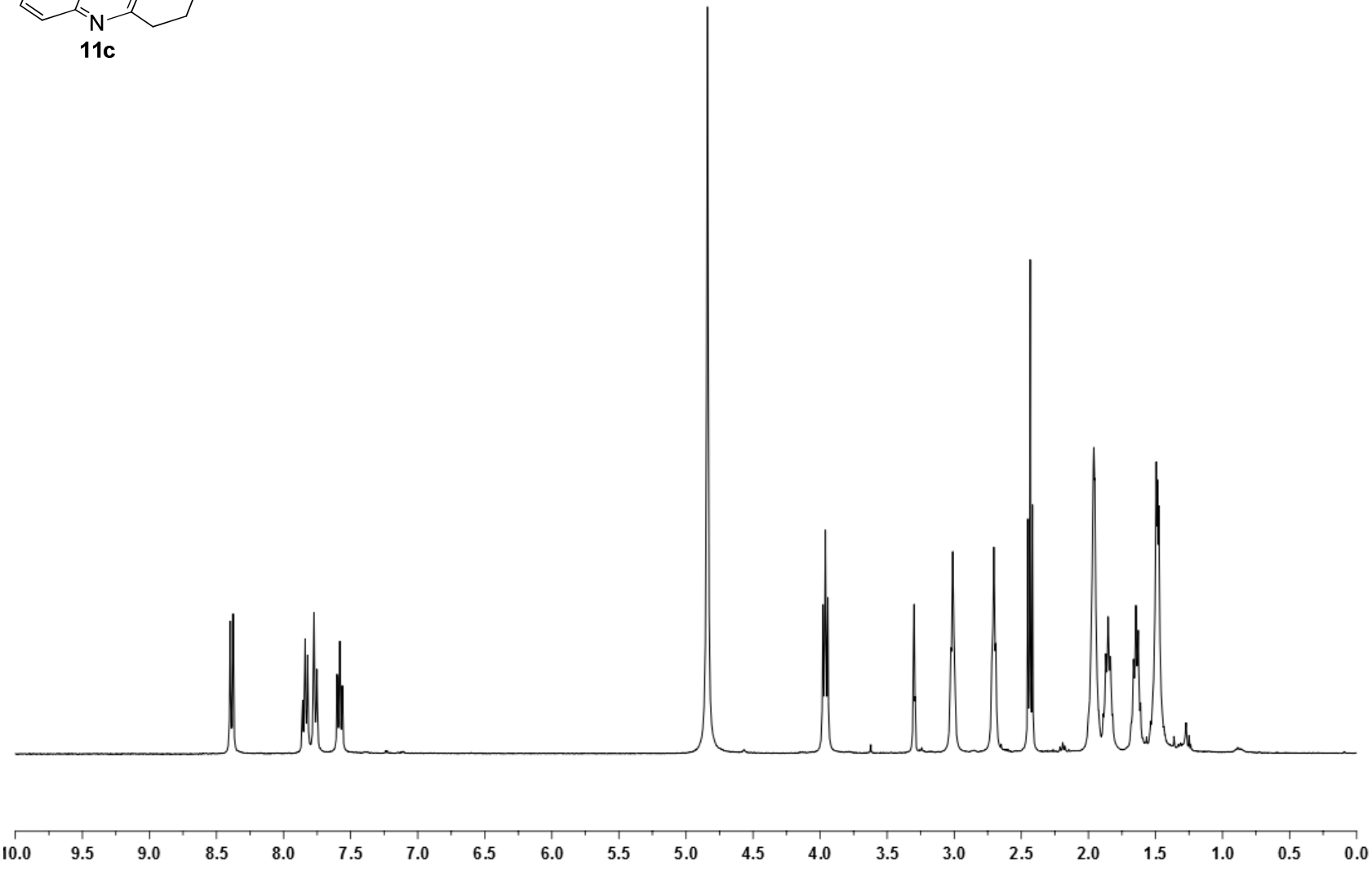

^{1}H NMR (400 MHz, CD_3OD)

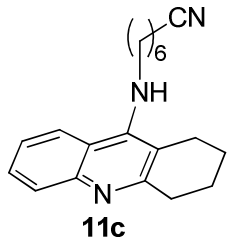

11c

^{13}C NMR (100.6 MHz, CD_3OD)

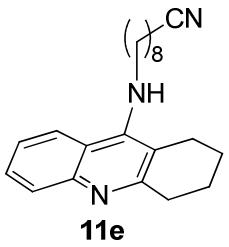

11e

^{1}H NMR (400 MHz, CD_3OD)

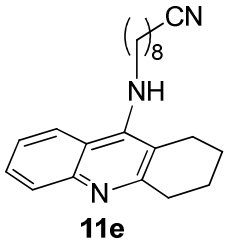

11e

^{13}C NMR (100.6 MHz, CD_3OD)

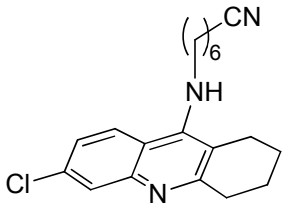

12c

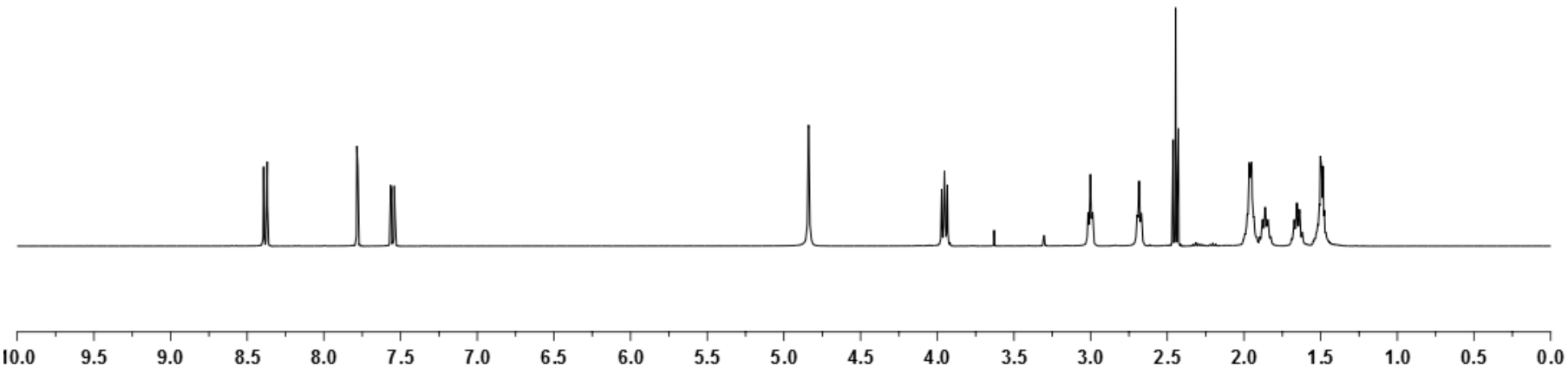

^{1}H NMR (400 MHz, CD_3OD)

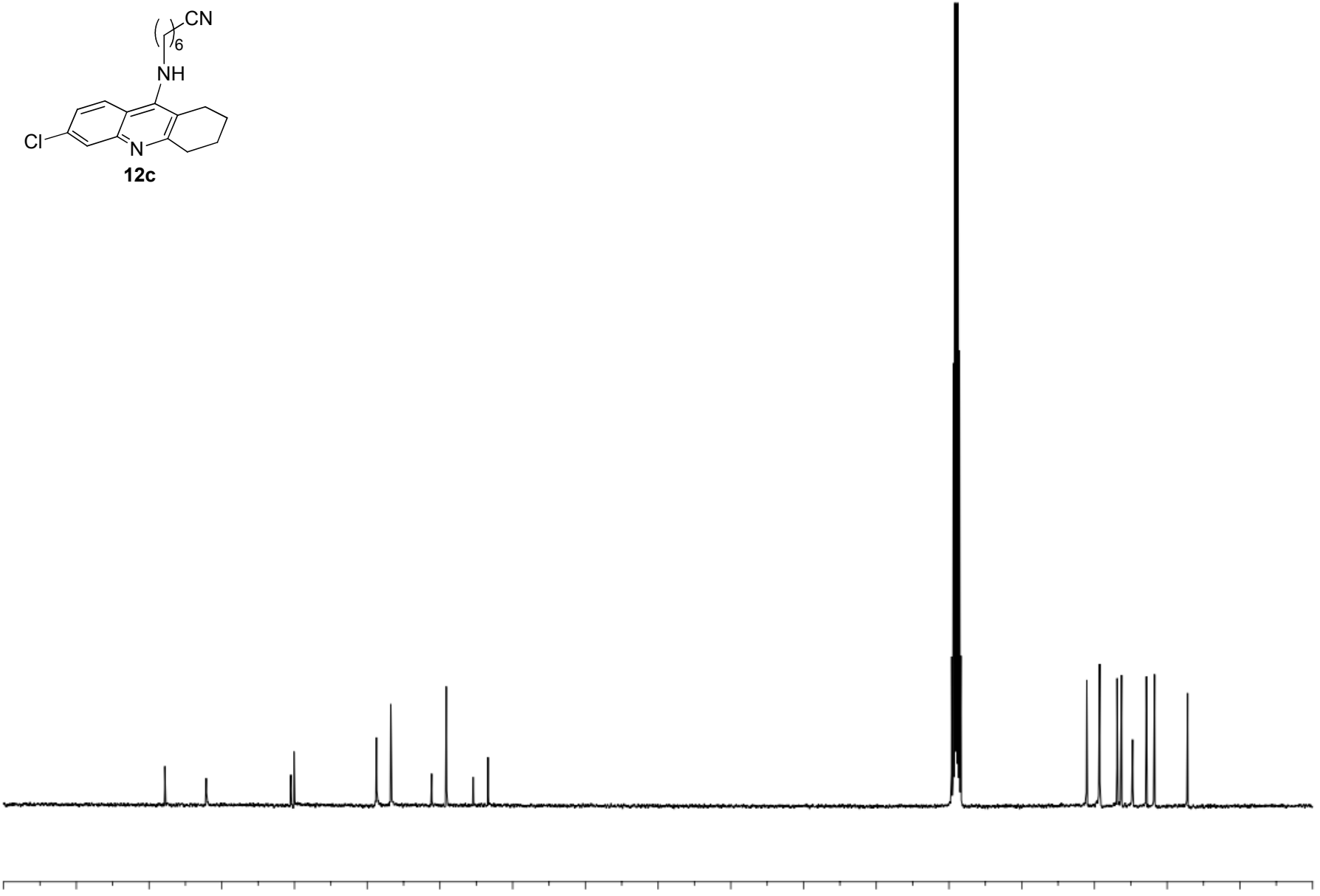

12c

^{13}C NMR (100.6 MHz, CD_3OD)

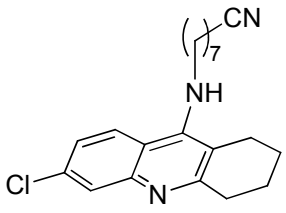

12d

^{1}H NMR (400 MHz, CD_3OD)

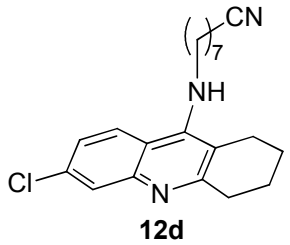

12d

^{13}C NMR (100.6 MHz, CD_3OD)

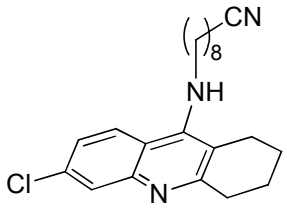

12e

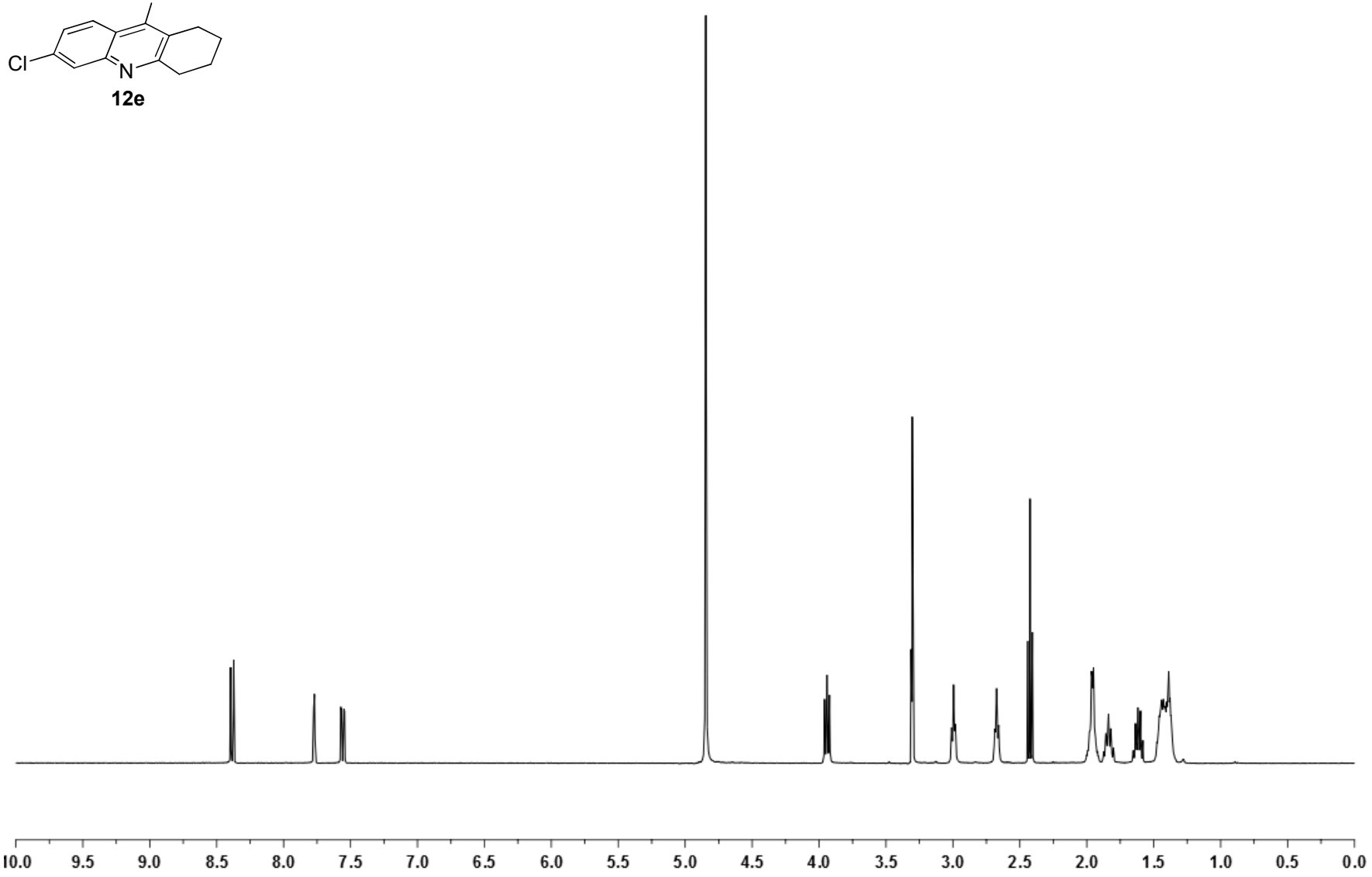

^{1}H NMR (400 MHz, CD_3OD)

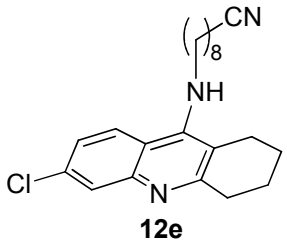

12e

^{13}C NMR (100.6 MHz, CD_3OD)

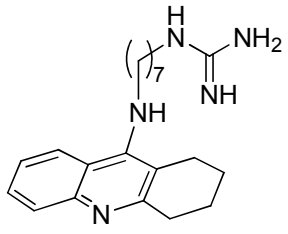

15c

^{1}H NMR (400 MHz, CD_3OD)

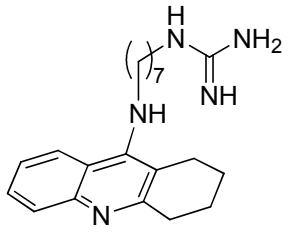

15c

^{13}C NMR (100.6 MHz, CD_3OD)

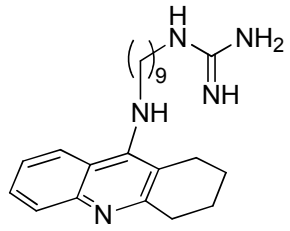

15e

^{1}H NMR (400 MHz, CD_3OD)

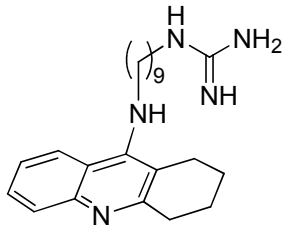

15e

^{13}C NMR (100.6 MHz, CD_3OD)

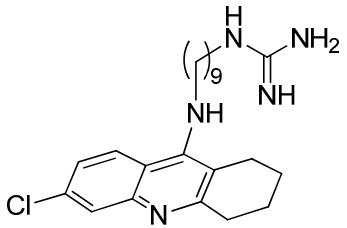

16e

^{1}H NMR (400 MHz, CD_3OD)

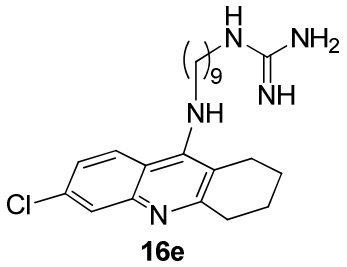

16e

^{13}C NMR (100.6 MHz, CD_3OD)

CHAPTER 7

Ongoing battle against drug resistant malaria

7.1. PfG6PD, a new target to combat drug resistant malaria

Because the occurrence of resistances from *P. falciparum* strains[437,438,439] as well as side effects with antimalarial drugs[440,441] become more and more frequent, new drug targets are urgently needed in order to gain the battle against malaria. In this regard, the enzyme glucose-6-phosphate dehydrogenase−6-phosphogluconolactonase of *P. falciparum* (*Pf*GluPho) has emerged as an intriguing new drug target candidate for antimalarial drug development on the basis of several recent findings.[334] Very interestingly, deficiency in the human glucose-6-phosphate dehydrogenase (hG6PD) enzyme, which affects around 400 million people worldwide,[442] has been associated with protection from severe malaria infections since a few decades ago.[287,309,317a] Although the biological significance of *Pf*GluPho and hG6PD is not totally elucidated, it is suggested that both enzymes play an important role in the development and survival of malaria parasites in human RBCs, depending on the pentose phosphate pathway both in *Plasmodium falciparum* and its human host.[287,334,443]

As we have mentioned in ***chapter 3***, *Pf*GluPho is a unique bifunctional enzyme, bearing glucose-6-phosphate and 6-phosphogluconolactonase domains, exclusively found in *Plasmodium* species and catalyzes the first two steps of the pentose phosphate pathway (PPP) which is supposed to be the major NADPH source[318] for these parasites (**Figure 7.1**), which are highly sensitive to oxidative stress.[267] Particularly, PPP activity in infected RBCs is greatly increased (78-fold) compared to non-infected ones, and the parasite PPP is responsible for 82% of this activity.[443] Moreover, silencing of *Pf*GluPho with RNA interference (RNAi) resulted in arrested parasite growth at the trophozoite stage, increased gametocyte formation, and enhanced transcription

[267] Becker, K. *et al.* Ed. Sherman, I. W. ASM Press, Washington, D.C, **2005**, 365−383.
[287] Luzzatto, L. *Haematologica* **2006**, *91*, 1303−1306.
[309] Ruwende, C.; Khoo, S. C.; Snow, R. W. *et al*. *Nature* **1995**, *376*, 246–249.
[317a] Cappadoro, M.; Giribaldi, G.; O'Brien, E. *et al*. *Blood* **1998**, *92*, 2527−2534.
[318] Preuss, J.; Jortzik, E.; Becker, K. *IUBMB Life* **2012**, *64*, 603–611.
[334] Jortzik, E.; Mailu, B. M., Preuss, J. *et al. Biochem. J*. **2011**, *436*, 641–650.
[437] Trape, J. F. *Am. J. Trop. Med. Hyg*. **2001**, *64*, 12−17.
[438] Marks, F.; von Kalckreuth, V.; Kobbe, R. *et al*. *J. Infect. Dis.* **2005**, *192*, 1962−1965.
[439] Egan, T. J.; Kaschula, C. H. *Curr. Opin. Infect. Dis*. **2007**, *20*, 598−604.
[440] Gottschall, J. L.; Elliot, W.; Lianos, E. *et al. Blood* **1991**, *77*, 306−310.
[441] Veinot, J. P.; Mai, K. T.; Zarychanski, R. *J. Rheumatol*. **1998**, *25*, 1221−1225.
[442] Nkhoma, E. T.; Poole, C.; Vannappagari, V. *et al. Blood Cells Mol. Dis.* **2009**, *42*, 267−278.
[443] Atamna, H.; Pascarmona, G.; Ginsburg, H. *Mol. Biochem. Parasitol*. **1994**, *67*, 79–89.

of thioredoxin reductase.[444] However, since the RNAi machinery is missing in *Plasmodium*[445] the significance of these studies must be considered cautiously. However, a recent report by Lopez-Barragan *et al*. claimed that antisense RNA may be an important factor in *P. falciparum*'s regulation of gene expression,[446] thus strengthening the results of the previous RNAi-based study.

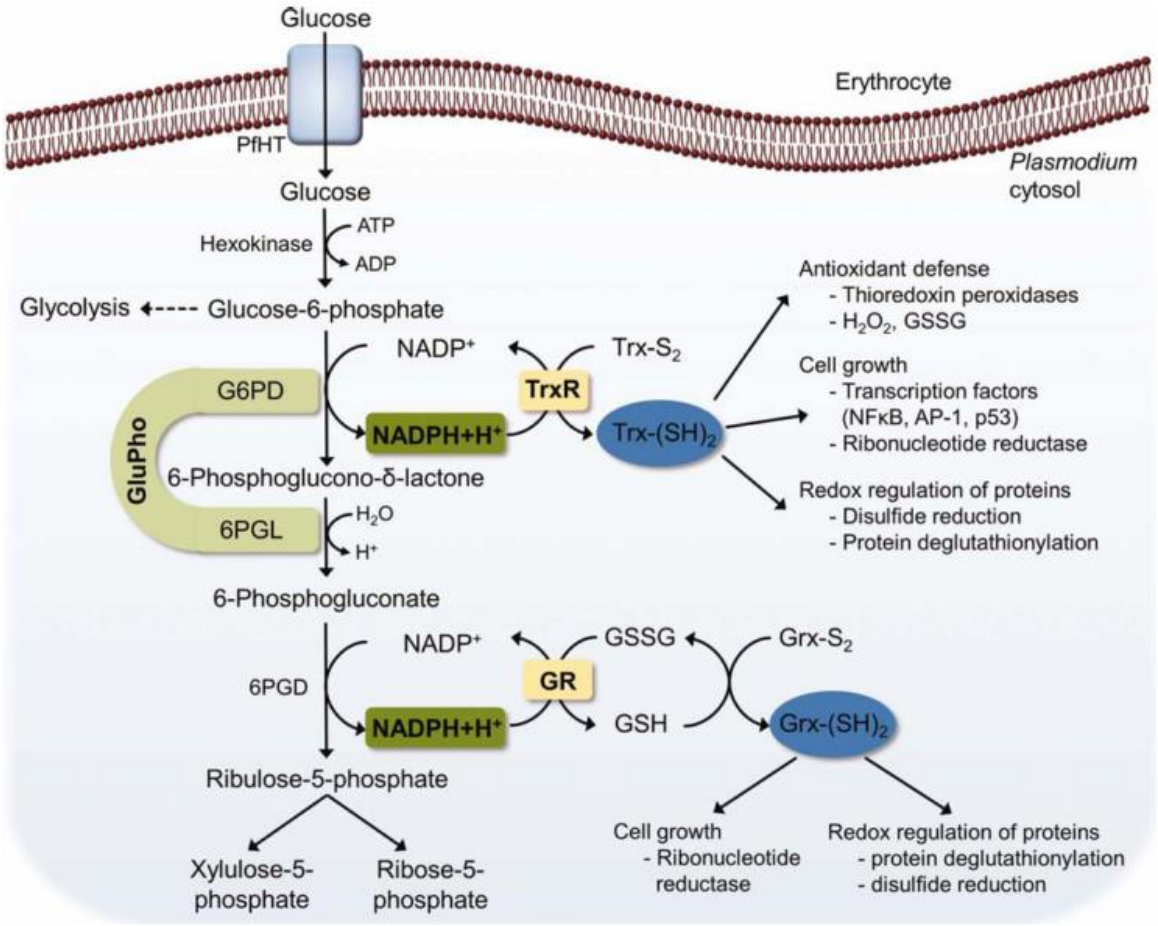

Figure 7.1. The Plasmodium pentose phosphate pathway. The pentose phosphate pathway provides NADPH for the thioredoxin and the GSH (glutathione) system in *P. falciparum*. NAPDH formed by *Pf*GluPho and 6PGD can be used by both thioredoxin reductase (TrxR) and GSH reductase (GR) for the reduction of their substrates thioredoxin (Trx) and glutaredoxin (Grx). Trx and Grx from *P. falciparum* can reduce a broad range of protein substrates and are thus involved in the redox regulation of many cellular processes. 6PGD, 6-phosphogluconate dehydrogenase; 6PGL, 6-phosphogluconolactonase; G6PD, glucose-6-phosphate dehydrogenase; GluPho,

[444] Crooke, A.; Diez, A.; Mason, P. J. *et al*. *FEBS J*. **2006**, *273*, 1537−1546.
[445] Baum, J.; Papenfuss, A. T.; Mair, G. R. *et al*. *Nucleic Acids Res*. **2009**, *37*, 3788–3798.
[446] Lopez-Barragan, M. J.; Lemieux, J.; Quinones, M. *et al. BMC Genomics* **2011**, *12*, 587.

glucose-6-phosphate dehydrogenase 6-phosphogluconolactonase; *Pf*HT, *P. falciparum* hexose transporter (Image source: Preuss, J.; Jortzik, E.; Becker, K. *IUBMB Life* **2012**, *64*, 603–611).

Furthermore, taking into account that an essential feature for a molecule to be considered as a potential drug target is that it must be distinguishable from its homologues in the human host, *Pf*GluPho also prove valuable in this respect as mammals do not express this enzyme and it presents considerable structural differences compared to hG6PD, potentially allowing selective targeting.[332,333] *Pf*GluPho is 107 kDa in size and found as stable tetrameric structure, rather large compared with the 59-kDa hG6PD which exist as dimer or tetramer, with the dimer probably being the predominant form *in vivo*. *Pf*GluPho differs in substrate affinity and kinetic mechanism from the human enzyme too.[333,334]

In spite of the importance of the role *Pf*GluPho appears to play in the parasites PPP as well as in overcoming oxidative stress, studies using *Pf*GluPho have been restricted in the past to the enzyme purified from parasite extracts, which is not only limiting in terms of the quantity of the enzyme required for inhibitor testing, crystal screening, and biochemical characterization of the enzyme, but also contains a high excess of the RBC G6PD. However, Becker and co-workers has recently succeeded in the cloning, heterologous overexpression, purification, and kinetic characterization of both enzymatic activities of full-length *Pf*GluPho,[334] which has allowed them to further substantiate the characterization of *Pf*GluPho as a drug target through a large screening of novel inhibitors in a high-throughput format. In fact, the only efforts reported so far aimed at seeking *Pf*GluPho inhibitors belong to Becker's research group. Thus, the HTS-screening of a large library of compounds resulted in the identification of the first selective inhibitor, being active at the low micromolar range and non-competitive with respect to G6P and $NADP^+$ (**Figure 7.2**).[447,448,449,450]

[332] Clarke, J. L.; Sodeinde, O.; Mason, P. J. *Mol. Biochem. Parasitol.* **2003**, *127*, 1–8.
[333] Clarke, J. L.; Scopes, D. A.; Sodeinde, O. *et al*. *Eur. J. Biochem*. **2001**, *268*, 2013–2019.
[334] Jortzik, E.; Mailu, B. M., Preuss, J. *et al. Biochem. J.* **2011**, *436*, 641–650.
[447] Preuss, J.; Maloney, P.; Peddibhotla, S. *et al. J. Med. Chem.* **2012**, *55*, 7262−7272.
[448] Preuss, J.; Hedrick, M.; Sergienko, E. *et al. J. Biomol. Screening* **2012**, *17*, 738−751.
[449] Maloney, P.; *et al*. A selective inhibitor of *Pf*G6PD. http://www.ncbi.nlm.nih.gov/books/NBK143548/
[450] Maloney, P.; *et al*. A 2nd selective inhibitor of *Pf*G6PD. http://www.ncbi.nlm.nih.gov/books/NBK184495/

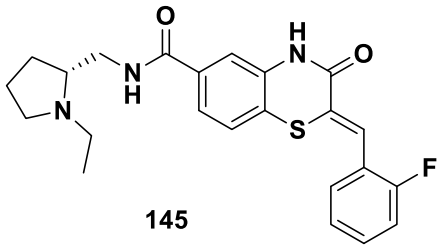

145

*Pf*G6PD IC_{50}: **889 nM**

hG6PD IC_{50}: **2.6 µM**

Selectivity index: **≈ 3**

Figure 7.2. First selective inhibitor of the G6PD activity of *Pf*GluPho (*Pf*G6PD).

A recent double crossover knock-out study performed by Becker *et al*.[451] in 2015 reaffirmed the role of *Pf*GluPho as an excellent antimalarial drug target, showing that the parasite enzyme is indeed essential for the survival of intraerythrocytic forms of *P. falciparum*.

Before having knowledge about these findings from Becker's research group, in the light of a new report that ascribed a strong positive selection on human survival against malaria to the G6PD-Mahidol mutation over the past 1500 years in Southeast Asians,[312a] encouraged the group of Dr. F. Javier Luque (Universitat de Barcelona) to develop an homology model of *Pf*G6PD, which, in collaboration with our group, would be followed by the design and synthesis of potential inhibitors.

7.2. Substrate analog inhibitors of PfG6PD designed from an enzyme homology model (Draft of the manuscript)

The rational design of a novel class of *Pf*GluPho inhibitors was envisioned according to an initial hypothesis that the structure of the G6PD domain in *P. falciparum* should be closely related to its human homologous, hG6PD, and thus computational studies were performed within the *Pf*G6PD domain. Intriguingly, the modelling studies from the homology model of *Pf*G6PD revealed a mutation of the residue 365 that caused the substitution of an arginine, positively charged at physiological pH, within the catalytic site of hG6PD, for an aspartate residue, negatively charged at physiological pH, within *Pf*G6PD (**Figure 7.3**).

[312a] Louicharoen, C.; Patin, E.; Paul, R. *et al*. *Science* **2009**, *326*, 1546−1549.
[451] Allen, S. M.; Lim, E. E.; Jortzik, E. *et al*. *FEBS J.* **2015**, *282*, 3808−3823.

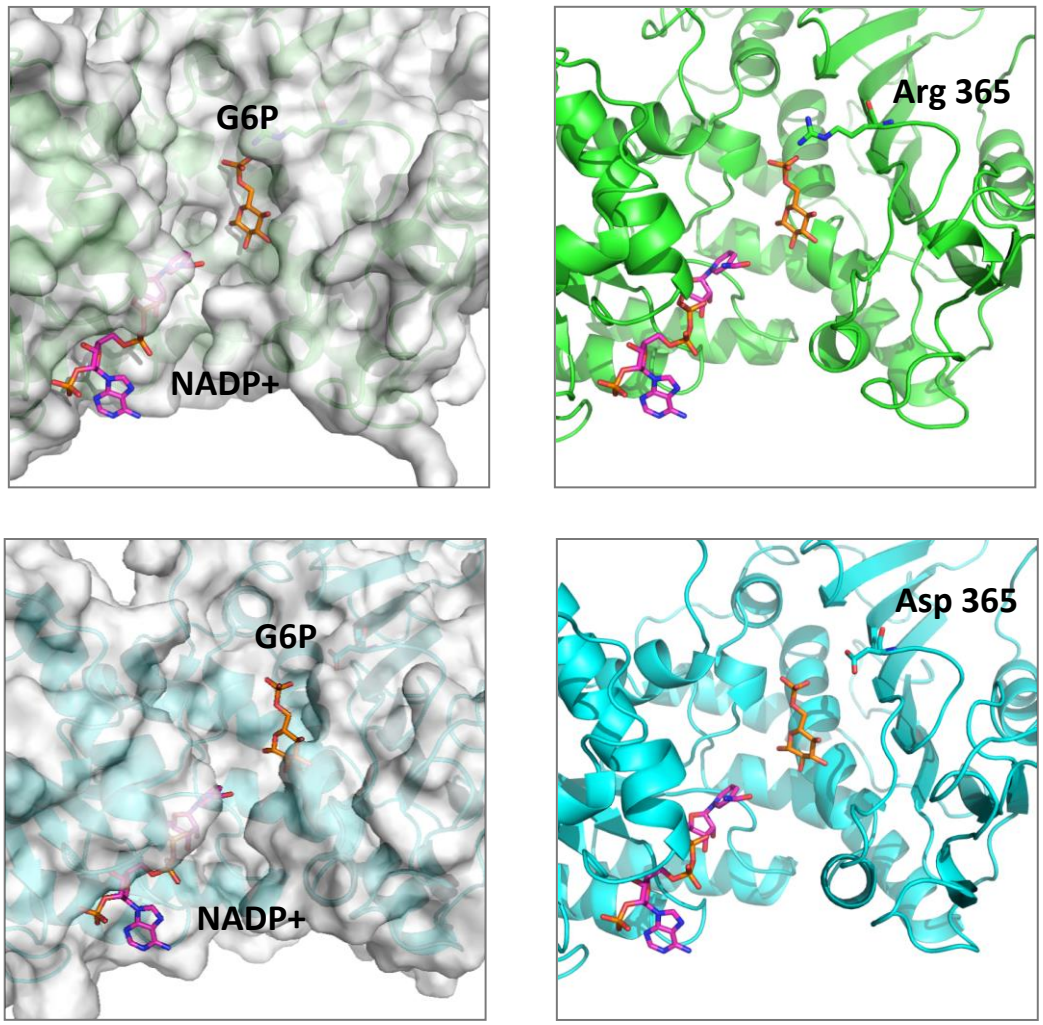

Figure 7.3. Images of the hG6PD (up) and *Pf*G6PD enzymes (down) with its natural substrates, G6P and $NADP^+$.

On the basis of this striking finding, the design of a novel class of *Pf*G6PD inhibitors was devised as a small set of compounds based on a D-glucose core, aimed at mimicking the natural substrate G6P at the catalytic site of *Pf*G6PD, and derivatized at position 6 with a side chain terminating with a basic group, protonatable at physiological pH (**Figure 7.4**).

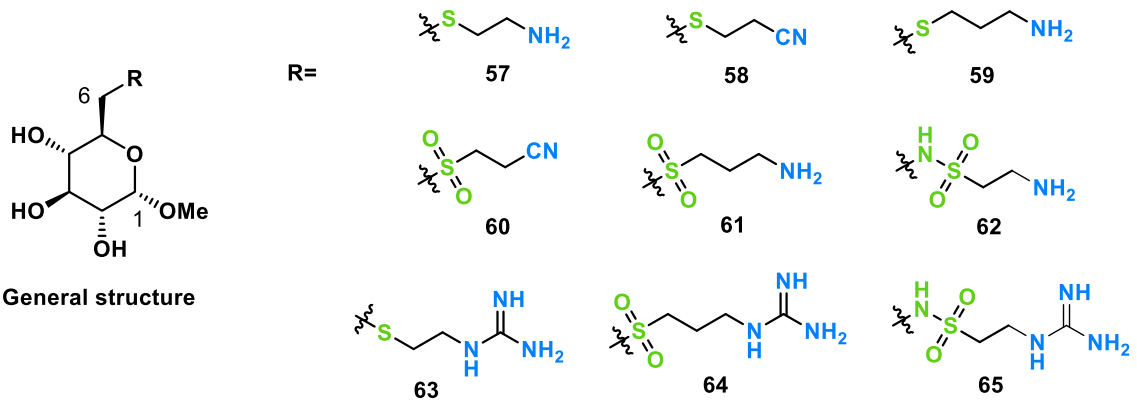

Figure 7.4. Structure of the potential substrate analog inhibitors of *Pf*G6PD **57**–**65**.

7.2.1 Synthesis of substrate analog PfG6PD inhibitors

For the preparation of this series of compounds, methyl α-D-glucopyranoside was chosen as a starting material, because it facilitates the synthetic routes by keeping the anomeric position protected, and the methoxy group is thought to be small enough to not disrupt the set of interactions within the catalytic site of the enzyme. Moreover, methyl α-D-glucopyranoside is more lipophilic than D-glucose, and, hence, was expected to enable an easier handling of the resulting derivatives.

In order to derive structure–activity relationships (SAR), the methyl α-D-glucopyranoside core was decorated at position 6 with a thioether, sulfone, or sulfonamide attached to an ethyl or a propyl chain that terminates with an amine or a guanidine group (**Figure 7.4**). Although the design made for these compounds was based on the presence of a basic group, protonatable at physiological pH, in order to promote the interaction with the aspartate residue within the catalytic site of *Pf*G6PD, the cyano intermediates (**58** and **60**) were also tested for comparison purposes.

For the preparation of the above depicted compounds methyl 6-chloro-6-deoxy-α-D-glucopyranoside, **67**, was used as a common intermediate. The chloroderivative **67** was prepared by reaction of methyl α-D-glucopyranoside, **66**, with 2 equiv of methanesulfonyl chloride in anhydrous DMF at a controlled internal temperature of 65 ^{o}C, and posterior treatment with a 25% solution of NaOMe in MeOH (**Scheme 7.1**).

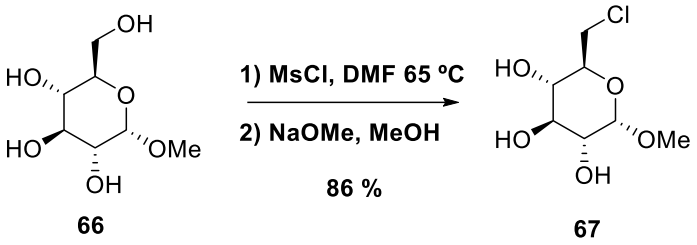

Scheme 7.1. Preparation of the common intermediate methyl 6-chloro-6-deoxy-α-D-glucopyranoside, **67**.

Then, for the obtention of thioethers **57**–**59** and **63**, the chloroderivative **67** was reacted with commercially available cysteamine hydrochloride in the presence of NaH for 48 h to afford the aminothioether **57**,[452] which was thereafter treated with 1*H*-pyrazole-1-carboxamidine hydrochloride, **146**, and Et_3N to provide guanidinothioether **63**. On the other hand, **67** was treated with more than 2 equiv of 3-mercaptopropanenitrile, **147**, freshly prepared from its dimer 3,3'-dithiobis(propanenitrile),[453] in presence of NaH to afford the cyanothioether **58**, which was in turn transformed into the aminothioether **59** by hydrogenation with Raney-Ni catalyst at 16 atm overnight (**Scheme 7.2**).

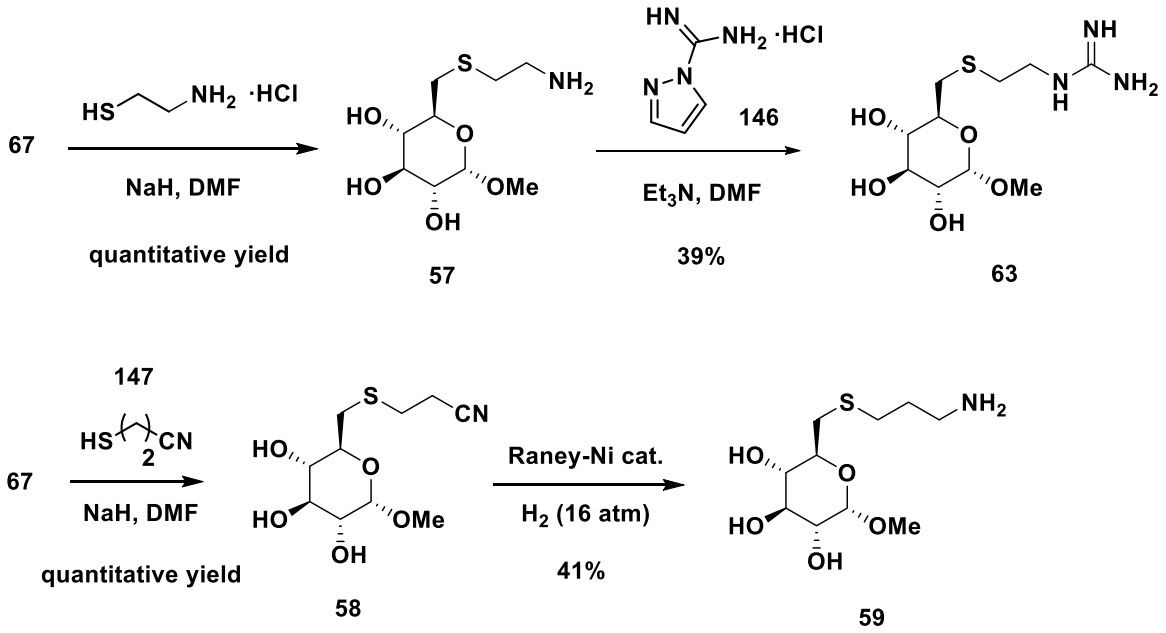

Scheme 7.2. Preparation of thioether derivatives **57**–**59** and **63**.

[452] Gómez-García, M.; Benito, J. M.; Gutiérrez-Gallego, R. *et al*. *Org. Biomol. Chem.* **2010**, *8*, 1849–1860.
[453] Klose, J.; Reese, C. B.; Song, Q. *Tetrahedron* **1997**, *53*, 14411–14416.

For the obtention of sulfones **60**, **61**, and **64**, the cyanothioether **58** was first oxidized with *meta*-chloroperoxybenzoic acid (MCPBA) and $NaHCO_3$ in CH_2Cl_2 to provide cyanosulfone **60**, which was subsequently reduced to aminosulfone **61** by hydrogenation with Raney-Ni under the same conditions described above. Then, **61** was reacted with 1*H*-pyrazole-1-carboxamidine hydrochloride, **146**, and Et_3N in CH_3CN for 6 h to afford guanidinosulfone **64** (**Scheme 7.3**).

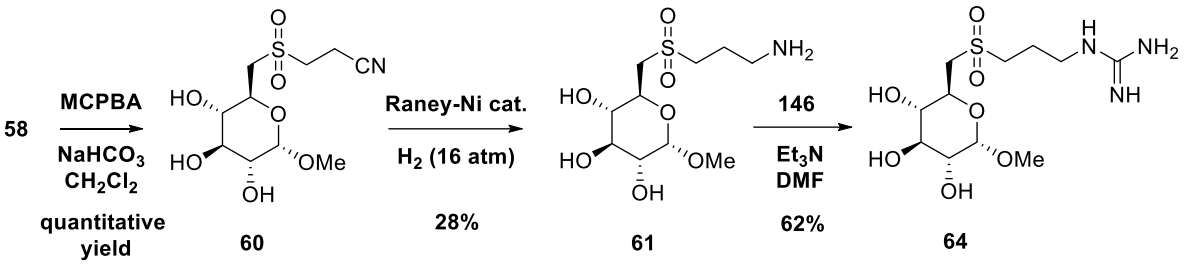

Scheme 7.3. Preparation of sulfones **60**, **61**, and **64**.

A different synthetic route was followed for the preparation of sulfonamide compounds **62** and **65**, comprising a nucleophilic substitution of **67** with potassium phthalimide in DMF for 7 days to provide the phthalimido derivative **148** in moderate yield, and posterior phthalimide cleavage by hydrazinolysis to give methyl 6-amino-6-deoxy-α-D-glucopyranoside, **149**, through a conventional Gabriel synthesis, in a different manner from the previously reported procedure for **149**.[454] Then, amine **149** was treated with sulfonyl chloride **150**, which was readily prepared from taurine,[455] to obtain the phthalimidosulfonamide **151** in excellent yield. Hydrazinolysis of **151** led to the target aminosulfonamide **62** in low yield, likely due to retention on the stationary phase (silica gel) during column chromatography purification of the crude reaction product, because of its high polarity. Finally, guanidinosulfonamide **65** was obtained from **62** through the usual conditions with reagent **146** (**Scheme 7.4**).

[454] Burland, P. A.; Osborn, H. M.; Turkson, A. *Bioorg. Med. Chem.* **2011**, *19*, 5679–5692.
[455] Zarchi, M. A. K.; Tayefi, M.; Tirgir, F. *et al*. *J. Appl. Polym. Sci*. **2011**, *121*, 2573–2583.

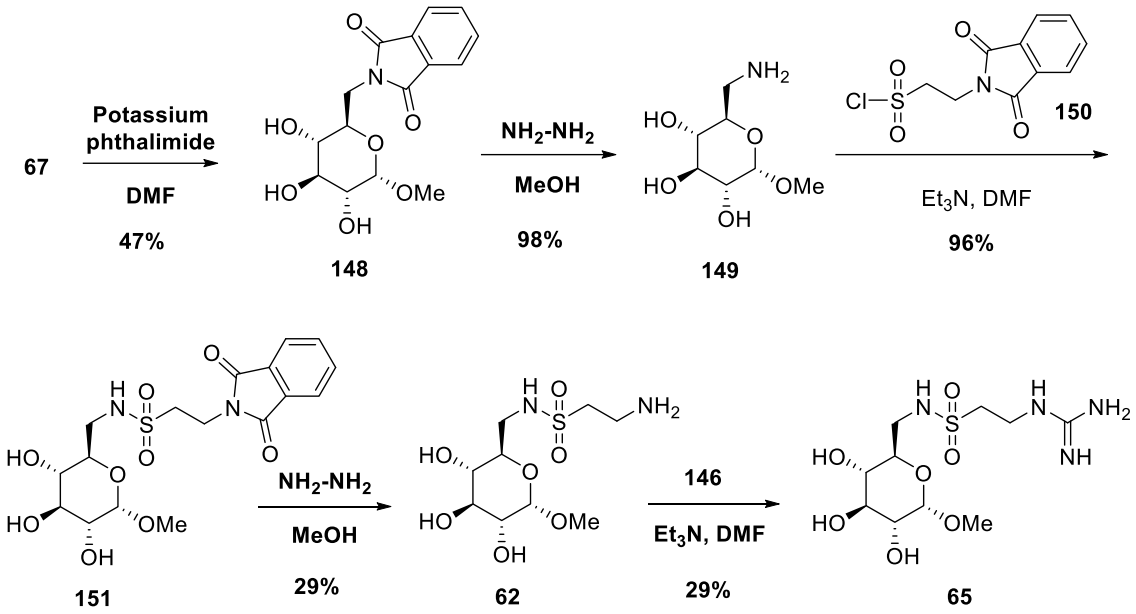

Scheme 7.4. Preparation of sulfonamides **62** and **65**.

7.2.2 In vitro biological profiling of substrate analog PfG6PD inhibitors

The *in vitro* evaluation of the putative *Pf*G6PD inhibitors against isolated *Pf*G6PD and hG6PD, the phenotypic assays against *Plasmodium falciparum*, and the cytotoxicity tests with HEPG2 human hepatoma cells were carried out by the group of Dr. José Manuel Bautista (Universidad Complutense de Madrid).

All the compounds showed a millimolar activity in *in vitro* cultures of *P. falciparum*. Compounds bearing a propyl chain as **59** and **61** showed the lowest growth inhibition potencies with IC_{50} values higher than 2 mM. On the other hand, compounds functionalized with a guanidine group displayed the highest antiplasmodial potencies, with IC_{50} values below 1 mM, namely guanidinotioether **63** has an IC_{50} of 588 µM against cultured *P. falciparum* and guanidinosulfonamide **65** exhibited the lowest IC_{50} value (339 µM). However, guanidinosulfone **64** showed an IC_{50} value of 1.57 mM, clearly higher than those of guanidines **63** and **65**.

Kinetics studies of the enzymatic inhibition of *Pf*G6PD and hG6PD by the most active compounds **57** and **62** suggested a selective inhibition of *Pf*G6PD for both inhibitors, being competitive for G6P and not affecting cofactor $NADP^+$ function. Particularly, compound **57** displayed a K_i of 76 µM for *Pf*G6PD inhibition with G6P substrate and a K_i of 364 µM at varying concentration of $NADP^+$, while a lowest inhibition was found for hG6PD with a K_i value higher than 2 mM for both, G6P and $NADP^+$. Compound **62** also displayed a micromolar inhibition of *Pf*G6PD at varying

concentration of G6P (22.8 μM) or $NADP^+$ (269 μM), and a less potent inhibition of hG6PD with G6P (440 μM) and $NADP^+$ (1260 μM). In conclusion, both compounds displayed moderate micromolar affinity toward *Pf*G6PD and favourable *Pf*G6PD *versus* hG6PD selectivity, in agreement with the design strategy based on the homology model of *Pf*G6PD.

Moreover, another phenotypic study aimed at characterizing the amount of pyknotic forms after 48h treatment of *P. falciparum* with the most potent inhibitors (**58**, **60**, **63** and **65**) was carried out. It was observed an accumulation of pyknotic forms of the parasite mostly in mature stages (trophozoite) upon incubation with the four selected compounds, revealing a different mechanism of action than that observed after chloroquine treatment (CQ, **Figure 7.5**). These results are in accordance with those found after RNAi treatment[444] where a major afectation for the mature trophozoite parasites was also observed. This finding point out firstly the mechanism of action of the inhibitors, which it was preserved for all compounds even the chemical modifications, producing a complete absence of live due to the appearance of pyknotic forms, and secondly the major affectation in trophozoit forms (pyknotic mature) will stimulate an immune response, because of these forms delay the parasite clearance. In conclusion, it makes these inhibitors of therapeutic interest as potential anti-malarial drugs with an additional immunomodulatory effect.

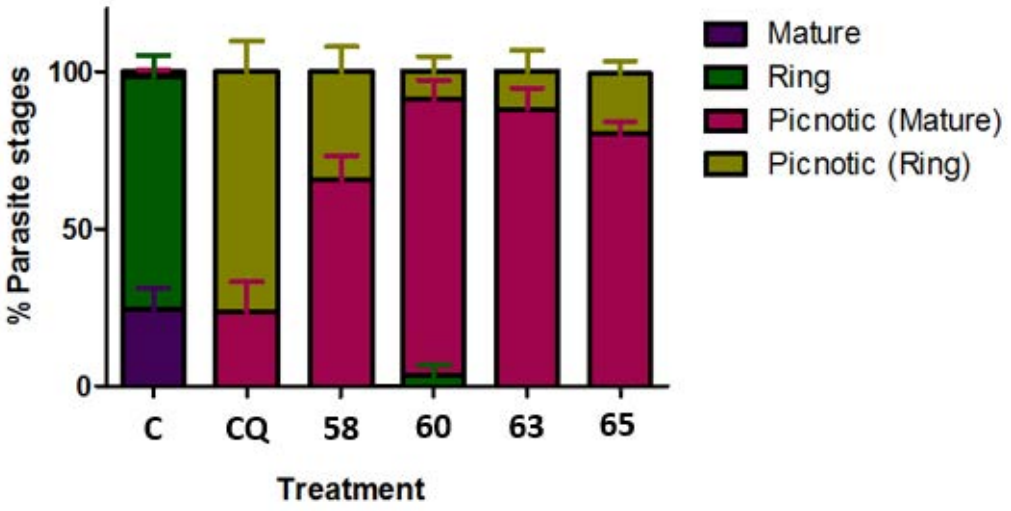

Figure 7.5. Study of remaining parasitic forms after treatment with compounds **58**, **60**, **63** and **65** at 2 mM concentration, compared with chloroquine treatment (10 μM).

[444] Crooke, A.; Diez, A.; Mason, P. J. *et al*. M. *FEBS J*. **2006**, *273*, 1537−1546.

Finally, regarding cytotoxicity evaluation, the compounds did not show significant loss of viability of HEPG2 human hepatoma cells below 80% when given at concentrations between 0.2 and 1.0 mM. Moreover, most of the inhibitors that showed K_i values for hG6PD above 200 μM (**57**, **58**, **60**, **62** and **63**) still maintained these viability values at 2 mM. Nevertheless, those inhibitors showing K_i values for hG6PD below 200 μM (**59**, **61**, **64** and **65**) decreased cell viability below 80% at concentrations between 1.5 and 2 mM.

In summary, we have successfully exploited a significant structural difference at the catalytic site of *Pf*G6PD relative to the human enzyme, to design and synthesize a series of substrate analogs that display a clear selectivity towards the *P. falciparum* enzyme, together with a micromolar affinity, in the range as that displayed by the substrate, G6P. The higher IC_{50} values found in the phenotypic screening against cultured *P. falciparum* might be ascribed to unfavourable physicochemical/pharmacokinetic properties, an issue which should be addressed in future endeavours in this project.

7. A.

Draft of the manuscript

Discovery of selective substrate analog inhibitors of *Plasmodium falciparum* glucose-6-phosphate dehydrogenase as novel antimalarial agents

Nelson Alencar,[†,‡] Irene Sola,[§,‡] María Linares,[#,‡] Caterina Pont,[§] Cristina Sampedro,[§] Jordi Juárez-Jiménez,[†] Paloma Abad,[#] Susana Pérez-Benavente,[#] Jerónimo Lameira,[¶] José M. Bautista,[#] Diego Muñoz-Torrero,[,§] and F. Javier Luque[*,†]*

[†] Department of Nutrition, Food Science and Gastronomy, Faculty of Pharmacy and Food Sciences, and Institute of Biomedicine (IBUB), University of Barcelona, Av. Prat de la Riba 171, E-08921 Santa Coloma de Gramenet, Spain

[§] Laboratory of Pharmaceutical Chemistry (CSIC Associated Unit), Faculty of Pharmacy and Food Sciences and IBUB, University of Barcelona, Av. Joan XXIII 27-31, E-08028, Barcelona, Spain

[#] Departamento de Bioquímica y Biología Molecular IV and Instituto de Investigación Hospital 12 de Octubre, Universidad Complutense de Madrid, Avda. Puerta de Hierro s/n, Ciudad Universitaria, 28040-Madrid, Spain

[¶] Laboratório de Planejamento e Desenvolvimento de Fármacos-LPDF, Instituto de Ciências Exatas e Naturais- ICEN, Universidade Federal do Pará – UFPA, Av. Augusto Correa, Nº 1- Bairro: Guamá, Cep: 66.075-900, Belém-Pará, Brazil

ABSTRACT: Despite the ongoing efforts for malaria control, *Plasmodium* parasites are closer to win the fight between the efficacy of antimalarial drugs and the development of resistance. This issue intensifies the desperate need for safe and affordable new drugs, which are effective against multiple parasite life cycle stages, but are also endowed with mechanisms of action different from those of current antimalarial drugs in order to avoid resistances. The enzyme glucose-6-phosphate dehydrogenase (G6PD) of *P. falciparum* has emerged as a promising and attractive target for antimalarial drug discovery, in the light of its key role in parasite development and survival and of the protective effect against malaria infection observed under human G6PD deficiency conditions. Here we describe the construction of a homology model of *Pf*G6PD, which has enabled the identification of key structural differences as compared with the human enzyme. We have exploited these changes to rationally design a novel family of substrate analog-based inhibitors that can display selectivity towards *Pf*G6PD. A series of glucose derivatives featuring an α-methoxy group at the anomeric position and different side chains at position 6 terminating with different basic functionalities has been synthesized and their *Pf*G6PD and hG6PD inhibitory activities and their toxicity against parasite and mammalian cells has been assessed. Several compounds have been found to display micromolar affinity (K_i up to 23 μM), nice selectivity (up to > 26-fold), and low cytotoxicity, but only high micromolar IC_{50} values in the phenotypic assays with *P. falciparum* cultures, likely as a result of a poor internalization of the compounds in the parasite cell. Future hit optimization should focus on improving the physicochemical / pharmacokinetic properties of this class of compounds.

INTRODUCTION

Malaria remains one of the major causes of death worldwide, with an estimated 214 million new infections and 438,000 deaths only in 2015, accounting for about 70% early child deaths (under 5 years).[1] Over the millenia malaria, first described for Hippocrates around 400 B.C., has shaped the human genome.[2] Malaria parasites, mainly *P. falciparum* and *P. vivax*, have exerted intense selective pressure on the cellular phenotype of human erythrocytes, driving to the strongest known evolutionary selection behind sickle-cell trait, thalassemia, glucose-6-phosphate dehydrogenase deficiency (G6PDd), and other erythrocyte pathologies that coexist in areas where malaria is present.[3-5]

Since the discovery of G6PDd about 60 years ago as an outgrowth of investigations of hemolytic anemia induced by antimalarial drug primaquine, many thousands of papers documenting clinical events, population distribution, biochemical characteristics, and molecular biology have been published.[6,7] G6PDd is the commonest human enzymopathy, affecting 400 million people throughout the world, mostly in Africa, South Europe, the Middle East, and Southeast Asia. G6PDd is an X-linked recessive hereditary genetic disorder of red blood cells (RBC) caused by missense mutations at the so-called "housekeeping" G6PD gene. Altogether more than 160 mutations have been described for this deficiency, giving rise to a broad classification in accordance with the World Health Organization, depending on the severity of the biochemical and clinical phenotype, from class I to class IV with low to normal enzyme activity, and class V with increased activity respect non-G6PD deficient phenotype.[8,9] Although G6PD deficiency is associated with a number of hematologic disorders, such as neonatal jaundice, kernicterus, chronic non-spherocytic haemolytic anemia and favism, amongst others, its clinical penetrance is exceedingly low. Hemizygote males show the

severe phenotype. Homozygote females are least commonly affected, while heterozygote females with only one affected X-chromosome vary in severity depending on the balance between the expression of the normal and abnormal X chromosomes.[10,11] The striking similarity between the global distribution of G6PD-deficient alleles and the malaria endemic areas lends support to the malaria protection hypothesis, which is suggested to be the consequence of natural selection processes.[12-14]

G6PD is a crucial enzyme that catalyzes the first and rate limiting step of the pentose phosphate pathway (PPP), converting glucose-6-phosphate (G6P) into 6-phosphogluconolactone, thereby allowing the production of nicotinamide adenine dinucleotide phosphate (NADPH). In a second step, 6-phosphogluconolactonase (6PL) transforms the product into 6-phosphogluconate, which is converted into ribulose-5-phosphate by the following enzyme in the PPP, 6-phosphogluconate dehydrogenase, producing another molecule of NADPH. NADPH is required for several biosynthetic reactions and plays a key role as a reducing agent preserving the balance of reduced/oxidized states of glutathione. The reduced form of glutathione is essential for the reduction of hydrogen peroxide and oxygen radicals and the maintenance of hemoglobin and other RBC proteins in the reduced state.[7,9,16] Thus, NADPH affords cell protection against oxidative damage, which is of particular importance in RBC, since they do not contain mitochondria and therefore any other source of NADPH.[16]

Although a clinical protective effect in G6PDd carriers against fulminating malaria infection (*P. falciparum*) has been shown mainly in Africa,[17-24] other reports have not found a clear association and regarding *P. vivax* malaria, a non-lethal infection spread over India, Latin America, and parts of the Eastern Mediterranean, it has not been accurately tested and remains anecdotal.[25-27] The precise mechanism of this selective advantage remains uncertain, it seems to be related to the effects on RBC by increasing

oxidative stress. Reduced erythrocyte invasion by the parasite, decreased intra-erythrocytic parasite growth rate, enhanced phagocytosis of parasite-infected erythrocytes at an early stage of parasite maturation, and increased immune response against parasite-infected erythrocytes are putative mechanisms that may explain the role of G6PD-deficient alleles in the resistance to *P. falciparum* malaria.[28-33]

Decades ago it was hypothesized that the parasites make use of the host enzyme to carry out the initial reaction of the PPP in which G6P is oxidized by G6PD.[34] Nowadays there is the evidence that *P. falciparum* has several potential pathways to generate NADPH.[35-38] The cytosolic enzyme glutamate dehydrogenase and the mitochondrial isocitrate dehydrogenase are involved in NADPH production, however, glutamate dehydrogenase is dispensable for asexual stage growth[39] and the contribution of isocitrate dehydrogenase is still unclear.[40] In addition of NADPH formation, the PPP pathway serves for the generation of nucleotides and nucleic acids. Contrary to human G6PD (hG6PD), the bifunctional enzyme *P. falciparum* glucose-6-phosphate dehydrogenase–6-phosphogluconolactonase (*Pf*GluPho), exclusively found in *Plasmodium* species, combines G6PD and 6PGL functions of the PPP with unique structural and functional features, thus catalyzing the two first reactions in the PPP. The *Plasmodium* enzyme shows remarkable differences from its human counterpart, being 107 kDa in size and found as stable tetramers, rather large compared with the 59 kDa hG6PD, which exists as a dimer or a tetramer, with the dimer probably being the predominant form *in vivo*. *Pf*GluPho also differs in substrate affinity as well as kinetic mechanism from the human enzyme.[41-43] Particularly, PPP activity in infected RBCs is greatly increased (78-fold) compared to non-infected ones, with the parasite PPP being responsible for 82% of this activity.[44] Furthermore, RNA-mediated gene silencing of *Pf*GluPho in cell culture caused arrest of the parasite life cycle at the trophozoite stage

and enhanced gametocyte formation.[45] Although the biological significance of *Pf*GluPho is not fully elucidated, the overall findings point out not only the structural dissimilarity compared with its human homologous, but also the importance of this enzyme in the parasite infection cycle and in the response of the parasite to oxidative stress, thereby making *Pf*GluPho an ideal target for novel antimalarial drugs.

Recently, Becker *et al.* have identified some selective inhibitors of *Pf*G6PD after a high throughput screening (HTS) of a large library of compounds, which are active at the submicromolar range and non-competitive with respect to G6P and $NADP^+$ (Fig. 1).[46-49] However, the lack of a tridimensional structure of *Pf*G6PD precludes the structure-based rational design of inhibitors.

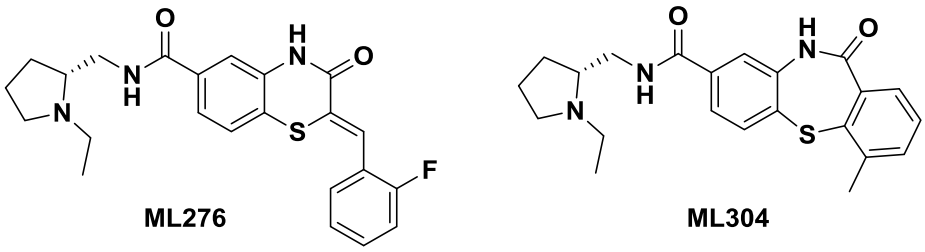

Figure 1. Chemical structures of the selective *Pf*G6PD inhibitors ML276 and ML304.

Here, we describe the construction of a homology model of the *Pf*G6PD enzyme and the synthesis and evaluation of *Pf*G6PD and hG6PD inhibition, antiplasmodial, and cytotoxic activities of a novel class of substrat analog inhibitors of *Pf*G6PD, which have been rationally designed on the basis of the homology model.

RESULTS AND DISCUSSION

Design of inhibitors based on the *Pf*G6PD homology model. The homology model of *Pf*G6PD was built starting with the alignment between the primary sequences of G6PD

from different *Plasmodium* species, *Leuconostoc mesenteroides,* and the human enzyme. Molecular docking was carried out then to assess the binding mode of the substrate G6P within the modeled structure of *Pf*G6PD, using the PDB structures of the complexes of *L. mesenteroides* and human G6PD with G6P.

Comparison between the X-ray structure of the hG6PD–G6P and the docked structure of the *Pf*G6PD–G6P complexes revealed that residue 365, close to the substrate G6P site of the catalytic pocket, was mutated from an arginine in hG6PD to a shorter and oppositely charged aspartate in *Pf*G6PD (Fig. 2). On the basis of this finding, we inferred that introduction at position 6 of a glucose moiety of a short side chain terminating with a basic functionality, protonatable at physiological pH might enable an ionic interaction with Asp365 of *Pf*G6PD, whereas that side chain should be detrimental for the interaction with Arg365 of the human enzyme due to both steric clash and electrostatic repulsion, thereby making it possible the selective inhibition of the parasite enzyme.

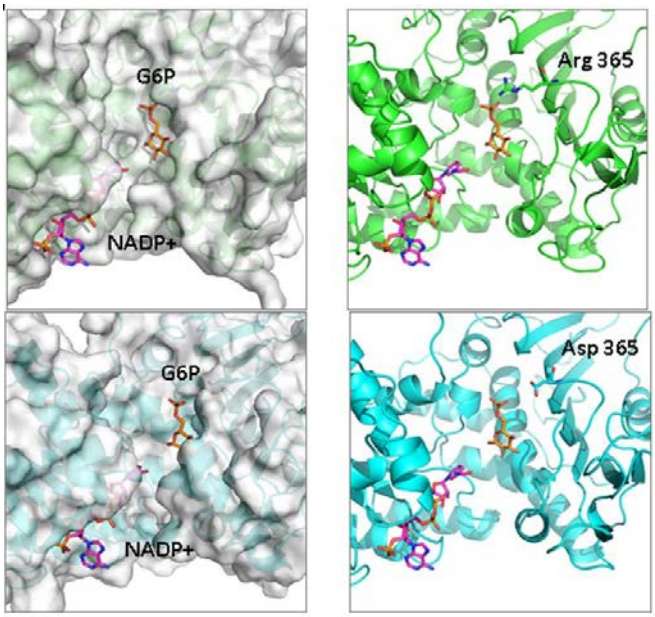

Figure 2. hG6PD (up) and *Pf*G6PD (down) in complex with the natural substrates, G6P and $NADP^+$.

Chemistry. We envisaged the synthesis of several substrate (G6P) analogs in which the phosphate group was replaced by different hydrogen bond donor and/or acceptor groups, namely thioether or sulfone (Scheme 1) or sulfonamide (Scheme 2), with short side chains terminating with protonatable amino or guanidino groups. For comparison purposes, some nitrile precursors, i.e. nitriles **4** and **6** (Scheme 1), were also subjected to biological evaluation.

The synthesis of thioether derivatives **2**–**5** and sulfones **6**–**8** was undertaken starting from the known chloroderivative **1**,[50] which was readily prepared by reaction of commercially available methyl α-D-glucopyranoside with methanesulfonyl chloride in DMF at 65 ºC.[51] Amine **2**, a compound recently described as an intermediate for the preparation of glycoclusters,[52] was prepared in quantitative yield by nucleophilic substitution reaction of chloroderivative **1** with cisteamine (Scheme 1). The novel guanidine **3** was synthesized from amine **2** upon reaction with 1*H*-pyrazole-1-carboxamidine hydrochloride and Et_3N in refluxing acetonitrile, and isolated in the form of its hydrochloride salt.

Reaction of chloroderivative **1** with the thiolate formed by deprotonation of 3-mercaptopropanenitrile with NaH in DMF afforded the novel cyanothioether **4** in quantitative yield, from which the novel thioether **5** and sulfones **6**–**8** were subsequently synthesized following standard procedures (Scheme 1). Thus, hydrogenation at 16 atm of cyanothioether **4** using Raney-Ni as the catalyst afforded the aminothioether **5** in moderate yield. *M*-Chloroperbenzoic acid oxidation of cyanothioether **4** gave in quantitative yield the corresponding cyanosulfone, **6**, from which the aminosulfone **7** was synthesized by Raney-Ni-catalyzed hydrogenation. Treatment of **7** with 1*H*-pyrazole-1-carboxamidine hydrochloride and Et_3N in refluxing acetonitrile afforded the guanidinosulfone **8** in 68% yield.

Scheme 1. Synthesis of thioether and sulfone derivatives 2–8[a]

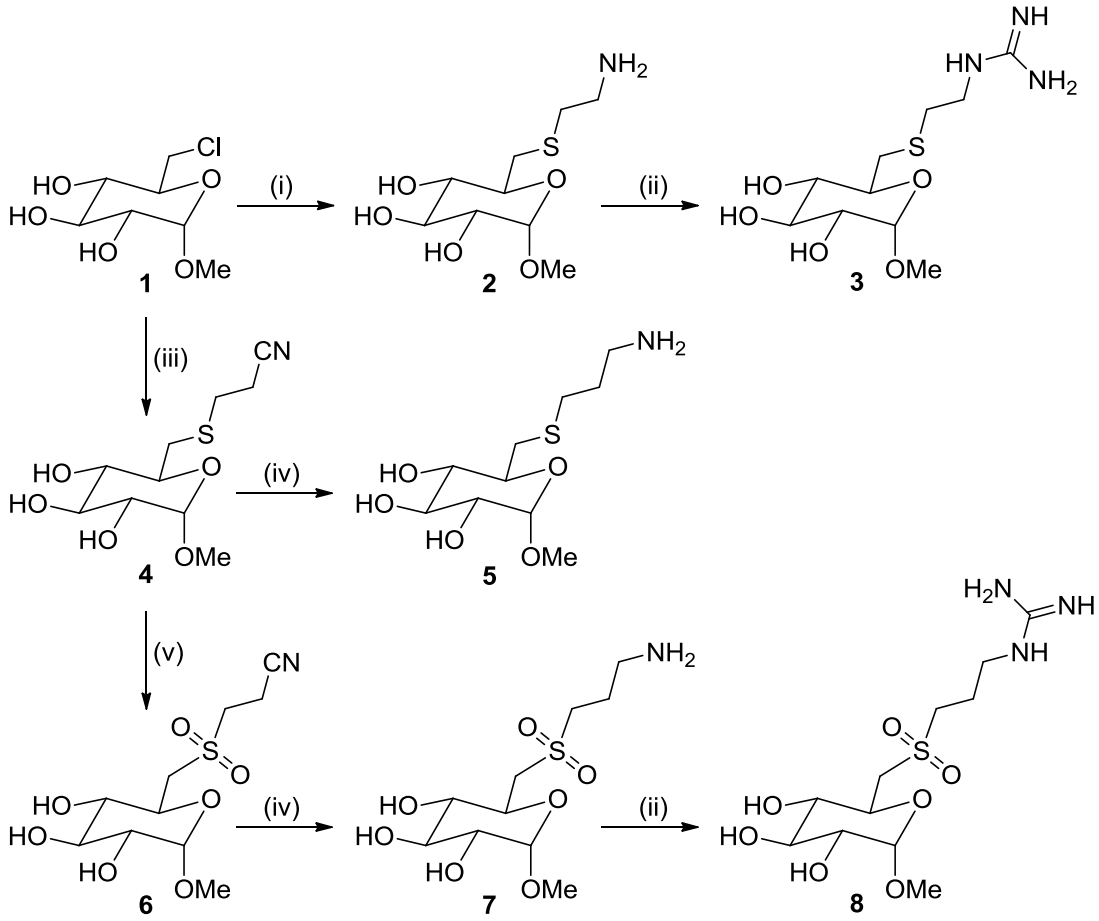

[a]Reagents and conditions: (i) cysteamine hydrochloride, NaH, DMF, 0 ºC, 10 min; then, **1**, room temperature, 48 h, quantitative yield; (ii) 1*H*-pyrazole-1-carboxamidine hydrochloride, Et_3N, acetonitrile, reflux, 6 h to overnight; then, HCl/MeOH, 39% yield (**3**·HCl), 62% (**8**·HCl); (iii) 3-mercaptopropanenitrile, NaH, DMF, 0 ºC, 10 min; then, **1**, room temperature, 72 h, quantitative yield; (iv) H_2 (16 atm), Raney-Ni, MeOH, room temperature, overnight, 41% yield (**5**), 28% yield (**7**); (v) *m*-chloroperbenzoic acid, $NaHCO_3$, CH_2Cl_2, 0 ºC; then, room temperature, 3 h, quantitative yield.

For the synthesis of the novel amino- and guanidinosulfonamides **11** and **12**, the known methyl 6-amino-6-deoxy-α-D-glucopyranoside,[53] **9**, was used as starting material

(Scheme 2). In turn, amine **9** was readily synthesized by reaction of chloroderivative **1** with potassium phthalimide in DMF at 100 ºC for 7 days, followed by hydrazinolysis. Reaction of amine **9** with 2-phthalimidoethanesulfonyl chloride,[54] previously prepared by reaction of taurine with phthalic anhydride, followed by reaction with PCl_5, gave in excellent yield the phthalimidosulfonamide **10**. Hydrazinolysis of **10** in refluxing MeOH afforded aminosulfonamide **11**, in low yield, after two tedious silica gel column chromatography purifications. Finally, aminosulfonamide **11** was converted into the corresponding guanidinosulfonamide, **12**, under the usual guanidinylation conditions (Scheme 2).

Scheme 2. Synthesis of sulfonamido derivatives 11 and 12[a]

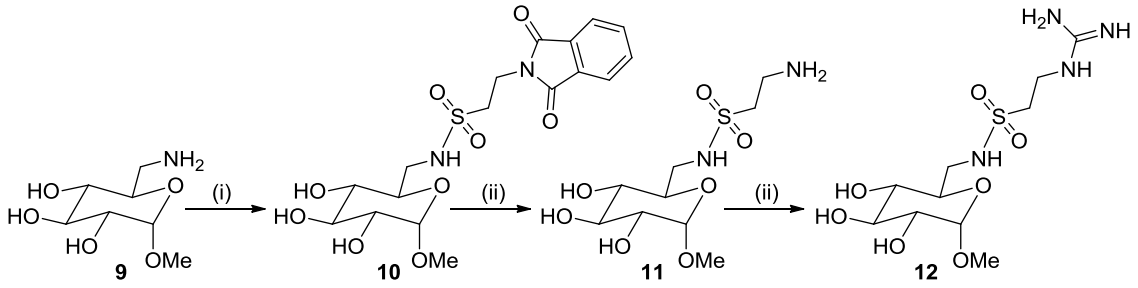

[a]Reagents and conditions: (i) 2-phthalimidoethanesulfonyl chloride, Et_3N, DMF, 0 ºC; then, room temperature, 6 days, 96% yield; (ii) hydrazine monohydrate, MeOH, reflux, overnight, 29% yield; (iii) 1*H*-pyrazole-1-carboxamidine hydrochloride, Et_3N, acetonitrile, reflux, 6 h; then, HCl/MeOH, 29% yield.

Biological Profiling. The novel compounds designed to differentially bind at the G6P site of the catalytic pocket of the dual *P. falciparum* enzyme glucose-6-phosphate dehydrogenase–6-phosphogluconolactonase were tested for *in vitro* inhibition of the parasite enzyme and the homologous human enzyme. Four out of the 9 tested

compounds displayed a considerably higher affinity towards the parasite enzyme, i.e. lower K_i^{G6P} values in the parasite enzyme than in the human enzyme. Thus, compounds **2**, **3**, **6**, and **11** showed K_i^{G6P} values between 23 and 76 μM in the parasite dual enzyme but > 200 μM to > 2000 μM in the human enzyme (Table 1). Conversely, the human enzyme was significantly inhibited by compounds **7**, **8**, and **12** at K_i^{G6P} values below 40 μM, very similar or even lower to the K_i^{G6P} values obtained for the malaria parasite enzyme.

As expected, those compounds that feature a terminal protonatable amino or guanidine group display higher affinities than those with a nonbasic cyano group, and among them, amino derivatives are more selective than guanidino derivatives for *Pf*G6PD over hG6PD. Regarding the inner functionality of the side chain at position 6, the affinity towards *Pf*G6PD follows the order sulfonamide > sulfone > thioether, with the sulfonyl oxygen atoms of sulfonamides and sulfones likely mimicking the hydrogen acceptor capability of the phosphate oxygen atoms of the substrate G6P.

Kinetic studies with compounds **2** and **11** within *Pf*G6PD or hG6PD, using a fixed concentration of NADP (200 μM) and variable concentrations of G6P and *viceversa*, have shown that these compounds are competitive with the substrate G6P but not with $NADP^+$. Indeed, regarding the parasite enzyme, the K_i^{G6P} values are clearly lower than the K_i^{NADP} values (76 μM vs 364 μM for compound **2**; 23 μM vs 269 μM for compound **11**). A similar situation is found for hG6PD, with compound **11** displaying K_i^{G6P} and K_i^{NADP} values of 440 μM and 1260 μM, respectively, whereas in compound **2** both K_i values were above 2000 μM.

Table 1. Affinity Values toward *Pf*G6PD and hG6PD and Antiplasmodial Activity of the Novel Compounds[a]

compd	K_i^{G6P} (μM) [*Pf*G6PD–6PGL]	K_i^{G6P} (μM) [hG6PD]	IC_{50} (mM) *P. falciparum*
2	76.1	> 2000	1.75
3	45.6	> 200	0.59
4	259	> 200	1.02
5	289	129	> 2
6	68.8	> 200	0.96
7	34.4	35.4	> 2
8	42.9	22.3	1.57
11	22.8	> 400	1.47
12	32.4	16.8	0.33

[a] K_i values are those of the forward enzymatic reaction using G6P as non-saturating substrate (between 10 and 300 μM) and saturating NADP concentrations (200 μM) using the purified parasite (K_i^{G6P} [*Pf*G6PD–6PGL]) or human (K_i^{G6P} [hG6PD]) enzyme. IC_{50} values were obtained in triplicate in *P. falciparum* cultures in human erythrocytes.

The *in vivo* phenotypic assay of the novel compounds on *P. falciparum* cultures showed curves clearly indicating a dose response effect, although with IC_{50} values in the high micromolar range from 330 μM to 1.75 mM (Table 1). To trace the targeting of the inhibitors on the *P. falciparum* intraerythrocytic cycle, the phenotype of the parasites growing in some selected inhibitors (**3**, **4**, **6**, and **12**) was analysed at 2 mM (Fig. 3). Interestingly, these G6PD–6PGL inhibitors showed a full effect in killing the parasites since upon 48 h incubation most parasite forms showed unviable pyknotic forms, mostly in mature stages (trophozoites). This result suggests a different mechanism to that of chloroquine, which kills the parasite at the stage of rings, the immature form, i.e. earlier than the new inhibitors.

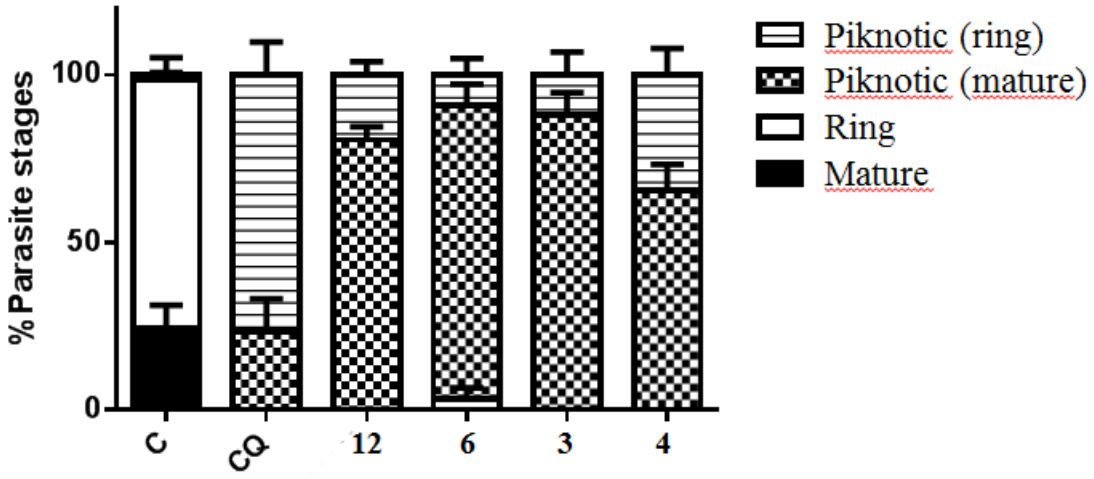

Figure 3. Phenotypic analysis of *P. falciparum* intraerythrocytic cycle upon exposure to compounds **3**, **4**, **6**, and **12** in comparison to chloroquine and a control. *In vitro* culture of *P. falciparum* during a complete erythrocytic cycle (48 h) was performed starting from young rings and incubated with the G6PD-6PGL inhibitors at 2 mM concentration and chloroquine (CQ) at 10 μM in parallel to a control culture (C) in the absence of inhibitors.

Cytotoxicity of the novel G6PD–6PGL inhibitors towards mammalian cells was also assayed using HEPG2 human hepatoma cells and concentrations of the inhibitors between 0.2 and 2.0 mM (Fig. 4). The novel compounds did not show significant loss of viability of HEPG2 human hepatoma cells, which showed percentages of survival above 80% for the range of inhibitor concentrations between 0.2 and 1.0 mM. Moreover, most of the inhibitors showing selectivity towards *Pf*G6PD, with K_i^{G6P} values for the human enzyme above 200 μM (**2**, **3**, **4**, **6**, and **11**) still maintained these viability values at the highest tested concentration of 2 mM. Nevertheless, those inhibitors showing a higher selectivity towards hG6PD, with K_i^{G6P} values for the human enzyme below 200 μM (**5**, **7**, **8**, and **12**) decreased cell viability below 80% at 1.5 and 2 mM concentrations.

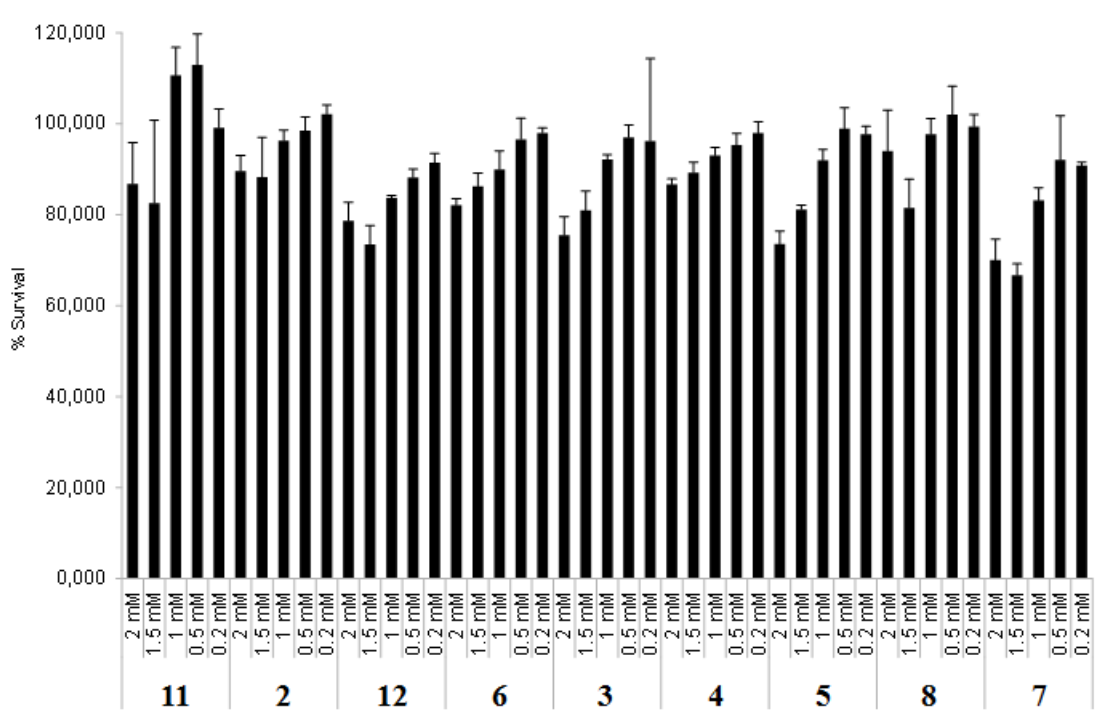

Figure 4. Cytotoxicity assays of the G6PD–6PGL inhibitors. HEPG2 human hepatoma cells were incubated with the inhibitors at four different concentrations (0.2, 0.5, 1.0, 1.5, and 2.0 mM). Viability of the HEPG2 human hepatoma cells after 24 h is plotted in comparison with 100% viability of control cultures in the absence of inhibitors.

CONCLUSIONS

Selective inhibition of the enzyme G6PD of *P. falciparum* has recently emerged as a promising novel therapeutic approach, which is expected to derive new drugs that may circumvent one of the main drawbacks of the current antimalarial drugs, namely the emergence of resistance. Only one family of selective inhibitors of *Pf*G6PD has been reported so far. These compounds were discovered after a HTS campaign and hit-to-lead optimization. In the absence of a X-ray 3D structure of *Pf*G6PD, we have built an homology model of this enzyme and used it to rationally design a family of analogs of the substrate G6P as selective *Pf*G6PD inhibitors, on the basis of a key structural difference between the human and parasite enzymes close to the G6P binding site,

which results from the change of the Arg365 residue in the human enzyme, positively charged at physiological pH, to a shorter and negatively charged Asp365 residue. In agreement with our working hypothesis, several compounds display moderate two-digit micromolar affinity and up to > 26-fold selectivity for *Pf*G6PD over hG6PD. These compounds seem to be competitive with regard to the substrate G6P but not to $NADP^+$ and are nontoxic to mammalian cells up to a concentration as high as 2 mM. In phenotypic assays with cultured *P. falciparum* parasites, the compounds exhibit submillimolar to low millimolar IC_{50} values, i.e. their antiplasmodial activity is one order of magnitude lower than their affinity towards *Pf*G6PD. These results likely reflect a poor permeation of the compounds across cell membranes, as a consequence of their high polarity. Interestingly, these compounds seem to act at a different stage of the parasite development than chloroquine, killing the parasites at the mature stages instead of at the earlier ring stage, thereby paving the way for potential combination therapies with sequential action at different stages of the parasite life cycle, once the physicochemical / pharmacokinetic issues are addressed in future lead optimization endeavors.

EXPERIMENTAL SECTION

Chemistry. General methods

Melting points were determined in open capillary tubes with a MFB 595010M Gallenkamp melting point apparatus. 400 MHz ^1H/ 100.6 MHz ^{13}C NMR spectra were recorded on a Varian Mercury 400 spectrometer at the Centres Científics i Tecnologics of the University of Barcelona (CCiTUB). The chemical shifts are reported in ppm (δ scale) relative to solvent signals (CD_3OD at 3.31 and 49.0 ppm in the ^1H and ^{13}C NMR

spectra, respectively), and coupling constants are reported in Hertz (Hz). Assignments given for the NMR spectra of the new compounds have been carried out by comparison with the NMR data of compounds **4**, **6**, and **10**, which in turn, were assigned on the basis of DEPT, COSY $^{1}H/^{1}H$ (standard procedures), and COSY $^{1}H/^{13}C$ (gHSQC and gHMBC sequences) experiments. IR spectra were run on a Perkin Elmer Spectrum RX I spectrophotometer. Absorption values are expressed as wavenumbers (cm^{-1}); only significant absorption bands are given. Optical rotations were measured on a PerkinElmer model 241 polarimeter. Column chromatography was performed on silica gel 60 AC.C (40−60 mesh, SDS, ref 2000027). Thin-layer chromatography was performed with aluminium-backed sheets with silica gel 60 F_{254} (Merck, ref 1.05554), and spots were visualized with UV light and 1% aqueous solution of $KMnO_4$. High resolution mass spectra was carried out at the CCiTUB with a LC/MSD TOF Agilent Technologies spectrometer.

Methyl 6-[(2-aminoethyl)thio]-6-deoxy-α-D-glucopyranoside, 2. A solution of cysteamine hydrochloride (235 mg, 2.07 mmol) in anhydrous DMF (9 mL) was cooled at 0 ºC with an ice bath, and then treated portionwise with NaH (60% dispersion in oil, 166 mg, 4.14 mmol). After stirring the mixture for 10 min, chloroderivative **1** (400 mg, 1.88 mmol) was added. The reaction mixture was stirred at room temperature for 48 h and evaporated under reduced pressure to give a yellow solid (877 mg), which was purified through column chromatography (40–60 μm silica gel, CH_2Cl_2 / MeOH / 50% aq. NH_4OH mixtures, gradient elution). On elution with CH_2Cl_2 / MeOH / 50% aq. NH_4OH 80:20:0 to 75:25:1, amine **2** (508 mg, quantitative yield) was isolated as a beige very hygroscopic solid; R_f 0.04 (CH_2Cl_2 / MeOH 7:3).

2·HCl: $[\alpha]^{20}_{D}$ = + 74 (*c* 0.88, MeOH); IR (ATR) *v* 3500–2500 (max at 3221, 2907, 2839, OH, $^{+}$NH, CH st) cm^{-1}; ^{1}H NMR (400 MHz, CD_3OD) δ 2.74 (dd, *J* = 14.4 Hz, *J'* = 8.0 Hz, 1H, 6-H_a), 2.88 (dd, *J* = 14.0 Hz, *J'* = 7.6 Hz, 1H, 1'-H_a), 2.92 (dd, *J* = 14.0

Hz, *J'* = 7.6 Hz, 1H, 1'-H_b), 3.00 (dd, *J* =14.4 Hz, *J'* =2.0 Hz, 1H, 6-H_b), 3.16 (t, *J* = 6.8 Hz, 2H, 2'-H_2), 3.25 (dd, *J* = *J'* = 9.6 Hz, 1H, 4-H), 3.39 (dd, *J* = 9.6 Hz, *J'* = 3.6 Hz, 1H, 2-H), 3,43 (s, 3H, 1-OCH_3), 3.59 (dd, *J* = *J'* = 9.6 Hz, 1H, 3-H), 3.68 (ddd, *J* = 9.6 Hz, *J'* = 8.0 Hz, *J''* = 2.0 Hz, 1H, 5-H), 4.66 (d, *J* = 3.6 Hz, 1H, 1-H), 4.85 (s, OH, $^{+}NH_3$); ^{13}C NMR (100.6 MHz, CD_3OD) δ 31.1 (CH_2, C1'), 34.2 (CH_2, C6), 39.9 (CH_2, C2'), 55.7 (CH_3, 1-OCH_3), 73.50 (CH), 73.54 (CH) (C2, C5), 74.3 (CH, C4), 74.9 (CH, C3), 101.3 (CH, C1); HRMS (ESI), calcd for ($C_9H_{19}NO_5S + H^+$) 254.1057, found 254.1056.

Methyl 6-deoxy-6-[(2-guanidinoethyl)thio]-α-D-glucopyranoside, 3. To a suspension of amine **2** (77 mg, 0.30 mmol) in acetonitrile (3 mL), Et_3N (0.04 mL, 29 mg, 0.29 mmol) and 1*H*-pyrazole-1-carboxamidine hydrochloride (58 mg, 0.40 mmol) were added. The reaction mixture was stirred under reflux overnight and cooled to room temperature. The solvent was poured off and the precipitate was dried in vacuo. The resulting brown sticky solid (46 mg) was taken in MeOH (5 mL), treated with methanolic HCl (0.5 N, 5 mL), and filtered through a 0.2 μm NYL filter. The filtrate was evaporated under reduced pressure, washed successively with CH_3CN (2 × 3 mL), CH_2Cl_2 (2 × 5 mL), and pentane (2 × 3 mL), and finally dried at 35 ºC / 30 Torr, to provide guanidine **3**·HCl (39 mg, 0.12 mmol, 39% yield) as a brownish hygroscopic solid; $[\alpha]^{20}_D$ = + 72 (*c* 2.2, MeOH); IR (ATR) *v* 3500–2500 (max at 3303, 3173, 2918, OH, ^{+}NH, NH, CH st), 1659, 1643, 1617 (C=N st) cm^{-1}; ^1H NMR (400 MHz, CD_3OD) δ 2.71 (dd, *J* = 14.4 Hz, *J'* = 8.0 Hz, 1H, 6-H_a), 2.81 (dt, *J* = 13.6 Hz, *J'* = 6.8 Hz, 1H, 1'-H_a), 2.86 (dt, *J* = 13.6 Hz, *J'* = 6.8 Hz, 1H, 1'-H_b), 3.00 (dd, *J* = 14.4 Hz, *J'* = 2.4 Hz, 1H, 6-H_b), 3.24 (dd, *J* = 9.6 Hz, *J'* = 9.2 Hz, 1H, 4-H), 3.39 (dd, *J* = 9.6 Hz, *J'* = 3.6 Hz, 1H, 2-H), 3.42 (t, *J* = 6.8 Hz, 2H, 2'-H_2), 3.43 (s, 3H, 1-OCH_3), 3.59 (dd, *J* = 9.6 Hz, *J'* = 9.2 Hz, 1H, 3-H), 3.66 (ddd, *J* = 9.6 Hz, *J'* = 8.0 Hz, *J''* = 2.4 Hz, 1H, 5-H), 4.65 (d, *J*

= 3.6 Hz, 1H, 1-H), 4.84 (s, OH, NH, NH_2, $^+NH_2$); ^{13}C NMR (100.6 MHz, CD_3OD) δ 33.0 (CH_2, C1'), 34.5 (CH_2, C6), 42.1 (CH_2, C2'), 55.6 (CH_3, 1-OCH_3), 73.5 (CH, C2), 73.7 (CH, C5), 74.4 (CH, C4), 74.9 (CH, C3), 101.1 (CH; C1), 158.6 (C, guanidine C); HRMS (ESI), calcd for ($C_{10}H_{21}N_3O_5S + H^+$) 296.1275, found 296.1279.

Methyl 6-[(2-cyanoethyl)thio]-6-deoxy-α-D-glucopyranoside, 4. A solution of 3-mercaptopropanenitrile (646 mg, 7.41 mmol) in anhydrous DMF (12 mL) was cooled at 0 ºC with an ice bath, and then treated portionwise with NaH (60% dispersion in oil, 296 mg, 7.40 mmol). After stirring the mixture for 10 min, chloroderivative **1** (700 mg, 3.29 mmol) was added. The reaction mixture was stirred at room temperature for 72 h and evaporated under reduced pressure to give a yellow solid (2.05 g), which was purified through column chromatography (40–60 μm silica gel, CH_2Cl_2 / MeOH mixtures, gradient elution). On elution with CH_2Cl_2 / MeOH 92:8 to 90:10, nitrile **4** (891 mg, quantitative yield) was isolated as a beige solid; R_f 0.34 (CH_2Cl_2 / MeOH 9:1).

A solution of **4** (50 mg, 0.19 mmol) in MeOH (5 mL) was filtered through a 0.20 μm NYL filter and evaporated under reduced pressure. After washing the resulting solid successively with CH_2Cl_2 (2 × 5 mL) and pentane (2 × 3 mL), and drying at 35 ºC / 30 Torr, the analytical sample of **4** (43 mg) was obtained as a yellowish hygroscopic solid; $[\alpha]^{20}_D$ = + 143 (*c* 0.86, MeOH); IR (ATR) *ν* 3335, 3192 (OH st), 2251 (CN st) cm^{-1}; ^1H NMR (400 MHz, CD_3OD) δ 2.73 (dd, *J* = 14.4 Hz, *J'* = 8.0 Hz, 1H, 6-H_a), 2.78 (t, *J* = 7.2 Hz, 2H, 2'-H_2), 2.86 (dd, *J* = 13.6 Hz, *J'* = 7.2 Hz, 1H, 1'-H_a), 2.93 (dd, *J* = 13.6 Hz, *J'* = 7.2 Hz, 1H, 1'-H_b), 3.03 (dd, *J* = 14.4 Hz, *J'* = 2.4 Hz, 1H, 6-H_b), 3.24 (dd, *J* = *J'* = 9.6 Hz, 1H, 4-H), 3.40 (dd, *J* = 9.6 Hz, *J'* = 3.6 Hz, 1H, 2-H), 3.44 (s, 3H, 1-OCH_3), 3.58 (dd, *J* = *J'* = 9.6 Hz, 1H, 3-H), 3.66 (ddd, *J* = 9.6 Hz, *J'* = 8.0 Hz, *J''* = 2.4 Hz, 1H, 5-H), 4.65 (d, *J* = 3.6 Hz, 1H, 1-H), 4.84 (s, OH); ^{13}C NMR (100.6 MHz, CD_3OD) δ 19.3 (CH_2, C2'), 29.9 (CH_2, C1'), 34.7 (CH_2, C6), 55.6 (CH_3, 1-OCH_3), 73.6

(CH, C2), 73.8 (CH, C5), 74.4 (CH, C4), 75.0 (CH, C3), 101.2 (CH, C1), 120.2 (C, CN); HRMS (ESI), calcd for ($C_{10}H_{17}NO_5S + NH_4^+$) 281.1166, found 281.1166.

Methyl 6-[(3-aminopropyl)thio]-6-deoxy-α-D-glucopyranoside, 5. A mixture of nitrile **4** (213 mg, 0.81 mmol) and Raney-Ni (50% water, 300 mg) in MeOH (80 mL) was reacted with hydrogen (16 atm) at room temperature overnight in a Parr stirred reactor. The resulting suspension was filtered through Celite® and rinsed with MeOH (25 mL). The solvent was removed in vacuo to afford a brownish oil (205 mg), which was purified through column chromatography (40–60 μm silica gel, CH_2Cl_2 / MeOH / 50% aq. NH_4OH mixtures, gradient elution). On elution with CH_2Cl_2 / MeOH / 50% aq. NH_4OH 75:25:1 to 65:35:1, amine **5** (88 mg, 41% yield) was isolated as a colourless sticky solid; R_f 0.11 (CH_2Cl_2 / MeOH / 50% aq. NH_4OH 7:3:0.1).

A solution of **5** (40 mg, 0.15 mmol) in MeOH (5 mL) was filtered through a 0.20 μm NYL filter, treated with methanolic HCl (0.5 N, 1.35 mL) and evaporated under reduced pressure. The resulting solid was washed successively with CH_2Cl_2 (2 × 5 mL) and pentane (2 × 3 mL) to give, after drying at 35 ºC / 30 Torr, **5**·HCl (44 mg) as a yellowish hygroscopic solid; $[\alpha]^{20}_D$ = + 171 (*c* 0.46, MeOH); IR (ATR) *v* 3500–2500 (max at 3301, 2912, 2854, 2839, OH, $^+$NH, CH st) cm^{-1}; ^{1}H NMR (400 MHz, CD_3OD) δ 1.99 (tt, $J = J' = 8.0$ Hz, 2H, 2'-H_2), 2.66 (dd, $J = 14.0$ Hz, $J' = 8.0$ Hz, 1H), 2.68 (dd, $J = 14.0$ Hz, $J' = 8.0$ Hz, 1H), 2.73 (m, 1H) (6-H_a, 1'-H_a, 1'-H_b), 2.98 (dd, $J = 14.0$ Hz, $J' = 2.8$ Hz, 1H, 6-H_b), 3.13 (t, $J = 8.0$ Hz, 2H, 3'-H_2), 3.22 (dd, $J = 9.6$ Hz, $J' = 8.8$ Hz, 1H, 4-H), 3.38 (dd, $J = 9.6$ Hz, $J' = 3.6$ Hz, 1H, 2-H), 3.42 (s, 3H, 1-OCH_3), 3.58 (dd, $J = 9.6$ Hz, $J' = 8.8$ Hz, 1H, 3-H), 3.65 (br dd, $J = 9.6$ Hz, $J' = 8.0$ Hz, 1H, 5-H), 4.63 (d, $J = 3.6$ Hz, 1H, 1-H), 4.85 (s, OH, $^+NH_3$); ^{13}C NMR (100.6 MHz, CD_3OD) δ 27.1 (CH_2, C2'), 30.6 (CH_2, C1'), 34.4 (CH_2, C6), 47.9 (CH_2, C3'), 55.6 (CH_3, 1-OCH_3), 73.5 (CH,

C2), 73.6 (CH, C5), 74.5 (CH, C4), 75.0 (CH, C3), 101.1 (CH, C1), HRMS (ESI), calcd for ($C_{10}H_{21}NO_5S + H^+$) 268.1213, found 268.1214.

Methyl 6-[(2-cyanoethyl)sulfonyl]-6-deoxy-α-D-glucopyranoside, 6. A suspension of nitrile **4** (210 mg, 0.80 mmol) and $NaHCO_3$ (181 mg, 2.16 mmol) in CH_2Cl_2 (3.5 mL) was cooled at 0 ºC with an ice bath and treated with *m*-chloroperbenzoic acid (77% purity, 483 mg, 2.16 mmol). The reaction mixture was stirred at room temperature for 3 h and evaporated under reduced pressure to give a solid residue (726 mg), which was purified through column chromatography (40–60 μm silica gel, CH_2Cl_2 / MeOH mixtures, gradient elution). On elution with CH_2Cl_2 / MeOH 92:8 to 88:12, slightly impure cyanosulfone **6** (289 mg, quantitative yield) was isolated; R_f 0.57 (CH_2Cl_2 / MeOH 8:2). A solution of **6** (21 mg, 0.07 mmol) in MeOH (5 mL) was filtered through a 0.20 μm NYL filter and evaporated under reduced pressure. The analytical sample of **6** (18 mg) was obtained by washing the resulting solid successively with CH_2Cl_2 (2 × 5 mL) and pentane (2 × 3 mL), and drying at 35 ºC / 30 Torr; mp 151–153 ºC; $[\alpha]^{20}_D = +127$ (*c* 0.38, MeOH); IR (ATR) *v* 3378, 3308 (OH st), 2270 (CN st), 1295, 1137, 1115 (SO_2 st) cm^{-1}; ^1H NMR (400 MHz, CD_3OD) δ 3.00 (t, J = 7.2 Hz, 2H, 2'-H_2), 3.16 (dd, J = 9.6 Hz, J' = 8.8 Hz, 1H, 4-H), 3.41 (dd, J = 9.6 Hz, J' =3.6 Hz, 1H, 2-H), superimposed in part 3.46 (dd, J = 14.0 Hz, J' = 2.4 Hz, 1H, 6-H_a), 3.47 (s, 3H, 1-OCH_3), superimposed in part 3.51 (dd, J = 14.0 Hz, J' = 9.6 Hz, 1H, 6-H_b), 3.53 (m, 1 H, 1'-H_a), 3.58 (dd, J = 14.0 Hz, J' = 7.2 Hz, 1H, 1'-H_b), 3.62 (dd, J = 9.6 Hz, J' = 8.8 Hz, 1H, 3-H), 4.06 (ddd, $J = J'$ = 9.6 Hz, J''= 2.4 Hz, 1H, 5-H), 4.71 (d, J = 3.6 Hz, 1H, 1-H), 4.85 (s, OH); ^{13}C NMR (100.6 MHz, CD_3OD) δ 11.5 (CH_2, C2'), 51.3 (CH_2, C1'), 56.0 (CH_2, C6), 56.4 (CH_3, 1-OCH_3), 68.7 (CH, C5), 73.2 (CH, C2), 74.1 (CH, C4), 74.7 (CH, C3), 101.6 (CH, C1), 118.6 (C, CN); HRMS (ESI), calcd for ($C_{15}H_{17}NO_7S + NH_4^+$) 313.1064, found 313.1062.

Methyl 6-[(3-aminopropyl)sulfonyl]-6-deoxy-α-D-glucopyranoside, 7. A mixture of cyanosulfone **6** (289 mg, 0.98 mmol) and Raney-Ni (50% water, 300 mg) in MeOH (80 mL) was reacted with hydrogen (16 atm) at room temperature overnight in a Parr stirred reactor. The resulting suspension was filtered through Celite® and rinsed with MeOH (25 mL). The solvent was removed in vacuo to afford a yellow oil (186 mg), which was purified through column chromatography (40–60 μm silica gel, CH_2Cl_2 / MeOH mixtures, gradient elution). On elution with CH_2Cl_2 / MeOH 82:18 to 78:22, aminosulfone **7** (82 mg, 28% yield) was isolated; R_f 0.09 (CH_2Cl_2 / MeOH / 50% aq. NH_4OH 7:3:0.1).

A solution of **7** (29 mg, 0.10 mmol) in MeOH (5 mL) was filtered through a 0.20 μm NYL filter, treated with methanolic HCl (0.5 N, 0.87 mL) and evaporated under reduced pressure. The resulting solid was washed successively with CH_2Cl_2 (2 × 5 mL) and pentane (2 × 3 mL) to give, after drying at 35 ºC / 30 Torr, **7**·HCl (19 mg) as a yellowish hygroscopic solid; $[\alpha]^{20}_{D}$ = + 147 (*c* 1.3, MeOH); IR (ATR) *ν* 3500–2500 (max at 3241, 2916, 2844, OH, $^{+}$NH, CH st), 1280, 1132, 1102 (SO_2 st) cm^{-1}; ^{1}H NMR (400 MHz, CD_3OD) *δ* 2.19 (tt, *J* = *J'* = 7.6 Hz, 2H, 2'-H_2), 3.13 (t, *J* = 7.6 Hz, 2H, 3'-H_2), 3.15 (dd, *J* = 9.6 Hz, *J'* = 8.8 Hz, 1H, 4-H), superimposed in part with the solvent signal 3.22 (dt, *J* = 14.0 Hz, *J'* = 7.6 Hz, 1H, 1'-H_a), superimposed in part with the solvent signal 3.33 (dt, *J* = 14.0 Hz, *J'* = 7.6 Hz, 1H, 1'-H_b), 3.40 (dd, *J* = 10.0 Hz, *J'* = 3.6 Hz, 1H, 2-H), superimposed in part 3.45 (dd, *J* = 12.0 Hz, *J'* = 8.0 Hz, 1H, 6-H_a), superimposed in part 3.459 (dd, *J* = 12.0 Hz, *J'* = 4.0 Hz, 1H, 6-H_b), 3.460 (s, 3H, 1-OCH_3), 3.62 (dd, *J* = 10.0 Hz, *J'* = 8.8 Hz, 1H, 3-H), 4.06 (ddd, *J* = 9.6 Hz, *J'* = 8.0 Hz, *J''* = 4.0 Hz, 1H, 5-H), 4.69 (d, *J* = 3.6 Hz, 1H, 1-H), 4.85 (s, OH, $^{+}NH_3$); ^{13}C NMR (100.6 MHz, CD_3OD) *δ* 21.3 (CH_2, C2'), 39.5 (CH_2, C3'), 53.0 (CH_2, C1'), 55.9 (CH_2,

C6), 56.3 (CH_3, 1-OCH_3), 68.6 (CH, C5), 73.3 (CH, C2), 74.2 (CH, C4), 74.7 (CH, C3), 101.5 (CH, C1); HRMS (ESI), calcd for ($C_{10}H_{21}NO_7S + H^+$) 300.1111; found 300.1114.

Methyl 6-deoxy-6-[(3-guanidinopropyl)sulfonyl]-α-D-glucopyranoside, 8. To a suspension of aminosulfone **7** (27 mg, 0.09 mmol) in acetonitrile (1 mL), Et_3N (0.02 mL, 15 mg, 0.14 mmol) and 1*H*-pyrazole-1-carboxamidine hydrochloride (16 mg, 0.11 mmol) were added. The reaction mixture was stirred under reflux for 6 h and cooled to room temperature. The solvent was poured off and the precipitate was dried in vacuo. The resulting yellow sticky solid (39 mg) was taken in MeOH (2 mL), treated with methanolic HCl (0.5 N, 2 mL), and filtered through a 0.2 μm NYL filter. The filtrate was evaporated under reduced pressure, washed successively with CH_3CN (2 × 2 mL), CH_2Cl_2 (2 × 2 mL), and pentane (2 × 2 mL), and dried at 35 ºC / 30 Torr, to provide guanidine **8**·HCl (21 mg, 0.05 mmol, 62% yield) as a yellowish hygroscopic solid; $[\alpha]^{20}_D$ = + 155 (*c* 0.80, MeOH); IR (ATR) *ν* 3500–2500 (max at a 3335, 3313, 3160, 2928, 2912, OH, NH^+, NH, CH st), 1644, 1630 (C=N st), 1293, 1104 (SO_2 st) cm^{-1}; ^1H NMR (400 MHz, CD_3OD) *δ* 2.10 (tt, *J* = *J'* = 7.6 Hz, 2H, 2'-H_2), 3.15 (dd, *J* = 9.6 Hz, *J'* = 9.2 Hz, 1H, 4-H), 3.24–3.35 (complex signal, 2H, 1'-H_a, 1'-H_b), 3.35 (t, *J* = 7.6 Hz, 2H, 3'-H_2), 3.41 (dd, *J* = 9.6 Hz, *J'* = 4.0 Hz, 1H, 2-H), 3.42–3.48 (complex signal, 2H, 6-H_a, 6-H_b), 3.46 (s, 3H, 1-OCH_3), 3.62 (dd, *J* = 9.6 Hz, *J'* = 9.2 Hz, 1H, 3-H), 4.06 (ddd, *J* = *J'* = 9.6 Hz, *J''* = 5.6 Hz, 1H, 5-H), 4.70 (d, *J* = 4.0 Hz, 1H, 1-H), 4.85 (s, OH, NH, NH_2, $^+NH_2$); ^{13}C NMR (100.6 MHz, CD_3OD) *δ* 22.7 (CH_2, C2'), 40.9 (CH_2, C3'), 53.0 (CH_2, C1'), 55.9 (CH_2, C6), 56.3 (CH_3, 1-OCH_3), 68.6 (CH, C5), 73.3 (CH, C2), 74.2 (CH, C4), 74.7 (CH, C3), 101.5 (CH, C1), 158.7 (C, guanidine C); HRMS (ESI), calcd for ($C_{11}H_{23}N_3O_7S + H^+$) 342.1329; found 342.1367.

Methyl 6-deoxy-6-(2-phthalimidoethanesulfonamido)-α-D-glucopyranoside, 10. A solution of amine **9** (500 mg, 2.59 mmol) and Et_3N (0.51 mL, 370 mg, 3.66 mmol) in

anhydrous DMF (15 mL) was cooled at 0 ºC with an ice bath and treated with 2-phthalimidoethanesulfonyl chloride (744 mg, 2.72 mmol). The reaction mixture was stirred at room temperature for 6 days, treated with NH_4Cl (5 mL), and evaporated under reduced pressure to give a solid residue (2.51 g), which was purified through column chromatography (40–60 μm silica gel, CH_2Cl_2 / MeOH mixtures, gradient elution). On elution with CH_2Cl_2 / MeOH 90:10, phthalimidosulfonamide **10** (1.07 g, 96% yield) was isolated as a white solid; R_f 0.52 (CH_2Cl_2 / MeOH 9:1); mp 143–145 ºC; $[\alpha]^{20}_D$ = + 100 (*c* 0.28, MeOH); IR (ATR) *v* 3449, 3311 (OH, NH st), 1770, 1705 (C=O st), 1316, 1142 (SO_2 st) cm^{-1}; ^1H NMR (400 MHz, CD_3OD) δ superimposed in part 3.23 (dd, *J* = 9.6 Hz, *J'* = 8.8 Hz, 1H, 4-H), 3.24 (dd, *J* = 14.0 Hz, *J'* = 6.8 Hz, 1H, 6-H_a), superimposed in part 3.42 (dd, *J* = 9.6 Hz, *J'* = 3.6 Hz, 1H, 2-H), 3.43 (s, 3H, 1-OCH_3), 3.47 (dt, *J* = 12.0 Hz, *J'* = 6.8 Hz, 1H, 1'-H_a), 3.49 (dt, *J* = 12.0 Hz, *J'* = 6.8 Hz, 1H, 1'-H_b), 3.52 (dd, *J* = 14.0 Hz, *J'* = 2.8 Hz, 1H, 6-H_b), 3.59 (ddd, *J* = 9.6 Hz, *J'* = 6.8 Hz, *J''* = 2.8 Hz, 1H, 5-H), 3.61 (dd, *J* = 9.6 Hz, *J'* = 8.8 Hz, 1H, 3-H), 4.12 (t, *J* = 6.8 Hz, 2H, 2'-H_2), 4.71 (d, *J* = 3.6 Hz, 1H, 1-H), 4.84 (s, OH, NH), 7.80 (m, 2H, phthalimide H_{meta}), 7.87 (m, 2H, phthalimide H_{ortho}); ^{13}C NMR (100.6 MHz, CD_3OD) δ 33.8 (CH_2, C2'), 45.1 (CH_2, C6), 50.2 (CH_2, C1'), 55.8 (CH_3, 1-OCH_3), 72.1 (CH, C5), 72.9 (CH, C4), 73.5 (CH, C2), 74.9 (CH, C3), 101.3 (CH, C1), 124.3 (2CH, phthalimide C_{ortho}), 133.4 (2C, phthalimide C_{ipso}), 135.5 (2CH, phthalimide C_{meta}), 169.4 (2C, phthalimide CO); HRMS (ESI), calcd for ($C_{17}H_{22}N_2O_9S + H^+$) 431.1119; found 431.1120.

Methyl 6-(2-aminoethanesulfonamido)-6-deoxy-α-D-glucopyranoside, 11. To a solution of phthalimidosulfonamide **10** (473 mg, 1.10 mmol) in MeOH (3.3 mL), hydrazine monohydrate (0.07 mL, 72 mg, 1.44 mmol) was added, and the reaction mixture was stirred under reflux overnight. The resulting mixture was evaporated under

reduced pressure to give a solid residue (516 mg). After two consecutive column chromatography purifications (40–60 μm silica gel, CH_2Cl_2 / MeOH / 50% aq. NH_4OH mixtures, gradient elution), aminosulfonamide **11** (95 mg, 29% yield) was isolated on elution with CH_2Cl_2 / MeOH / 50% aq. NH_4OH 80:20:0.2; R_f 0.06 (CH_2Cl_2 / MeOH / 50% aq. NH_4OH 8:2:0.05).

A solution of **11** (95 mg, 0.32 mmol) in MeOH (1 mL) was filtered through a 0.2 μm NYL filter, treated with methanolic HCl (0.5 N, 2.84 mL), and evaporated under reduced pressure. The resulting solid was washed with pentane (3 × 3 mL) and dried at 35 ºC / 30 Torr, to provide **11**·HCl (85 mg) as a brown highly hygroscopic solid; mp 72–76 ºC; $[\alpha]^{20}_{D}$ = + 6 (*c* 0.52, MeOH); IR (ATR) *ν* 3500–2500 (max at 3221, 3141, 2902, 2839, OH, NH^+, NH, CH st), 1310, 1141 (SO_2 st) cm^{-1}; ^1H NMR (400 MHz, CD_3OD) *δ* 3.19 (dd, *J* = 9.6 Hz, *J'* = 9.2 Hz, 1H, 4-H), 3.26 (dd, *J* = 14.0 Hz, *J'* = 6.8 Hz, 1H, 6-H_a), 3.39 (dd, *J* = 9.2 Hz, *J'* = 4.0 Hz, 1H, 2-H), 3.37–3.40 (complex signal, 2H), 3.43–3.48 (complex signal, 2H) (1'-H_a, 1'-H_b, 2'-H_2), 3.43 (s, 3H, 1-OCH_3), 3.53 (dd, *J* = 14.0 Hz, *J'* = 2.8 Hz, 1H, 6-H_b), 3.59 (ddd, *J* = 9.6 Hz, *J'* = 6.8 Hz, *J''* = 2.8 Hz, 1H, 5-H), 3.61 (dd, *J* = *J'* = 9.2 Hz, 1H, 3-H), 4.70 (d, *J* = 4.0 Hz, 1H, 1-H), 4.85 (s, OH, NH); ^{13}C NMR (100.6 MHz, CD_3OD) *δ* 35.9 (CH_2, C2'), 45.0 (CH_2, C6), 50.2 (CH_2, C1'), 55.8 (CH_3, 1-OCH_3), 72.1 (CH, C5), 72.8 (CH, C4), 73.5 (CH, C2), 74.9 (CH, C3), 101.3 (CH, C1); HRMS (ESI), calcd for ($C_9H_{20}N_2O_7S + H^+$) 301.1064; found 301.1060.

Methyl 6-deoxy-6-(2-guanidinoethanesulfonamido)-α-D-glucopyranoside, 12. To a suspension of aminosulfonamide **11** (67 mg, 0.22 mmol) in acetonitrile (2 mL), Et_3N (0.06 mL, 44 mg, 0.43 mmol) and 1*H*-pyrazole-1-carboxamidine hydrochloride (38 mg, 0.26 mmol) were added. The reaction mixture was stirred under reflux for 6 h and cooled to room temperature. The solvent was poured off and the precipitate was dried in

vacuo. The resulting brown sticky solid (65 mg) was taken in MeOH (5 mL), treated with methanolic HCl (0.5 N, 5 mL), and filtered through a 0.2 μm NYL filter. The filtrate was evaporated under reduced pressure, washed successively with CH_3CN (2 × 3 mL), CH_2Cl_2 (2 × 5 mL), and pentane (2 × 3 mL), and dried at 35 ºC / 30 Torr, to provide guanidine **12**·HCl (24 mg, 0.06 mmol, 29% yield) as a brownish highly hygroscopic solid; $[\alpha]^{20}_{D}$ = + 17 (*c* 0.35, MeOH); IR (ATR) *v* 3500–2500 (max at 3340, 3174, 2907, 2844, OH, $^{+}$NH, NH, CH st), 1650, 1643, 1630 (C=N st), 1309, 1139 (SO_2 st) cm^{-1}; ^{1}H NMR (400 MHz, CD_3OD) δ superimposed in part 3.20 (dd, *J* = 9.6 Hz, *J'* = 9.2 Hz, 1H, 4-H), 3.24 (dd, *J* = 14.0 Hz, *J'* = 7.2 Hz, 1H, 6-H_a), 3.34–3.39 (complex signal, 2H, 1'-H_a, 1'-H_b), superimposed in part 3.42 (dd, *J* = 9.6 Hz, *J'* = 4.0 Hz, 1H, 2-H), 3.43 (s, 3H, 1-OCH_3), 3.52 (dd, *J* = 14.0 Hz, *J'* = 2.8 Hz, 1H, 6-H_b), superimposed in part 3.59 (ddd, *J* = 9.6 Hz, *J'* = 7.2 Hz, *J''* = 2.8 Hz, 1H, 5-H), 3.61 (dd, *J* = 9.6 Hz, *J'* = 9.2 Hz, 1H, 3-H), 3.66 (t, *J* = 6.0 Hz, 2H, 2'-H_2), 4.69 (d, *J* = 4.0 Hz, 1H, 1-H), 4.85 (s, OH, NH, NH_2, $^{+}NH_2$); ^{13}C NMR (100.6 MHz, CD_3OD) δ 37.6 (CH_2, C2'), 44.9 (CH_2, C6), 51.9 (CH_2, C1'), 55.8 (CH_3, 1-OCH_3), 72.1 (CH, C5), 72.7 (CH, C4), 73.4 (CH, C2), 74.8 (CH, C3), 101.2 (CH, C1), 158.6 (C, guanidine C); HRMS (ESI), calcd for ($C_{10}H_{22}N_4O_7S$ + H^+) 343.1282; found 343.1280.

***In vitro* culture of *Plasmodium falciparum*.** *P. falciparum* strain Dd2 (clone MRA-150; Malaria Research and Reference Reagent Resource Center: http://www.mr4.org), maintained in continuous culture following the protocol previously described.[55] The culture media consisted of standard RPMI 1640 (Sigma-Aldrich) supplemented with 0.5 % Albumax I (Gibco), 100 μM hypoxanthine (Sigma-Aldrich), 25 mM HEPES (Sigma-Aldrich), 12.5 μg/mL gentamicine (Sigma-Aldrich), and 25 mM $NaHCO_3$ (Sigma-Aldrich), and incubated in 5% CO_2 at 37 ºC in tissue culture flasks (Iwaki). The progress of growth in the culture was determined by microscopy in thin blood smears

stained with Wright's eosin methylene blue solution (Merck), using the freely available Plasmoscore software[56] to monitor the parasitaemia. The detailed description of the culture and synchronization methods used have been reported previously.[55]

Antimalarial drug activity assay. Drug activity was assayed by the PicoGreen microfluorimetric DNA-based assay monitoring parasite growth inhibition at different drug concentrations.[57] PicoGreen (P7589) was purchased from Invitrogen and diluted as indicated by the manufacturer in TE buffer (10 mM Tris-HCl, 1 mM EDTA, pH 7.5). Synchronized rings from stock cultures were used to test serial dilutions of the inhibitors in 96-well culture microplates. Thus, 150 µL of parasites at 2% hematocrit and 1% parasitemia were allowed to grow for 48 h in 5% CO_2 at 37 ºC. The parasites were then centrifuged at 600 × g for 10 min and resuspended in saponin (0.15%, wt/vol, in phosphate-buffered saline (PBS)) to lyse the erythrocytes and release the malaria parasites. To eliminate all traces of hemoglobin, the pellet was washed by the addition of 200 µL of PBS followed by centrifugation at 600 × g. The washing step was repeated twice to ensure complete removal of hemoglobin. Finally, pellets were resuspended in 100 µL of PBS. A 100-µL volume of PicoGreen diluted in TE was added to each well. Plates were incubated for 30 to 60 min in the dark, and the fluorescence intensity was measured at 485-nm excitation and 528-nm emission. Growth inhibition defining the half maximal inhibitory concentration (IC_{50}) was calculated as previously described.[57] Upon treatment, the parasite morphology was evaluated by microscopic analysis of thin blood smears stained with Wright's stain. Smears from drug-free cultures were used as a control.

Steady-state enzymatic assays to characterize human and parasite G6PD inhibition. To compare the mechanism of action of the inhibitors, the kinetic parameters of human and *P. falciparum* G6PD were determined in a range of concentrations in the linear portion of the Lineweaver-Burk plots in the presence and absence of inhibitor for analysis and curve fitting into the Michaelis-Menten equation. These assays were run in triplicate in a 900 μL of a mixture containing 0.1 M Tris (pH 8.0) and varying concentrations of glucose-6-phosphate (10–300 μM) or $NADP^+$ (5–200 μM) at the corresponding saturating concentrations of the other substrate: $NADP^+$ or glucose-6-phosphate (200 μM). The inhibitor was added to the mixture without prior incubation at concentrations between 40 and 160 μM. In all experiments the exact concentrations of the solutions of glucose-6-phosphate and $NADP^+$ were enzymatically determined. The assays were carried out at 25 ºC in a Perkin-Elmer LS-50B spectrofluorimeter, and the linear increase in fluorescence intensity of the NADPH levels were observed at 450 nm emission (excitation at 340 nm). Care was taken to ensure that initial rates were measured along the time length of the assay (5–10 min). K_i, K_M and V_{max} values were calculated using Graphpad Prism software.
Recombinant human G6PD was obtained as previously reported.[58] *P. falciparum* G6PD was partially purified from cultures at 80–90% trophozoites according to previously reported procedures.[59]

***In vitro* cell viability assay.** HEPG2 human hepatoma cells were cultured 24 h in triplicate in 96-well flat-bottomed microplates in DMEM Glutamax (GIBCO) growth medium in a final volume of 100 μL per well. Cells grown in the presence of medium alone were used as controls. To evaluate the potential cytotoxic effect of the G6PD inhibitors, one set of plates received serial dilutions from 0.2 to 2 mM of each inhibitor.

Cells were seeded during 24 h and 48 h in triplicate in 96-well flat-bottomed microplates at a density of 5×10^3 cells per well in 100 μL growth medium. Treatment and control in growth medium was performed after 24 h and during further 24 h incubation in a final volume of 200 μL (100 μL cells + 100 μL medium with or without treatment). Following treatment, cell viability was determined by means of the colorimetric EZ4U (Biomedica, Vienna, Austria) according to the manufacturers instructions, and absorbance at 490/610 nm was measured spectrophotometrically in a Cary 50 BIO Microplate Reader 50MPR (Varian).

Homology modeling. Homology modeling was used to build up the tertiary structure of *Pf*G6PD. The FASTA sequence of *Pf*G6PD was obtained in UNIPROT Data Bank with code Q8IKU0. An alignment between primary sequence of *Pf*G6PD from different *Plasmodium* species, *L. mesenteroides,* and human enzymes was made. The human enzyme (PDB code: 2BLH)[60] was used to build the tertiary structure of *Pf*G6PD (41% sequence identity). The result of this alignment is shown in Fig. 5. The Modeller[61] program was applied to generate 10 satisfactory models for the hOGA. This program uses an automated modeling technique that significantly improves the accuracy of loop predictions in protein structures.[62] The stereochemical quality of the structures was evaluated using Molprobity,[63] while the distribution of residual energy was evaluated with Anolea.[64] Finally, the model with the lowest energy and lowest restraint violation was selected for MD simulations.

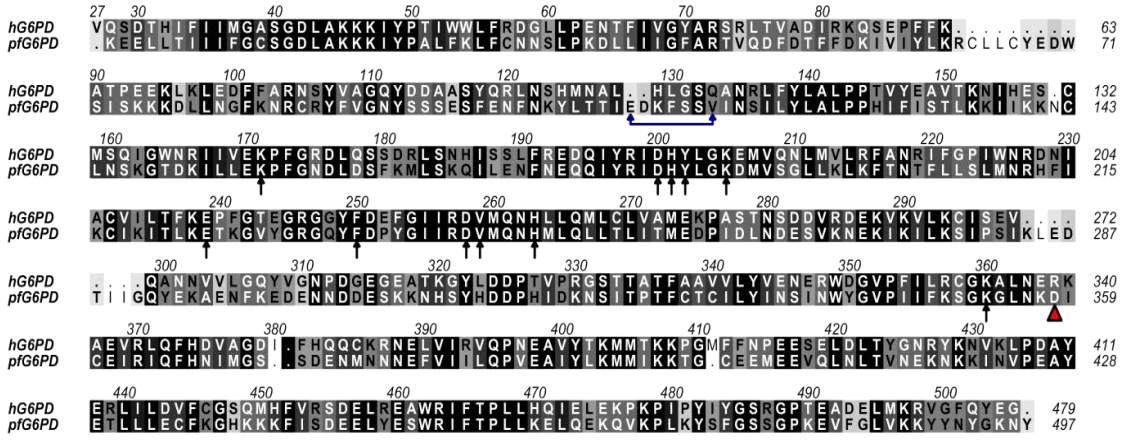

Figure 5. Alignment between primary sequences of humanized *Pf*G6PD and hG6PD enzymes.

Molecular docking. The molecular docking was conducted using the modeled structure of the *Pf*G6PD enzyme and the PDB structures of the G6PD−G6P complex from *L. mesenteroides* and human species. The molecular docking was found to be standard by the Molegro Virtual Docker (MVD) software. The algorithm used was the MolDock score ($E_{score} = E_{inter} + E_{intra}$), an adaptation of the differential evolution algorithm, where Einter is the ligand–protein interaction energy and Eintra is the internal energy of the ligand.[65,66] The binding orientations and geometries for G6P re-docked in the hG6PD active site can be superimposed and are consistent with the published X-ray structure. With the goal of validating the theoretical model, the MolDock score (kcal/mol) from G6P binding and analogues was close to that obtained from G6P binding to hG6PD.

Molecular dynamics. The computational model for the MD calculations was taken from the models of *Pf*G6PD obtained by homology modeling with the G6P substrate and the docked ligands. Classical molecular dynamics (MD) simulations were performed with the CUDA-accelerated version of the PMEMD module as implemented

in AMBER12[67] software package. All ligands in study were parametrized using gaff and parm99SB force field.[68] For all compounds the atomic point charges were determined using the RES procedure by fitting the HF/6-31G(d) electrostatic potential. Each ligand was immersed in an octahedral box of TIP3P water molecules, and the Xleap module was used to add the proper number of Cl- counter ions to neutralize the overall charge of the simulated system. Prior to the production runs, the energy of each system was minimized, and then the system was equilibrated by rising the temperature from 50 to 298 K in 200 ps at constant volume. Finally, the density of the system was equilibrated in a subsequent 200 ps run using the NPT (298 K, 1 bar) ensemble.

AUTHOR INFORMATION

Corresponding Authors

* For F.J.L.: phone: +34-934033788; E-mail: fjluque@ub.edu.

* For D.M.-T.: phone: +34-934024533; E-mail: dmunoztorrero@ub.edu.

Author Contributions

‡ These authors contributed equally.

Notes

The authors declare no competing financial interest.

ACKNOWLEDGMENTS

This work was supported by Ministerio de Economía y Competitividad (MINECO) (SAF2014-57094-R) and Generalitat de Catalunya (GC) (2014SGR52, 2014SGR1189). Fellowships from GC to I.S. and C.P., from FIS to J.J.-J., and the ICREA support to F.J.L. are gratefully acknowledged. The Center for Scientific and Academic Services of Catalonia (CESCA) is acknowledged for providing access to computational facilities.

ABBREVIATIONS USED

G6P, glucose-6-phosphate; G6PD, glucose-6-phosphate dehydrogenase; G6PDd, glucose-6-phosphate dehydrogenase deficiency; hG6PD, human glucose-6-phosphate dehydrogenase; HTS, high throughput screening; MD, molecular dynamics; NADPH, nicotinamide adenine dinucleotide phosphate; PBS, phosphate-buffered saline; *Pf*G6PD, *Plasmodium falciparum* glucose-6-phosphate dehydrogenase; *Pf*GluPho, *P. falciparum* glucose-6-phosphate dehydrogenase–6-phosphogluconolactonase; 6PL, 6-phosphogluconolactonase; PPP, pentose phosphate pathway; RBC, red blood cells.

REFERENCES

(1) World Malaria Report 2015; World Health Organization: Geneva, 2015; http://apps.who.int/iris/bitstream/10665/200018/1/9789241565158_eng.pdf?ua=1.

(2) Cunhaa, C. B.; Cunha, B. A. Brief history of the clinical diagnosis of malaria: from Hippocrates to Osler. *J. Vector Dis.* **2008**, *45*, 194−199.

(3) Fortin, A.; Stevenson, M. M.; Gros, P. Susceptibility to malaria as a complex trait: big pressure from a tiny creature. *Hum. Mol. Genet*. **2002**, *11*, 2469–2478.

(4) Kwiatkowski, D. P. How malaria has affected the human genome and what human genetics can teach us about malaria. *Am. J. Hum. Genet.* **2005**, *77*, 171–190.

(5) Winzeler, E. A. Malaria research in the post-genomic era. *Nature* **2008**, *455*, 751−756.

(6) Beutler, E. G6PD deficiency. *Blood* **1994**, *84*, 3613-3636.

(7) Beutler, E. Glucose-6-phosphate dehydrogenase deficiency: a historical perspective. *Blood* **2008**, *111*, 16−24.

(8) WHO Working Group. Glucose-6-phosphate dehydrogenase deficiency. *B. World Health Organ.* **1989**, *67*, 601−611.

(9) Beutler, E. GGPD: Population genetics and clinical manifestations. *Blood Rev.* **1996**, *10*, 45−52.

(10) Luzzatto, L. Glucose 6-phosphate dehydrogenase deficiency: from genotype to phenotype. *Haematologica* **2006**, *91*, 1303−1306.

(11) Mason, P. J.; Bautista, J. M.; Gilsanz, F. G6PD deficiency: the genotype-phenotype association. *Blood Rev.* **2007**, *21*, 267–283.

(12) Tishkoff, S. A.; Varkonyi, R.; Cahinhinan, N.; Abbes, S.; Argyropoulos, G.; Destro-Bisol, G.; Drousiotou, A.; Dangerfield, B.; Lefranc, G.; Loiselet, J.; Piro, A.; Stoneking, M.; Tagarelli, A.; Tagarelli, G.; Touma, E. H.; Williams, S. M.; Clark, A. G. Haplotype diversity and linkage disequilibrium at human G6PD: recent origin of alleles that confer malarial resistance. *Science* **2001**, *293*, 455−462.

(13) Nkhoma, E. T.; Poole, C.; Vannappagari, V.; Hall, S. A.; Beutler, E. The global prevalence of glucose-6-phosphate dehydrogenase deficiency: a systematic review and meta-analysis. *Blood Cells Mol. Dis.* **2009**, *42*, 267−278.

(14) Manganelli, G.; Masullo, U.; Passarelli, S.; Filosa, S. Glucose-6-phosphate dehydrogenase deficiency: disadvantages and possible benefits. *Cardiovasc. Hematol. Disord. Drug Targets*, **2013**, *13*, 73−82.

(16) Cappellini, M. D.; Fiorelli, G. Glucose-6-phosphate dehydrogenase deficiency. *Lancet* **2008**, *371*, 64−74.

(17) Allison, A. C.; Clyde, D. F. Malaria in African children with G6PD-deficient erythrocyte glucose-6-phosphate dehydrogenase. *Br. Med. J.* **1961**, *1*, 1346−1349.

(18) Kruatrachue, M.; Charoenlarp, P.; Chongsuphajaisiddhi, T.; Harina-suta, C. Erythrocyte glucose-6-phosphate dehydrogenase and malaria in Thailand. *Lancet* **1962**, *2*, 1183−1186.

(19) Bienzle, U.; Ayeni, O.; Lucas, A. O.; Luzzatto, L. Glucose-6-phosphate dehydrogenase and malaria. Greater resistance of females heterozygous for enzyme deficiency and of males with non-deficient variant. *Lancet* **1972**, *1*, 107−110.

(20) Kar, S.; Seth, S.; Seth, P. K. Prevalence of malaria in Ao Nagas and its association with G6PD and HbE. *Hum. Biol.* **1992**, *64*, 187−197.

(21) Ruwende, C.; Khoo, S. C.; Snow, R. W.; Yates, S. N. R.; Kwiatkowski, D.; Gupta, S.; Warn, P.; Allsopp, C. E. M.; Gilbert, S. C.; Peschu, N.; Newbold, C. I.; Greenwood, B. M.; Marsh, K.; Hill, A. V. S. Natural selection of hemi- and heterozygotes for G6PD deficiency in Africa by resistance to severe malaria. *Nature* **1995**, *376*, 246−249.

(22) Mombo, L.; Ntoumi, F.; Bisseye, C.; Ossari, S.; Lu, C.; Nagel, R. L.; Krishnamoorthy, R. Human genetic polymorphisms and asymptomatic *Plasmodium falciparum* malaria in Gabonese schoolchildren. *Am. J. Trop. Med. Hyg.* **2003**, *68*, 186−190.

(23) Guindo, A.; Fairhurst, R. M.; Doumbo, O. K.; Wellems, T. E.; Diallo, D. A. X-Linked G6PD deficiency protects hemizygous males but not heterozygous females against severe malaria. *Plos Med.* **2007**, *4*, e66.

(24) Ouattara, A. K.; Bisseye, C.; Bazie, B. V.; Diarra, B.; Compaore, T. R.; Djigma, F.; Pietra, V.; Moret, R.; Simpore, J. Glucose-6-phosphate dehydrogenase (G6PD) deficiency is associated with asymptomatic malaria in a rural community in Burkina Faso. *Asian. Pac. J. Trop. Biomed.* **2014**, *4*, 655−658.

(25) Louicharoen, C.; Patin, E.; Paul, R.; Nuchprayoon, I.; Witoonpanich, B.; Peerapittayamongkol, C.; Casademont, I.; Sura, T.; Laird, N. M.; Singhasivanon, P.; Quintana-Murci, L.; Sakuntabhai, A. Positively selected G6PD-Mahidol mutation reduces *Plasmodium vivax* density in southeast Asians. *Science* **2009**, *326*, 1546−1549.

(26) Peixoto, H. M.; Brito, M. A. M.; Romero, G. A. S.; Monteiro, W. M.; de Lacerda, M. V. G.; de Oliveira, M. R. F. G6PD deficiency in male individuals infected by *Plasmodium vivax* malaria in the Brazilian Amazon: a cost study. *Malaria J.* **2015**, *14*, 126−134.

(27) Khim, N.; Benedet, C.; Kim, S.; Kheng, S.; Siv, S.; Leang, R.; Lek, S.; Muth, S.; Chea, N.; Chuor, C. M.; Duong, S.; Kerleguer, A.; Tor, P.; Chim, P.; Canier. L.; Witkowski, B.; Taylor, W. R. J.; Ménard, D. G6PD deficiency in *Plasmodium falciparum* and *Plasmodium vivax* malaria-infected Cambodian patients, *Malaria J.* **2013**, *12*, 171−180.

(28) Luzzatto, L.; Usanga, E. A; Reddy, S. Glucose-6-phosphate dehydrogenase deficient red cells: Resistance to infection by malarial parasites. *Science* **1969**, *164*, 839−842.

(29) Cappadoro, M.; Giribaldi, G.; O'Brien, E.; Turrini, F.; Mannu, F.; Ulliers, D.; Simula, G.; Luzzatto, L.; Arese, P. Early phagocytosis of glucose-6-phosphate dehydrogenase (G6PD)-deficient erythrocytes parasitized by *Plasmodium falciparum* may explain malaria protection in G6PD deficiency. *Blood* **1998**, *92*, 2527−2534.

(30) Becker, K.; Koncarevic, S.; Hunt, N. H.: Oxidative stress and antioxidant defense in malarial parasites. In Molecular Approaches to Malaria, Sherman, I. W. (Ed.), *American Society of Microbiology Press* **2005**, 365−383.

(31) Arese, P.; Turrini, F.; Schwarzer, E. Band 3/complement-mediated recognition and removal of normally senescent and pathological human erythrocytes. *Cell. Physiol. Biochem*. **2005**, *16*, 133−146.

(32) López, C.; Saravia, C.; Gomez, A.; Hoebeke, J.; Patarroyo, M. A. Mechanisms of genetically-based resistance to malaria. *Gene* **2010**, *467*, 1–12.

(33) Méndez, D.; Linares, M.; Diez, A.; Puyet, A.; Bautista, J. M. Stress response and cytoskeletal proteins involved in erythrocyte membrane remodeling upon *Plasmodium falciparum* invasion are differentially carbonylated in G6PD A$^-$ deficiency. *Free Radic. Biol. Med*. **2011**, *50*, 1305−1313.

(34) Eckman J.; Eaton, J. W. Dependence of *Plasmodium* glutathione metabolism on the host cell. *Nature* **1979**, *278*, 754−756.

(35) Langer, B. W.; Phisphumvidhi, P.; Friedlander, Y. Malaria parasite metabolism: the pentose cycle in *Plasmodium berghei*. *Exp. Parasitol.* **1967**, *20*, 68−76.

(36) Hempelmann, E.; Wilson, R. J. M. Detection of glucose-6-phosphate dehydrogenase in malarial parasites. *Mol. Biochem. Parasitol.* **1981**, *2*, 197−204.

(37) Preuss, J.; Jortzik, E.; Becker, K. Glucose-6-phosphate metabolism in *Plasmodium falciparum*. *IUBMB Life* **2012**, *64*, 603−611.

(38) Bozdech, Z.; Ginsburg, H. Data mining of the transcriptome of *Plasmodium falciparum*: the pentose phosphate pathway and ancillary processes. *Malaria J.* **2005**, *4*, 17−28.

(39) Storm, J.; Perner, J.; Aparicio, I.; Patzewitz, E. M.; Olszewski, K.; Llinas, M.; Engel, P. C.; Müller, S. *Plasmodium falciparum* glutamate dehydrogenase a is dispensable and not a drug target during erythrocytic development. *Malaria J.* **2011**, *10*, 193−204.

(40) Wrenger, C.; Müller, S. Isocitrate dehydrogenase of *Plasmodium falciparum*: Energy metabolism or redox control? *Eur. J. Biochem.* **2003**, *270*, 1775–1783.

(41) Clarke, J. L.; Scopes, D. A.; Sodeinde, O.; Mason, P. J. Glucose-6-phosphate dehydrogenase-6-phosphogluconolactonase. A novel bifunctional enzyme in malaria parasites. *Eur. J. Biochem.* **2001**, *268*, 2013−2019.

(42) Jortzik, E.; Mailu, B. M.; Preuss, J.; Fischer, M.; Bode, L.; Rahlfs, S.; Becker, K. Glucose-6-phosphate dehydrogenase-6-phosphogluconolactonase: a unique bifunctional enzyme from *Plasmodium falciparum*. *Biochem. J.* **2011**, *436*, 641−650.

(43) Allen, S. M.; Lim, E. E.; Jortzik, E.; Preuss, J.; Chua, H. H.; MacRae, J. I.; Rahlfs, S.; Haeussler, K.; Downton, M. T.; McConville, M. J.; Becker, K.; Ralph, S. A. *Plasmodium falciparum* glucose-6-phosphate dehydrogenase 6-phosphogluconolactonase is a potential drug target. FEBS J. **2015**, *282*, 3808−3823.

(44) Atamna, H.; Pascarmona, G.; Ginsburg, H. Hexose monophosphate shunt activity in intact *Plasmodium falciparum*-infected erythrocytes and in free parasites. *Mol. Biochem. Parasitol.* **1994**, *67*, 79−89.

(45) Crooke, A.; Diez, A.; Mason, P. J.; Bautista, J. M. Transient silencing of *Plasmodium falciparum* bifunctional glucose-6-phosphate dehydrogenase-6-phosphogluconolactonase. *FEBS J.* **2006**, *273*, 1537−1546.

(46) Preuss, J.; Hedrick,M.; Sergienko, E.; Pinkerton,A.; Mangravita-Novo, A.; Smith, L.; Marx, C.; Fischer, E.; Jortzik, E.; Rahlfs, S.; Becker, K.; Bode, L. High-throughput screening for small- molecule inhibitors of *Plasmodium falciparum* glucose-6-phosphate dehydrogenase 6-phosphogluconolactonase. *J. Biomol. Screening* **2012**, *17*, 738−751.

(47) Maloney, P.; Peddibhotla, S.; Hedrick, M. P.; Hershberger, P.; Gosalia, P.; Milewski, M.; Li, Y. L.; Sugarman, E.; Hood, B.; Suyama, E.; Nguyen, K.; Vasile, S.; Sergienko, E.; Mangravita-Novo, A.; Vicchiarelli, M.; McAnally, D.; Smith, L. H.; Roth, G. P.; Diwan, J.; Chung, T. D. Y.; Jortzik, E.; Rahlfs, S.; Becker, K.; Pinkerton, A. B.; Bode, L.; Preuss, J. Discovery of a *Plasmodium falciparum* glucose-6-phosphate dehydrogenase 6-phosphogluconolactonase inhibitor (*R*,*Z*)-*N*-((1-Ethylpyrrolidin-2-yl)methyl)-2-(2-fluorobenzylidene)-3-oxo-3,4-dihydro-2*H*-benzo[*b*][1,4]thiazine-6-carboxamide (ML276) that reduces parasite growth *in vitro*. *J. Med. Chem.* **2012**, *55*, 7262−7272.

(48) Maloney, P.; Hedrick, M.; Peddibhotla, S.; Hershberger, P.; Milewski, M.; Gosalia, P.; Li, L.; Preuss, J.; Sugarman, E.; Hood, B.; Suyama, E.; Nguyen, K.; Vasile, S.; Sergienko, E.; Salanawil, S.; Stonich, D.; Su, Y.; Dahl, R.; Mangravita-Novo, A.; Vicchiarelly, M.; McAnally, D.; Smith, L. H.; Roth, G.; Diwan, J.; Chung, T. D. Y.; Pinkerton, A. B.; Bode, L.; Becker, K. A selective inhibitor of *Plasmodium falciparum* glucose-6-phosphate dehydrogenase (*Pf*G6PDH). Probe Reports from the NIH

Molecular Libraries Program, Bethesda (MD), http://www.ncbi.nlm.nih.gov/books/NBK143548/, **2010**.

(49) Maloney, P.; Hedrick, M.; Peddibhotla, S.; Hershberger, P.; Milewski, M.; Gosalia, P.; Li, L.; Preuss, J.; Sugarman, E.; Hood, B.; Suyama, E.; Nguyen, K.; Vasile, S.; Sergienko, E.; Salanawil, S.; Stonich, D.; Su, Y.; Dahl, R.; Mangravita-Novo, A.; Vicchiarelly, M.; McAnally, D.; Smith, L. H.; Roth, G.; Diwan, J.; Chung, T. D. Y.; Pinkerton, A. B.; Bode, L.; Becker, K. A 2nd selective inhibitor of *Plasmodium falciparum* glucose-6-phosphate dehydrogenase (*Pf*G6PDH) - Probe 2, Probe Reports from the NIH Molecular Libraries Program, Bethesda (MD), http://www.ncbi.nlm.nih.gov/books/NBK184495/, **2010**.

(50) Sinclair, H. B. An improved method for the preparation of methyl 6-chloro-6-deoxy-α-D-glucopyranoside. *J. Org. Chem.* **1965**, *30*, 1283–1284.

(51) Evans, M. E.; Long, L., Jr.; Parrish, F. W. Reaction of carbohydrates with methylsulfonyl chloride in *N*,*N*-dimethylformamide. Preparation of some methyl 6-chloro-6-deoxyglycosides. *J. Org. Chem.* **1968**, *33*, 1074–1076.

(52) Gómez-García, M.; Benito, J. M.; Gutiérrez-Gallego, R.; Maestre, A.; Ortiz Mellet, C.; García Fernández, J. M.; Jiménez Blanco, J. L. Comparative studies on lectin–carbohydrate interactions in low and high density homo- and heteroglycoclusters. *Org. Biomol. Chem.* **2010**, *8*, 1849–1860.

(53) García Fernández, J. M.; Ortiz Mellet, C.; Fuentes, J. Chiral 2-thioxotetrahydro-1,3-*O*,*N*-heterocycles from carbohydrates. 2. Stereocontrolled synthesis of oxazoline pseudo-*C*-nucleosides and bicyclic oxazine-2-thiones. *J. Org. Chem.* **1993**, *58*, 5192–5199.

(54) Zarchi, M. A. K.; Tayefi, M.; Tirgir, F.; Sabzalian, M. R. An environmentally compatible synthesis of polyesters derived from 5-(2-phthalimidoethanesulfonamido) isophthalic acid as a novel diacid monomer. *J. Appl. Polym. Sci.* **2011**, *121*, 2573–2583.

(55) Radfar, A.; Méndez, D.; Moneriz, C.; Linares, M.; Marín-García, P.; Puyet, A.; Diez, A.; Bautista, J. M. Synchronous culture of *Plasmodium falciparum* at high parasitemia levels. *Nat. Protoc.* **2009**, *4*, 1899–1915.

(56) Proudfoot, O.; Drew, N.; Scholzen, A.; Xiang, S.; Plebanski, M. Investigation of a novel approach to scoring Giemsa-stained malaria-infected thin blood films. *Malar. J.* **2008**, *7*, 62.

(57) Moneriz, C.; Marín-García, P.; Bautista, J. M.; Diez, A.; Puyet, A. Haemoglobin interference and increased sensitivity of fluorimetric assays for quantification of low-parasitaemia *Plasmodium* infected erythrocytes. *Malar. J.* **2009**, *8*, 279.

(58) Bautista, J. M.; Mason, P. J.; Luzzatto, L. Purification and properties of human glucose-6-phosphate dehydrogenase made in *E. coli*. *Biochim. Biophys. Acta* **1992**, *1119*, 74–80.

(59) Kurdi-Haidar, B.; Luzzatto, L. Expression and characterization of glucose-6-phosphate dehydrogenase of *Plasmodium falciparum*. *Mol. Biochem. Parasitol.* **1990**, *41*, 83–91.

(60) Kotaka, M.; Gover, S.; Vandeputte-Rutten, L.; Au, S. W. N.; Lam, V. M. S.; Adams, M. J., Structural studies of glucose-6-phosphate and $NADP^+$ binding to human glucose-6-phosphate dehydrogenase. *Acta Crystallographica Section D* **2005**, *61*, 495−504.

(61) Sali, A.; Blundell, T. L. Comparative protein modelling by satisfaction of spatial restraints. *J. Mol. Biol.* **1993**, *234*, 779−815.

(62) Fiser, A.; Do, R. K.; Sali, A. Modeling of loops in protein structures. *Protein Sci.* **2000**, *9*, 1753−1773.

(63) Davis, I. W.; Murray, L. W.; Richardson, J. S.; Richardson, D. C. MOLPROBITY: Structure validation and all-atom contact analysis for nucleic acids and their complexes. *Nucleic Acids Res.* **2004**, *32*, 615−619.

(64) Melo, F.; Feytmans, E. Assessing protein structures with a non-local atomic interaction energy. *J. Mol. Biol.* **1998**, *277*, 1141−1152.

(65) Thomsen, R.; Christensen, M. H. MolDock: a new technique for high-accuracy molecular docking. *J. Med. Chem.* **2006**, *49*, 3315–3321.

(66) Sobral Sampaio, L. F.; Pantoja Mesquita, F.; Monteiro de Sousa, P. R.; Lameira Silva, J.; Nahum Alves, C. The melatonin analog 5-MCA-NAT increases endogenous dopamine levels by binding NRH:quinone reductase enzyme in the developing chick retina. *Int. J. Dev. Neurosci.* **2014**, *38*, 119–126.

(67) Case, D. A.; Darden, T. A.; Cheatham, T. E., III; Simmerling, C. L.; Wang, J.; Duke, R. E.; Luo, R.; Walker, R. C.; Zhang, W.; Merz, K. M.; Roberts, B.; Hayik, S.; Roitberg, A.; Seabra, G.; Swails, J.; Goetz, A. W.; Kolossváry, I.; Wong, K. F.; Paesani, F.; Vanicek, J.; Wolf, R. M.; Liu, J.; Wu, X.; Brozell, S. R.; Steinbrecher, T.; Gohlke, H.; Cai, Q.; Ye, X.; Wang, J.; Hsieh, M.-J.; Cui, G.; Roe, D. R.; Mathews, D. H.; Seetin, M. G.; Salomon-Ferrer, R.; Sagui, C.; Babin, V.; Luchko, T.; Gusarov, S.; Kovalenko, A.; Kollman, P. A. *AMBER 12*, University of California, San Francisco, CA, 2012.

(68) Lindorff-Larsen, K.; Piana, S.; Palmo, K.; Maragakis, P.; Klepeis, J. L.; Dror, R. O.; Shaw, D. E. Improved side-chain torsion potentials for the Amber ff99SB protein force field. *Proteins* **2010**, *78*, 1950−1958.

Conclusions

✶ The first objective of this PhD thesis involved the design, synthesis and *in vitro* and *in vivo* pharmacological evaluation of two novel classes of multitarget anti-Alzheimer drug candidates that might hit additional key targets beyond cholinesterase and Aβ aggregation, which differentiate them to the rest of dual binding site AChEIs developed over the last decade in our research group.

Firstly, a series of **rhein–huprine hybrids**, (±)-**74a–h**, was prepared containing a unit of racemic huprine Y, (±)-**11**, as the AChE active site interacting unit connected through an amide-containing oligomethylene or aromatic linker to an anthraquinone fragment derived from rhein, **75**, expected to inhibit tau protein aggregation and to interact with the peripheral site of AChE. These novel rhein–huprine hybrids were pharmacologically evaluated against several key targets of interest for AD treatment. (±)-**74a–h** turned out to be potent hAChEIs (IC_{50} = 1.07–18.2 nM) and moderately potent inhibitors of hBChE (IC_{50} = 620–1460 nM), and they were also shown to significantly inhibit both AChE-induced (29–52% inhibition at 100 μM) and self-induced Aβ aggregation, the latter both *in vitro* (32–41% inhibition at 10 μM) and in *E. coli* cells overexpressing the peptide (40–68% inhibition at 10 μM). Finally, some of these hybrids also turned out to be potent inhibitors of Aβ formation, with IC_{50} values toward BACE-1 in the nanomolar or low micromolar range (from 120 nM to 2 μM), also to significantly inhibit tau protein aggregation in *E. coli* cells overexpressing the protein (23–57% inhibition at 10 μM), and were predicted to be able to cross the BBB and enter the CNS using the *in vitro* PAMPA-BBB assay, thereby making them promising anti-Alzheimer drug candidates. The excellent results found for the nonamethylene-linked rhein-huprine hybrid, (±)-**74e**, in particular its outstanding BACE-1 inhibition (IC_{50} = 120 nM), prompted us to carry out the synthesis of both enantiomers (+)- and (–)-**74e**, their *ex vivo* assessment using hippocampal slices from 2-month-old C57bl6 mice and a further *in vivo* study with a double AβPP and PS-1 mutant (AβPPswe/PS1) transgenic mouse model. A relevant decrease in the levels of toxic Aβ42 peptide and amyloid 42/40 ratio in the hippocampus of transgenic mice was observed after treatment with hybrid (+)-**74e**, in accordance with the remarkable *in vitro* BACE-1 inhibition (IC_{50} = 80 nM). In agreement with the design rationale, both biological assays as well as molecular modeling studies demonstrated that the rhein–huprine hybrids and, in particular, hybrid (+)-**74e**, act as multitarget agents, which establish a dual site binding not only within

AChE, but also within BACE-1, in the latter case involving a so far unexplored secondary binding site, which is adjacent to the catalytic site.

A second family of multipotent anti-Alzheimer drug candidates was designed and synthesized in the present PhD Thesis work, named the **levetiracetam–huprine** [(2*S*,7'''*S*,11'''*S*)-**92** and (2*S*,7'''*R*,11'''*R*)-**93**] and **levetiracetam–(6-chloro)tacrine hybrids** [(±)-, (*R*)-, and (*S*)-**84**, and (±)-**85**], which consisted of a moiety of huprine Y, tacrine or 6-chlorotacrine, as the AChE active site interacting unit, and a fragment derived from the antiepileptic drug levetiracetam (Keppra®), aimed at interacting with the peripheral site of AChE together with tackling the aberrant epileptiform activity, as one of the mechanisms by which Aβ exerts its neurotoxic effects. For the preparation of the enantiomeric levetiracetam-based hybrids, the enantiopure levetiracetam fragment (*S*)-**86** was firstly synthesized through resolution of the racemic acid precursor of levetiracetam, **86**, by treatment with the chiral auxiliary (*S*)-*N*-phenylpantolactam in order to provide a diastereomeric mixture which was then purified to provide diastereopure esters, that were finally hydrolyzed to give the desired enantiopure carboxylic acid, (*S*)-**86**. All levetiracetam-based hybrids were pharmacologically evaluated toward cholinesterases and Aβ and tau aggregation. The enantiopure levetiracetam–huprine hybrid (2*S*,7'''*S*,11'''*S*)-**92** turned out to show the best pharmacological profile with moderately potent dual Aβ42 and tau antiaggregation effect in the *E. coli* cell aggregation model (36% and 54% of inhibition, respectively), besides being one of the most potent and selective AChE inhibitors (AChE IC_{50} = 4.2 nM, and BChE IC_{50} = 232 nM). Interestingly, the novel hybrids also exhibited significant antiepileptic activity after a 4-week treatment with a 5 mg/kg dose in transgenic APP/PS1 mice. Moreover, hybrid (±)-**84** bearing a tacrine moiety and (2*S*,7'''*S*,11'''*S*)-**92** led to a clear cognitive improvement in APP/PS1 mice after 4 days without receiving the compounds, which is indicative of a disease-modifying effect. In the case of the lead levetiracetam–huprine hybrid (2*S*,7'''*S*,11'''*S*)-**92**, its effect on epileptiform activity was also complemented with a direct effect on amyloid and tau pathologies, neuroinflammation, and cholinesterases, thereby emerging as a very promising disease-modifying anti-Alzheimer drug candidate.

✶ The second objective of this PhD thesis involved the repurposing of huprine Y, **11**, a highly potent anticholinesterasic compound (IC_{50} = 0.61 nM) originally developed as a potential anti-Alzheimer agent, towards the development of new HAT therapies, on the basis of the astonishing trypanocidal activity found for this compound (*T. brucei* IC_{50} = 0.61 μM and IC_{90}= 2.94 μM).

The trypanocidal activity of several series of huprine-based homo- and heterodimers was first explored due to the fact that molecular dimerization had been reported to increase antiprotozoal activity and/or overcome drug resistance, mainly in the malaria field due to a more efficient trapping in the acidic digestive vacuole of the parasite and prevention of heme polymerization. Firstly, the preparation of a series of ***bis*(+)-huprines**, (+)-**101a–e,** was carried out by a one-pot double nucleophilic substitution reaction with 2 equiv. of (+)-(7*R*,11*R*)-huprine Y, (+)-**11**, and 1 equiv. of the corresponding α,ω-dihaloalkane, **104a**–**e**, using KOH as the base in DMSO at r. t. for three days, and the subsequent isolation by silica gel column chromatography. All *bis*(+)-huprines, (+)-**101a–e**, showed similar *in vitro* potencies against cultured bloodstream forms of *T. brucei* (IC_{50} = 0.50–0.89 μM and IC_{90} ≈ 1 μM), being significantly more potent than the parent huprine Y (IC_{90} = 2.94 μM).

A screening against cultured bloodstream forms of *T. brucei* of a small in-house library of huprine- or tacrine-based heterodimeric compounds, belonging to three distinct structural classes (**series I–III** described in chapter 6), which had been previously developed in our research group as AChE inhibitors, was performed. On the basis of the biological activity results of these screened series, with series **I** emerging as the most interesting, we carried out the synthesis of the novel **heterodimeric compounds 102−103g** and **131−132f,g**, and the evaluation of their trypanocidal activity. The preparation of these compounds involved synthetic methodologies already used on our research group, based on nucleophilic substitutions at the exocyclic amino group of the quinoline scaffold.

Finally, a **side chain modification at the exocyclic primary amino group of huprine** was also explored, with the aim of optimizing the antitrypanosomal activity profile with regard to the parent huprine Y and the huprine-based homo- and heterodimers. For that purpose, it was firstly screened a small in-house library of 16 *N*-alkylhuprines functionalized either with a cyano or an amino group at the end of an oligomethylene chain, containing in some cases a *p*-phenylene ring (**77a–h**, **76a–h**, and **133**) against cultured bloodstream forms of *T. brucei* and rat myoblast L6 cells. Afterwards, a second generation of modified side chain analogs was synthesized based on the results of the pharmacological evaluation of the firstly screened

compounds, involving the preparation of novel *N*-cyano, *N*-amino, and *N*-guanidinoalkylated derivatives of huprine (**134b,e**), tacrine (**135, 137**, and **139c,f**), or 6-chlorotacrine (**136, 138**, and **140c,f**), and the preparation of the *N*-piperidinopropyl and *N*-morpholinopropyl substituted huprines, **141** and **142**.

Overall, the drug repurposing approach from huprine Y suggests that this compound represents a suitable template for the search of quinoline-based anti-trypanosomatid agents. For instance, the novel dodecamethylene-linked bis(+)-huprine Y, **101d**, achieved a three-fold enhancement of the selectivity of the parent huprine Y, **11**, (SI= 13) with an IC_{50} value against *T. brucei* of 0.76 μM and a selectivity index of 37.5. Interestingly, the lead heterodimeric compounds **102d** and **103d** comprising also two quinoline moieties connected in both cases with a nonamethylene linker, achieved a greater trypanocidal potency and selectivity than **101d** (**102 d**, *T. brucei* IC_{50} = 0.21 μM and SI = 34; **103d**, *T. brucei* IC_{50} = 0.24 μM and SI = 167). Finally, the side chain modification strategy on the huprine scaffold gave rise to one of the most potent and less cytotoxic compounds ever synthesized in our research group, exhibiting a *T. brucei* IC_{50} value of 0.12 μM and a selectivity index of 133. Additionaly, using PAMPA-BBB assay, all compounds were predicted to be able to cross the blood–brain barrier, making them of considerable interest in the treatment of late stage HAT, when parasites invade human CNS and produce a host of symptoms including psychiatric, motor and sensorial disorders along with abnormal reflexes, and eventually death if untreated.

✶ The third objective of this PhD Thesis involved the development of novel potential antimalarial drugs with a novel mechanism of action that may overcome parasite resistance. This challenging project was born on the basis of recent findings that pointed out the bifunctional enzyme glucose-6-phosphate dehydrogenase–6-phosphogluconolactonase of *P. falciparum* (*Pf*GluPho) as a promising antimalarial target, in the light of the protective effect against malaria infection conferred by the deficiency of human glucose-6-phosphate dehydrogenase (hG6PD). Starting from a homology model of *Pf*G6PD, built by the group of Prof. F. J. Luque, we have exploited the structural differences found at the catalytic site between the parasite and human G6PD enzymes to rationally design and synthesize a family of substrate analog selective inhibitors of the *Pf*G6PD domain of the *Pf*GluPho enzyme.

A short series of nine **glycosidic compounds** (**57** − **65**), decorated at position 6 with a sulfide, sulfone, or sulfonamide group and derivatized either with an ethyl or a propyl side chain terminating with a cyano, an amine, or a guanidine group, was prepared by straightforward synthetic routes which involve the common starting material methyl 6-chloro-6-deoxy-α-D-glucopyranoside, **67**. The novel compounds were screened against the parasite and human G6PD enzymes, cultured *P. falciparum* parasites, and mammalian cells. Several compounds showed a greater selectivity against *Pf*G6PD with K_i values within the micromolar range, from 32 μM to higher than 200 μM; for instance, compound **57** showed the best profile with a K_i value of 76 μM for *Pf*G6PD, while a clearly lowest affinity was found for hG6PD with a K_i value higher than 2 mM. In addition, the most potent inhibitors also showed a greater inhibitory activity of the *P. falciparum* growth in culture (IC_{50} values from 339 μM to 2 mM). Furthermore, phenotypic assays at 48 h upon treatment determined that schizont was the most sensitive intraerythrocytic parasite form to this family of compounds, which is indicative of a mechanism of action different from that of chloroquine. Finally, the absence of *in vitro* cytotoxicity against mammalian cells complements the biological profile of these new molecules as promising antimalarial hits. Current optimization endeavors in this class of compounds are being carried out by the PhD student Katia Pont, who is pursuing the improvement of the physicochemical/pharmacokinetic properties of these molecules.

References

[1] 2015 Facts and Figures. Alzheimer's Association Home Page. https://www.alz.org (accessed February 2, 2016)

[2] Cummings, J. L.; Askin-Edgar, S. Evidence for psychotropic effects of acetylcholinesterase inhibitors. *CNS Drugs* **2000**, *13*, 385−395.

[3] Leonard, B. E. Advances in the drug treatment of Alzheimer's disease. *Hum*. *Psycopharmacol*. **1998**, *13*, 83−90.

[4] Tayeb, H. O.; Yang, H. K.; Price, B. H.; Tarazi, F. Y. Pharmacotherapies for Alzheimer's diseases: Beyond cholinestrase inhibitors. *Pharmacol. Ther.* **2012**, *134*, 8–25.

[5] World Alzheimer Report 2015: The Global Impact of Dementia - An analysis of prevalence, incidence, cost and trends. Alzheimer's Disease International Home Page. http://www.alz.co.uk (accessed January 12, 2016).

[6] Stelzmann, R. An English translation of Alzheimer's 1907 paper, "Ü ber eine eigenartige erkankung der hirnrinde". *Clinical Anat.* **1995**, *1*, 429−431.

[7] Katzman R. The prevalence and malignancy of Alzheimer disease: A major killer. *Arch. Neurol.* **1976**, *33*, 217–218.

[8] a) Tomiyama, T.; Shoji, A.; Kataoka, K.; Suwa, Y.; Asano, S.; Kaneko, H.; Endo, N. Inhibition of amyloid beta protein aggregation and neurotoxicity by rifampicin. Its possible function as a hydroxyl radical scavenger. *J. Biol. Chem*. **1996**, *271*, 6839–6844. b) Lahiri, D. K.; Farlow, M. R.; Sambamurti, K.; Greig, N. H.; Giacobini, E.; Schneider, L. S. A critical analysis of new molecular targets and strategies for drug developments in Alzheimer's disease. *Curr. Drug Targets* **2003**, *4*, 97–112. c) Cummings, J. Treatment of Alzheimer's disease: Current and future therapeutic approaches. *Rev. Neurol. Dis.* **2004**, *1*, 60–69. d) Bartolini, M.; Bertucci, C.; Bolognesi, M. L.; Cavalli, A.; Melchiorre, C.; Andrisano, V. Insight into the kinetic of amyloid β (1−42) peptide self-aggregation: Elucidation of inhibitors' mechanism of action. *ChemBioChem* **2007**, *8*, 2152–2161. e) Gauthier, S.; Poirier, J. Current and future management of Alzheimer's disease. *Alzheimers Dement.* **2008**, *4* (Suppl. 1), S48–50.

[9] Krall, W. J.; Sramek, J. J.; Cutler, N. Cholinesterase inhibitors: a therapeutic strategy for Alzheimer disease. *Ann. Pharmacother.* **1999**, *33*, 441–450.

[10] Hardy, J; Allson, D. Amyloid deposition as the central event in the aetiology of Alzheimer's disease. *Trends Pharmacol. Sci.* **1991**, *12*, 383−388.

[11] Masters, C. L; Simms, G.; Weinman, N. A.; Multhaup, G.; McDonald, B.L.; Beyreuther, K. Amyloid plaque core protein in Alzheimer disease and Down syndrome. *Proc. Natl. Acad. Sci. USA* **1985**, *82*, 4245–4249.

[12] Kang, J.; Lemaire, H. G.; Unterbeck, A.; Salbaum, J. M.; Masters, C. L.; Grzes- chik, K. H.; Multhaup, G.; Beyreuther, K.; Muller-Hill, B. The precursor of Alzheimer's disease amyloid A4 protein resembles a cell-surface receptor. *Nature* **1987**, *325*, 733–736.

[13] Churcher, I. Tau Therapeutic Strategies for the Treatment of Alzheimer's Disease. *Curr. Top. Med. Chem.* **2006**, *6*, 579−595.

[14] Ferrer, I.; Gomez-Isla, T.; Puig, B.; Freixes, M.; Ribé, E.; Dalfó, E.; Avila, J. Current advances on different kinases involved in tau phosphorylation, and implications in Alzheimer's disease and tauopathies. *Curr. Alzheimer Res.* **2005**, *2*, 3-18.

[15] Ballard, C.; Gauthier, S.; Corbett, A.; Brayne, C.; Aarsland, D.; Jones, E. Alzheimer's disease. *Lancet* **2011**, *377*, 1019–1031.

[16] Hardy, J.; Selkoe, D. J. The amyloid hypothesis of Alzheimer's disease: Progress and problems on the road to therapeutics. *Science* **2002**, *297*, 353−356.

[17] Knopman, D. S.; Parisi, J. E.; Salviati, A.; Floriach-Robert, M.; Boeve, B. F.; Ivnik, R. J.; Smith, G. E.; Dickson, D. W.; Johnson, K. A.; Petersen, L. E.; McDonald, W. C.; Braak, K.; Petersen, R. C. Neuropathology of cognitively normal elderly. *J. Neuropathol. Exp. Neurol*. **2003**, *62*, 1087–1095.

[18] a) Fagan, A. M.; Mintun, M. A.; Shah, A. R.; Aldea, P.; Roe, C. M.; Mach, R. H.; Marcus, D.; Morris, J. C.; Holtzman, D. M. Cerebrospinal fluid tau and ptau181 increase with cortical amyloid deposition in cognitively normal individuals: Implications for future clinical trials of Alzheimer's disease. *EMBO Mol. Med*. **2009**, *1*, 371–380. b) Morris, J. C.; Roe, C. M.; Grant, E. A.; Head, D.; Storandt, M.; Goate,

A. M.; Fagan, A. M.; Holtzman, D. M.; Mintun, M. A. Pittsburgh compound B imaging and prediction of progression from cognitive normality to symptomatic Alzheimer disease. *Arch. Neurol*. **2009**, *66*, 1469–1475. c) Rentz, D. M.; Rentz, D.; Locascio, J. J.; Becker, J. A.; Moran, E. K.; Eng, E.; Buckner, R. L.; Sperling, R. A.; Johnson, K. A. Cognition, reserve, and amyloid deposition in normal aging. *Ann. Neurol.* **2010**, *67*, 353–364.

[19] Rissman, R. A.; Poon, W. W.; Blurton-Jones, M.; Oddo, S.; Torp, R.; Vitek, M. P.; LaFerla, F. M.; Rohn, T. T.; Cotman, C. W. Caspase-cleavage of tau is an early event in Alzheimer disease tangle pathology. *J. Clin. Invest.* **2004**, *114*, 121–130.

[20] Dickson, D. W. Apoptotic mechanisms in Alzheimer neurofibrillary degeneration: cause or effect? *J. Clin. Invest.* **2004**, *114*, 23−27.

[21] Camps, P.; Muñoz-Torrero, D. Cholinergic drugs in pharmacotherapy of Alzheimer's disease. *Mini-Rev. Med. Chem*. **2002**, *2*, 11−25.

[22] Decker, M. W.; McGaugh, J. L. The role of interactions between the cholinergic system and other neuromodulatory systems in learning and memory. *Synapse* **1991**, *7*, 151–168.

[23] Terry, A. V.; Buccafusco, J. J. The cholinergic hypothesis of age and Alzheimer's disease-related cognitive deficits: recent challenges and their implications for novel drug development. *J. Pharmacol. Exp. Ther.* **2003**, *306*, 821−827.

[24] Savini, L.; Gaeta, A.; Fattorusso, C.; Catalanotti, B.; Campiani, G.; Chiasserini, L.; Pellerano, C.; Novellino, E.; McKissic D.; Saxena, A. Specific targeting of acetylcholinesterase and butyrylcholinesterase recognition sites. Rational design of novel, selective, and highly potent cholinesterase inhibitors. *J. Med. Chem*. **2003**, *46*, 1−14.

[25] Sussman, J. L.; Harel, M.; Frolow, F.; Oefner, C.; Goldman, A.; Toker, L.; Silman, I. Atomic structure of acetylcholinesterase from Torpedo californica: a prototypic acetylcholine-binding protein. *Science*, **1991**, *253*, 872−879.

[26] Macdonald, I. R.; Rockwood, K.; Martin, E.; Darvesh, S. Cholinesterase inhibition in Alzheimer's disease: Is specificity the answer? *J. Alzheimers Dis*. **2014**, *42*, 379−384.

[27] Perry, E. K.; Perry, R. H.; Blessed, G.; Tomlinson, B. E. Changes in brain cholinesterases in senile demetia of Alzheimer type. *Neuropathol. Appl. Neurobiol.* **1978**, *4*, 273−277.

[28] Lane, R. M.; Potkin, S. G.; Enz, A. Targeting acetylcholinesterase and butyrylcholinesterase in dementia. *Int. J. Neuropsychopharmacol.* **2006**, *9*, 101−124. −1317.

[29] Fernández-Bachiller, M. I.; Pérez, C.; Monjas, L.; Rademann, J.; Rodríguez-Franco, M. I. New tacrine-4-oxo-4*H*-chromene hybrids as multifunctional agents for the treatment of Alzheimer's disease, with cholinergic, antioxidant, and β-amiloid-reducing properties. *J. Med. Chem*. **2012**, *55*, 1303−1317.

[30] Mesulam, M. M.; Geula, C. Butyrylcholinesterase reactivity differentiates the amyloid plaques of aging from those of dementia. *Ann. Neurol.* **1994**, *36*, 722−727.

[31] a) Guillozet, A. L.; Smiley, J. F.; Mash, D. C.; Mesulam, M. M. Butyrylcholinesterase in the life cycle of amyloid plaques. *Ann. Neurol.* **1997**, *42*, 909−918. b) Geula, C.; Darvesh, S. Butyrycholinesterase, cholinergic neurotransmission and the pathology of Alzheimer's disease. *Drugs Today* **2004**, *40*, 711−721. c) Ballard C. G.; Greig, N. H.; Guillozet-Bongaarts A. L.; Enz, A.; Darvesh, S. Cholinesterases: roles in the brain during health and disease. *Curr. Alzheimer Res.* **2005**, *2*, 307−318. d) Anand, P.; Singh, B. A review on cholinesterase inhibitors for Alzheimer's disease. *Arch. Pharm. Res.* **2013**, *36*, 375–399.

[32] Greig, N. H.; Utsuki, T.; Ingram, D. K.; Wang, Y.; Pepeu, G.; Scali, C.; Yu, Q. S.; Mamczarz, J.; Holloway, H. W.; Giordano, T.; Chen, D., Furukawa, K.; Sambamurti, K.; Brossi, A.; Lahiri, D. K. Selective butyrylcholinesterase inhibition elevates brain acetylcholine, augments learning and lowers Alzheimer β-amyloid peptide in rodent. *Proc. Natl. Acad. Sci. U. S. A.* **2005**, *102*, 17213−17218.

[33] Haass, C.; Lemere, C. A.; Capell, A.; Citron, M.; Seubert, P.; Schenk, D.; Lannfelt, L.; Selkoe, D. J. The Swedish mutation causes early-onset Alzheimer's disease by β-secretase cleavage within secretory pathway. *Nat. Med.* **1995**, *1*, 1291−1296.

[34] Jahn, H. Memory loss in Alzheimer's disease. *Dialogues Clin. Neurosci*. **2013**, *15*, 445−454.

[35] Citron, M.; Eckman, C. B.; Diehl, T. S.; Corcoran, C.; Ostaszewski, B. L.; Xia, W.; Levesque, G.; St George Hyslop, P.; Younkin, S. G.; Selkoe, D. J. Additive effects of PS1 and APP mutations on secretion of the 42-residue amyloid β-Protein. *Neurobiol. Dis.* **1998**, *5*, 107−116.

[36] Raber, J.; Huang, Y.; Ashford, J. W. ApoE genotype accounts for the vast majority of AD risk and AD pathology. *Neurobiol. Aging* **2004**, *25*, 641–650.

[37] Jonsson, T.; Atwal, J. K.; Steinberg, S.; Snaedal, J.; Jonsson, P. V.; Bjornsson, S.; Stefansson, H.; Sulem, P.; Gudbjartsson, D.; Maloney, J.; Hoyte, K.; Gustafson, A.; Liu, Y.; Lu, Y.; Bhangale, T.; Graham, R. R.; Huttenlocher, J.; Bjornsdottir, G.; Andreassen, O. A.; Jönsson, E. G.; Palotie, A.; Behrens, T. W.; Magnusson, O. T.; Kong, A.; Thorsteinsdottir, U.; Watts, R. J.; Stefansson, K. A mutation in APP protects against Alzheimer's disease and age-related cognitive decline. *Nature* **2012**, *488*, 96−99.

[38] Den Dunnen, W. F.; Brouwer, W. H.; Bijlard, E.; Kamphuis, J.; van Linschoten, K.; Eggens-Meijer, E.; Holstege, G. No disease in the brain of a 115-year-old woman. *Neurobiol. Aging* **2008**, *29*, 1127−32.

[39] Narayan, P.; Ehsani, S.; Lindguist, S. Combating neurodegenerative disease with chemical probes and model systems. *Nat. Chem. Biol.* **2014**, *10*, 911−920.

[40] Schmitt, B.; Bernhardt, T.; Moeller, H. J.; Heuser, I.; Frölich, L. Combination therapy in Alzheimer's disease. A review of current evidence. *CNS Drugs* **2004**, *18*, 827−844.

[41] Berk, C.; Sabbagh, M. N. Successes and failures for drugs in late-stage development for Alzheimer's disease. *Drugs Aging* **2013**, *30*, 783–792.

[42] Lipton, S. A. Turning down but not off. *Nature* **2004**, *428*, 473.

[43] Waxman, E. A.; Lynch, D. R. N-Methyl-D-aspartate receptor subtypes: multiple roles in excitotoxicity and neurological disease. *Neuroscientist* **2005**, *11*, 37−49.

[44] Gualtieri, F.; Dei, S.; Manetti, D.; Romanelli, M. N. The medicinal chemistry of Alzheimer's and Alzheimer-like diseases with emphasis on the cholinergic hypothesis. *Farmaco* **1995**, *50*, 489−503.

[45] Davis, K. L.; Thal, L. J.; Gamzu, E. R.; Davis, C. S.; Woolson, R. F.; Gracon, S. I.; Drachman, D. A.; Schneider, L. S.; Whitehouse, P .J.; Hoover, T. M. A double-blind, placebo-controlled multicenter study of tacrine for Alzheimer's disease. *N. Engl. J. Med.* **1992**, *327*, 1253−1259.

[46] Marx, J. Searching for drugs that combat Alzheimer's. *Science* **1996**, *273*, 50−53.

[47] Sugimoto, H.; Iimura, Y.; Yamanishi, Y.; Yamatsu, K. Synthesis and structure-activity relationships of acetylcholinesterase inhibitors: 1-benzyl-4-[(5,6-dimethoxy-1-oxoindan-2-yl)methyl]piperidine hydrochloride and related compounds. *J. Med. Chem.* **1995**, *38*, 4821−4829.

[48] Polinsky, R. J. Clinical pharmacology of rivastigmine: a new-generation acetylcholinesterase inhibitor for the treatment of Alzheimer's disease. *Clin. Ther.* **1998**, *20*, 634−647.

[49] Sramek, J. J.; Frackiewicz, E. J.; Cutler, N. R. Review of the acetylcholinesterase ihibitor galanthamine. *Expert Opin. Inv. Drug.* **2000**, *9*, 2393−2402.

[50] Giacobini, E. Cholinesterase inhibitors: new roles and terapeutic alternatives. *Pharmacol. Res.* **2004**, *50*, 433−440.

[51] Lemstra, A. W.; Richard, E.; van Gool, W. A. Cholinesterase inhibitors in dementia: yes, no, or maybe? *Age Aging* **2007**, *36*, 625–627.

[52] Connelly, P. J.; Prentice, N. P.; Fowler, K. G. Predicting the outcome of cholinesterase inhibitor treatment in Alzheimer's disease. *J. Neurol. Neurosur. Ps.* **2005**, *76*, 320–324.

[53] Bizzarro, A.; Marra, C.; Acciarri, A.; Valenza, A.; Tiziano, F. D.; Brahe, C.; Masullo, C. Apolipoprotein E ε4 allele differentiates the clinical response to donepezil in Alzheimer's disease. *Dement. Geriatr. Cogn.* **2005**, *20*, 254–261.

[54] Choi, S. H.; Kim, S. Y.; Na, H. R.; Kim, B. K.; Yang, D. W.; Kwon, J. C., Park, M. Y. Effect of ApoE genotype on response to donepezil in patients with Alzheimer's disease. *Dement. Geriatr. Cogn*. **2008**, *25*, 445–450.

[55] Zemek, F.; Drtinova, L.; Nepovimova, E.; Sepsova, V.; Korabecny, J.; Klimes, J.; Kuca, K. Outcomes of Alzheimer's disease therapy with acetylcholinesterase inhibitors and memantine. *Expert Opin. Drug Saf.* **2014**, *13*, 759−774.

[56] Watkins, P. B.; Zimmerman, H. J.; Knapp, M. J.; Gracon, S. I.; Lewis K. W. Hepatotoxic effects of tacrine administration in patients with Alzheimer's disease. *JAMA* **1994**, *271*, 992–998.

[57] Winker, M. A. Tacrine for Alzheimer's disease. Which patient, what dose? *JAMA* **1994**, *271*, 1023–1024.

[58] Giacobini, E. Cholinesterase inhibitors stabilize Alzheimer disease. *Neurochem. Res.* **2000**, *25*, 1185−1190.

[59] Mohs, R. C.; Doody, R. S.; Morris, J. C.; Ieni, J. R.; Rogers, S. L.; Perdomo, C. A.; Pratt, R. D.; "312" Study Group. A 1-year, placebo-controlled preservation of function survival study of donepezil in AD patients. *Neurology* **2001**, *57*, 481–488.

[60] Winblad, B.; Engedal, K.; Soininen, H.; Verhey, F.; Waldemar, G.; Wimo, A.; Wetterholm, A. L.; Zhang, R.; Haglund, A.; Subbiah, P.; Donepezil Nordic Study Group. A 1-year, randomized, placebo-controlled study of donepezil in patients with mild to moderate AD. *Neurology* **2001**, *57*, 489–495.

[61] McGaughy, J.; Everitt, B. J.; Robbins, T. W.; Sarter, M. The role of cortical cholinergic afferent projections in cognition: impact of new selective immunotoxins. *Behav. Brain Res.* **2000**, *115*, 251–263.

[62] Cutuli, D.; Foti, F.; Mandolesi, L.; De Bartolo, P.; Gelfo, F.; Federico, F.; Petrosini, L. Cognitive performances of cholinergically depleted rats following chronic donepezil administration. *J. Alzheimers Dis.* **2009**, *17*, 161–176.

[63] Wang, X. D.; Chen, X. Q.; Yang, H. H.; Hu, G. Y. Comparison of the effects of cholinesterase inhibitors on [^{3}H]MK-801 binding in rat cerebral cortex. *Neurosci. Lett.* **1999**, *272*, 21−24.

[64] Takada-Takatori, Y.; Kume, T.; Sugimoto, M.; Katsui, H.; Sugimoto, H.; Akaike, A. Acetylcholinesterase inhibitors used in treatment of Alzheimer's disease prevent glutamate neurotoxicity via nicotinic acetylcholine receptors and phosphatidylinositol 3-kinase cascade. *Neuropharmacology* **2006**, *51*, 474−486.

[65] Kihara, T.; Sawada, H.; Nakamizo, T.; Kanki, R.; Yamashita, H.; Maelicke, A.; Shimohama, S. Galantamine modulates nicotinic receptor and blocks Aβ-enhanced glutamate toxicity. *Biochem. Biophys. Res. Commun.* **2004**, *325*, 976−982.

[66] Meunier, J.; Ieni, J.; Maurice, T. The anti-amnesic and neuroprotective effects of donepezil against amyloid $\beta_{25\text{-}35}$ peptide-induced toxicity in mice involve an interaction with σ1receptor. *Br. J. Pharmacol.* **2006**, *149*, 998−1012.

[67] Massoulié, J.; Pezzementi, L.; Bon, S.; Krejci, E.; Vallette, F. M. Molecular and cellular biology of cholinesterases. *Prog. Neurobiol*. **1993**, *41*, 31–91.

[68] García-Ayllón, M. S.; Small, D. H.; Avila, J.; Sáez-Valero, J. Revisiting the role of acetylcholinesterase in Alzheimer's disease: cross-talk with P-tau and β-amyloid. *Front. Mol. Neurosci*. **2011**, *4*, 22.

[69] a) Greig, N.; Utsuki, T.; Ingram, D.; Wang, Y.; Pepeu, G.; Scali, C.; Yu, Q. S.; Mamczarz, J.; Holloway, H. W.; Giordano, T.; Chen, D.; Furukawa, K.; Sambamurti, K.; Brossi, A.; Lahiri, D. Selective butyrylcholinesterase inhibition elevates brain acetylcholine, augments learning and lowers Alzheimer beta-amyloid peptide in rodent. *Proc. Natl. Acad. Sci. U.S.A*. **2005**, *102*, 17213−17218. b) Lane, R. M.; Potkin, S. G.; Enz, A. Targeting acetylcholinesterase and butyrylcholinesterase in dementia. *Int. J. Neuropsychoph.* **2006**, *9*, 101−124. c) Venneri, A.; Lane, R. Effects of cholinesterase inhibition on brain white matter volume in Alzheimer's disease. *Neuroreport* **2009**, *20*, 285−288.

[70] Shanks, M.; Kivipelto, M.; Bullok, R.; Lane, R. Cholinesterase inhibition: is there evidence for disease-modifying effects? *Curr. Med. Res. Opin.* **2009**, *25*, 2439−2446.

[71] Muñoz-Torrero, D. Acetylcholinesterase inhibitors as disease-modifying therapies for Alzheimer's disease. *Curr. Med. Chem.* **2008**, *15*, 2433−2455.

[72] Inestrosa, N. C.; Alvarez, A.; Pérez, C. A.; Moreno, R. D.; Vicente, M.; Linker, C.; Casanueva, O. I.; Soto, C.; Garrido, J. Acetylcholinesterase accelerates assembly of amyloid-beta-peptides into Alzheimer's fibrils: possible role of the peripheral site of the enzyme. *Neuron* **1996**, *16*, 881−891.

[73] Alvarez, A.; Opazo, C.; Alarcon, R.; Garrido, J.; Inestrosa, N. C. Acetylcholinesterase promotes the aggregation of amyloid-beta-peptide fragments by forming a complex with the growing fibrils. *J. Mol. Biol.* **1997**, *272*, 348−361.

[74] Alvarez, A.; Alarcón, R.; Opazo, C.; Campos, E. O.; Muñoz, F. J.; Calderón, F. H.; Dajas, F.; Gentry, M. K.; Doctor, B. P.; De Mello, F. G.; Inestrosa, N. C. Stable complexes involving acetylcholinesterase and amyloid-beta peptide change the biochemical properties of the enzyme and increase the neurotoxicity of Alzheimer's fibrils. *J. Neurosci.* **1998**, *18*, 3213−3223.

[75] Inestrosa, N. C.; Sagal, J. P.; Colombres, M. Acetylcholinesterase interaction with Alzheimer amyloid beta. *Subcell Biochem.* **2005**, *38*, 299−317.

[76] Inestrosa, N. C.; Dinamarca, M. C.; Alvarez, A. Amyloid-cholinesterase interactions. Implications for Alzheimer's disease. *FEBS J.* **2008**, *275*, 625−632.

[77] Chacón, M. A.; Reyes, A. E.; Inestrosa, N. C. Acetylcholinesterase induces neuronal cell loss, astrocyte hypertrophy and behavioral deficits in mammalian hippocampus. *J. Neurochem.* **2003**, *87*, 195−204.

[78] Reyes, A. E.; Chacón, M. A.; Dinamarca, M. C.; Cepa, W.; Morgan, C.; Inestrosa, N. C. Acetylcholinesterase-Aβ complexes are more toxic than Aβ fibrils in rat hippocampus: effect on rat β-amyloid aggregation, laminin expression, reactive astrocytosis, and neuronal cell loss. *Am. J. Pathol.* **2004**, *164*, 2163−2174.

[79] Dinamarca, M. C.; Arrázola, M.; Toledo, E.; Cerpa, W. F.; Hancke, J.; Inestrosa, N. C. Release of acetylcholinesterase (AChE) from beta-amyloid plaques assemblies improves the spatial memory impairments in APP-transgenic mice. *Chem. Biol. Interact*. **2008**, *175*, 142−149.

[80] Muñoz, F. J.; Inestrosa, N. C. Neurotoxicity of acetylcholinesterase amyloid β-peptide aggregates is dependent on the type of Aβ peptide and the AChE concentration present in the complexes. *FEBS Lett*. **1999**, *450*, 205−209.

[81] De Ferrari, G. V.; Canales, M. A.; Shin, I.; Weiner, L. M.; Silman, I.; Inestrosa, N. C. A structural motif of acetylcholinesterase that promotes amyloid β-peptide fibril formation. *Biochemistry* **2001**, *40*, 10447−10457.

[82] Castro, A.; Martínez, A. Targeting β-amyloid pathogenesis through acetylcholinesterase inhibitors. *Curr. Pharm. Design* **2006**, *12*, 4377−4387.

[83] Brogi, S.; Butini, S.; Maramai, S.; Colombo, R.; Verga, L.; Lanni, C.; De Lorenzi, E.; Lamponi, S.; Andreassi, M.; Bartolini, M.; Andrisano, V.; Novellino, E.; Campiani, G.; Brindisi, M.; Gemma, S. Disease-modifying anti-Alzheimer's drugs: Inhibitors of human cholinesterases interfering with β-amyloid aggregation. *CNS Neurosci. Ther.* **2014**, *20*, 624−632.

[84] a) Pang, Y. P.; Quiram, P.; Jelacic, T.; Hong, F.; Brimijoin, S. Highly potent, selective, and low cost *bis*-tetrahydroaminacrine inhibitors of acetylcholinesterase. Steps toward novel drugs for treating Alzheimer's disease. *J. Biol. Chem*. **1996**, *271*, 23646−23649. b) Carlier, P. R.; Han, Y. F.; Chow, E. S.; Li, C. P.; Wang, H.; Lieu, T. X.; Wong, H. S.; Pang, Y. P. Evaluation of short-tether *bis*-THA AChE inhibitors. A further test of the dual binding site hypothesis. *Bioorg. Med. Chem.* **1999**, *7*, 351−357. c) Bolognesi, M. L.; Cavalli, A.; Valgimigli, L.; Bartolini, M.; Rosini, M.; Andrisano, V.; Recanatini, M.; Melchiorre, C. Multi-target-directed drug design strategy: from a dual binding site acetylcholinesterase inhibitor to a trifunctional compound against Alzheimer's disease. *J. Med. Chem*. **2007**, *50*, 6446−6449.

[85] Piazzi, L.; Rampa, A.; Bisi, A.; Gobbi, S.; Belluti, F.; Cavalli, A.; Bartolini, M.; Andrisano, V.; Valenti, P.; Recanatini, M. 3-(4-[[Benzyl(methyl)amino]methyl]phenyl)-6,7-dimethoxy-2H-2-chromenone (AP2238) inhibits both acetylcholinesterase and acetylcholinesterase-induced β-amyloid aggregation: a dual function lead for Alzheimer's disease therapy. *J. Med. Chem*. **2003**, *46*, 2279−2282.

[86] Muñoz-Ruiz, P.; Rubio, L.; García-Palomero, E.; Dorronsoro, I.; del Monte-Millán, M.; Valenzuela, R.; Usán, P.; de Austria, C.; Bartolini, M.; Andrisano, V.; Bidon-Chanal, A.; Orozco, M.; Luque, F. J.; Medina, M.; Martínez, A. Design, synthesis, and biological evaluation of dual binding site acetylcholinesterase inhibitors: new disease-modifying agents for Alzheimer's disease. *J. Med. Chem*. **2005**, *48*, 7223−7233.

[87] a) Camps, P.; El Achab, R.; Görbig, D. M.; Morral, J.; Muñoz-Torrero, D.; Badia, A.; Baños, J. E.; Vivas, N. M.; Barril, X.; Orozco, M.; Luque, F. J. Synthesis, in vitro pharmacology, and molecular modeling of very potent tacrine-huperzine A hybrids as acetylcholinesterase inhibitors of potential interest for the treatment of Alzheimer's disease. *J. Med. Chem.* **1999**, *42*, 3227−3242. b) Muñoz-Torrero, D.; Camps, P. Huprines for Alzheimer's disease drug development. *Expert Opin. Drug Dis.* **2008**, *3*, 65−81.

[88] a) Camps, P.; Formosa, X.; Galdeano, C.; Muñoz-Torrero, D.; Ramírez, L.; Gómez, E.; Isambert, N.; Lavilla, R.; Badia, A.; Clos, M. V.; Bartolini, M.; Mancini, F.; Andrisano, V.; Arce, M. P.; Rodríguez-Franco, M. I.; Huertas, O.; Dafni, T.; Luque, F.J. Pyrano[3,2-c]quinoline-6-chlorotacrine hybrids as a novel family of acetylcholinesterase- and β-amyloid-directed anti-Alzheimer compounds. *J. Med. Chem.* **2009**, *52*, 5365−5379. b) Galdeano, C.; Viayna, E.; Sola I.; Formosa, X.; Camps, P.; Badia, A.; Clos, M. V.; Relat, J.; Ratia, M.; Bartolini, M.; Mancini, F.; Andrisano, V.; Salmona, M.; Minguillón C.; González-Muñoz, G. C.; Rodríguez-Franco, M. I.; Bidon-Chanal, A.; Luque, F. J.; Muñoz-Torrero, D. Huprine-tacrine heterodimers as anti-amyloidogenic compounds of potential interest against Alzheimer's and prion diseases. *J. Med. Chem*. **2012**, *55*, 661−669. c) Viayna, E.; Sabate, R.; Muñoz-Torrero, D. Dual inhibitors of β-amyloid aggregation and acetylcholinesterase as multi-target anti-Alzheimer drug candidates. *Curr. Top. Med. Chem*. **2013**, *13*, 1820−1842.

[89] a) Camps, P.; Muñoz-Torrero, D.; Formosa, X.; Scarpellini, M. Acetylcholinesterase-inhibiting compounds for treating Alzheimer's disease. WO 2007/122274A1. b) Camps, P.; Formosa, X.; Galdeano, C.; Gómez, T.; Muñoz-Torrero, D.; Scarpellini, M.; Viayna, E.; Badia A.; Clos, M. V.; Camins, A.; Pallàs, M.; Bartolini, M.; Mancini, F.; Andrisano, V.; Estelrich, J.; Lizondo, M.; Bidon-Chanal, A.; Luque, F. J. Novel donepezil-based inhibitors of acetyl- and butyrylcholinesterase and acetylcholinesterase-induced β-amyloid aggregation. *J. Med. Chem*. **2008**, *51*, 3558−3598. c) Muñoz-Torrero, D.; Camps, P.; Gómez, T.; Viayna, E.; Galdeano, C. Multifunctional compounds modifying Alzheimer's disease for the treatment of said disease. WO 2011/076969A1. d) Viayna, E.; Gómez, T.; Galdeano, C.; Ramírez, L.; Ratia, M.; Badia, A.; Clos, M. V.; Verdaguer, E.; Junyent, F.;

Camins, A.; Pallàs, M.; Bartolini, M.; Mancini, F.; Andrisano, V.; Arce, M. P.; Rodríguez-Franco, M. I.; Bidon-Chanal, A.; Luque, F. J.; Muñoz-Torrero, D. Novel huprine derivatives with inhibitory activity toward amyloid β-aggregation and formation as disease-modifying anti-Alzheimer drug candidates. *ChemMedChem* **2010**, *5*, 1855−1870. e) Sola, I.; Viayna, E.; Gómez, T.; Galdeano, C.; Cassina, M.; Camps, P.; Romeo, M.; Diomede, L.; Salmona, M.; Franco, P.; Schaeffer, M.; Colantuono, D.; Robin, D.; Brunner, D.; Taub, N.; Hutter-Paier, B.; Muñoz-Torrero, D. Multigram synthesis and in vivo efficacy studies of a novel multitarget anti-Alzheimer's compounds. *Molecules* **2015**, *20*, 4492−4515.

90 Melnikova, I. Therapies for Alzheimer's disease. *Nat. Rev. Drug Discov.* **2007**, *6*, 341−342.

91 Skovronsky, D. M.; Lee, V. M.; Trojanowski, J. Q. Neurodegenerative diseases: new concepts of pathogenesis and their therapeutic implications. *Annu. Rev. Pathol.* **2006**, *1*, 151−170.

92 De Strooper, B.; Vassar, R.; Golde, T. The secretases: enzymes with therapeutic potential in Alzheimer disease. *Nat. Rev. Neurol*. **2010**, *6*, 99−107.

93 Jonsson, T.; Atwal, J. K.; Steinberg, S.; Snaedal, J.; Jonsson, P. V.; Bjornsson, S.; Stefansson, H.; Sulem, P.; Gudbjartsson, D.; Maloney, J.; Hoyte, K.; Gustafson, A.; Liu, Y.; Lu, Y.; Bhangale, T.; Graham, R. R.; Huttenlocher, J.; Bjornsdottir, G.; Andreassen, O. A.; Jönsson, E. G.; Palotie, A.; Behrens, T. W.; Magnusson, O. T.; Kong, A.; Thorsteinsdottir, U.; Watts, R. J.; Stefansson, K. A mutation in APP protects against Alzheimer's disease and age-related cognitive decline. *Nature* **2012**, *488*, 96–99.

94 a) May, P. C.; Dean, R. A.; Lowe, S. L.; Martenyi, F.; Sheehan, S. M.; Boggs, L. N.; Monk, S. A.; Mathes, B. M.; Mergott, D. J.; Watson, B. M.; Stout, S. L.; Timm, D. E.; Smith Labell, E.; Gonzales, C. R.; Nakano, M.; Jhee, S. S.; Yen, M.; Ereshefsky, L.; Lindstrom, T. D.; Calligaro, D. O.; Cocke, P. J.; Greg Hall, D.; Friedrich, S.; Citron, M.; Audia, J. E. Robust central reduction of amyloid-β in humans with an orally available, non-peptidic β-secretase inhibitor. *J. Neurosci.* **2011**, *31*, 16507−16516. b) Stone, J.; Kleijn, H. J.; Dockendorf, M.; Ma, L.; Palcza, J.; Tseng, J.; Tanen, M.; Forman, M. Consistency of Bace inhibitor-mediated brain amyloid production inhibition by MK-8931 in Alzheimer's disease patients and healthy young adults. *Alzheimer's Dementia* **2013**, 9(4) Supplement, P690–P691.

95 Kacker, P.; Bottegoni, G.; Cavalli, A. Computational methods in the discovery and design of BACE-1 inhibitors. *Curr. Med. Chem*. **2012**, *19*, 6095−6111.

96 a) Cheret, C.; Willem, M.; Fricker, F. R.; Wende, H.; Wulf-Goldenberg, A.; Tahirovic, S.; Nave, K. A.; Saftig, P.; Haass, C.; Garratt, A. N.; Bennett, D. L.; Birchmeier, C. Bace1 and Neuregulin-1 cooperate to control formation and maintenance of muscle spindles. *EMBO J*. **2013**, *32*, 2015–2028. b) Kandalepas, P. C.; Vassar, R. Identification and biology of β-secretase. *J. Neurochem*. **2012**, *120* (Suppl 1), 55–61. c) Kuhn, P. H.; Koroniak, K.; Hogl, S.; Colombo, A.; Zeitschel, U.; Willem, M.; Volbracht, C.; Schepers, U.; Imhof, A.; Hoffmeister, A.; Haass, C.; Rossner, S.; Brase, S.; Lichtenthaler, S. F. Secretome protein enrichment identifies physiological BACE1 protease substrates in neurons. *EMBO J*. **2012**, *31*, 3157–3168. d) Zhou, L.; Barao, S.; Laga, M.; Bockstael, K.; Borgers, M.; Gijsen, H.; Annaert, W.; Moechars, D.; Mercken, M.; Gevaert, K.; De Strooper, B. The neural cell adhesion molecules L1 and CHL1 are cleaved by BACE1 protease in vivo. *J. Biol. Chem*. **2012**, *287*, 25927–25940. e) Cai, J.; Qi, X.; Kociok, N.; Skosyrski, S.; Emilio, A.; Ruan, Q.; Han, S.; Liu, L.; Chen, Z.; Rickman, C. B.; Golde, T.; Grant, M. B.; Saftig, P.; Serneels, L.; De Strooper, B.; Joussen, A. M.; Boulton, M. E. β-Secretase (BACE1) inhibition causes retinal pathology by vascular dysregulation and accumulation of age pigment. *EMBO Mol. Med*. **2012**, 4, 980–991. f) Alzforum. "Cloistered Retreat Takes the Pulse of BACE Research." http://www.alzforum.org/news/conference-coverage/cloistered-retreat-takes-pulse-bace-research. February 18, 2016.

97 Willem, M.; Garratt, A. N.; Novak, B.; Citron, M.; Kaufmann, S.; Rittger, A.; De Strooper, B.; Saftig, P.; Birchmeier, C.; Haass, C. Control of peripheral nerve myelination by the beta-secretase BACE1. *Science* **2006**, *314*, 664–666.

98 Fielden, M. R.; Werner, J.; Coppi, A.; Dunn, R. T.; Trueblood, E.; Afshari, C. A.; Lightfoot-Dunn, R.; Jamison, J. A.; Hickman, D.; Zhou, L., Retinal Toxicity Induced by a Novel β- Secretase Inhibitor in the Sprague−Dawley Rat. *Toxicol. Pathol.* **2015**, *43*, 581−592.

99 Lilly Voluntarily Terminates Phase II Study for LY2886721, a Beta Secretase Inhibitor, Being Investigated as a Treatment for Alzheimer's Disease; Eli Lilly Pharmaceuticals: Indianapolis, IN, June 13, 2013; https://investor.lilly.com/releaseDetail.cfm?ReleaseID=771353.

100 Vassar, R. BACE1 inhibitor drugs in clinical trials for Alzheimer's disease. *Alzheimers Res. Ther*. **2014**, *6*, 89.

[101] McDonald, R. J. Multiple combinations of co-factors produce variants of age-related cognitive decline: a theory. *Can. J. Exp. Psychol*. **2002**, *56*, 221–339.

[102] a) Hopkins, A. L. Network pharmacology. *Nat. Biotechnol.* **2007**, *25*, 1110−1111. b) Hopkins, A. L. Network pharmacology: the next paradigm in drug discovery. *Nat. Chem. Biol.* **2008**, *4*, 682−690. c) Janga, S. C.; Tzakos, A. Structure and organization of drug-targets networks: insights from genomic approaches for drug discovery. *Mol. BioSyst.* **2009**, *5*, 1536−1548.

[103] a) Buccafusco, J. J.; Terry, A. V., Jr. Multiple Central Nervous System Targets for Eliciting Beneficial Effects on Memory and Cognition. *J. Pharmacol. Exp. Ther.* **2000**, *295*, 438−446. b) Youdim, M. B.; Buccafusco, J. J. CNS Targets for multifunctional drugs in the treatment of Alzheimer's and Parkinson's Diseases. *J. Neural Transm.* **2005**, *112*, 519−537. c) Nicolotti, O.; Giangreco, I.; Introcaso, A.; Leonetti, F.; Stefanachi, A.; Carotti, A. Strategies of Multi-Objective Optimization in Drug Discovery and Development. *Expert Opin. Drug Dis.* **2011**, *6*, 871−884.

[104] a) Morphy, R.; Rankovic, Z. Designed multiple ligands. An emerging drug discovery paradigm. *J. Med. Chem.* **2005**, *48*, 6523−6543. b) Morphy, R.; Rankovic, Z. Fragments, network biology and designing multiple ligands. *Drug Discov. Today* **2007**, *12*, 156–160. c) Bottegoni, G.; Favia, A. D.; Recanatini, M.; Cavalli, A. The role of fragment-based and computational methods in polypharmacology. *Drug Discov. Today* **2012**, *17*, 23–34. d) Viayna, E.; Sola, I.; Di Pietro, O.; Muñoz-Torrero, D. Human disease and drug pharmacology, complex as real life. *Curr. Med. Chem.* **2013**, *20*, 1623−1634.

[105] Recent reviews: a) Cavalli, A.; Bolognesi, M. L.; Minarini, A.; Rosini, M.; Tumiatti, V.; Recanatini, M.; Melchiorre, C. Multi-target-directed ligands to combat neurodegenerative diseases. *J. Med. Chem.* **2008**, *51*, 347−372. b) Carmo Carreiras, M.; Mendes, E.; Jesus Perry, M.; Paula Francisco, A.; Marco-Contelles, J.; Carreiras, M.; Perry, M.; Francisco, A. The multifactorial nature of Alzheimer's disease for developing potential therapeutics. *Curr. Top. Med. Chem*. **2013**, *13*, 1745−1770. c) Rampa, A.; Gobbi, S.; Belluti, F.; Bisi, A. Emerging targets in neurodegeneration: New opportunities for Alzheimer's disease treatment? *Curr. Top. Med. Chem*. **2013**, *13*, 1879−1904. d) Geldenhuys, W. J.; Van der Schyf, C. J. Rationally designed multi-targeted agents against neurodegenerative diseases. *Curr. Med. Chem*. **2013**, *20*, 1662−1672. e) Chen, X.; Decker, M. Multi-target compounds acting in the central nervous system designed from natural products. *Curr. Med. Chem.* **2013**, *20*, 1673−1685. f) Guzior, N.; Wieckowska, A.; Panek, D.; Malawska, B. Recent development of multifunctional agents as potential drug candidates for the treatment of Alzheimer's disease. *Curr. Med. Chem.* **2015**, *22*, 373−404.

[106] Recent examples: a) Farina, R.; Pisani, L.; Catto, M.; Nicolotti, O.; Gadaleta, D.; Denora, N.; Soto-Otero, R.; Mendez-Alvarez, E.; Passos, C.S.; Muncipinto, G.; Altomare, C. D.; Nurisso, A.; Carrupt, P. A.; Carotti, A. Structure-Based Design and Optimization of Multitarget-Directed 2H-Chromen-2-one Derivatives as Potent Inhibitors of Monoamine Oxidase B and Cholinesterases. *J. Med. Chem*. **2015**, *58*, 5561−5578. b) Prati, F.; De Simone, A.; Bisignano, P.; Armirotti, A.; Summa, M.; Pizzirani, D.; Scarpelli, R.; Perez, D. I.; Andrisano, V.; Perez-Castillo, A.; Monti, B.; Massenzio, F.; Polito, L.; Racchi, M.; Favia, A. D.; Bottegoni, G.; Martinez, A.; Bolognesi, M. L.; Cavalli, A. Multitarget drug discovery for Alzheimer's disease: Triazinones as BACE-1 and GSK-3β inhibitors. *Angew. Chem. Int. Ed.* **2015**, *54*, 1578−1582. c) Rochais, C.; Lecoutey, C.; Gaven,F.; Giannoni, P.; Hamidouche, K.; Hedou, D.; Dubost, E.; Genest, D.; Yahiaoui, S.; Freret, T.; Bouet, V.; Dauphin, F.; Sopkova de Oliveira Santos, J.; Ballandonne, C.; Corvaisier, S.; Malzert-Fréon, A.; Legay, R.; Boulouard, M.; Claeysen, S.; Dallemagne, P. Novel multitarget-directed ligands (MTDLs) with acetylcholinesterase (AChE) inhibitory and serotonergic subtype 4 receptor (5-HT4R) agonist activities as potential agents against Alzheimer's disease: The design of donecopride. *J. Med. Chem.* **2015**, *58*, 3172−3187. d) Guzior, N.; Bajda, M.; Skrok, M.; Kurpiewska, K.; Lewinski, K.; Brus, B.; Pislar, A.; Kos, J.; Gobec, S.; Malawska, B. Development of multifunctional, heterodimeric isoindoline-1,3-dione derivatives as cholinesterase and β-amyloid aggregation inhibitors with neuroprotective properties. *Eur. J. Med. Chem*. **2015**, *92*, 738−749. e) Xie, S.S.; Lan, J.S.; Wang, X.B.; Jiang, N.; Dong, G.; Li, Z.R.; Wang, K. D. G.; Guo, P.P.; Kong, L.Y. Multifunctional tacrine−trolox hybrids for the treatment of Alzheimer's disease with cholinergic, antioxidant, neuroprotective and hepatoprotective properties. *Eur. J. Med. Chem*. **2015**, 93, 42−50. f) Sang, Z.; Qiang, X.; Li, Y.; Yuan, W.; Liu, Q.; Shi, Y.; Wei, A.; Luo, Y.; Tan, Z.; Deng, Y. Design, synthesis and evaluation of scutellarein-O-alkylamines as multifunctional agents for the treatment of Alzheimer's disease. *Eur. J. Med. Chem*. **2015**, *94*, 348−366. g) Benchekroun, M.; Bartolini, M.; Egea, J.; Romero, A.; Soriano,E.; Pudlo, M.; Luzet, V.; Andrisano, V.; Jimeno, M.-L.; López, M. G.; Wehle, S.; Gharbi, T.; Refouvelet, B.; de

Andrés, L.; Herrera- Arozamena, C.; Monti, B.; Bolognesi, M. L.; Rodríguez-Franco, M. I.; Decker, M.; Marco-Contelles, J.; Ismaili, L. Novel tacrine-grafted Ugi adducts as multipotent anti-Alzheimer drugs: A synthetic renewal in tacrine−ferulic acid hybrids. *ChemMedChem* **2015**, *10*, 523−539. h) Liu, Q.; Qiang, X.; Li, Y.; Sang, Z.; Li, Y.; Tan, Z.; Deng, Y. Design, synthesis and evaluation of chromone-2-carboxamidoalkyl- benzylamines as multifunctional agents for the treatment of Alzheimer's disease. *Bioorg. Med. Chem*. **2015**, *23*, 911−923.

107 Melchiorre, C.; Andrisano, V.; Bolognesi, M. L.; Budriesi, R.; Cavalli, A.; Cavrini, V.; Rosini, M.; Tumiatti, V.; Recanatini, M. Acetylcholinesterase inhibitors based on a polyamine backbone for potential use against Alzheimer's disease. *J. Med. Chem*. **1998**, *41*, 4186−4189.

108 a) Bolognesi, M.; Andrisano, V.; Bartolini, M.; Banzi, R.; Melchiorre, C. Propidium-based polyamine ligands as potent inhibitors of acetylcholinesterase and acetylcholinesterase-induced amyloid-β aggregation. *J. Med. Chem*. **2005**, *48*, 24−27. b) Huang, W.; Tang, L.; Shi, Y.; Huang, S.; Xu, L.; Sheng, R.; Wu, P.; Li, J.; Zhou, N.; Hu, Y. Searching for the multi-target-directed ligands against Alzheimer's disease: discovery of quinoxaline-based hybrid compounds with AChE, H3R and BACE 1 inhibitory activities. *Bioorg. Med. Chem*. **2011**, *19*, 7158−7167. c) Li, Y.; Peng, P.; Tang, L.; Hu, Y.; Hu, Y.; Sheng, R. Design, synthesis and evaluation of rivastigmine and curcumin hybrids as site-activated multitarget-directed ligands for Alzheimer's disease therapy. *Bioorg. Med. Chem*. **2014**, *22*, 4717−4725. d) Rosini, M.; Simoni, E.; Bartolini, M.; Cavalli, A.; Ceccarini, L.; Pascu, N.; Mcclymont, D. W.; Tarozzi, A.; Bolognesi, M. L.; Minarini, A.; Tumiatti, V.; Andrisano, V.; Mellor, I. R.; Melchiorre, C. Inhibition of acetylcholinesterase, β-amyloid aggregation, and NMDA receptors in Alzheimer's disease: a promising direction for the multi-target- directed ligands gold rush. *J. Med. Chem*. **2008**, *51*, 4381−4384.

109 a) Holmquist, L.; Stuchbury, G.; Berbaum, K.; Muscat, S.; Young, S.; Hager, K.; Engel, J.; Münch, G. Lipoic acid as a novel treatment for Alzheimer's disease and related dementias. *Pharmacol. Ther.* **2007**, *113*, 154−164. b) Bolognesi, M. L.; Rosini, M.; Andrisano, V.; Bartolini, M.; Minarini, A.; Tumiatti, V.; Melchiorre, C. MTDL design strategy in the context of Alzheimer's disease: from lipocrine to memoquin and beyond. *Curr. Pharm. Des.* **2009**, *15*, 601−613.

110 a) Sterling, J.; Herzig, Y.; Goren, T.; Finkelstein, N.; Lerner, D.; Goldenberg, W.; Miskolczi, I.; Molnar, S.; Rantal, F.; Tamas, T.; Toth, G.; Zagyva, A.; Zekany, A.; Lavian, G.; Gross, A.; Friedman, R.; Razin, M.; Huang, W.; Krais, B.; Chorev, M.; Youdim, M. B.; Weinstock, M. Novel dual inhibitors of AChE and MAO derived from hydroxy aminoindan and phenethylamine as potential treatment for Alzheimer's disease. *J. Med. Chem*. **2002**, *45*, 5260−5279. b) Youdim, M. B.; Amit, T.; Bar-Am, O.; Weinreb, O.; Yogev-Falach, M. Implications of co-morbidity for etiology and treatment of neurodegenerative diseases with multifunctional neuroprotective-neurorescue drugs: ladostigil. *Neurotoxic. Res.* **2006**, *10*, 181−192. c) Bolea, I.; Gella, A.; Unzeta, M. Propargylamine-derived multitarget-directed ligands: fighting Alzheimer's disease with mono- amine oxidase inhibitors. *J. Neural Transm*. **2013**, *120*, 893−902. d) Pisani, L.; Catto, M.; Leonetti, F.; Nicolotti, O.; Stefanachi, A.; Campagna, F.; Carotti, A. Targeting monoamine oxidases with multipotent ligands: an emerging strategy in the search of new drugs against neurodegenerative diseases. *Curr. Med. Chem*. **2011**, *18*, 4568−4587.

111 Marco-Contelles, J.; León, R.; de Los Ríos, C.; Guglietta, A.; Terencio, J.; López, M. G.; García, A. G.; Villarroya, M. Novel multipotent tacrine-dihydropyridine hybrids with improved acetylcho-linesterase inhibitory and neuroprotective activities as potential drugs for the treatment of Alzheimer's disease. *J. Med. Chem.* **2006**, *49*, 7607−7610.

112 Cavalli, A.; Bolognesi, M. L.; Capsoni, S.; Andrisano, V.; Bartolini, M.; Margotti, E.; Cattaneo, A.; Recanatini, M.; Melchiorre, C. A small molecule targeting the multifactorial nature of Alzheimer's disease. *Angew. Chem., Int. Ed. Engl.* **2007**, *46*, 3689−3692.

113 Simarro, P. P.; Diarra, A.; Ruiz-Postigo, J. A.; Franco, J. R.; Jannin, J. The Human African trypanosomiasis control and surveillance programme of the World Health Organization 2000–2009: the way forward. *PLoS Negl. Trop. Dis*. **2011**, *5*, e1007.

114 WHO: Trypanosomiasis, human African (sleeping sickness). http://www.who.int/mediacentre/factsheets/fs259/en/ (Accessed November 27, 2015)

115 DNDi: About Human African Trypanosomiasis. http://www.dndi.org/diseases-projects/hat/ (Accessed December 15, 2015)

116 Maurice, J. New WHO plan targets the demise of sleeping sickness. *Lancet* **2013**, *381*, 13−14.

117 World Health Organization. *Working to Overcome the Global Impact of Neglected Tropical Diseases: First WHO Report on Neglected Tropical Diseases* **2010**.

[118] World Health Organization. *Investing to Overcome the Global Impact of Neglected Tropical Diseases: Third WHO Report on Neglected Tropical Diseases* **2015**.

[119] Fèvre, E. M.; Wissmann, B. V.; Weburn, S. C.; Lutumba, P. The burden of human African trypanosomiasis. *PLoS Negl. Trop. Dis*. **2008**, *2*, e333.

[120] Welburn, S. C.; Maudlin, I.; Simarro, P. P. Controlling sleeping sickness – a review. *Parasitology* **2009**, *136*, 1943–1949.

[121] Barrett, M. P. The rise and fall of sleeping sickness. *Lancet* **2006**, *367*, 1377–1378.

[122] Simarro, P. P.; Jannin, J. G.; Cattand, P. Eliminating human African trypanosomiasis: where do we stand and what comes next? *PLoS Med.* **2008**, *5*, e55.

[123] Franco, J. R.; Simarro, P. P.; Diarra, A.; Jannin, J. G. Epidemiology of human African tripanosomiasis. *Clin. Epidemiol*. **2014**, *6*, 257−275.

[124] Brun, R.; Blum, J.; Chappuis, F.; Burri, C. Human African trypanosomiasis. *Lancet* **2010**, *375*, 148–59.

[125] Hoare, C. A. The mammalian trypanosomes of Africa. *The African trypanosomiasis*. George Allen and Unwin LTD, London, **1970**, 3−23.

[126] Malvy, D.; Chappuis, F. Sleeping sickness. *CMI* **2011**, *17*, 986–995.

[127] Barrett, M. P.; Burchmore R. J. S.; Stich, A.; O'Lazzari, J.; Frasch, A. C.; Cazzulo, J. J.; Krishna, S. The trypanosomiases. *Lancet* **2003**, *362*, 1469–1480.

[128] Kennedy, P. G. E. The fatal sleep: Africa's killer disease that went undiscovered for centuries. Reviewed by Donelson, L. G.; Donelson, J. E. Edinburgh: Luath Press, **2010**.

[129] Picozzi, K.; Fèvre, E. M.; Odiit, M.; Carrington, M.; Eisler, M. C.; Maudlin, I.; Welburn, S. C. Sleeping sickness in Uganda: a thin line between two fatal diseases. *BMJ* **2005**, *331*, 1238–1241.

[130] Malvy, D.; Djossou, F.; Longy-Boursier, M.; Le Bras, M.; Weill, F. X.; Chapuis, P. Human West African trypanosomiasis with chancre presentation. *Eur. J. Dermatol.* **2000**, *10*, 561–562.

[131] Gautret, P.; Clerinx, J.; Caumes, E.; Simon, F.; Jensenius, M.; Loutan, L.; Sclagenhauf, P.; Castelli, F.; Freedman, D.; Miller, A.; Bronner, U.; Parola, P. Imported human African trypanosomiasis in Europe, 2005–2009. *Euro Surveill*. **2009**, *14*, 19327.

[132] Kennedy, P. G. E. Clinical features, diagnosis, and treatment of human African trypanosomiasis (sleeping sickness). *Lancet Neurol*. **2013**, *12*, 186−194.

[133] Welburn, S. C.; Maudlin, I. Chapter 4-Priorities for the Elimination of Sleeping Sickness. *Adv. Parasitol.* **2012**, *79*, 299–337.

[134] Nagle, A. S.; Khare, S.; Kumar, A. B.; Supek, F.; Buchynskyy, A.; Mathison, C. J. N.; Chennamaneni, N. K.; Pendem, N.; Buckner, F. S.; Gelb, M. H.; Molteni, V. Recent developments in drug discovery for leishmaniasis and human African trypanosomiasis. *Chem. Rev.* **2014**, *114*, 11305−11347.

[135] Atouguia, J. L. M.; Kennedy, P. G. E.; Davis, L. E. Neurological aspects of human African trypanosomiasis. Butterworth-Heinemann, Oxford, **2000**, 321−372.

[136] Blum, J.; Schmid, C.; Burri, C. Clinical aspects of 2541 patients with second stage human African trypanosomiasis. *Acta Tropica* **2006**, *97*, 55−64.

[137] Bentovoglio, M.; Grassi-Zucconi, G.; Olsson, T.; Kristensson, K. *Trypanosoma brucei* and the nervous system. *Trends Neurosci*. **1994**, *17*, 325−329.

[138] Lundkvist, G.B.; Kristensson, K.; Bentivoglio, M. Why trypanosomes cause sleeping sickness. *Physiology* **2004**, *19*, 198−206.

[139] MacGregor, P.; Savill, N. J.; Hall, D.; Matthews, K. R. Transmission stages dominate trypanosome within-host dynamics during chronic infections. *Cell Host Microbe* **2011**, *9*, 310–318.

[140] Rotureau, B.; Subota, I.; Buisson, J.; Bastin, P. A new asymmetric division contributes to the continuous production of infective trypanosomes in the tsetse fly. *Development* **2012**, *139*, 1842–1850.

[141] Bethony, J. M.; Cole, R. N.; Guo, X. T.; Kamhawi, S.; Lightowlers, M. W.; Loukas, A.; Petri, A.; Reed, S.; Valenzuela, J. G.; Hotez, P. J. Vaccines to combat the neglected tropical diseases. *Immunol. Rev*. **2011**, *239*, 237–270.

[142] Delespaux, V.; de Koning, H. P. Drugs and drug resistance in African trypanosomiasis. *Drug Resist. Updates* **2007**, *10*, 30−50.

[143] Rodgers, J. Human African trypanosomiasis, chemotherapy and CNS disease. *J. Neuroimmunol*. **2009**, *211*, 16−22.

[144] Priotto, G.; Kasparian, S.; Mutombo, W.; Ngouama, D.; Ghorashian, S.; Arnold, U.; Ghabri, S.; Baudin, E.; Buard, V.; Kazadi-Kyanza, S.; Ilunga, M.; Mutangala, W.; Pohlig, G.; Schmid, C.; Karunakara, U.; Torreele, E.; Kande, V. Nifurtimox–eflornithine combination therapy for second-

stage African *Trypanosoma brucei gambiense* trypanosomiasis: a multicentre, randomised, phase III, non-inferiority trial. *Lancet* **2009**, *374*, 56–64.

145 Burri, C. Chemotherapy against human African trypanosomiasis: is there a road to success? *Parasitology* **2010**, *137*, 1987–1994.

146 Fairlamb, A. H. Chemotherapy of human African trypanosomiasis: current and future prospects. *Trends Parasitol*. **2003**, *19*, 488−494.

147 DNDi: http://www.dndi.org (Accessed December 15, 2015).

148 Goupil, L. S.; McKerrow, J. H. Introduction: drug discovery and development for neglected diseases. *Chem. Rev.* **2014**, *114*, 11131–11137.

149 Njoroge, M.; Njuguna, N. M.; Mutai, P.; Ongarora, D. S. B.; Smith, P. W.; Chibale, K. Recent approaches to chemical discovery and development against malaria and the neglected tropical diseases human African trypanosomiasis and schistosomiasis. *Chem. Rev.* **2014**, *114*, 11138–11163.

150 Renslo, A. R.; McKerrow, J.H. Drug discovery and development for neglected parasitic diseases. *Nat. Chem. Biol.* **2006**, *2,* 701–710.

151 Swinney, D. C.; Anthony, J. How were new medicines discovered? *Nat. Rev. Drug Discov*. **2011**, *10*, 507−519.

152 Gilbert, I. H. Drug Discovery for Neglected Diseases: Molecular Target-Based and Phenotypic Approaches. *J. Med. Chem.* **2013**, *56*, 7719−7726.

153 Kotz, J. Phenotypic screening, take two. *SciBX* **2012**, *5*, 1−3.

154 Kuettel, S.; Mosimann, M.; Mäser, P.; Kaiser, M.; Brun, R.; Scapozza, L.; Perozzo, R. Adenosine Kinase of *T. b. rhodesiense* identified as the putative target of 4-[5-(4-phenoxyphenyl)-2H-pyrazol-3-yl]morpholine using chemical proteomics. *PLoS Negl. Trop. Dis*. **2009**, *3*, e506.

155 Mercer, L.; Bowling, T.; Perales, J.; Freeman, J.; Nguyen, T.; Bacchi, C.; Yarlett, N.; Don, R.; Jacobs, R.; Nare, B. 2,4-Diaminopyrimidines as potent inhibitors of *Trypanosoma brucei* and identification of molecular targets by a chemical proteomics approach. *PLoS Negl. Trop. Dis.* **2011**, *5*, e956.

156 König, J.; Wyllie, S.; Wells, G.; Stevens, M. F.; Wyatt, P. G.; Fairlamb, A. H. Antitumor Quinol PMX464 is a cytocidal anti-trypanosomal inhibitor targeting trypanothione metabolism. *J. Biol. Chem.* **2011**, *286*, 8523-8533.

157 Brun, R.; Don, R.; Jacobs, R. T.; Wang, M. Z.; Barrett, M. P. Development of novel drugs for human African trypanosomiasis. *Future Microbiol*, **2011**, *6*, 677−691.

158 Jones, A. J.; Avery, V. M. Whole-organism high-throughput screening against *Trypanosoma brucei brucei*. *Expert Opin. Drug Discov.* **2013**, *8*, 495−507.

159 Torreele, E.; Bourdin, T. B.; Tweats, D.; Kaiser, M.; Brun, R.; Mazué, G.; Bray, M. A.; Pécoul, B. Fexinidazole – a new oral nitroimidazole drug candidate entering clinical development for the treatment of sleeping sickness. *PLoS Negl. Trop. Dis.* **2010**, *4*, e923.

160 Jacobs, R. T.; Nare, B.; Wring, S. A.; Orr, M. D.; Chen, D.; Sligar, J. M.; Jenks, M. X.; Noe, R. A.; Bowling, T. S.; Mercer, L. T.; Rewerts, C.; Gaukel, E.; Owens, J.; Parham, R.; Randolph, R.; Beaudet, B.; Bacchi, C. J.; Yarlett, N.; Plattner, J. J.; Freund, Y.; Ding, C.; Akama, T.; Zhang, Y. K.; Brun, R.; Kaiser, M.; Scandale, I.; Don, R. SCYX-7158, an orally-active benzoxaborole for the treatment of stage 2 human African trypanosomiasis. *PLoS Negl. Trop. Dis*. **2011**, *5*, e1151.

161 DNDi: *Oxaborole SCYX-7158*. http://www.dndi.org/diseases-projects/portfolio/oxaborole-scyx-7158.html. (Accessed 15 January 2016).

162 Berriman, M.; Ghedin, E.; Hertz-Fowler, C.; Blandin, G.; Renauld, H.; Bartholomeu, D. C.; Lennard, N. J.; Caler, E.; Hamlin, N. E.; Haas, B.; Böhme, U.; Hannick, L.; Aslett, M. A.; Shallom, J.; Marcello, L.; Hou, L.; Wickstead, B.; Alsmark, U. C.; Arrowsmith, C.; Atkin, R. J.; Barron, A. J.; Bringaud, F.; Brooks, K.; Carrington, M.; Cherevach, I.; Chillingworth, T. J.; Churcher, C.; Clark, L. N.; Corton, C. H.; Cronin, A.; Davies, R. M.; Dogget, J.; Djikeng, A.; Feldblyum, T.; Field, M. C.; Fraser, A.; Goodhead, I.; Hance, Z.; Harper, D.; Harris, B. R.; Hauser, H.; Hostetler, J.; Ivens, A.; Jagels, K.; Johnson, D.; Johnson, J.; Jones, K.; Kerhornou, A. X.; Koo, H.; Larke, N.; Landfear, S.; Larkin, C.; Leech, V.; Line, A.; Lord, A.; MacLeod, A.; Mooney, P. J.; Moule, S.; Martin, D. M.; Morgan, G. W.; Mungall, K.; Norbertczak, H.; Ormond, D.; Pai, G.; Peacock, C. S.; Peterson, J.; Quail, M. A.; Rabbinowitsch, E.; Rajandream, M. A.; Reitter, C.; Salzberg, S. L.; Sanders, M.; Schobel, S.; Sharp, S.; Simmonds, M.; Simpson, A. J.; Tallon, L.; Turner, C. M.; Tait, A.; Tivey, A. R.; Van Aken, S.; Walker, D.; Wanless, D.; Wang, S.; White, B.; Whitehead, S.; Woodward, J.; Wortman, J.; Adams, M. D.; Embley, T. M.; Gull, K.; Ullu, E.; Barry, J. D.; Fairlamb, A. H.; Opperdoes, F.; Barrell, B. G.; Donelson, J. E.; Hall, N.; Fraser, C. M.; Melville, S. E.; El-Sayed, N. M. The genome of the African trypanosome *Trypanosoma brucei*. *Science* **2005**, *309*, 416−422.

[163] Gilbert, I. H. Target-based drug discovery for human African trypanosomiasis: selection of molecular target and chemical matter. *Parasitology* **2014**, *141*, 28–36.

[164] Hannaert, V. Sleeping Sickness Pathogen (Trypanosoma brucei) and Natural Products: Therapeutic Targets and Screening Systems. *Planta Med.* **2011**, *77*, 586–597.

[165] Jones, A. J.; Grkovic, T.; Sykes, M. L.; Avery, V. M. Trypanocidal Activity of Marine Natural Products. *Mar. Drugs* **2013**, *11*, 4058–4082.

[166] Croft, S. L.; Barrett, M. P.; Urbina, J. A. Chemotherapy of trypanosomiases and leishmaniasis. *Trends Parasitol.* **2005**, *21,* 508–512.

[167] Steverding, D.; Tyler, K. M. Novel antitrypanosomal agents. *Expert Opin. Investig. Drugs* **2005**, *14*, 939–955.

[168] Barrett, M. P.; Croft, S. L. Management of trypanosomiasis and leishmaniasis. *Br. Med. Bull.* **2012**, *104*, 175–196.

[169] Tang, S. C.; Shapiro, T. A. Newly Identified Antibacterial Compounds Are Topoisomerase Poisons in African Trypanosomes. *Antimicrob. Agents Chemother.* **2010**, *54*, 620–62629.

[170] Patel, G.; Karver, C. E.; Behera, R.; Guyett, P. J.; Sullenberger, C.; Edwards, P.; Roncal, N. E.; Mensa-Wilmot, K.; Pollastri, M. P. Kinase Scaffold Repurposing for Neglected Disease Drug Discovery: Discovery of an Efficacious, Lapatanib-Derived Lead Compound for Trypanosomiasis. *J. Med. Chem.* **2013**, *56*, 3820−3832.

[171] Munos, B. Lessons from 60 years of pharmaceutical innovation. *Nat. Rev. Drug Discov.* **2009**, *8*, 959−968.

[172] Paul, S. M.; Mytelka, D. S.; Dunwiddie, C. T.; Persinger, C. C.; Munos, B. H.; Lindborg, S. R.; Schacht, A. L. How to improve R&D productivity: the pharmaceutical industry's grand challenge. *Nat. Rev. Drug Discov*. **2010**, *9*, 203−214.

[173] Bleicher, K. H.; Böhm, H. J.; Müller, K.; Alanine, A. I. Hit and lead generation: beyond high-throughput screening. *Nat. Rev. Drug Discov.* **2003**, *2*, 369−378.

[174] Fattori, D. Molecular recognition: the fragment approach in lead generation. *Drug Discov. Today* **2004**, *9*, 229−238.

[175] De Simone, R. W.; Currie, K. S.; Mitchell, S. A.; Darrow, J. W.; Pippin, D. A. Privileged structures: applications in drug discovery. *Comb. Chem. High Throughput Screen*. **2004**, *7*, 473−494.

[176] Bongarzone, S.; Bolognesi, M. L. The concept of privileged structures in rational drug design: focus on acridine and quinoline scaffolds in neurodegenerative and protozoan diseases. *Expert Opin. Drug Discov.* **2011**, *6*, 251−268.

[177] Welsch, M. E.; Snyder, S. A.; Stockwell, B. R. Privileged scaffolds for library design and drug discovery. *Curr. Opin. Chem. Biol.* **2010**, *14*, 347−361.

[178] O'Neil, P. M.; Ward, S. A.; Berry, N. G.; Jeyadevan, J. P.; Biagini, G. A.; Asadollaly, E.; Park, B. K.; Bray, P. G. A medicinal chemistry perspective on 4-aminoquinoline antimalarial drugs. *Curr. Top. Med. Chem*. **2006**, *6*, 479−507.

[179] Kaur, K.; Jain, M.; Reddy, R. P.; Jain, R. Quinolines and structurally related heterocycles as antimalarials. *Eur. J. Med. Chem.* **2010**, *45*, 3245–3264.

[180] Musiol, R.; Serda, M.; Hensel-Bielowka, S.; Polanski, J. Quinoline-based antifungals. *Curr. Med. Chem*. **2010**, *17*, 1960−1973.

[181] López, A. E. Privileged scaffolds in medicinal chemistry: Design, synthesis, evaluation. Chapter 6 − Quinolines: Privileged scaffolds in medicinal chemistry. Bräse, S. (Ed.) Royal Society of Chemistry Publishing, **2015**, 132−146.

[182] Högberg, T.; Frimurer, T. M.; Sasmai, P. K. Melanin concentrating hormone receptor (MCHR1) antagonists − still a viable approach for obesity treatment? *Bioorg. Med. Chem. Lett*. **2012**, *22*, 6039−6047.

[183] Afzal, O.; Kumar, S.; Haider, M. R.; Ai, M. R.; Kumar, R.; Jaggi, M.; Bawa, S. A review on anticancer potential of bioactive heterocycle quinoline. *Eur. J. Med. Chem*. **2015**, *97*, 871−910.

[184] Becherer, J. D.; Boros, E. E.; Carpenter, T. Y.; Cowan, D. J.; Deaton, D. N.; Haffner, C. D.; Jeune, M. R.; Kaldor, I. W.; Poole, J. C.; Preugschat, F.; Rheault, T. R.; Schulte, C. A.; Shearer, B. G.; Shearer, T. W.; Shewchuk, L. M.; Smalley Jr., T. L.; Stewart, E. L.; Stuart, D.; Ulrich, J. C. Discovery of 4-Amino-8-quinoline carboxamides as novel, submicromolar inhibitors of NAD-hydrolyzing enzyme CD38. *J. Med. Chem*. **2015**, *58*, 7021−7056.

[185] Okamura, N.; Suemoto, T.; Furumoto, S.; Suzuki, M.; Shimadzu, H.; Akatsu, H.; Yamamoto, T.; Fujiwara, H; Nemoto, M.; Maruyama, M.; Arai, H.; Yanai, K.; Sawada, T.; Kudo, Y. Quinoline and

benzimidazole derivatives: candidate probes for in vivo imaging of tau pathology in Alzheimer's disease. *J. Neurosci.* **2005**, *25*, 10857−10862.

[186] Adlard, P. A.; Cherny, R. A.; Finkelstein, D. I.; Gautier, E.; Robb, E.; Cortes, M.; Volitakis, I.; Liu, X.; Smith, J. P.; Perez, K.; Laughton, K.; Li, Q. X.; Charman, S. A.; Nicolazzo, J. A.; Wilkins, S.; Deleva, K.; Lynch, T.; Kok, G.; Ritchie, C. W.; Tanzi, R. E.; Cappai, R.; Masters, C. L.; Barnham, K. J.; Bush, A. I. Rapid restoration of cognition in Alzheimer's transgenic mice with 8-hydroxy quinoline analogs is associated with decreased interstitial Abeta. *Neuron.* **2008**, *59*, 43−55.

[187] Navarrete, L. P.; Guzmán, L.; San Martín, A.; Astudillo-Saavedra, L.; Maccioni, R. B. Molecules of the quinoline family block tau self-aggregation: implications toward a therapeutic approach for Alzheimer's disease. *J. Alzheimers Dis.* **2012**, *29*, 79−88.

[188] Alzforum: Clioquinol. http://www.alzforum.org/therapeutics/clioquinol (Accessed 14 February **2016**).

[189] Musonda, C. C.; Gut, J.; Rosenthal, P. J.; Yardley, V.; Carvalho de Souza, R. C.; Chibale, K. Application of multicomponent reactions to antimalarial drug discovery. Part 2: New antiplasmodial and antitrypanosomal 4-aminoquinoline gamma- and delta-lactams via a 'catch and release' protocol. *Bioorg. Med. Chem.* **2006**, *14*, 5605–5615.

[190] Musonda, C. C.; Yardley, V.; de Souza, R. C. C.; Ncokazi, K.; Egan, T. J.; Chibale, K. Antiplasmodial, β-hematin inhibition, antitrypanosomal and cytotoxic activity in vitro of novel 4-aminoquinoline 2-imidazolines. *Org. Biomol. Chem.* **2008**, *6*, 4446–4451.

[191] Glans, L.; Hu, W.; Jöst, C.; de Kock, C.; Smith, P. J.; Haukka, M.; Bruhn, H.; Schatzschneider, U.; Nordlander, E. Synthesis and biological activity of cymantrene and cyrhetrene 4-aminoquinoline conjugates against malaria, leishmaniasis, and trypanosomiasis. *Dalton Trans.* **2012**, *41*, 6443–6450.

[192] Gehrke, S. S.; Pinto, E. G; Steverding, D.; Pleban, K.; Temponed, A. G.; Hider, R. C.; Wagner, G. K. Conjugation to 4-aminoquinoline improves the anti-trypanosomal activity of Deferiprone-type iron chelators. *Bioorg. Med. Chem.* **2013**, *21*, 805–813.

[193] Leverrier, A.; Bero, J.; Frédérich, M.; Quetin-Leclercq, J.; Palermo, J. Antiparasitic hybrids of *Cinchona* alkaloids and bile acids. *Eur. J. Med. Chem*. **2013**, *66*, 355−363.

[194] Coa, J. C.; Castrillón, W.; Cardona, W.; Carda, M.; Ospina, V.; Muñoz, J. A.; Vélez, I. D.; Robledo, S.M. Synthesis, leishmanicidal, trypanocidal and cytotoxic activity of quinoline-hydrazone hybrids. *Eur. J. Med. Chem.* **2015**, *101*, 746–753.

[195] Kouznetsov, V. V.; Gomez-Barrio, A. Recent developments in the design and synthesis of hybrid molecules based on aminoquinoline ring and their antiplasmodial evaluation. *Eur. J. Med. Chem.* **2009**, *44*, 3091−3113.

[196] Muregi, F. W.; Ishih, A. Next-generation antimalarial drugs: hybrid molecules as a new strategy in drug design. *Drug Dev. Res.* **2010**, 71, 20−32.

[197] Gemma, S.; Camodeca, C.; Sanna Coccone, S.; Joshi, B. P.; Bernetti, M.; Moretti, V.; Brogi, S.; Bonache de Marcos, M. C.; Savini, L.; Taramelli, D.; Basilico, N.; Parapini, S.; Rottman, M.; Brun, R.; Lamponi, S.; Caccia, S.; Guiso, G.; Summers, R. L.; Martin, R. E.; Saponara, S., Gorelli, B.; Novellino, E.; Campiani, G.; Butini, S. Optimization of 4-aminoquinoline/clotrimazole-based hybrid antimalarials: further structure–activity relationships, in vivo studies, and preliminary toxicity profiling. *J. Med. Chem.* **2012**, *55*, 6948−6967.

[198] Fisher, G. M.; Tanpure, R. P.; Douchez, A.; Andrews, K. T.; Poulsen, S. A. Synthesis and evaluation of antimalarial properties of novel 4-aminoquinoline hybrid compounds. *Chem. Biol. Drug Des.* **2014**, *84*, 462−472.

[199] Kannan, M.; Raichurkar, A. V.; Khan, F. R.; Iyer, P. S. Synthesis and *in vitro* evaluation of novel 8-aminoquinoline-pyrazolopyrimidine hybrids as potent antimalarial agents. *Bioorg. Med. Chem. Lett.* **2015**, *25*, 1100−1103.

[200] Davis, T. M.; Hung, T. Y.; Sim, I. K.; Karunajeewa, H. A.; Ilett, K. F. Piperaquine: a resurgent antimalarial drug. *Drugs* **2005**, *65*, 75−87.

[201] Camps, P.; El Achab, R.; Morral, J.; Muñoz-Torrero, D.; Badia, A.; Banos, J. E.; Vivas, N. M.; Barril, X.; Orozco, M.; Luque, F. J. New tacrine-huperzine A hybrids (huprines): highly potent tight-binding acetylcholinesterase inhibitors of interest for the treatment of Alzheimer's disease. *J. Med. Chem.* **2000**, *43*, 4657–4666.

[202] Oluwafemi, A. J.; Okanla, E. O.; Camps, P.; Muñoz-Torrero, D.; Mackey, Z. B.; Chiang, P. K.; Seville, S.; Wright, C. W. Evaluation of cryptolepine and huperzine derivatives as lead compounds towards new agents for the treatment of human african trypanosomiasis. *Nat. Prod. Commun.* **2009**, *4*, 193–198.

[203] Upadhayaya, R. S.; Dixit, S. S.; Földesi, A.; Chattopadhyaya, J. New antiprotozoal agents: their synthesis and biological evaluation. *Bioorg. Med. Chem. Lett*. **2013**, *23*, 2750.

[204] Rashad, A. A.; Jones, A. J.; Avery, V. M.; Baell, J.; Keller, P. A. Facile synthesis and preliminary structure-activity analysis of new sulfonamides against *Trypanosoma brucei. ACS Med. Chem. Lett*. **2014**, *5*, 496−500.

[205] Mushtaque, S. Reemergence of chloroquine (CQ) analogs as multi-targeting antimalarials agents: A review. *Eur. J. Med. Chem*. **2015**, *90*, 280−295.

[206] Defaux, J.; Sala, M.; Formosa, X.; Galdeano, C.; Taylor, M. C.; Alobaid, W. A. A.; Kelly, J. M.; Wright, C. W.; Camps, P.; Muñoz-Torrero, D. Huprines as a new family of dual acting trypanocidal–antiplasmodial agents. *Bioorg. Med. Chem.* **2011**, *19*, 1702–1707.

[207] Di Pietro, O.; Viayna, E.; Vicente-García, E.; Bartolini, M.; Ramón, R.; Juárez-Jiménez, J.; Clos, M. V.; Pérez, B.; Andrisano, V.; Luque, F.J.; Lavilla, R.; Muñoz-Torrero, D. 1,2,3,4-Tetrahydrobenzo[*h*][1,6]naphthyridines as a new family of potent peripheral-to-midgorge-site inhibitors of acetylcholinesterase: synthesis, pharmacological evaluation and mechanistic studies. *Eur. J. Med. Chem.* **2014**, *73*, 141−152.

[208] Di Pietro, O.; Vicente-García, E.; Taylor, M. C.; Berenguer, D.; Viayna, E.; Lanzoni, A.; Sola, I.; Sayago, H.; Riera, C.; Fisa, R.; Clos, M. V.; Pérez, B.; Kelly, J. M.; Lavilla, R.; Muñoz-Torrero, D. Multicomponent reaction-based synthesis and biological evaluation of tricyclic heterofused quinolines with multi-trypanosomatid activity. *Eur. J. Med. Chem.* **2015**, *105*, 120–137.

[209] World Malaria Report 2015, World Health Organization Home Page. (http://apps.who.int/iris/bitstream/10665/200018/1/9789241565158_eng.pdf, accessed February 2016)

[210] Murray, C. J.; Rosenfeld, L. C.; Lim, S. S; Andrews, K. G.; Foreman, K. J.; Haring, D.; Fullman, N.; Lozano, R.; Lopez, A. D. Global malaria mortality between 1980 and 2010: a systematic analysis. *Lancet* **2012**, *379*, 413−431.

[211] Fernando, S. D.; Rodrigo, C.; Rajapakse, S. The 'hidden' burden of malaria: cognitive impairment following infection. *Malar. J*. **2010**, *9*, 366.

[212] Marsh, K.; Forster, D.; Waruiru, C.; Mwangi, I.; Winstanley, M.; Marsh, V.; Newton, C.; Winstanley, P.; Warn, P.; Peshu, N.; Pasvol, G.; Snow, R. Indicators of life-threatening malaria in African children. *N. Engl. J. Med*. **1995**, *332*, 1399–1404.

[213] Boivin, M. J.; Bangirana, P.; Byarugaba, J.; Opoka, R. O.; Idro, R.; Jurek, A. M.; John, C. C. Cognitive impairment after cerebral malaria in children: a prospective study. *Pediatrics* **2007**, *119*, e360–e366.

[214] Sacks, J.; Malaney, P. The economic and social burden of malaria. *Nature* **2002**, *415*, 680–685.

[215] Overview of malaria elimination. World Health Organization Home Page. (http://www.who.int/malaria/areas/elimination/overview/en/, accessed February 2016).

[216] Snow, R. W.; Guerra, C. A.; Noor, A. M.; Myint, H. Y.; Hay, S. I. The global distribution of clinical episodes of *Plasmodium falciparum* malaria. *Nature* **2005**, *434*, 214–217.

[217] Flannery, E. L.; Chatterjee, A. K.; Winzeler, E. A. Antimalarial drug discovery – approaches and progress towards new medicines. *Nat. Rev. Microbiol.* **2013**, *11*, 849−862.

[218] Kumar, S.; Kumari, R.; Pandey, R. *Protoplasma* **2015**, *252*, 717−753.

[219] Hay, S. I; Guerra, C. A.; Tatem, A. J.; Noor, A. M.; Snow, R. W. The global distribution and population at risk of malaria: past, present, and future. *Lancet Infect. Dis*. **2004**, *4*, 327–336.

[220] WHO releases new guidance on insecticide-treated mosquito nets: Recent data from Kenya "ends the debate" about how to deliver the nets. WHO Home Page: http://www.who.int/mediacentre/news/releases/2007/pr43/en/index.html, accessed February 2016.

[221] Zucker, J. R. Changing patterns of autochthonous malaria transmission in the United States: a review of recent outbreaks. *Emerg. Infect. Dis*. **1996**, *2*, 37–43

[222] Gething, P. W.; Patil, A. P.; Smith, D. L.; Guerra, C. A.; Elyazar, I. R.; Johnston, G. L.; Tatem, A. J.; Hay, S. I. A new world malaria map: *Plasmodium falciparum* endemicity in 2010. *Malar. J.* **2011**, *10*, 378.

[223] Zimmerman, P. A.; Ferreira, M. U.; Howes, R. E.; Mercereau-Puijalon, O. Red Blood Cell Polymorphism and Susceptibility to Plasmodium vivax. *Adv. Parasitol*. **2013**, *81*, 27−76.

[224] Baird, J. K. Neglect of Plasmodium vivax malaria. *Trends Parasitol.* **2007**, *23*, 533–539.

[225] Guerra, C. A.; Howes, R. E.; Patil, A. P.; Gething, P. W.; van Boeckel, T. P.; Temperley, W. H.; Kabaria, C. W.; Tatem, A. J.; Manh, B. H.; Elyazar, I. R.; Baird, J. K.; Snow, R. W.; Hay, S. I. The international limits and population at risk of Plasmodium vivax transmission in 2009. *PLoS Negl. Trop. Dis.* **2010**, *4*, e774.

[226] Rahimi, B. A.; Thakkinstian, A.; White, N. J.; Sirivichayakul, C.; Dondorp, A. M.; Chokejindachai, W. Severe vivax malaria: a systematic review and meta-analysis of clinical studies since 1900. *Malar. J.* **2014**, *13*, 481.

[227] Battle, K. E.; Gething, P. W.; Elyazar, I. R.; Moyes, C. L.; Sinka, M. E.; Howes, R. E.; Guerra, C. A.; Price, R. N.; Baird, K. J.; Hay, S. I. The global public health significance of *Plasmodium vivax*. *Adv. Parasitol.* **2012**, 80, 1−111.

[228] Singh, B.; Sung, K. L.; Matusop, A.; Radhakrishnan, A.; Shamsul, S. S.; Cox-Singh, J.; Thomas, A.; Conway, D. J. A large focus of naturally acquired *Plasmodium knowlesi* infections in human beings. *Lancet* **2004**, *363*, 1017–1024.

[229] Singh, B.; Daneshvar, C. Human infections and detection of *Plasmodium knowlesi*. *Clin. Microbiol*. *Rev*. **2013**, *26*, 165–184.

[230] Stresman, G. H. Beyond temperature and precipitation: Ecological risk factors that modify malaria transmission. *Acta Trop.* **2010**, *116*, 167–172.

[231] Sturm, A.; Amino, R.; Van de Sand, C.; Regen, T.; Retzlaff, S.; Rennenberg, A.; Krueger, A.; Pollok, J. M.; Menard, R.; Heussler, V. T. Manipulation of host hepatocytes by the malaria parasite for delivery into liver sinusoids. *Science* **2006**, *313*, 1287–1290.

[232] Biamonte, M. A.; Wanner, J.; Le Roch, K. G. Recent advances in malaria drug discovery. *Bioorg. Med. Chem. Lett.* **2013**, *23*, 2829−2843.

[233] Gardner, M. J.; Hall, N.; Fung, E.; White, O.; Berriman, M.; Hyman, R. W.; Carlton, J. M.; Pain, A.; Nelson, K. E.; Bowman, S.; Paulsen, I. T.; James, K.; Eisen, J. A.; Rutherford, K.; Salzberg, S. L.; Craig, A.; Kyes, S.; Chan, M. S.; Nene, V.; Shallom, S. J.; Suh, B.; Peterson, J.; Angiuoli, S.; Pertea, M.; Allen, J.; Selengut, J.; Haft, D.; Mather, M. W.; Vaidya, A. B.; Martin, D. M. A.; Fairlamb, A. H.; Fraunholz, M. J.; Roos, D. S.; Ralph, S. A.; McFadden, G. I.; Cummings, L. M.; Subramanian, G. M.; Mungall, C.; Venter, C. J.; Carucci, D. J.; Hoffman, S. L.; Newbold, C.; Davis, R. W.; Fraser, C. M.; Barrell, B. Genome sequence of the human malaria parasite Plasmodium falciparum. *Nature* **2002**, *419*, 498–511.

[234] Greenwood, B. M.; Fidock, D. A.; Kyle, D. E.; Kappe, S. H. I.; Alonso, P. L.; Collins, H. F.; Duffy, P. E. Malaria: progress, perils, and prospects for eradication. *J. Clin. Invest.* **2008**, *118*, 1266−1276.

[235] Faurant, C. From bark to weed: The history of artemisinin. *Parasite* **2011**, *18*, 215−218.

[236] Achan, J.; Talisuna, A. O.; Erhart, A.; Yeka, A.; Tibenderana, J. K.; Baliraine, F. N.; Rosenthal, P. J.; d'Alessandro, U. Quinine, an old-antimalarial drug in modern world: role in the treatment of malaria. *Malar. J.* **2011**, *10*, 144.

[237] White, N. J. Quinghaosu (Artemisinin): The Price of Success. *Science* **2008**, *230*, 330−334.

[238] Morris, C. A.; Duparc, S.; Borghini-Fuhrer, I.; Jung, D.; Shin, C. S.; Fleckenstein, L. Review of the clinical pharmacokinetics of artesunate and its active metabolite dihydroartemisinin following intravenous, intramuscular, oral or rectal administration. *Malar. J.* **2011**, *10*, 263.

[239] Ro, D. K.; Paradise, E. M.; Ouellet, M.; Fisher, K. J.; Newman, K. L.; Ndungu, J. M.; Ho, K. A.; Eachus, R. A.; Ham, T. S.; Kirby, J.; Chang, M. C.; Withers, S. T.; Shiba, Y.; Sarpong, R.; Keasling, J. D. Production of the antimalarial drug precursor artemisinic acid in engineered yeast. *Nature* **2006**, *440*, 940−943.

[240] Djimdé, A.; Lefèvre, G. Understanding the pharmacokinetics of Coartem. *Malar. J.* **2009**, *8* (Suppl. 1), S4.

[241] Beutler, E. The hemolytic effect of primaquine and related compounds: a review. *Blood* **1959**, *14*, 103–139.

[242] Verma, R.; Khanna, P.; Chawla, S. Malaria vaccine can prevent millions of deaths in the world. *Hum. Vaccin. Immunother*. **2013**, *9*, 1268−1271.

[243] WHO Home Page. Tables of malaria vaccine projects globally «The Rain- bow Tables» 2015. (http://www.who.int/immunization/research/development/Rainbow_tables/en/, accessed February 2016)

[244] Aponte, J. J.; Aide, P.; Renom, M.; Mandomando, I.; Bassat, Q.; Sacarlal, J.; Manaca, M. N.; Lafuente, S.; Barbosa, A.; Leach, A.; Lievens, M.; Vekemans, J.; Sigauque, B.; Dubois, M. C.; Demolitié, M. A.; Sillman, M.; Savarese, B.; McNeil, J. G.; Macete, E.; Ballou, W. R.; Cohen, J.; Alonso, P. L. Safety of the RTS,S/AS02D candidate malaria vaccine in infants living in a highly endemic area of Mozambique: a double blind randomised controlled phase I/IIb trial. *Lancet* **2007**, *370*, 1543–1551.

[245] WHO Home Page. Weekly epidemiological record, 29th January 2016, 91, 33–52 (http://www.who.int/wer/2016/wer9104.pdf?ua=1, accessed February 2016)

[246] Todryk, S. M.; Hill, A. V. S. Malaria vaccines: the stage we are at. *Nat. Rev. Microbiol*. **2007**, *5*, 487–489.

[247] Baird, J. K. Effectiveness of antimalarial drugs. *N. Engl. J. Med.* **2005**, *352*, 1565–1577.

[248] Alam, A.; Goyal, M.; Igbal, M. S.; Pal, C.; Dey, S.; Bindu, S.; Maity, P.; Bandyopadhay, U. Novel antimalarial drug targets: hope for new antimalarial drugs. *Expert Rev. Clin. Pharmacol*. **2009**, *2*, 469–489.

[249] Price, R. N.; Cassar, C.; Brockman, A.; Duraisingh, M.; van Vugt, M.; White, N. J.; Nosten, F.; Krishna, S. The pfmdr1 gene is associated with a multidrug-resistant phenotype in *Plasmodium falciparum* from the western border of Thailand. *Antimicrob. Agents Chemother*. **1999**, *43*, 2943–2949.

[250] Olliaro, P. Mode of action and mechanisms of resistance for antimalarial drugs. *Pharmacol. Ther*. **2001**, *89*, 207–219.

[251] Fidock, D. A.; Nomura, T.; Talley, A. K.; Cooper, R. A.; Dzekunov, S. M.; Ferdig, M. T.; Ursos, L. M.; Sidhu, A. B.; Naudé, B.; Deitsch, K. W.; Su, X. Z.; Wootton, J. C.; Roepe, P. D.; Wellems, T. E. Mutations in the *P. falciparum* digestive vacuole transmembrane protein *Pf*CRT and evidence for their role in chloroquine resistance. *Mol. Cell.* **2000**, *6*, 861–871.

[252] Syafruddin, D.; Siregar, J. E.; Marzuki, S. Mutations in the cytochrome b gene of *Plasmodium berghei* conferring resistance to atovaquone. *Mol. Biochem. Parasitol.* **1999**, *104*, 185–194.

[253] Plowe, C. V.; Kublin, J. G.; Doumbo, O. K. *P. falciparum* dihydrofolate reductase and dihydropteroate synthase mutations: epidemiology and role in clinical resistance to antifolates. *Drug Resist. Updat*. **1998**, *1*, 389–396.

[254] Daily, J. P. Antimalarial drug therapy: the role of parasite biology and drug resistance. *J. Clinical Pharmacol.* **2006**, *46*, 1487−1497.

[255] Mugittu, K.; Genton, B.; Mshinda, H.; Beck, H. P. Molecular monitoring of Plasmodium falciparum resistance to artemisinin in Tanzania. *Malar. J.* **2006**, *5*, 126.

[256] Birkholtz, L.; van Brummelen, A. C.; Clark, K.; Niemand, J.; Maréchal, E.; Llinás, M.; Louw, A. I. Exploring functional genomics for drug target and therapeutics discovery in *Plasmodia*. *Acta Trop.* **2008**, *105*, 113–123.

[257] Durand, P. M.; Naidoo, K.; Coetzer, T. L. Evolutionary patterning: a novel approach to the identification of potential drug target sites in *Plasmodium falciparum*. *PLoS ONE* **2008**, *3*, e3685.

[258] Johnson, P. C.; Higgins, A. J. Precise phenotypic anchoring for drug target identification, validation and biomarker discovery using an advanced system biology approach. *Drug Discovery World Summer* **2004**, 55–62.

[259] Wuchty, S. Rich-club phenomenon in the interactome of *P. falciparum* – artifact or signature of a parasitic life style? *PLoS ONE* **2007**, *2*, e335.

[260] Jiang, Z.; Zhou, Y. Using Gene networks to drug target identification. *J. Integr. Bioinform.* **2005**, *2*, 14.

[261] Jana, S.; Paliwal, J. Novel molecular targets for antimalarial chemotherapy. *Int. J. Antimicrob. Agents* **2007**, *30*, 4–10.

[262] Allen, R. J.; Kirk, K. Cell volume control in the *Plasmodium*-infected erythrocyte. *Trends Parasitol.* **2004**, *20*, 7–10.

[263] Becker, K.; Tilley, L.; Vennerstrom, J. L.; Roberts, D.; Rogerson, S.; Ginsburg, H. Oxidative stress in malaria parasite-infected erythrocytes: host–parasite interactions. *Int. J. Parasitol.* **2004**, *34*, 163–189.

[264] Cowman, A. F.; Crabb, B. S. Invasion of red blood cells by malaria parasites. *Cell* **2006**, *124*, 755–766.

[265] Choi, S R.; Mukherjee, P.; Avery, M. A. The fight against drug-resistant malaria: novel plasmodial targets and antimalarial drugs. *Curr. Med. Chem.* **2008**, *15*, 161–171.

[266] Biagini, G. A.; O'Neill, P. M.; Nzila, A.; Ward, S. A.; Bray, P. G. Antimalarial chemotherapy: young guns or back to the future? *Trends Parasitol.* **2003**, *19*, 479−487.

[267] Becker, K.; Koncarevic, S.; Hunt, N. H. Oxidative stress and antioxidant defence in malaria parasites. Ed. Sherman, I. W. Molecular Approaches to Malaria. ASM Press, Washington, D.C, **2005**, 365−383.

[268] Egan, T. J.; Combrinck, J. M.; Egan, J.; Hearne, G. R.; Marques, H. M.; Ntenteni, S.; Sewell, B. T.; Smith, P. J.; Taylor, D.; van Schalkwyk, D. A.; Walden, J. C. Fate of haem iron in the malaria parasite *Plasmodium falciparum*. *Biochem J*. **2002**, *365*, 343–347.

[269] Slater, A. F.; Cerami, A. Inhibition by chloroquine of a novel haem polymerase enzyme activity in malaria trophozoites. *Nature* **1992**, *355*, 167–169.

[270] Zhang, F.; Schmidt, W. G.; Hou, Y.; Williams, A. F.; Jacobson, K. Spontaneous incorporation of the glycosyl-phosphatidylinositol-linked protein Thy-1 into cell membranes. *Proc. Natl. Acad. Sci. USA* **1992**, *89*, 5231–5235.

[271] Loria, P.; Miller, S.; Foley, M.; Tilley, L. Inhibition of the peroxidative degradation of haem as the basis of action of chloroquine and other quinoline antimalarials. *Biochem J*. **1999**, *339*, 363–370.

[272] Ginsburg, H.; Famin, O.; Zhang, J.; Krugliak, M. Inhibition of glutathione dependent degradation of heme by chloroquine and amodiaquine as a possible basis for their antimalarial mode of action. *Biochem. Pharmacol.* **1998**, *56*, 1305–1313.

[273] Goldberg, D. E. Hemoglobin degradation. *Curr. Top. Microbiol. Immunol*. **2005**, *295*, 275–291.

[274] Ginsburg, H.; Ward, S. A.; Bray, P. G. An integrated model of chloroquine action. *Parasitol. Today* **1999**, *15*, 357–360.

[275] O'Neill, P. M.; Posner, G. H. A medicinal chemistry perspective on artemisinin and related endoperoxides. *J. Med. Chem*. **2004**, *47*, 2945–2964.

[276] Rahlfs, S.; Becker, K. Thioredoxin peroxidases of the malarial parasite *Plasmodium falciparum*. *Eur. J. Biochem*. **2001**, *268*, 1404–1409.

[277] Müller, S. Redox and antioxidant systems of the malaria parasite *Plasmodium falciparum*. *Mol. Microbiol.* **2004**, 53, 1291−1305.

[278] Kruger, N. J.; von Shaewen, A. The oxidative pentose phosphate pathway: structure and organization. *Curr. Opin. Plant. Biol.* **2003**, *6*, 236−246.

[279] Berg, J. M.; Tymoczko, J. L.; Stryer, L. The pentose phosphate pathway generates NADPH and synthesizes five-carbon sugars. Biochemistry, 5th edn. New York, Freeman, W. H., **2002**.

[280] Cappellini, M. D.; Fiorelli, G. Glucose-6-phosphate dehydrogenase deficiency. *Lancet* **2008**, *371*, 64–74.

[281] Luzzatto, L.; Metha, A.; Vulliamy, T. Glucose 6-phosphate dehydrogenase deficiency. Eds. Scriver, C. R., Beaudet, A. L., Sly, W. S., et al, The metabolic and molecular bases of inherited disease, 8th ed. Columbus: McGraw-Hill, **2001**: 4517–4553.

[282] Naylor, C. E.; Rowland, P.; Basak, K.; Gover, S.; Mason, P. J.; Bautista, J. M.; Vulliamy, T. J.; Luzzatto, L.; Adams, M. J. Glucose 6-phosphate dehydrogenase mutations causing enzyme deficiency in a model of the tertiary structure of the human enzyme. *Blood* **1996**, 87, 2974–2982.

[283] Au, S. W. N.; Gover, S.; Lam, V. M. S.; Adams, M. J. Human glucose-6-phosphate dehydrogenase: the crystal structure reveals a structural NADP+ molecule and provides insights into enzyme deficiency. *Structure* **2000**, *8*, 293–303.

[284] Battistuzzi, G.; d'Urso, M.; Toniolo, D.; Persico, G. M.; Luzzatto, L. Tissue-specific levels of G6PD correlate with methylation of specific sites at the 3´ end of the gene. *Proc. Natl. Acad. Sci. USA* **1985**, *82*, 1465–1469.

[285] Gaetani, G. D.; Parker, G. C.; Kirkman, H. N. Intracellular restraint: a new basis for the limitation in response to oxidative stress in human erythrocytes containing low-activity variants of glucose-6-phosphate dehydrogenase. *Proc. Natl. Acad. Sci. USA* **1974**, *71*, 3584–3587.

[286] Beutler, E.; Yeh, M.; Fairbanks, V. F. The normal human female as a mosaic of X chromosome activity: studies using the genes of G6PD deficiency as a marker. *Proc. Natl. Acad. Sci. USA* **1962**, *48*, 9–16.

[287] Luzzatto, L. Glucose 6-phosphate dehydrogenase deficiency: from genotype to phenotype. *Haematologica* **2006**, *91*, 1303−1306

[288] Mason, P. J.; Bautista, J. M.; Gilsanz, F. G6PD deficiency: the genotype-phenotype association. *Blood Rev.* **2007**, *21*, 267–283.

[289] Beutler, E. The red cell: A tiny dynamo, in Wintrobe, M. M., ed. *Blood Pure and Eloquent*, McGraw-Hill, New York, **1980**, 141−168.

[290] Dern, R. J.; Beutler, E.; Alving, A. S. The hemolytic effect of primaquine. V. Primaquine sensitivity as a manifestation of a multiple drug sensitivity. *J. Lab. Clin. Med.* **1955**, *45*, 30-39.

[291] Beutler, E. GGPD: Population genetics and clinical manifestations. *Blood Rev.* **1996**, *10*, 45−52.

[292] Beutler, E. The genetics of glucose-6-phosphate dehydrogenase deficiency. *Semin. Hematol*. **1990**, *27*, 137–164.

[293] Beutler, E. Red cell metabolism: A manual of biochemical methods, 3rd edn. Grune and Stratton New York, **1984**.

[294] Betke, K.; Brewer, G. J.; Kirkman, H. N.; Luzzatto, L.; Motulsky, A. G.; Ramot, B.; Siniscalco, M.; Beutler, E.; Standley, C. C. et al. Standardization of procedures for the study of glucose-6-phosphate

dehydrogenase: report of a WHO Scientific Group. *World Health Organ. Tech. Rep. Ser.* **1967**, *366*, 1–53.

[295] WHO working group. Glucose-6-phosphate dehydrogenase deficiency. *Bull. World Health Organ.* **1989**, *67*, 601–611.

[296] Zanella, A.; Colombo, M. B.; Rossi, F.; Merati, G.; Sirchia, G. Congenital non-spherocytic haemolytic anaemias. *Haematologica* **1989**, *74*, 387−396.

[297] Beutler, E. Glucose-6-phosphate dehydrogenase deficiency and other enzyme abnormalities, in Beutler, E., Lichtman, M. A., Coller, B. S., Kipps, T. J. (eds): Williams Hematology. New York, NY, McGraw- Hill. **1995**, 564.

[298] Valentine, W. N.; Paglia, D. E. Erythroenzymopathies and hemolytic anemia: The many faces of inherited variant enzymes. *J. Lab. Clin. Med*. **1990**, *115*, 12−20.

[299] Valentine, W. N.; Tanaka, K. R.; Paglia, D. E. Hemolytic anemias and erythrocyte enzymopathies. *Ann. Intern. Med.* **1985**, *103*, 245−257.

[300] Frank, J. E. Diagnosis and management of G6PD deficiency. *Am. Fam. Physician.* **2005**, *72*, 1277–1282.

[301] Greene, L. S. G6PD deficiency as protection against *falcipurum* malaria: An epidemiologic critique of population and experimental studies. *Yearbook Phys. Anthropol*. **1993**, 17 (suppl 3), 153−178.

[302] Motulsky, A. G. Glucose-6-phosphate dehydrogenase deficiency haemolytic disease of the newborn, and malaria. *Lancet* **1961**, *277*, 1168−1169.

[303] Allison, A. C. Glucose 6-phosphate dehydrogenase deficiency in red blood cells of East Africans. *Nature* **1960**, *186*, 531−532.

[304] Allison, A C.; Clyde, D. F. Malaria in African children with deficient erythrocyte glucose-6-phosphate dehydrogenase. *Br. Med. J.* **1961**, *1*, 1346−1349.

[305] Siniscalco, M.; Bemini, L.; Filippi, G.; Lane, B.; Meera-Khan, P.; Piomelli, S.; Rattazzi, M. Population genetics of haemoglobin variants, thalassaemia and glucose-6- phosphate dehydrogenase deficiency, with particular reference to the malaria hypothesis. *Bull World Health Organ*. **1966**, *34*, 379−393.

[306] Luzzatto, L.; Usanga, E. A.; Reddy, S. Glucose 6-phosphate dehydrogenase deficient red cells: Resistance to infection by malarial parasites. *Science* **1969**, *164*, 839−842.

[307] Luzzatto, L.; Bienzle, U. The malaria/G6PD hypothesis. *Lancet* **1979**, *1*, 1183–1184.

[308] Luzzatto, L.; O'Brien, S.; Usanga, E.; Wanachiwanawin, W. Origin of G6PD polymorphism: Malaria and G6PD deficiency, in Yoshida, A., Beutler, E. (eds): Glucose-6-Phosphate Dehydrogenase, Orlando, FL, Academic, **1986**, 181.

[309] Ruwende, C.; Khoo, S. C.; Snow, R. W.; Yates, S. N. R.; Kwiatkowski, D.; Gupta, S.; Warn, P.; Allsopp, C. E. M.; Gilbert, S. C.; Peschu, N.; Newbold, C. I.; Greenwood, B. M.; Marsh, K.; Hill, A. V. S. Natural selection of hemi and heterozygotes for G6PD deficiency in Africa by resistance to severe malaria. *Nature* **1995**, *376*, 246–249.

[310] Ruwende, C.; Hill, A. Glucose-6-phosphate dehydrogenase deficiency and malaria. *J. Mol. Med.* **1998**, *76*, 581–588.

[311] a) Kruatrachue, M.; Charoenlarp, P.; Chongsuphajaisiddhi, T.; Harina-suta, C. Erythrocyte glucose-6-phosphate dehydrogenase and malaria in Thailand. *Lancet* **1962**, *2*, 1183−1186. b) Bienzle, U.; Ayeni, O.; Lucas, A. O.; Luzzatto, L. Glucose-6-phosphate dehydrogenase and malaria. Greater resistance of females heterozygous for enzyme deficiency and of males with non-deficient variant. *Lancet* **1972**, *1*, 107−110. c) Kar, S.; Seth, S.; Seth, P. K. Prevalence of malaria in Ao Nagas and its association with G6PD and HbE. *Hum. Biol.* **1992**, *64*, 187−197. d) Mombo, L.; Ntoumi, F.; Bisseye, C.; Ossari, S.; Lu, C.; Nagel, R. L.; Krishnamoorthy, R. Human genetic polymorphisms and asymptomatic *Plasmodium falciparum* malaria in gabonese schoolchildren. *Am. J. Trop. Med. Hyg.* **2003**, *68*, 186−190. e) Guindo, A.; Fairhurst, R. M.; Doumbo, O. K.; Wellems, T. E.; Diallo, D. A. X-Linked G6PD Deficiency Protects Hemizygous Males but Not Heterozygous Females against Severe Malaria. *Plos Med.* **2007**, *4*, e66. f) Ouattara, A. K.; Bisseye, C.; Bazie, B. V.; Diarra, B.; Compaore, T. R.; Djigma, F.; Pietra, V.; Moret, R.; Simpore, J. Glucose-6-phosphate dehydrogenase (G6PD) deficiency is associated with asymptomatic malaria in a rural community in Burkina Faso. *Asian. Pac. J. Trop. Biomed.* **2014**, *4*, 655−658.

[312] a) Louicharoen, C.; Patin, E.; Paul, R.; Nuchprayoon, I.; Witoonpanich, B.; Peerapittayamongkol, C.; Casademont, I.; Sura, T.; Laird, N. M.; Singhasivanon, P.; Quintana-Murci, L.; Sakuntabhai, A. Positively Selected G6PD-Mahidol Mutation Reduces *Plasmodium vivax* Density in Southeast Asians. *Science* **2009**, *326*, 1546−1549. b) Khim, N.; Benedet, C.; Kim, S.; Kheng, S.; Siv, S.; Leang, R.; Lek, S.;

Muth, S.; Chea, N.; Chuor, C. M.; Duong, S.; Kerleguer, A.; Tor, P.; Chim, P.; Canier. L.; Witkowski, B.; Taylor, W. R. J.; Ménard, D. G6PD deficiency in *Plasmodium falciparum* and *Plasmodium vivax* malaria-infected Cambodian patients. *Malaria J.* **2013**, *12*, 171−180. c) Peixoto, H. M.; Brito, M. A. M.; Romero, G. A. S.; Monteiro, W. M.; de Lacerda, M. V. G.; de Oliveira, M. R. F. G6PD deficiency in male individuals infected by *Plasmodium vivax* malaria in the Brazilian Amazon: a cost study. *Malaria J.* **2015**, *14*, 126−134.

313 Turrini, F.; Schwarzer, E.; Arese, P. The involvement of hemozoin toxicity in depression of cellular immunity. *Parasitol. Today* **1993**, *9*, 297-300.

314 Miller, J.; Golenser, J.; Kullgren, B.; Spira, D. T. *Plasmodium falciparum*: thiol status and growth in normal and deficient human erythrocytes. *Exp. Parasitol.* **1984**, *57*, 239−247.

315 Golenser, J.; Miller, J.; Spira, D. T.; Kosower, N. S.; Vande Waa, J. A.; Jensen, J. B. Inhibition of intraerythrocytic development of *Plasmodium falciparum* in glucose-6-phosphate dehydrogenase deficient erythrocytes is enhanced by oxidants and crisis form factor. *Trop. Med. Parasitol.* **1988**, *39*, 273−276.

316 Janney, S. K.; Joist, J. H.; Fitch, C. D. Excess release of ferrriheme in G6PD-deficient erythrocytes: possible cause of hemolysis and resistance to malaria. *Blood* **1986**, *67*, 331−333.

317 a) Cappadoro, M.; Giribaldi, G.; O'Brien, E.; Turrini, F.; Mannu, F.; Ulliers, D.; Simula, G.; Luzzatto, L.; Arese, P. Early phagocytosis of glucose-6-phosphate dehydrogenase (G6PD)-deficient erythrocytes parasitized by *Plasmodium falciparum* may explain malaria protection in G6PD deficiency. *Blood* **1998**, *92*, 2527−2534. b) Arese, P.; Turrini, F.; Schwarzer, E. Band 3/Complement-mediated Recognition and Removal of Normally Senescent and Pathological Human Erythrocytes. *Cell. Physiol. Biochem*. **2005**, *16*, 133−146. c) López, C.; Saravia, C.; Gomez, A.; Hoebeke, J.; Patarroyo, M. A. Mechanisms of genetically-based resistance to malaria. *Gene* **2010**, *467*, 1–12. d) Méndez, D.; Linares, M.; Diez, A.; Puyet, A.; Bautista, J. M. Stress response and cytoskeletal proteins involved in erythrocyte membrane remodeling upon Plasmodium falciparum invasion are differentially carbonylated in G6PD A^{-} deficiency. *Free Radic. Biol. Med*. **2011**, *50*, 1305−1313.

318 Preuss, J.; Jortzik, E.; Becker, K. Glucose-6-phosphate metabolism in *Plasmodium falciparum. IUBMB Life* **2012**, *64*, 603**–**611.

319 Wrenger, C.; Müller, S. Isocitrate dehydrogenase of Plasmodium Falciparum: Energy metabolism or redox control? *Eur. J. Biochem.* **2003**, *270*, 1775**–**1783.

320 Storm, J.; Perner, J.; Aparicio, I.; Patzewitz, E. M.; Olszewski, K.; Llinas, M.; Engel, P. C.; Müller, S. *Plasmodium falciparum* glutamate dehydrogenase a is dispensable and not a drug target during erythrocytic development. *Malaria J.* **2011**, *10*, 193−204.

321 Langer, B. W.; Phisphumvidhi, P.; Friedlander, Y. Malaria parasite metabolism: the pentose cycle in *Plasmodium berghei*. *Exp. Parasitol.* **1967**, *20*, 68−76.

322 Sherman, I. W. Biochemistry of *Plasmodium* (malaria parasites). *Microbiol. Rev.* **1979**, *43*, 453−495.

323 Fletcher, K. A.; Canning, M. V.; Theakston, R. D. G. Electrophoresis of glucose-6-phosphate and 6-phosphogluconate dehydrogenase in erythrocytes from malaria infected animals. *Ann. Trop. Med. Parasitol.* **1977**, *71*, 125−130.

324 Eckman, J.; Eaton, J. W. Dependence of Plasmodium glutathione metabolism on the host cell. *Nature* **1979**, *278*, 754−756.

325 Hempelmann, E.; Wilson, R. J. M. Detection of glucose-6-phosphate dehydrogenase in malaria parasites. *Mol. Biochem. Parasitol*. **1981**, *2*, 197−204.

326 Ling, I. T., Wilson, R. J. M. Glucose 6-phosphate-dehydrogenase activity of the malaria parasite *Plasmodium falciparum. Mol. Biochem. Parasitol*. **1988**, *31*, 47−56.

327 Kurdi-Haidar, B.; Luzzatto, L. Expression and characterization of glucose-6-phosphate dehydrogenase of Plasmodium fulciparum. *Mol. Biochem. Parasitol*. **1990**, *41*, 83−91.

328 Shahabuddin, M.; Rawlings, D. J.; Kaslow, D. C. A novel glucose-6-phosphate dehydrogenase in *Plasmodium falciparum*: cDNA and primary protein structure. *Biochim. Biophys. Acta.* **1994**, *1219*, 191−194.

329 O'Brien, E.; Kurdihaidar, B.; Wanachiwanawin, W.; Carvajal, J. L.; Vulliamy, T. J.; Cappadoro, M.; Mason, P. J.; Luzzatto, L. Cloning of the glucose 6-phosphate dehydrogenase gene from *Plasmodium falciparum. Mol. Biochem. Parasitol.* **1994**, *64*, 313−326.

330 Jeffery, J.; Persson, B.; Wood, I.; Bergman, T.; Jeffery, R.; Jornvall, H. Glucose-6-phosphate dehydrogenase. Structure-function relationships and the *Pichia jadinii* enzyme structure. *Eur. J. Biochem*. **1993**, *212*, 41−49.

[331] Scopes, D. A.; Bautista, J. M.; Vulliamy, T. J.; Mason, P. J. *Plasmodium falciparum* Glucose-6-phosphate dehydrogenase (G6PD) − the N-terminal portion is homologous to a predicted protein encoded near to Glucose-6-Phosphate dehydrogenase in *Haemophilus Influenzae*. *Mol. Microbiol.* **1997**, *23*, 847−848.

[332] Clarke, J. L.; Sodeinde, O.; Mason, P. J. A unique insertion in *Plasmodium berghei* glucose-6-phosphate dehydrogenase-6-phosphogluconolactonase: evolutionary and functional studies. *Mol. Biochem. Parasitol.* **2003**, *127*, 1–8.

[333] Clarke, J. L.; Scopes, D. A.; Sodeinde, O.; Mason, P. J. Glucose-6-phosphate dehydrogenase-6-phosphogluconolactonase: A novel bifunctional enzyme in malaria parasites. *Eur. J. Biochem*. **2001**, *268*, 2013**–**2019.

[334] Jortzik, E.; Mailu, B. M., Preuss, J.; Fischer, M.; Bode, L.; Rahlfs, S.; Becker, K. Glucose-6-phosphate dehydrogenase-6-phosphogluconolactonase: a unique bifunctional enzyme from Plasmodium falciparum. *Biochem. J*. **2011**, *436*, 641**–**650.

[335] Stover, N. A.; Dixon, T. A.; Cavalcanti, A. R. Multiple independent fusions of glucose-6-phosphate dehydrogenase with enzymes in the pentose phosphate pathway. *PLoS ONE* **2011**, *6*, e22269.

[336] Bozdech, Z.; Ginsburg, H. Data mining of the transcriptome of *Plasmodium falciparum*: the pentose phosphate pathway and ancillary processes. *Malar. J*. **2005**, *4*, 17.

[337] Bajda, M.; Guzior, N.; Ignasik, M.; Malawska, B. Multi-target- directed ligands in Alzheimer's disease treatment. *Curr. Med. Chem*. **2011**, *18*, 4949−4975.

[338] Russo, P.; Frustaci, A.; Del Bufalo, A.; Fini, M.; Cesario, A. Multitarget drugs of plants origin acting on Alzheimer's disease. *Curr. Med. Chem.* **2013**, *20*, 1686−1693.

[339] Muñoz-Torrero, D. Complexity against complexity: Multitarget drugs. *Curr. Med. Chem*. **2013**, *20*, 1621−1622.

[340] Kung, H. F. The β-amyloid hypothesis in Alzheimer's disease: seeing is believing. *ACS Med. Chem*. *Lett*. **2012**, *3*, 265−267.

[341] Pimplikar, S. W. Reassessing the amyloid cascade hypothesis of Alzheimer's disease. *Int. J. Biochem. Cell Biol.* **2009**, *41*, 1261−1268.

[342] Citron, M. Alzheimer's disease: strategies for disease modification. *Nat. Rev. Drug Discov.* **2010**, *9*, 387−398.

[343] Du, D. M.; Carlier, P. R. Development of bivalent acetylcholinesterase inhibitors as potential therapeutic drugs for Alzheimer's disease. *Curr. Pharm. Des.* **2004**, *10*, 3141−3156.

[344] Recanatini, M.; Valenti, P. Acetylcholinesterase inhibitors as a starting point towards improved Alzheimer's disease therapeutics. *Curr. Pharm. Des.* **2004**, *10*, 3157−3166.

[345] Li, W. M.; Kan, K. K. W.; Carlier, P. R.; Pang, Y. P.; Han, Y. F. East meets West in the search for Alzheimer's therapeutics novel dimeric inhibitors from tacrine and huperzine A. *Curr. Alzheimer Res*. **2007**, *4*, 386−396.

[346] Holzgrabe, U.; Kapková, P.; Alptüzün, V.; Scheiber, J.; Kugelmann, E. Targeting acetylcholinesterase to treat neurodegenera- tion. *Expert Opin. Ther. Targets* **2007**, *11*, 161−179.

[347] Musial, A.; Bajda, M.; Malawska, B. Recent developments in cholinesterases inhibitors for Alzheimer's disease treatment. *Curr. Med. Chem.* **2007**, *14*, 2654−2679.

[348] Haviv, H.; Wong, D. M.; Silman, I.; Sussman, J. L. Bivalent ligands derived from huperzine A as acetylcholinesterase inhibitors. *Curr. Top. Med. Chem.* **2007**, *7*, 375−387.

[349] Rampa, A.; Belluti, F.; Gobbi, S.; Bisi, A. Hybrid-based multitarget ligands for the treatment of Alzheimer's disease. *Curr. Top. Med. Chem*. **2011**, *11*, 2716−2730.

[350] Bolognesi, M. L. Polypharmacology in a single drug: multitarget drugs. *Curr. Med. Chem*. **2013**, *20*, 1639−1645.

[351] Morphy, R.; Rankovic, Z. The physicochemical challenges of designing multiple ligands. *J. Med. Chem*. **2006**, *49*, 4961−4970.

[352] Weinreb, O.; Amit, T.; Bar-Am, O.; Youdim, M.B.H. Ladostigil: A novel multimodal neuroprotective drug with cholinesterase and brain-selective monoamine oxidase inhibitory activities for Alzheimer's disease treatment. *Curr. Drug Targets* **2012**, *13*, 483−494.

[353] Di Pietro, O.; Viayna, E.; Vicente-García, E.; Bartolini, M.; Ramón, R.; Juárez-Jiménez, J.; Clos, M. V.; Pérez, B.; Andrisano, V.; Luque, F. J.; Lavilla, R.; Muñoz-Torrero, D. 1,2,3,4-Tetrahydrobenzo[h][1,6]naphthyridines as a new family of potent peripheral-to-midgorge-site inhibitors of acetylcholinesterase: Synthesis, pharmacological evaluation and mechanistic studies. *Eur. J. Med. Chem.* **2014**, *73*, 141−152.

[354] Fu, H.; Li, W.; Luo, J.; Lee, N. T. K.; Li, M.; Tsim, K. W. K.; Pang, Y.; Youdim, M. B. H.; Han, Y. Promising anti-Alzheimer's dimer bis(7)-tacrine reduces β-amyloid generation by directly inhibiting BACE-1 activity. *Biochem. Biophys. Res. Commun.* **2008**, *366*, 631−636.

[355] Galdeano, C.; Viayna, E.; Arroyo, P.; Bidon-Chanal, A.; Blas, J. R.; Muñoz-Torrero, D.; Luque, F. J. Structural determinants of the multifunctional profile of dual binding site acetylcholinesterase inhibitors as anti-Alzheimer agents. *Curr. Pharm. Des*. **2010**, *16*, 2818−2836.

[356] Pickhardt, M.; Gazova, M.; von Bergen, M.; Khlistunova, I.; Wang, Y.; Hascher, A.; Mandelkow, E. M.; Biernat, J.; Mandelkow, E. J. Anthraquinones inhibit tau aggregation and dissolve Alzheimer's paired helical filaments in vitro and in cells. *Biol. Chem*. **2005**, *5*, 3628−3635.

[357] von Bergen, M.; Friedhoff, P.; Biernat, J.; Heberle, J.; Mandelkow, E. M.; Mandelkow, E. Assembly of tau protein into Alzheimer paired helical filaments depends on a local sequence motif ((306)VQIVYK(311))forming beta structure. *Proc. Natl. Acad. Sci. U. S. A.* **2000**, *97*, 5129−5134.

[358] von Bergen, M.; Barghorn, S.; Li, L.; Marx, A.; Biernat, J.; Mandelkow, E. M.; Mandelkow, E. Mutations of tau protein in frontotemporal dementia promote aggregation of paired helical filaments by enhancing local beta-structure. *J. Biol. Chem*. **2001**, *276*, 48165−48174.

[359] Friedhoff, P.; Schneider, A.; Mandelkow, E. M.; Mandelkow, E. Rapid assembly of Alzheimer-like paired helical filaments from microtubule-associated protein tau monitored by fluorescence in solution. *Biochemistry* **1998**, *37*, 10223−10230.

[360] Bulic, B.; Pickhardt, M.; Schmidt, B.; Mandelkow, E. M.; Waldmann, H.; Mandelkow, E. Development of tau aggregation inhibitors for Alzheimer's disease. *Angew. Chem. Int. Ed*. **2009**, *48*, 1740−1752.

[361] Freiedhoff, P.; von Bergen, M.; Mandelkow, E. M.; Davies, P.; Mandelkow, E. A nucleated assembly of Alzheimer paired helical filaments*.Proc. Natl. Acad. Sci. U. S. A*. **1998**, *95*, 15712−15717.

[362] National Institute on Aging (NIH) website. The hallmarks of AD. (https://www.nia.nih.gov/alzheimers/publication/part-2-what-happens-brain-ad/hallmarks-ad, accessed on March 2016)

[363] Yang, X.; Sun, G.; Yang, C.; Wang, B. Novel rhein analogues as potential anticancer agents. *ChemMedChem* **2011**, *6*, 2294−2301.

[364] Martson, F. A. The purification of eukaryotic polypeptides synthesized in *Escherihia coli*. *Biochem. J.* **1986**, *240*, 1−12.

[365] Waldo, G. S.; Standish, B. M.; Berendzen, J.; Terwilliger, T. C. Rapid protein-folding using green fluorescent protein. *Nat. Biotechnol*. **1999**, *17*, 691−695.

[366] Di, L.; Kerns, E. H.; Fan, K.; McConnell, O. J.; Carter, G. T. High throughput artificial membrane permeability assay for blood- brain barrier. *Eur. J. Med. Chem.* **2003**, *38*, 223−232.

[367] May, P. C.; Dean, R. A.; Lowe, S. L.; Martenyi, F.; Sheehan, S. M.; Boggs, L. N.; Monk, S. A.; Mathes, B. M.; Mergott, D. J.; Watson, B. M.; Stout, S. L.; Timm, D. E.; Smith LaBell, E.; Gonzales, C. R.; Nakano, M.; Jhee, S. S.; Yen, M.; Ereshefsky, L.; Lindstrom, T. D.; Calligaro, D. O.; Cocke, P. J.; Hall, D. G.; Friedrich, S.; Citron, M.; Audia, J. E. Robust central reduction of amyloid-β in humans with an orally available, non-peptidic β-secretase inhibitor*. J. Neurosci.* **2011**, *31*, 16507−16516.

[368] Serrano-Pozo, A.; Frosch, M, P.; Masliah, E.; Hyman, B. T. Neuropathological alterations in Alzheimer disease. *Cold Spring Harb. Perspect. Med.* **2011**, *1*, a006189.

[369] Garcia-Alloza, M.; Robbins, E. M.; Zhang-Nunes, S. X.; Purcell, S. M.; Betensky, R. A.; Raju, S.; Prada, C.; Greenberg, S. M.; Bacskai, B. J.; Frosch, M. P. Characterization of amyloid deposition in the APPswe/PS1dE9 mouse model of Alzheimer disease. *Neurobiol. Dis.* **2006***, 24*, 516−524.

[370] Walsh, D. M.; Klyubin, I.; Fadeeva, J. V.; Cullen, W. K.; Anwyl, R.; Wolfe, M. S.; Rowan, M. J.; Selkoe, D. J. Naturally secreted oligomers of amyloid beta protein potently inhibit hippocampal long-term potentiation in vivo. *Nature* **2002**, *416*, 535−539.

[371] Selkoe, D. J. Alzheimer's disease is a synaptic failure. *Science* **2002**, *298*, 789−791.

[372] Shankar, G. M.; Li, S.; Mehta, T. H.; Garcia-Muñoz, A.; Shepardson, N. E.; Smith, I.; Brett, F. M.; Farrell, M. A.; Rowan, M. J.; Lemere, C. A.; Regan, C. M.; Walsh, D. M.; Sabatini, B. L.; Selkoe, D. J. Amyloid-beta protein dimers isolated directly from Alzheimer's brains impair synaptic plasticity and memory. *Nat. Med*. **2008**, *14*, 837−842.

[373] Selkoe, D. J. Soluble oligomers of the amyloid beta-protein impair synaptic plasticity and behavior. *Behav. Brain Res*. **2008**, *192*, 106−113.

[374] Ashe, K. H. Learning and memory in transgenic mice modeling Alzheimer's disease. *Learn Mem.* **2001**, *8*, 301−308.

[375] Martin, S. J.; Grimwood, P. D.; Morris, R. G. Synaptic plasticity and memory: an evaluation of the hypothesis. *Annu. Rev. Neurosci.* **2000**, *23*, 649−711.

[376] Whitlock, J. R.; Heynen, A. J.; Shuler, M. G.; Bear, M. F. Learning induces long-term potentiation in the hippocampus. *Science* **2006**, *313*, 1093−1097.

[377] Morris, R. G.; Anderson, E.; Lynch, G. S.; Baudry, M. Selective impairment of learning and blockade of long-term potentiation by an N-methyl-D-aspartate receptor antagonist, AP5. *Nature* **1986**, *319*, 774−776.

[378] Caroni, P.; Donato, F.; Muller, D. Structural plasticity upon learning: regulation and functions. *Nat. Rev. Neurosci.* **2012**, *13*, 478−490.

[379] Morris, R. G.; Garrud, P.; Rawlins, J. N.; O'Keefe, J. Place navigation impaired in rats with hippocampal lesions. *Nature* **1982**, *297*, 681−683.

[380] Hommet, C.; Mondon, K.; Camus, V.; De Toffol, B.; Constans, T. Epilepsy and dementia in the elderly. *Dement. Geriatr. Cogn. Disord.* **2008**, *25*, 293−300.

[381] Mendez, M.; Lim, G. Seizures in elderly patients with dementia: epidemiology and management. *Drugs Aging* **2003***, 20,* 791−803*.*

[382] Palop, J. J.; Mucke, L. Epilepsy and cognitive impairments in Alzheimer disease. *Arch. Neurol.* **2009**, *66*, 435−440

[383] Palop, J. J.; Mucke, L. Amyloid-β-induced neuronal dysfunction in Alzheimer's disease: from synapses toward neural networks. *Nat. Neurosci.* **2010**, *13*, 812−818.

[384] Vossel, K. A.; Beagle, A. J.; Rabinovici, G. D.; Shu, H.; Lee, S. E.; Naasan, G.; Hegde, M.; Cornes, S. B.; Henry, M. L.; Nelson, A. B.; Seeley, W. W.; Geschwind, M. D.; Gorno-Tempini, M. L.; Shih, T.; Kirsch, H. E.; Garcia, P. A.; Miller, B. L.; Mucke, L. Seizures and epileptiform activity in the early stages of Alzheimer disease. *JAMA Neurol.* **2013**, *70*, 1158−1166.

[385] McCarron, M.; Gill, M.; McCallion, P.; Begley, C. Health comorbidities in ageing persons with Down syndrome and Alzheimer's dementia. *J. Intellect. Disabil. Res.* **2005**, *49*, 560−566.

[386] Palop, J. J.; Chin, J.; Roberson, E. D.; Wang, J.; Thwin, M. T.; Bien-Ly, N.; Yoo, J.; Ho, K. O.; Yu, G. Q.; Kreitzer, A.; Finkbeiner, S.; Noebels, J. L.; Mucke, L. Aberrant excitatory neuronal activity and compensatory remodeling of inhibitory hippocampal circuits in mouse models of Alzheimer's disease. *Neuron* **2007**, *55*, 697−711.

[387] Sanchez, P. E.; Zhu, L.; Verret, L.; Vossel, K. A.; Orr, A. G.; Cirrito, J. R.; Devidze, N.; Ho, K.; Yu, G. Q.; Palop, J. J.; Mucke, L. Levetiracetam suppresses neuronal network dysfunction and reverses synaptic and cognitive deficits in an Alzheimer's disease model. *Proc. Natl. Acad. Sci. U. S. A.* **2012***, 109,* E2895−E2903.

[388] Shi, J. Q.; Wang, B. R.; Tian, Y. Y.; Xu, J.; Gao, L.; Zhao, S. L.; Jiang, T.; Xie, H. G.; Zhang, Y. D. Antiepileptics topiramate and levetiracetam alleviate behavioral deficits and reduce neuropathology in APPswe/PS1dE9 transgenic mice. *CNS Neurosci. Ther*. **2013**, *19*, 871−881.

[389] Bakker, A.; Krauss, G. L.; Albert, M. S.; Speck, C. L.; Jones, L. R.; Stark, C. E.; Yassa, M. A.; Bassett, S. S.; Shelton, A. L.; Gallagher, M. Reduction of hippocampal hyperactivity improves cognition in amnestic mild cognitive impairment. *Neuron* **2012**, *74*, 467−474.

[390] Lynch, B. A.; Lambeng, N.; Nocka, K.; Kensel-Hammes, P.; Bajjalieh, S. M.; Matagne, A.; Fuks, B. The synaptic vesicle protein SV2A is the binding site for the antiepileptic drug levetiracetam. *Proc. Natl. Acad. Sci. U. S. A.* **2004**, *101*, 9861−9866.

[391] Vogl, C.; Mochida, S.; Wolff, C.; Whalley, B. J.; Stephens, G. J. The synaptic vesicle glycoprotein 2A ligand levetiracetam inhibits presynaptic Ca2+ channels through an intracellular pathway. *Mol. Pharmacol.* **2012**, *82*, 199−208.

[392] Meehan, A. L.; Yang, X.; McAdams, B. D.; Yuan, L.; Rothman, S. M. A new mechanism for antiepileptic drug action: vesicular entry may mediate the effects of levetiracetam*. J. Neurophysiol.* **2011**, *106*, 1227−1239.

[393] Ueda, Y.; Doi, T.; Nagatomo, K.; Tokumaru, J.; Takaki, M.; Willmore, L. J. Effect of levetiracetam on molecular recognition of hippocampal glutamate and GABA transporters in rats with chronic seizures induced by amygdalar $FeCl_3$ injection. *Brain Res*. **2007**, *1151*, 55−61.

[394] Godoy, J. A.; Rios, J. A.; Zolezzi, J. M.; Braidy, N.; Inestrosa, N. C. Signaling pathway cross talk in Alzheimer's disease. *Cell Commun. Signal.* **2014**, *12*, 1−12.

[395] Lanni, C.; Lenzken, S. C.; Pascale, A.; Del Vecchio, I.; Racchi, M.; Pistoia, F.; Govoni, S. Cognition enhancers between treating and doping the mind. *Pharmacol. Res.* **2008**, *57*, 196**–**213.

[396] Croisile, B.; Trillet, M.; Fondarai, J.; Laurent, B.; Mauguière, F.; Billardon, M. Long-term and high-dose piracetam treatment of Alzheimer's disease. *Neurology* **1993**, *43*, 301**–**305.

[397] Waegemans, T.; Wilsher, C. R.; Danniau, A.; Ferris, S. H.; Kurz, A.; Winblad, B. Clinical efficacy of piracetam in cognitive impairment: a meta-analysis. *Dement. Geriatr. Cogn. Disord*. **2002**, *13*, 217–224.

[398] Giurgea, C. E. The nootropic concept and its prospective implications. *Drug Dev. Res.* **1982**, *2*, 441–446.

[399] Müller, W. E.; Eckert, G. P.; Eckert, A. Piracetam: novelty in a unique mode of action. *Pharmacopsychiatry* **1999**, *32*, Suppl 1: 2–9.

[400] Valzelli, L.; Bernasconi, S.; Sala, A. Piracetam activity may differ according to the age of the recipient mouse. *Int. Pharmacopsychiatry* **1980**, *15*, 150–156.

[401] Müller, W. E.; Koch, S.; Scheuer, K.; Rostock, A.; Bartsch, R. Effects of piracetam on membrane fluidity in the aged mouse, rat, and human brain. *Biochem. Pharmacol.* **1997**, *53*, 135–140.

[402] Boschi, F.; Camps, P.; Comes-Franchini, M.; Muñoz-Torrero, D.; Ricci, A.; Sánchez, L. A synthesis of levetiracetam based on (S)-N-phenylpantolactam as a chiral auxiliary. *Tetrahedron: Asymmetry* **2005**, *16*, 3739−3745.

[403] Carlier, P. R.; Chow, E. S. H.; Han, Y.; Liu, J.; El Yazal, J.; Pang, Y. P. Heterodimeric tacrine-based a cetylcholinesterase inhibitors: Investigating ligand−peripheral site interactions. *J. Med. Chem.* **1999**, *42*, 4225−4231.

[404] Camps, P.; Contreras, J.; Font-Bardia, M.; Morral, J.; Muñoz-Torrero, D.; Solans, X. Enantioselective synthesis of tacrine−huperzine A hybrids. Preparative chiral MPLC separation of their racemic mixtures and absolute configuration assignments by X-ray diffraction analysis. *Tetrahedron: Asymmetry* **1998**, *9*, 835−849.

[405] Prati, F.; Uliassi, E.; Bolognesi, M. L. Two diseases, one approach: multitarget drug discovery in Alzheimer's and neglected tropical diseases. *Med. Chem. Commun*. **2014**, *5*, 853–861.

[406] Morphy, R.; Kay, C.; Rankovic, Z. From magic bullets to designed multiple ligands. *Drug Discov. Today*, **2004**, *9*, 641–651.

[407] Cherny, R. A.; Atwood, C. S.; Xilinas, M. E.; Gray, D. N.; Jones, W. D.; McLean, C. A.; Barnham, K. J.; Volitakis, I.; Fraser, F. W.; Kim, Y.; Huang, X.; Goldstein, L. E.; Moir, R. D.; Lim, J. T.; Beyreuther, K.; Zheng, H.; Tanzi, R. E.; Masters, C. L.; Bush, A. I. Treatment with a copper-zinc chelator markedly and rapidly inhibits beta-amyloid accumulation in Alzheimer's disease transgenic mice. *Neuron* **2001**, *30*, 665−676.

[408] Ritchie, C. W.; Bush, A. I.; Mackinnon, A.; Macfarlane, S.; Mastwyk, M.; MacGregor, L.; Kiers, L.; Cherny, R.; Li, Q. X.; Tammer, A.; Carrington, D.; Mavros, C.; Volitakis, I.; Xilinas, M., Ames, D.; Davis, S.; Beyreuther, K.; Tanzi, R. E.; Masters, C. L. Metal-protein attenuation with iodochlorhydroxyquin (clioquinol) targeting Abeta amyloid deposition and toxicity in Alzheimer disease: a pilot phase 2 clinical trial. *Arch. Neurol.* **2003**, *60*, 1685−1691.

[409] LeVine H. 3rd.; Ding, Q.; Walker, J. A.; Voss, R. S.; Augelli-Szafran, C. E. Clioquinol and other hydroxyquinoline derivatives inhibit Abeta(1-42) oligomer assembly. *Neurosci. Lett.* **2009**, *465*, 99−103.

[410] Chibale, K. Economic drug discovery and rational medicinal chemistry for tropical diseases. *Pure Appl. Chem.* **2005**, *77*, 1957−1964.

[411] Egan, T. J. Haemozoin formation as a target for the rational design of new antimalarials. *Drug Des. Rev. Online* **2004**, *1*, 93–110.

[412] Onyeibor, O.; Croft, S. L.; Dodson, H. I.; Feiz-Haddad, M.; Kendrick, H.; Millington, N. J.; Parapini, S.; Phillips, R. M.; Seville, S.; Shnyder, S. D.; Taramelli, D.; Wright, C. W. Synthesis of some cryptoleine analogues, assessment of their antimalarial and cytotoxic activities, and consideration of their antimalarial mode of action. *J. Med. Chem*. **2005**, *48*, 2701−2709.

[413] Girault, S.; Grellier, P.; Berecibar, A.; Maes, L.; Mouray, E.; Lemière, P.; Debreu, M. A.; Davioud-Charvet, E.; Sergheraert, C. Antimalarial, antitrypanosomal, and antileishmanial activities and cytotoxicity of bis(9-amino-6-chloro-2-methoxyacridines):influence of the linker. *J. Med. Chem*. **2000**, *43*, 2646−2654.

[414] Ellman, G. L.; Courtney, K. D.; Andres, V., Jr.; Featherstone, R. M. A new and rapid colorimetric determination of acetylcholinesterase activity. *Biochem. Pharmacol*. **1961**, *7*, 88−95.

[415] Doak, B. C.; Zheng, J.; Dobritzsch, D.; Kihlberg, J. How Beyond Rule of 5 Drugs and Clinical Candidates Bind to Their Targets. *J. Med. Chem.* **2016**, *59*, 2312−2327.

[416] Gregor, V. E.; Emmerling, M. R.; Lee, C.; Moore, C. J. The synthesis and in vitro acetylcholinesterase and butyrylcholinesterase inhibitory activity of tacrine (Cognex®) derivatives. *Bioorg. Med. Chem. Lett*. **1992**, *2*, 861−864.

[417] Ma, M.; Mehta, J.; Williams, L. D.; Carlier, P. R. Pd-catalyzed amination as an alternative to nucleophilic aromatic substitution for the synthesis of N-alkyltacrines and analogs. *Tetrahedron Lett*. **2011**, *52*, 16−919.

[418] Ronco, C.; Jean, L.; Outaabout, H.; Renard, P.-Y. Palladium-catalyzed preparation of N-alkylated tacrine and huprine compounds. *Eur. J. Org. Chem*. **2011**, 302−310.

[419] Camps, P.; Formosa, X.; Muñoz-Torrero, D.; Petrignet, J.; Badia, A.; Clos, M. V. Synthesis and pharmacological evaluation of huprine-tacrine heterodimers: Subnanomolar dual binding site acetylcholinesterase inhibitors. *J. Med. Chem.* **2005**, *48*, 1701−1704.

[420] Hu, M. K.; Lu, C. F. A Facile Synthesis of Bis-Tacrine Isosteres. *Tetrahedron Lett.* **2000**, *41*, 1815–1818.

[421] Michalson, E. T.; D'Andrea, S.; Freeman, J. P.; Szmuszkovicz, J. The Synthesis of 9-(1-Azetidinyl)-1,2,3,4-tetrahydroacridine. *Heterocycles* **1990**, *30*, 415–425.

[422] Eberle, C.; Burkhard, J. A.; Stump, B.; Kaiser, M.; Brun, R.; Krauth-Siegel, R. L.; Diederich, F. Synthesis, inhibition potency, binding mode, and antiprotozoal activities of fluorescent inhibitors of trypanothione reductase based on mepacrine-conjugated diaryl sulfide scaffolds. *ChemMedChem* **2009**, *4*, 2034−2044.

[423] Krauth-Siegel, R. L.; Inhoff, O. Parasite-specific trypanothione reductase as a drug target molecule. *Parasitol. Res*. **2003**, *90*, S77−85.

[424] Spinks, D.; Shanks, E. J.; Cleghorn, L. A. T.; McElroy, S.; Jones, D.; James, D.; Fairlamb, A. H.; Frearson, J. A.; Wyatt, P. G.; Gilbert, I. H. Investigaton of trypanothione reductase as a drug target *in Trypanosoma brucei. ChemMedChem* **2009**, *4*, 2060−2069.

[425] Chibale, K.; Haupt, H.; Kendrick, H.; Yardley, V.; Saravanamuthu, A.; Fairlamb, A. H.; Croft, S. L. Antiprotozoal and cytotoxicity evaluation of sulfonamide and urea analogues of quinacrine. *Bioorg. Med. Chem. Lett.* **2001**, *11*, 2655−2657.

[426] Saravanamuthu, A.; Vickers, T. J.; Bond, C. S.; Peterson, M. R.; Hunter, W. N.; Fairlamb, A. H. Two interacting binding sites for quinacrine derivatives in the active site of trypanothione reductase: a template for drug design. *J. Biol. Chem.* **2004**, *279*, 29493−29500.

[427] Bonnet, B.; Soullez, D.; Davioud-Charvet, E.; Landry, V.; Horvath, D.; Sergheraert, C. New spermine and spermidine derivatives as potent inhibitors of *Trypanosoma cruzi* trypanothione reductase. *Bioorg. Med. Chem.* **1997**, *5*, 1249−1256.

[428] Girault, S.; Baillet, S.; Horvath, D.; Lucas, V.; Davioud-Charvet, E.; Tartar, A.; Sergheraert, C. New potent inhibitors of trypanothione reductase from *Trypanosoma cruzi* in the 2-aminodiphenylsulfide series. *Eur. J. Med. Chem.* **1997**, *32*, 39−52.

[429] Girault, S.; Davioud-Charvet, T. E.; Maes, L.; Dubremetz, J. F.; Debreu, M. A.; Landry, V.; Sergheraert, C. Potent and specific inhibitors of trypanothione reductase from *Trypanosoma cruzi*: bis(2-aminodiphenylsulfides) for fluorescent labeling studies. *Bioorg. Med. Chem*. **2001**, *9*, 837−846.

[430] Walton, J. G. A.; Jones, D. C.; Kiuru, P.; Durie, A. J.; Westwood, N. J.; Fairlamb, A. H. Synthesis and evaluation of indatraline-based inhibitors for trypanothione reductase. *ChemMedChem* **2011**, *6*, 321−328.

[431] Basilico, N.; Pagani, E.; Monti, D.; Olliaro, P.; Taramelli, D. A microtitre-based method for measuring the haem polymerization inhibitory activity (HPIA) of antimalarial drugs. *J. Antimicrob. Chemother.* **1998**, *42*, 55−60.

[432] Parapini, S.; Basilico, N.; Pasini, E.; Egan, T. J.; Olliaro, P.; Taramelli, D.; Monti, D. Standardization of the physicochemical parameters to assess *in vitro* the beta-hematin inhibitory activity of antimalarial drugs. *Exp. Parasitol*. **2000**, *96*, 249−256.

[433] Best, M.; Gifford, A. N.; Kim, S. W.; Babst, B.; Piel, M.; Rösch, F.; Fowler, J. S. Rapid radiosynthesis of [11C] and [14C]azelaic, suberic, and sebacic acids for in vivo mechanistic studies of systemic acquired resistance in plants. *J. Labelled Compd. Radiopharm*. **2012**, *55*, 39−43.

[434] Taber, D. F.; Kong, S. Alkylation of acetonitrile. *J. Org. Chem.* **1997**, *62*, 8575−8576.

[435] Lethesh, K. C.; Van Hecke, K.; Van Meervelt, L.; Nockemann, P.; Kirchner, B.; Zahn, S.; Parac-Vogt, T. N.; Dehaen, W.; Binnemans, K. Nitrile-functionalized pyridinium, pyrrolidinium, and piperidinium ionic liquids. *J. Phys. Chem. B* **2011**, *115*, 8424−8438.

[436] Chang, C. S.; Su, C. C.; Zhuang, J. R.; Tsai, S. W. Enhancement of enantioselectivity on the synthesis of (S)-naproxen morpholinoalkyl ester prodrugs in organic solvents using isopropanol-dried immobilized lipase. *J. Mol. Catal. B. Enzym.* **2004**, *30*, 151–157.

[437] Trape, J. F. The public health impact of chloroquine resistance in Africa. *Am. J. Trop. Med. Hyg*. **2001**, *64*, 12−17.

[438] Marks, F.; von Kalckreuth, V.; Kobbe, R.; Adjei, S.; Adjei, O.; Horstmann, R. D.; Meyer, C. G.; May, J. Parasitological rebound effect and emergence of pyrimethamine resistance in Plasmodium falciparum after single-dose sulfadoxine-pyrimethamine. *J. Infect. Dis*. **2005**, *192*, 1962−1965.

[439] Egan, T. J.; Kaschula, C. H. Strategies to reverse drug resistance in malaria. *Curr. Opin. Infect. Dis*. **2007**, *20*, 598−604.

[440] Gottschall, J. L.; Elliot, W.; Lianos, E.; McFarland, J. G.; Wolfmeyer, K.; Aster, R. H. Quinine-induced immune thrombocytopenia associated with hemolytic uremic syndrome: a new clinical entity. *Blood* **1991**, *77*, 306−310.

[441] Veinot, J. P.; Mai, K. T.; Zarychanski, R. Chloroquine related cardiac toxicity. *J. Rheumatol*. **1998**, *25*, 1221−1225.

[442] Nkhoma, E. T.; Poole, C.; Vannappagari, V.; Hall, S. A.; Beutler, E. The global prevalence of glucose-6-phosphate dehydrogenase deficiency: a systematic review and meta-analysis. *Blood Cells Mol. Dis*. **2009**, *42*, 267−278.

[443] Atamna, H.; Pascarmona, G.; Ginsburg, H. Hexose-monophosphate shunt activity in intact *Plasmodium falciparum*-infected erythrocytes and in free parasites. *Mol. Biochem. Parasitol*. **1994**, *67*, 79–89.

[444] Crooke, A.; Diez, A.; Mason, P. J.; Bautista, J. M. Transient silencing of *Plasmodium falciparum* bifunctional glucose-6-phosphate dehydrogenase-6-phosphogluconolactonase. *FEBS J*. **2006**, *273*, 1537−1546.

[445] Baum, J.; Papenfuss, A. T.; Mair, G. R.; Janse, C. J.; Vlachou, D.; Waters, A. P.; Cowman, A. F.; Crabb, B. S.; de Koning-Ward, T. F. Molecular genetics and comparative genomics reveal RNAi is not functional in malaria parasites. *Nucleic Acids Res*. **2009**, *37*, 3788–3798.

[446] Lopez-Barragan, M. J.; Lemieux, J.; Quinones, M.; Williamson,K. C.; Molina-Cruz, A.; Cui, K.; Barillas-Mury, C.; Zhao, K.; Su, X. Z. Directional gene expression and antisense transcripts in sexual and asexual stages of *Plasmodium falciparum. BMC Genomics* **2011**, *12*, 587.

[447] Preuss, J.; Maloney, P.; Peddibhotla, S.; Hedrick, M. P.; Hershberger, P.; Gosalia, P.; Milewski, M.; Li, Y. L.; Sugarman, E.; Hood, B.; Suyama, E.; Nguyen, K.; Vasile, S.; Sergienko, E.; Mangravita-Novo, A.; Vicchiarelli, M.; McAnally, D.; Smith, L. H.; Roth, G. P.; Diwan, J.; Chung, T. D. Y.; Jortzik, E.; Rahlfs, S.; Becker, K.; Pinkerton, A. B.; Bode, L. Discovery of a *Plasmodium falciparum* Glucose-6-phosphate Dehydrogenase 6-phosphogluconolactonase Inhibitor (R,Z)-N-((1- Ethylpyrrolidin-2-yl)methyl)-2-(2-fluorobenzylidene)-3-oxo-3,4-dihydro‑2H‑benzo[b][1,4]thiazine-6-carboxamide (ML276) That Reduces Parasite Growth in Vitro. *J. Med. Chem.* **2012**, *55*, 7262−7272.

[448] Preuss, J.; Hedrick, M.; Sergienko, E.; Pinkerton, A.; Mangravita-Novo, A.; Smith, L.; Marx, C.; Fischer, E.; Jortzik, E.; Rahlfs, S.; Becker, K.; Bode, L. High-throughput screening for small- molecule inhibitors of *Plasmodium falciparum* glucose-6-phosphate dehydrogenase 6-phosphogluconolactonase. *J. Biomol. Screening* **2012**, *17*, 738−751.

[449] Maloney, P.; Hedrick, M.; Peddibhotla, S.; Hershberger, P.; Milewski, M.; Gosalia, P.; Li L.; Preuss, J.; Sugarman, E.; Hood, B.; Suyama, E.; Nguyen, K.; Vasile, S.; Sergienko, E.; Salanawil, S.; Stonich, D.; Su, Y.; Dahl, R.; Mangravita-Novo, A.; Vicchiarelli, M.; McAnally, D.; Smith, L. H.; Roth, G.; Diwan, J.; Chung, T. D. Y.; Pinkerton, A. B.; Bode, L.; Becker, K. (**2010**) A Selective Inhibitor of Plasmodium falciparum Glucose-6-Phosphate Dehydrogenase (PfG6PDH) in Probe Reports from the NIH Molecular Libraries Program, Bethesda (MD). http://www.ncbi.nlm.nih.gov/books/NBK143548/

[450] Maloney, P.; Hedrick, M.; Peddibhotla, S.; Hershberger, P.; Milewski, M.; Gosalia, P.; Li L.; Preuss, J.; Sugarman, E.; Hood, B.; Suyama, E.; Nguyen, K.; Vasile, S.; Sergienko, E.; Salanawil, S.; Stonich, D.; Su, Y.; Dahl, R.; Mangravita-Novo, A.; Vicchiarelli, M.; McAnally, D.; Smith, L. H.; Roth, G.; Diwan, J.; Chung, T. D. Y.; Pinkerton, A. B.; Bode, L.; Becker, K. (**2010**) A 2nd Selective Inhibitor of Plasmodium falciparum Glucose-6-Phosphate Dehydrogenase (PfG6PDH) - Probe 2 in Probe Reports from the NIH Molecular Libraries Program, Bethesda (MD). http://www.ncbi.nlm.nih.gov/books/NBK184495/

[451] Allen, S. M.; Lim, E. E.; Jortzik, E.; Preuss, J.; Chua, H. H.; MacRae, J. I.; Rahlfs, S.; Haeussler, K.; Downton, M. T.; McConville, M. J.; Becker, K.; Ralph, S. A. *Plasmodium falciparum* glucose-6-phosphate dehydrogenase 6-phosphogluconolactonase is a potential drug target. *FEBS J.* **2015**, *282*, 3808−3823.

[452] Gómez-García, M.; Benito, J. M.; Gutiérrez-Gallego, R.; Maestre, A.; Mellet, C. O.; Fernández, J. M.; Blanco, J. L. Comparative studies on lectin–carbohydrate interactions in low and high density homo- and heteroglycoclusters. *Org. Biomol. Chem.* **2010**, *8*, 1849−1860.

[453] Klose, J.; Reese, C. B.; Song, Q. Preparation of 2-(2-Cyanoethyl)sulfanyl-1*H*-isoindole-l,3-(2*H*)-dione and related sulfur-transfer agents. *Tetrahedron* **1997**, *53*, 14411−14416.

[454] Burland, P. A.; Osborn, H. M.; Turkson, A. Synthesis and glycosidase inhibitory profiles of functionalised morpholines and oxazepanes. *Bioorg. Med. Chem.* **2011**, *19*, 5679–5692.

[455] Zarchi, M. A. K.; Tayefi, M.; Tirgir, F.; Sabzalian, M. R. An environmentally compatible synthesis of polyesters derived from 5-(2-Phthalimidoethanesulfonamido) isophthalic acid as a novel diacid monomer. *J. Appl. Polym. Sci*. **2011**, *121*, 2573–2583.

Communication of results

OTHER JOURNAL PUBLICATIONS

- Di Pietro, O.; Alencar, N.; Esteban, G.; Viayna, E.; Szałaj, N.; Vázquez, J.; Juárez-Jiménez, J.; **Sola, I.**; Pérez, B., Solé, M.; Unzeta, M.; Muñoz-Torrero, D.; Luque, F. J. Design, synthesis and biological evaluation of *N*-methyl-*N*-[(1,2,3-triazol-4-yl)alkyl]propargylamines as novel monoamine oxidase B inhibitors. *Bioorg Med Chem.* **2016**, in press.

- **Sola**, **I**.; Viayna, E.; Gómez, T.; Galdeano, C.; Cassina, M.; Camps, P.; Romeo, M.; Diomede, L.; Salmona, M.: Franco, P.; Schaeffer, M.; Colantuono, D.; Robin, D.; Jud, D.; Hutter-Paier, B.; Muñoz-Torrero, D., Multigram synthesis and *in vivo* efficacy studies of the donepezil–huprine hybrid AVCRI104P4, a multi-target anti-Alzheimer compound. *Molecules* **2015**, *20*, 4492−4515.

- Di Pietro, O.; Vicente-García, E.; Viayna, E.; Lanzoni, A.; **Sola**, **I**.; Taylor; M. C.; Berenguer, D.; Fisa, R.; Riera, C.; Clos, M. V.; Pérez, B.; Kelly, J. M.; Lavilla, R.; Muñoz-Torrero, D., Multicomponent reaction-based synthesis and biological evaluation of tricyclic heterofused quinolines with multi-trypanosomatid activity. *Eur. J. Med. Chem.* **2015**, *105*, 120−137.

- Pouplana, S.; Espargaró, A.; Galdeano, C.; Viayna, E.; **Sola**, **I**.; Ventura, S.; Muñoz-Torrero, D.; Sabate, R., Thioflavin-S staining of bacterial inclusion bodies for the fast, simple, and inexpensive screening of amyloid aggregation inhibitors. *Curr. Med. Chem*. **2014**, *21*, 1152−1159.

- Galdeano, C.; Viayna, E.; **Sola**, **I**.; Formosa, X.; Camps, P.; Badia, A.; Clos, M.V.; Relat, J.; Ratia, M.; Bartolini, M.; Mancini, F.; Andrisano, V.; Salmona, M.; Minguillón, C.; González-Muñoz, G. C.; Rodríguez-Franco, M.I.; Bidon-Chanal, A.; Luque, F.J.; Muñoz-Torrero, D., Huprine-tacrine heterodimers as anti-amyloidogenic compounds of potential interest against Alzheimer's and prion diseases. *J. Med. Chem.* **2012**, *55*, 661−669.

- Viayna, E.; **Sola**, **I**.; Di Pietro, O.; Muñoz-Torrero, D., Human disease and drug pharmacology, complex as real life. *Curr. Med. Chem*. **2012**, *20*, 1623−1634.

- Muñoz-Torrero, D.; Pera, M.; Relat, J.; Ratia, M.; Galdeano, C.; Viayna, E.; **Sola**, **I**.; Formosa, X.; Camps, P.; Badia, A.; Clos, M.V., Expanding the multipotent profile of huprine-tacrine heterodimers as disease-modifying anti-Alzheimer agents. *Neurodegener. Dis.* **2012**, *9*, 96−99.

PATENTS

- Muñoz-Torrero D.; Ferrer, I.; **Sola**, **I**.; Aso, E. Multi-target drug compounds for the treatment of neurodegenerative disorders, WO 2014/206877 A1.

- Muñoz-Torrero D.; Inestrosa, N.C.; Viayna, E.; **Sola**, **I**.; Vázquez, S. Beta-amyloid-directed multitarget compounds for the treatment of Alzheimer's disease, US 9,238,626 B2.

PRESENTATIONS IN SCIENTIFIC MEETINGS

- **Sola**, **I**.; Aso, E.; Frattini, D.; López-González, I.; Espargaró, A.; Sabaté, R.; Clos, M. V.; Ferrer, I.; Muñoz-Torrero. D. Synthesis and *in vitro* & *in vivo* evaluation of a levetiracetam-huprine hybrid as a novel multitarget anti-Alzheimer drug candidate (Poster presentation). II Simposio de Jóvenes Investigadores de la Sociedad Española de Química Terapéutica (SEQT), Madrid, Spain, 2015.

- **Sola**, **I**.; Viayna, E.; Bartolini, M.; De Simone, A.; Andrisano, V.; Clos, M.; V.; Pérez, B.; Badia, A.; Sabaté, R.; Inestrosa,N.; Muñoz-Torrero, D. Synthesis and in vitro & in vivo evaluation of a novel rhein-huprine Y multi-target anti-alzheimer compounds (Oral communication). I Simposio de Jóvenes Investigadores de la Sociedad Española de Química Terapéutica (SEQT), Madrid, Spain, 2014.

- **Sola**, **I**.; Artigas, A.; Taylor, M.C.; Pérez, B.; Kelly, J.M.; Muñoz-Torrero, D. Bis-huprines as a new family of trypanocidal agents (Poster presentation). XVII National Meeting Sociedad Española de Química Terapéutica (SEQT) - Advances in Drug Discovery: Successes, Trends and Future Challenges, Madrid, Spain, 2013.

- Viayna, E.; **Sola, I**.; Bartolini, M.; De Simone, A.; Tapia-Rojas, C.; Carvajal, F.J.; Serrano, F.G.; Sabate, R.; Juárez, J.; Pérez, B.; Badia, A.; Luque, F.J.; Andrisano, V.; Clos, M.V.; Inestrosa, N.C.; Muñoz-Torrero, D. Synthesis, molecular modelling, in vitro biological profiling, and in vivo efficacy studies of a novel family of huprine-based multi-target anti-Alzheimer compounds (Poster presentation). XVII National Meeting Sociedad Española de Química Terapéutica (SEQT) - Advances in Drug Discovery: Successes, Trends and Future Challenges, Madrid, Spain, 2013.

- **Sola**, **I**.; Viayna, E.; Gómez, T.; Galdeano, C.; Camps, P.; Schaeffer, M.; Colantuono, D.; Robin, D.; Franco, P.; Jud, D.; Hutter-Paier, B.; Diomede, L.; Salmona, M.; Muñoz-Torrero, D. Multi-gram scale synthesis and in vivo efficacy studies of the multitarget anti-Alzheimer compound AVCRI104P4 (Poster presentation). XXIInd International Symposium on Medicinal Chemistry (ISMC 2012), Berlin, Germany, 2012.

- Viayna, E.; **Sola, I.**; Fullana, M. M.; Clos, M. V.; Pérez, B.; Badia, A.; Bartolini, M.; De Simone, A.; Andrisano, V.; Muñoz-Torrero, D. Synthesis and pharmacological evaluation of huprine-based multitarget anti-Alzheimer compounds (Poster presentation). XXIInd International Symposium on Medicinal Chemistry (ISMC 2012), Berlin, Germany, 2012.

- Clos, M.V.; Ratia, M.; Ramírez, V.; Olivares, I.; Viayna, E.; **Sola, I.**; Galdeano, C.; Camps, P.; Muñoz-Torrero, D.; Marutle, A.; Darreh-Shori, T.; Nordberg, A.; Badia, A.; Perez, B.; Giménez-Llort, L. AVCRI104P3, an huprine derivative, increases short- and long-term learning and memory in non-transgenic and restores cognitive deficits in 3xTg-AD mice (Poster presentation). FENS Forum 2012, Barcelona, Spain, 2012.

- Clos, M.V.; Olivares, I.; Ratia, M.; Ramírez, V.; Viayna, E.; **Sola, I.**; Galdeano, C.; Camps, P.; Muñoz-Torrero, D.; Marutle, A.; Darreh-Shori, T.; Nordberg, A.; Badia, A.; Pérez, B.; Giménez-Llort, L. Cognitive and molecular effects of AVCRI104P3, a multitarget anti-Alzheimer drug candidate, in 3xTg-AD mice (Poster presentation). 12th International Stockholm/Springfield Symposium on Advances in Alzheimer Therapy, Stockholm, Sweden, 2012.

- Galdeano, C.; Ragusa, M.I.; Viayna, E.; Moncada, F.; **Sola, I.**; Viayna, A.; Ferlito, V.; Guillou, C.; Muñoz-Torrero, D. Synthesis of huprine-based multitarget anti-Alzheimer compounds bearing an antioxidant pharmacophoric moiety (Poster presentation). 9th Spanish-Italian Symposium on Organic Chemistry (SISOC-IX), Tenerife, Spain, 2012.

- Muñoz-Torrero, D.; Viayna, E.; **Sola, I.**; Gómez, T.; Galdeano, C.; Camps, P.; Ratia, M.; Perez, B.; Badia, A.; Clos, M. V.; Bartolini, M.; Mancini, F.; Andriano, V. AVCRI104P4, a multitarget drug candidate for the disease-modifying treatment of Alzheimer's disease (Poster presentation). Global Alzheimer's Research Summit Madrid 2011 - Present and Future of Alzheimer's Research, Madrid, Spain, 2011.

- Clos, M. V.; Ratia, M.; Ramirez, V.; Viayna, E.; **Sola, I.**; Galdeano, C.; Camps, P.; Muñoz-Torrero, D.; Badia, A.; Perez, B.; Giménez-Llort, L. Behavioural effects of AVCRI104P3 in NTg and 3xTg-AD mice (Poster presentation). Global Alzheimer's Research Summit Madrid 2011 - Present and Future of Alzheimer's Research, Madrid, Spain, 2011.

- Muñoz-Torrero, D.; Galdeano, C.; Viayna, E.; **Sola, I.**; Formosa, X.; Camps, P.; Badia, A.; Clos, M. V.; Pera, M.; Ratia, M.; Bartolini, M.; Mancini, F.; Andrisano, V.; González-Muñoz, G. C.; Rodríguez-Franco, M. I.; Rivail, L.; Luque, F. J. A novel family of huprine derivatives with anti-amyloidogenic properties (Oral communication). The 10th International Conference on Alzheimer's & Parkinson's Diseases AD/PD 2011, Barcelona, Spain, 2011. Publication on Neurodegenerative Diseases 2011, 8, S1.

- Viayna, E.; Camps, P.; Formosa, X.; Galdeano, C.; Muñoz-Torrero, D.; **Sola, I.**; Badia, A.; Clos, M.V.; Pera, M.; Ratia, M.; Bartoloni, M.; Mancini, F.; Andrisano, V.; González-Muñoz, G.C.; Rodríguez-Franco, M.I.; Rivail, L.; Luque, F.J. Síntesi de nous compostos anti-Alzheimer basats en huprina (Oral communication). Sisena Trobada de Joves Investigadors dels Països Catalans, Valencia, Spain, 2010.